The Scientific World Journal

Impacts of Land Use Changes on Soil Properties and Processes

Guest Editors: Antonio Paz González, Cleide Aparecida de Abreu, Ana Maria Tarquis, and Eduardo Medina-Roldán

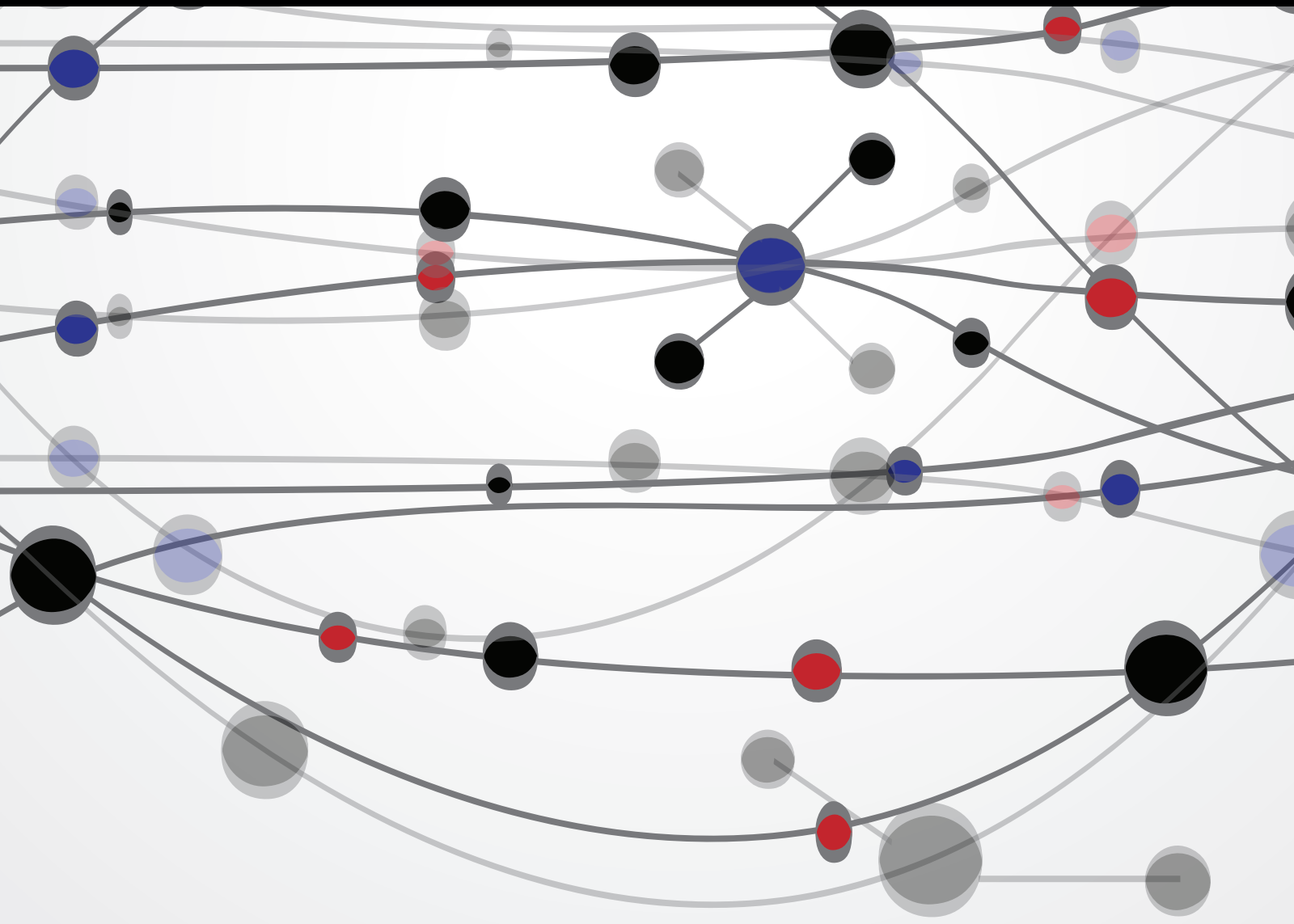

Impacts of Land Use Changes on Soil Properties and Processes

The Scientific World Journal

Impacts of Land Use Changes on Soil Properties and Processes

Guest Editors: Antonio Paz González, Cleide Aparecida de Abreu, Ana Maria Tarquis, and Eduardo Medina-Roldán

Contents

Hindawi Publishing Corporation
The Scientific World Journal
Volume 2014, Article ID 831975, 2 pages
http://dx.doi.org/10.1155/2014/831975

Editorial

Impacts of Land Use Changes on Soil Properties and Processes

Antonio Paz González,[1] Cleide Aparecida de Abreu,[2] Ana Maria Tarquis,[3,4] and Eduardo Medina-Roldán[5]

[1] *Soil Science Department, Faculty of Sciences, University of A Coruña (UDC), 15008 A Coruña, Spain*
[2] *Center for Soils and Environmental Resources, Agronomic Institute of Campinas (IAC), Avenida Barão de Itapura 1481, 13022902 Campinas, SP, Brazil*
[3] *Applied Mathematics Department, Polytechnical University of Madrid, Ciudad Universitaria, s/n, 28040 Madrid, Spain*
[4] *CEIGRAM, Polytechnical University of Madrid, Ciudad Universitaria, s/n, 28040 Madrid, Spain*
[5] *Department of Environmental Sciences, Xi'an Jiaotong-Liverpool University, Suzhou, Jiangsu 25123, China*

Correspondence should be addressed to Antonio Paz González; tucho@udc.es

Received 24 December 2014; Accepted 24 December 2014; Published 31 December 2014

Land use is one of the main drivers of many processes of environmental change, as it influences basic resources within the landscape, including the soil resources. Poor soil management can rapidly deteriorate vast amounts of land, which frequently becomes a major threat to rural subsistence in many developing and developed countries. Conversely, impact of land use changes on soil can occur so unnoticed that land managers hardly contemplate initiating ameliorative measures. Knowledge and understanding of soil properties and processes ensures remediation or reclamation of disturbed or damaged soils.

This special issue brought together an international group of scientists presenting results from field trials and data harvesting carried out in a range of different soils and environments, from Poland, Italy, Spain, and USA to China, Indonesia, Venezuela, Brazil, and Argentina, together with laboratory experiments, reviews, and modeling with advanced mathematical tools. The strength of such issue was derived from a mutual interest in the mechanisms that regulate the impact of land use and changes in land use on soil properties and processes and also in the development and use of the most advanced methods and procedures for assessing them.

Drawing on the latest research and opinion, first this issue contains one state-of-the-art review and two research articles highlighting the usefulness and efficiency of the approach adopted here in a general context. W. Zhou et al. reviewed the effect of paddy upland rotation on soil properties. W. Shangguan et al. addressed the soil pedodiversity of China, mapping the distribution and extent of different soil taxa; this allowed identification of nearly 90 endangered soils, also suggesting that at least two dozens of soils have already gone extinct due to inadequate land use. J. Rejman et al. addressed the role of land use change in soil losses and relief modification in Loess areas of Poland.

Various authors reported laboratory experiments aiming to clarify the role of external inputs (amendments, irrigation, etc.) in selected soil properties. More specifically, A. D. Karathanasis et al. used several amendment materials together with extracts from crop biomass to accelerate fragmentation of fragipans and, therefore, to increase the water holding capacity of these soils. L. Chu et al. assessed the potential of microsprinkler irrigation as a method to alleviate soil salinization, allowing crop growth. M. García-Albacete et al. conducted leaching experiments to analyse phosphorus mobility in both soil-compost ad soil-digestate systems, showing that phosphorus losses were higher for the former than for the latter; in addition this study provided evidence of the importance of waste's wettability for assessing P sorption mechanisms and risk of leaching losses. M. García-Sánchez et al. using a batch experiment showed that both organic amendments and a sulfur compound added to two

different Hg contaminated soils (luvisol and chernozem) were able to reduce Hg mobile fractions and increased availability of macro- and micronutrient.

The role of land use in soil organic matter and nitrogen dynamics has been illustrated by case studies carried out in contrasting soil and climatic conditions. A. F. González-Pedraza and N. Dezzeo studied soil nitrogen seasonality in the Western Llanos of Venezuela. S. Dori et al. addressed soil carbon dynamics in different regions of Europe and discussed the efficiency of management practices that control the potential of sequestration of soil organic carbon. A. Liang et al. analysed the mechanisms of soil organic carbon turnover on agricultural systems using a combination of isotopic tracer and physical fractionation under no-tillage and mouldboard ploughing; results showed that shot term impact of the studied tillage treatments varied in the different fractions analysed. D. A. McGranahan et al. analysed the reliability of carbon sequestration estimations associated with the effect of unexplained variability and due to interactions of vegetation, land use management, and soil properties with belowground ecosystem function; subsequently, even if rangeland soils are important carbon pools, it is unlikely that rangeland plant communities can be effectively categorized by their carbon sequestration potential.

Land use impacts on greenhouse gasses have been a major topic of this special issue. Z. S. Zhang et al. conducted a field trial to evaluate the effect of mulching from residues of a previous crop on paddy fields under no-tillage; this management system was found to significantly increase CO_2 and N_2O emissions, while decreasing CH_4 emissions. S. F. Smith and K. R. Brye reported results from a field trial on a silt loan soil under soybean, showing that the impact of irrigation on seasonal CO_2 emissions differed between years, whereas no-tillage management reduced seasonal CO_2 emissions; the tillage effect on total CO_2 emissions was not dependent on the irrigation scheme used. L. N. L. K. Choo and O. H. Ahmed used a lysimeter experiment to analyse both CO_2 emissions and dissolved organic carbon leaching in a drained peat land cropped to pineapple under tropical conditions. Y. Lu and H. Xu performed an incubation experiment to test the effects of soil temperature, flooding, and organic matter addition on N_2O emissions in a wetland soil.

Two manuscripts addressed the role of land use in soil organism. G. M. Siqueira et al. used the classical pitfall trap method to study the interactions between the soil arthropod community and land use and management of an entisol under semiarid climate in Brazil; the arthropod abundance under native forest was much lower than under native biomes with tropical climate. Agricultural land use strongly decreases the abundance of Formicidae compared to natural biome. E. E. Kuramae et al. studied the role of several land uses in the structure and composition of microbial communities in Netherlands using DNA analysis; the functional gene diversity found in different soils did not group the sites accordingly to land management, and the main factors driving differences in functional genes between land uses or management systems were carbon : nitrogen ratio, phosphatase activity, and total nitrogen.

New experimental and conceptual methods are needed to assess the effects of land use changes on soil properties and processes. J. L. M. P. de Lima et al. mapped soil surface macropores using infrared thermography; this technique is expected to provide a better understanding of the complex relationships between soil pores and soil physical and hydraulic properties. C. Moreno et al. developed an image analysis method to estimate the soil cover by different types of mulching materials during degradation in the field; particular attention was paid to thresholding methods in image treatment; proportion of areas lacking mulch have been automatically assessed. The applications of fractals and multifractals in soil and earth sciences are increasing, since many soil properties and processes have been shown to depend on complex interactions that could be assessed by fractal models. Also there is an increasing availability of data sets allowing computation and modelling using these mathematical tools. J. de Castro et al. described fractal analysis of Laplacian pyramidal and applied this method to segmentation of soil micromorphology; the algorithm used produced more reliable results than the commonly employed OTSU algorithm.

Geostatistics was used to evaluate the spatial variability of several soil properties as related to land use at various sampling scales. G. M. Siqueira et al. used soil apparent electrical conductivity for devising soil sampling schemes in an agricultural field that in a further step were analyzed by geostatistical techniques; as a result, a first manuscript was devoted to estimated spatial patterns of soil compaction and a second one provided insight into the spatial variability of selected general soil properties. L. A. Morales et al. studied the spatial distribution of ammonium-nitrogen, phosphorus, and potassium in a paddy field at Argentina during three different vegetative periods of the rice crop. X. Tan et al. analyzed the spatial variability of sixteen soil properties, including several soil enzymes, focusing on soil quality assessment; it was concluded that the spatial patterns of soil quality were better reflected using an integrated index based on soil enzyme activities. P. L. Aguado et al. used multifractal analysis to characterize a landscape, based on a high resolution digital elevation model; it was shown that the use of the multifractal approach with mean absolute gradient data is a useful tool for analyzing topographical features.

We believe that the present special issue reflects recent advances on the effects of land use over a range of soil properties and processes, complemented with insightful case studies using advanced mathematical techniques and new experimental methods for assessing soil surface characteristics.

Acknowledgment

We wish to thank all the authors for submitting their work in the issue and their patience during the review process.

Antonio Paz González
Cleide Aparecida de Abreu
Ana Maria Tarquis
Eduardo Medina-Roldán

Hindawi Publishing Corporation
The Scientific World Journal
Volume 2014, Article ID 712403, 11 pages
http://dx.doi.org/10.1155/2014/712403

Research Article

Using Multivariate Geostatistics to Assess Patterns of Spatial Dependence of Apparent Soil Electrical Conductivity and Selected Soil Properties

Glécio Machado Siqueira,[1] Jorge Dafonte Dafonte,[2] Montserrat Valcárcel Armesto,[2] and Ênio Farias França e Silva[3]

[1]*Centro de Ciências Agrárias e Ambientais, Universidade Federal do Maranhão, BR-222, Km 04, s/n, Boa Vista, 65500-000 Chapadinha, MA, Brazil*
[2]*Departamento de Ingeniería Agroforestal, Escuela Politécnica Superior, Universidad de Santiago de Compostela, Campus Universitario, s/n, 27002 Lugo, Spain*
[3]*Departamento de Engenharia Agrícola, Universidade Federal Rural de Pernambuco, Dois Irmãos, 52171-900 Recife, PE, Brazil*

Correspondence should be addressed to Glécio Machado Siqueira; gleciosiqueira@hotmail.com

Received 24 June 2014; Revised 26 August 2014; Accepted 28 August 2014; Published 31 December 2014

Academic Editor: Ana Maria Tarquis

The apparent soil electrical conductivity (EC_a) was continuously recorded in three successive dates using electromagnetic induction in horizontal (EC_a-H) and vertical (EC_a-V) dipole modes at a 6 ha plot located in Northwestern Spain. One of the EC_a data sets was used to devise an optimized sampling scheme consisting of 40 points. Soil was sampled at the 0.0–0.3 m depth, in these 40 points, and analyzed for sand, silt, and clay content; gravimetric water content; and electrical conductivity of saturated soil paste. Coefficients of correlation between EC_a and gravimetric soil water content (0.685 for EC_a-V and 0.649 for EC_a-H) were higher than those between EC_a and clay content (ranging from 0.197 to 0.495, when different EC_a recording dates were taken into account). Ordinary and universal kriging have been used to assess the patterns of spatial variability of the EC_a data sets recorded at successive dates and the analyzed soil properties. Ordinary and universal cokriging methods have improved the estimation of gravimetric soil water content using the data of EC_a as secondary variable with respect to the use of ordinary kriging.

1. Introduction

The quality of soil data collection for precision agriculture has a very important influence, since it has been found that acquisition of exhaustive information in this phase supports the use of geospatial technologies for the estimation of soil spatial variability and later on assists in the determination of "management units." However, for assessing the soil spatial variability, a large number of samples are generally needed, which considerably increases costs of sampling and analysis. Notwithstanding, the sampling process can be improved, using soil variables that can be recorded or measured quickly, which can help in enhancing the estimation of other soil properties more difficult to measure.

The measurement of apparent soil electrical conductivity (EC_a) allows the collection of information on the field and on the spatial distribution of other properties that are correlated. In accordance with Corwin and Rhoades [1] the main methods for the measurement of soil EC_a are contact and electromagnetic induction. McNeill [2], Sudduth et al. [3], Corwin and Lesch [4], and Kühn et al. [5] indicate that EC_a is mainly influenced by soil water content, texture, organic matter content, size and distribution of pores, salinity, cation exchange capacity, concentration of electrolytes dissolved in the soil solution, temperature, composition of soil colloids, and so on. Thus, the use of EC_a for soil classification allows recognition and delimitation of the physical, chemical, and biological soil properties that play an important role

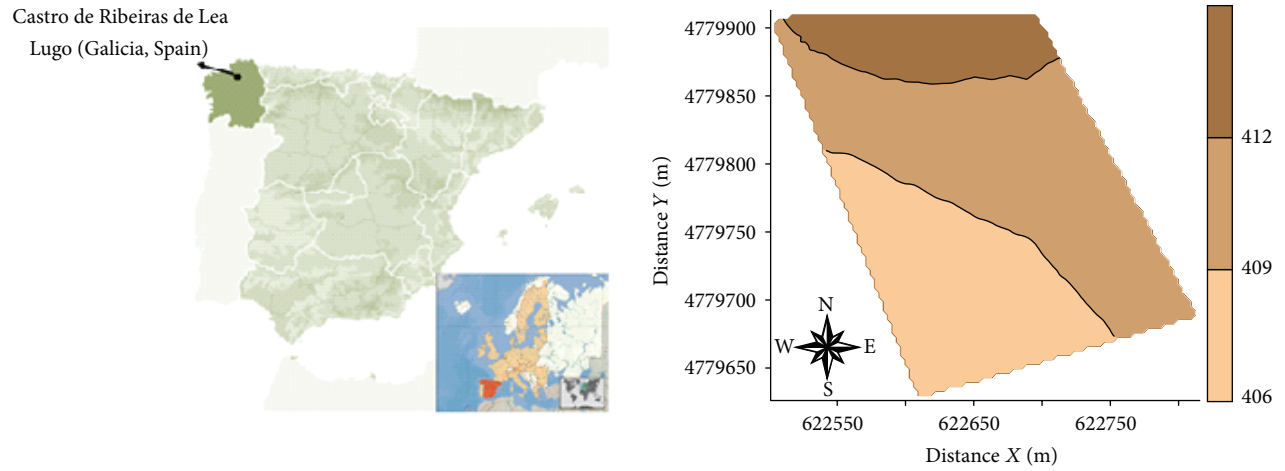

(a) (b)

Figure 1: Geographical location of the study area (a). Field digital elevation model (b).

in agricultural production and environmental conservation. Thus, these data are essential for monitoring the temporal condition of the soil and application management processes [6]. Therefore, the EC_a parameter is used as an aid in precision agriculture, to promote the evaluation of the spatial variability of soil and the definition of management units.

The use of geostatistics has great advantages because it allows the study of the spatial variability of soil properties. Kriging is a geostatistical method that can be used to predict the value of soil properties in unsampled locations, favouring the application of differentiated soil management in precision agriculture. Several authors have devised soil sampling schemes directed by properties that directly or indirectly influence crop yield [7–10], and the success of this approach depends on the use of variables that are quickly and easily measured, such as EC_a.

Based on the above rationale, the objectives of this work were as follows: (1) to analyze the spatial dependence of successive EC_a data sets, (2) to assess the spatial variability of soil texture attributes using a soil sampling scheme directed by soil EC_a, and (3) to improve the estimation of the spatial variability of soil variables such as soil water content through multivariate geostatistics using EC_a as secondary information.

2. Material and Methods

2.1. Study Site. The experimental field is 6 ha in surface and it is located in Castro Ribeiras de Lea (Lugo, NW Spain). Geographic coordinates are 43°09′49″N and 7°29′47″W, average elevation is 410 m, and mean slope is 2% (Figure 1).

The area where the field is located is considered to be representative of both the topographic patterns and the main soil type of the region "Terra Cha," which is characterized by an extensive livestock production, on a landscape with seasonal conditions of hydromorphy, due to impeded drainage.

The crop succession of the experimental site was fallow-silage corn (*Zea mays* L.) under no-till farming during the study year. Previously, this site had been under pasture for silage production. Field data recording and soil sampling were performed in spring 2008.

Table 1: Soil texture data for a representative profile of the study area.

Horizon	Depth (m)	Organic matter	Clay	Silt	Sand	Gravel
		g dm^{-3}	g kg^{-1}			
A_p	0.0–0.35	50.50	175	191	634	370
B_w	0.35–0.70	7.20	192	207	591	448
B_{tg}	>0.70	2.60	479	280	241	—

The soil was classified as a Gleyic Cambisol [11], and it was developed over Tertiary-Quaternary sediments; the parent material from the Quaternary has high gravel content and it is underlain by clayey Tertiary sediments with low saturated hydraulic conductivity [12]. According to Neira Seijo [13] the soil profile of the studied field is represented by the sequence A_p-B_w-B_{tg}, developed on successive sedimentary layers with heterogeneous soil particle size distribution (Table 1). The soil texture of the fine earth (<2.00 mm) was sandy-loam at the A_p horizon, sandy-clay-loam in B_w horizon, and clayey in the horizon B_{tg} and there was a general clay increase with soil depth. Moreover, the A_p and B_w horizons were characterized by a high content of gravel, attaining 37% and 45%, respectively. The organic matter content was rather high on the A_p horizon (5.05%) contrasting with the lower contents at the underlying horizons of the soil profile. The climate of the Terra Cha region is classified as maritime temperate climate (Cfb, according to Köppen), characterized by warm summers and no dry season; average annual rainfall is as high as 930 mm.

2.2. Apparent Soil Electrical Conductivity Measurements and Sampling Scheme. Apparent soil electrical conductivity (EC_a) was measured using electromagnetic induction equipment

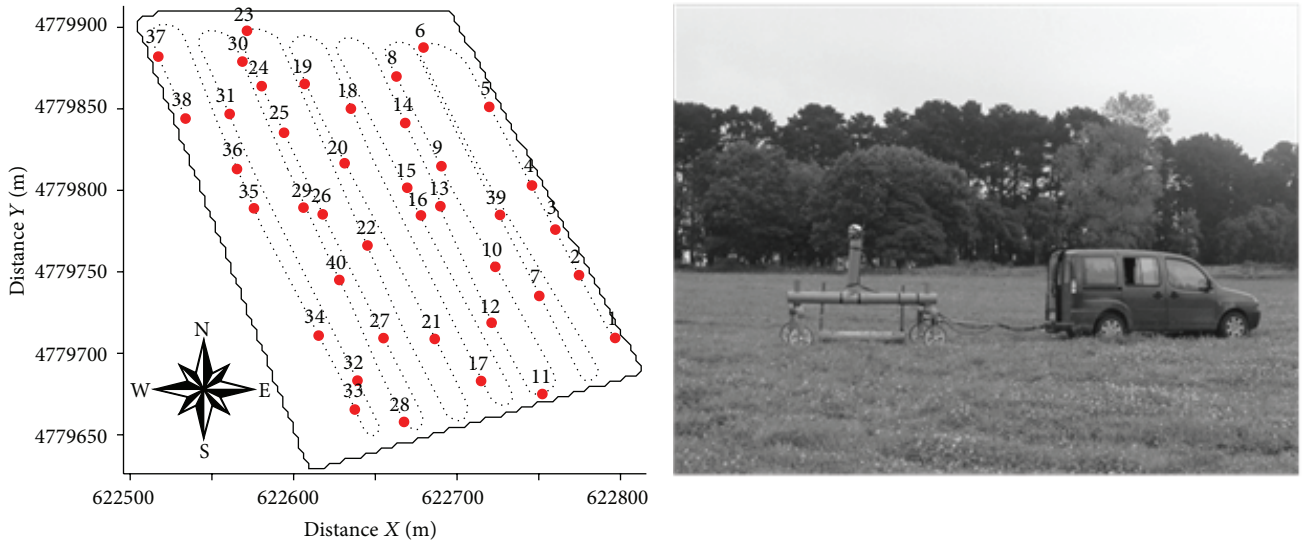

FIGURE 2: Scheme showing apparent electrical conductivity (EC_a) continuously recorded (line) and the location of 40 soil sampling points (circles) on 23/6/2008 (a) and cart containing the EM38-DD equipment and GPS (b).

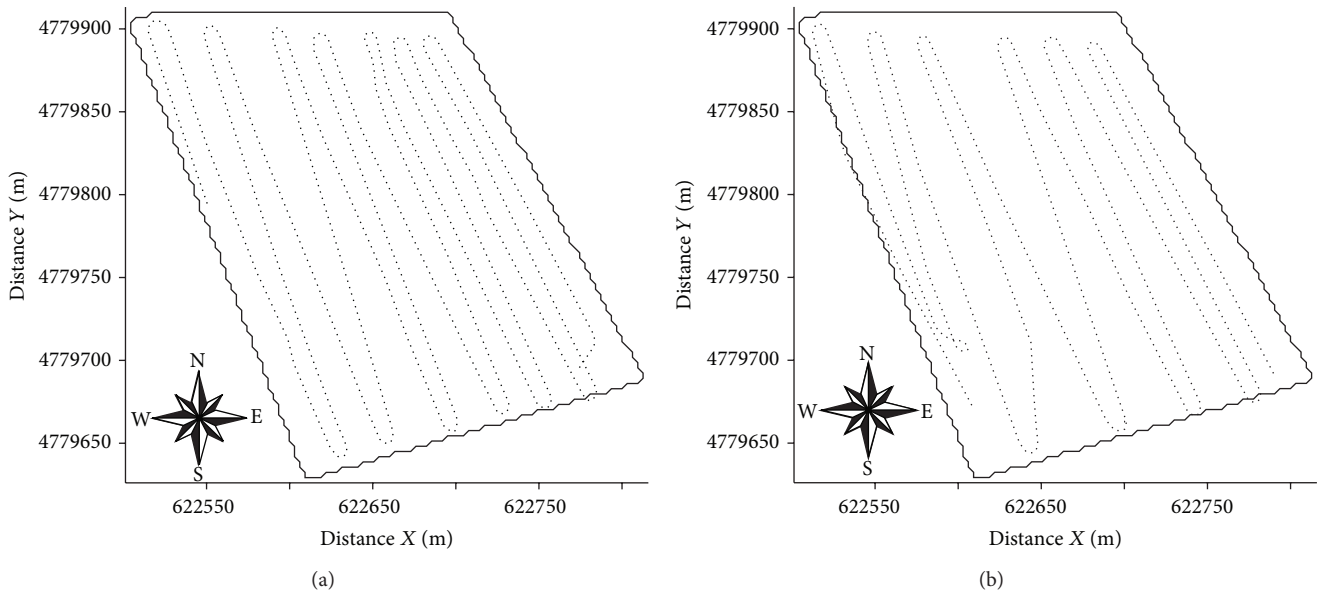

FIGURE 3: Scheme showing apparent electrical conductivity (EC_a) recorded during 14/3/2008 (a) and 3/4/2008 (b).

EM38-DD [14]. This device consists of two integrated EM38 units oriented in the horizontal and vertical dipole positions, providing simultaneous measurements for the two dipoles modes; in the vertical dipole mode, the primary magnetic field is thought to effectively penetrate to a depth of about 1.5 m, while in the horizontal dipole position EM38-DD is thought to be effective for a shallower soil depth estimated at about 0.75 m [14].

To complete continuous record of the apparent soil electrical conductivity in horizontal dipole (EC_a-H, mS m^{-1}) and in vertical dipole (EC_a-V, mS m^{-1}) (Figures 2(a) and 3), the EM38-DD was installed in a car built with plastic materials (Figure 2(b)). In addition, GPS RTK was used for georeferencing the recorded measures.

The reference measurements of EC_a-H and EC_a-V were performed on 23/6/2008 at 1859 sampling points following the scheme presented in Figure 2(a). The soil sampling scheme was devised using the software tool ESAP-RSSD (response surface sampling design), based on a multiple linear regression model [7, 9]. This software aims to optimize the position of new sampling points considering apparent soil electrical conductivity (EC_a) measured with horizontal (EC_a-H) and vertical dipoles (EC_a-V) (Figure 2(a)). The optimized soil sampling scheme consisted of 40 points. In

Table 2: Statistical parameters of the continuously recorded EC_a data sets and the soil properties analyzed.

Date	Variable	Unit	N	Min.	Max.	Mean ± SD	Variance	CV	Skew	Kurt	D
14/3/2008	EC_a-V	mS m^{-1}	1887	5.75	18.38	10.48 ± 1.19	1.42	11.35	0.527	0.124	0.045Ln
14/3/2008	EC_a-H	mS m^{-1}	1887	9.25	19.00	14.1 ± 0.77	0.60	5.46	0.065	1.810	0.040Ln
3/4/2008	EC_a-V	mS m^{-1}	1871	9.63	20.50	14.04 ± 2.15	4.64	15.31	0.662	0.083	0.073Ln
3/4/2008	EC_a-H	mS m^{-1}	1871	6.63	19.50	14.59 ± 0.77	0.60	5.28	0.160	10.51	0.095Ln
23/6/2008	EC_a-V	mS m^{-1}	1886	4.13	20.13	11.21 ± 2.47*	6.12	22.03	0.485	−0.243	0.071Ln
23/6/2008	EC_a-H	mS m^{-1}	1886	6.63	20.00	12.12 ± 1.79*	3.22	14.77	0.839	1.285	0.092Ln
23/6/2008	CE_e	mS m^{-1}	40	7.00	28.00	13.82 ± 5.09	25.94	36.83	1.200	1.008	0.159n
23/6/2008	Clay	g kg^{-1}	40	119.00	220.00	168.37 ± 30.92	956.54	18.36	−0.190	−1.321	0.153n
23/6/2008	Silt	g kg^{-1}	40	233.00	357.00	296.25 ± 35.06	1229.73	11.83	0.149	−1.041	0.098n
23/6/2008	Sand	g kg^{-1}	40	487.00	586.00	535.37 ± 22.53	507.72	4.21	0.055	−0.270	0.069n
23/6/2008	θg	%	38	13.41	45.67	26.74 ± 6.81	49.50	25.47	−2.904	6.510	0.085n

N: number of measurements; Min.: minimum value; Max.: maximum value; Mean ± SD: mean ± standard deviation; CV: coefficient of variation (%); Skew: skewness; Kurt: kurtosis; and D: normality of the data for test of Kolmogorov-Smirnov ($P < 0.01$, n: normality, and Ln: log normality). *Nonsignificant at 5% level of ANOVA (SNK).

addition continuous measurements of EC_a-H and EC_a-V were previously taken in the experimental field on 14/3/2008 and 3/4/2008, as shown in Figure 3. Note, however, that the schemes of the continuously recorded EC_a data sets taken in the three successive dates were different as shown in Figures 2(a), 3(a), and 3(b).

In the 40 points selected during the EC_a campaign of 23/6/2008, soil samples were taken at the 0.0–0.3 m depth with a manual soil probe. Soil texture, soil water content, and electrical conductivity of saturated paste extracts were determined using standard methods. Soil texture (clay, silt, and sand, in g kg^{-1}) was determined by the sieve-pipette method, following Camargo et al. [15]; in this method a mixture of sodium hydroxide and sodium hexametaphosphate was used as chemical dispersant. The gravimetric soil water content (θg, %) was obtained after weighing the mass of the wet and dry sample, according to Camargo et al. [15]. To determine the electrical conductivity of soil saturated extracts (EC_e), a mixture of soil and distilled water of 1 : 1 was prepared as proposed by USDA [16]; electrical conductivity measurements were performed using a conductivity meter ORION Model 122.

2.3. Statistical and Geostatistical Analysis. All the values were statistically analyzed using SPSS package 11.5 at 5% level of SNK (Student-Newman-Keuls) method ANOVA. The test of normality Kolmogorov-Smirnov was used to test the normality of data with probability of error 1% ($P < 0.01$). The correlation was calculated with the correlation coefficient of Pearson.

The analysis of the spatial variability of soil physical properties was conducted using the experimental variogram; the fitting of variogram model was performed using the method described by Vieira [17], based on cross-validation. Initial analysis showed that the variogram of any studied properties showed a trend, so the universal kriging was used in these cases, in which the residual variogram is required [18]. For those variables that showed no trend, ordinary kriging was used. The degree of spatial dependence (SD) was determined according to the following:

$$\text{SD}\,(\%) = \frac{C_0}{C_0 + C_1} * 100, \quad (1)$$

where C_0 is nugget effect and $(C_0 + C_1)$ is the sill $(C_0 + C_1)$ according to Cambardella et al. [19], which is considered as high (SD ≤ 25%), moderate (SD = 25–75%), and low (SD ≥ 75%).

Cross-variogram was used to study the spatial correlation between soil variables; when there was a trend in some of these variables, universal cokriging was used [18], instead of ordinary cokriging. The software used to perform ordinary kriging, universal kriging, and universal cokriging was Gstat [20]. In cokriging the covariance matrix must be positive and definite [18, 21–23]. The use of cokriging was used only for a couple of attributes that showed correlation coefficient values ($|r|$) greater than 0.5.

3. Results and Discussion

Statistical analysis of the data (Table 2) indicates that there is great variation between samples, in accordance with low (CV ≤ 12%) and middle (CV = 12–60%) variation coefficient values, by classification of Warrick and Nielsen [24]. It is verified that the apparent electrical conductivity of the soil (EC_a) measurement with the horizontal dipole (EC_a-H) has lower CV than the measurements with the vertical dipole (EC_a-V). This fact can be explained because the vertical dipole mode explores a larger volume of soil than the horizontal dipole, and there is greater heterogeneity in those variables that affect the EC_a values, mainly clay content, organic material, water content in the soil, porosity, salinity, and so forth [2–5].

Only data EC_a-V and EC_a-H sampling in 23/6/2008 did not show differentiation by the average test (ANOVA) between the different sampling dates.

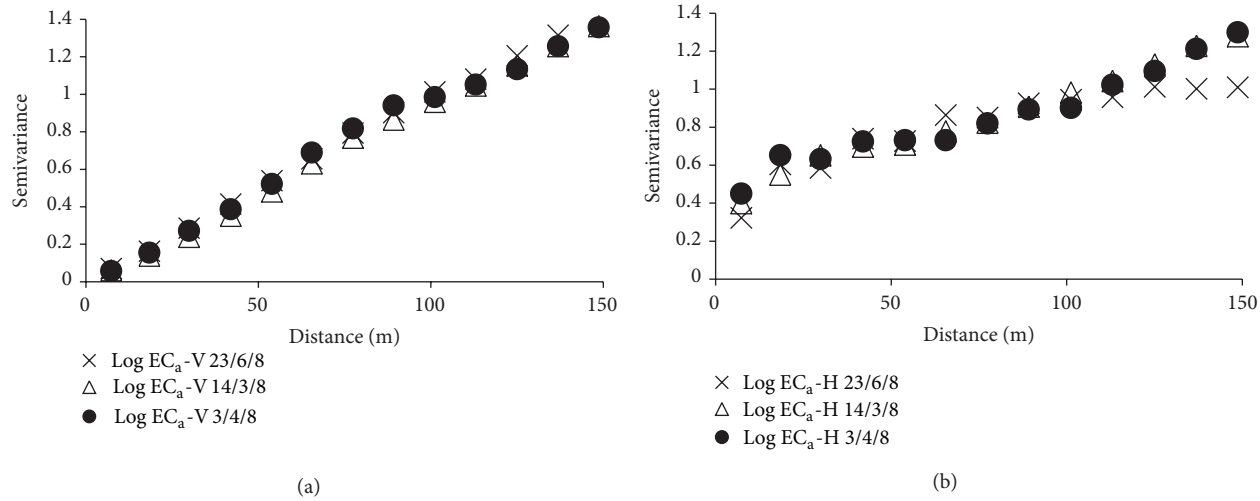

Figure 4: Standardized sample semivariogram for log EC_a-V (a) and log EC_a-H (b) recorded during three successive dates.

Table 3: Precipitation and reference evapotranspiration between successive dates, in which apparent soil electrical conductivity (CE_a-V and CE_a-H) was recorded.

Period	Precipitation (mm)	Reference evapotranspiration (mm)
15/2/2008–14/3/2008	52.6	38.0
14/3/2008–3/4/2008	80.4	37.1
3/4/2008–23/6/2008	397.8	214.6

The values of the electrical conductivity of the saturation paste extract of the soil (EC_e) are higher than the values of EC_a-V and EC_a-H; this fact is because EC_e is a parameter that depends on the content of anions and cations in the soil solution; the water content is homogeneous in all samples, because the sample is saturated with water, and the soil apparent electric conductivity values measured with the equipment EM38-DD (EC_a-V and EC_a-H) are very influenced by the soil water content [2, 3, 5]; and the water content in the soil is variable along the field.

EC_a-V and EC_a-H measured on several sampling dates (14/3/2008, 3/4/2008, and 23/6/2008) showed lognormal distribution (Table 2). Other attributes studied showed normal frequency distribution (EC_e, clay, silt, sand, and soil water content).

In the geostatistical analysis, lognormal transformation was used for properties that showed lognormal distribution. The highest values of coefficient of correlation between EC_a variables and clay and silt content are on the first measurement date (14/3/2008); on this date the soil moisture is lower coincided with data of precipitation and evapotranspiration (Table 3). Grandjean et al. [25] describe that soil with moisture lower is ideal for characterization of soil bulk density and of soil texture, using measurements of electrical conductivity.

The coefficient of correlation values between the apparent soil electrical conductivity (EC_a-V and EC_a-H) measurement on several sampling dates (14/3/2008, 3/4/2008, and 23/6/2008) presented moderate positive correlation coefficient values ($0.5 \leq r < 0.8$).

The coefficient of correlation between EC_a-$V_{23/6/2008} \times \theta g$ ($r = 0.685$) and EC_a-$H_{23/6/2008} \times \theta g$ ($r = 0.648$) was moderately positive ($0.5 \leq r < 0.8$), confirming the correlation between the values of EC_a-V and EC_a-H and the water content in soil, because according to Grandjean et al. [25], under wet conditions, electrical conductivity measurements are dominated by the effect of water content, which tends to hide the influence of the other factors.

The values of log EC_a-V are affected by the groundwater level, so the variogram follows the trend in the ground water level (Figure 4). As can be seen on standardized variograms with the value of the sample variance, data from EC_a-V measurement on 14/3/2008 and 3/4/2008 present a trend, following the same pattern of the digital elevation map of the area (Figure 1(b)). Analyzing standardized variograms for log EC_a-H data can be seen that only shows trend for the variogram of 14/3/2008 and 3/4/2008, but not for the variogram of 23/6/2008; on this date the water table was probably located below the depth of soil investigated with the horizontal dipole mode.

Corwin and Lesch [4] found higher values of correlation between data from log EC_a-V and log EC_a-H and electrical conductivity of the saturation extract (EC_e) and clay content, but lower than those found for log EC_a-V and log EC_a-H and the water content in soil. Martínez and Vanderlinden [26] described a higher correlation between EC_a and water content in loamy soils, while in clay soils the correlation was lower. The correlation coefficients for EC_e, silt, and clay with the log EC_a-H are greater than with the log-EC_a-V.

In order to improve the correlation between the values of EC_a-V and EC_a-H with clay content, soil water content should be as homogeneous as possible within the study area, better if

its value is closer to field capacity and unlike the water table is as low as possible, so the best time to take measurements under these conditions would be in the autumn, when there was heavy rainfall, although under these conditions the water table probably would not have ascended enough to be close to the surface.

The initial geostatistical data analysis showed that the physical properties of the soil (clay, silt, sand, and gravimetric water content) showed no trend, then being possible the estimate of the variable using the original data with ordinary kriging. Moreover, EC_e data and apparent electrical conductivity of the soil (EC_a-V and EC_a-H) on several sampling dates show trend in Figure 3; the semivariance value is not stabilized around variance value of data, and the universal kriging was used to construct the maps of spatial variability of these variables.

The fitted variogram parameters (Table 5) show that the spherical model was the fitted model to the properties under study, according to Cambardella et al. [19], Goovaerts [18], Vieira [17], and Siqueira et al. [27] describing this model; it is usually best fitted to the properties of soil and plant. All attributes had low values of nugget effect (C_0). Range values (a) varied from 40.00 m (log EC_a-H $\text{Residual}_{3/4/2008}$) to 130.00 m (clay, silt, and soil water content). The degree of spatial dependence between samples was high (SD $\leq$ 25.00%) across the study, the exception being log EC_a-H $\text{Residual}_{14/3/2008}$ which presented a moderate degree of spatial dependence (SD = 31.67%).

The spatial variability maps obtained with universal kriging (Figure 5) show that there is a similarity between the maps EC_a-V (Figures 5(a), 5(c), and 5(e)) and EC_a-H (Figures 5(b), 5(d), and 5(f)) on several sampling dates, with further differentiation of maps of EC_a-V and EC_a-H on the measured data on 23/6/2008 (Figures 5(e) and 5(f)) when the water table level was lower.

It is observed that the maps of EC_a-V and EC_a-H (Figure 5) and the map of the water content in soil (Figure 6(e)) obtained with ordinary kriging (Figure 6(e)) look similar, following the same pattern of digital elevation model (Figure 1(b)).

The map of the electrical conductivity of the saturation extract (EC_e, Figure 6(a)) shows inverse behaviour to maps EC_a-V and EC_a-H (Figure 5). Moreover, the map of spatial variability of clay content in the study area (Figure 6(b)) shows no similarity to maps EC_a-V and EC_a-H (Figure 5); this fact is also repeated with silt (Figure 6(c)) and sand (Figure 6(d)).

Table 6 presents the fitting parameters cross-variogram between $\theta g \times EC_a$-V ($r = 0.685$) and $\theta g \times EC_a$-H ($r = 0.648$). The cross-variograms were fitted to a spherical model with the same range compared to single variograms to obtain a linear model coregionalization (Table 6).

The spatial variability maps constructed using ordinary and universal cokriging (Figure 7) demonstrate that the use of the soil apparent electrical conductivity measured by electromagnetic induction (EC_a-V and EC_a-H) on 23/6/2008 was a secondary variable that improves the estimation of the soil water content using cokriging. This improvement in the estimation of θg can be observed in Table 7, where it showed an increase in the value of the correlation coefficient between the measured and the estimated values from cross-validation using ordinary cokriging with log-EC_a-V (0.746) and with log-EC_a-H (0.756) as secondary variables with respect to use of ordinary kriging (0.637). Moreover, in the case of the soil water content map obtained with ordinary cokriging using as secondary data EC_a-H (Figure 7(b)) is less smooth than the map obtained with ordinary kriging (Figure 6(e)).

4. Conclusions

When taking into account all the soil properties studied, EC_a and gravimetric soil water content measured at the same date, that is, 23/6/2008, showed the highest coefficients of correlation Table 4. Moreover, EC_a showed higher coefficients of correlation to clay and silt content than to silt content, and the strength of the correlation was higher for the first EC_a recording date, that is, 14/3/2008, when the soil moisture was lower. Thus, coefficient of correlation of EC_a with silt and clay content showed a trend to increase the soil moisture decreased; this result suggests the usefulness of recording EC_a on successive dates with different soil water contents.

The spatial patterns of spatial variability of the logarithmic values of apparent soil electrical conductivity (EC_a) and the electrical conductivity of the soil saturated paste (EC_e) were modeled by universal kriging, whereas those of sand, clay, silt, and gravimetric water content were modeled by ordinary kriging. The use of cokriging with EC_a data as secondary variable improved the estimation of the gravimetric soil water content with respect to the use of kriging.

Abbreviations

EC_a: Apparent soil electrical conductivity
EC_a-V: CE_a in vertical dipole
EC_a-H: CE_a in horizontal dipole
EC_e: Electrical conductivity of soil saturation extract.

Conflict of Interests

The authors declare that there is no conflict of interests regarding the publication of this paper. The referencing brands of commercial products in the paper do not imply that the authors recommend the equipment utilized in this study. The support funds presented by the Development Agencies do not show conflict of interests regarding the publication of this paper.

Acknowledgments

The authors are grateful to the Ministerial de Asuntos Exteriors y de Cooperation (MAEC-AECID) from Spain for the granting of scholarships for Ph.D. studies. This work has been funded by Ministerial de Education y Ciencia, within the framework of research Project CGL2005-08219-C02-02, and cofunded by Xunta de Galicia, within the framework of research Project PGIDIT06PXIC291062PN and by the European Regional Development Fund (ERDF). The authors acknowledge the provincial farm Gayoso Castro

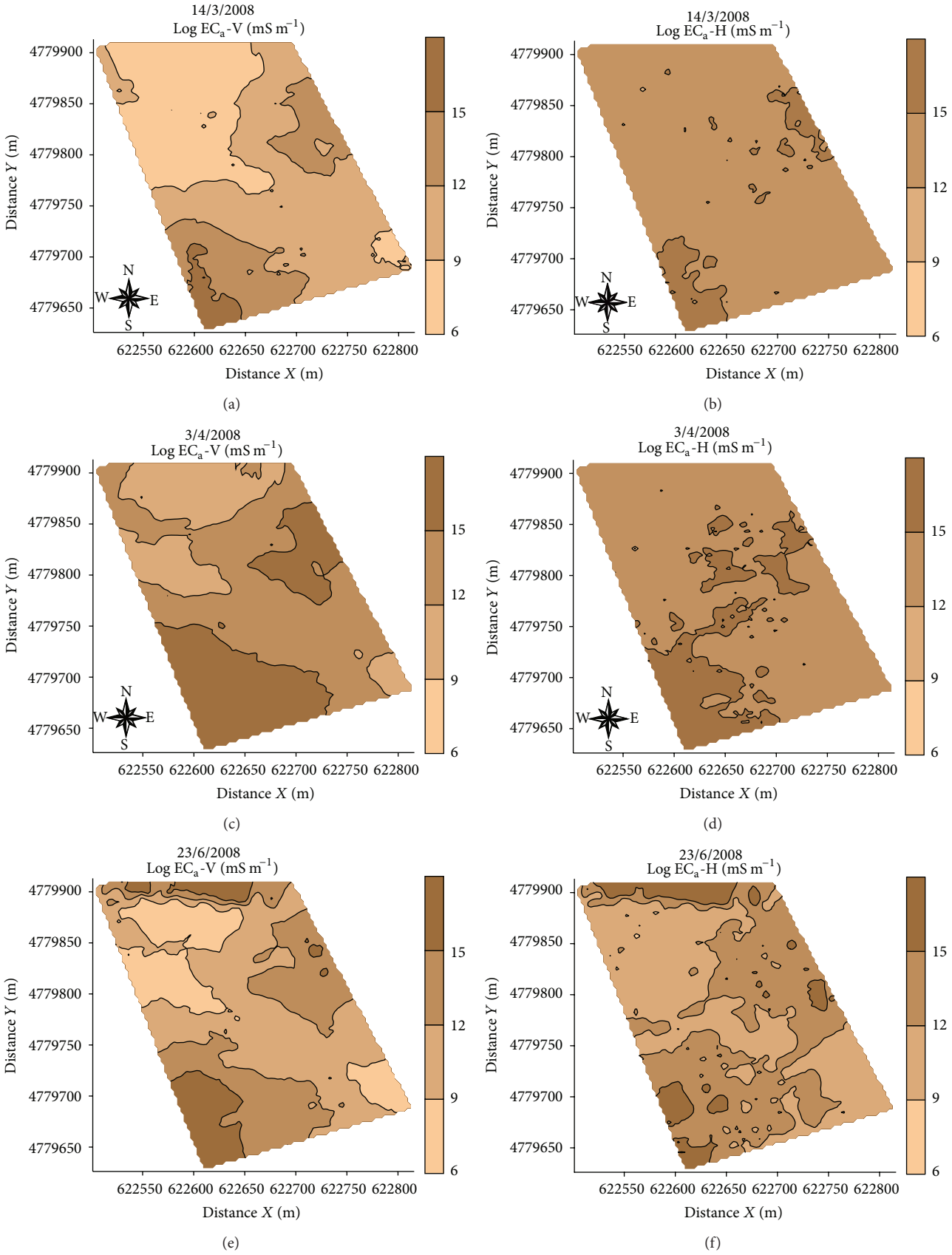

FIGURE 5: Kriging maps of apparent soil electrical conductivity (EC_a-V and EC_a-H) from the continuous records made in 14/3/2008, 3/4/2008, and 23/6/2008.

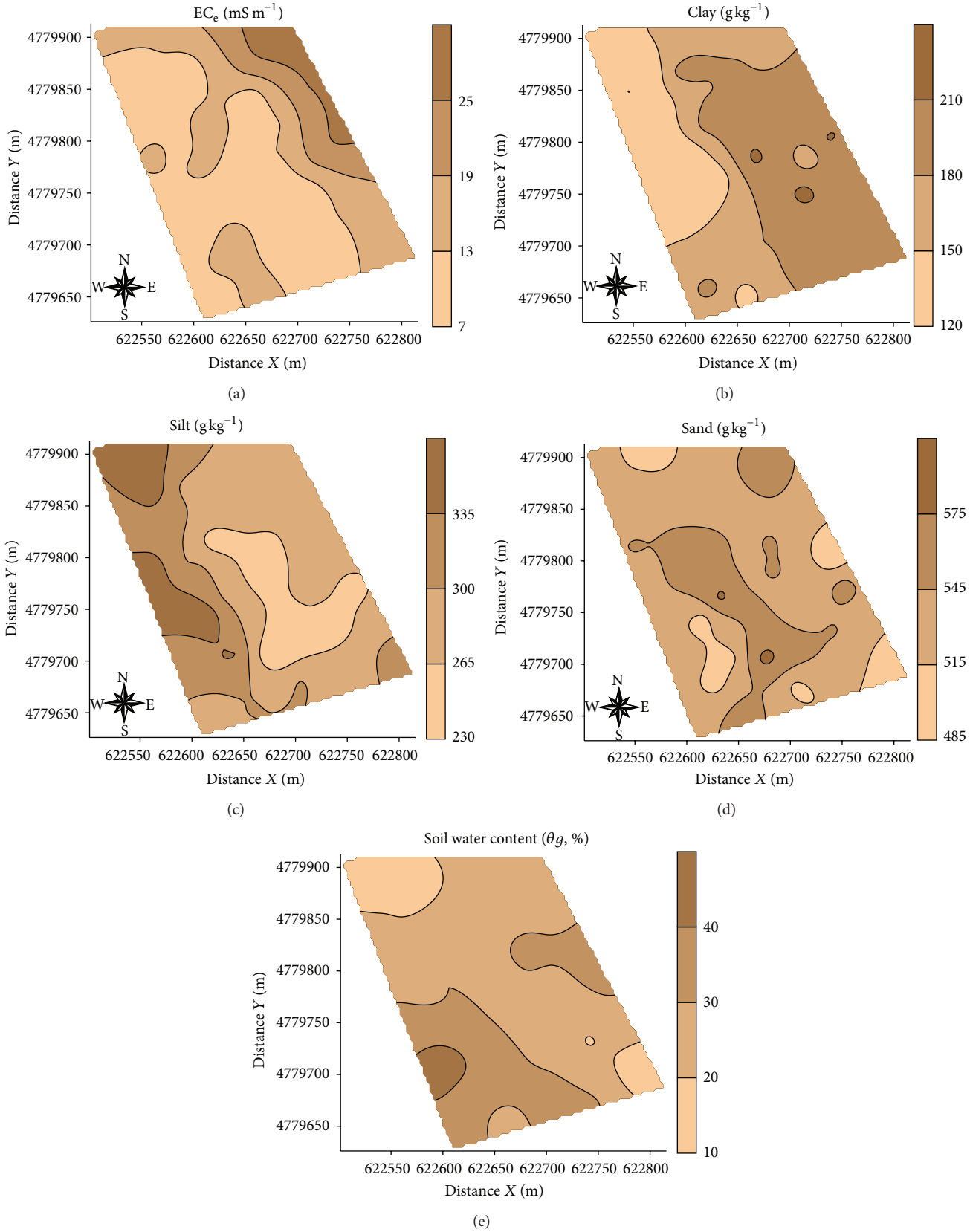

Figure 6: Kriging maps of the soil properties analyzed.

Table 4: Linear correlation matrix between the continuously recorded EC_a data sets and the soil properties analyzed.

		14/03/2008		03/04/2008		23/06/2008						
		Log EC_a-V	Log EC_a-H	Log EC_a-V	Log EC_a-H	Log EC_a-V	Log EC_a-H	EC_e	Clay	Silt	Sand	θg
14/03/2008	Log EC_a-V	1.000										
14/03/2008	Log EC_a-H	0.780	1.000									
03/04/2008	Log EC_a-V	0.972	0.759	1.000								
03/04/2008	Log EC_a-H	0.724	0.796	0.792	1.000							
23/06/2008	Log EC_a-V	0.861	0.729	0.855	0.688	1.000						
23/06/2008	Log EC_a-H	0.541	0.644	0.515	0.569	0.751	1.000					
23/06/2008	EC_e	0.127	0.185	−0.012	−0.141	0.156	0.224	1.000				
23/06/2008	Clay	0.344	0.495	0.252	0.197	0.253	0.346	0.221	1.000			
23/06/2008	Silt	−0.247	−0.423	−0.172	−0.216	−0.137	−0.228	−0.145	−0.773	1.000		
23/06/2008	Sand	−0.086	−0.012	−0.076	0.065	−0.133	−0.119	−0.076	−0.170	−0.494	1.000	
23/06/2008	θg	*	*	*	*	0.685	0.648	0.005	0.221	−0.145	−0.075	1.000

*Values were excluded in linear correlation analysis because the soil water content was only measured on 23/6/2006 and for this reason the coefficients of correlation were not calculated between soil water content and apparent electrical conductivity of the soil (EC_a-V and EC_a-H) for other sampling dates (14/3/2008 and 03/4/2008).

**To correlate the measurement of log EC_a-V and log EC_a-H for the measurement dates (14/3/2008 and 3/4/2008) with the measurements made on 23/6/2008, it was necessary to estimate the measurements of log EC_a, EC_e, clay, silt, and sand content using kriging in locations measured on 23/6/2008.

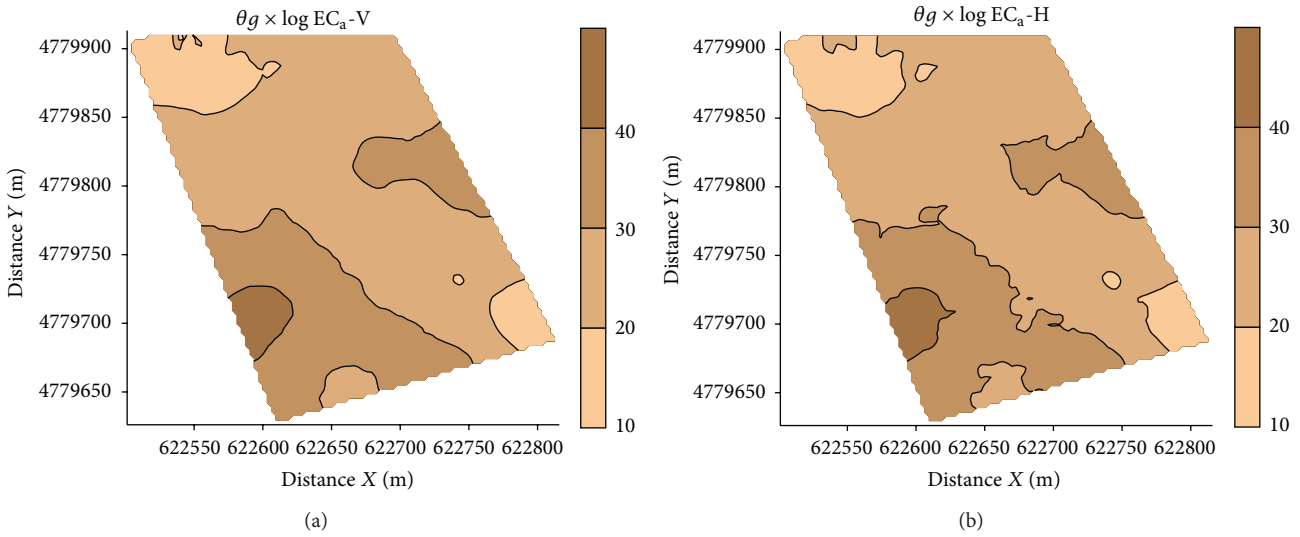

Figure 7: Map of gravimetric water content, θg, obtained by the universal cokriging.

Table 5: Fitted semivariogram parameters and respective models of the continuously recorded EC_a data sets and the soil properties analyzed.

Date	Variable	Geostatistical method	Model	C_0	C_1	a	SD
14/03/2009	Log EC_a-V residual	UK	Spherical	0.0001	3.14	105.00	0.00
	Log EC_a-H residual	UK	Spherical	0.14	0.302	44.00	31.67
03/04/2008	Log EC_a-V residual	UK	Spherical	0.00	5.10	145.00	0.00
	Log EC_a-H residual	UK	Spherical	0.10	0.32	40.00	23.80
23/06/2008	Log EC_a-V residual	UK	Spherical	0.001	0.01	130.00	9.09
	Log EC_a-H residual	UK	Spherical	0.001	0.005	130.00	1.96
	EC_e residual	UK	Spherical	0.00025	0.0018	100.00	9.09
	Clay	OK	Spherical	0.001	1060.00	130.00	0.00
	Silt	OK	Spherical	0.00	1400.00	130.00	0.00
	Sand	OK	Spherical	0.00	510.00	70.00	0.00
	θg	OK	Spherical	0.001	60.00	130.00	0.00

UK: universal kriging; OK: ordinary kriging; C_0: nugget effect; C_1: structural variance; a: range (m); and SD: spatial dependence (%).

Table 6: Fitted cross-semivariogram models and respective parameters between gravimetric water content (principal variable) and log EC_a (secondary variable).

	Variable	Geostatistical method	Model	C_0	C_1	a (m)
23/6/2008	$\theta g \times \log EC_a$-V	Universal cokriging	Spherical	1.00	20.00	130.00
23/6/2008	$\theta g \times \log EC_a$-H	Ordinary cokriging	Spherical	0.00	15.00	130.00

C_0: nugget effect; C_1: structural variance; and a: range (m).

Table 7: Correlation coefficients between measured gravimetric water content and data estimated by kriging and cokriging.

θg (ordinary kriging)	0.637	$\theta g \times \log EC_a$-V (universal cokriging)	0.746
		$\theta g \times \log EC_a$-H (ordinary cokriging)	0.756

of the Deputation of Lugo for allowing the use of their facilities to carry out this work. The authors thank the CNPq (National Council for Scientific and Technological Development (Brazil)) and FACEPE (Fundação de Amparo à Ciência e Tecnologia do Estado de Pernambuco (Brazil)) and they also thank CNPq for the scholarship DCR—Regional Scientific Development awarded to the first author. Also thanks are given to FAPEMA, MA, Brazil, for funding the publication of this paper. The authors would like to thank two anonymous reviewers for the comments that undoubtedly improved the quality of this paper.

References

[1] D. L. Corwin and J. D. Rhoades, "Measurement of inverted electrical conductivity profiles using electromagnetic induction,"

Soil Science Society of America Journal, vol. 48, no. 2, pp. 288–291, 1984.

[2] J. D. McNeill, "Electrical conductivity of soils and rocks," Technical Note TN-5, Geonics Limited, Ontario, Canada, 1980, http://www.geomatrix.co.uk/tools/application-notes/tn5.pdf.

[3] K. A. Sudduth, N. R. Kitchen, W. J. Wiebold et al., "Relating apparent electrical conductivity to soil properties across the north-central USA," *Computers and Electronics in Agriculture*, vol. 46, no. 1, pp. 263–283, 2005.

[4] D. L. Corwin and S. M. Lesch, "Characterizing soil spatial variability with apparent soil electrical conductivity: I. Survey protocols," *Computers and Electronics in Agriculture*, vol. 46, no. 1–3, pp. 103–133, 2005.

[5] J. Kühn, A. Brenning, M. Wehrhan, S. Koszinski, and M. Sommer, "Interpretation of electrical conductivity patterns by soil properties and geological maps for precision agriculture," *Precision Agriculture*, vol. 10, no. 6, pp. 490–507, 2009.

[6] C. K. Johnson, J. W. Doran, H. R. Duke, B. J. Wienhold, K. M. Eskridge, and J. F. Shanahan, "Field-scale electrical conductivity mapping for delineating soil condition," *Soil Science Society of America Journal*, vol. 65, no. 6, pp. 1829–1837, 2001.

[7] S. M. Lesch, D. J. Strauss, and J. D. Rhoades, "Spatial prediction of soil salinity using electromagnetic induction techniques. 1. Statistical prediction models: a comparison of multiple linear regression and cokriging," *Water Resources Research*, vol. 31, no. 2, pp. 373–386, 1995.

[8] J. W. van Groenigen, W. Siderius, and A. Stein, "Constrained optimisation of soil sampling for minimisation of the kriging variance," *Geoderma*, vol. 87, no. 3-4, pp. 239–259, 1999.

[9] S. M. Lesch, J. D. Rhoades, and D. L. Corwin, "The ESAP version 2.01r user manual and tutorial guide," Research Report, Salinity Laboratory, Riverside, Calif, USA, 2000.

[10] B. Minasny, A. B. McBratney, and D. J. J. Walvoort, "The variance quadtree algorithm: use for spatial sampling design," *Computers and Geosciences*, vol. 33, no. 3, pp. 383–392, 2007.

[11] Fao-Isric, "World reference base for soil resources," Roma y Wageningen, p. 161, 2014, http://www.fao.org/docrep/w8594e/w8594e00.HTM.

[12] A. C. Gegunde and F. Diaz-Fierros, *Os solos da Terra Chá. Tipos, xénese e aproveitamento*, Publicación Diputación Provincial de Lugo, Lugo, Spain, 1992.

[13] X. X. Neira Seijo, *Desenrolo de técnicas de manexo de auga axeitadas a um uso racional de regadíos [Ph.D. thesis]*, USC/EPS, 1993.

[14] Geonics, *EMD38-DD Ground Conductivity Meter-Dual Dipole Version*, Geonics, Ontario, Canada, 2005.

[15] O. A. Camargo, A. C. Moniz, J. A. Jorge, and J. M. A. S. Valadares, "Methods of chemical, mineralogical and physical analyses of soils," *Technical Bulletim of the Agronomic Institute of Campinas, Campinas*, no. 106, p. 94, 1986 (Portuguese).

[16] USDA, *Soil Quality Test Kit Guide*, USDA, Washington, DC, USA, 1999 (Spanish), http://www.nrcs.usda.gov/Internet/FSE_DOCUMENTS/stelprdb1044786.pdf.

[17] S. R. Vieira, "Geoestatística em estudos de variabilidade espacial do solo," in *Tópicos em Ciência do solo*, R. F. Novais, V. H. Alvarez, and G. R. Schaefer, Eds., vol. 1, pp. 1–54, Sociedade Brasileira de Ciência do Solo, Viçosa, Brazil, 2000.

[18] P. Goovaerts, *Geostatistics for Natural Resources Evaluation*, Oxford University Press, New York, NY, USA, 1997.

[19] C. A. Cambardella, T. B. Moorman, J. M. Novak et al., "Field-scale variability of soil properties in central Iowa soils," *Soil Science Society of America Journal*, vol. 58, no. 5, pp. 1501–1511, 1994.

[20] E. J. Pebesma, "Gstat user's manual," Department of Physical Geography, Utrecht University, 2014, http://www.gstat.org/gstat.pdf.

[21] P. Goovaerts, "Geostatistics in soil science: state-of-the-art and perspectives," *Geoderma*, vol. 89, no. 1-2, pp. 1–45, 1999.

[22] C. V. Deutsch and A. G. Journel, *GSLIB-Geostatistical Software Library and User's Guide*, Oxford University Press, New York, NY, USA, 2nd edition, 1998.

[23] J.-P. Chilès and P. Delfiner, *Geostatistics: Modeling Spatial Uncertainty*, Wiley Series in Probability and Statistics: Applied Probability and Statistics, Wiley-Interscience, New York, NY, USA, 1999.

[24] A. W. Warrick and R. R. Nielsen, "Spatial variability of soil physical properties in the field," in *Applications of Soil Physics*, D. Hillel, Ed., Academic Press, New York, NY, USA, 1980.

[25] D. Grandjean, I. Cousin, M. Seger et al., *From Geophysical Parameters to Soil Characteristics*, FP7—DIGISOIL Project Deliverable D2.1, 2009, http://eusoils.jrc.ec.europa.eu/projects/Digisoil/Documents/Digisoil-D2.1.pdf.

[26] G. Martínez and K. Vanderlinden, "Análisis de la relación espacial entre la humedad gravimétrica del suelo y la conductividad eléctrica aparente," in *Tendencias Actuales de la Ciencia del Suelo*, N. Bellinfante and A. Jordán, Eds., pp. 29–36, Universidad de Sevilla, Sevilla, Spain, 2007.

[27] G. M. Siqueira, S. R. Vieira, and M. B. Ceddia, "Variability of soil physical attributes determined by different methods," *Bragantia*, vol. 67, no. 1, pp. 203–211, 2008 (Portuguese).

Hindawi Publishing Corporation
The Scientific World Journal
Volume 2014, Article ID 514204, 11 pages
http://dx.doi.org/10.1155/2014/514204

Research Article

Effects of Land Use Change and Seasonality of Precipitation on Soil Nitrogen in a Dry Tropical Forest Area in the Western Llanos of Venezuela

Ana Francisca González-Pedraza[1,2] and Nelda Dezzeo[2]

[1] *Universidad Nacional Experimental Sur del Lago "Jesús María Semprum" (UNESUR), Programa Ingeniería de la Producción Agropecuaria, Laboratorio de Suelos, Santa Bárbara, Municipio Colón 5148, Estado Zulia, Venezuela*

[2] *Instituto Venezolano de Investigaciones Científicas (IVIC), Centro de Ecología, Laboratorio de Ecología de Suelos, Km 11, Carretera Panamericana, Altos de Pipe 1020, Estado Miranda, Venezuela*

Correspondence should be addressed to Ana Francisca González-Pedraza; gonzalezan@unesur.edu.ve

Received 16 July 2014; Revised 4 September 2014; Accepted 1 October 2014; Published 31 December 2014

Academic Editor: Antonio Paz González

We evaluated changes of different soil nitrogen forms (total N, available ammonium and nitrate, total N in microbial biomass, and soil N mineralization) after conversion of semideciduous dry tropical forest in 5- and 18-year-old pastures (YP and OP, resp.) in the western Llanos of Venezuela. This evaluation was made at early rainy season, at end rainy season, and during dry season. With few exceptions, no significant differences were detected in the total N in the three study sites. Compared to forest soils, YP showed ammonium losses from 4.2 to 62.9% and nitrate losses from 20.0 to 77.8%, depending on the season of the year. In OP, the ammonium content increased from 50.0 to 69.0% at the end of the rainy season and decreased during the dry season between 25.0 and 55.5%, whereas the nitrate content increased significantly at early rainy season. The net mineralization and the potentially mineralizable N were significantly higher ($P < 0.05$) in OP than in forest and YP, which would indicate a better quality of the substrate in OP for mineralization. The mineralization rate constant was higher in YP than in forest and OP. This could be associated with a reduced capacity of these soils to preserve the available nitrogen.

1. Introduction

Soil nitrogen (N) is a key element in primary productivity and soil fertility of ecosystems [1, 2]. N dynamics in tropical dry forest have been related to the rapid rate of mineralization, high available mineral concentrations, and the low efficiency of plant nutrient use [3–5]. Great effort has been dedicated to understand the dynamics of this element after clear-cutting and burning of these forests [1, 6].

The N mineralization involves a series of actions mainly mediated by soil microorganisms [7]. Therefore, this is a sensitive process to disturbance in most forest ecosystems [1, 6]. In a tropical forest, N mineralization depends on the amount and type of organic matter and microbial activity, as well as on soil physicochemical properties and soil moisture content [8].

When the tropical dry forest is cut down and burned to be converted into pasture, the soil temperature increases, causing rapid ammonification and nitrification. Consequently, great losses of N by volatilization, erosion, and leaching occur. Additionally, vegetation absorption and microorganism immobilization are insufficient to prevent these losses [9]. Later, during the early stages of revegetation under pasture, the mineralization and nitrification rates are lower than those in the original forest [5, 10].

The tropical dry forest has been considered one of the world's most threatened ecosystems [11–14]. However, there is little information about land use changes effects for this

ecosystem. Most of the studies on this topic have been conducted in rainforest areas [4, 5, 10, 15–20].

Tropical dry forests are characterized by the marked seasonality of rainfall that influences its primary productivity [2, 13, 21]. In Venezuela, this ecosystem represents the most important life zone of land and includes large areas covered by dense seasonal dry forests developed on relatively fertile soils. These forests have been subjected to a high pressure of use associated with population growth and the expansion of the agricultural frontier. After tree cutting, one of the main uses has been the establishing of pastures. However, there is no detailed information about changes occurred in the soil nitrogen once the forests have been cleared and converted into pasture. This information is necessary to anticipate deforestation consequences and to design effective pasture management.

The objective of this research is to evaluate changes in the total N, soil available N (ammonium and nitrate), total N in microbial biomass, and soil N mineralization due to transformation of semideciduous tropical dry forest into pastures in an area located in the western Llanos, Venezuela.

2. Materials and Methods

2.1. Study Site. The study area was located in the western Llanos of Venezuela, at approximately 120 m asl, between 40°01′10″ and 40°59′10″ north latitude and 91°57′30″ and 91°25′18″ west longitude. The average annual rainfall in this region is 1243.7 mm, with a rainy season from April to December and a dry season from January to March. The average annual temperature is 26.8°C, with a maximum of 28.9°C between March and April and a minimum of 25.5°C between December and January. The relief is flat with a slope between 0 and 2% [22]. According to Holdridge [23], the area belongs to tropical dry forest with dominant deciduous vegetation. The soil parent material is from alluvial origin, consisting of a sandy-clay-loam texture, with kaolinite as dominant clay mineral [22]. In this region, large areas of natural forest were converted into pasture by slash-and-burn. Estrella grass (*Cynodon nlemfuensis* L.) grows for cattle use.

Specifically, the study was carried out in an area of tropical dry forest with dominant deciduous vegetation and in two adjacent pastures of 5 and 18 years old (YP and OP, resp.). The pastures were never fertilized, but annually they were cut down with machinery to control weeds and to promote grass growth. The original forest was manually cut down and burnt out, and Estrella grass was planted. Young pasture (YP) was established 5 years before starting this study. At sampling time, species of the original forest that could not be cut by hand, as well as vegetation of secondary growth, like palms and some species of legumes were observed in this pasture. The bovine cattle were introduced for grazing during dry season and at early and at end of rainy seasons. At each season the cattle remained in this pasture until they consumed the entire grass.

The old pasture (OP) was established after remotion of the original forest with machinery. Bovine cattle remained in this pasture during 3–7 days, while consuming the entire grass. The rotation time of cattle in this pasture was every 1-2 months. Weed control was similar to YP.

According to González-Pedraza and Dezzeo [24], in the study site the soils present fine texture with particular predominance of silt. Forest and OP soils show similar clay and sand contents, while YP soils have significantly higher clay content (up to 18%) than forest and OP soils. In general, the soil properties in the studied sites tended to be relatively similar (Table 1).

2.2. Soil Sample Collection. Soils were sampled in a natural forest and in two adjacent pastures of 5 and 18 years old. At each site, soil samples were taken from a 600 m^2 plot (20 × 30 m). The distance between the three sites was approximately 1–3 km. At each plot, three transects were traced, and on each transect four soil samples were taken.

For determining total nitrogen in microbial biomass (Nmic), soil available nitrogen (ammonium and nitrate), and soil nitrogen mineralization, 12 soil samples were collected at 0–5 cm depth with a 5 cm diameter soil core on three periods along the year: at early rainy season (May), at end rainy season (November), and during dry season (March). To determine total nitrogen (TN), 12 samples were additionally collected at each site with the soil core at 0–5, 5–10, 10–20, 20–30, and 30–40 cm depth. These last soil samples were collected only at the end of rainy season.

2.3. Laboratory Analyses. The total nitrogen (TN) was determined by digestion of the samples with concentrated sulfuric acid and oxidation with hydrogen peroxide (H_2O_2) and colorimetrically determined by Keeney and Nelson [26] method. The ammonium and nitrate contents were extracted with a solution of potassium chloride (KCl) 2N and colorimetrically measured at a wavelength of 655 and 410 nm, respectively, following the method proposed by Keeney and Nelson [26].

Total nitrogen in microbial biomass (Nmic) was extracted by the chloroform fumigation extraction method in field moist samples [27] using 0.5N K_2SO_4. In these extracts, all N was converted to nitrate using the alkaline persulfate oxidation method [28] and colorimetrically determined by using the Keeney and Nelson [26] method.

Nmic was determined using the following equation:

$$\text{Nmic} = \left(\text{Nmic fumigated} - \text{Nmic unfumigated}\right) * 1.85, \quad (1)$$

where Nmic fumigated is total nitrogen in microbial biomass in $CHCl_3$-fumigated samples and Nmic unfumigated is Nmic in nonfumigated controls.

A correction factor of 1.85 was used to account for incomplete release of microbial biomass N during the 24 h fumigation period [27].

The soil nitrogen mineralization was determined by Stanford and Smith [29] method. Every two weeks (during 15 weeks) at an incubation temperature of 35°C and under laboratory conditions, the nitrogen mineralized in soils samples was extracted with a calcium chloride ($CaCl_2$) 0.01 M solution. To ensure the necessary nutrients for maintaining

Table 1: Soil properties in the study sites (according to González-Pedraza and Dezzeo [24, 25]).

Component	Depth (cm)	Forest	YP	OP
Bulk density (g cm^{-3})	0–5	1.2 ± 0.0^{a}	1.1 ± 0.1^{a}	1.1 ± 0.0^{a}
%Humidity	0–5	31.4 ± 1.0^{a}	37.9 ± 1.7^{b}	33.9 ± 0.9^{ab}
%Sand	0–5	19.8 ± 1.7^{a}	12.5 ± 2.3^{b}	22.3 ± 1.6^{a}
%Silt	0–5	49.7 ± 1.8^{a}	44.8 ± 1.8^{a}	47.1 ± 1.3^{a}
%Clay	0–5	30.5 ± 2.8^{a}	42.7 ± 3.1^{b}	30.6 ± 1.9^{a}
pH H_2O	0–5	5.4 ± 0.1^{a}	5.0 ± 0.14^{ab}	4.8 ± 0.1^{b}
SOC (g C m^{-2})	0–5	1389.9 ± 251.9^{a}	1472.7 ± 400.2^{a}	1516.7 ± 249.9^{a}

Mean values ± standard deviation. Different lowercase letters indicate significant differences between sites ($P < 0.05$). YP: 5-year-old pasture; OP: 18-year-old pasture; SOC: soil organic carbon.

the activity of microbial populations during incubation time, an N free nutrient solution was used.

The ammonium and nitrate mineralized every two weeks were determined by Keeney and Nelson [26] method and the absorbance was colorimetrically measured at a wavelength of 655 and 410 nm, respectively.

From the ammonium and nitrate mineralized during 15 weeks of incubation, the N mineralized (N_m), the potentially mineralizable N (N_0), and the constant mineralization rate (k) were calculated according to the Stanford and Smith [29] methodology. N_m resulted of summing the ammonium and nitrate determined in each incubation interval. The cumulative N mineralized was obtained summing all N mineralized during 15 weeks of incubation. The net N mineralized every two weeks was linearly related to the square root of time through 15 weeks of incubation and N_0 and k were obtained according to Stanford and Smith [29] equation:

$$N_m = N_0 \left(1 - e^{-kt}\right), \quad (2)$$

where N_m = N mineralized in time t (g m^{-2}), N_0 = potentially mineralizable N (g m^{-2}), k = mineralization rate constant of first-order kinetics (weeks^{-1}), and t = time of incubation (weeks).

Total N, Nmic, available, and mineralized N (ammonium and nitrate) values were corrected to dry soil and the results were expressed in g N-NH_4^+ and g N-NO_3^- by m^{-2}, based on the soil bulk density (kg m^{-3}) and depth (m). Nitrogen losses were calculated by comparing the values found in pastures with the original forest values.

2.4. Statistical Analysis. Statistical analysis of data was carried out by an analysis of variance (ANOVA). The soil clay content showed significant differences between forest and pastures (Table 1), so it was used as a covariable to adjust data. Means were separated with Tukey's test when statistical differences ($P < 0.05$) were observed. When necessary, the data was transformed in order to homogenize variances, and when that did not meet this assumption ($P > 0.05$) according to Levenne's test, a nonparametric Mann-Whitney test was applied. To relate variables at sites of interest, a simple linear regression analysis was used. All statistics were computed using STATISTICA for Windows 6.0 [30].

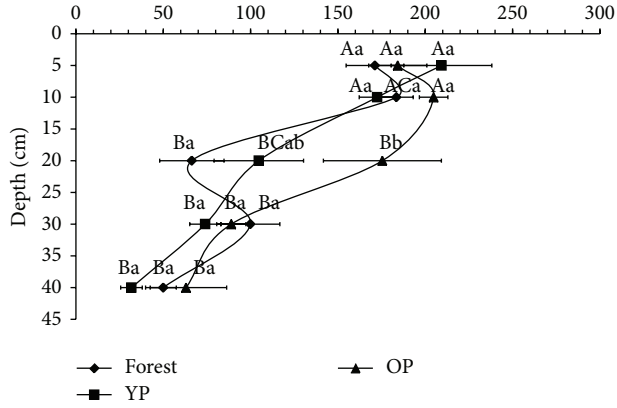

Figure 1: Total nitrogen (g m^{-2}) in the forest and pastures soils. All points are mean values with standard error bars across forest and pastures. Different lowercase letters indicate significant differences between sites ($P < 0.05$). Different capital letters indicate significant differences between depths ($P < 0.05$). YP: 5-year-old pasture; OP: 18-year-old pasture.

3. Results

3.1. Total Nitrogen (TN). No significant differences ($P > 0.05$) were detected (Figure 1) in the TN in forest, YP, and OP, with the exception of the 10–20 cm soil depths, where TN was 164.5% significantly ($P < 0.05$) higher in OP than in forest. Figure 1 also shows an uneven distribution of TN, with decreases and increases through the soil profile. It was observed that TN tends to decrease with soil depth in the three sites, except for OP at 5–10 cm soil depth and forest at 5–10 cm and at 20–30 cm soil depth.

3.2. Available Soil Nitrogen (Ammonium and Nitrate). The seasonal changes of the ammonium content are shown in Table 2. At end of rainy season, the ammonium content was significantly higher ($P < 0.05$) in OP than in YP and forest. During dry season, the ammonium content was significantly higher in forest than in YP and OP. At early rainy season no statistical differences were observed in the ammonium content between sites.

Between seasons, it was noted that, with few exceptions, the ammonium content was higher at the end of the rainy

Table 2: Seasonal changes in the available soil ammonium in the forest and pastures.

Season	Depth (cm)	Available ammonium ($N\text{-}NH_4^+$), $g\,m^{-2}$		
		Forest	YP	OP
End rainy season	0–5	3.3 ± 1.7^{Aa}	2.8 ± 1.1^{Aa}	5.6 ± 0.9^{Ab}
Dry season	0–5	2.7 ± 1.0^{Aa}	1.0 ± 0.3^{Bb}	1.2 ± 0.3^{Bb}
Early rainy season	0–5	0.7 ± 0.2^{Ba}	0.6 ± 0.1^{Ba}	0.7 ± 0.2^{Ba}

Mean values ± standard deviation. Different lower case letters indicate significant differences between sites ($P < 0.05$). Different capital letters indicate significant differences between seasons ($P < 0.05$). YP: 5-year-old pasture; OP: 18-year-old pasture.

Table 3: Seasonal changes in the available soil nitrate in the forest and pastures.

Season	Depth (cm)	Available nitrate ($N\text{-}NO_3^-$), $g\,m^{-2}$		
		Forest	YP	OP
End rainy season	0–5	0.9 ± 0.7^{Aba}	0.2 ± 0.2^{Ab}	1.4 ± 0.5^{Aa}
Dry season	0–5	1.4 ± 1.0^{Aab}	0.5 ± 0.3^{Ba}	1.7 ± 1.2^{Ab}
Early rainy season	0–5	0.5 ± 0.1^{Ba}	0.4 ± 0.2^{ABa}	1.0 ± 0.3^{Ab}

Mean values ± standard deviation. Different lowercase letters indicate significant differences between sites ($P < 0.05$). Different capital letters indicate significant differences between seasons ($P < 0.05$). YP: 5-year-old pasture; OP: 18-year-old pasture.

Table 4: Soil microbial nitrogen (Nmic) in the forest and pastures.

Season	Depth (cm)	Nmic ($g\,m^{-2}$)		
		Forest	YP	OP
End rainy season	0–5	2.4 ± 1.2^{Aa}	0.2 ± 0.1^{Ab}	1.4 ± 0.3^{Aa}
Dry season	0–5	0.7 ± 0.7^{Ba}	1.1 ± 0.6^{Ba}	1.0 ± 0.7^{Ba}
Early rainy season	0–5	1.3 ± 0.4^{Ba}	1.2 ± 0.5^{Ba}	2.0 ± 0.5^{Cb}

Mean values ± standard deviation. Different lowercase letters indicate significant differences between sites ($P < 0.05$). Different capital letters indicate significant differences between seasons ($P < 0.05$). YP: 5-year-old pasture; OP: 18-year-old pasture.

Table 5: Microbial nitrogen percentage in the total soil nitrogen in forest and pastures.

Season	Depth (cm)	Nmic/TN (%)		
		Forest	YP	OP
End rainy season	0–5	1.3 ± 0.9^{Aa}	0.2 ± 0.1^{Ab}	0.7 ± 0.4^{Aab}
Dry season	0–5	0.5 ± 0.5^{Ba}	0.7 ± 0.4^{Ba}	0.5 ± 0.4^{Aa}
Early rainy season	0–5	0.8 ± 0.4^{ABab}	0.6 ± 0.3^{Ba}	1.1 ± 0.3^{Bb}

Mean values ± standard deviation. Different lowercase letters indicate significant differences between sites ($P < 0.05$). Different capital letters indicate significant differences between seasons ($P < 0.05$). Nmic: microbial nitrogen; TN: total nitrogen; YP: 5-year-old pasture; OP: 18-year-old pasture.

season than in the dry season and at early rainy season (Table 2).

According to the results shown in Table 3, the nitrate content at the end of rainy season was lower in YP than in forest and OP. During dry season, the nitrate content was significantly higher than the value corresponding to YP, but similar to the forest value. At early rainy season, the nitrate content was significantly higher in OP than in forest and in YP, whereas between forest and YP no differences were observed.

The nitrate content in forest was higher at the end of rainy season and in dry season than at early rainy season. The nitrate content in YP was higher during dry season than in the two other seasons. In OP, no differences were observed between seasons (Table 3).

The land use change significantly affected the ammonium and nitrate content in the soils. Compared to forest soils, YP showed ammonium losses from 4.2 to 62.9% and nitrate losses from 20.0 to 77.8%, depending on the season of the year. In OP, the ammonium content increased from 50.0 to 69.0% at end of rainy season and decreased during dry season between 25.0 and 55.5%, whereas the nitrate content increased significantly at early rainy season.

3.3. Soil Microbial Nitrogen (Nmic). At end of the rainy season the Nmic was significantly ($P < 0.05$) lower in YP than in forest and OP. During dry season no differences were observed between sites, while at early rainy season the Nmic was higher in OP than in forest and YP (Table 4).

Between seasons, Nmic in the forest was the highest at the end of rainy season, while between the dry season and at early rainy season no differences were observed. YP showed Nmic lower at the end of rainy season, while between dry season and early rainy season no differences were detected. Meanwhile, the Nmic in OP was significantly different ($P < 0.05$) between seasons. The highest Nmic value in OP was observed at early rainy season and the lowest value during the dry season (Table 4).

The Nmic accounted between 0.07 and 1.57% of the NT in the soils of forest, YP, and OP. At the end of the rainy season Nmic/TN ratio was significantly lower ($P < 0.05$) in YP than in forest, while the values of OP showed no differences with those of forest and YP. During dry season, no differences were observed between sites. At early rainy season the Nmic/TN ratio was significantly lower in YP than in OP, while the forest showed no differences in relation to YP and OP (Table 5).

The Nmic/TN ratio in forest soils was lower during dry season compared to the end of rainy season, while in the other sample periods no differences were observed. YP showed lower Nmic/TN ratio at the end of rainy season, and no differences were observed in the wet season. In OP the Nmic/TN ratio was lower during the dry season compared to early rainy season (Table 5).

The relationship between Nmic values with the Cmic data reported by González-Pedraza and Dezzeo [25] are shown in Table 6. According to the results, the Cmic/Nmic ratio was significantly higher in YP than in forest and OP at the end of rainy season ($P < 0.05$), while between forest and OP there were no differences. During dry season, no differences were evident between sites. However, at early rainy season the Cmic/Nmic ratio was higher in forest than in pastures.

Between seasons, a significant decrease ($P < 0.05$) in the Cmic/Nmic ratio in YP soils was observed from the end of rainy season to dry season and to the early rainy season.

Table 6: Relationship between soil microbial carbon and soil microbial nitrogen in the forest and pastures.

Season	Depth (cm)	Cmic/Nmic		
		Forest	YP	OP
End rainy season	0–5	16.1 ± 7.2^{Aa}	169.4 ± 68.1^{Ab}	27.6 ± 9.5^{Aba}
Dry season	0–5	29.9 ± 29.3^{Aa}	34.1 ± 25.6^{Ba}	36.4 ± 16.0^{Aa}
Early rainy season	0–5	26.5 ± 8.3^{Aa}	16.2 ± 9.7^{Bb}	16.1 ± 7.4^{Bb}

Mean values ± standard deviation. Different lowercase letters indicate significant differences between sites ($P < 0.05$). Different capital letters indicate significant differences between seasons ($P < 0.05$). YP: 5-year-old pasture; OP: 18-year-old pasture. Cmic: microbial carbon; Nmic: microbial nitrogen.

Table 7: Net nitrogen mineralized by week throughout 15 weeks of incubation in the soil forest and pastures.

Week	Depth (cm)	Net nitrogen mineralized, g m^{-2}		
		Forest	YP	OP
2	0–5	2.4 ± 0.6^{a}	2.1 ± 1.0^{a}	4.0 ± 0.4^{b}
4		4.4 ± 1.7^{a}	1.9 ± 1.8^{b}	4.3 ± 2.6^{a}
6		0.8 ± 0.5^{a}	1.1 ± 0.8^{a}	2.4 ± 0.5^{b}
8		1.1 ± 0.4^{a}	0.9 ± 0.7^{a}	1.9 ± 0.6^{b}
10		0.6 ± 0.3^{a}	0.9 ± 0.4^{ab}	1.1 ± 0.4^{b}
12		0.4 ± 0.2^{a}	0.6 ± 0.3^{a}	0.8 ± 0.2^{b}
15		0.2 ± 0.3^{a}	0.2 ± 0.2^{a}	0.3 ± 0.3^{a}

Mean values ± standard deviation. Different lowercase letters indicate significant differences between sites at the same week ($P < 0.05$). YP: 5-year-old pasture; OP: 18-year-old pasture.

Table 8: Parameters derived from the N mineralization kinetics by applying the first-order equation $N_m = N_0[(1 - \exp^{-kt})]$.

Parameter from the N mineralization kinetics	Depth (cm)	Forest	YP	OP
N_m (g m^{-2})	0–5	9.8 ± 3.5^{a}	7.8 ± 4.2^{a}	14.8 ± 2.6^{b}
k (1/week)	0–5	0.1 ± 0.0^{a}	0.3 ± 0.2^{b}	0.2 ± 0.1^{a}
N_0 (g m^{-2})	0–5	13.0 ± 4.9^{a}	10.1 ± 5.3^{a}	18.5 ± 4.7^{b}
R^2	0–5	0.97	0.93	0.96

Mean values ± standard deviation. Different lowercase letters indicate significant differences between sites ($P < 0.05$). YP: 5-year-old pasture; OP: 18-year-old pasture. N_m = mineralized nitrogen accumulated during 15 weeks of incubation, k = constant rate of nitrogen mineralization, N_0 = potentially mineralizable nitrogen, and R^2 = coefficient of the determination.

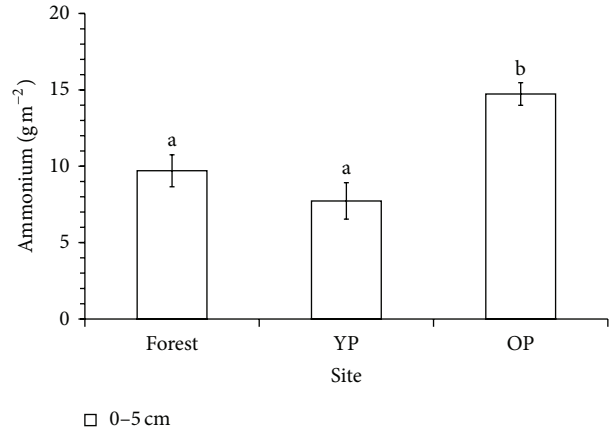

Figure 2: Mineralized ammonium accumulated during 15 weeks of the incubation experiment in laboratory conditions in forest and pastures soils. Mean values with standard error bars across forest and pastures. Different lowercase letters indicate significant differences between sites ($P < 0.05$). YP: 5-year-old pasture; OP: 18-year-old pasture.

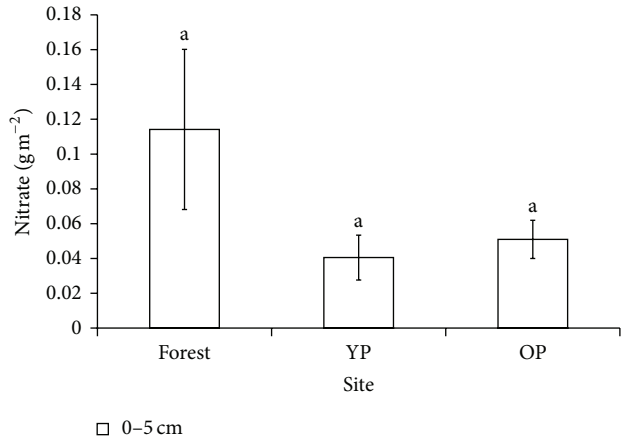

Figure 3: Mineralized nitrate accumulated during 15 weeks of the incubation experiment in laboratory conditions in forest and pastures' soils. Mean values with standard error bars across forest and pastures. Different lowercase letters indicate significant differences between sites ($P < 0.05$). YP: 5-year-old pasture; OP: 18-year-old pasture.

Forest showed no significant differences between seasons, while the Cmic/Nmic ratio in OP decreased from the dry period to early rainy season (Table 6).

3.4. Mineralized Ammonium and Nitrate throughout 15 Weeks of Incubation. The ammonium content was statistically ($P < 0.05$) higher in OP than in forest and YP. Between forest and YP no statistical differences were found (Figure 2). The nitrate content mineralized during 15 weeks of incubation did not differ between sites (Figure 3).

3.5. The Net N Mineralization. The net N mineralization rate decreased during the incubation period. During the first two weeks there was a rapid N release, which was significantly higher ($P < 0.05$) in OP than in forest and YP, while between forest and YP no differences were observed. This behavior, with few exceptions, did not change throughout the incubation period. The initial flow of mineralized N during the first two weeks of incubation was 68.8% for forest, 51.9% for YP, and 56.3% for OP (Table 7).

3.6. Parameters of the Nitrogen Mineralization Kinetics. The N_m, N_0, and k mean values obtained from application of the first-order equation proposed by Stanford and Smith [29] to describe the N mineralization kinetics are given in Table 8. N_m was significantly higher ($P < 0.05$) in OP than in forest

Table 9: Relationship between soil ammonium and nitrate in relation to the total mineralized N accumulated throughout 15 weeks of incubation in forest and pastures.

Parameter	Depth (cm)	Site		
		Forest	YP	OP
%Ammonium/N_m	0–5	98.2 ± 3.7^a	99.4 ± 0.6^a	99.6 ± 0.3^a
%Nitrate/N_m	0–5	1.8 ± 3.7^a	0.6 ± 0.6^a	0.4 ± 0.3^a

Mean values ± standard deviation. Different lowercase letters indicate significant differences between sites ($P < 0.05$). YP: 5-year-old pasture; OP: 18-year-old pasture. N_m = mineralized nitrogen accumulated throughout 15 weeks of incubation.

Table 10: Percentage of the mineralized N accumulated in relation to total nitrogen soil in forest and pastures.

	Depth (cm)	Site		
		Forest	YP	OP
N_m/NT (%)	0–5	6.1 ± 2.3^{ab}	4.6 ± 3.9^a	8.5 ± 2.6^b

Mean values ± standard deviation. Different lowercase letters indicate significant differences between sites ($P < 0.05$). YP: 5-year-old pasture; OP: 18-year-old pasture. N_m = N mineralized accumulated; TN = total nitrogen.

and YP, while between forest and YP no differences were observed. The k values varied significantly between the study sites, and the mineralized N per week ranged from 0.1 to 0.3%. In forest soils the model predicts that at 35°C and 9.1 ± 0.0 weeks (1/0.11), the obtained N_0 (13.0 ± 4.9 g N m^{-2}) was mineralized at a rate of 11% per week. In YP and OP the obtained N_0 was mineralized at a rate of 32 and 19%, respectively (Table 8).

According to the results shown in Table 8, the estimated time by the mineralization of N_0 was 3.12, 5.26, and 9.09 weeks for YP, OP, and forest, respectively.

In all studied sites, N_0 was higher than N_m. In that sense, it can be said that the estimated time in weeks (2.3 to 9.1 weeks) for mineralization of N_0 in the three study sites was lower than the 15 weeks used in this experiment to obtain the N_m (Table 8). In general, the accumulated N_m and N_0 were significantly higher ($P < 0.05$) in OP than in forest and YP. Between forest and YP no differences were found in these parameters; however, k was higher in YP than in forest and OP (Table 8).

3.7. Ammonium and Nitrate Percentage in Relation to N_m. The ammonium content accounted around 98-99% of N_m, while the nitrate content was only about 0.4 to 3.4% (Table 9). The soils of OP showed the highest N_m/TN percentages (Table 10).

4. Discussion

4.1. Effect of Land Use Change on Total Nitrogen (TN). The TN content in the soils of forest and pastures was relatively higher than that reported for other deciduous tropical forest soils [18, 31–34]. According to these results, it is clear that transformation of semideciduous dry tropical forest into pasture caused an increase in the TN, and this is not consistent with some reported data [5, 31, 35]. However, a similar trend was observed by Hassink [36], who found a higher N organic content in pastures over 10 years old than in young pastures (1–3 years old) and forest soils.

In many cases the management conditions can exert an important role in the soil nitrogen dynamic, especially if the pastures are fertilized. The pastures in the study site were never fertilized and they are not subjected to overgrazing. However, it is important to emphasize that star grass (*Cynodon nlemfuensis* L.) is a species with stoloniferous growth and abundant roots production. According to observations made in OP soils during the field sampling, star grass formed a layer on the ground composed by leaves and remnant stems, which could enhance the soil organic matter and, consequently, the total nitrogen of soil. Another factor that could explain the enhanced soil nitrogen, especially in YP, is related to an additional input of organic matter from the remaining plants of the original forest and from the secondary forest vegetation that continued regrowth.

The soil organic matter is the main N source in the soils [37], and it exerts an important effect on the dynamics of this element into the soil. According to González-Pedraza and Dezzeo [25], the soil organic carbon (SOC) for the studied sites was higher in pastures than in forest (Table 1). Additionally, the positive correlations found between SOC data and TN in forest and OP ($r = 0.82$ and 0.65, resp.) evidenced that the TN is closely related to the SOC in these sites. Therefore, the factors affecting the SOC help to explain the dynamics of TN in these soils.

The soil texture is another factor that could influence the TN behavior. According to González-Pedraza and Dezzeo [24], the YP soil showed higher clay percentage (%C) compared to forest. In that sense, a correlation was made between the TN and %C data, and a positive correlation in YP ($r = 0.73$, $P < 0.05$) was found. This indicates that the clay in the soil is protecting the soil nitrogen through organic matter. Similar results were reported by Hassink [36], who found a positive relationship between the organic N and the clay content.

4.2. Effect of Seasonality and Land Use Change on Available Nitrogen (Ammonium and Nitrate). The land use change significantly affected the ammonium and nitrate content in soils. As mentioned in the results, YP showed ammonium and nitrate losses compared to the forest, while OP showed nitrate increases and ammonium increases or decreases, depending on the sample period. Similar results were reported by Johnson and Wedin [5], Neill et al. [10], and Ellingson et al. [20], who found that in pastures, especially young pastures, the ammonification and nitrification are lower than in original forest. During early stages of the pastures establishing, the large losses of nitrate have been associated with volatilization, erosion, and leaching due to a decrease in the absorption rate by vegetation and immobilization of soil microorganisms [1, 6, 9].

N availability also has been positively correlated with the C and N levels in savannas, pastures, and agricultural crops' soils [38]. For example, Johnson and Wedin [5] pointed out that in contrast to the low efficiency in the use of nutrients

that characterize woody species in tropical forests, perennial grasses, particularly those adapted to fire, generally have a high C/N ratio in senescent aerial and underground tissues, allowing them to immobilize N during decomposition. García-Oliva et al. [31] and Hassink [36] also found higher C/N ratio in pastures than in forest soils.

The pastures age is another important factor affecting the nitrogen availability in the soil. In this study, the general trend towards an increase in the ammonium and nitrate content in relation to the pasture age is comparable with the data reported by Hassink [36], who found an increase in the total available N and a decrease in the C/N ratio in pastures soils with over 10 years old than in those between 1 and 3 years old.

The N transformation in the soils is mainly mediated by microorganisms [39, 40], and the microbial activity depends mainly on the substrate quantity, quality, and availability. It also depends on temperature and soil humidity [6, 41]. In this study, the ammonium and nitrate content increased with the increasing substrate availability and microbial activity, as indicated by Booth et al. [41]. Likewise, the nitrate content increase in pastures soils has been associated with a higher microbial transformation of ammonium and a low rate of absorption by grass plants [20]. In addition, it is possible that in OP the best quality of the substrate and major humidity percentage stimulated the microbial activity compared to forest.

The soil moisture content has a positive effect on the ammonium and nitrate content in the soils. [8, 42, 43]. During rainy season, the environmental conditions promote the activation of soil microbial processes [43, 44], which explains the higher ammonium content found in this study at the end of this season. It is very important to point out that in the western Llanos, the wet season ranges from 6 to 8 months along the year, and the samples of this study were taken at the end of rainy season, which favored the soil N availability, especially ammonium.

However, it is probable that at early rainy season both the ammonium and nitrate could be lost due to lixiviation and runoff. It is also possible that during the growing season, usually associated with the rainy months, a greater plant uptake occurs. This, perhaps, may explain the significant low contents found at early rainy season in relation to those at end of rainy season and during the dry period. In addition, it is probable that with the beginning of the rain the competition between soil microorganisms and plants to take the available nutrients increases, causing a decrease in the soil nitrogen availability.

On the other hand, the nitrate content increase evaluated during dry season in the three sites could be attributed to a decrease in the plant nutrient demand and also to microbial death [45].

4.3. Effect of Seasonality and Land Use Change on Soil Microbial Nitrogen (Nmic). Land use change and the seasonality in the precipitation regimen affected the Nmic behavior. Nmic values found in this study are lower than those reported for tropical dry forests, cultivated pastures, and savannas [8, 31, 44, 45]. However, these values are similar to those obtained by Jensen et al. [34] for savanna soils. Meanwhile, the Nmic/TN ratio values are lower than those reported by García-Oliva et al. [31] and by Jensen et al. [34] for areas with similar climatic conditions and vegetation.

For the study area, González-Pedraza and Dezzeo [25] pointed out that the microbial populations respond differently to changes in the soil moisture content throughout the year. These authors also showed that soil microbial activity was affected by vegetation type, seasonality of rainfall, and pasture age. This could indicate possible physiological differences between microbial communities in the three study sites, which can be associated with the fact that each site responded differently to changes in soil moisture content. González-Pedraza and Dezzeo [25] concluded that in YP soils, microorganisms were apparently less efficient to decompose the organic matter, while in OP the best quality of the substrate stimulated the microbial activity. Besides, the old age of OP allowed greater stability of soil microbial activity.

It is possible that the higher Nmic shown in OP at early rainy season could be related to the fact that the organic matter in this period was more palatable and had an easier decomposition for microbial populations, which allows it to be more active [46–51]. The Nmic increase in YP and decrease in forest and OP during the dry season reflect that the microbial populations respond differently to moisture content variations.

The Nmic decrease during dry season and increase with early rains can be associated with the microbial activation after the low activity during dry season due to the reduced soil moisture availability [52]. Additionally, at early rainy season many nutrients from the microbial biomass and soil organic matter are solubilized, becoming more accessible to the microorganisms [52].

Microbial biomass activity depends on factors such as humidity, temperature, soil texture, and the quantity and quality of plant material used as a substrate [47, 49, 51–56]. In this study, the Nmic in forest soil was significantly and positively correlated with the ammonium content ($r = 0.95$; $P < 0.05$) during dry season. On the other hand, at early rainy season Nmic was positively correlated with both the clay percentage ($r = 0.84$; $P < 0.05$) and the ammonium content ($r = 0.90$; $P < 0.05$).

The Nmic in pasture soils was related to the Cmic data reported by González-Pedraza and Dezzeo [25] and showed a high Cmic/Nmic ratio, especially at end of rainy season and during dry season. This result clearly shows differences in the composition of microbial communities on these soils. For example, the high Cmic/Nmic ratio found in YP soils at the end of rainy season reflects a strong limitation of available N during this season. This is also supported by the low content of TN, ammonium, and nitrate found in YP (Table 5).

In addition, a negative correlation ($r = -0.68$; $P < 0.05$) was found between the ammonium content and Nmic in YP soils. This could be due to a low substrate quality which could inhibit the metabolic process of soil microorganisms. Otherwise, in YP soils the microorganisms are, apparently, less efficient to decompose the organic matter and mineralize soil nitrogen [25]. It is also probable that

the TN pool in YP can be immobilized in plant tissues due to stress conditions, such as defoliation by cattle, and therefore it could be inaccessible to microorganisms [53]. As a consequence, the YP showed low contents of available N and Nmic.

At the end of the rains the Nmic was lower in the pasture than in forest soil, contrary to what happened in dry season. This suggests that at the end of rainfall the available N fractions are immobilized by microorganisms, absorbed by plants, or lost by leaching and/or erosion.

4.4. Effect of Seasonality and Land Use Change on Soil Nitrogen Mineralization. According to the results shown in Table 9, in the three studied sites ammonium was the predominant form of N mineralized during 15 weeks of incubation, while nitrate was very low both in the forest and pastures. This indicates that ammonification was the main privileged process, not nitrification. It is probable that the nitrification can be inhibited under slight acidic soils with soil pH < 6.0 [24], as those of the study area.

The N_m/TN values are higher than those reported by Arias de Estrada [56] for some dry tropical forest and pasture soils in western Llanos (Portuguesa and Barinas states), but relatively similar to those found by Sánchez et al. [57] for deciduous dry tropical forest and savannas of central Llanos (Guárico state). The highest N_m/TN found in OP would indicate that these soils are more able to mineralize nitrogen than forest and YP.

The land use change from forest to pasture affected the soil nitrogen mineralization. The mineralization pattern appears to be similar in the three sites, but the mineralization magnitude was different between forest and pastures. More than 50% of the available N into the soil was mineralized at the first two weeks of incubation. This accelerated flow has been associated with drying and physical disturbance of the soil samples, which cause death of a portion of the microbial population and their rapidly mineralization when soil is rewetting [52, 58, 59]. This could also be associated with the presence of N forms susceptible of being decomposed. Besides, the physical disturbance of the soil organic matter due to handling can contribute to accelerating the nitrogen mineralization of compounds highly sensitive to this process [59–61].

Because of depletion of the more labile soil organic matter fraction, the net N mineralization decreased in relation to the incubation time. This has been associated with the decrease of the potentially mineralizable N and the microbial population size during incubation time under laboratory conditions [61].

The N_m found in OP soils was significantly higher than that in forest and YP. Although no statistical differences were found in the TN values between sites, OP had 22.3% more TN than the forest. In addition, OP also presented the highest N_m/TN ratio, which would indicate that N in this pasture is more available for being mineralized than in forest and in YP. Moreover, it is probable that this old pasture could have a gradual and prolonging nutrient cycling in the ecosystem, which could allow more efficiency in the use of this substrate by the soil microorganisms.

In a previous section it was discussed that in pastures with a longer established time, an increase in the total N content and mineralization rate [36] can occur. It was also mentioned that the ammonium and nitrate mineralization was higher with increases in the substrate availability and in the microbial activity [41].

The N_0 in OP was 42.3% higher than in forest. This clearly indicates that in OP there was a larger pool of potentially available N. This could be associated with the pasture established time. Higher values of N_m and N_0 found in OP could also be indicating a better quality substrate for mineralization in pastures soils.

The relatively N_0 low values found in YP are, probably, due to a lower efficiency of microorganisms to compete with plants for nitrogen demand. Similarly, the short establishment time and the continuous pasture grazing have, probably, led to a depletion of available soil N because the microorganisms are highly selective and they use first labile forms of organic matter.

Because of a lower substrate quality, the high k values found in YP could be related to a reduced ability to preserve the available nitrogen in these soils resulting in a grass survival strategy under those conditions. In this sense, although YP had a lower N_0, its mineralization rate was higher.

5. Conclusions

Land use change from forest into pasture led to an increase in TN in almost all soil depths. Among the pastures, OP had a greater TN content than YP. The TN increase in YP topsoil was influenced by clay percentage. In OP, the established time has allowed a greater input and easier organic matter degradation, reflected in a higher content of N into the soil. During the three seasons, soil ammonium mineralization was the most important process in these soils resulting in the highest proportion of this nitrogen form in relation to TN.

The pasture establishment led to a decrease of ammonium and nitrate content and also to a decrease of soil microbial activity. The youngest pasture presented lower values of ammonium, nitrate, Nmic, N_0, and N_m in comparison with forest and old pasture. This pasture also had a higher mineralization rate (k). This leads to the conclusion that after the forest cutting and burning, the initial establishment of pastures negatively impacted on the soil N dynamics. This is reflected in the decrease of quality substrate and microorganisms efficiency to use this substrate. Therefore, the capacity of preserving the available N is reduced, and this can lead to N exhaustion. The higher values of N_m and N_0 found in OP are indicating a better quality of the substrate in this pasture.

Seasonality in precipitation had a marked effect on the soil N dynamics in the studied site. Prolonged rainy season privileged microbial processes that allowed a greater ammonium and nitrate mineralization and a higher Nmic. At early rainy season, ammonium and nitrate losses were associated with leaching and runoff caused by the first rainfall and by a nutrient demand increase for vegetation to grow. The nitrate increase during dry season was associated with

the lower nutrient demand of plants and microorganisms and with microbial population decrease in the three evaluated sites.

Conflict of Interests

The authors declare no conflict of interests regarding the publication of this paper.

Acknowledgments

This study was financially supported by the Planning Office of the University Sector (OPSU) in Venezuela. The authors wish to thank the technical staff of Soil Ecology Laboratory of Venezuelan Scientific Research Institute (IVIC). Thanks are also due to the owner of "El Mangón," where soil samples were taken, and to "Jesús María Semprum" Experimental National University (UNESUR) for their support to this research.

References

[1] P. M. Vitousek and J. M. Melillo, "Nitrate losses from disturbed forests: patterns and mechanisms," *Forest Science*, vol. 25, no. 4, pp. 605–619, 1979.

[2] A. Martínez-Yríza, "Biomass distribution and primary productivity of tropical dry forests," in *Seasonally Dry Tropical Forest*, S. H. Bullock, H. A. Mooney, and E. Medina, Eds., pp. 326–345, Cambridge University Press, Cambridge, Mass, USA, 1995.

[3] P. M. Vitousek, "Litterfall, nutrient cycling, and nutrient limitation in tropical forests," *Ecology*, vol. 65, no. 1, pp. 285–298, 1984.

[4] P. A. Matson, P. M. Vitousek, J. J. Ewel, M. J. Mazzarino, and G. P. Robertson, "Nitrogen transformations following tropical forest felling and burning on a volcanic soil.," *Ecology*, vol. 68, no. 3, pp. 491–502, 1987.

[5] N. C. Johnson and D. A. Wedin, "Soil carbon, nutrients, and mycorrhizae during conversion of dry tropical forest to grassland," *Ecological Applications*, vol. 7, no. 1, pp. 171–182, 1997.

[6] P. M. Vitousek and P. A. Matson, "Disturbance, nitrogen availability, and nitrogen losses in an intensively managed loblolly pine plantation," *Ecology*, vol. 66, no. 4, pp. 1360–1376, 1985.

[7] C. Campbell, R. Myers, and K. Weier, "Potentially mineralizable nitrogen, decomposition rates and their relationship to temperature for five Queensland soil," *Soil Science Research*, vol. 19, pp. 323–332, 1981.

[8] C. Anaya, F. García-Oliva, and V. Jaramillo, "Rainfall and labile carbon availability control litter nitrogen dynamics in a tropical dry forest," *Oecologia*, vol. 150, no. 4, pp. 602–610, 2007.

[9] E. A. Davidson, P. A. Matson, P. M. Vitousek et al., "Processes regulating soil emissions of NO and N_2O in a seasonally dry tropical forest," *Ecology*, vol. 74, no. 1, pp. 130–139, 1993.

[10] C. Neill, M. C. Piccolo, C. C. Cerri, P. A. Steudler, J. M. Melillo, and M. Brito, "Net nitrogen mineralization and net nitrification rates in soils following deforestation for pasture across the southwestern Brazilian Amazon Basin landscape," *Oecologia*, vol. 110, no. 2, pp. 243–252, 1997.

[11] D. H. Janzen, "Tropical dry forest: the most endangered major tropical ecosystem," in *Biodiversity*, E. O. Wilson and F. M. Peter, Eds., p. 521, National Academy Press, Washington, DC, USA, 1988.

[12] R. A. Houghton, D. S. Lefkowitz, and D. L. Skole, "Changes in the landscape of Latin America between 1850 and 1985 I. Progressive loss of forests," *Forest Ecology and Management*, vol. 38, no. 3-4, pp. 143–172, 1991.

[13] P. G. Murphy and A. E. Lugo, "Ecology of tropical dry forest," *Annual Review of Ecology and Systematics*, vol. 17, pp. 67–88, 1986.

[14] D. K. Kennard, "Secondary forest succession in a tropical dry forest: patterns of development across a 50-year chronosequence in lowland Bolivia," *Journal of Tropical Ecology*, vol. 18, no. 1, pp. 53–66, 2002.

[15] F. Montagnini and R. Buschbacher, "Nitrification rates in two undisturbed tropical rain forests and three slash-and-burn sites of the Venezuelan Amazon," *Biotropica*, vol. 21, no. 1, pp. 9–14, 1989.

[16] M. C. Piccolo, C. Neill, and C. Cerri, "Net nitrogen mineralization and net nitrification along a tropical forest-to-pasture chronosequence," *Plant and Soil*, vol. 162, no. 1, pp. 61–70, 1994.

[17] C. Neill, J. M. Melillo, P. A. Steudler et al., "Soil carbon and nitrogen stocks following forest clearing for pasture in the southwestern Brazilian Amazon," *Ecological Applications*, vol. 7, no. 4, pp. 1216–1225, 1997.

[18] S. Brown and A. E. Lugo, "Effects of forest clearing and succession on the carbon and nitrogen content of soils in Puerto Rico and US Virgin Islands," *Plant and Soil*, vol. 124, no. 1, pp. 53–64, 1990.

[19] F. García-Oliva, I. Casar, P. Morales, and J. M. Maass, "Forest-to-pasture conversion influences on soil organic carbon dynamics in a tropical deciduous forest," *Oecologia*, vol. 99, no. 3-4, pp. 392–396, 1994.

[20] L. J. Ellingson, J. B. Kauffman, D. L. Cummings, R. L. Sanford Jr., and V. J. Jaramillo, "Soil N dynamics associated with deforestation, biomass burning, and pasture conversion in a Mexican tropical dry forest," *Forest Ecology and Management*, vol. 137, no. 1–3, pp. 41–51, 2000.

[21] P. G. Murphy and A. E. Lugo, "Dry forest of Central America and the Caribbean," in *Seasonally Dry Tropical Forest*, S. H. Bullock, H. A. Mooney, and E. Medina, Eds., pp. 9–34, Cambridge University Press, Cambridge, Mass, USA, 1995.

[22] J. J. Ewel, A. Madriz, and J. A. Tosi Jr., "Zonas de vida de Venezuela," in *Memória Explicativa Sobre el Mapa Ecológico*, p. 265, Ministério de Agricultura y Cria, Fondo Nacional de Investigaciones Agropecuárias, Caracas, Venezuela, 2nd edition, 1968.

[23] L. R. Holdridge, "Determination of world plant formations from simple climatic data," *Science*, vol. 105, no. 2727, pp. 367–368, 1947.

[24] A. F. González-Pedraza and N. Dezzeo, "Efecto del cambio de uso de la tierra sobre las características de algunos suelos en los Llanos Occidentales de Venezuela," *Interciencia*, vol. 36, no. 2, pp. 135–141, 2011.

[25] A. González-Pedraza and N. Dezzeo, "Changes in the labile and recalcitrant organic matter fractions due to transformation of semi-deciduous dry tropical forest to pasture in the Western Llanos, Venezuela," in *Dry Forests: Ecology, Species Diversity and Sustainable Management*, F. E. Greer, Ed., chapter 4, pp. 105–132, Nova Science, New York, NY, USA, 2014.

[26] D. R. Keeney and D. W. Nelson, "Nitrogen-inorganic forms," in *Methods of Soil Analysis: Part II-Chemical and Microbiological Properties*, A. L. Page, R. H. Miller, and D. R. Keeney, Eds., Agronomy Monograph 9, pp. 643–698, American Society of

Agronomy and Soil Science Society of America, Wisconsin, Wis, USA, 1982.

[27] P. C. Brookes, A. Landman, G. Pruden, and D. S. Jenkinson, "Chloroform fumigation and the release of soil nitrogen: a rapid direct extraction method to measure microbial biomass nitrogen in soil," *Soil Biology and Biochemistry*, vol. 17, no. 6, pp. 837–842, 1985.

[28] M. L. Cabrera and M. H. Beare, "Alkaline persulfate oxidation for determining total nitrogen in microbial biomass extracts," *Soil Science Society of America Journal*, vol. 57, no. 4, pp. 1007–1012, 1993.

[29] G. Stanford and S. J. Smith, "Nitrogen mineralization potentials of soils," *Soil Science Society American Procedure*, vol. 36, pp. 465–472, 1972.

[30] Statistica, *Basic Statistical Analysis Methods*, Versión 6.0, StatSoft, Tulsa, Okla, USA, 2001.

[31] F. García-Oliva, J. F. G. Lancho, N. M. Montaño, and P. Islas, "Soil carbon and nitrogen dynamics followed by a forest-to-pasture conversion in western Mexico," *Agroforestry Systems*, vol. 66, no. 2, pp. 93–100, 2006.

[32] J. J. San José, R. A. Montes, and C. Rocha, "Neotropical savanna converted to food cropping and cattle feeding systems: soil carbon and nitrogen changes over 30 years," *Forest Ecology and Management*, vol. 184, no. 1–3, pp. 17–32, 2003.

[33] C. P. Giardina, R. L. Sanford Jr., and I. C. Døckersmith, "Changes in soil phosphorus and nitrogen daring slash-and-burn clearing of a dry tropical forest," *Soil Science Society of America Journal*, vol. 64, no. 1, pp. 399–405, 2000.

[34] M. Jensen, A. Michelsen, and M. Gashaw, "Responses in plant, soil inorganic and microbial nutrient pools to experimental fire, ash and biomass addition in a woodland savanna," *Oecologia*, vol. 128, no. 1, pp. 85–93, 2001.

[35] A. L. Sandoval-Pérez, M. E. Gavito, F. García-Oliva, and V. J. Jaramillo, "Carbon, nitrogen, phosphorus and enzymatic activity under different land uses in a tropical, dry ecosystem," *Soil Use and Management*, vol. 25, no. 4, pp. 419–426, 2009.

[36] J. Hassink, "Effects of soil texture and grassland management on soil organic C and N and rates of C and N mineralization," *Soil Biology and Biochemistry*, vol. 26, no. 9, pp. 1221–1231, 1994.

[37] K. R. Kelley and F. J. Stevenson, "Forms and nature of organic N in soil," in *Fertilizer Research*, N. Ahmad, Ed., vol. 42 of *Nitrogen Economy in Tropical Soils*, pp. 1–11, Kluwer Academic, Dodrecht, The Netherlands, 1995.

[38] J. R. Salinas-García, F. M. Hons, and J. E. Matocha, "Long-term effects of tillage and fertilization on soil organic matter dynamics," *Soil Science Society of America Journal*, vol. 61, no. 1, pp. 152–159, 1997.

[39] G. Bengtsson, P. Bengtson, and K. F. Månsson, "Gross nitrogen mineralization-, immobilization-, and nitrification rates as a function of soil C/N ratio and microbial activity," *Soil Biology and Biochemistry*, vol. 35, no. 1, pp. 143–154, 2003.

[40] T. Rosswall, "Microbiological regulation of the biogeochemical nitrogen cycle," *Plant and Soil*, vol. 67, no. 1–3, pp. 15–34, 1982.

[41] M. S. Booth, J. M. Stark, and E. Rastetter, "Controls on nitrogen cycling in terrestrial ecosystems: a synthetic analysis of literature data," *Ecological Monographs*, vol. 75, no. 2, pp. 139–157, 2005.

[42] M. L. Cabrera, "Modeling the flush of nitrogen mineralization caused by drying and rewetting soils," *Soil Science Society of America Journal*, vol. 57, no. 1, pp. 63–66, 1993.

[43] G. García-Méndez, J. M. Maass, P. A. Matson, and P. M. Vitousek, "Nitrogen transformations and nitrous oxide flux in a tropical deciduous forest in México," *Oecologia*, vol. 88, no. 3, pp. 362–366, 1991.

[44] J. S. Singh, A. S. Raghubanshi, R. S. Singh, and S. C. Srivastava, "Microbial biomass acts as a source of plant nutrients in dry tropical forest and savanna," *Nature*, vol. 338, no. 6215, pp. 499–500, 1989.

[45] V. J. Jaramillo and R. L. Sanford, "Nutrient cycling in tropical deciduous forests," in *Seasonally Dry Tropical Forest*, S. H. Bullock, H. A. Mooney, and E. Medina, Eds., pp. 346–361, Cambridge University Press, Cambridge, Mass, USA, 1995.

[46] L. Galicia and F. García-Oliva, "Remnant tree effects on soil microbial carbon and nitrogen in tropical seasonal pasture in western Mexico," *European Journal of Soil Biology*, vol. 44, no. 3, pp. 290–297, 2008.

[47] K. Potthast, U. Hamer, and F. Makeschin, "Impact of litter quality on mineralization processes in managed and abandoned pasture soils in Southern Ecuador," *Soil Biology and Biochemistry*, vol. 42, no. 1, pp. 56–64, 2010.

[48] A. R. Maharning, A. A. S. Mills, and S. M. Adl, "Soil community changes during secondary succession to naturalized grasslands," *Applied Soil Ecology*, vol. 41, no. 2, pp. 137–147, 2009.

[49] E. Paterson, G. Osler, L. A. Dawson, T. Gebbing, A. Sim, and B. Ord, "Labile and recalcitrant plant fractions are utilised by distinct microbial communities in soil: independent of the presence of roots and mycorrhizal fungi," *Soil Biology and Biochemistry*, vol. 40, no. 5, pp. 1103–1113, 2008.

[50] G. P. Sparling, P. B. S. Hart, J. A. August, and D. M. Leslie, "A comparison of soil and microbial carbon, nitrogen, and phosphorus contents, and macro-aggregate stability of soil under native forest and after clearance for pastures and plantation forest," *Biology and Fertility of Soils*, vol. 17, no. 2, pp. 91–100, 1994.

[51] R. L. Tate, *Soil Microbiology*, John Wiley & Sons, New York, NY, USA, 2nd edition, 2000.

[52] T. L. Kieft, E. soroker, and M. K. firestone, "Microbial biomass response to a rapid increase in water potential when dry soil is wetted," *Soil Biology and Biochemistry*, vol. 19, no. 2, pp. 119–126, 1987.

[53] K. Jangid, M. A. Williams, A. J. Franzluebbers et al., "Relative impacts of land-use, management intensity and fertilization upon soil microbial community structure in agricultural systems," *Soil Biology and Biochemistry*, vol. 40, no. 11, pp. 2843–2853, 2008.

[54] J. W. Raich and A. Tufekcioglu, "Vegetation and soil respiration: correlations and controls," *Biogeochemistry*, vol. 48, no. 1, pp. 71–90, 2000.

[55] W. B. McGill, K. R. Cannon, J. A. Robertson, and F. D. Cook, "Dynamics of soil microbial biomass and water-soluble organic C in Breton L after 50 years of cropping to two rotations," *Canadian Journal of Soil Science*, vol. 66, no. 1, pp. 1–19, 1986.

[56] T. Arias de Estrada, *Mineralización de nitrógeno en suelos cultivados y con bosques naturales, de los estados Barinas y Portuguesa [Trabajo de Grado para optar al título de Magíster Scientiarum en Biología, mención Ecología]*, Instituto Venezolano de Investigaciones Científicas (IVIC), 1990.

[57] L. F. Sánchez, J. García-Miragaya, and N. Chacón, "Nitrogen mineralization in soils under grasses and under trees in a protected Venezuelan savanna," *Acta Oecologica*, vol. 18, no. 1, pp. 27–37, 1997.

[58] T. Marumoto, J. P. E. Anderson, and K. H. Domsch, "Mineralization of nutrients from soil microbial biomass," *Soil Biology and Biochemistry*, vol. 14, no. 5, pp. 469–475, 1982.

[59] C. Wang, S. Wan, X. Xing, L. Zhang, and X. Han, "Temperature and soil moisture interactively affected soil net N mineralization in temperate grassland in Northern China," *Soil Biology & Biochemistry*, vol. 38, no. 5, pp. 1101–1110, 2006.

[60] D. S. Powlson, "Effect of cultivation on the mineralization of nitrogen in soil," *Plant and Soil*, vol. 57, no. 1, pp. 151–153, 1980.

[61] K. Robertson, J. Schnorer, M. Clarholm, T. A. Bonde, and T. Rosswall, "Microbial biomass in relation to C and N mineralization during laboratory incubations," *Soil Biology and Biochemistry*, vol. 20, no. 3, pp. 281–286, 1988.

Hindawi Publishing Corporation
The Scientific World Journal
Volume 2014, Article ID 135906, 12 pages
http://dx.doi.org/10.1155/2014/135906

Research Article

Spatial Distribution and Temporal Variability of Ammonium-Nitrogen, Phosphorus, and Potassium in a Rice Field in Corrientes, Argentina

Luis Alberto Morales,[1] Eva Vidal Vázquez,[2] and Jorge Paz-Ferreiro[2]

[1] *Faculty of Agricultural Sciences, National University of the Northeast, Sargento Cabral 2131, 3400 Corrientes, Argentina*
[2] *Faculty of Sciences, University of A Coruña, Zapateira Campus, 15008 A Coruña, Spain*

Correspondence should be addressed to Jorge Paz-Ferreiro; jpaz@udc.es

Received 16 July 2014; Revised 11 September 2014; Accepted 16 October 2014; Published 31 December 2014

Academic Editor: Antonio Paz González

Proper and effective management of soil nutrients requires assessment of their variability at the field scale. We compare the effects of lime amendment rate on the spatial variability of three macronutrient forms (NH_4^+-N, Olsen P, and Mehlich-1 K) in a paddy soil at three different dates during the growth period of a rice crop. The field work was carried out near Corrientes, Argentina. Lime treatments were 0, 625, and 1250 kg ha^{-1} dolomite, and each liming dose was applied to a 1.7 ha field. Ninety-three soil samples per treatment were first collected in aerobic conditions and then two more times after flooding, at bunch formation and flowering. Soil NH_4^+-N increased along time, whereas P was highest at bunch formation and K steadily decreased along the rice growth period. Dolomite addition increased macronutrient availability at the first and second samplings, but its effects at the third sampling depended on the element. The three soil nutrients analyzed displayed strong patterns of spatial dependence for the three lime treatments and at the three periods studied. The areas with relative high or low macronutrient concentrations within each field were not stable throughout the rice growth period. Seasonality in the spatial distribution of macronutrients may be of agronomic value for site specific management.

1. Introduction

Macronutrients (N, P and K) play an important role in crop production. Inadequate fertilizer management limits crop yield, results in nutrient mining, and causes loss of soil productivity. A satisfactory nutrient status saves the soil, a limited natural resource, and also prevents environmental pollution [1]. Proper and effective management of macronutrients and assessment of their effects on environmental quality requires an understanding of their variability in concentration across the fields. Moreover, knowledge about spatial and temporal behaviour in the variability of nutrient status is the key for site specific management trough precision agriculture techniques. Site specific management can help to minimize fertilizer inputs thought the whole field without prejudicing yields, which would contribute to bridge economic with environmental advantages [2, 3].

The spatial variability of soil properties is the outcome of the interaction of several soil forming factors and processes and in agricultural and forest fields involves also effects of management practices [3–5]. There has been a growing interest in the study of the spatial variability of soil characteristics, including macronutrients, using geostatistics since the 1980s [4–8]. More recently, the value of spatial measurements of soil properties coupled with geostatistical techniques to develop site specific management practices also has been widely acknowledged [2, 9, 10]. Indeed, geostatistical analysis has been carried out to assess heterogeneity in paddy soils, focussing either on soil properties and/or crop yield [5, 11] or on soil properties and/or nutrients [12–17].

In paddy soils, spatial variability has been shown to occur over distances of meters or tens of meters. Because these soils are characterized by a relatively flat topography and seasonal flooding, in the past they have been thought to be

apparently homogeneous. However, large spatial variability in soil properties has been reported for paddy fields of different countries [5, 11, 12, 14, 16], even if at a first sight this might be considered as a quite unexpected result. However, more recently it has also been shown that factors such as small differences in elevation after land-levelling [18] and redistribution of soil components and/or nutrients by lateral water movement across neighbouring small fields surrounded by ridges [19, 20] may drive heterogeneity of crop yield and soil properties at different scales. Temporal oscillations in the spatial patterns of variability of soil properties or soil nutrients in rice fields have been also previously reported [12, 13, 16, 20], even if this issue has been less frequently addressed.

Successful rice production requires an adequate soil fertility status and especially satisfactory levels of N, P, and K. In flooded soils major chemical and electrochemical changes occur that have a profound influence on soil nutrient availability. In this way, under submerged condition as in paddy rice cultivation ammonium (NH_4^+), rather than nitrate (NO_3^-), has been found to be the main source of N for crop growth. This is because NO_3^- (if present) can be depleted rapidly after flooding due to denitrification, while NH_4^+ tends to accumulate with time of submergence due to lack of O_2 for nitrification. Therefore, ammonium is likely to be the main form of nitrogen in flooded soils [21, 22]. Both forms of nitrogen, but especially NO_3^-, are very mobile and may show a marked seasonal change in concentrations during the growing season, owing to the unstable physicochemical properties, for example, redox potential, or to variations in microbial activity.

Phosphorus availability to rice mainly depends on soil pH. Flooding increases pH of acid soils and decreases pH of calcareous and sodic soils. In acid soils P is associated with Fe and Al compounds, whereas in soils, with pH higher than 6.5, P is primarily associated with calcium and magnesium. Flooding rice soils generally moderates the pH towards a neutral pH condition and consequently the availability of P is promoted [23, 24].

Several forms of soil potassium have been identified in paddy soils. Exchangeable K is considered mostly readily available, but other slowly available forms, which mainly depend on clay mineralogy and physicochemical properties, have been also identified in paddy soils [25]. The removal rate of K with rice grain and straw is rather high. Notwithstanding, either paddy farmers do not use K fertilizers or the used amount is insufficient to balance K removal [26]. Therefore, K availability of flooded rice soils is mainly affected by fertilizer application and straw management practices. Therefore, K deficiencies have been found to occur, even if only to a limited extent, in several types of lowland rice soils in association with small concentrations of exchangeable K, or to inactivation of K release by clay components.

Soil variability occurs across a continuum of spatial and temporal scales. Nutrient maps based on intensive soil sampling are a means to implement field-proven decision criteria for managing precision fertilizer input [5, 27, 28]. Experimental work was conducted on a paddy field in Corrientes, Argentina, to test the effect of lime amendment on the spatial distribution patterns of soil pH and Eh and on macro- and micronutrients. Three successive sampling campaigns were carried out to assess the stability of the spatial distribution along the growing season of the studied soil properties. Results reported on previous work for pH and Eh [17] and for extractable Fe, Mn, and Zn [12] showed a rather strong seasonality in the spatial distribution of these variables with changing patterns between sampling dates. Seasonal stability of nutrient maps has been considered as a prerequisite for efficient precision agriculture management [20]. On the other hand, several soil properties and nutrient in paddy soils previously have been shown to vary along the rice growing period [12, 17, 22, 24, 25]. Therefore, the first objective of this study was to conduct a field-scale analysis of the spatial variability of ammonium-N and available phosphorus and potassium, using the unpublished data sets of the above mentioned trial. The second objective was to investigate stability in the spatial distributions of ammonium-N, Olsen P, and Mehlich-1 K along the rice growth season.

2. Material and Methods

2.1. Site, Sampling Collection, and Laboratory Analysis. The study was conducted on a paddy field located near Corrientes, Argentina, cropped to rice (*Oryza sativa*, L.). The experimental site and the sampling procedure have been described before [12, 17] and therefore this information will be briefly summarized here. The climate is warm, subtropical with mean temperature of 20.1°C and mean yearly rainfall of about 1200 mm. The soil was classified as a typic Plintacualf [29], and it was an acidic soil (pH = 3.7, before liming), silt-loamy textured.

A field experiment was conducted to assess the influence of liming on several soil properties. The study site was an irrigated field with two previous years under lowland rice when this study was started. The entire field was subdivided in three parcels of 1.7 ha surface each, which received dolomite amendments in amounts of 0 (control), 625 kg ha^{-1}, and 1250 kg ha^{-1}. Each parcel was surrounded by a 10 m wide road and enclosed 32 plots of 50 m × 11.9 m, limited by 1.9 m width water channels (Figure 1). The experimental field was fertilized at sowing time using an N-P-K mixture with 35 kg of urea, 47 kg of superphosphate, and 95 kg of KCl. The fertilizer was uniformly broadcasted over the rice field.

Soil samples were collected at three different stages during the rice growth period. The first sampling was performed in aerobic conditions, just before sowing, the second sampling at bunch formation, that is, 28 days after flooding, and the third sampling at flowering stage, that is, 56 days after flooding. Ninety-three samples per liming treatment were taken at each of the three sampling dates. The basic sample grid was 11.9 × 20 m (Figure 1). Therefore, three soil samples were taken from each of the 32 single plots of a given parcel or treatment.

The soil was collected to a depth of 15 cm. Soil samples were air-dried and sieved (2 mm mesh). Ammonium-N was extracted with 2 M KCl and determined using methods described in [30]. Available P was extracted using bicarbonate [31]; phosphorus concentrations were determined colorimetrically using ascorbic acid-ammonium molybdate reagents.

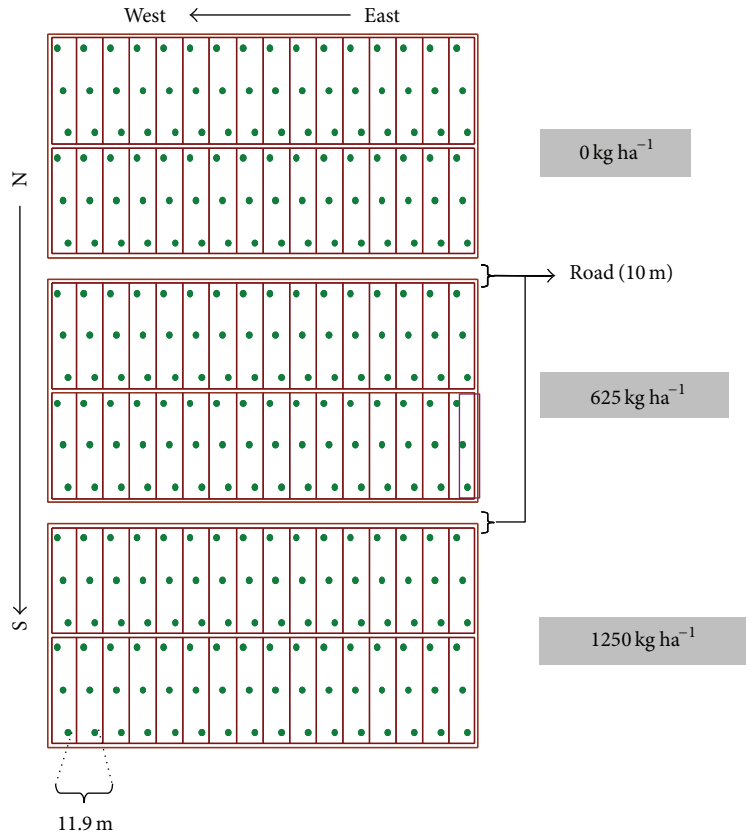

Figure 1: Sampling grid with 96 sampling positions per treatment.

Table 1: Mean ± standard deviation for pH and Eh at three sampling dates and on three different lime treatments. (Mean values followed by a diffferent lowercase letter in the column and different capital letter in the row are significantly different).

Dolomite	1st sampling (before sowing)	2nd sampling (day 28)	3rd sampling (day 56)
pH			
0 kg ha^{-1}	4.2 ± 0.09^{aA}	5.7 ± 0.28^{bB}	6.6 ± 0.24^{cC}
620 kg ha^{-1}	4.3 ± 0.07^{aA}	5.8 ± 0.30^{bB}	6.7 ± 0.22^{cC}
1250 kg ha^{-1}	4.4 ± 0.07^{aA}	5.9 ± 0.24^{bB}	6.8 ± 0.12^{cC}
Eh (mV)			
0 kg ha^{-1}	554.4 ± 7.4^{aA}	−16.4 ± 19.7^{aB}	−186.2 ± 31.9^{aC}
620 kg ha^{-1}	539.7 ± 10.6^{aA}	−25.8 ± 15.5^{bB}	−189.5 ± 29.7^{aC}
1250 kg ha^{-1}	532.4 ± 10.6^{aA}	−30.1 ± 13.5^{bB}	−210.3 ± 31.1^{bC}

Available K was extracted with the Mehlich-1 solution [32] and measured by atomic absorption spectrometry.

Mean values of pH and redox potential (Eh), reported in [17], are summarized in Table 1. On average, mean pH increased by 2.3 units along the rice growth period. Moreover, as expected, mean pH ranked as control <625 kg ha^{-1} dolomite <1250 kg ha^{-1} dolomite, at the three sampling dates. Redox potential decreased along the rice growth period with increasing duration of the anaerobic conditions; the effect of dolomite addition was to decrease mean soil redox potential on the three sampling dates.

2.2. Statistical and Geostatistical Analysis. The 27 data sets studied (3 nutrients × 3 lime treatments × 3 sampling dates) were first analyzed for normality by means of the Kolmogorov-Smirnov test. Then, descriptive statistics including mean, variance, coefficient of variation, maximum, minimum, skewness, and kurtosis were determined. Pearson correlation coefficients were also calculated to determine the relationship between soil properties.

Geostatistical analysis is based on the assumption that measurements separated by small distances are more likely to be similar to each other than those farther apart, meaning that spatial autocorrelation exists. This hypothesis can be verified through examination of semivariograms for the attributes under investigation. Moreover, the statistical tool used to measure the autocorrelation between samples is called the semivariogram. An experimental semivariogram can be obtained from semivariance values calculated as a function of the distance, $\gamma(h)$, which are given by the following equation:

$$\gamma(h) = \frac{1}{2N(h)} \sum_{i=1}^{N(h)} \left[Z(x_i) - Z(x_i + h)\right]^2, \quad (1)$$

where $Z(x_i)$ and $Z(x_i+h)$ are the actual values of the variable, Z, at places x_i and $(x_i + h)$, and $N(h)$ is the total number of

data pairs separated by a distance h. Thus, the experimental or sample variogram is obtained by changing h.

The experimental semivariogram must be fitted by a model that mathematically describes the spatial variation. Several standard models (i.e., spherical, exponential, Gaussian, etc.) are currently available. In this work, calculation of sample variogram and fitting of models were made using accredited criteria and procedures [2, 33]. The cross-validation technique was used for model fitting [34]. Then, agreement between experimental and modelled semivariograms was judged by various indicators, including determination coefficient (r^2), mean error (ME), and no dimensional mean square error (NMSE).

Semivariogram models were described using the following basic parameters: the distance h, the sill variance ($C_0 + C_1$), and the range of spatial dependence (a). The sill variance eventually reaches an upper bound; this parameter consists of a spatially correlated or structural variance (C_1) and may include a nugget variance (C_0), which represents the variation that has not been resolved at the scale of sampling. The degree of spatial dependence can be expressed by the ratio of nugget variance (C_0) to the threshold ($C_0 + C_1$) variance. The nugget to sill ratio was used to qualitatively classify the spatial dependence into strong (<25%), moderate (25 to 75%), and weak (>75%) following accredited criteria [6].

Based on the best fitting semivariogram model, the kriging approximation was used for interpolation and mapping purposes. Kriging is an optimal method of prediction in the sense that it is unbiased and the predictions have minimum variance [27, 28].

3. Results and Discussion

3.1. Statistical Analysis of Soil Macronutrients. Descriptive summary statistics of the 27 data sets studied are presented in Table 2. Concentrations of soil NH_4^+-N just before flooding ranged from 20.07 to 28.87 mg kg^{-1} and those at rice flowering (56 days after flooding) ranged from 37.74 to 43.92 mg kg^{-1}. The latter were significantly higher than the former ($P < 0.05$) and this was for the three liming treatments. The average increase in NH_4^+-N concentrations between the first and the third sampling period was 88%. Ammonium-N accumulation in anaerobic conditions is an expected result, due to the lack of conversion of organic N into mineral N in paddy soils [21, 22], as stated before. However the amounts of ammonium and nitrate nitrogen determined at the second sampling date, which ranged from 24.73 to 28.50 mg kg^{-1}, were not much different from those of the first sampling date, even if the rate of NH_4^+-N accumulation was not negligible for the control treatment during this period. Moreover, comparison between the first and the second sampling dates showed small but significant ($P < 0.05$) ammonium-N losses and increases at the 625 kg ha^{-1} and 1250 kg ha^{-1} treatments, respectively. The net increase in NH_4^+-N after flooding is the result of the net balance from accumulation (owing to the lack of O_2 for nitrification) and losses (owing mainly to plant uptake but also to denitrification processes).

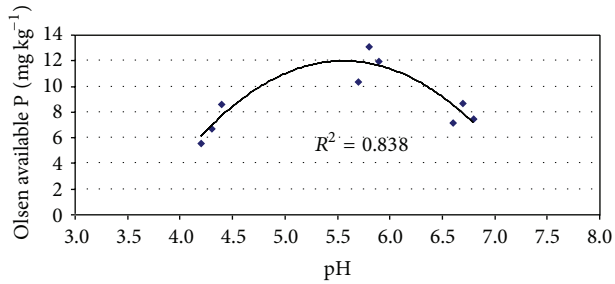

Figure 2: Relationship between average pH and average Olsen extractable phosphorus.

There were positive effects of lime amendment on NH_4^+-N concentration, both at sowing and at bunch formation, as the differences between the control treatment and the two treatments amended with dolomite were significant ($P < 0.05$). Nevertheless, concentrations of NH_4^+-N within each sampling period were considerably stable, as shown by the smaller range of values among liming treatments than among sampling dates.

Coefficients of variation of the NH_4^+-N data sets studied ranged from 9.7 to 20.3% and showed a trend to decrease for the successive sampling periods. This seasonal reduction in the statistical variability of NH_4^+-N concentrations throughout the rice growth period could be the result of more uniformity in microbiological activity across the field, which in turn may be due to a higher homogeneity of the redox conditions (Table 1). All the ammonium-N data sets studied were normally distributed. These distributions were slightly negatively or positively skewed, as the skewness parameter ranged from −0.462 to 0.654.

The mean concentrations of Olsen extractable P ranged from 5.52 to 8.57 mg kg^{-1} at the first sampling, in aerobiosis, from 10.36 to 13.12 mg kg^{-1} at the second sampling, 28 days after flooding, and from 7.14 to 8.67 mg kg^{-1} at the third sampling, 56 days after flooding. These results are in accordance with the fact that P availability has been found to be optimal when the soil pH is between 6.0 and 6.5. Figure 2 shows the relationships between mean pH and mean Olsen available P in the studied treatments. The initial concentrations of Olsen P in the very acid soil (in anaerobic conditions) were low [24, 31], but these increased rapidly after flooding, in all the liming treatments. Thus Olsen P increased with increasing soil pH and was highest for mean pH values between 5.7 and 5.9 recorded at the second sampling period. Subsequently, concentrations of Olsen P measured in the third period were lower compared to the second period, in accordance with the mean pH values ranging from 6.6 to 6.8. Therefore, the highest available P concentrations were recorded at bunch formation, owing to soil pH ranges near optimum values [24, 31]. However, available P was depleted throughout the late growing season, owing mainly to pH increases above to the 6.5 threshold, but also to the plant uptake.

Liming significantly ($P < 0.05$) increased Olsen P availability in aerobic conditions before flooding. Also, at the second sampling the mean concentration of Olsen P was

Table 2: Summary statistics for NH_4^+-N, P, and K concentrations on different sampling dates and liming treatments (Var.: variance; CV: coefficient of variation).

Lime (Kg ha^{-1})	Code	Mean (mg kg^{-1})	Var.	CV	Minimum (mg kg^{-1})	Maximum (mg kg^{-1})	Skewness	Kurtosis
Ammonium nitrogen, NH_4^+-N								
First sampling								
0	NH_4-10	20.07^{a,A}	14.67	19.1	11.16	28.80	−0.047	−0.405
625	NH_4-11	28.87^{c,B}	17.09	14.3	20.42	39.72	0.159	−0.435
1250	NH_4-12	27.30^{b,A}	30.56	20.3	11.62	43.63	0.064	0.856
Second sampling								
0	NH_4-20	24.73^{a,B}	15.29	15.8	17.09	35.28	0.319	−0.530
625	NH_4-21	27.36^{b,A}	11.21	12.2	21.43	37.38	0.654	−0.036
1250	NH_4-22	28.50^{c,B}	12.56	12.4	19.79	36.94	0.099	−0.775
Third sampling								
0	NH_4-30	37.74^{a,C}	24.14	13.0	28.84	48.52	0.433	−0.820
625	NH_4-31	43.92^{b,C}	31.23	12.7	30.38	55.38	−0.462	−0.251
1250	NH_4-32	38.84^{c,C}	14.25	9.7	29.60	48.54	0.126	−0.033
Phosphorus, P								
First sampling								
0	P-10	5.52^{a,A}	1.75	24.0	2.50	8.04	0.041	−0.730
625	P-11	6.72^{b,A}	2.03	21.2	3.74	10.72	0.450	−0.346
1250	P-12	8.57^{c,A}	2.60	18.8	5.04	12.33	−0.160	−0.274
Second sampling								
0	P-20	10.36^{a,C}	4.75	21.0	6.61	18.45	1.069	1.562
625	P-21	13.12^{b,C}	6.50	19.4	7.30	18.43	0.012	−0.670
1250	P-22	11.93^{c,C}	3.39	15.4	8.72	17.34	0.502	0.037
Third sampling								
0	P-30	7.14^{a,B}	3.39	25.8	3.50	14.26	0.894	1.633
625	P-31	8.67^{b,B}	2.72	19.1	4.79	13.17	0.194	−0.319
1250	P-32	7.45^{a,B}	3.02	23.3	4.05	10.69	0.111	−0.883
Potassium, K								
First sampling								
0	K-10	38.15^{a,C}	47.95	18.2	26.56	64.64	1.012	1.551
625	K-11	44.41^{b,C}	36.93	13.7	34.26	65.21	0.822	0.897
1250	K-12	50.41^{c,C}	35.78	11.9	38.24	70.53	0.380	0.387
Second sampling								
0	K-20	32.09^{a,B}	23.54	15.1	22.01	42.35	0.004	−0.969
625	K-21	36.46^{b,B}	86.97	25.6	19.86	59.87	0.277	−0.860
1250	K-22	40.44^{c,B}	57.47	18.8	28.73	59.68	0.355	−0.649
Third sampling								
0	K-30	19.41^{b,A}	7.48	14.1	12.43	25.30	0.019	−0.647
625	K-31	18.01^{a,A}	5.78	13.4	12.42	23.95	0.137	−0.022
1250	K-32	17.25^{a,A}	9.56	17.9	11.34	23.23	0.177	−1.038

Mean values followed by different small letters and different capital letters are significantly different ($P < 0.05$) for liming treatment and sampling date, respectively.

significantly lower ($P < 0.05$) in the control treatment than in the two dolomite amended treatments. However, at the third sampling date, the highest mean Olsen P values were recorded at the 625 kg ha^{-1} dolomite treatment. In general, and in agreement with the trends observed before for ammonium-N, Olsen P concentrations showed smaller differences among liming treatments than among sampling dates (Figure 2).

Coefficients of variation for Olsen P ranged from 15.4 to 25.8% and, therefore, showed a similar order of magnitude for the different treatments and sampling dates studied. The seasonal stability in the statistical variability of available P probably reflects the influence of pH as main factor driving the dynamics of P in paddy rice soils. All the Olsen P data sets studied also were normally distributed. The coefficients of skewness for these distributions ranged from 0.169 to 1.069

and were positive for 8 out of 9 data sets. Positively skewed distributions indicate the presence of some few extreme high values of available P.

The critical value of Olsen extractable P across a wide range of soil types has been established at 6.0 mg kg^{-1} [23]. Subcritical P levels are expected to cause reductions of production under intensive rice cropping. Available phosphorus concentrations before flooding ranged from very low to low and become moderate after the additional release promoted by the soil pH increase due to flooding. No visual symptoms of P deficiencies were observed in the rice crop studied. Therefore, the applied supply of P, as superphosphate, may be sufficient for the agricultural practices and rice production levels of the local area. Moreover, the 625 kg ha^{-1} dolomite treatment was more efficient than the 1250 kg ha^{-1} dolomite treatment for releasing available Olsen P, in anaerobic conditions, as shown by mean values at the second and third sampling dates.

Concentrations of available K extracted with Mehlich-1 are reported in Table 2 and ranged from 28.15 to 50.41 mg kg^{-1}, 32.09 to 40.44 mg kg^{-1}, and 17.25 to 19.41 mg kg^{-1} at the first, second, and third sampling dates, respectively. Therefore, available K concentrations steadily decreased throughout the crop period, from sowing to bunch formation and then to flowering. On average Mehlich-1 extractable K was more than two times higher just before flooding than after 56 days of submersion. Available K depletion probably was mainly due to the plant uptake, so that it is expected to increase again after rice harvesting and straw mineralization. Notwithstanding, the dynamic of K along the rice vegetative period could be also affected by soil intrinsic factors such as clay mineralogical composition and physicochemical characteristics.

Mean extractable K concentrations in the soil measured at sowing and at bunch formation also increased significantly ($P < 0.05$) with rate of dolomite application. Hence, in the two first sampling dates, mean Mehlich-1 K values for the three dolomite treatments ranked as control < 625 kg ha^{-1} < 1250 kg ha^{-1}. At the third sampling date, however, the mean extractable K concentrations measured at the control treatment were significantly lower than those at the two dolomite amended treatments, but no significant differences were found between the two treatments with dolomite amendment. The control treatment had the lowest mean extractable K level before flooding and the highest after 58 days of flooding; in contrast the 1250 kg ha^{-1} treatment had the highest mean extractable K level before flooding and the lowest after 58 days of flooding. Hence, the rate of diminution in soil available K throughout the crop growth period was greater for the dolomite amended treatments than for the control treatment. Therefore, seasonal changes in available K under paddy rice cultivation were not similar for all the treatments, suggesting specific K fixation or depletion depending on soil reaction.

Coefficients of variation for Mehlich-1 K have been found to vary between 11.4 and 25.6%, and they were smaller than 20% in eight out of nine data sets. On average, CVs for Mehlich-1 extractable K were lower than those obtained for

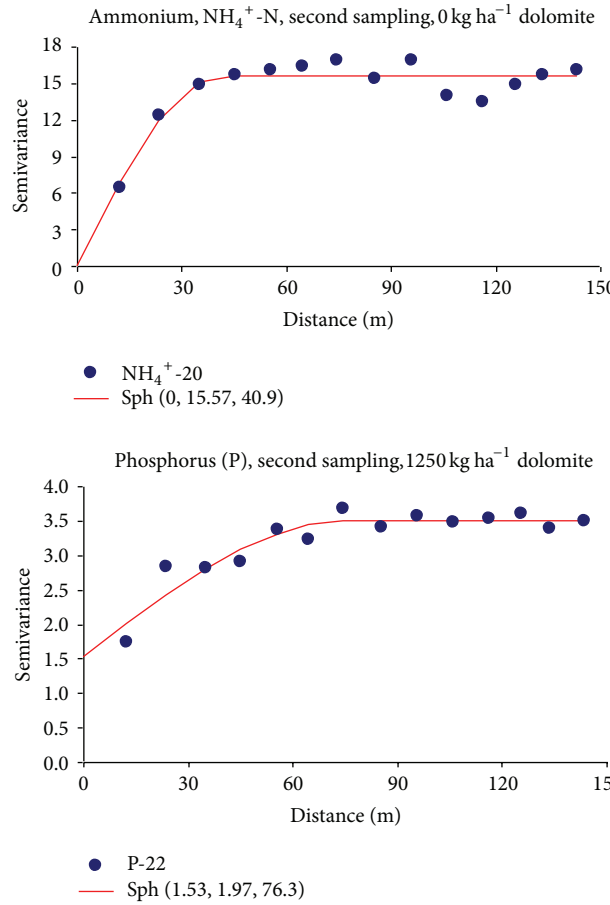

Figure 3: Selected examples of semivariograms corresponding to experimental data sets without nugget effect and with the highest nugget effect modelled.

Olsen P. Again, all the available K data sets studied were normally distributed. Moreover, the distributions of extractable K for all the data sets analyzed were positively skewed, with skewness coefficients ranging from 0.004 to 1.012. The highest values of extractable K exhibited by distributions with the largest skewness coefficients may be associated with locations with the highest straw residues left after crop harvesting.

Mehlich-1 extractable K concentrations below 50 mg kg^{-1} are considered to be low for an intensive high-yielding rice crop [28]. Thus, according to these soil tests, the amount of K fertilizer applied was not sufficient to maintain a good nutritional status during the entire growth season. No visual deficiencies were detected for K in our experimental field. Consequently, the applied K can be considered to be sufficient to maintain current rice yields of about 4–6 t ha^{-1} in the studied area.

3.2. Spatial Dependence and Kriging Maps of Soil Macronutrients. Selected examples of semivariograms are presented in Figure 3. They correspond to one of the data sets with the highest degree of spatial dependence (no nugget effect) and to the data set with the lowest degrees of spatial dependence, meaning the highest nugget to sill ratio, that is,

Table 3: Semivariogram model type, parameters for best fitted model (C_0: nugget; C_1: structural variance; a: range), and cross-validation indicators (r^2: determination coefficient; ME: mean error, NMSE: no dimensional mean square error) of the studied NH_4-N, P, and K data sets.

Lime	Code	Model	C_0	C_1	$C_0/(C_0 + C_1)$	a (m)	r^2	ME	NMSE
Ammonium nitrogen, NH_4^+-N									
First sampling									
0	NH_4-10	Spherical	1.09	14.20	7.1	47.0	0.923	0.003	1.004
625	NH_4-11	Spherical	6.37	10.41	38.0	45.1	0.663	−0.011	0.994
1250	NH_4-12	Spherical	13.58	19.05	41.6	68.9	0.932	−0.016	0.926
Second sampling									
0	NH_4-20	Spherical	0.00	15.57	0.0	40.9	0.876	−0.003	1.147
625	NH_4-21	Exponential	0.00	12.25	0.0	59.5	0.912	−0.005	0.992
1250	NH_4-22	Exponential	0.00	13.08	0.0	49.8	0.869	−0.019	1.000
Third sampling									
0	NH_4-30	Spherical	1.95	24.15	7.5	53.2	0.639	−0.001	0.813
625	NH_4-31	Spherical	0.00	33.96	0.0	71.9	0.907	0.002	0.922
1250	NH_4-32	Spherical	2.60	13.92	15.7	84.6	0.972	−0.008	0.937
Phosphorus, P									
First sampling									
0	P-10	Spherical	0.23	1.59	12.6	51.7	0.835	−0.052	1.060
625	P-11	Spherical	0.61	1.54	28.4	64.0	0.836	−0.003	1.020
1250	P-12	Spherical	0.44	2.29	16.1	53.0	0.850	0.002	0.903
Second sampling									
0	P-20	Spherical	0.42	4.86	8.0	65.2	0.951	−0.000	1.097
625	P-21	Spherical	0.43	6.24	6.4	47.7	0.944	−0.019	0.996
1250	P-22	Spherical	1.53	1.97	43.7	76.3	0.908	−0.014	1.029
Third sampling									
0	P-30	Spherical	1.41	2.30	38.0	73.9	0.976	0.002	0.848
625	P-31	Spherical	0.74	2.11	26.0	57.7	0.843	0.027	0.855
1250	P-32	Spherical	0.89	2.25	28.3	60.0	0.912	0.001	0.941
Potassium, K									
First sampling									
0	K-10	Spherical	4.97	46.74	9.6	59.7	0.861	0.011	1.184
625	K-11	Spherical	6.55	33.12	16.5	54.2	0.903	−0.005	0.948
1250	K-12	Spherical	15.96	21.35	42.8	51.4	0.925	0.013	0.901
Second sampling									
0	K-20	Spherical	6.73	18.65	26.5	65.5	0.891	0.006	0.954
625	K-21	Spherical	14.61	75.20	16.3	52.3	0.887	0.049	0.863
1250	K-22	Spherical	16.56	43.79	27.4	58.9	0.783	0.004	0.782
Third sampling									
0	K-30	Spherical	1.46	6.66	18.0	63.1	0.899	−0.024	0.882
625	K-31	Spherical	2.46	3.71	39.9	68.2	0.921	0.003	1.075
1250	K-32	Spherical	3.52	6.84	34.0	76.8	0.960	−0.008	0.690

$(C_0)/(C_0+C_1)$. The geostatistical parameters for the best fitted semivariogram models describing the spatial dependence of the soil macronutrients studied are listed in Table 3, together with the cross-validation parameters used for assessing the goodness of fit. All the semivariograms modelled increased with lag distance (h), until a more or less constant value was reached, at a given separation distance, that is, the sill or total semivariance ($C + C_0$); this separation distance (a) is called the range of spatial dependence. Note that the nugget variance, C_0, is the semivariance at $h = 0$. Experimental semivariograms of the NH_4^+-N concentrations measured at the three lime treatments and during the three periods studied could be described quite well by either spherical or exponential models with a nugget component (C_0) plus a spatial component (C_1) with a range of spatial dependence varying between 40.9 and 84.6 m. For Olsen P and Mehlich-1 K, all experimental semivariograms were described by spherical models with a range between 51.4 and 76.8 m.

Theoretical models were fitted to experimental semivariograms based both on subjective visual inspection and on the following parameters obtained by cross-validation: determination coefficients of the regression between calculated and kriging estimated values (r^2), mean errors (ME), and no dimensional mean square errors (NMSE). Goodness of fit was assessed by proximity to ideal values of these parameters for a perfect fit, that is; $r^2 = 1$, ME = 0, and NMSE = 1 [12, 33]. Determination coefficients were $r^2 \geq 0.639$, mean errors were ME ≤ 0.059, and no dimensional mean square errors were $0.813 < \text{NMSE} < 1.189$. Therefore, the values of these parameters suggest that all models adequately fitted the spatial dependence of the studied macronutrient data sets.

Note also that in most of the cases studied the experimental semivariograms were best described by a spherical model. The exception was for two NH_4^+-N data sets corresponding to the 625 kg ha^{-1} and 1250 kg ha^{-1} treatments during the second sampling, which were best fitted by exponential models. Other soil properties studied before in our experimental field (pH, Eh, extractable Fe, Mn, and Zn) also have been found to fit mostly spherical models and otherwise exponential models [12, 13, 17].

The nugget variance represents either experimental variability induced by potential laboratory errors or field random variability that can not be detected at the scale of sampling. The nugget to sill ratio, $C_0/(C + C_0)$, ranged between 0 and 43.7% for all the data sets studied. This ratio was zero at four data sets, was smaller than 25% at 11 data sets, and ranged from 25 to 50% at 12 data sets, indicating in most of the cases a strong to moderate degree of spatial dependence, according to the authorized criteria [6] previously quoted. Moreover, the magnitude of the nugget variance showed no dependence of the liming treatment or the sampling date. Altogether, the small to moderate nugget effects indicate that the sampling grid used was proper to reflect the spatial dependence of the studied macronutrients.

The sill value ($C + C_0$) reflects the total variance for very large distances; the sill is given by the sum of the nugget semivariance (C), which may be zero, plus the portion of the semivariance that is spatially structured (C_0). As expected, for each data set, the value of the sill modeled was of the same order of magnitude as the value of statistical variance. The sill value ranged from 12.35 to 32.63 (mg kg^{-1})^2 for NH_4^+-N, from 1.82 to 6.67 (mg kg^{-1})^2 for Olsen P, and from 6.17 to 89.81 (mg kg^{-1})^2 for Mehlich-1 K, indicating that Olsen P had the weakest pattern of spatial variability. Mean sill values were lowest for NH_4^+-N at the second sampling date; however in this sampling they were highest for available P and K. Main factors responsible for the differences in semivariance for very large distances, that is, for the sill value, of the data sets studied here could be: (a) seasonal variations, driven by the different biogeochemical processes during aerobic and anaerobic conditions, (b) nutrient uptake by the rice crop, and (c) management effects such as liming.

The values for the range of spatial dependence of the semivariogram models were of the same order of magnitude for the three nutrients studied, varying from 40.9 to 84.6 m for NH_4^+-N, from 47.7 to 76.3 m for Olsen P, and from 51.4 to 76.8 m for Mehlich-1 K. Highest values of this parameter were about two times larger than smallest values. The range of spatial dependence showed a slight trend to increase throughout the rice growth period. This suggests the area of similarity of the nutrient content becomes larger during the rice growing season. Note also that this area may embrace several individual rice plots of 50×10 m size (Figure 1). Moreover, the values of the range of spatial dependence for ammonium-N and extractable P and K were also similar to those previously reported for pH and Eh [17] and for extractable Fe, Mn, and Zn [12, 13] at the same experimental field. Sample locations separated by distances smaller than the range are more alike and are spatially correlated, whereas those separated by distances greater than the range are spatially uncorrelated. Summarizing, there were some similarities in the range of spatial dependence for soil chemical properties measured under different lime treatments at different sampling dates, but differences in range also were found with the same frequency as similarities.

Spatial dependence at paddy fields of various sizes [5, 11–15] and also at the scale of a whole district cropped with rice [16] has been reported for several soil properties. Semivariograms depend on the sampling scale, sampling design, and support of the underlying data sets; thus, there is no "absolute" semivariogram for a soil property. Since all these factors vary between published studies, it becomes difficult to compare the results by different authors. Moreover, in our experimental field the soil properties analysed in the present and in previous work, namely, pH, Eh, and macro- and micronutrient concentrations [12, 13, 17], showed seasonal modifications in the patterns of spatial dependence. A seasonal pattern of variability, which may depend upon local conditions, is an additional drawback to compare results from different filed trials.

Until now, the temporal oscillation in the variability of soil properties has mainly been reported for soil biological properties, as, for example, soil enzymes, soil biological activity, and soil fauna, and for soil quality indices based on these properties [35, 36]. However, in this work and in previous work carried out at our experimental field [12, 13, 17], we described seasonality in the spatial patterns of variability of soil general properties or soil nutrient content in rice fields, which has been also demonstrated by field trials conducted in other different areas [20, 37].

Spatial variability of soil properties depends both on soil forming factors and processes and on management practices, as stated before. In our case study, climate, topography, and water level were homogeneous throughout the experimental fields. The parent material consisted of sedimentary rocks characterised by various particle size distributions, which could draw spatial variability at the decameter scale [12]. Element speciation and concentrations of macro- and micronutrients at a given location within a field also depend on various soil properties, such as organic matter content, total element composition, pH, and redox potential (Eh), on plant nutrient uptake, and on management practices. In a previous work pH and Eh of the studied field have been demonstrated to undergo seasonal variability. On the other hand, the fertilizer use efficiency of rice is very low

when all fertilizers are applied as base dressing, as in this field experiment; therefore nutrient uptake by rice plants cannot be viewed as a major source of variability in our conditions. However, current management practices of the rice crop, associated with the irrigation system employed, may result in uneven water application [20] and also may drive redistribution of elements by lateral flow across the smallest production units [19, 20]. Therefore redistribution by unsteady flooding and lateral water movement could be considered as a main source of spatial variability, even if all the experimental units were managed similarly. In addition the role of microrelief heterogeneities has been also stressed as an essential source of variability in soil properties under rice cultivation [20, 37].

Therefore, the results of this work together with those reported in previous work [12, 13, 17] suggest that texture, soil mineral and organic composition, and liming dose may be possible factors influencing the spatial variability of soil macronutrients at the studied parcel. In addition, seasonality or temporal variability of the patterns of spatial variability of the studied macronutrients and other soil properties may be mainly driven by uneven flooding associated with irrigation, lateral flow between small plots, and microtopographic irregularities.

Examples of kriging maps for ammonium-N, Olsen P, and Mehlich-1 K are shown in Figures 4, 5, and 6, respectively. The selected examples correspond to the three successive sampling dates of the control treatment. These maps illustrate areas with varied spatial and temporal concentrations of nutrient throughout the experimental fields. Concentrations of ammonium-N ranged from 11 to 29 mg kg^{-1}, 17 to 38 mg kg^{-1}, and 30 to 48 mg kg^{-1} at the first, second, and third sampling dates, respectively. Similarly Olsen P ranged from 3 to 9 mg kg^{-1}, from 6 to 20 mg kg^{-1}, and from 5 to 12 mg kg^{-1} in these sampling periods, whereas the respective ranges of variation for Mehlich-1 K were from 20 to 70 mg kg^{-1}, 24 to 44 mg kg^{-1}, and 15 to 17 mg kg^{-1}. Differences between patches with the lowest and the highest concentrations ranged approximately between 1.5 and 3.5. Kriging maps also clearly illustrated the presence of small scale variability for NH_4^+-N, Olsen P, and Mehlich-1 K within each liming treatment (data not shown) and during each of the three sampling dates.

The patterns of spatial distribution of the three nutrients presented in the maps of Figures 4, 5, and 6 are characterized by small zones, that is, discrete patches, with heterogeneous values of the studied variables. For a given area, differences in concentration among sampling dates are clearly shown, so that areas with relative high or low macronutrient concentrations within each field were not stable throughout the rice growth period. Thus, there was a lack of temporal stability for the macronutrients studied, similar to that previously described for pH and Eh [17] and for Fe, Mn, and Zn [12, 13].

Our results also showed that seasonality changed the patterns of distribution of ionic species with different degrees of mobility such as ammonium, phosphate, or potassium. Subsequently, seasonal variability in soil macronutrient concentration (N, P, K) was not only present but potentially of agronomic importance.

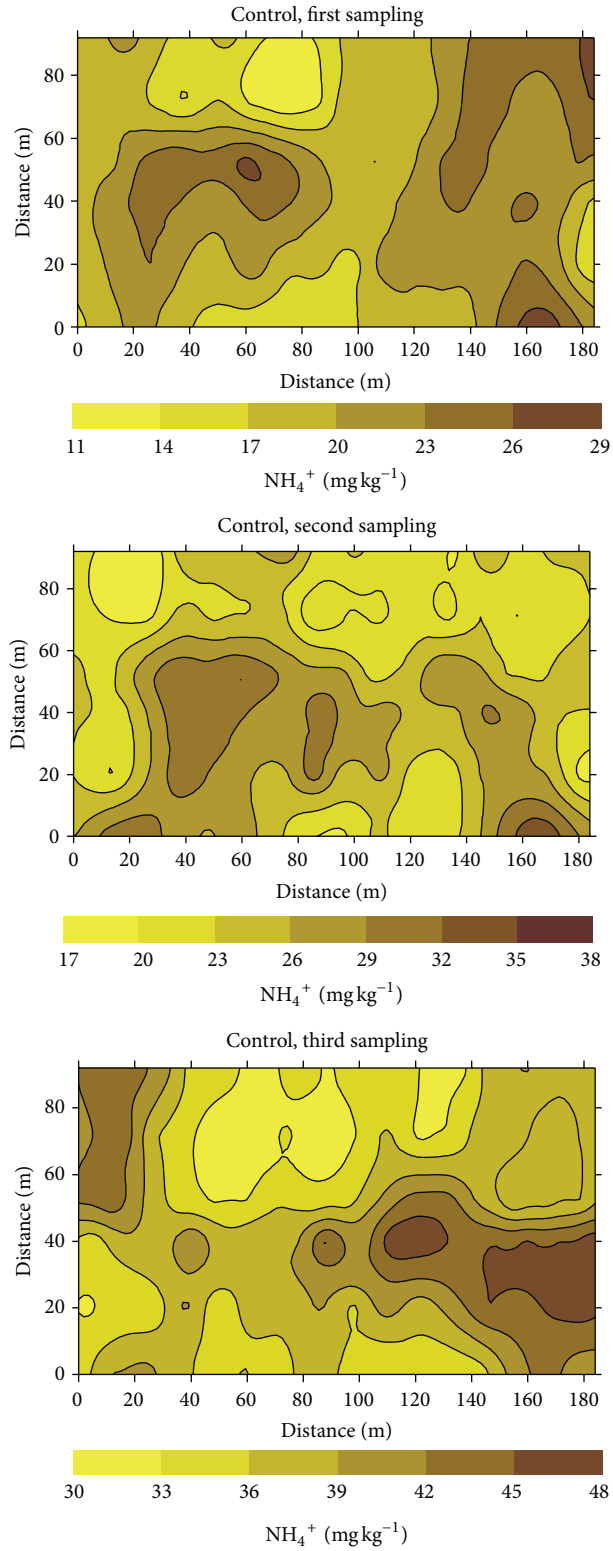

Figure 4: Kriging maps for ammonium-nitrogen (NH_4^+-N) at the control treatment, for successive sampling dates.

Our macronutrient maps were based on an intensive sampling on a 50 × 11.9 m grid. Farmers cannot afford this level of investment in sampling and often rely on data from satellites

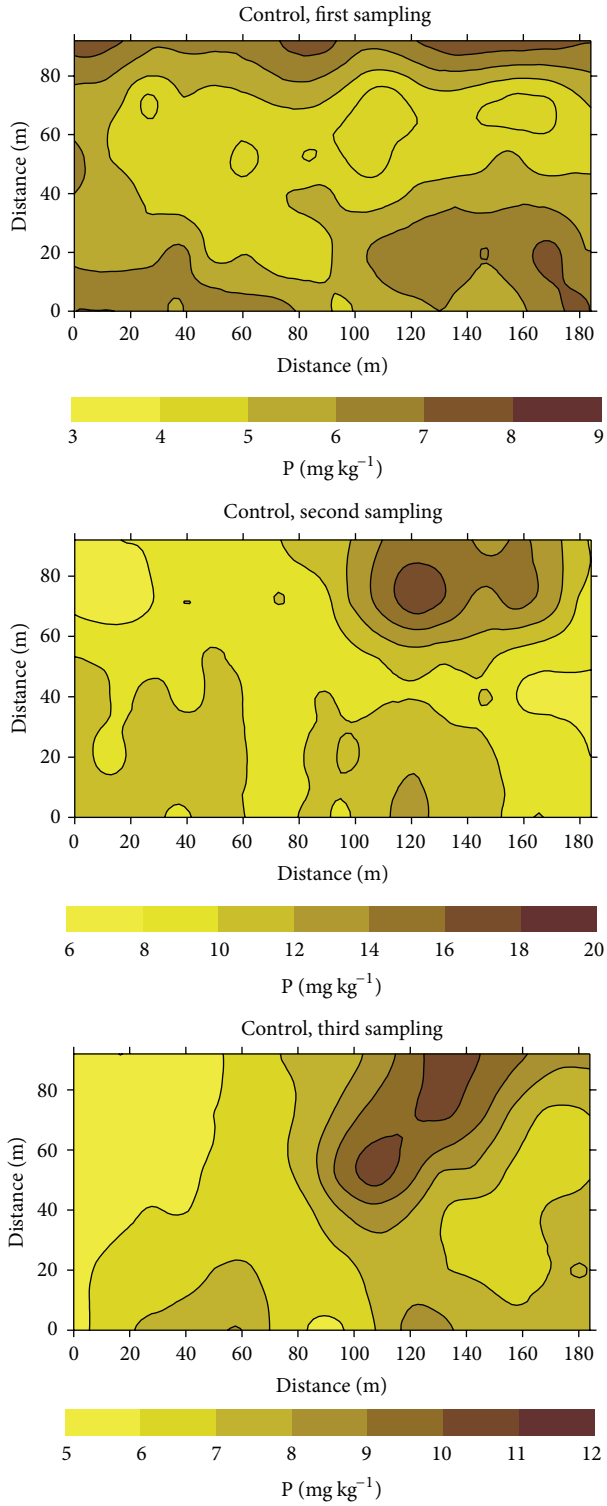

Figure 5: Kriging maps for Olsen extractable phosphorus (P) at the control treatment, for successive sampling dates.

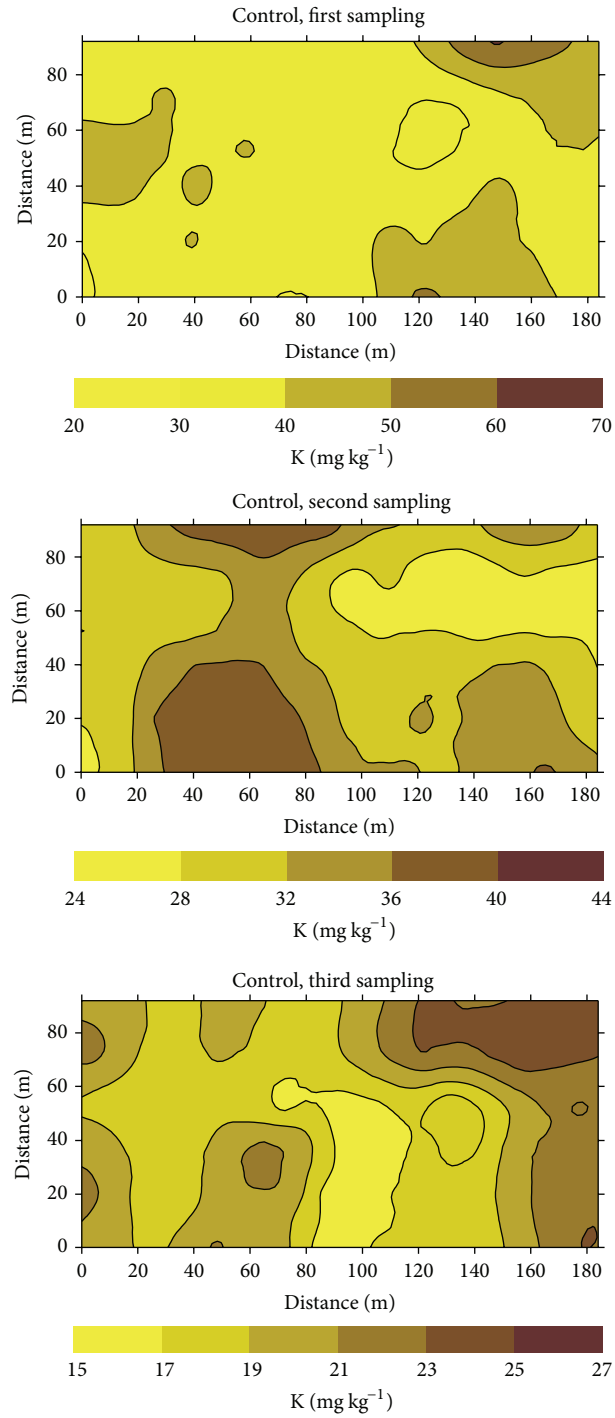

Figure 6: Kriging maps for Mehlich-1 extractable potassium (K) at the control treatment, for successive sampling dates.

or aircraft or from tractor-borne equipment. However, and in spite of significant technological advances, nowadays a lack of decision criteria still remains for an efficient site specific management of fertilizer inputs on several crops, and this is the case for lowland rice. To overcome this deficit nutrient maps based on intensive soil sampling are required. Therefore, kriging maps are useful for optimizing soil sampling and for delineating management units. They have been widely used in rainfed agriculture as a straightforward approach for precise management of phosphorus and potassium, since these nutrients show comparatively stable spatial distribution patterns in aerobic conditions [2, 3, 6, 7].

In our lowland paddy soil, marked seasonal changes in mean concentrations and in the spatial distribution of ions with wide differences in mobility such as ammonium-N, phosphate, and potassium were detected. This information may be potentially very useful both for site specific management and for environmental purposes. In general, recommendations for fertilizer application to rice crops are based on correlation between soil test values of the target nutrient measured on samples collected before flooding. The above results suggest that the efficiency of site specific management practices in rice fields would increase if the observed patterns of seasonal changes in macronutrient concentration are taken into account. This is in agreement also with recent work [20].

On the other hand, analysis of soil spatial variability also provides valuable knowledge for environmental management. For example, if only mean values of macronutrients were taken into account, the low concentrations of ammonium-N and available P and K across the rice growth period were unlikely to have any adverse effects on the environment; however the presence of spots with nutrient concentrations higher than the average could be critical for ponding water and ground water quality.

4. Conclusions

Mean values of ammonium-N, Olsen P, and Mehlich-1 K sampled during three different dates along the rice growth period, and under three dolomite treatments, in an acid paddy soil, varied both seasonally and as a function of the liming rate. Increasing rates of dolomite amendment increased ammonium-N, Olsen P, and Mehlich-1 K, both before sowing (aerobic conditions) and 28 days after flooding (anaerobic conditions). Meanwhile, after 56 days of flooding effects of dolomite amendment on the concentration of the studied nutrients were dissimilar.

Ammonium-N accumulated in anaerobic conditions and was highest at the third sampling date, 56 days after flooding. Olsen P availability increased with increasing pH after flooding, but this effect was reversed for pH values higher than 6.5 measured at the flowering stage of the rice crop. Mehlich-1 K steadily decreased along the growth period of rice.

The spatial variability of NH_4^+-N, P, and K on rice fields with three different rates of dolomite amendment and at three different crop stages was best described mainly by spherical models and otherwise with exponential models. The nugget to sill ratio ranged from 0 to 43.7% for all the data sets studied, showing strong to moderate pattern of spatial dependence. The small to moderate nugget effects also indicate that the sampling grid used was proper to reflect the spatial dependence of the studied macronutrients.

Kriging maps clearly showed the presence of small scale variability for NH_4^+-N, Olsen P, and Mehlich-1 K within each liming treatment and during each of the three sampling dates. Also the position of patches with high and low concentrations of the studied macronutrients changed between successive sampling dates, providing evidence of the lack of temporal stability in the patterns of spatial distribution. Seasonality in the spatial distribution of macronutrients should be considered as an important factor for an efficient site specific management.

Conflict of Interests

The authors declare that there is no conflict of interests regarding the publication of this paper.

Acknowledgment

This study was partly financed by Spanish Ministry of Foreign Affairs, AECID Agency, Grant B/6921/08.

References

[1] A. E. Johnston, "The value of long-term field experiments in agricultural, ecological and environmental research," *Advances in Agronomy*, vol. 59, pp. 291–333, 1997.

[2] D. L. Corwin and S. M. Lesch, "Application of soil electrical conductivity to precision agriculture: theory, principles, and guidelines," *Agronomy Journal*, vol. 95, no. 3, pp. 455–471, 2003.

[3] B. Koch, R. Khosla, W. M. Frasier, D. G. Westfall, and D. Inman, "Economic feasibility of variable-rate nitrogen application utilizing site-specific management zones," *Agronomy Journal*, vol. 96, no. 6, pp. 1572–1580, 2004.

[4] S. R. Vieira, J. L. Hatfield, D. R. Nielsen, and J. W. Biggar, "Geostatistical theory and application to variability of some agronomical properties," *Hilgardia*, vol. 51, no. 3, pp. 1–75, 1983.

[5] B. B. Trangmar, R. S. Yost, M. K. Wade, G. Uehara, and M. Sudjadi, "Spatial variation of soil properties and rice yield on recently cleared land," *Soil Science Society of America Journal*, vol. 51, no. 3, pp. 668–674, 1987.

[6] C. A. Cambardella, T. B. Moorman, J. M. Novak et al., "Field-scale variability of soil properties in central Iowa soils," *Soil Science Society of America Journal*, vol. 58, no. 5, pp. 1501–1511, 1994.

[7] A. Paz, M. T. Taboada, and M. J. Gómez, "Spatial variability in topsoil micronutrient contents in a one-hectare cropland plot," *Communications in Soil Science and Plant Analysis*, vol. 27, no. 3-4, pp. 479–503, 1996.

[8] A. Paz-Gonzalez, M. T. Taboada Castro, and S. R. Vieira, "Geostatistical analysis of heavy metals in a one-hectare plot under natural vegetation in a serpentine area," *Canadian Journal of Soil Science*, vol. 81, no. 4, pp. 469–479, 2001.

[9] M. D. Cahn, J. W. Hummel, and B. H. Brouer, "Spatial analysis of soil fertility for site-specific crop management," *Soil Science Society of America Journal*, vol. 58, no. 4, pp. 1240–1248, 1994.

[10] M. Oliver, Ed., *Geostatistical Applications for Precision Agriculture*, Springer, 2010.

[11] J. Yanai, C. Keun Lee, T. Kaho et al., "Geostatistical analysis of soil chemical properties and rice yield in a paddy field and application to the analysis of yield-determining factors," *Soil Science and Plant Nutrition*, vol. 47, no. 2, pp. 291–301, 2001.

[12] L. A. Morales, E. V. Vázquez, and J. Paz-Ferreiro, "Spatial and temporal variability of Mehlich-1 extractable Fe, Mn and Zn over a rice field as a function of lime amendment," *Stochastic Environmental Research and Risk Assessment*, vol. 25, no. 8, pp. 1039–1048, 2011.

[13] L. A. Morales, E. V. Vázquez, and J. Paz-Ferreiro, "Influence of liming on the spatial and temporal variability of Mehlich-1 extractable Fe in a rice field," *Journal of Geochemical Exploration*, vol. 109, no. 1–3, pp. 78–85, 2011.

[14] X. Liu, J. Xu, M. Zhang, B. Si, and K. Zhao, "Spatial variability of soil available Zn and Cu in paddy rice fields of China," *Environmental Geology*, vol. 55, no. 7, pp. 1569–1576, 2008.

[15] L. Wang, J.-P. Wu, Y.-X. Liu, H.-Q. Huang, and Q.-F. Fang, "Spatial variability of micronutrients in rice grain and paddy soil," *Pedosphere*, vol. 19, no. 6, pp. 748–755, 2009.

[16] Y. Zhao, X. Xu, J. L. Darilek, B. Huang, W. Sun, and X. Shi, "Spatial variability assessment of soil nutrients in an intense agricultural area, a case study of Rugao County in Yangtze River Delta Region, China," *Environmental Geology*, vol. 57, no. 5, pp. 1089–1102, 2009.

[17] L. A. Morales, J. Paz-Ferreiro, S. R. Vieira, and E. V. Vázquez, "Spatial and temporal variability of EH and PH over a rice field as related to lime addition," *Bragantia*, vol. 69, pp. 67–76, 2010.

[18] N. Moritsuka, J. Yanai, M. Umeda, and T. Kosaki, "Spatial relationships among different forms of soil nutrients in a paddy field," *Soil Science and Plant Nutrition*, vol. 50, no. 4, pp. 565–573, 2004.

[19] B. Lennartz, R. Horn, R. Duttmann et al., "Ecological safe management of terraced rice paddy landscapes," *Soil & Tillage Research*, vol. 102, no. 2, pp. 179–192, 2009.

[20] M. B. Simmonds, R. E. Plant, J. M. Peña-Barragán, C. van Kessel, J. Hill, and B. A. Linquist, "Underlying causes of yield spatial variability and potential for precision management in rice systems," *Precision Agriculture*, vol. 14, no. 5, pp. 512–540, 2013.

[21] F. N. Ponnamperuma, "The chemistry of submerged soils," *Advances in Agronomy*, vol. 24, pp. 29–96, 1972.

[22] W. H. Patrick Jr. and A. Jugsujinda, "Sequential reduction and oxidation of inorganic nitrogen, manganese, and iron in flooded soil," *Soil Science Society of America Journal*, vol. 56, no. 4, pp. 1071–1073, 1992.

[23] N. K. Fageria and V. C. Baligar, "Growth and nutrient concentrations of common bean, lowland rice, corn, soybean, and wheat at different soil pH on an Inceptisol," *Journal of Plant Nutrition*, vol. 22, no. 9, pp. 1495–1507, 1999.

[24] B. Linquist and M. Ruark, "Re-evaluating diagnostic phosphorus tests for rice systems based on soil phosphorus fractions and field level budgets," *Agronomy Journal*, vol. 103, no. 2, pp. 501–508, 2011.

[25] A. Raheb and A. Heidari, "Effects of clay mineralogy and physico-chemical properties on potassium availability under soil aquic conditions," *Journal of Soil Science and Plant Nutrition*, vol. 12, no. 4, pp. 747–761, 2012.

[26] C. Witt and S. M. Haefele, "Paddy soils," in *Encyclopedia of Soils in the Environment*, D. Hilel, Ed., vol. 3, pp. 141–150, Academic Press, Columbia University, New York, NY, USA, 2005.

[27] R. Caridad-Cancela, E. V. Vázquez, S. R. Vieira, C. A. Abreu, and A. P. González, "Assessing the spatial uncertainty of mapping trace elements in cultivated fields," *Communications in Soil Science and Plant Analysis*, vol. 36, no. 1–3, pp. 253–274, 2005.

[28] S. R. Vieira and A. P. Gonzalez, "Analysis of the spatial variability of crop yield and soil properties in small agricultural plots," *Bragantia*, vol. 62, no. 1, pp. 127–138, 2003.

[29] Soil Survey Staff, *Key to Soil Taxonomy*, Natural Resources Conservation Service, Washington, DC, USA, 11th edition, 2010.

[30] D. R. Keeney and D. W. Nelson, "Nitrogen—inorganic forms," in *Methods of Soil Analysis, Part 2*, A. L. Page, Ed., Agronomy Monograph no. 9, pp. 643–698, ASA and SSSA, Madison, Wis, USA, 2nd edition, 1982.

[31] S. R. Olsen and L. E. Sommers, "Phosphorus," in *Methods of Soil Analysis*, A. L. Page, R. H. Miller, and D. R. Keeney, Eds., Agronomy Monograph, pp. 403–430, ASA and ASSA, Madison, Wis, USA, 2nd edition, 1982.

[32] A. Mehlich, *Determination of P, Ca , Mg, K, Na and* NH_4, North Carolina Soil Test Division, Raleigh, NC, USA, 1953.

[33] S. R. Vieira, "Geoestatistics in soil spatial variability studies," in *Topics in Soil Science*, R. F. Novais, V. H. Álvarez, and G. R. Schaefer, Eds., pp. 1–54, Brazilian Society of Soil Science, Viçosa, Brazil, 2000, (Portuguese).

[34] S. R. Vieira, J. R. P. de Carvalho, and A. P. González, "Jack knifing for semivariogram validation," *Bragantia*, vol. 69, pp. 97–105, 2010.

[35] J. Paz-Ferreiro, D. Baez-Bernal, J. Castro-Insúa, and M. I. García-Pomar, "Temporal variability of soil biological properties in temperate grasslands and croplands amended with organic and inorganic fertilizers," *Communications in Soil Science and Plant Analysis*, vol. 44, no. 1–4, pp. 19–27, 2013.

[36] J. Paz-Ferreiro and S. Fu, "Biological indices for soil quality evaluation: perspectives and limitations," *Land Degradation & Development*, 2013.

[37] K. Shoji, T. Kawamura, H. Horio, K. Nakayama, and N. Kobayashi, "Variability of micro-elevation, yield, and protein content within a transplanted paddy field," *Precision Agriculture*, vol. 6, no. 1, pp. 73–86, 2005.

Hindawi Publishing Corporation
The Scientific World Journal
Volume 2014, Article ID 416074, 8 pages
http://dx.doi.org/10.1155/2014/416074

Research Article

Factors Controlling Carbon Metabolism and Humification in Different Soil Agroecosystems

S. Doni, C. Macci, E. Peruzzi, B. Ceccanti, and G. Masciandaro

Institute of Ecosystem Studies, National Research Council (CNR), Via Moruzzi 1, 56124 Pisa, Italy

Correspondence should be addressed to S. Doni; serena.doni@ise.cnr.it

Received 5 June 2014; Revised 3 October 2014; Accepted 6 November 2014; Published 31 December 2014

Academic Editor: Eduardo Medina-Roldán

The aim of this study was to describe the processes that control humic carbon sequestration in soil. Three experimental sites differing in terms of management system and climate were selected: (i) Abanilla-Spain, soil treated with municipal solid wastes in Mediterranean semiarid climate; (ii) Puch-Germany, soil under intensive tillage and conventional agriculture in continental climate; and (iii) Alberese-Italy, soil under organic and conventional agriculture in Mediterranean subarid climate. The chemical-structural and biochemical soil properties at the initial sampling time and one year later were evaluated. The soils under organic (Alberese, soil cultivated with *Triticum durum* Desf.) and nonintensive management practices (Puch, soil cultivated with *Triticum aestivum* L. and *Avena sativa* L.) showed higher enzymatically active humic carbon, total organic carbon, humification index (B/E_3s), and metabolic potential (dehydrogenase activity/water soluble carbon) if compared with conventional agriculture and plough-based tillage, respectively. In Abanilla, the application of municipal solid wastes stimulated the specific β-glucosidase activity (extracellular β-glucosidase activity/extractable humic carbon) and promoted the increase of humic substances with respect to untreated soil. The evolution of the chemical and biochemical status of the soils along a climatic gradient suggested that the adoption of certain management practices could be very promising in increasing SOC sequestration potential.

1. Introduction

Soil systems are exposed to a variety of environmental stresses, of a natural and anthropogenic origin, which can potentially affect soil functioning. For this reason, there is growing recognition for the need to develop sensitive indicators of soil quality that reflect the effects of land management on soil and assist land managers in promoting long-term sustainability of terrestrial ecosystems [1, 2]. Soil organic matter, (SOM) providing energy, substrates, and biological diversity necessary to sustain numerous soil functions, has been considered one of the most important soil properties that contributes to soil quality and fertility [3, 4].

The SOM consists of chemical components differing in biological degradability: (i) rapid and medium turnover fractions and (ii) more recalcitrant forms that turn over slowly. The former provide immediate and short-term sources of carbon substrate for the soil biota and contribute more to nutrient cycling. The latter, on the other hand, represent long-term reservoirs of energy that serve to sustain the system in the longer term and they improve soil structure.

In order to understand the temporal dynamics of SOM in managed systems, it is therefore vital to characterize soil organic carbon quantity and quality.

In particular, by providing nutrients and physical protection for enzymes and microorganisms, soil humic carbon content has widely been recognized as an important fraction of SOM that can be used to study soil quality in ecosystems influenced by agricultural practices or adverse climate conditions. Humic substances are able to bind extracellular enzymes (humic-enzyme complexes) and preserve them from proteolysis and chemical degradation. As suggested by other studies [5, 6], the relationship between enzyme activity and humic carbon content might reflect the potential for enzyme immobilisation in soil and, therefore, the potential for soil resilience. β-glucosidase activity may be a particularly useful enzyme for soil quality monitoring because of its central role in SOM cycling. In particular, this enzyme,

catalysing the hydrolysis of cellulose to glucose, provides an indication of the potential for soil organic matter decomposition.

Humic-β-glucosidase activity has been considered an important indicator of changes in soil quality resulting from environmental stress in agricultural systems [6, 7].

Agricultural management systems affect organic carbon turnover and can modify the structural composition of SOM [8].

Characterization of SOM quality in soil can be obtained by using various analytical methodologies, such as infrared, ultraviolet-visible, nuclear magnetic resonance spectroscopy, oxidative reductive polymeric degradation, and gel column filtration. Several researchers have used pyrolysis-gas chromatography (Py-GC) as a reproducible and relatively rapid technique for studying qualitative changes in the structure of SOM under different agronomic uses [9, 10]. Different peaks corresponding to the major volatile pyrolytic fragments can be used to interpret the structural evolution of SOM in terms of sources, decomposition, and stability.

Based on chemical composition, the following group of compounds can be identified: (i) aliphatics, fatty acids and sterols, (ii) carbohydrates, (iii) lignin, (iv) aromatic compounds and polycyclic aromatic hydrocarbons (PAHs), and (v) N-containing compounds.

On the other hand, other soil easily measurable descriptors can be used to study the processes related to the active labile carbon pool in soil. For instance, dehydrogenase activity, indicating the status of soil microbial activity, gives information on soil metabolism. This enzyme activity has been proposed as a valid indicator of soil quality under different agronomic practices and climatic conditions [11, 12].

Also total β-glucosidase activity, involved in cellulose degradation in soil, has been proposed as an early indicator of changes in organic matter status and turnover [1, 13].

Due to the complex interactions and dynamics of these soil properties, many researchers have emphasised the need to develop indices of soil quality through a combination of variables which reflect a range of soil functions, such as humification and mineralization processes, metabolism, and nutrient cycling [14].

The aim of this study was to (i) describe properties and processes that control soil organic carbon accumulation and decrease turnover rate and (ii) illustrate the importance of conservation practices and management systems that reverse the trend to degradation and facilitate carbon sequestration in soil.

These objectives may be achieved by analysing chemical, chemicophysical, and biochemical properties in order to define the most important indicators that describe organic carbon dynamics in relation to the management practices adopted in the different pedoclimatic conditions.

2. Materials and Methods

2.1. Sampling Locations

2.1.1. Abanilla Experimental Site in Murcia, Spain. The site is located in Abanilla (38°12′N, 01°02′W) in open scrubland not used for agricultural purposes. The climate is Mediterranean semiarid. The mean annual rainfall is 300 mm y^{-1} and the mean annual temperature is 18°C. The studied soil is poorly developed with an ochric epipedon as the diagnostic horizon and is classified as a Haplic Calcisol (World Reference Base classification). The Abanilla site has a sandy clay loam soil (USDA classification) and it is characterized by a TOC and TIC content of 0.5% and 9%, respectively, and a pH of 6.5.

In this site, six fields of 85 m^2 each, three treated with the organic fraction of a municipal solid waste (S-WOF treatment) and three untreated fields (S-C, control), were set up. The waste organic fraction addition was made, 16 years before soil sampling, in such a dose as to increase the SOM by 1.5%. This fraction was incorporated into the top 15 cm of the soil using a rotovator. In the S-WOF, plant cover developed spontaneously (60–70% plant coverage), while very scant vegetation grew in the control soil (20–30% plant coverage). The vegetation of the area is the typical of Mediterranean semiarid lowlands: *Pinus halepensis* Mill. and natural shrubs.

2.1.2. Alberese Experimental Site in Tuscany, Italy. The site is located in Alberese (42°40′N, 11°06′E), characterized by a Mediterranean semiarid climate. The soils were taken at two agricultural areas: an organic area (I-BA) and a conventional area (I-CA). Both areas had durum wheat (*Triticum durum* Desf.) as a monoculture. In the organic area, three fields were fertilized with 100 kg ha^{-1} y^{-1} of commercial green manure, while, in the conventional area, three fields were fertilized with ammonium nitrate at a total rate of 200 kg ha^{-1} y^{-1}. Organic and conventional management systems were carried out for five years. Each plot was 200 m^2.

The Alberese site has a sandy clay loam soil (USDA classification) and it is characterized by a TOC and TIC content of 0.15% and 2.1%, respectively and a pH of 7.8. The soil is an Chromic Cambisol (World Reference Base classification). The main vegetation of the area is *Quercus ilex* L. and natural shrubs. The annual precipitation is 600 mm y^{-1} and the mean temperature is 15°C.

2.1.3. Puch Experimental Site in Bavaria, Germany. The fields in Puch are located about 40 km north-west of Munich (48°10′N, 11°13′E). In this site, plant cover has been intentionally modified during the last 50 years in a long term experiment. Three plots under intensive tillage (P-IT) have been kept without plants since 1953 by ploughing twice a year and by repeated grubbing; these soils are not fertilized and are ploughed whenever vegetation appears. As a result, there is no input from plants and the SOM is constantly exposed to aeration. Three plots under conventional agriculture (P-CA) were cultivated with wheat (*Triticum aestivum* L.) and oats (*Avena sativa* L.); these soils received regular tillage, which allows some plant cover to establish itself. Three unmanaged soils were used as control soil (P-C); the control soil was abandoned and covered by low density of spontaneous vegetation. Each treated plot and each untreated (control) plot are about 200 m^2 (total area per treatment 600 m^2) with a sandy loam texture (USDA classification) and it is characterized by a TOC and TIC content of 1.1% and 0.03%, respectively, and a pH of 6.6. The soil is an Haplic Luvisol (World Reference Base classification), the vegetation of the area is the typical

of Continental climate with a predominance of *Picea abies* (L.) H.Karst. and *Abies alba*. Mill. The annual precipitation is 900 mm y^{-1} and the mean temperature is 8°C.

The monitoring of each soil ecosystem consisted in samplings carried out once a year. In this paper, the results of the initial sampling (T1) and one year later (T2) are reported. The T1 and T2 sampling were done at the same time for the different experimental sites, even if the treatments started in different periods for the different sites.

Each soil sample was a composite of nine bulk soil subsamples randomly collected from the top layer (15 cm; 150 cm^3 soil cores) of an homogenous area. Three composite soil samples per each replicate treatment were taken, air-dried, sieved (<2 mm), and stored at room temperature prior determining chemical, physical, and biochemical properties.

2.2. Methods

2.2.1. Chemical, Biological, and Physical Analysis. Total organic carbon (TOC) and the total inorganic carbon (TIC) contents were measured with a LECO, U.S.A. RC-412 Multiphase Carbon/Hydrogen/Moisture Determinator. Total Nitrogen (TN) content was determined by a LECO, U.S.A. FP-528 Protein/Nitrogen Determinator. Water Soluble Carbon (WSC) was extracted using the method reported by [15]. Sodium pyrophosphate (0.1 M, pH 7.1) at 37°C for 24 h under shaking at 200 oscillation min^{-1} was used to extract Total Humic Carbon (THC) [8]. The extract was filtered on a 0.22 μm Millipore membrane and passed through an ultrafiltration AMICON PM10 cut-off membrane to obtain the enzymatically active fraction >10^4 Da (active humic carbon, AHC). The C content of WSC, THC, and AHC was determined by dichromate oxidation [16].

Total (TG) and extracellular (EG) β-glucosidase activities were determined on whole soil [17] and soil pyrophosphate extract fraction >10^4 Da [8], respectively, using 0.05 M disodium (4-nitrophenyl) phosphate hexahydrate (PNG) as substrate. The 4-nitrophenol (PNP) produced by hydrolysis was extracted and determined spectrophotometrically at 398 nm [18]. Dehydrogenase activity was determined by the method of Masciandaro et al. [19], using 3-(4-iodophenyl)-2-(4-nitrophenyl)-5-phenyl-2*H*-tetrazol-3-ium chloride (INT) as electron acceptor and detecting spectrophotometrically the 1-(4-iodophenyl)-5-(4-nitrophenyl)-3-phenylformazan at 490 nm. Total porosity was determined by the method by Lowell and Shields [20].

2.2.2. Chemicostructural Analyses (Pyrolysis-Gas Chromatography). The Py-GC is based on a rapid decomposition of organic matter under a controlled high flash of temperature, in an inert atmosphere of gaseous N_2 carrier. A gas chromatograph is used for the separation and quantification of pyrolytic fragments. Fifty micrograms of an air-dried and ground (<100 mesh) soil sample and 300 μL of sodium pyrophosphate (0.1 M, pH 7.1) extract were introduced into pyrolysis quartz microtubes in a CDS Pyroprobe 190. The analysis of sodium pyrophosphate extracts gives more reliable information on native SOM.

Pyrolysis was carried out at 800°C for 10 s, with a heating rate of 10°C ms^{-1} (nominal conditions). The probe was coupled directly to a Carlo Erba 6000 gas chromatograph with a flame ionization detector (FID). Chromatographic conditions were as follows: a 3 m × 6 mm, 80–100 mesh, SA 1422 (Supelco Inc.) poropak Q packed column; the temperature program was 60°C, increasing to 240°C by 8°C min^{-1}. Pyrograms were interpreted by quantification of seven peaks corresponding to the major volatile pyrolytic fragments [21]: acetonitrile (E_1), acetic acid (K), benzene (B), pyrrole (O), toluene (E_3), furfural (N), and phenol (Y). Acetonitrile (E_1) is derived from the pyrolysis of aminoacids, proteins, and microbial cells. Furfural (N) is principally derived from cellulose and other aliphatic organic compounds. Acetic acid (K) is preferentially derived from pyrolysis of lipids, fats, waxes, cellulose and other carbohydrates. Phenol (Y) is derived from fresh or condensed (humic) lignocellulosic structures. Benzene (B) and toluene (E_3) are basically derived from condensed aromatic structures of stable (humified) organic matter, particularly for benzene, since toluene must come from rings with aliphatic chains, albeit short. Pyrrole (O) is derived from nitrogenated compounds, such as nucleic acids, proteins, and microbial cells [22]. Peak areas were normalized, so that the area under each peak referred to the percentage of the total of the selected seven peaks (relative abundances). The alphabetic code used was conventional and has already been employed in previous papers [21, 23]. Peak purity of the selected major volatile fragments was checked by coupling the same chromatographic system to a mass detector HP 8000A in the same operative conditions confirming the reliability of the working conditions.

Some ratios between relative abundances of some of the peaks were determined [21]: (i) N/O: mineralization index. This index expresses the ratio between furfural, which is the pyrolytic product arising from polysaccharides, and pyrrole, which derives from nitrogenous compounds, humified organic matter, and microbial cells. The higher the ratio, the lower the mineralization of organic matter.

(ii) B/E_3: humification index. The higher the ratio, the higher the humification of organic matter, because benzene is derived mostly from pyrolytic degradation of condensed aromatic structures, while toluene comes from aromatic uncondensed rings with aliphatic chains [21].

2.3. Statistical Analyses. The Statistica 7.0 software (StatSoft Inc., Tulsa, Oklahoma, USA) was used for the statistical analysis. All results are the means of three field replicates. Differences among treatments within each site were tested by analysis of variance (one way ANOVA). The means were compared by using least significant differences calculated at $P < 0.05$ (Fisher's test). In addition, the results were studied using principal component analysis (PCA), a multivariate statistical data analysis technique, which reduces a set of raw data to a number of principal components that retain most of the variance within the original variables, in order to identify possible patterns or clusters between objects and variables [24]. All raw data used in the PCA analysis were subjected to pretreatment in order to remove or reduce irrelevant sources of variation or "noise" which may interfere in the

Table 1: Chemical and physical properties at T1 and T2 sampling times. For each site, different letters indicate statistically different values among the treatments ($P < 0.05$).

		TOC g kg^{-1}	THC g kg^{-1}	AHC g kg^{-1}	TN g kg^{-1}	WSC g kg^{-1}	Porosity mm^3 g^{-1}
				T1			
Abanilla-Spain	S-C	5.1^b	0.81^b	0.58^b	0.72^b	82^a	192^b
	S-WOF	27.6^a	2.82^a	1.96^a	3.28^a	225^b	203^a
Alberese-Italy	I-CA	12.6^b	1.35^b	0.89^b	1.14^b	63^b	131^b
	I-BA	18.7^a	1.93^a	1.35^a	1.38^a	70^a	147^a
Puch-Germany	P-CA	20.0^a	3.09^a	1.59^a	1.79^a	128^a	204^a
	P-IT	10.3^b	2.05^c	1.13^c	0.80^c	98^b	161^b
	P-C	11.5^b	2.45^b	1.34^b	0.98^b	96^b	160^b
				T2			
Abanilla-Spain	S-C	5.9^b	0.91^b	0.52^b	0.75^b	76^b	198^b
	S-WOF	24.0^a	2.63^a	1.49^a	2.52^a	154^a	217^a
Alberese-Italy	I-CA	13.1^b	1.38^a	0.69^b	0.81^b	46^b	142^b
	I-BA	18.2^a	1.41^a	0.95^a	1.64^a	53^a	154^a
Puch-Germany	P-CA	17.3^a	2.56^a	1.58^a	1.53^a	75^a	210^a
	P-IT	8.0^c	2.19^c	1.08^c	0.57^c	65^b	174^b
	P-C	11.4^b	2.40^b	1.51^a	1.18^b	58^c	167^b

TOC, total organic carbon; THC, total humic carbon; AHC, active humic carbon; TN, total nitrogen; WSC, water soluble carbon.
C, control; WOF, waste organic fraction added; CA, conventional agriculture; BA, organic agriculture; IT, intensive tillage. T1, initial sampling time; T2, one year later.

analysis. Firstly, the raw data were log transformed to reduce data heterogeneity; following this, the transformed data were standardized.

Finally, a correlation matrix of the data was also calculated in order to determine the relationship between the indicators. The significant levels reported ($P < 0.05$) are based on the Student's distribution.

3. Results and Discussion

The chemical, physical (Table 1), and biochemical (Table 2) variables showed very similar values at T1 and T2, which are the times corresponding to the two sampling periods, indicating the stability of soil characteristics in a short period of time.

Total organic carbon (TOC) was closely related to soil type and management systems. There were, in fact, significant differences ($P < 0.05$) in TOC content among the treatments in the three geographic areas (Table 1). The lowest TOC was found in the Abanilla unmanaged soil (control), being located in a predesertic dry area (Southern-Eastern Spain). This soil can be defined as a biologically "poor soil" [25, 26] having a low content of organic matter and microbial activity (Tables 1 and 2). The effect of waste organic fraction application on organic carbon content in the Abanilla soil was still clear 16 years later. Beneficial effects of applying organic materials on SOM are well known from several long-term experiments [27–29]. In particular, a higher content of water soluble carbon (S-WSC) was observed where organic amendment was added (S-WOF treatment), in contrast to the control soil (Table 1). In the S-WOF treated soil, plant cover developed spontaneously, while very scant vegetation grew in the control soil. The maintenance of a vegetation cover in the S-WOF soil probably had a positive influence on the input of WSC through root exudates and plant remains [30]. This labile organic carbon fraction, which is considered easily degradable by soil microorganisms [31], determined, as expected, the activation of the resident microbial populations. Beneficial effects of plants on microbial stimulation through organic exudates at the root-soil interface have been widely reported [32]. Soil dehydrogenase and total β-glucosidase activities were, in fact, significantly greater ($P < 0.05$) in the managed than in the control soil (Table 2). As usually reported, a positive correlation between dehydrogenase activity and WSC ($P < 0.05$, $r = 0.75$) [30, 33, 34] and β-glucosidase activity and WSC ($P < 0.05$, $r = 0.92$) [35] was observed.

The dehydrogenase activity, especially when referred to the energetic and immediately available C substrate, gives an idea of the metabolic potentiality of soil rehabilitation. This metabolic potential, calculated as the ratio between the activity of the viable microbial community (dehydrogenase activity) and the sources of energy for microorganisms (water soluble carbon concentration), was higher in the S-WOF with respect to the control soil.

Moreover, the higher total humic carbon (THC) and enzymatically-active humic carbon (AHC) observed in the S-WOF with respect to the control soil indicated the positive impact of organic matter addition on the maintenance of the stable carbon pool. The higher AHC also suggested the higher capacity of this stable humic fraction >10^4 molecular weight to preserve the extracellular enzymes in an active form, as confirmed by the significantly ($P < 0.01$) higher specific extracellular β-glucosidase activity, calculated as the ratio between extracellular β-glucosidase activity and associated AHC; this specific activity allows evaluating the accumulation of

Table 2: Biochemical properties at T1 and T2 sampling times. For each site, different letters indicate statistically different values among the treatments ($P < 0.05$).

		EG mg PNP kg^{-1} h^{-1}	TG mg PNP kg^{-1} h^{-1}	DH-ase mg INTF kg^{-1} h^{-1}
		T1		
Abanilla-Spain	S-C	3.3^{b}	117^{a}	1.08^{b}
	S-WOF	44.1^{a}	405^{b}	3.21^{a}
Alberese-Italy	I-CA	6.7^{a}	511^{b}	2.10^{b}
	I-BA	6.6^{a}	883^{a}	2.52^{a}
Puch-Germany	P-CA	16.1^{b}	95^{b}	4.67^{a}
	P-IT	4.4^{c}	82^{c}	1.38^{c}
	P-C	44.7^{a}	182^{a}	2.26^{b}
		T2		
Abanilla-Spain	S-C	3.6^{b}	75^{b}	1.78^{b}
	S-WOF	31.3^{a}	438^{a}	5.06^{a}
Alberese-Italy	I-CA	6.3^{a}	639^{b}	2.98^{b}
	I-BA	6.4^{a}	823^{a}	3.58^{a}
Puch-Germany	P-CA	15.8^{b}	145^{b}	4.31^{a}
	P-IT	4.3^{c}	50^{c}	1.22^{c}
	P-C	40.4^{a}	190^{a}	2.86^{b}

EG, extracellular β-glucosidase activity; TG, total β-glucosidase activity; DH-ase, dehydrogenase activity.
C, control; WOF, waste organic fraction addition; CA, conventional agriculture; BA, organic agriculture; IT, intensive tillage. T1, initial sampling time; T2, one year later.

enzymatically active humic pool. The preservation of the humic-enzyme complexes represents an important condition for soil resilience and their presence has been defined as a necessary condition to make the soil able to counteract the irreversible degradation (soil desertification) [36].

Significant differences in chemical and biochemical indicators related to the carbon cycle were also observed between organic (I-BA) and conventional (I-CA) agricultural soils in the Alberese site. The organic management stimulated soil metabolic potential, expressed by the ratio between the dehydrogenase activity and water soluble carbon [1, 37] (Table 2), and increased total organic carbon (TOC) and nitrogen contents (TN) and available forms of carbon (WSC, THC, AHC) (Table 1). However, the specific β-glucosidase, both total (expressed by the ratio between the total β-glucosidase activity and TOC) and extracellular (expressed by the ratio between the extracellular β-glucosidase activity and AHC), showed no significant difference ($P > 0.05$) between the organic and conventionally managed soils (Table 2). In general, the presence of abundant cereal crops causes less soil disturbance and stimulates microbial activity more than uncropped or intermittently cropped soil [38].

The Puch soils showed a decrease in the amount of TOC in the intensively tilled soil (P-IT), with respect to the control (P-C) and conventionally cropped (P-CA) soils. In particular, P-IT showed a lower content of active humic carbon fraction (AHC) and specific extracellular β-glucosidase activity (EG/AHC) (Table 2). Also the P-CA soil, although it presented higher values of chemical indicators, showed a reduced specific extracellular β-glucosidase activity (EG/AHC) with respect to the P-C. As already observed [38], these results indicated that the conversion of plough tillage (P-IT) to a no-till agricultural farming system (P-CA), involving a frequent use of cover crops in the rotation cycle along with adoption of integrated nutrient management, is a practice able to restore and maintain a substantial organic carbon pool in soils.

The carbon turnover may be assessed also through the chemicostructural composition of SOM as determined by the pyrolytic technique. The ratio between benzene (B) and toluene (E_3) pyrolytic fragments, which has been considered as a "humification index," and the ratio between furfural (N) and pyrrole (O), which has been interpreted as a "mineralization index" [8, 34], showed the same trend in the whole soil and soil extract (Table 3).

In the Abanilla site, B/E_3 resulted higher in the organically treated soil (S-WOF) than in the control soil (S-C), suggesting the activation of humification by organic amendment; root exudates, as previously described for WSC, seem to be responsible for the low value of the N/O index found in the whole soil of the S-WOF treatment (Table 3).

Also in the Alberese site, the increase of B/E_3 in the organic with respect to the conventional agriculture system confirmed the prevalence of the humification process over mineralization. According to the humification index, the furfural/pyrrole (N/O) ratio showed higher values in the I-BA-treated soil, thus indicating the presence of more evolved

Table 3: Pyrolytic indices of mineralization (N/O) and humification (B/E_3). For each site, different letters indicate statistically different values among the treatments ($P < 0.05$).

		Whole soil		AHC extract	
		N/O	B/E_3	N/O	B/E_3
Abanilla-Spain	S-C	1.49[a]	0.547[b]	1.21[a]	0.581[b]
	S-WOF	1.23[b]	0.827[a]	1.16[a]	0.732[a]
Alberese-Italy	I-CA	0.85[b]	0.645[b]	0.93[b]	0.796[b]
	I-BA	0.96[a]	0.738[a]	1.13[a]	0.977[a]
Puch-Germany	P-CA	1.39[a]	0.930[a]	1.28[a]	0973[a]
	P-IT	1.04[c]	0.768[b]	1.13[b]	0.910[b]
	P-C	1.25[b]	0.765[b]	1.31[a]	0.911[b]

N/O, furfural/pyrrole; B/E_3, benzene/toluene; AHC, active humic carbon. C, control; WOF, waste organic fraction addition; CA, conventional agriculture; BA, organic agriculture; IT, intensive tillage. Data reported as mean values of T1 (initial sampling time) and T2 (one year later), coefficient of variation of the two sampling times ranging from 2 to 10%.

Table 4: Principal components (PC) and component loadings related to physical, chemical, and biochemical properties determined in the different soils.

	PC1	PC2	PC3
TOC	**0.745***	0.518	0.355
THC	**0.892***	−0.175	0.184
AHC	**0.892***	0.007	0.281
TN	0.585	0.496	0.611
EG	**0.762***	−0.005	0.402
TG	0.196	**0.910***	−0.111
WSC	0.288	−0.091	**0.877***
DH-ase	**0.722***	0.419	0.261
B/E_3s	**0.879***	0.164	−0.169
N/Os	0.101	**−0.710***	0.233
porosity	0.057	−0.331	**0.822***
Var. Sp.	4.498	2.196	2.382
Prp. Tot.	0.409	0.200	0.217

TOC: total organic carbon; THC: total humic carbon; AHC: active humic carbon; TN: total nitrogen; EG: extracellular β-glucosidase activity; TG: β-glucosidase activity; WSC: water soluble carbon; DH-ase: dehydrogenase activity; B/E_3s: benzene/toluene whole soil; N/Os: furfural/pyrrole whole soil. Var. Sp.: explained variance; Prp. Tot.: total proportionality.
*Variables with component loadings used to interpret the PCs; threshold level: 0.7.

(less mineralizable) humic matter in both the whole soil and soil extract (Table 3).

In the Puch soils, significative differences were found ($P < 0.05$) in the humification index (B/E_3) between the intensively tilled soil (P-IT), the control soil (P-C), and the conventional agriculture (P-CA). P-IT treatment, showing the lower values ($P < 0.05$), seems to be exposed to mineralization.

By considering the three management systems which were expected to negatively affect soil properties, that is, Abanilla control soil S-C, Alberese conventional agriculture I-CA, and Puch control soils P-C or P-IT, one can, on the basis of all the indicators measured, rank the soils in a decreasing order of degradation: Abanilla ≫ Alberese > Puch. In addition, being the climate one of the most important factors affecting SOM turnover, the soil degradation reflected the geographical distribution of the three selected sites, from driest to more humid places.

Therefore, Abanilla could be expected to show a slower metabolism than the other soils, which may be reflected in a different carbon turnover, and this was actually found. The management with ameliorating practices, instead, undoubtedly slows down, arrests, or even reverses soil degradation. In order to explain more clearly the factors (TOC, THC, AHC, TN, total and extracellular β-glucosidase, dehydrogenase, WSC, porosity, B/E_3, and N/O) controlling carbon metabolism and humification process in the three ecosystems, principal component analysis (PCA) was performed.

Soil properties can be summarized in three independent PCs, which explained 83% of the total variance (Table 4). The first PC (PC1, 41% of the total variance) included TOC, AHC, THC, EG, Dh-ase, and B/E_3. The statistically significant positive relation between AHC, THC, and TOC (indicators denoting significance on the same PC with the same sign) indicated the great influence of TOC on humic carbon evolution. In addition, the positive loading between these indicators and DH-ase suggests the presence of an active metabolism sustained by the readily decomposable SOM that promotes the synthesis of persistent *site-specific* humic substances (as part of humus-soil own organic matter). The evolution of the stable organic C fraction (AHC) is relevant since it determines the capability resistance and/or resilience of soils to degradation processes, particularly in extreme environments [36]. It is generally known that humic substances such as AHC, which are capable of binding active enzymes, may express both a biochemico-functional role, stabilizing extracellular enzymes also in extreme environmental conditions [31], and a chemicostructural role, their importance being related to mineral particle stabilization and the fact that they constitute a slow release nutrient source in soil ecosystems [39]. In view of this, a relationship between AHC and the functional-structural indicators (B/E_3, total organic carbon and extracellular enzyme activity) could be expected. However, the statistically significant negative relation between TG and N/Os on the second PC suggested that the mineralization process is increased by the microbial activation of carbon cycle.

Although cause-effect relations are difficult to establish given the collinearity of variables, the positive loading of WSC and porosity on the third PC suggested a relationship between decomposable organic matter inputs and soil porosity improvement.

Figure 1 provides the biplot of the PCA analysis obtained using the first two PCs. This plot gives a graphical representation of clusters of soils with similar physical-chemical and biochemical properties. The biplot indicated that organic management positively affected the soil organic carbon evolution; in fact, I-BA and S-WOF were shifted in relation to the I-CA and S-C, respectively, along positive values of PC1, which was positively associated with the indicators indicative of humification processes. These organically managed soils were also shifted along positive values of PC2, confirming

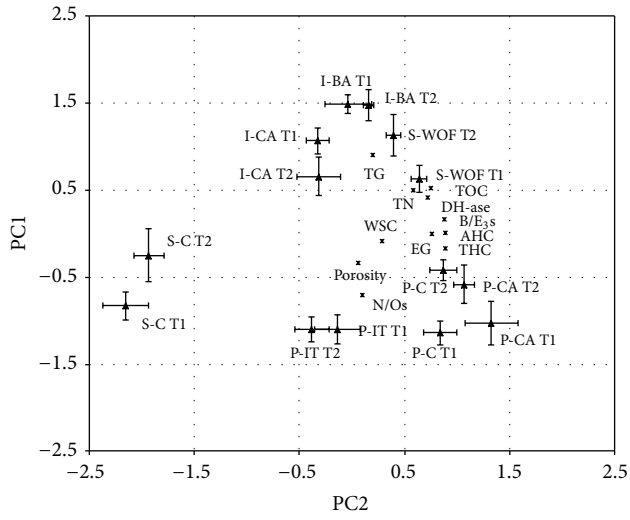

Figure 1: Biplot of factor scores and loadings at each sampling time (T1 and T2), in each treatment. TOC: total organic carbon; THC: total extractable carbon; AHC: extractable carbon fraction >10.000 Da; TN: total nitrogen; EG: extracellular β-glucosidase activity; TG: β-glucosidase activity; WSC: water soluble carbon; DH-ase: dehydrogenase activity; B/E_3s: benzene/toluene whole soil; and N/Os: furfural/pyrrole whole soil.

their higher ability in protecting humic carbon from mineralization.

Similarly, the different Puch treatments were spread on the PC1. In particular, the P-IT treatment was shifted with respect to P-C and P-CA along negative values indicating the establishment of mineralization processes.

4. Conclusions

The adoption of organic (Alberese site, I-BA) and/or nonintensive management (Puch site, P-CA) practices in comparison with conventional agriculture (Alberese site, I-CA) or plough-based tillage methods (Puch site, P-IT) provoked a considerable stimulation of metabolic potential (dehydrogenase activity/water soluble carbon) and an increase of humic carbon and humic-associated enzymes.

In Abanilla site, the application of municipal solid wastes (S-WOF) stimulated the specific β-glucosidase activity (extracellular β-glucosidase activity/extractable humic carbon) with respect to untreated soil and promoted the stabilization of SOM, as showed by the increase of humic substances.

The PCA analysis was able to assess the evolution of the carbon cycle and the shift of metabolic processes towards humification or mineralization pathways in the different soil ecosystems.

The AHC showed a positive dependence on TOC and microbial activity, indicating an active metabolism sustained by the decomposable SOM, which promoted the synthesis of persistent *site-specific* humic substances. On the other hand, the negative relation between N/O index and TG indicated that the microbial activation of the carbon cycle regulates the decomposition of SOM. These results, marking the biochemical evolution and chemical status of the soils, are particularly important because they suggest that the adoption of certain management practices under different climate could have a great impact in maximizing SOC sequestration.

Conflict of Interests

The authors declare that there is no conflict of interests regarding the publication of this paper.

Acknowledgment

The study was carried out within the framework of the EU project "Indicators and thresholds for desertification, soil quality, and remediation" INDEX (STREP Contract no. 505450 2004/2006).

References

[1] A. K. Bandick and R. P. Dick, "Field management effects on soil enzyme activities," *Soil Biology and Biochemistry*, vol. 31, no. 11, pp. 1471–1479, 1999.

[2] R. E. Masto, P. K. Chhonkar, D. Singh, and A. K. Patra, "Alternative soil quality indices for evaluating the effect of intensive cropping, fertilisation and manuring for 31 years in the semi-arid soils of India," *Environmental Monitoring and Assessment*, vol. 136, no. 1–3, pp. 419–435, 2008.

[3] J. W. Doran and T. B. Parking, "Defining and assessing soil quality," in *Defining Soil Quality for a Sustainable Environment*, J. W. Doran, D. C. Coleman, D. F. Bezdicek, and B. A. Stewart, Eds., pp. 3–21, Soil Science Society of America and American Society of Agronomy, Madison, Wis, USA, 1994.

[4] R. Lal, "Challenges and opportunities in soil organic matter research," *European Journal of Soil Science*, vol. 60, no. 2, pp. 158–169, 2009.

[5] M. D. Busto and M. Perez-Mateos, "Characterization of β-D-glucosidase extracted from soil fractions," *European Journal of Soil Science*, vol. 51, no. 2, pp. 193–200, 2000.

[6] B. Ceccanti, S. Doni, C. Macci, G. Cercignani, and G. Masciandaro, "Characterization of stable humic-enzyme complexes of different soil ecosystems through analytical isoelectric focussing technique (IEF)," *Soil Biology and Biochemistry*, vol. 40, no. 9, pp. 2174–2177, 2008.

[7] S. Doni, C. Macci, H. Chen, G. Masciandaro, and B. Ceccanti, "Isoelectric focusing of β-glucosidase humic-bound activity in semi-arid Mediterranean soils under management practices," *Biology and Fertility of Soils*, vol. 48, no. 2, pp. 183–190, 2012.

[8] G. Masciandaro and B. Ceccanti, "Assessing soil quality in different agro-ecosystems through biochemical and chemico-structural properties of humic substances," *Soil and Tillage Research*, vol. 51, no. 1-2, pp. 129–137, 1999.

[9] K. G. J. Nierop, M. M. Pulleman, and J. C. Y. Marinissen, "Management induced organic matter differentiation in grassland and arable soil: a study using pyrolysis techniques," *Soil Biology & Biochemistry*, vol. 33, no. 6, pp. 755–764, 2001.

[10] B. Ceccanti, G. Masciandaro, and C. Macci, "Pyrolysis-gas chromatography to evaluate the organic matter quality of a mulched soil," *Soil and Tillage Research*, vol. 97, no. 1, pp. 71–78, 2007.

[11] B. Ceccanti, B. Pezzarossa, F. J. Gallardo-Lancho, and G. Masciandaro, "Biotests as markers of soil utilization and fertility," *Geomicrobiology Journal*, vol. 11, no. 3-4, pp. 309–316, 1993.

[12] R. Doi and S. L. Ranamukhaarachchi, "Correlations between soil microbial and physicochemical variations in a rice paddy: implications for assessing soil health," *Journal of Biosciences*, vol. 34, no. 6, pp. 969–976, 2009.

[13] C. M. Monreal and D. W. Bergstrom, "Soil enzymatic factors expressing the influence of land use, tillage system and texture on soil biochemical quality," *Canadian Journal of Soil Science*, vol. 80, no. 3, pp. 419–428, 2000.

[14] D. de la Rosa, "Soil quality evaluation and monitoring based on land evaluation," *Land Degradation and Development*, vol. 16, no. 6, pp. 551–559, 2005.

[15] C. García, M. T. Hernández, and F. Costa, "Study on water extract of sewage sludge compost," *Soil Science Plant and Nutrition*, vol. 37, pp. 399–408, 1990.

[16] J. C. Yeomans and J. M. Bremner, "A rapid and precise method for routine determination of organic carbon in soil," *Communications in Soil Science and Plant Analysis*, vol. 19, no. 13, pp. 1467–1476, 1988.

[17] C. García, M. T. Hernández, F. Costa, B. Ceccanti, G. Masciandaro, and M. Calcinai, "Evaluation of the organic matter of raw and composted municipal wastes," *Soil Science and Plant Nutrition*, vol. 39, pp. 99–108, 1993.

[18] G. Masciandaro, B. Ceccanti, and C. García, "Anaerobic digestion of straw and piggery wastewaters: II. Optimization of the process," *Agrochimica*, vol. 38, no. 3, pp. 195–203, 1994.

[19] G. Masciandaro, B. Ceccanti, V. Ronchi, and C. Bauer, "Kinetic parameters of dehydrogenase in the assessment of the response of soil to vermicompost and inorganic fertilisers," *Biology and Fertility of Soils*, vol. 32, no. 6, pp. 479–483, 2000.

[20] S. Lowell and J. E. Shields, "Influence of contact angle on hysteresis in mercury porosimetry," *Journal of Colloid And Interface Science*, vol. 80, no. 1, pp. 192–196, 1981.

[21] B. Ceccanti, J. M. Alcaniz-Baldellou, M. Gispert-Negrell, and M. Gassiot-Matas, "Characterization of organic matter from two different soils by pyrolysis-gas chromatography and isoelectric focusing," *Soil Science*, vol. 142, no. 2, pp. 83–90, 1986.

[22] J. M. Bracewell and G. W. Robertson, "A pyrolysisgas chromatography method for discrimination of soil humus types," *Journal of Soil Science*, vol. 24, pp. 421–428, 1976.

[23] J. M. Alcañiz, A. Seres, and M. Gassiot-Matas, "Diferenciacion entre humus mull carbonatado y mull evolucionado por Py-GC," in *Proceedings of the National Conference Ciencia del Suelo*, pp. 217–228, Madrid, Spain, 1984.

[24] S. Carroll, A. Goonetilleke, and L. Dawes, "Framework for soil suitability evaluation for sewage effluent renovation," *Environmental Geology*, vol. 46, no. 2, pp. 195–208, 2004.

[25] G. Masciandaro, B. Ceccanti, and C. Garcia, "Soil agro-ecological management: fertirrigation and vermicompost treatments," *Bioresource Technology*, vol. 59, no. 2-3, pp. 199–206, 1997.

[26] G. Masciandaro, V. Bianchi, C. Macci, S. Doni, B. Ceccanti, and R. Iannelli, "Potential of on-site vermicomposting of sewage sludge in soil quality improvement," *Desalination and Water Treatment*, vol. 23, no. 1–3, pp. 123–128, 2010.

[27] M. Diacono and F. Montemurro, "Long-term effects of organic amendments on soil fertility. A review," *Agronomy for Sustainable Development*, vol. 30, no. 2, pp. 401–422, 2010.

[28] J. R. Brown, "The Sanborn field experiment," in *Long-Term Experiments in Agriculture and Ecological Sciences*, R. A. Leigh and A. E. Johnson, Eds., pp. 39–51, CAB International, Wallingford, UK.

[29] J. Dorado, M. C. Zancada, G. Almendros, and C. López-Fando, "Changes in soil properties and humic substances after long-term amendments with manure and crop residues in dryland farming systems," *Journal of Plant Nutrition and Soil Science*, vol. 166, no. 1, pp. 31–38, 2003.

[30] C. Garcia, A. Roldan, and T. Hernandez, "Changes in microbial activity after abandonment of cultivation in a semiarid Mediterranean environment," *Journal of Environmental Quality*, vol. 26, no. 1, pp. 285–291, 1997.

[31] B. D. Cook and D. L. Allan, "Dissolved organic carbon in old field soils: total amounts as a measure of available resources for soil mineralization," *Soil Biology and Biochemistry*, vol. 24, no. 6, pp. 585–594, 1992.

[32] C. Macci, S. Doni, E. Peruzzi, G. Masciandaro, C. Mennone, and B. Ceccanti, "Almond tree and organic fertilization for soil quality improvement in southern Italy," *Journal of Environmental Management*, vol. 95, pp. S215–S222, 2012.

[33] F. Bastida, J. L. Moreno, T. Hernández, and C. García, "The long-term effects of the management of a forest soil on its carbon content, microbial biomass and activity under a semi-arid climate," *Applied Soil Ecology*, vol. 37, no. 1-2, pp. 53–62, 2007.

[34] G. Masciandaro, B. Ceccanti, and J. F. Gallardo-Lancho, "Organic matter properties in cultivated versus set-aside arable soils," *Agriculture, Ecosystems and Environment*, vol. 67, no. 2-3, pp. 267–274, 1998.

[35] F. Bastida, G. G. Barberá, C. García, and T. Hernández, "Influence of orientation, vegetation and season on soil microbial and biochemical characteristics under semiarid conditions," *Applied Soil Ecology*, vol. 38, no. 1, pp. 62–70, 2008.

[36] B. Ceccanti and G. Masciandaro, "Stable humus-enzyme nucleus: the last barrier against soil desertification," in *Preserving Soil Quality and Soil Biodiversity—The Role of Surrogate Indicators*, M. C. Lobo and J. J. Ibanez, Eds., pp. 77–82, CSIC-IMIA, Madrid, Spain, 2003.

[37] S. Marinari, G. Masciandaro, B. Ceccanti, and S. Grego, "Influence of organic and mineral fertilisers on soil biological and physical properties," *Bioresource Technology*, vol. 72, no. 1, pp. 9–17, 2000.

[38] R. Lal and J. M. Kimble, "Conservation tillage for carbon sequestration," *Nutrient Cycling in Agroecosystems*, vol. 49, no. 1–3, pp. 243–253, 1997.

[39] B. Ceccanti and C. García, "Coupled chemical and biochemical methodologies to characterize a composting process and the humic substances," in *Humic Substances in the Global Environment and Implications on Human Health*, N. Senesi and T. M. Miano, Eds., pp. 1279–1284, 1994.

Hindawi Publishing Corporation
The Scientific World Journal
Volume 2014, Article ID 341804, 11 pages
http://dx.doi.org/10.1155/2014/341804

Research Article

The Effect of Land Use Change on Transformation of Relief and Modification of Soils in Undulating Loess Area of East Poland

Jerzy Rejman,[1] Anna Rafalska-Przysucha,[1] and Jan Rodzik[2]

[1] *Institute of Agrophysics, Polish Academy of Sciences, Str. Doświadczalna 4, 20-290 Lublin, Poland*
[2] *Faculty of Earth Sciences and Spatial Management, University of Maria Curie-Skłodowska, al. Kraśnicka 2c, 20-718 Lublin, Poland*

Correspondence should be addressed to Jerzy Rejman; rejman@ipan.lublin.pl

Received 18 July 2014; Revised 15 October 2014; Accepted 21 October 2014; Published 31 December 2014

Academic Editor: Antonio Paz González

The change of primary forest areas into arable land involves the transformation of relief and modification of soils. In this study, we hypothesized that relatively flat loess area was largely transformed after the change of land use due to erosion. The modifications in soil pedons and distribution of soil properties were studied after 185 years of arable land use. Structure of pedons and solum depth were measured in 128 and soil texture and soil organic carbon in 39 points. Results showed that soils of noneroded and eroded profiles occupied 14 and 50%, respectively, and depositional soils 36% of the area. As a consequence, the clay, silt, and SOC concentration varied greatly in the plowed layer and subsoil. The reconstructed profiles of eroded soils and depositional soils without the accumulation were used to develop the map of past relief. The average inclination of slopes decreased from 4.3 to 2.2°, and slopes >5° vanished in the present topography. Total erosion was 23.8 Mg ha^{-1} year^{-1}. From that amount, 88% was deposited within the study area, and 12% was removed outside. The study confirmed the hypothesis of the significant effect of the land use change on relief and soils in loess areas.

1. Introduction

Any change in land use or even in crop rotation affects the intensity of water or tillage erosion, the processes that provide redistribution of soil material and changes in soil properties. However, the scale of soil changes in space and time is weakly recognized. Loess areas with high soil erodibility, long lasting arable land use, and rolling landscape belong to the regions of the highest water erosion risk in Europe [1]. Mechanical tillage has increased the human pressure on soil and started to constitute an important part of total erosion. While water erosion dominated on longer slopes, soil translocation due to tillage transformed the upper areas of cultivated hillslopes [2–4].

Erosion and deposition resulted in a large modification of soils developed from loess. To describe the changes, Turski et al. [5] proposed a classification of soils based on reduction of pedon of Haplic Luvisols. The classification included noneroded soils, four classes of erosion, and depositional soils. To distinguish erosion classes, the illuvial horizon B was separated in three parts (Bt1, Bt2, and BC) that were easily recognized in the field by the identification of the B subhorizon located below the plowed layer. The studies showed a mosaic type of localization of noneroded, eroded, and depositional soils located on slopes and within the plateau of the Lublin Upland [5–7]. Houben [8] showed a similar lack of spatial pattern in location of soils in loess catchment of Southern Germany. One of the reasons for uncertainty in localization of soils could be a large density of open and closed depression in loess areas and different degree in filling of the depressions by deposited material. The density of depressions is assessed within the range from 1 to 16 per km^{-2} [9, 10]. The modification of pedons resulted in redistribution of soil material and changes in soil properties [6, 11–13].

Analysis of spatial distribution of soil properties is important for evaluation of landscape evolution after the change of land use from natural forest into arable land [8, 14]. The studies concern the comparison of present and past topography and try to find a rate of landscape transformation. Topography of the past is reconstructed on the basis of

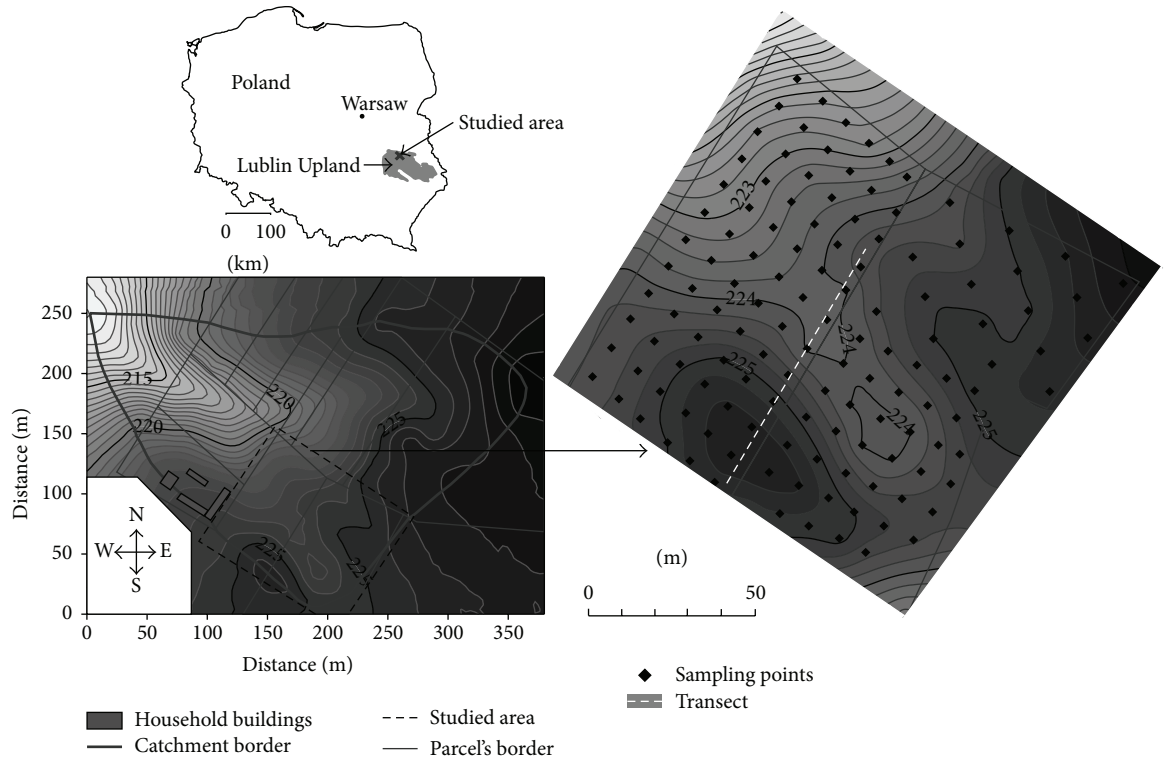

Figure 1: Location of the study area and localization of sampling points for soil profiles analyses and soil transect.

point-measurements of erosion and deposition, and the studies enable calculating erosion budget for catchments [15, 16]. Radionuclide caesium 137 (^{137}Cs) is the most widespread method in evaluation of distribution of erosion and deposition. Description of soil profiles is weakly represented and needs an accurate description of noneroded soil profiles and establishment of the relations between soil depth and topographical features, that is, slope, aspect, upslope area, relative height difference, and so forth [17–19]. However, the studies did not give a clear response of the relations [8, 20, 21]. The assumption that erosion processes under natural forests did not introduce significant changes to soil profiles was the basis of reconstruction of the past relief. Studies under old forest in loess areas showed that soil profiles were not affected by erosion outside the gullied areas and confirmed the assumption [20, 22].

Previous studies in loess belt of the Lublin Upland were limited to recognition of the state of soil profile modification and its effect on soil properties [5–7]. However, evaluation of the changes that were introduced to soil and relief needs more comprehensive attitude that should also include a reconstruction of the past topography and analysis of changes in relief.

The purpose of the studies was evaluation of the changes that were introduced to the relief and soils after 185 years of arable land use of loess area. In this study, we hypothesized that relatively flat loess area at present was largely transformed due to erosion and deposition. The hypothesis was tested by assessment of changes in the depth of soil solum and soil properties, and geostatistical techniques were used to study the spatial pattern of soil attributes. Description of soil profiles in relation to the soil position in the landscape was used to reconstruct the depth of eroded profiles and the past topography. The reconstruction of the past topography was used to calculate erosion and deposition and evaluation of slope transformation in the studied area.

2. Methods

2.1. Site Description. The study area is located in the northern part of the Lublin Upland (51°19′53″N latitude, 22°23′19″E longitude). Loess deposits in this part of the region are about 10–30 m thick. The mean annual rainfall is 550.6 mm and the mean daily air temperature 7.4°C. Both precipitation and temperature are not uniformly distributed over the year. The highest monthly precipitation of 81.7 mm occurs in July and the lowest of 23.4 mm in January. Snow represents about 15% of total precipitation, and the average duration of snow cover is about 90 days. Annual rainfall erosivity evaluated on the basis of the *R*-factor of the USLE [23] is relatively low and ranges from 590 to 1850 MJ mm ha^{-1} h^{-1} [24]. The mean air temperature ranges from −3.4 in January to 17.9°C in July. Dry forest (*Tilio-Carpinetum*) was a natural vegetation of the area [25], and Haplic Luvisols developed from loess were typical soils [26].

The study area of 1.3 ha occupies part of two parcels and is located near the watershed zone in the southern part of small catchment of dry basin type (Figure 1). The study area represents a rolling type of relief with relatively

small differences of relative height that ranges from 221 to 226 m a.s.l. The site was deforested in 1820 and from that time remains under arable land use. The change of land use was reflected on topographical maps from 1804 and 1830. Present arrangement of parcels was established after land consolidation in 1932. Typical crop rotation included sugar beets (*Beta vulgaris* L.) or potatoes (*Solanum tuberosum* L.), spring barley (*Hordeum vulgare* L.) or spring wheat (*Triticum aestivum* L.), red clover (*Trifolium pretense* L.), and winter wheat (*Triticum aestivum* L.) or, earlier, rye (*Secale cereale* L.). In the early 1990s, red clover was removed from the rotation. Tillage included a mouldboard ploughing once or twice a year, and a chisel ploughing in spring. Mouldboard ploughing is performed to the depth of 25 cm in the autumn, and to 15 cm after cereal harvest, the same depth as chisel. Mechanical tillage has been started from the 80s of the last century.

A detailed topographic survey of the study area was carried out with a tachymeter in the autumn of 2005. On the basis of measurements, topographic maps were produced with Surfer version 10 [27]. Analysis of map showed that inclination of slopes varied from 0 to 5° with a mean of 2.2° within the study area.

2.2. Soil Characteristics. Thickness of soil horizons was established on the basis of description of intact soil cores of 2.5 cm diameter. Soil cores were taken to the depth of calcareous loess in noneroded and eroded soils, and to the lower border of BC horizon in depositional soils. The horizons were separated by difference in soil color and consistency. On the basis of measurements, depth of soil solum, that is, the cumulative thickness of soil horizons from Ap to BC, was established. The border between decalcified and calcareous loess was determined with 10% HCl. The soils were classified according to Turski et al. [5]. Noneroded soils characterized the full sequence of horizons typical for Haplic Luvisol, that is, Ap-E-Bt1-Bt2-BC-C-Ck. With reduction of soil profile, three erosion classes were distinguished. Slightly eroded soil characterized the loss of E horizon, and the profile had the following sequence: Ap-Bt1-Bt2-BC-C-Ck. With the loss of deeper horizons, the soils were classified as moderately (Ap-Bt2-BC-C-Ck) and severely (Ap-BC-C-Ck) eroded. Separation of the illuvial B horizon in three parts (Bt1, Bt2, and BC) is a difference to the standard description of Haplic Luvisol provided by WRB [26] and the Polish Soil Systematic System [28]. In this study, in contrast to previous work of Turski et al. [5], all soils with accumulated soil material that overlay the original soil were classified as depositional soils. Generally, the sequence of horizons of depositional soils was Ap-C1-Ab-E-Bt1-Bt2-BC-C-Ck. Contribution of soils in the study area was calculated as a percentage of soils to the total number of soil cores.

Samples for analysis of soil texture and soil organic carbon (SOC) were taken from the plowed layer (0–26 cm) and subsoil (26–50 cm). The samples were air-dried and sieved on 2 mm mesh. The particle size distribution was determined by areometric method [29], and SOC by wet combustion with dichromate solution [30].

Sampling for profile description and soil properties was performed in a regular grid of 20 m × 20 m (in total 39 measuring points). Then, density of sampling for profile description was increased and adjusted to the expected changes in soil redistribution that were visible by change of color of the plowed layer. Finally, sampling was performed in a grid 10 m × 10 m for majority of the studied area, and the total number of soil cores was 128. Location of sampling points was established with a type on the basis of the measured distance from the borders of parcels. Sampling was performed in the autumn of 2003 and 2004. Additionally, distribution of soil depth was studied along a transect located along the border of two parcels (Figure 1). Within the transect of the total length of 85 m, 4 ditches of the length from 9 to 18 m were made to the depth of 2 m. The ditches were separated by a distance of about 10 m.

2.3. Reconstruction of the Past Relief and Calculation of Erosion and Accumulation. Elaboration of the map without accumulated layer in depositional soils was the first step in reconstruction of the past topography. To develop a map, the depth of deposition was subtracted from the relative height in each of the sampling points. The map was developed with Surfer using kriging with linear model. The soils were separated according to the position in the landscape in four groups: soils in top of hill's position, flat area, on slopes of the southern and northern exposition, and the floor of depressions. Then, the depth of solum of noneroded and buried soils was analyzed for separated locations. Mean depth of solum of the soils was used to reconstruct the depth of soils with eroded profiles. In the reconstruction, the depth of the past plowed layer Ab was assumed on 13 cm. To minimize the effect of possible errors, the reconstruction of profiles was limited only to the depth of the first disturbed horizon. It means that only depth of E and Bt1 was reconstructed for slightly eroded soils, and depth of deeper horizons was accepted without any changes. Similar procedure was used for moderately and severely eroded soils; that is, for the former the depth of E, Bt1, and Bt2 and for the latter the depth of E, Bt1, Bt2, and BC were reconstructed. The calculations were made in Excel. Depth of lost part of reconstructed profiles was added to the relative height in measured points. Then, a map of the past topography was developed on the basis of relative heights of reconstructed profiles and profiles without deposition. The map was produced using kriging with linear model, and distribution of slopes was analyzed. Amount of erosion was calculated from the difference in the depth of reconstructed and preserved soil profiles and deposition from the depth of accumulated material within the studied area.

2.4. Statistical Analyses. Experimental data were statistically analyzed using Statistica version 8 [31]. Geostatistical analyses were performed with GS+ [32, 33]. Selection of variograms was based on residual sums of squares (RSS) and determination coefficients (R^2). Semivariance models were used to produce soil maps with Surfer version 10 [27]. Before the performance of geostatistical analyses, the data were checked for trend and normality. A uniform lag interval of 10 and

Table 1: Mean depth and standard deviation (SD) of soil horizons of noneroded and eroded soils.

Soil	Soil horizon											
	Ap		E		Bt1		Bt2		BC		C	
	Mean	SD	Mean	SD	Mean	SD	Mean	SD	Mean	SD	Mean	SD
	(m)											
Noneroded (n = 25)	0.27	0.02	0.14	0.07	0.42	0.11	0.34	0.11	0.37	0.07	0.11	0.03
Slightly eroded (n = 38)	0.27	0.02	—	—	0.22	0.11	0.32	0.11	0.34	0.10	0.10	0.04
Moderately eroded (n = 15)	0.25	0.02	—	—	—	—	0.20	0.10	0.29	0.08	0.08	0.02
Severely eroded (n = 11)	0.27	0.03	—	—	—	—	—	—	0.27	0.10	0.10	0.05

20 m was used in geostatistical analyses for soil properties and solum depth, respectively. Rotation of semivariance was tested independently.

3. Results

3.1. Soil Erosion Classes and Depth of Soil Solum. Measurements of intact soil cores showed that the processes of soil erosion and deposition largely modified the soils within the studied area. Depositional and slightly eroded soils were the most frequent and their contribution amounted to 36 and 30% of the total number of cores, respectively. Noneroded soils were represented by 14, moderately eroded soils by 12, and severely eroded soils by 9% of cores.

Taking into account all the studied soils, depth of solum (Ap-BC) ranged from 0.50 to 4.61 m with a mean of 1.52 and coefficient of variation (CV) of 50.9%. Depth of solum of noneroded soils ranged from 1.28 to 1.85 m, with a mean of 1.55 cm. Erosion and loss of parts or the whole soil genetic horizons resulted in decrease of mean depth of solum to 1.15, 0.74, and 0.55 m in slightly, moderately, and severely eroded soils, respectively (Figure 2). The differences in soil depth among the studied soils were statistically significant.

All the studied soils have similar depth of the plowed layer (Table 1). Assuming the depth of horizons of noneroded soils as a standard, the mean profile of slightly eroded soil was reduced not only by the loss of the whole E horizon, but also by the loss of 48% of Bt1 horizon. Moderately eroded soils characterize the loss of the E, Bt1 and 38% of Bt2 horizon, and severely eroded soils the loss of E, Bt1, Bt2 and 7% of BC horizons. Depth of decalcified layer C was similar among the studied soils and ranged from 0.04 to 0.23 m with a mean of 0.10 cm. Decalcified layer of soil overlaid the calcareous loess.

Depositional soils characterized the largest differentiation of solum depth that ranged from 1.2 to 4.61 m with a mean of 2.28 m. Three groups could be distinguished within depositional soils: initial, typical, and disturbed (Table 2). The initial group of depositional soils included the soils of deeper plowed layer than the depth of plow at present. Present and older plowed layer differed by soil consistency; however they had similar dark grey color. Soils of this group represent a transient form between noneroded and typical depositional soils. Larger depth of plowed layer indicates that accumulation of soil material has started in the locations of these soils. Separation of this group enables a more precise determination of the zones of accumulation. Depth

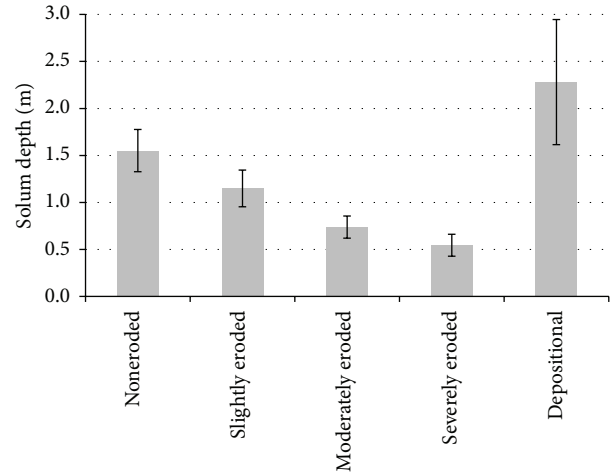

Figure 2: Mean depth and standard deviation of soil solum (Ap-BC) of the studied soils.

of solum of the soils ranged from 1.2 to 2.16 m, and after substraction of the depth of present plowed layer Ap, it ranged from 0.95 to 1.86 m. Typical depositional soils consisted of soils where accumulated material covered the buried soils of full sequence of horizons characteristic of Haplic Luvisols. Present and buried plowed layers were separated by accumulated material that differed by color. Depth of solum of these soils ranged from 1.62 to 4.61 m, and thickness of accumulated material (Ap-C1) from 0.1 to 1.51 m with a mean of 0.53 m. Depth of old plowed layer Ab ranged from 0.07 to 0.34 with a mean of 0.14 m and coefficient of variation (CV) of 46%. Disturbed depositional soils consisted of profiles where accumulated material was settled on previously eroded soils. Three profiles represented this group, one with the loss of Ab and two others with the loss of Ab, E, and part of Bt1 horizon. Depth of solum of the disturbed depositional soils ranged from 1.62 to 2.06 m.

Distribution of soil solum showed a spatial structure of variability within the study area. The structure was best described by spherical isotropic model of semivariance with a range of autocorrelation of 31.9 m, nugget and sill of 0.0001 and 0.28 m^2, respectively. The solum data were fitted to the model with coefficient of determination R^2 = 0.87, and anisotropy ratio was 1.75. Distribution of solum depth was presented in Figure 3.

Table 2: Number and mean depth (m) of horizons of depositional soils (standard deviation in brackets).

Depositional soils	Sequence of horizons	n	Soil horizon							Solum
			Ap	C1	Ab	E	Bt1	Bt2	BC	Ap-BC
			(m)							
Initial	Ap-Ab-E-Bt1-Bt2-BC-C-Ck	15	0.27	—	0.10	0.14	0.52	0.42	0.37	1.82
			(0.02)	—	(0.05)	(0.09)	(0.15)	(0.12)	(0.06)	(0.22)
Typical	Ap-C1-Ab-E-Bt1-Bt2-BC-C-Ck	28	0.26	0.53	0.14	0.16	0.50	0.65	0.37	2.58
			(0.02)	(0.42)	(0.07)	(0.06)	(0.14)	(0.29)	(0.05)	(0.68)
Disturbed	Ap-C1-E-Bt1-Bt2-BC-C-Ck	1	0.28	0.56	—	0.14	0.24	0.42	0.42	2.06
			(0.00)	(0.00)	—	(0.00)	(0.00)	(0.00)	(0.00)	(0.00)
	Ap-C1-Bt1-Bt2-BC-C-Ck	2	0.26	0.22	—	—	0.35	0.50	0.37	1.69
			(0.00)	(0.13)	—	—	(0.24)	(0.19)	(0.01)	(0.07)

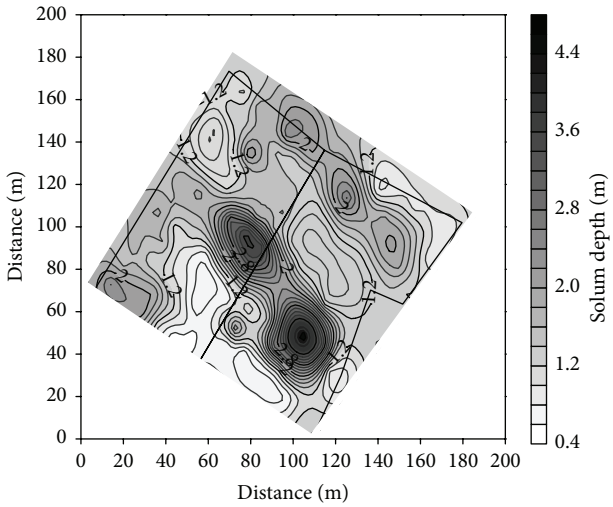

Figure 3: Distribution of soil solum (Ap-BC).

3.2. Soil Texture Fractions and Soil Organic Carbon. The modification of pedon of Haplic Luvisols resulted in differentiation of soil texture and SOC concentration in both the plowed layer and subsoil of the studied soils. The most significant changes concerned the clay, silt, and SOC (Table 3). The clay concentration was the smallest in the plowed layer of noneroded soil and gradually increased in slightly, moderately, and severely eroded soils. The latter contained 2 times more clay than the plowed layer of noneroded soil. In subsoil, the largest concentration of clay was found in slightly eroded soil, and then it gradually decreased in moderately and severely eroded soil. Generally, the clay content in subsoil was larger than in the plowed layer of the studied soils. Severely eroded soil was the exception, as it contained more clay in the plowed layer in comparison to the subsoil. Silt concentration showed a reverse relation to the soil erosion class in comparison to the clay. The largest concentration of SOC was in the plowed layer of depositional and noneroded soils, and the smallest in severely eroded soil. The SOC concentration in subsoil of depositional soils was 2-fold larger in comparison to the others.

Clay and SOC concentration characterized the largest variation in the plowed layer, and the variation of both parameters in subsoil was even larger (Table 4). Content of clay was negatively linearly correlated with silt, and coefficients of determination R^2 were 0.91 and 0.97 in the plowed layer and subsoil, respectively. All studied soil properties showed a spatial structure of variability. Isotropic spherical models of semivariance with anisotropy ratio below 2.3 best described the structure (Table 4). The data were better fitted to the models for the plowed layer than subsoil, and determination coefficients R^2 ranged from 0.45 to 0.95. Generally, the ranges of autocorrelation for textural fractions varied from 32 to 36 m in the plowed layer and from 27 to 32 m in subsoil (apart of sand). The ranges of autocorrelation for SOC in the plowed layer and subsoil were 42 and 32 m, respectively. The calculated semivariograms were used in point ordinary kriging to produce the maps of clay and SOC distribution.

Distribution of clay in the plowed layer well corresponds to the distribution of soil solum. The zones of high content of clay are the zones of shallow soils (Figures 4(a) and 2). The similarity is disturbed in subsoil, where only part of the zones of high clay content covers the area of shallow soils (Figures 4(b) and 2). The zones of the smallest content of clay correspond mainly with the area of deep depositional soils. Distribution of silt showed a reverse relation to the soil depth (not showed in the paper). Distribution of SOC is also related with distribution of soil solum (Figures 5 and 2). The relation between the zones of high SOC concentration and deep soils is better visible in subsoil than in the plowed layer.

3.3. Reconstruction of the Past Relief and Balance of Erosion and Deposition. Topography of the studied area without accumulated material was presented in Figure 6(a). Noneroded and buried soils (i.e., depositional soils after removal of deposition layer) of the full sequence of horizons typical for Haplic Luvisol were represented by 60 profiles. From that amount, soils located at hill top position were represented by 2, at flat area by 10, at slopes of N exposition by 14, at slopes of S exposition by 18, and at floor of depressions by 16 profiles (Table 5). Statistical analysis showed that the soils could be separated in 3 groups. The first group consisted of soils located at hill top position and slopes of southern aspect. The depth of the former ranged from 0.95 to 1.13 m, and the latter from 1.09 to 1.54 m. The second group consisted

Table 3: Soil particle fractions and SOC concentration in the plowed layer and subsoil of the studied soils and results of ANOVA; means were separated by Tukey's HSD test.

Soil	Sand (2–0.05 mm)		Silt (0.05–0.002 mm)		Clay (<0.002 mm)		SOC	
	Mean	CV	Mean	CV	Mean	CV	Mean	CV
	g/kg	%	g/kg	%	g/kg	%	g/kg	%
				Plowed layer				
Noneroded (n = 5)	148	8	764^{a}	1	88^{a}	13	9.6^{ab}	7.3
Slightly eroded (n = 13)	158	4	701^{b}	3	142^{b}	13	8.8^{b}	12.5
Moderately eroded (n = 4)	165	9	688^{b}	2	148^{b}	14	9.5^{ab}	13.9
Severely eroded (n = 2)	150	0	685^{b}	1	165^{b}	3	7.9^{b}	9.1
Depositional (n = 15)	160	7	743^{a}	24	97^{a}	24	10.9^{a}	11.9
				Subsoil				
Noneroded (n = 5)	154	3	752^{a}	3	100^{a}	28	3.6^{a}	7.6
Slightly eroded (n = 13)	161	8	629^{bc}	4	212^{bc}	9	3.4^{a}	22.3
Moderately eroded (n = 4)	163	3	650^{bc}	4	188^{bc}	13	3.3^{a}	25.5
Severely eroded (n = 2)	160	13	710^{ab}	3	130^{ab}	0	3.0^{a}	4.0
Depositional (n = 15)	159	6	741^{a}	6	100^{a}	44	7.6^{b}	36.6

Mean values of solum followed by different letters are significantly different at $P \leq 0.05$.

Table 4: Statistics of soil properties and parameters of isotropic spherical models of semivariance.

Soil property	Soil layer	Min.	Max.	Mean	CV	Skewness	Kurtosis	Nugget	Sill	Range of autocorrelation	Anisotropy ratio
			(g kg^{-1})		(%)			(g kg^{-1})^2		(m)	
Sand	Plowed	140	180	157.7	6.4	0.32	−0.43	0.1	103	36.0	1.50
	Subsoil	140	180	159.5	6.9	0.34	−0.32	52.9	278	310.6	2.22
Silt	Plowed	670	780	721.5	4.6	0.12	−1.26	1	1121	37.6	1.42
	Subsoil	590	780	690.8	9.0	0.04	−1.55	10	3912	32.2	1.41
Clay	Plowed	70	180	120.8	27.4	0.04	−1.19	1	1119	31.6	1.47
	Subsoil	70	240	147.2	41.9	0.03	−1.66	10	3773	26.8	1.31
SOC	Plowed	6.7	13.7	9.7	15.6	0.28	−0.13	0.23	2.39	41.5	1.49
	Subsoil	1.2	10.8	5.0	55.5	1.05	−0.42	0.0001	0.27	31.6	1.41

of soils located on relatively flat areas and slopes of northern aspect. The depth of solum of these soils ranged from 1.28 to 1.74 and from 1.51 to 1.86 m, respectively. Finally, the third group represented the deepest soils located at the floor of open and closed depressions, and the solum depth varied from 1.68 to 2.68 m. Soils with eroded profiles were classified at the same way. Eroded soils at flat position were represented by 17 profiles, and soils on slopes of southern and northern exposition by 20 and 26 profiles, respectively. Lost depth of eroded soils was calculated from the difference of the mean depth of noneroded and buried soils and preserved depth of eroded soils. The calculations were made taking into account the position of the soils in the landscape. The difference was added to the present relative height of the eroded sites. Then, the map of the past topography of the site was developed. The map is based on the reconstructed profiles and profiles without soil accumulation (Figure 6(b)).

Database of reconstructed and overbuilt profiles enabled calculating the amount of erosion and accumulation within the study area. Sum of accumulated and eroded soil material for all studied profiles was 29.52 and 32.59 m, respectively. The amounts divided by total number of profiles showed that the average profile was overbuilt by 0.23 m and eroded by 0.26 m. Assuming that soil density is 1.3 Mg m^{-3} [13] total erosion was 4394 Mg. From that amount, 88% was deposited within the study area, and 12% removed outside. Taking into account the period of arable land use of the area (185 years), total soil erosion was 23.8 Mg ha^{-1} year^{-1} in the studied area, that is, 1.41 mm year^{-1}.

3.4. Transformation of Slopes of the Past Relief. Analysis of slopes reflects the changes between present and past relief (Figure 7). Slopes in the range from 2.5 to 4.5° prevailed in the past topography, whereas slopes from 1 to 3° at present. In the latter, slopes above 5° were absent, whereas these slopes amounted to 30% of total slopes in the past relief. The average inclination of slopes decreased by about a half, that is, from 4.3 to 2.2° at the past and present topography.

3.5. Location of Soils in Transect. Soil distribution in transect that crossed the study area is an evidence of the changes of relief (Figure 8). Soils on slopes and top of the hills were eroded, and depression was filled with accumulated

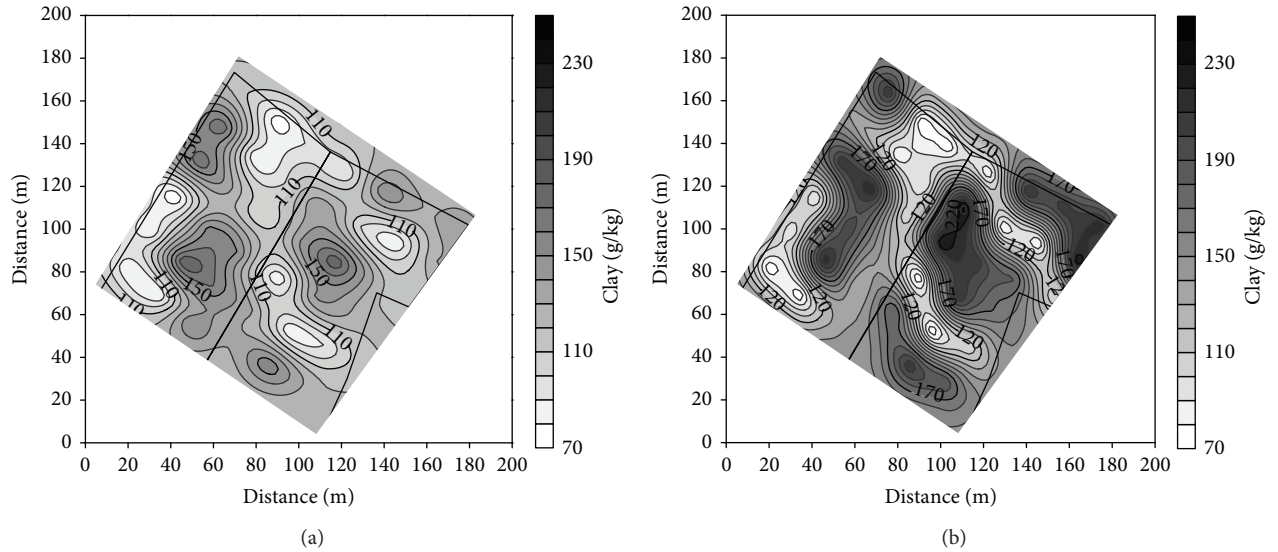

Figure 4: Distribution of clay (g kg^{-1}) in the plowed layer (a) and subsoil (b).

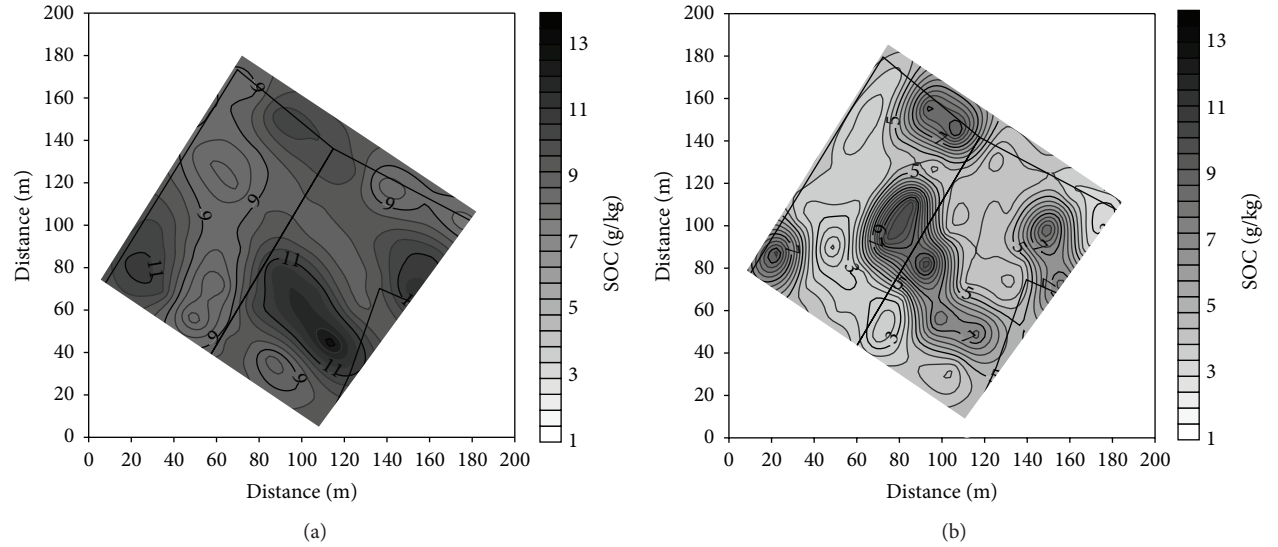

Figure 5: Distribution of SOC (g/kg) in the plowed layer (a) and subsoil (b).

Table 5: Depth of soil horizons in noneroded (apart from Ap horizon) and buried soils, depth of soil solum, and results of ANOVA; means were separated by Tukey's HSD test.

Soil position and number of profiles	Depth of horizons										Depth of solum	
	Ab		E		Bt1		Bt2		BC		Ab-BC	
	Mean (m)	CV (%)	Mean (m)	CV (%)	Mean (m)	CV (%)	Mean (m)	CV (%)	Mean (m)	CV (%)	Mean (m)	CV (%)
Top (n = 2)	0.11	22.2	0.09	7.7	0.26	13.7	0.29	34.5	0.30	20.0	1.04[a]	8.7
Flat area (n = 10)	0.10	43.6	0.19	33.7	0.56	27.9	0.43	17.2	0.36	21.1	1.64[b]	6.2
Slope-aspect S (n = 14)	0.09	27.5	0.11	43.2	0.42	28.8	0.34	25.0	0.35	16.5	1.31[a]	10.3
Slope-aspect N (n = 18)	0.12	16.7	0.14	59.9	0.48	18.8	0.41	29.2	0.38	16.3	1.52[b]	8.8
Floor (n = 16)	0.16	43.8	0.18	33.0	0.51	26.8	0.80	34.0	0.40	6.2	2.05[c]	15.7

Mean values of solum followed by different letters are significantly different at $P \leq 0.05$.

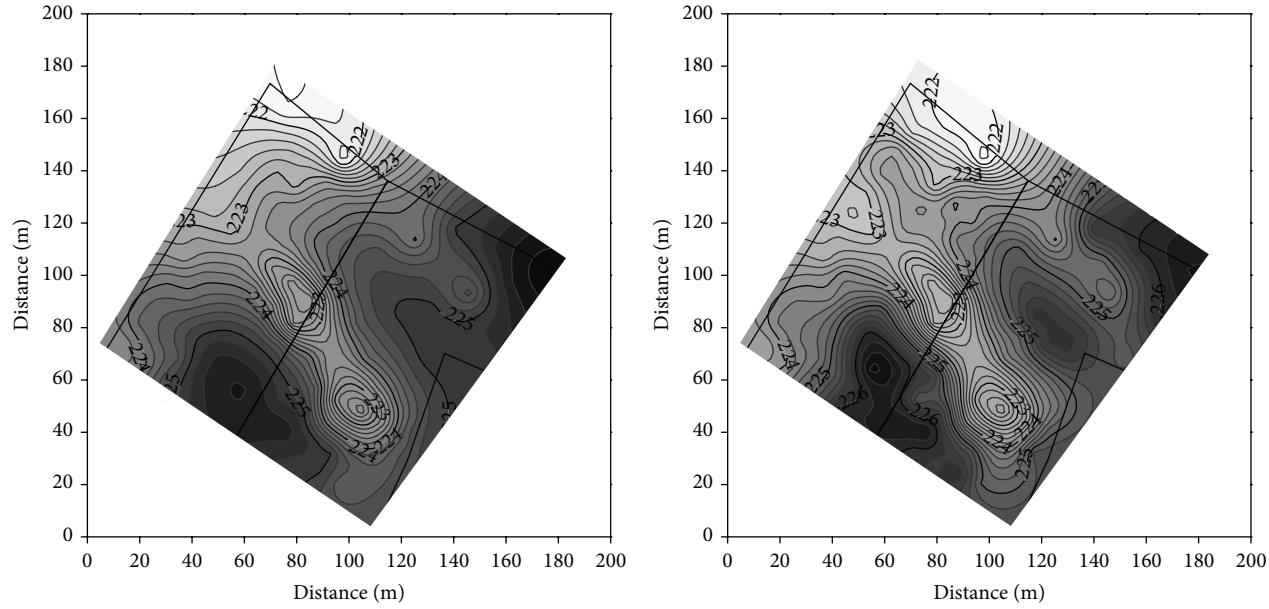

Figure 6: Topography of studied area without accumulated soil material (a) and the past relief (b).

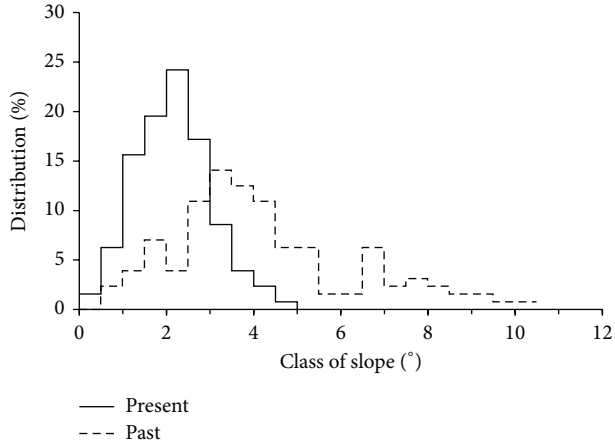

Figure 7: Distribution of slope classes in the present and past relief.

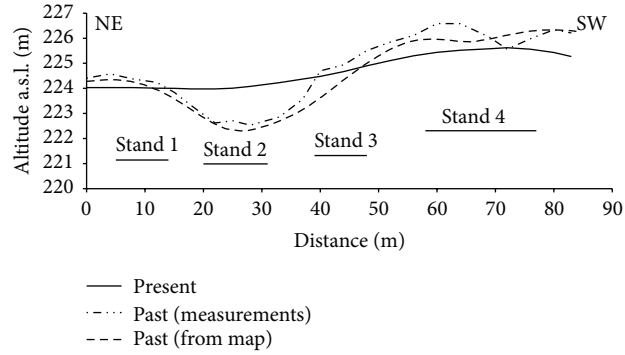

Figure 8: Present and past topography of the transect in the study area with localization of four soil pitches.

soil material. Maximum reduction of the soil was about 1.25 m, and maximum accumulation 1.45 m. At the distance of 85 m, the difference of relative height decreased from 4 m of the past relief to 1.5 m at present. Within stand 1, slightly eroded soil prevailed and changed to noneroded soil at the distance of 14 m. Depositional soils that overlaid the buried soil of full sequence of horizons typical for Haplic Luvisol were present in stand 2, and the depth of accumulation was 1.5 m. Within stand 3, noneroded soils were present at the transect distance of 45–48 m and changed to moderately eroded at the end of the stand. Large differentiation of soil depth within a relatively small distance was observed within stand 4 (Figure 9). Soil distribution pointed that the area of this stand was a part of depression of the past relief. The depression vanished during the agricultural use of the area and erosion, and the changes in soil depth are the only evidence of its existence. An inversion of topography was the result of transformation of relief in the stand. Past slopes of SSW aspect were inverted to present NNE slopes, and vice versa. The center of depression is located at present border of watershed. The changes in soil cover within stand 4 were not reflected in the reconstructed map, as sampling points were located in positions that omitted the centre of depression. Localization of transect within the study area was presented in Figure 1.

4. Discussion

Studies showed that soils were largely modified after 185 years of arable land use of the studied area. Noneroded soils were scarce (14% of profiles), depositional soil more frequent (30%), and soils of eroded profiles the most frequent (56%).

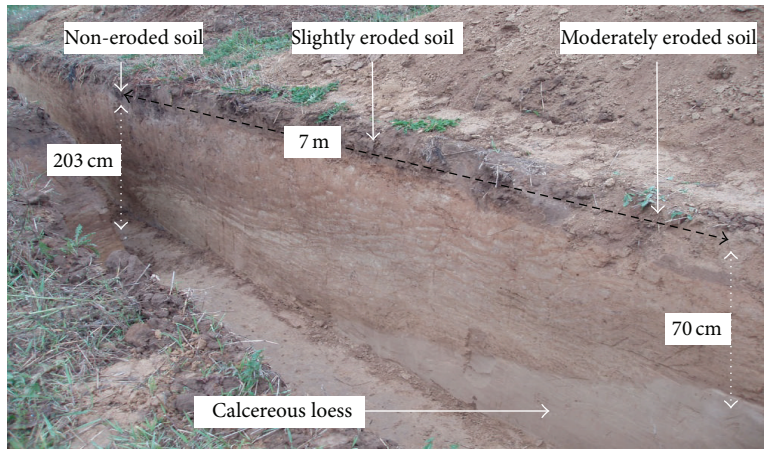

Figure 9: Changes in the depth of soil in transect at the distance of 66–70 m (part of the stand 4) (Photo J. Rejman).

Such large differentiation in soils seems to be typical for some part of loess area of the Lublin Upland. The percentage of noneroded soils ranged from 10 to 21%, eroded soils from 41 to 48%, and depositional soils from 31 to 49% in two other sites of the Upland [5, 7]. Different distribution of soils was reported by Rodzik et al. [34] with larger percentage of noneroded soils that amounted to 35% and smaller percentage of depositional soils that amounted to 18%. The difference could be related to topography of the studied areas. The former studies were performed at the area that consisted of hill's top, slope of southern exposition, and part of valley, and the latter were limited to the slope of northern exposition.

Modification of soils due to erosion and accumulation affected the content of textural fractions and SOC concentration in both the ploughed layer and subsoil. The most significant changes concerned the content of clay. In the ploughed layer, the mean clay concentration in noneroded soil was 88 g kg^{-1} and increased with reduction of profile to the value of 165 in severely eroded soil. Within a subsoil, clay content in noneroded soil was 100 g kg^{-1} and increased to 212 in slightly eroded soils and then decreased to the value of 130 g kg^{-1} in severely eroded soil. The changes well corresponded to the vertical distribution of clay in the profile of noneroded Haplic Luvisol. Similar changes of clay content in noneroded and eroded soils were reported by Turski et al. [5]. The changes are related with excavation of the illuvial horizon B due to erosion and its gradual contribution to the plowed layer. Larger changes are reported in soils of the postglacial area. Heckrath et al. [3] found that clay content in the ploughed layer ranged from 10 to 60%. Similar large differences were observed in the areas of shallow loess that covered clay-reach bedrock [12, 35].

Generally, the reaccumulation of soil material due to water erosion concerns at first the fine material, so higher content of SOC and clay should be observed in the depositional soils. Concentration of SOC follows this tendency, whereas clay content, although higher in the plowed layer of depositional soils, is similar in subsoil layer of noneroded and depositional soils. The explanation could be that some part of the soil material (12%) was removed from the studied area and some part of clay could be washed down the profile of depositional soils. The latter could take place especially in depressions, where stagnation of water was usually observed during the snow melting. The vertical movement of clay particles could follow the same way as pedogenic processes that provided the enrichment of clay in the illuvial Bt horizon. However this hypothesis needs to be confirmed in further studies.

Distribution of soil solum, soil texture fractions, and SOC showed a spatial structure of variability best described by isotropic spherical models of semivariance with a range of autocorrelation of 30–40 m, about half of the distance between the hills of the past relief. Miller et al. [11] showed a similar close relation of range of spatial dependence of soil properties and average distance between hills.

High percentage of soils with eroded profiles is an evidence of strong erosion. However, the calculated annual soil erosion rates were not large and amounted to 1.41 mm ha^{-1}. The calculated rate is smaller than the range of annual erosion (2–7 mm) in the Lublin Upland [36–39]. The pattern of soil redistribution with the zones of eroded soils is separated by depositional soils fits to the areas where soil translocation due to tillage is a dominant part of erosion [40, 41]. The measurements of water erosion on runoff plots of various lengths also point to supremacy of soil transport on short distance in the studied area with annual rates up to 5 mm [42, 43]. It seems that both processes of tillage and water erosion participated in reduction of pedon. Measurements of deposited soil material showed that a majority of the eroded soil was maintained within the study area. Similar amounts of erosion and deposition resulted in large smoothing of the studied area, and the average slope decreased by about a half, that is, from 4.3 to 2.2° after 185 years of arable land use. The final effect of erosion and accumulation processes would be transformation of the complex sloping area into a uniform gentle slope. Maruszczak and Uziak [44] found such stadium of transformation of soil catena in loess area of the Lublin Upland.

5. Conclusions

The results of the study showed that the change of land use from forest to arable area introduced significant changes to relief and soils in loess area. After about 185 years of cultivation, the relief was largely smoothed, and majority of soil pedons were reduced due to erosion or overbuilt by accumulation. Soils of noneroded pedons were scarce and maintained mainly at the lower part of the slopes at the places of equilibrium between erosion and deposition. Total soil erosion was assessed on 4394 Mg, and 88% from that amount was deposited inside the studied area. Such large deposition resulted in transformation of slopes. The average slope inclination decreased from 4.3 to 2.3°, and slopes above 5° (that constituted 30% of the past topography) vanished at present.

The modification of pedons resulted in large variation of soil properties in both the plowed layer and subsoil, and development of spatial structure of distribution of soil textural fractions and soil organic carbon. Spherical isotropic models of semivariance best described the spatial pattern of soil attributes, and ranges of autocorrelation were 30–40 m, about half the distance between the hills of the past relief. The study proved that present-day relatively flat loess areas had much larger differentiated relief in the past, and distribution of soil solum is the only evidence of the changes.

Conflict of Interests

The authors declare that there is no conflict of interests regarding the publication of this paper.

References

[1] O. Cerdan, G. Govers, Y. le Bissonnais et al., "Rates and spatial variations of soil erosion in Europe: a study based on erosion plot data," *Geomorphology*, vol. 122, no. 1-2, pp. 167–177, 2010.

[2] G. Govers, K. Vandaele, P. Desmet, J. Poesen, and K. Bunte, "The role of tillage in soil redistribution on hillslopes," *European Journal of Soil Science*, vol. 45, no. 4, pp. 469–478, 1994.

[3] G. Heckrath, J. Djurhuus, T. A. Quine, K. van Oost, G. Govers, and Y. Zhang, "Tillage erosion and its effect on soil properties and crop yield in Denmark," *Journal of Environmental Quality*, vol. 34, no. 1, pp. 312–324, 2005.

[4] K. van Oost, W. van Muysen, G. Govers, J. Deckers, and T. A. Quine, "From water to tillage erosion dominated landform evolution," *Geomorphology*, vol. 72, no. 1–4, pp. 193–203, 2005.

[5] R. Turski, J. Paluszek, and A. Slowinska-Jurkiewicz, "The effect of erosion on the spatial differentiation of the physical properties of Orthic Luvisols," *International Agrophysics*, vol. 6, no. 3-4, pp. 123–136, 1992.

[6] J. Rejman, "Redistribution of basic physical properties and water content of soils in a loess catchment," *Acta Agrophysica Monographiae*, vol. 5, pp. 1–107, 2013.

[7] J. Rejman, R. Turski, and J. Paluszek, "Spatial and temporal variations in erodibility of loess soil," *Soil and Tillage Research*, vol. 46, no. 1-2, pp. 61–68, 1998.

[8] P. Houben, "Scale linkage and contingency effects of field-scale and hillslope-scale controls of long-term soil erosion: anthropogeomorphic sediment flux in agricultural loess watersheds of Southern Germany," *Geomorphology*, vol. 101, no. 1-2, pp. 172–191, 2008.

[9] T. Vanwalleghem, J. Poesen, I. Vitse et al., "Origin and evolution of closed depressions in central Belgium, European loess belt," *Earth Surface Processes and Landforms*, vol. 32, no. 4, pp. 574–586, 2007.

[10] R. Kołodyńska-Gawrysiak and L. Chabudziński, "Morphometric features and distribution of closed depressions on the Nałęczów Plateau (Lublin Upland, SE Poland)," *Annales Universitatis Mariae Curie-Sklodowska Sectio B*, vol. 67, no. 1, pp. 45–61, 2012.

[11] M. P. Miller, M. J. Singer, and D. R. Nielsen, "Spatial variability of wheat yield and soil properties on complex hills," *Soil Science Society of America Journal*, vol. 52, no. 4, pp. 1133–1141, 1988.

[12] D. J. Timlin, Y. Pachepsky, V. A. Snyder, and R. B. Bryant, "Spatial and temporal variability of corn grain yield on a hillslope," *Soil Science Society of America Journal*, vol. 62, no. 3, pp. 764–773, 1998.

[13] J. Rejman, I. Iglik, J. Paluszek, and J. Rodzik, "Soil redistribution and crop productivity in loess areas (Lublin Upland, Poland)," *Soil and Tillage Research*, vol. 143, pp. 77–84, 2014.

[14] I. Peeters, T. Rommens, G. Verstraeten et al., "Reconstructing ancient topography through erosion modelling," *Geomorphology*, vol. 78, no. 3-4, pp. 250–264, 2006.

[15] D. E. Walling, M. A. Russell, R. A. Hodgkinson, and Y. Zhang, "Establishing sediment budgets for two small lowland agricultural catchments in the UK," *Catena*, vol. 47, no. 4, pp. 323–353, 2002.

[16] G. Verstraeten, T. Rommens, I. Peeters, J. Poesen, G. Govers, and A. Lang, "A temporarily changing Holocene sediment budget for a loess-covered catchment (Central Belgium)," *Geomorphology*, vol. 108, no. 1-2, pp. 24–34, 2009.

[17] K. Dalsgaard, E. Baastrup, and B. T. Bunting, "The influence of topography on the development of Alfisols on calcareous clayey till in Denmark," *CATENA*, vol. 8, no. 1, pp. 111–136, 1981.

[18] T. Rommens, G. Verstraeten, J. Poesen et al., "Soil erosion and sediment deposition in the Belgian loess belt during the Holocene: establishing a sediment budget for a small agricultural catchment," *Holocene*, vol. 15, no. 7, pp. 1032–1043, 2005.

[19] T. Vanwalleghem, J. Poesen, A. McBratney, and J. Deckers, "Spatial variability of soil horizon depth in natural loess-derived soils," *Geoderma*, vol. 157, no. 1-2, pp. 37–45, 2010.

[20] D. J. Pennock, "Multi-site assessment of cultivation-induced soil change using revised landform segmentation procedures," *Canadian Journal of Soil Science*, vol. 83, no. 5, pp. 565–580, 2003.

[21] F. J. Young and R. D. Hammer, "Soil-landform relationships on a loess-mantled upland landscape in Missouri," *Soil Science Society of America Journal*, vol. 64, no. 4, pp. 1443–1454, 2000.

[22] T. Vanwalleghem, H. R. Bork, J. Poesen et al., "Prehistoric and Roman gullying in the European loess belt: a case study from central Belgium," *Holocene*, vol. 16, no. 3, pp. 393–401, 2006.

[23] W. H. Wischmeier and D. D. Smith, "Predicting rainfall erosion losses—a guide to conservation planning," in *Agricultural Handbook 537*, pp. 1–58, Department of Agriculture, Washington, DC, USA, 1978.

[24] J. Rejman, R. Brodowski, and I. Iglik, "Annual variations of soil erodibility of silt loam developed from less based on 10-years runoff-plot studies," *Annals of Warsaw University of Life Sciences SGGW, Series of Land Reclamation*, vol. 39, pp. 77–83, 2008.

[25] J. Flisiak and K. Flisiak, "Bogucin through the centuries," *Polihymnia*, pp. 1–95, 2008 (Polish).

[26] IUSS Working Group WRB, "World reference base for soil resources 2006, first update 2007," World Soil Resources Reports 103, FAO, Rome, Italy, 2007.

[27] *Surfer ver. 10.3. Surfer Surface Mapping System*, Golden Software Inc., Golden, Colo, USA, 2011.

[28] J. Marcinek and J. Komisarek, "Systematic of polish soils," *Roczniki Gleboznawcze*, vol. 62, no. 3, pp. 1–178, 2011.

[29] T. Lityński, H. Jurkowska, and E. Gorlach, *Agricultural Chemical Analyses, Soils and Fertilizers*, PWN Press, Warsaw, Poland, 1976 (Polish).

[30] N. V. Tiurin, *Methodology of Analysis of Soil Humus Content*, Studia of Organic Compounds of Soils, Moscow, 1951.

[31] StatSoft, "STATISTICA (data analysis software system), version 8.0," 2008, http://www.statsoft.com/.

[32] *GS+: Geostatistics for the Environmental Studies. Version 9.0*, Gamma Design Software, LLC., Plainwell, Mich, USA, 2008, http://www.gammadesign.com/.

[33] G. P. Robertson, *GS+: Geostatistics for the Environmental Sciences*, Gamma Design Software, Plainwell, Mich, USA, 2008.

[34] J. Rodzik, P. Mroczek, and T. Wiśniewski, "Pedological analysis as a key for reconstructing primary loess relief —a case study from the magdalenian site in klementowice (eastern poland)," *Catena*, vol. 117, pp. 50–59, 2014.

[35] F. J. Arriaga and B. Lowery, "Corn production on an eroded soil: effects of total rainfall and soil water storage," *Soil & Tillage Research*, vol. 71, no. 1, pp. 87–93, 2003.

[36] S. Ziemnicki and Z. Mazur, "Slope transect as a exposure of soil erosion," *Annales Universitatis Mariae Curie-Skłodowska. Sectio E. Agricultura*, vol. 10, no. 3, pp. 77–160, 1955 (Polish).

[37] Z. Mazur, "Change of relief on loess slopes in Elizówka," *Annales UMCS E*, vol. 27, no. 10, pp. 169–198, 1972 (Polish).

[38] S. Pałys and Z. Mazur, "Changes of relief on eroded loess under controlled and uncontrolled conditions," *Bibliotheca Fragmenta Agronomica*, vol. 4B, pp. 295–305, 1998 (Polish).

[39] W. Zgłobicki, M. Kozieł, L. Lata, A. Plak, and M. Reszka, "Application of geochemical markers as a test for assessment of intensity of contemporary colluvial and alluvial sedimentation," *Annales UMCS Sectio B*, vol. 63, pp. 87–103, 2008 (Polish).

[40] D. A. Lobb, R. G. Kachanoski, and M. H. Miller, "Tillage translocation and tillage erosion in the complex upland landscapes of southwestern Ontario, Canada," *Soil & Tillage Research*, vol. 51, no. 3-4, pp. 189–209, 1999.

[41] S. de Alba, M. Lindstrom, T. E. Schumacher, and D. D. Malo, "Soil landscape evolution due to soil redistribution by tillage: A new conceptual model of soil catena evolution in agricultural landscapes," *Soil and Tillage Research*, vol. 58, no. 1, pp. 77–100, 2004.

[42] J. Rejman, "The effect of water and tillage erosion on the transformation of loess soils and slopes," *Acta Agrophysica Monographiae*, vol. 3, pp. 1–90, 2006.

[43] J. Rejman and B. Usowicz, "Evaluation of soil-loss contribution areas on loess soils in Southeast Poland," *Earth Surface Processes and Landforms*, vol. 27, no. 13, pp. 1415–1423, 2002.

[44] H. Maruszczak and S. Uziak, "Effect of microrelief of loess regions on the differentiation of soil-forming processes," *Roczniki Gleboznawcze*, vol. 29, pp. 159–173, 1978 (Polish).

Hindawi Publishing Corporation
The Scientific World Journal
Volume 2014, Article ID 535768, 11 pages
http://dx.doi.org/10.1155/2014/535768

Research Article

County-Scale Spatial Distribution of Soil Enzyme Activities and Enzyme Activity Indices in Agricultural Land: Implications for Soil Quality Assessment

Xiangping Tan,[1] Baoni Xie,[1] Junxing Wang,[1] Wenxiang He,[1] Xudong Wang,[1] and Gehong Wei[2]

[1] *College of Natural Resources and Environment, Northwest A&F University, Yangling, Shaanxi 712100, China*
[2] *College of Life Science, Northwest A&F University, Yangling, Shaanxi 712100, China*

Correspondence should be addressed to Wenxiang He; wenxianghe@nwsuaf.edu.cn

Received 26 May 2014; Revised 25 July 2014; Accepted 15 August 2014; Published 31 December 2014

Academic Editor: Antonio Paz González

Here the spatial distribution of soil enzymatic properties in agricultural land was evaluated on a county-wide (567 km^2) scale in Changwu, Shaanxi Province, China. The spatial variations in activities of five hydrolytic enzymes were examined using geostatistical methods. The relationships between soil enzyme activities and other soil properties were evaluated using both an integrated total enzyme activity index (TEI) and the geometric mean of enzyme activities (GME). At the county scale, soil invertase, phosphatase, and catalase activities were moderately spatially correlated, whereas urease and dehydrogenase activities were weakly spatially correlated. Correlation analysis showed that both TEI and GME were better correlated with selected soil physicochemical properties than single enzyme activities. Multivariate regression analysis showed that soil OM content had the strongest positive effect while soil pH had a negative effect on the two enzyme activity indices. In addition, total phosphorous content had a positive effect on TEI and GME in orchard soils, whereas alkali-hydrolyzable nitrogen and available potassium contents, respectively, had negative and positive effects on these two enzyme indices in cropland soils. The results indicate that land use changes strongly affect soil enzyme activities in agricultural land, where TEI provides a sensitive biological indicator for soil quality.

1. Introduction

Soil is a natural resource playing key roles in organic matter (OM) decomposition, nutrient cycling, and water retention and release [1]. Soils are subject to natural or environmental degradation, often accompanied by erosion and leaching. Degradation of soils occurs even without the intervention of human agricultural practices [2, 3], thus threatening this valuable resource. Soil quality, particularly in arid and semiarid areas, needs to be preserved and improved for food security and environmental protection [4]. Previously, a variety of quantitative measures, including soil physicochemical properties indicative of the fundamental context of soil functions, have been extensively used to assess soil quality [5]. However, most soil physicochemical properties change slowly in response to the environmental stress, with significant changes commonly detected only after many years. By contrast, soil biological properties are sensitive indicators for soil quality, which rapidly respond to minor environmental changes in the soil [6].

Soil enzyme activity is a potential indicator of soil quality due to its high sensitivity to external interference and the ease of measurement [7]. The activities of hydrolytic enzymes are frequently measured to evaluate the effect of land use on biological processes in soils related to carbon (C), nitrogen (N), phosphate (P), and sulfur (S) cycling [8, 9]. Soil invertase deserves special recognition because its substrate, sucrose, is one of the most abundant soluble sugars in plants and is partially responsible for the breakdown of plant litter in soils [10]. Urease enzyme is responsible for the hydrolysis of urea fertilizer into NH_3 and CO_2 with a concomitant rise in soil pH [11]. Phosphatases are a broad group of enzymes that catalyze hydrolysis of esters and anhydrides of phosphoric acid. Apart from being a good indicator of soil fertility,

phosphatase enzymes play key roles in the soil system [8]. Additionally, dehydrogenase enzyme activity is commonly used as an indicator of biological activity in soils [11]. Catalase activity in soils is considered to be an indicator of aerobic microbial activity and has been related to both the number of aerobic microorganisms and soil fertility [12].

Enzyme activity generally increases with the rise of soil organic matter (OM) content. Higher enzyme activity indicates larger microbial communities and greater stability of enzymes adsorbed on humic materials [13]. The activities of extracellular enzymes in soil vary significantly with seasons and geographical locations [14], as well as soil depth [15, 16]. Together these findings indicate that soil enzyme activities have broad-scale spatial variability depending on the environmental conditions. Due to seasonal and spatial variability, single biological properties cannot be accurate measures of soil quality [17, 18]. Therefore, multiparametric indices are recommended for environmental impact assessment of agroecosystems and nonagricultural soils [19, 20]. In fact, existing multiparametric indices have been found less sensitive to seasonal variations [21] than single properties.

Conventional statistical procedures assume that variations in soil properties are randomly distributed within sampling units. However, soil properties are continuous variables whose values at any location are expected to vary to different extents according to the direction and spacing of sampling points. Therefore, increasing emphasis has been put on the fact that variations in a soil property are not entirely random within a field. Such spatial structure of soil property should be taken into account in processing data [22]. Knowledge regarding the spatial distribution of soil enzyme activity across the landscape has great implications for interpreting the spatial pattern of OM decomposition and the rate of nutrient mineralization at regional scales [23]. When taking biological properties as the indicator of soil quality, it is necessary to consider the spatial variability of biological properties themselves as well as the underlying influencing factors [24]. Most studies have investigated the spatial variability of soil enzyme activities based on pot and/or microplot experiments [25, 26], while few reports are available at regional scales [22–24, 27–29]. Because the experimental data are not always applicable to actual field conditions, it is necessary to carry out field studies on the spatial variability of soil enzyme activity, especially in arid and semiarid areas associated with serious soil erosion.

The present study was conducted on China's Loess Plateau, which is known for its deep deposits of loess. Frequent and long-term anthropogenic activities have negatively affected the soil environment on the Loess Plateau, resulting in significant degradation of natural vegetation and intense soil erosion [30, 31]. Although a number of surveys have quantified soil erosion and the spatial variability of soil properties in the plateau region [32, 33], there is little information on the spatial distribution of soil enzyme activities across the large-scale landscape. The responses of soil enzyme activities to geographical locations on the Loess Plateau remain unclear, and related research is urged to provide reference data for integrated soil quality management.

The objectives of this study were (1) to quantify the activities of five soil enzymes (invertase, urease, phosphatase, catalase, and dehydrogenase) and selected soil physicochemical properties across an entire county (Changwu) on the Loess Plateau; (2) to investigate the spatial variability of soil enzyme activities in a representative area in the Hilly-Gully Region of Loess Plateau; and (3) to explore the relationships between soil enzyme activities and physicochemical properties using an integrated soil enzyme activity index (TEI) and to compare it with the geometric mean of enzyme activities (GME).

2. Materials and Methods

2.1. Study Area. Changwu County (567 km^2) is located in Xianyang City, Shaanxi Province, China (34°59′–35°8′N, 107°17′–107°58′E) (Figure 1). This county is part of the Hilly-Gully Region of Loess Plateau. It mainly consists of low, rolling hills and deep, narrow gullies. The dominant soil types are Cumuli-Ustic Isohumosols (dark loessial soil) and Loessi-Orthic Primosols (cultivated loessial soils). The altitude ranges from 847 to 1274 m.a.s.l. Changwu has a continental semiarid monsoon climate, with mean monthly temperatures ranging from −9.9°C in January to 24.4°C in July. The annual average temperature is 9.2°C, and the annual precipitation is 573 mm. Heavy rainstorms occasionally occur in this county, mainly between June and September. The driest season is during winter, from December to February.

2.2. Soil Sampling and Chemical Analysis. In late October 2008, soils were sampled at the 0–20 cm depth from 245 locations in 171 villages of Changwu (Figure 1). The samples from croplands were taken randomly in every village and those from apple orchards were randomly taken in every two villages across the county. The sampling locations were identified using a global positioning system (GARMIN GPS72). One soil sample in the cropland consisted of five individual subsamples which were taken randomly within a 10 m radius from each sampling point. Similarly, for a sample in apple orchard, five subsamples were taken from each of three rows. There were 170 soil samples from croplands and 75 from apple orchards. All soil samples were air-dried at room temperature and then passed through a 1.0 mm sieve.

Soil physicochemical analysis was conducted on 0.25 mm sieved samples using routine analytical methods [34]. The OM content was determined by oxidation with $K_2Cr_2O_7$/H_2SO_4. Total N content was analyzed following the Kjeldahl digestion procedure. Alkali-hydrolyzable N content was measured using the alkaline hydrolysis diffusion method. For total P and K analyses, the samples were decomposed with sodium hydroxide (solid) at 720°C and extracted with hot water, followed by molybdenum blue spectrophotometry and atomic absorption spectrophotometry, respectively. Available P was extracted with 0.5 $mol \cdot L^{-1}$ sodium bicarbonate and quantified by molybdenum antimony blue spectrophotometry. Available K was extracted with 1 $mol \cdot L^{-1}$ ammonium acetate and quantified by atomic absorption spectrophotometry. Soil particle size distribution was determined using a pipette method. Cation exchange capacity (CEC) was

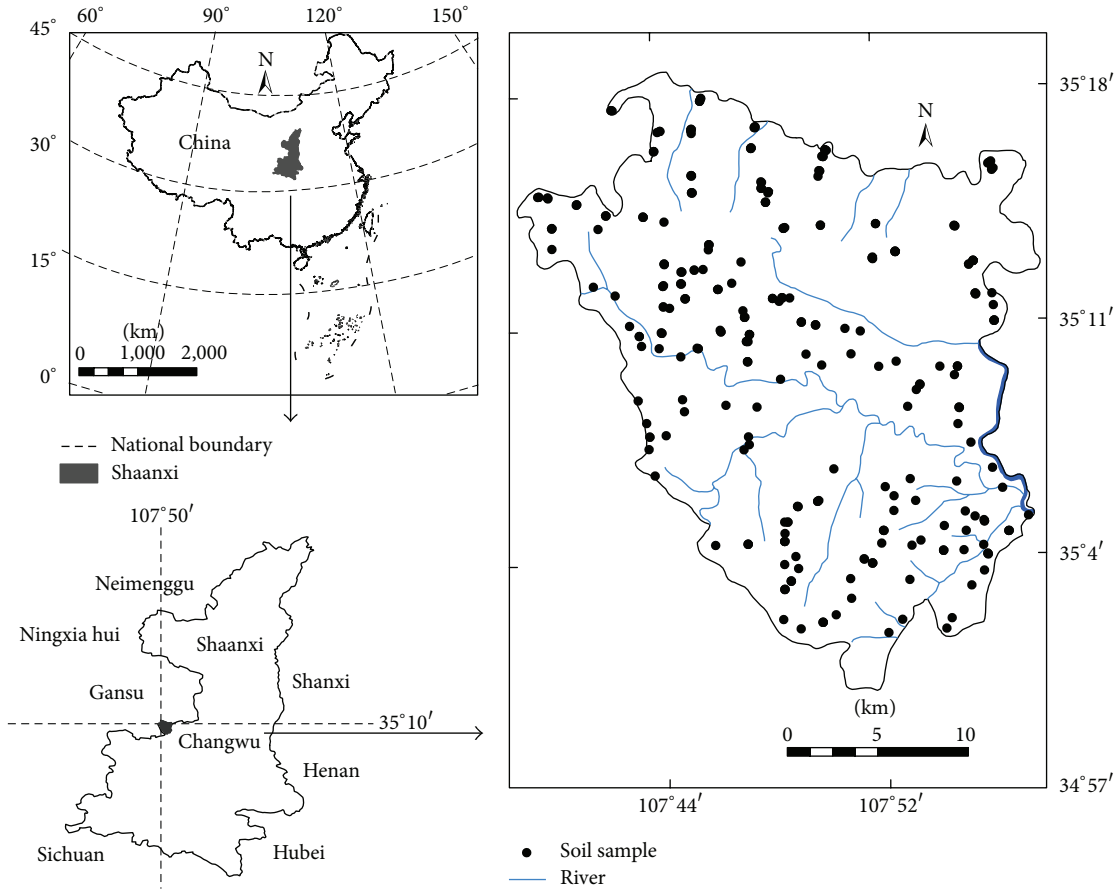

Figure 1: Location of Changwu County and distribution of sampling points in the study area.

quantified using a 1 mol·L^{-1} ammonium acetate exchange method. Soil pH was measured in a 5 : 1 water to soil slurry with an electronic pH meter (Mettler Toledo FE20).

2.3. Soil Enzyme Activity Assays. Enzyme activities were measured with 1 mm sieved soil samples in unbuffered extract solutions meant to simulate the field conditions.

Invertase activity was determined as described by [35]. Briefly, 5 g of air-dried soil was mixed together with 15 mL of 8% sucrose solution, 5 mL of distilled water, and 5 drops of toluene. After incubation for 24 h, at 37°C, the soil solution was centrifuged at 4000 rpm for 5 min and a 1 mL aliquot was transferred to a volumetric flask containing 3 mL of 3,5-dinitrosalicylic acid. The mixture was heated for 5 min. When the solution reached room temperature, glucose content was quantified colorimetrically at 508 nm on a spectrophotometer (INESA 722N). Invertase activity was expressed as μg glucose·g^{-1} soil·h^{-1}.

For the urease activity assay, 5 g of air-dried soil was mixed with 5 mL of toluene, 20 mL of distilled water, and 10 mL of 10% urea solution. After incubation at 37°C for 24 h, the soil suspension was centrifuged at 4000 rpm for 5 min and a 1 mL aliquot was treated with 4 mL of sodium phenol solution (containing 100 mL of 6.6 M phenol solution and 100 mL of 6.8 M NaOH) and 3 mL of 0.9% sodium hypochlorite solution. The ammonium released into the solution was quantified colorimetrically at 578 nm on a spectrophotometer. Urease activity was expressed as μg NH_4-N·g^{-1} soil·h^{-1} [35].

For phosphatase activity assay, 5 g of air-dried soil was mixed with 5 drops of toluene, 10 mL of disodium phenyl phosphate solution, and 10 mL of distilled water. The suspension was incubated for 24 h, at 37°C, and then centrifuged at 4000 rpm for 5 min. The supernatant was colored with 0.25 ammonia-ammonium chloride buffer, at pH 9.6, 0.5 mL of 2% 4-aminoantipyrine, and 0.5 mL of 8% potassium ferrocyanide. The phenol content was determined colorimetrically at 510 nm on a spectrophotometer. Phosphatase activity was expressed as μg phenol·g^{-1} soil·h^{-1} [35].

Catalase and dehydrogenase activities were assayed using the method of [11]. For catalase activity assay, 2 g of air-dried soil was mixed with 40 mL of distilled water and 5 mL of 0.3% H_2O_2. The soil slurry was shaken for 20 min at 150 rpm. The remaining peroxide was stabilized by adding 5 mL of 1.5 M sulfuric acid and the solution was then immediately centrifuged at 4000 rpm for 5 min. The peroxide in the supernatant was titrated with 0.05 M $KMnO_4$. Catalase activity was expressed as mL $KMnO_4$·g^{-1} soil·h^{-1}.

For dehydrogenase activity assay, 3 g of air-dried soil was mixed with a 3% triphenyl tetrazolium chloride solution

as the substrate and 1.25 to 1.75 mL of distilled water. The soil slurry was mixed thoroughly and incubated at 37°C for 24 h. Thereafter, triphenyl formazan was extracted with methanol and quantified by colorimetric analysis at 485 nm. Dehydrogenase activity was expressed as μg TPF·g^{-1} soil·h^{-1} [11] and all enzyme activities were calculated as the mean of two replicates.

2.4. Statistical and Geostatistical Analyses. Descriptive statistics (arithmetic mean, maximum and minimum, median, standard deviation, coefficient of variation, skewness, and kurtosis), and Pearson product moment correlation analysis were conducted using SPSS 18 for Windows (SPSS Inc., Chicago, IL, USA). Data normality was tested by one-sample Kolmogorov-Smirnov test.

The semivariogram analysis was used to assess the spatial structure of the studied variables. Then, the Ordinary Kriging interpolation was used to estimate the unknown values at unsampled locations and to map the spatial variability of soil properties and TEI [36]. The sample semivariogram was calculated using

$$\gamma(h) = \frac{1}{2N(h)} \sum_{i=1}^{N(h)} \left[Z(x_i) - Z(x_i + h)\right]^2, \quad (1)$$

where $\gamma(h)$ is the semivariance for interval distance class h, that is, the distance separating sample points x_i and $x_i + h$, $N(h)$ is the number of sample couples for the lag interval h, and $Z(x_i)$ and $Z(x_i + h)$ are measured values at points i and $i + h$, respectively.

Three variogram models (spherical, Gaussian, and exponential) were fitted to the sample semivariograms in this research. The best fitted model should have the smallest residual sum of squares (RSS) and the largest coefficient of determination (R^2) between predicted values and the measured values of soil properties. Then the best fitted models were used to provide input parameters for Kriging interpolation. The estimated values were obtained using

$$Z^*(x_0) = \sum_{i=1}^{n} \lambda_i Z(x_i), \quad (2)$$

where $Z^*(x_0)$ is the predicted value at point x_0, $Z(x_i)$ are the measured values at sampling location x_i, λ_i is the weight to be assigned to sample x_i, and n is the number of sites within the neighborhood searched for the interpolation.

Here log or Box-Cox transformation was used when the original data was not normally distributed. Semivariance calculations of the soil properties were conducted based on the maximum sampling distance of 17 km, which was divided into 15 lag distance classes separated by an average of 1.1 km. No significant anisotropy was considered, because the anisotropy ratio was less than 2.5 [37]. The cross validation procedure was used to assess the models fitted to experimental semivariograms. After a semivariogram model has been obtained, the Kriging technique was applied to obtain a map of estimates. The geostatistical analysis was performed in ArcGIS (version 10.0, ERIS, Redlands, CA, USA).

2.5. Calculation of Soil Enzyme Activity Indices. The integrated total enzyme activity index (TEI) was calculated using the following equation [20]:

$$\mathrm{TEI} = \sum_{n=1}^{i} \frac{X_i}{\overline{X_i}} \quad (n = 1, 2, 3, 4, 5), \quad (3)$$

where X_i is the activity of soil enzyme i and $\overline{X_i}$ is the mean activity of enzyme i in all samples.

The geometric mean of enzyme activities (GME) was calculated by (4) discussed elsewhere [38] as

$$\mathrm{GME} = \sqrt[5]{\mathrm{Invertase} \times \mathrm{Urease} \times \mathrm{Phosphatase} \times \mathrm{Catalase} \times \mathrm{Dehydrogenase}}. \quad (4)$$

3. Results

3.1. Descriptive Statistics of Soil Properties. The OM content of surface soil samples averaged 12.57 g·kg^{-1} and the total N concentration averaged 0.89 g·kg^{-1} across the county. Both parameters varied substantially, from 5.16 to 18.25 g·kg^{-1} for OM content and from 0.28 to 1.37 g·kg^{-1} for total N content. The soils were mostly fine in texture, with an average clay content of 33%. Soil pH ranged from 7.80 to 9.09, with a mean of 8.59 (Table 1).

Invertase activity of surface soil samples (0–20 cm depth) ranged from 102 to 707 μg glucose·g^{-1} h^{-1}, with a mean of 379 μg glucose·g^{-1} h^{-1}. Urease activity ranged from 3.16 to 108 μg NH_4^+-N·g^{-1} h^{-1}, with a mean of 25.0 μg NH_4^+-N·g^{-1} h^{-1}. Phosphatase activity ranged from 15.1 to 71.6 μg phenol·g^{-1} soil·h^{-1}, with a mean of 34.88 μg phenol·g^{-1} soil·h^{-1}. Catalase activity ranged from 4.58 to 13.1 mL $KMnO_4$·g^{-1} soil·h^{-1}, with a mean of 8.79 mL $KMnO_4$·g^{-1} soil·h^{-1}. Dehydrogenase activity ranged from 0.15 to 3.06 μg TPF·g^{-1} h^{-1}, with a mean of 25.0 μg TPF·g^{-1} h^{-1} (Table 1). The coefficients of variation (CV) were 28% for invertase activity, 53% for urease activity, 25% for phosphatase activity, 22% for catalase activity, and 49% for dehydrogenase activity.

The activities of all enzymes and the levels of OM, AN, AK, and CEC were normally distributed (one-sample Kolmogorov-Smirnov test, $P > 0.05$). Total N and pH levels were negatively skewed and nonnormally distributed, whereas total P, total K, available P, and clay contents were positively skewed and nonnormally distributed. The underlying reasons for normal or nonnormal distribution of these variables were unknown, but management and spatial effects seemed to play a role.

3.2. Relationships of Soil Physicochemical Properties and Enzymatic Activities. Results of the correlation analysis in all soil samples showed that the OM content was significantly correlated with invertase, urease, phosphatase, and dehydrogenase activities ($P < 0.01$) but not with catalase activity ($P > 0.05$). The alkali-hydrolyzable N content was strongly

Table 1: Descriptive statistics of selected soil physicochemical properties and enzyme activities in surface horizon (0–20 cm) of Changwu County, Shaanxi Province, China ($n = 245$).

Parameters	Range	Minimum	Maximum	Mean	Standard deviation	K-S Z Asymp. Sig. (2-tailed)		Skewness	Kurtosis
OM/g kg^{-1}	13.09	5.16	18.25	12.57	2.22	1.21	0.11	−0.52	1.4
Total N/g kg^{-1}	1.09	0.28	1.37	0.89	0.19	2.64	0.00	−0.46	0.78
Total P/g kg^{-1}	1.45	0.17	1.62	0.67	0.26	2.51	0.00	1.14	1.95
Total K/g kg^{-1}	11.42	16.68	28.1	22.23	1.95	2.23	0.00	0.19	0.1
Alkali-hydrolyzable N/mg kg^{-1}	85.75	19.25	105	59.68	15.72	1.01	0.26	0.02	−0.04
Available P/mg kg^{-1}	46.71	2.54	49.25	17.06	10.51	1.66	0.01	1.53	1.88
Available K/mg kg^{-1}	450	63.13	513.13	199.36	94.22	0.76	0.62	0.8	−0.09
CEC/cmol kg^{-1}	16.84	6.68	23.52	13.91	3.29	1.08	0.19	0.73	−0.12
Clay/%	33.09	17.41	50.5	33.19	5.14	1.59	0.01	0.51	2.27
pH	1.20	7.89	9.09	8.59	0.23	1.81	0.00	−0.64	0.14
Invertase/μg glucose·g^{-1} soil·h^{-1}	605.1	102.07	707.18	379.26	106.34	0.79	0.55	0.32	0.04
Urease/μg NH_4-N g^{-1} soil·h^{-1}	104.7	3.16	107.86	37.86	20.07	1.38	0.05	0.77	0.3
Phosphatase/μg phenol·g^{-1} soil·h^{-1}	56.55	15.12	71.67	34.88	8.83	0.79	0.57	0.57	1.24
Catalase/mL $KMnO_4$·g^{-1} soil·h^{-1}	8.55	4.58	13.13	8.79	1.97	0.86	0.44	0.11	−0.64
Dehydrogenase/μg TPF·g^{-1} soil·h^{-1}	2.91	0.15	3.06	1.29	0.63	0.99	0.28	0.48	−0.28

K-S Z, Kolmogorov-Smirnov Z; OM, organic matter; N, nitrogen; P, phosphorous; K, potassium; and CEC, cation exchange capacity.

correlated with invertase, urease, phosphatase, catalase, and dehydrogenase activities ($P < 0.01$). No significant correlation was found between soil pH and phosphatase activity ($P > 0.05$). However, soil pH was positively correlated with dehydrogenase activity ($P < 0.05$) and negatively correlated with invertase, urease, and catalase activities ($P < 0.01$; Table 2). Additionally, soil phosphatase activity was extremely significantly correlated with invertase ($r = 0.409$, $P < 0.01$) and urease activities ($r = 0.228$, $P < 0.01$), and catalase activity was significantly correlated with invertase ($r = 0.146$, $P < 0.05$) and urease activities ($r = 0.144$, $P < 0.05$). Soil dehydrogenase activity was significantly correlated with invertase ($r = 0.519$, $P < 0.01$), phosphatase ($r = 0.649$, $P < 0.01$), and catalase activities ($r = -0.174$, $P < 0.01$).

3.3. Spatial Structure of Soil Properties. Semivariance analysis showed that the soil properties generally had spatial dependence (Table 3). The semivariograms all exhibited spatial structure. The experimental semivariograms for soil dehydrogenase activity, available K content, CEC level, and clay content were fitted by exponential models. The experimental semivariogram for total K content was fitted by a spherical model. The experimental semivariograms for other soil properties were fitted by the Gaussian models.

The spatial dependence of the data was confirmed by total variance (Sill) composed of structural (C) and nugget variances (Co). Nugget to sill ratio ([Co/Sill]) for soil enzyme activities was 67% and that for soil physicochemical properties was 54%. Nugget to sill ratios of urease and dehydrogenase activities accounted for 85% and 71% of the total variance, respectively. These values were significantly higher than sill and nugget effects. Available K content had the largest nugget to sill ratio among all soil properties. The effective ranges of phosphatase and urease activities were greater than those of invertase, catalase, and dehydrogenase activities (3.9, 5.3, and 2 km, resp.).

The Kriging maps showed that soil OM, total N, and CEC levels showed similar spatial distribution patterns, with the lowest values occurring in the center of the county (Figures 2(a), 2(b), and 2(h)). Soil alkali-hydrolyzable N, available P contents, and pH value were highest in the central and southern parts and lowest in the northern part of Changwu (Figures 2(e), 2(f), and 2(j)). In contrast, total P content increased from the south to the northwest (Figure 2(c)). Soil total K, available K, and clay contents had no obvious variation trends across the county (Figures 2(d), 2(g), and 2(i)). The distribution of these three properties did not correspond to the topographical feature of the study area or to the spatial distribution of the other soil properties. Soil invertase, urease, and catalase activities were highest in the northern area in Changwu County, followed by the central and southern areas (Figures 2(k), 2(l), and 2(n)). Soil phosphatase activity was highest in the center of the county (Figure 2(m)). Dehydrogenase activity decreased from the southwest to the northeast (Figure 2(o)).

3.4. Enzymatic Activity Indices. A main novelty of this study was to introduce the integrated index TEI as a dimensionless parameter for easy comparison of the combined enzyme activity and the quality of each soil sample. We also compared this index with the commonly used GME index. The TEI values of total, orchard, and cropland soil samples varied from 1.87 to 7.43, 2.7 to 7.4, and 1.8 to 7.4, with a median value of 5.07, 4.9, and 5.07, respectively. The mean TEI value of all soil samples was estimated to be 5. The GME values of total, orchard, and cropland soil samples varied from 6.9 to 33, 10

Table 2: Correlation coefficients (Pearson r value) between soil physicochemical properties and enzyme activities in surface horizon (0–20 cm) of Changwu County ($n = 245$).

	Invertase	Urease	Phosphatase	Catalase	Dehydrogenase
OM	0.547**	0.386**	0.580**	−0.06	0.469**
Total N	0.300**	0.431**	0.243**	0.255**	0.03
Total P	−0.06	0.317**	−0.176**	0.315**	−0.325**
Total K	0.11	0.11	0.12	−0.213**	0.246**
Alkali-hydrolyzable N	0.393**	0.192**	0.486**	−0.462**	0.552**
Available P	0.05	0.366**	0.09	−0.186**	−0.02
Available K	0.00	0.358**	0.147*	0.09	−0.06
CEC	0.11	0.291**	−0.13	0.718**	−0.322**
Clay	0.11	0.127*	0.02	0.297**	−0.10
pH	−0.167**	−0.380**	0.05	−0.529**	0.154*

* and ** represent statistical significances at the 5% and 1% levels, respectively; OM, organic matter; N, nitrogen; P, phosphorous; K, potassium; and CEC, cation exchange capacity.

Table 3: Parameters for variogram models of soil physicochemical properties, enzyme activities, and TEI in surface horizon (0–20 cm) of Changwu County ($n = 245$).

Parameters	Model	C_0	$C_0 + C$	$[C_0/(C_0 + C)]100$	Range/km	RMSS
OM	Gaussian	3.03	4.36	69.53	9.3	1.09
Total N	Gaussian	0.02	0.04	57.05	7.49	1.05
Total P	Gaussian	0.04	0.05	77.74	6.26	1.05
Total K	Spherical	0.89	3.07	28.83	3.31	1.01
Alkali-hydrolyzable N	Gaussian	100.93	243.7	41.41	11.33	1.06
Available P	Gaussian	0.26	0.32	81.78	15.63	1.08
Available K	Exponential	0.19	0.21	89.89	10.27	1.01
CEC	Exponential	0.01	0.04	31.06	10.46	1.01
Clay	Exponential	7.18	24.64	29.14	5.23	0.97
pH	Gaussian	0.02	0.05	37.78	9.36	1.03
Invertase	Gaussian	16.89	27.93	60.45	3.89	1.00
Urease	Gaussian	8.87	10.4	85.34	9.36	1.02
Phosphatase	Gaussian	1.59	2.6	61.31	12.99	1.01
Catalase	Gaussian	1.32	2.44	54.27	5.33	0.98
Dehydrogenase	Exponential	0.19	0.27	71.26	1.99	0.96
TEI	Gaussian	0.65	1.30	50.15	0.84	1.07

C_0, nugget variance; C, structural variance; $C_0 + C$, sill; RMSS, root-mean-square standardized; OM, organic matter; N, nitrogen; P, phosphorous; K, potassium; and CEC, cation exchange capacity.

to 30, and 22 to 33, with a median value of 21.6, 20.8 and 22.1, respectively. The mean GME values of different groups of soil samples were estimated to be 21.3, 20.5, and 21.7, respectively.

The TEI and GME values were most correlated with the activities of invertase, urease, phosphatase, catalase, and dehydrogenase, except orchard soil catalase activity (Table 4). Pearson correlation analysis showed that TEI and GME were positively correlated with soil OM, total N, and alkali-hydrolyzable N contents but negatively correlated with pH level. In addition, the TEI and GME values of total and orchard soil samples were positively correlated with total K content. The TEI and GME values of total and cropland soil samples were positively correlated with available P and K contents. The TEI values of total and cropland soil samples were positively correlated with CEC (Table 4).

Multivariate regression analysis was carried out to investigate the relationship between soil physicochemical properties and enzyme activity indices (TEI and GME) (Table 5). Among the soil properties measured in this equation, soil OM content had the strongest positive effect while soil pH had a negative effect on the two indices. Additionally, total P content had a positive effect on TEI and GME in orchard soils. The alkali-hydrolyzable N and available K contents had negative and positive effects on TEI and GME in cropland soils while the alkali-hydrolyzable N and available P contents had positive and negative effects on both enzyme activity indices in total soils.

4. Discussion

4.1. Spatial Structure of Soil Enzyme Activities. Wilding [39] previously described a classification scheme for identifying the variability of soil properties based on their CV values.

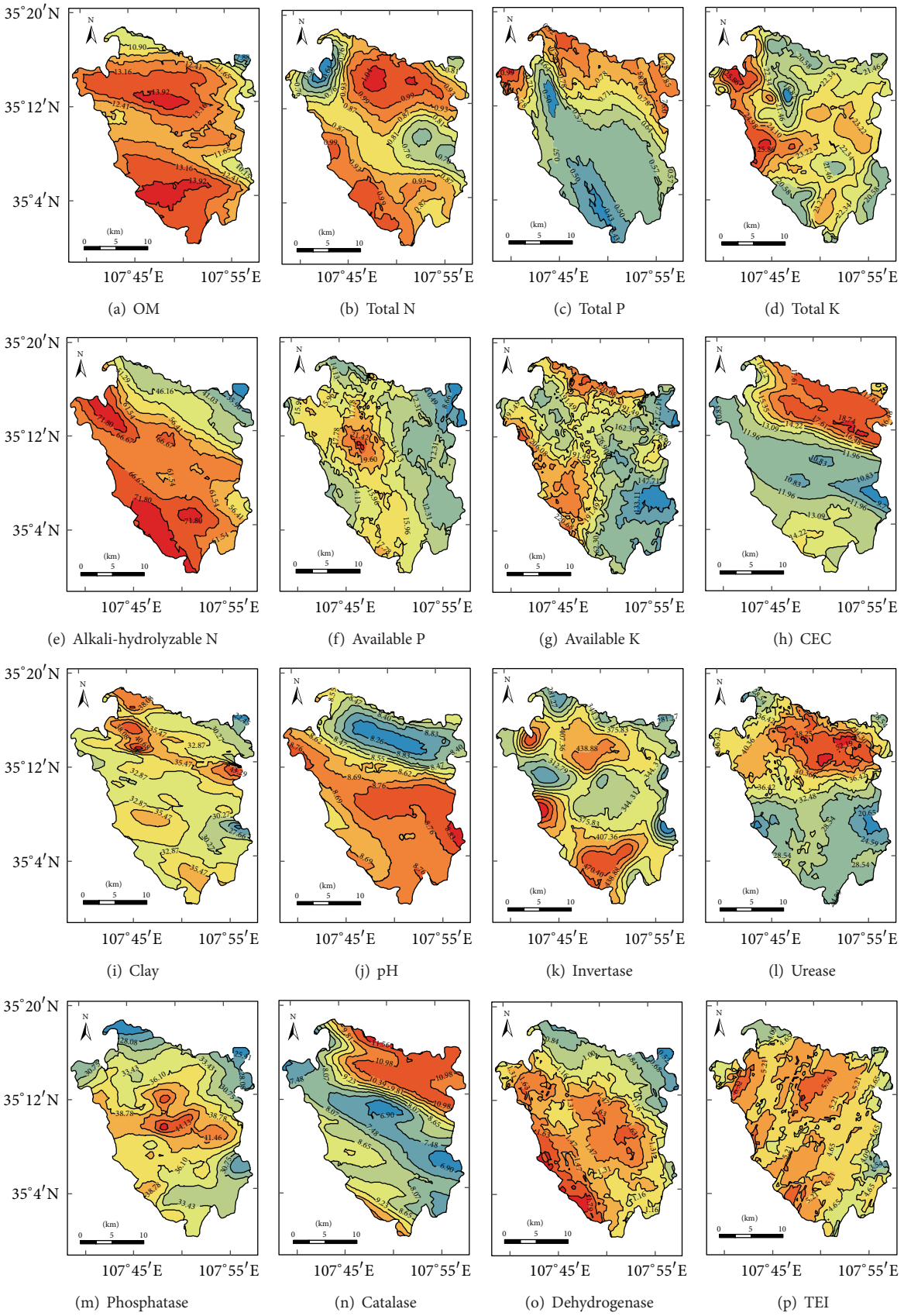

Figure 2: Spatial distribution patterns of soil physicochemical properties and enzyme activities and TEI in surface horizon of Changwu County.

Table 4: Pearson correlation coefficients between soil physicochemical properties and enzyme activity indices in surface horizon (0–20 cm) of Changwu County.

	Samples					
	Orchard ($n = 75$)		Cropland ($n = 170$)		Total ($n = 245$)	
Enzyme activity index	TEI	GME	TEI	GME	TEI	GME
OM	0.566**	0.569**	0.696**	0.693**	0.659**	0.655**
Total N	0.299**	0.315**	0.459**	0.448**	0.407**	0.395**
Total P	−0.103	−0.09	0.095	0.054	0.021	−0.021
Total K	0.291*	0.252*	0.137	0.118	0.179**	0.142*
Alkali-hydrolyzable N	0.314**	0.287*	0.543**	0.574**	0.459**	0.461**
Available P	0.074	0.086	0.353**	0.355**	0.187**	0.139*
Available K	0.217	0.217	0.267**	0.238**	0.235**	0.175**
CEC	0.092	0.109	0.174*	0.137	0.148*	0.121
Clay	0.063	0.057	0.12	0.091	0.103	0.086
pH	−0.280*	−0.294*	−0.277**	−0.259**	−0.271**	−0.243**
Invertase	0.707**	0.688**	0.655**	0.661**	0.663**	0.673**
Urease	0.501**	0.486**	0.739**	0.699**	0.624**	0.559**
Phosphatase	0.749**	0.751**	0.725**	0.729**	0.712**	0.737**
Catalase	0.149	0.174	0.267**	0.232**	0.225**	0.219**
Dehydrogenase	0.811**	0.801**	0.681**	0.705**	0.690**	0.729**
GME	0.990**	1	0.986**	1	0.981**	1

∗ and ∗∗ represent statistical significances at the 5% and 1% levels, respectively; OM, organic matter; N, nitrogen; P, phosphorous; K, potassium; CEC, cation exchange capacity; GME, geometric mean of enzyme activities; and TEI, total enzyme activity.

Table 5: Multiple linear regressions between soil physicochemical properties and enzyme activity indices in surface horizon (0–20 cm) of Changwu County.

Samples	Multiple regression equation	R^2	P
Orchard ($n = 75$)	$\log_{10}\text{TEI} = 1.214 + 0.722 \times \log_{10}\text{OM} - 0.157 \times \text{pH} - 0.131 \times \log_{10}\text{Total P}$	0.491	<0.001
	$\log_{10}\text{GME} = 1.911 + 0.792 \times \log_{10}\text{OM} - 0.176 \times \text{pH} - 0.136 \times \log_{10}\text{Total P}$	0.483	<0.001
Cropland ($n = 170$)	$\log_{10}\text{TEI} = 1.116 + 0.409 \times \log_{10}\text{OM} - 0.197 \times \text{pH} - 0.358 \times \log_{10}\text{AN} + 0.09 \times \log_{10}\text{Available K}$	0.63	<0.001
	$\log_{10}\text{GME} = 1.788 + 0.399 \times \log_{10}\text{OM} - 0.216 \times \text{pH} - 0.444 \times \log_{10}\text{AN} + 0.084 \times \log_{10}\text{Available K}$	0.628	<0.001
Total ($n = 245$)	$\log_{10}\text{TEI} = 0.736 + 0.607 \times \log_{10}\text{OM} - 0.126 \times \text{pH} + 0.38 \times \log_{10}\text{AN} - 0.061 \times \log_{10}\text{Available P}$	0.53	<0.001
	$\log_{10}\text{GME} = 1.592 + 0.638 \times \log_{10}\text{OM} - 0.159 \times \text{pH} + 0.256 \times \log_{10}\text{AN} - 0.046 \times \log_{10}\text{Available P}$	0.528	<0.001

According to Wilding's classification, the CV values of soil invertase, phosphatase, and catalase activities are relatively small (22–28%), whereas those of urease and dehydrogenase activities (49–53%) are at the medium level. Soil enzyme activities have close relationships with soil biology and are sensitive in discriminating among soil management practices, such as fertilization by means of animal manure or green manures/crop residues and municipal refuse amendment, as well as among tillage treatments. However, a previous report indicated that dehydrogenase and cellulose activities in the surface soil horizon of an arable land (2 km^2) had small CV values (18% and 26%, resp.) [26]. Bonmati et al. [25] observed that the CV values for soil urease, phosphatase, and protease activities ranged from 28% to 60% in a 15 m × 40 m meadow. Smith and Halvorson [24] reported the CV values of 33% for phosphatase activity and 36% for dehydrogenase activity in agricultural land ($n = 220$). These findings confirmed that the spatial variability of soil enzyme activities varied in different ecosystems.

Knowledge regarding the spatial variability of soil biological properties is critical for the management and improvement of agricultural soil quality. Reliable information on the range of spatial relationships makes it possible to define the sampling strategy needed for accurately mapping soil biological properties [22]. In the present study, the best model of semivariogram varied depending on the kinds of soil enzymes, and the effective ranges of soil enzymes decreased in the order of phosphatase → urease → catalase → invertase → dehydrogenase (Table 3). Semivariograms for enzyme activities exhibited spatial correlated distances that ranged from 2 to 13 km (Table 3). Likewise, Aşkın and Kızılkaya [22] recently had reported that the zone (4500 × 4500 m) of influence of soil urease activity was approximately 19.3 km. In general, however, field-scale (50 ha) studies

indicate that the effective ranges of soil dehydrogenase and cellulose activities are 84.3–93.3 m [26]. The difference among those studies may depend highly on the size of sample area and the sampling distance. Both soil properties and scale effect have strong effects on the spatial distribution of enzyme activity. The spatial structure of soil properties is complex and contrasting range values have been reported. Therefore, future research should consider the size of study area and the distances between sampling points. The most appropriate sampling scheme and the separation distance between sampling points for future data collection are highly important and should be determined in preliminary studies [23].

The ratio of nugget to sill can be used as a criterion to classify the strength of the spatial dependence of soil properties (<25%, strong spatial dependence; 25–75%, moderate spatial dependence; and >75%, weak spatial dependence) [40]. In the present study, the nugget to sill ratios descended in the order of urease activity (85%) > dehydrogenase activity (71%) > phosphatase activity (61%) > invertase activity (60%) > catalase activity (54%). The activities of invertase, phosphatase, dehydrogenase, and catalase are more spatially dependent than urease activity. The moderate spatial dependence of invertase, phosphatase, dehydrogenase, and catalase activities indicates that these enzyme activities are primarily controlled by specific geological factors and have better correlation. The weak spatial dependence of soil urease activities indicates that the environment has a stronger impact than geographical distance on the spatial distribution of relevant microbial communities. Similarly, high nugget effects have been observed for dehydrogenase activity in no-till field which was cropped with corn (*Zea mays* L.) and soybean (*Glycine max* (L.) Merr.) (62.7%) [40], Cambisol soil under winter wheat (68.4%) [26], and no-till wheat crop soil (70.7%) [41]. The variability of weakly spatially dependent parameters may be caused by agricultural practices, such as application of fertilizers and tillage, whereas strongly spatially dependent parameters are influenced by variations in innate soil characteristics such as texture and mineralogy [40]. The differences in spatial dependency of soil enzyme activities may be related to different spatial distribution of various microbial groups and soil fertilizer, which reflects the influence of different soil topography, vegetation, and agricultural practices.

Visualizing the spatial distribution of soil biotic components contributes to the understanding of spatial structure and thus may help with accurate prediction and mapping of soil microbial properties [42]. The activities of five soil enzymes in Changwu County showed patchy distribution related to soil physicochemical properties tested (Figure 2). For example, invertase, urease, and catalase activities were generally highest in the northern part of Changwu. As for soil properties, the OM, total N, total P, and CEC levels were high while the alkali-hydrolyzable N, available P, available K, and soil pH levels were relatively low in the northern part of Changwu. Spatially different distribution of the enzymatic activity is related to the variations in soil OM content, the activity of related living organisms, and the intensity of biological processes [22]. Therefore, it is not surprising that microbial properties show cross-dependence among themselves and with other soil properties depending on the ecosystem [42]. Understanding of the spatial distribution of physicochemical indicators for soil quality is an important step for explaining the spatial variability of biological parameters. The statistical results analysis showed that there were highly significant correlations between soil enzyme activities (invertase, urease, phosphatase, catalase, and dehydrogenase) and several physicochemical properties (OM, total N, total P, alkali-hydrolyzable N, CEC, and pH levels) in Changwu. These strong relationships confirm that soil enzyme activities provide a meaningful integrative measure of soil physicochemical properties and biological soil fertility, which thus may play a role in monitoring soil biological quality [43].

4.2. Implications for Assessing Soil Quality by a Biological or an Integrated Enzyme Activity Index. Results of the multivariate regression analysis indicated that soil OM and pH levels, respectively, had stronger positive and negative effects than other soil properties on TEI and GME. Meanwhile, TEI and GME had stronger positive correlation with soil physicochemical properties than individual enzyme activities (Table 4). Generally, the OM content positively affects extracellular enzyme activity in soil [42, 43]. The adsorption of enzyme molecules to soil particles and OM materials possibly protected the enzymes against soil pH changes. Alternatively, this could be attributed to the dependence of microbial activity (hence enzyme production) on the supply of organic substrate (organic C availability). In such cases, the organic C content and enzyme activity would be related to each other via microbial biomass [26].

Soil biological properties are highly sensitive to environmental stress and thus can be used to assess quality. Any soil quality index should include several biological variables so as to better reflect the complex processes affecting soil quality and to compensate for the wide variations occurring in individual properties [44]. For instance, the TEI values showed more similar spatial distribution patterns with soil physicochemical properties (Figure 2(p), $n = 245$). As the TEI index introduced in this study involves only five soil enzymes, further large-scale studies are recommended to verify the applicability of TEI as an integrated activity index of soil enzymes in different ecosystems. A more comprehensive and accurate biological indicator for changes in soil quality can be obtained by taking into consideration more enzyme components and/or microbial parameters that are indicative of key soil biological processes. These indicators must be quantified on a local and landscape basis as a means for making small-scale and regional management decisions [24]. In view of the limitations of single soil biological properties, it is recommended to develop and use multiparametric indices such as TEI for providing and integrating more information on soil quality.

5. Conclusion

Results of the conventional and geostatistical analyses indicate that the spatial variability of agricultural soil properties is complex in Changwu County. Spatial distribution maps show that soil invertase, urease, and catalase activities are high in

the northern area, soil phosphatase activity is high in the central area, and soil dehydrogenase activity is high in the southwestern area of the county. The spatial patterns of soil quality are better reflected using an integrated soil enzyme index, which provides a sensitive biological indicator for soil quality as compared with the single enzyme activities.

Conflict of Interests

The authors declare that there is no conflict of interests regarding the publication of this paper.

Authors' Contribution

Xiangping Tan contributed to data analysis, laboratory assay, and paper preparation; Baoni Xie contributed to data analysis; Junxing Wang contributed to laboratory assay; Wenxiang He contributed to experiment design and paper preparation and revision; Xudong Wang and Gehong Wei provided paper revision and experiment design.

Acknowledgments

This work was supported by the National Hi-tech Research and Development Program of China (no. 2012AA101402), the Chinese Universities Scientific Fund, and the Knowledge Innovation Project of Chinese Academy of Sciences (KSCX-YW-09-07).

References

[1] K. Ritz, H. I. J. Black, C. D. Campbell, J. A. Harris, and C. Wood, "Selecting biological indicators for monitoring soils: a framework for balancing scientific and technical opinion to assist policy development," *Ecological Indicators*, vol. 9, no. 5, pp. 1212–1221, 2009.

[2] M. M. Mikha and C. W. Rice, "Tillage and manure effects on soil and aggregate-associated carbon and nitrogen," *Soil Science Society of America Journal*, vol. 68, no. 3, pp. 809–816, 2004.

[3] K. Jin, S. Sleutel, D. Buchan et al., "Changes of soil enzyme activities under different tillage practices in the Chinese Loess Plateau," *Soil and Tillage Research*, vol. 104, no. 1, pp. 115–120, 2009.

[4] K. Nosrati, "Assessing soil quality indicator under different land use and soil erosion using multivariate statistical techniques," *Environmental Monitoring and Assessment*, vol. 185, no. 4, pp. 2895–2907, 2013.

[5] E. Puglisi, A. A. M. Del Re, M. A. Rao, and L. Gianfreda, "Development and validation of numerical indexes integrating enzyme activities of soils," *Soil Biology and Biochemistry*, vol. 38, no. 7, pp. 1673–1681, 2006.

[6] J. A. Pascual, C. Garcia, T. Hernandez, J. L. Moreno, and M. Ros, "Soil microbial activity as a biomarker of degradation and remediation processes," *Soil Biology and Biochemistry*, vol. 32, no. 13, pp. 1877–1883, 2000.

[7] A. K. Bandick and R. P. Dick, "Field management effects on soil enzyme activities," *Soil Biology and Biochemistry*, vol. 31, no. 11, pp. 1471–1479, 1999.

[8] R. P. Dick, "Soil enzyme activities as indicators of soil quality," in *Defining Soil Quality for a Sustainable Environment*, J. W. Doran, D. C. Coleman, D. F. Bezdicek, and B. A. Stewart, Eds., pp. 107–124, SSSA, Madison, Wis, USA, 1994.

[9] E. Kandeler and E. Murer, "Aggregate stability and soil microbial processes in a soil with different cultivation," *Geoderma*, vol. 56, no. 1–4, pp. 503–513, 1993.

[10] W. T. Frankenberger Jr. and J. B. Johanson, "Factors affecting invertase activity in soils," *Plant and Soil*, vol. 74, no. 3, pp. 313–323, 1983.

[11] R. G. Burns, *Soil Enzymes*, Academic Press, London, UK, 1978.

[12] C. Trasar-Cepeda, F. Camiña, M. C. Leirós, and F. Gil-Sotres, "An improved method to measure catalase activity in soils," *Soil Biology and Biochemistry*, vol. 31, no. 3, pp. 483–485, 1999.

[13] S. Marinari and L. V. Antisari, "Effect of lithological substrate on microbial biomass and enzyme activity in brown soil profiles in the northern Apennines (Italy)," *Pedobiologia*, vol. 53, no. 5, pp. 313–320, 2010.

[14] J. Paz-Ferreiro, C. Trasar-Cepeda, M. C. Leirós, S. Seoane, and F. Gil-Sotres, "Effect of management and climate on biochemical properties of grassland soils from Galicia (NW Spain)," *European Journal of Soil Biology*, vol. 46, no. 2, pp. 136–143, 2010.

[15] C. Wittmann, M. A. Kähkönen, H. Ilvesniemi, J. Kurola, and M. S. Salkinoja-Salonen, "Areal activities and stratification of hydrolytic enzymes involved in the biochemical cycles of carbon, nitrogen, sulphur and phosphorus in podsolized boreal forest soils," *Soil Biology and Biochemistry*, vol. 36, no. 3, pp. 425–433, 2004.

[16] E. Alarcón-Gutiérrez, C. Floch, C. Augur, J. L. Petit, F. Ziarelli, and S. Criquet, "Spatial variations of chemical composition, microbial functional diversity, and enzyme activities in a Mediterranean litter (Quercus ilex L.) profile," *Pedobiologia*, vol. 52, no. 6, pp. 387–399, 2009.

[17] R. P. Dick and V. V. S. R. Gupta, "A conceptual model for the role of abiontic soil enzymes in microbial ecology: a potential analogue for soil quality," in *Soil Biota: Management in Sustainable Farming Systems*, C. E. Pankhurst, B. M. Doube, V. V. S. R. Gupta, and P. R. Grace, Eds., pp. 167–168, CSIRO Publications, East Melbourne, Australia, 1994.

[18] P. Nannipieri, S. Grego, and B. Ceccanti, "Ecological significance of biological activity," in *Soil Biochemistry*, J. M. Bollag and G. Stotzky, Eds., pp. 293–355, Marcel Dekker, New York, NY, USA, 1990.

[19] J. Paz-Ferreiro and S. Fu, "Biological indices for soil quality evaluation: perspectives and limitations," *Land Degradation & Development*, 2014.

[20] W. He, X. Tan, X. Wang, M. Tang, and M. Hao, "Study on total enzyme activity index in soil," *Acta Pedologica Sinica*, vol. 47, no. 6, pp. 211–215, 2010 (Chinese).

[21] J. Paz-Ferreiro, C. Trasar-Cepeda, M. del Carmen Leirós, S. Seoane, and F. Gil-Sotres, "Intra-annual variation in biochemical properties and the biochemical equilibrium of different grassland soils under contrasting management and climate," *Biology and Fertility of Soils*, vol. 47, no. 6, pp. 633–645, 2011.

[22] T. Aşkın and R. Kızılkaya, "The spatial variability of urease activity of surface agricultural soils within urban area," *Journal of Central European Agriculture*, vol. 6, no. 2, pp. 161–166, 2005.

[23] A. Piotrowska, J. Długosz, B. Namysłowska-Wilczyńska, and R. Zamorski, "Field-scale variability of topsoil dehydrogenase and cellulase activities as affected by variability of some physicochemical properties," *Biology and Fertility of Soils*, vol. 47, no. 1, pp. 101–109, 2011.

[24] J. L. Smith and J. J. Halvorson, "Field scale studies on the spatial variability of soil quality indicators in Washington State, USA," *Applied and Environmental Soil Science*, vol. 2011, Article ID 198737, 7 pages, 2011.

[25] M. Bonmati, B. Ceccanti, and P. Nanniperi, "Spatial variability of phosphatase, urease, protease, organic carbon and total nitrogen in soil," *Soil Biology & Biochemistry*, vol. 23, no. 4, pp. 391–396, 1991.

[26] S. Smoliński, J. Długosz, A. Piotrowska, and R. Zamorski, "Spatial variability of soil dehydrogenases and cellulases activities in a field scale," *Polish Journal of Soil Science*, vol. 41, no. 1, pp. 73–80, 2008.

[27] Y. Gao, P. Zhou, L. Mao, Y. Zhi, C. Zhang, and W. Shi, "Effects of plant species coexistence on soil enzyme activities and soil microbial community structure under Cd and Pb combined pollution," *Journal of Environmental Sciences*, vol. 22, no. 7, pp. 1040–1048, 2010.

[28] K. Wallenius, H. Rita, A. Mikkonen et al., "Effects of land use on the level, variation and spatial structure of soil enzyme activities and bacterial communities," *Soil Biology and Biochemistry*, vol. 43, no. 7, pp. 1464–1473, 2011.

[29] Z. Hossain and S.-I. Sugiyama, "Geographical structure of soil microbial communities in northern Japan: effects of distance, land use type and soil properties," *European Journal of Soil Biology*, vol. 47, no. 2, pp. 88–94, 2011.

[30] H. Shi and M. Shao, "Soil and water loss from the Loess Plateau in China," *Journal of Arid Environments*, vol. 45, no. 1, pp. 9–20, 2000.

[31] F.-S. Chen, D.-H. Zeng, and X.-Y. He, "Small-scale spatial variability of soil nutrients and vegetation properties in semi-arid Northern China," *Pedosphere*, vol. 16, no. 6, pp. 778–787, 2006.

[32] Y. Wang, B. Fu, Y. Lü, C. Song, and Y. Luan, "Local-scale spatial variability of soil organic carbon and its stock in the hilly area of the Loess Plateau, China," *Quaternary Research*, vol. 73, no. 1, pp. 70–76, 2010.

[33] B. Fu and L. Chen, "Agricultural landscape spatial pattern analysis in the semi-arid hill area of the Loess Plateau, China," *Journal of Arid Environments*, vol. 44, no. 3, pp. 291–303, 2000.

[34] R. K. Lu, *Analytical Methods of Soil and Agricultural Chemistry*, China Agricultural Science and Technology Press, Beijing, China, 1999.

[35] S. Y. Guan, D. S. Zhang, and Z. M. Zhang, *Soil Enzyme and Their Research Methods*, China Agricultural Science and Technology Press, Beijing, China, 1987.

[36] D. G. Krige, "A statistical approach to some basic mine valuation problems on the witwatersrand," *Journal of the Chemical, Metallurgical and Mining Society of South Africa*, vol. 52, no. 6, pp. 119–139, 1952.

[37] B. B. Trangmar, R. S. Yost, and G. Uehara, "Application of geostatistics to spatial studies of soil properties," *Advances in Agronomy*, vol. 38, no. 1, pp. 45–94, 1985.

[38] M. B. Hinojosa, R. García-Ruíz, B. Viñegla, J. A. Carreira, R. García-Ruíz, and B. Viñegla, "Microbiological rates and enzyme activities as indicators of functionality in soils affected by the Aznalcóllar toxic spill," *Biology and Fertility of Soils*, vol. 36, no. 10, pp. 1637–1644, 2004.

[39] L. Wilding, "Spatial variability: its documentation accomodation and implication to soil surveys," in *Soil Spatial Variability*, D. R. Nielsen and J. Bouma, Eds., pp. 166–194, Pudoc, Wageningen, The Netherlands, 1985.

[40] C. A. Cambardella, T. B. Moorman, J. M. Novak et al., "Field-scale variability of soil properties in central Iowa soils," *Soil Science Society of America Journal*, vol. 58, no. 5, pp. 1501–1511, 1994.

[41] W. J. Staddon, M. A. Locke, and R. M. Zablotowicz, "Spatial variability of cyanazine dissipation in soil from a conservation-managed field," in *Water Quality Assessments in the Mississippi Delta Regional Solutions*, M. T. Nett, M. A. Locke, and D. A. Pennington, Eds., pp. 179–193, National Scope, Washington, DC, USA, 2004.

[42] E. Katsalirou, S. Deng, D. L. Nofziger, A. Gerakis, and S. D. Fuhlendorf, "Spatial structure of microbial biomass and activity in prairie soil ecosystems," *European Journal of Soil Biology*, vol. 46, no. 3-4, pp. 181–189, 2010.

[43] T. Aşkın and R. Kızılkaya, "Assessing spatial variability of soil enzyme activities in pasture topsoils using geostatistics," *European Journal of Soil Biology*, vol. 42, no. 4, pp. 230–237, 2006.

[44] C. Trasar-Cepeda, C. Leirós, F. Gil-Sotres, and S. Seoane, "Towards a biochemical quality index for soils: an expression relating several biological and biochemical properties," *Biology and Fertility of Soils*, vol. 26, no. 2, pp. 100–106, 1998.

Hindawi Publishing Corporation
The Scientific World Journal
Volume 2014, Article ID 269480, 12 pages
http://dx.doi.org/10.1155/2014/269480

Research Article

Using Soil Apparent Electrical Conductivity to Optimize Sampling of Soil Penetration Resistance and to Improve the Estimations of Spatial Patterns of Soil Compaction

Glécio Machado Siqueira,[1] Jorge Dafonte Dafonte,[2] Javier Bueno Lema,[2] Montserrat Valcárcel Armesto,[2] and Ênio Farias França e Silva[3]

[1]*Centro de Ciências Agrárias e Ambientais, Universidade Federal do Maranhão, BR-222, KM 04, s/n, Boa Vista, 65500-000 Chapadinha, MA, Brazil*
[2]*Escuela Politécnica Superior, Universidad de Santiago de Compostela (USC), Campus Universitario, 27002 Lugo, Spain*
[3]*Departamento de Engenharia Agrícola, Universidade Federal Rural de Pernambuco (UFPRE), Rua D. Manuel de Medeiros, s/n, 52171-900 Recife, PE, Brazil*

Correspondence should be addressed to Glécio Machado Siqueira; gleciosiqueira@hotmail.com

Received 8 July 2014; Revised 26 September 2014; Accepted 7 October 2014; Published 31 December 2014

Academic Editor: Antonio Paz González

This study presents a combined application of an EM38DD for assessing soil apparent electrical conductivity (EC_a) and a dual-sensor vertical penetrometer Veris-3000 for measuring soil electrical conductivity (EC_{veris}) and soil resistance to penetration (PR). The measurements were made at a 6 ha field cropped with forage maize under no-tillage after sowing and located in Northwestern Spain. The objective was to use data from EC_a for improving the estimation of soil PR. First, data of EC_a were used to determine the optimized sampling scheme of the soil PR in 40 points. Then, correlation analysis showed a significant negative relationship between soil PR and EC_a, ranging from −0.36 to −0.70 for the studied soil layers. The spatial dependence of soil PR was best described by spherical models in most soil layers. However, below 0.50 m the spatial pattern of soil PR showed pure nugget effect, which could be due to the limited number of PR data used in these layers as the values of this parameter often were above the range measured by our equipment (5.5 MPa). The use of EC_a as secondary variable slightly improved the estimation of PR by universal cokriging, when compared with kriging.

1. Introduction

Soil physical properties play an important role on crop growth, if not the most important [1]. On the other hand, soil cultivation under different land uses may cause changes in soil spatial variability, depending on tillage intensity [2].

The use of farm machinery in agricultural production systems disturbs the soil structure and often may generate soil compacted layers that affect soil aeration and infiltration capacity. Different soil management systems produce different levels of soil compaction, depending on water content, type of soil, and agricultural machinery operations.

Soil penetration resistance has been found to be well correlated with root growth, and these two variables are inversely proportional. When soil water content decreases, soil mechanical resistance increases, because of the diminution of cohesion within the solid fraction of soil [3–5]. Several authors have shown that root growth can be restricted or even impeded when PR values vary between 1.0 and 3.5 MPa [6, 7]; however others quoted threshold between 2.0 and 4.0 MPa [8] for limitations to root grow.

Hill and Meza-Montalvo [9] concluded that agricultural machinery traffic during the crop growth cycle may increase the values of soil density and soil resistance to penetration to 50%. For this reason, the quantification of soil PR changes caused by soil management is an important parameter for maintaining desirable levels of production and environmental sustainability.

Most farmers consider the soil as uniform for its management, but soil properties are variable in space and time. As a result of these variations, the use of the average value of a soil property could lead to wrong management decisions. This notwithstanding, conventional agriculture has been based on soil sampling with few samples [10].

The electrical conductivity (EC) is the property that has a material to transmit or conduct electrical current [11–14]. The apparent soil electrical conductivity (EC_a) is a measure of the bulk electrical conductivity of the soil and is influenced by various factors such as soil porosity, concentration of dissolved electrolytes, texture, quantity and composition of colloids, organic matter, and water content in the soil [11]. Recent research found that apparent soil electrical conductivity measurements using electromagnetic sensors can be used to make rapid measurements of soil water content, soil clay content, cation exchange capacity and levels of exchangeable calcium and magnesium, depth of horizons with a "pan" caused by compaction, organic matter content, and salt content in soil solution [14]. In this way, measurements of apparent soil electrical conductivity (EC_a) can be used to define specific management zones.

Rhoades et al. [11] and Nadler [12] claim that soils with high water content have a higher value of EC_a, which makes the interpretation of EC_a data difficult. This is because the water content varies with depth, even if the soil is uniform, which may cause strong EC_a variations as a function of depth. Moreover, temperature also affects the soil EC_a [11, 15]. This is because increased soil temperature has effect on water viscosity and therefore affects the mobility of dissolved electrolytes into the soil solution [16]. Summarizing, it is widely accepted that the main factors that influence EC_a are texture, soil water content, and salinity [14, 17–19]; there is good correlation between these soil properties and EC_a [20].

The aim of this study was to use apparent soil electrical conductivity data (EC_a), measured by EM38, first to generate optimal soil sampling designs and then to improve the spatial estimation of soil resistance to penetration (PR) on the studied field.

2. Material and Methods

The studied field is 6 ha in surface, and it is located at Castro Riberas de Lea, Lugo, Northwestern Spain. The geographical coordinates are 43°09′49″N and 7°29′47″W, average elevation is 410 m and average slope is 2%. The soil of the study area is classified according to FAO-ISRIC [21] as Gleyc Cambisol. At the sampling date, the field was cropped with maize for silage under no tillage; before maize, the field was devoted to permanent grassland for silage. A more thorough description of this area can be found in Siqueira et al. [22].

The apparent soil electrical conductivity (EC_a) was measured with an induction electromagnetic device, namely, EM38-DD (Geonics Limited). The EM38-DD is constructed by mechanically and electrically integrating two standard EM38 ground conductivity meters. The bottom instrument's transmitter-receiver dipoles are oriented parallel to the earth in horizontal dipole (EC_a-H), while for the top instrument, which controls the digital output of the whole instrument, the dipoles are oriented perpendicular to the earth surface in vertical dipole (EC_a-V). In the EC_a-V mode, the primary magnetic field can effectively penetrate to a depth of 1.5 m, while the EC_a-H mode is effective for shallower investigation (0.75 m) [12]. The data were collected on 23/6/2008 in 1859 points (Figure 1), using EM38DD a field computer and a GPS RTK to georeference EC_a data.

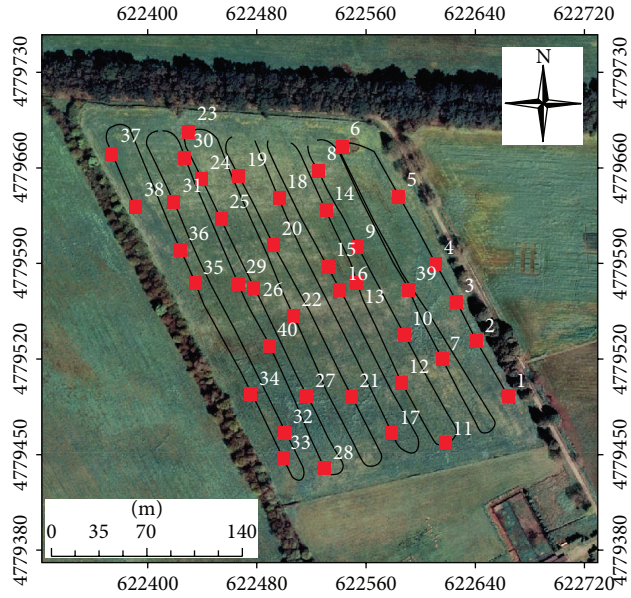

Figure 1: Continuous record of soil apparent electrical conductivity (EC_a) obtained by electromagnetic induction (line) and the optimized sampling scheme consisting 40 points (circles).

The EC_a data, together with the software ESAP-RSSD 2.35 [23], were used to identify the 40 optimal locations to perform measurements with the VERIS P3000 equipment (Figure 1). The penetrometer used in this research was the Profiler 3000, manufactured by Veris Technologies Inc. It was a self-contained, trailer mounted device, designed to be pulled through the field by a vehicle [24]. An onboard power unit and hydraulic cylinder were used to insert the penetrometer to a maximum depth of approximately 90 cm. Maximum insertion force was limited to approximately 5.5 MPa with the sensing tip, to prevent overload of the mechanical components and sensing system. A second hydraulic cylinder pivoted the penetrometer mast through a transverse arc, allowing approximately 90 cm of side-to-side displacement for acquiring data across in row and between row locations. Data collection was triggered every 2 cm. Soil electrical conductivity (EC_{veris}) was sensed immediately above the penetrometer tip. The penetrometer tip itself was electrically insulated from the penetrometer shaft with a thin dielectric ring. Electrical contact with the tip was by means of a small steel rod inside and insulated from the hollow shaft.

In this study the soil penetration resistance data was grouped into the following layers: 0.0-0.1 m ($PR_{0.0\text{-}0.1}$), 0.1-0.2 m ($PR_{0.1\text{-}0.2}$), 0.2-0.3 m ($PR_{0.2\text{-}0.3}$), 0.3-0.4 m ($PR_{0.3\text{-}0.4}$), 0.4-0.5 m ($PR_{0.4\text{-}0.5}$), 0.5-0.6 m ($PR_{0.5\text{-}0.6}$), 0.6-0.7 m

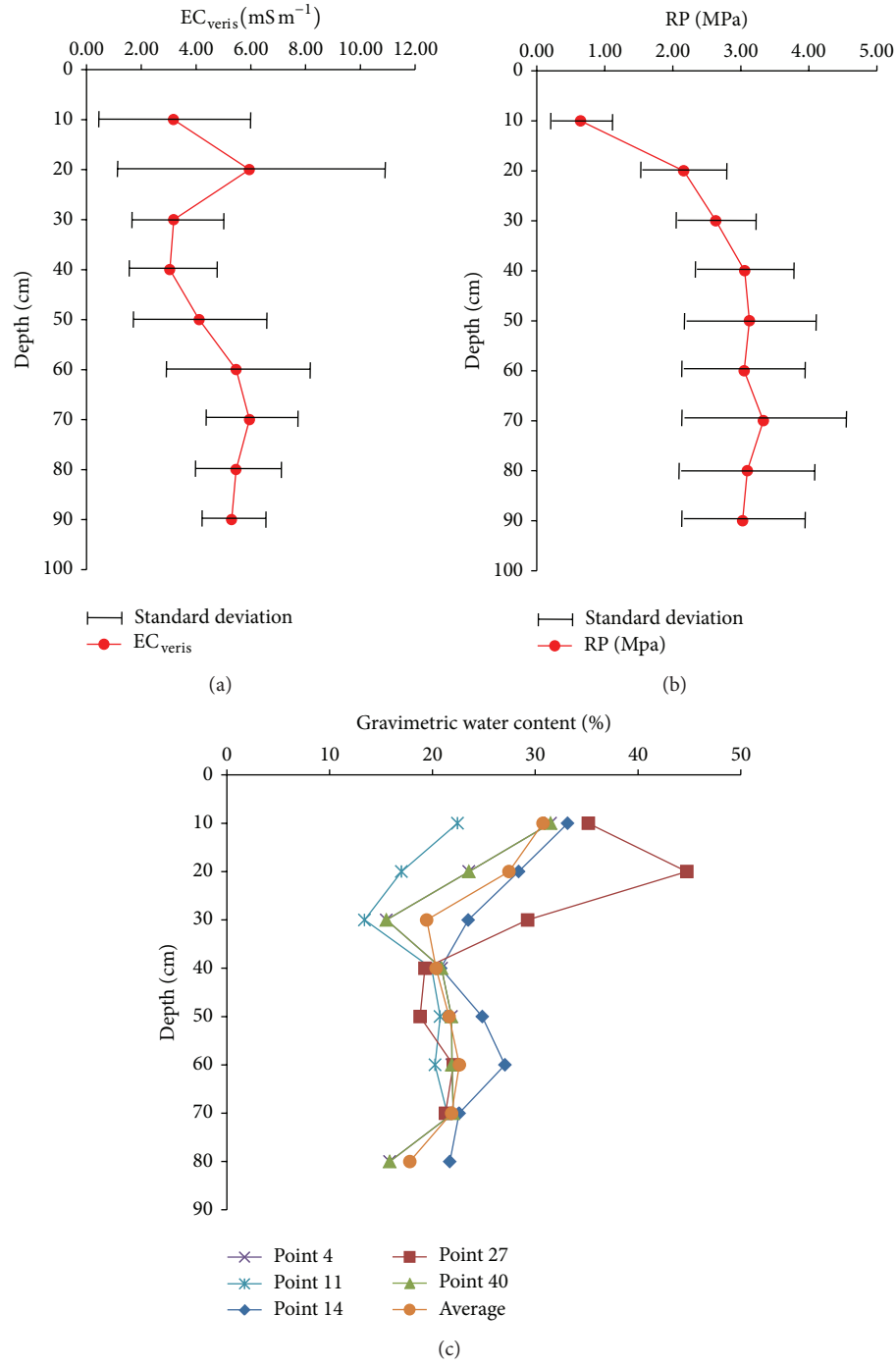

FIGURE 2: Mean values of EC_{veris} measured continuously, penetration resistance (PR) measured at 40 points, and gravimetric water content at five selected points.

($PR_{0.6\text{-}0.7}$), 0.7-0.8 m ($PR_{0.7\text{-}0.8}$), and 0.8-0.9 m ($PR_{0.8\text{-}0.9}$) (Figure 2). In each measurement location, the PR and EC_{veris} profile was measured in six near points. Therefore, the PR and EC_{veris} data showed for each location is the mean of the six profiles measured (Figures 2(a) and 2(b)).

Gravimetric soil water content was measured at these sampling points: 4, 11, 14, 27, and 40 (Figure 2(c)), in order to relate the EC_a values with the soil water content. Pearson's coefficients of correlation and significance levels were calculated between the data using pairs with the package "hmisc" [25].

The geostatistical analysis included preliminary statistical analysis, Kolmogorov-Smirnov normality test, analysis of trend, variogram modeling, and estimating values for unsampled locations using the kriging interpolation technique. Initial analysis showed that some variables had

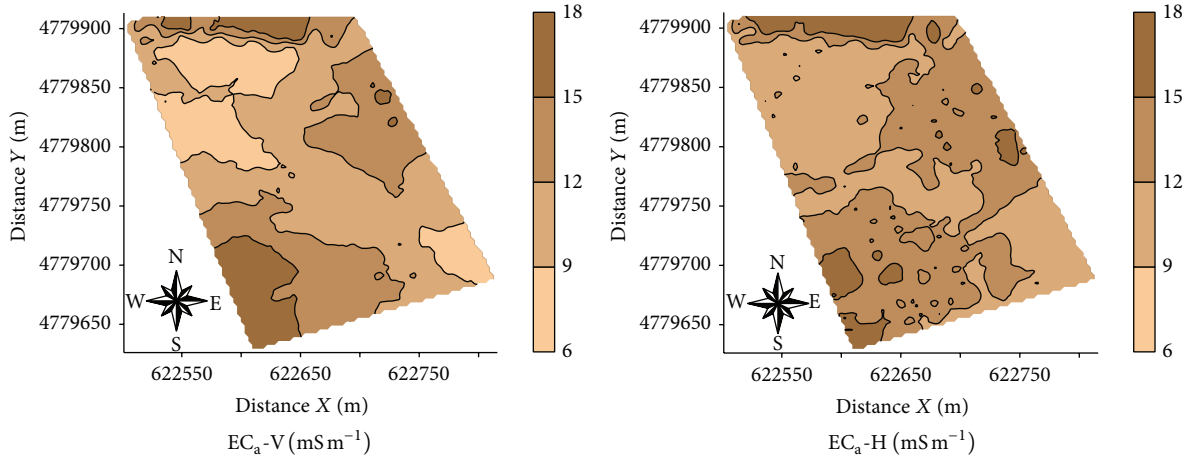

Figure 3: Maps of soil apparent electrical conductivity (EC_a-V and EC_a-H).

a trend; in this case the residual ordinary kriging was used.

Using geostatistics, there are two options to solve the problem created by the existence of a drift within the neighborhood search. On the one hand, it can be assumed that the drift is an equation with constant coefficients for the entire study area, which leads to residual kriging. On the other hand it can be assumed that coefficients of the drift equation vary by location of the study area, which results in universal kriging or kriging with trend model; this procedure simultaneously solves drift while kriging equations are solved. In this research the residual ordinary kriging was used (Table 3). The residual variograms were fitted to variogram models with cross validation using the package Gstat for R [26]; Surfer 7.0 software was used for the creation of the maps.

Some of the variables with a trend were interpolated by universal cokriging [27], instead of ordinary cokriging or cokriging with external drift. The software used to perform ordinary kriging, universal kriging, and universal cokriging was Gstat for R [26]. Using cokriging the covariance matrix must be positive definite [27–29].

3. Results and Discussion

Table 1 shows the statistical parameters for the apparent electrical conductivity (EC_a) measured with EM38-DD and soil resistance to penetration (PR) and electrical conductivity (EC_{veris}) measured with penetrometer Veris P3000 (Table 4). All studied properties showed log-normal distribution with statistical Kolmogorov-Smirnov test with significance level of 0.01.

Coefficient of variation of the studied properties had a moderate variability with values between 12 and 60%, according to the classification of Warrick and Nielsen [1]. The following data sets had high CV values (>60%): $EC_{veris\ 0\text{-}0.1}$; $EC_{veris\ 0.1\text{-}0.2}$; $EC_{veris\ average\ 0.0–0.4}$ y $PR_{0\text{-}0.1}$. The presence of high values of CV mainly for electrical conductivity (EC_{veris}) were expected since the number of measurements was much lower (maximum 140), compared to EC_a-V and EC_a-H data measured with the EM38-DD device (1859 measurements, Figure 3).

The small number of measurements obtained with Veris P3000 at the deepest soil layers (Table 1) was mainly because the equipment has a safety valve that prevents the measurement of soil PR above 5.5 MPa. The presence of a compacted layer or gravel in the soil profile was the main reason for because reducing the number of measurements at the deepest layers. Figure 2 shows the average values of the electrical conductivity (EC_{veris}, Figure 2(a)), penetration resistance (PR, Figure 2(b)), and gravimetric water content (%, Figure 2(c)) in the field studied.

The average values of the electrical conductivity measured with Veris penetrometer (EC_{veris}) showed an increase with increasing depth, which is in accordance with results presented by Johnson et al. [30] and Motavalli et al. [31]. Increasing values of water content and soil clay content in depth, contributed to increased values of EC_{veris} [32, 33]. The mean values of soil resistance to penetration (PR) increased in depth, but there was a slight decrease in the values of PR in depth below 0.5 m depth, because of a gravel layer located at this depth.

Figure 2(a) shows that the standard deviation of EC_{veris} data is higher in the surface layers, decreasing in the deeper layers, the opposite occurs with PR data because in depth the stone volume is larger causing PR values exceeding in many cases the equipment measurement limit of 5.5 MPa, as reflected in the smaller number of measurements in these layers of soil (Table 1).

Gravimetric soil moisture was measured at locations 4, 11, 14, 27, and 40 (Figure 2(c)); the choice of these locations was made on the basis of the topography of the area; these locations are representative for spatial variability of water content. It is seen that in the surface layers the water content

Table 1: Statistical parameters of the apparent electrical conductivity (EC_a) measured with EM38, in vertical and horizontal modes, and electrical conductivity (EC_{veris}) and soil resistance to penetration (PR) measured with VERIS P3000 at successive layers.

Variable	Units	N	Min.	Max.	Mean	Variance	CV	Skewness	Kurtosis	D
EC_a-V		1859	4.13	20.13	11.21	6.12	22.07	0.485	−0.243	0.071Ln
EC_a-H		1859	6.63	20.00	12.12	3.22	14.81	0.839	1.285	0.092Ln
$EC_{veris\,0.0\text{-}0.1}$		140	1.07	12.27	3.17	7.64	87.00	2.523	6.259	0.317Ln
$EC_{veris\,0.1\text{-}0.2}$		134	1.58	17.84	5.94	23.48	81.47	1.360	0.798	0.317Ln
$EC_{veris\,0.2\text{-}0.3}$		131	1.36	8.14	3.18	2.77	52.34	1.562	2.643	0.317Ln
$EC_{veris\,0.3\text{-}0.4}$		102	1.13	7.79	3.04	2.48	51.88	1.279	1.966	0.317Ln
$EC_{veris\,0.4\text{-}0.5}$	mS m^{-1}	84	0.62	9.30	4.11	6.02	59.65	−0.179	−1.739	0.330Ln
$EC_{veris\,0.5\text{-}0.6}$		72	0.80	9.41	5.46	6.76	47.57	−3.680	−10.143	0.361Ln
$EC_{veris\,0.6\text{-}0.7}$		63	2.79	8.05	5.95	2.83	28.29	−36.860	−197.233	0.404Ln
$EC_{veris\,0.7\text{-}0.8}$		32	2.13	7.31	5.45	2.49	28.92	−49.662	−418.618	0.432Ln
$EC_{veris\,0.8\text{-}0.9}$		27	3.17	6.81	5.29	1.27	21.34	−265.192	−7150.197	0.513Ln
$EC_{veris\,0.0–0.4}$		507	1.40	9.32	3.83	5.74	62.47	−1.511	−14.054	0.317Ln
$EC_{veris\,0.4–0.9}$		278	0.62	7.94	4.51	5.09	49.96	−39.185	−39.185	0.330Ln
$PR_{0.0\text{-}0.1}$		140	0.30	2.47	0.64	0.18	67.30	1.169	1.858	0.317Ln
$PR_{0.1\text{-}0.2}$		134	1.10	3.28	2.16	0.40	29.41	−26.517	−121.478	0.317Ln
$PR_{0.2\text{-}0.3}$		131	1.49	3.53	2.63	0.32	21.78	−0.423	−0.677	0.317Ln
$PR_{0.3\text{-}0.4}$		102	1.68	4.85	3.05	0.53	23.89	0.265	0.025	0.317Ln
$PR_{0.4\text{-}0.5}$		84	1.74	5.54	3.12	0.94	31.17	−0.211	4.172	0.330Ln
$PR_{0.5\text{-}0.6}$	MPa	72	1.92	5.32	3.04	0.86	30.43	−19.154	−60.403	0.381Ln
$PR_{0.6\text{-}0.7}$		63	1.60	5.59	3.33	1.46	36.31	−16.549	−88.761	0.404Ln
$PR_{0.7\text{-}0.8}$		32	1.54	4.85	3.09	0.99	36.26	−34.572	−285.556	0.432Ln
$PR_{0.8\text{-}0.9}$		27	1.62	4.43	3.02	0.87	30.87	−47.972	−495.883	0.449Ln
$PR_{average\,0.0–0.4}$		507	1.18	3.06	2.12	0.26	24.05	−48.771	−233.173	0.317Ln
$PR_{average\,0.4–0.9}$		278	1.95	5.54	3.40	0.98	29.21	−33.401	−207.070	0.330Ln

N: number of measures (maximum six measurements in each location for EC_{veris} and PR); Min.: minimum value; Max.: maximum value; CV: coefficient of variation (%); D: normality of the data for test of Kolmogorov-Smirnov ($P < 0.01$, n: normality and Ln: lognormality).

varies more than in the deeper layers. The topsoil has higher water content than in the deeper layers in the sampling date.

In Figure 2(a) it can be seen that the graph of EC_a is very similar to the soil water content graph (%, Figure 2(c)). Thus, EC_{veris} dataset obtained by the penetrometer Veris is an indirect way to obtain information about the soil water status, facilitating the interpretation of PR data, because the direct measurement of the volumetric water content of the soil is hard and slow, particularly in this type of soil with a high (>370,00 g kg^{-1}) amount of stones [34]. Motavalli et al. [31] studied the use of equipment Veris P3000 to detect the effects of compaction, and they found that the values of EC_a were correlated with soil compaction and clay content in the soil profile, thereby enabling to relate EC_a with PR.

Figure 4 shows the relationship between soil water content and EC_{veris} for the locations where soil water content was measured. It is apparent that there is no good correlation between EC_{veris} and gravimetric soil water for the selected points; to assess dependence between these two variables, more soil water content measurements would be needed.

Sudduth et al. [33] comparing the penetrometer Veris P3000 with ASAE Standard penetrometer found no significant differences between the values of soil resistance to penetration (PR) for different penetrometers studied. Canarache [6] showed that in addition to soil moisture, also PR is related

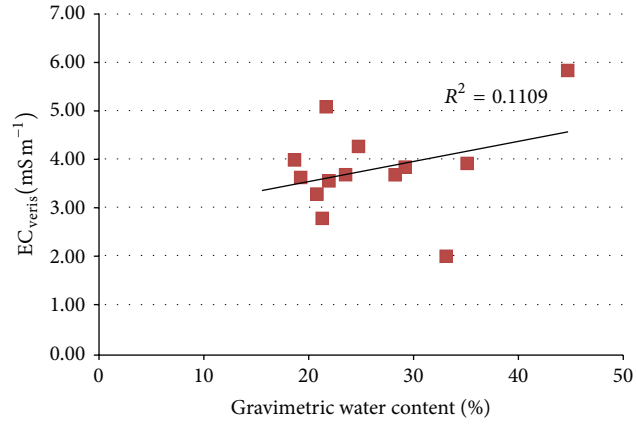

Figure 4: Correlation between EC_{veris} and gravimetric soil water content.

to other soil properties such as bulk density fine sand, sand, and clay contents. However, several authors claim that PR values are mainly related to moisture and soil bulk density [35–37]. In our case study, as soil sampling became difficult due to increasing gravel content in depth, PR measurements were essential to assess the physical status of the soil.

Summarizing, we showed that the joint use of EC_{veris} and PR data can detect changes in soil density and water content due to compaction, in addition to natural variations in soil texture.

Several authors provided different soil PR threshold values, regarding limitations for crop production. For example, Taylor and Gardner [37] reported that PR values greater than 2 MPa inhibit vegetative growth. Taylor and Burnett [38] studied the development of different crops (*Gossypium hirsutum, Sesamum indicum, Cyamopsis tetragonolobus, Sesbania exaltata, Phaseolus aureus, Vigna sinensis* var. Chinese Red, and *Sorghum vulgare* var. Sumac sorghum) with different tillage systems, these authors describe that values from 2.8 MPa began to restrict the root growth. Ehlers et al. [39] studied root growth of oats (*Avena sativa* L.) in the 0–0.25 m layer and found that root growth ceased when PR reached values between 3.6 and 4.9 MPa. Letey [40] and Bueno et al. [41] noted that soil PR values to higher than 2.0 MPa are restrictive to root growth.

Bennie [42] stated that more important than soil PR is the rate at which changes occur in soil bulk density until critical density values for vegetative growth are achieved. Bueno et al. [41] studied the PR in the 0–0.25 m layer at a field neighboring to our experimental field under no-till and conventional tillage and found PR values between 0.0 and 3.0 MPa depending on soil water content. In general, the mean value of PR for 0–0.4 m layer ($PR_{average\ 0.0–0.4}$) in this study was about 2.12 MPa. This value was close to the 2 MPa threshold, commonly cited as restrictive for crop growth. $PR_{average\ 0.4–0.9}$ was 3.40 MPa, exceeding the value of 2 MPa. However, the average soil water content of this layer is more stable over the study field, as shown in Figure 3, whereas the soil moisture content at 0.0–0.4 m layer varied considerably over this field.

Bueno [43] and Amiama [44], studying the PR at 0.0–0.4 m depth in a field near to the area studied here in several years, found similar values of PR, the higher values of PR were found in the depth layers. Amiama [44] found a moderate correlation between PR and soil water content values.

Table 2 shows the correlation matrix between the measured variables. There is a significant correlation between EC_a data EM38-DD and EC_{veris}, but the correlation s was not significant below 0.6 m depth. Probably, the lack of correlation at the deepest soil layers is related to the small number of sampling points in these layers obtained with the penetrometer Veris; in turn this is the result of the high content of gravel with depth.

Pearson's correlations between EC_a and PR show highly significant negative relationships. This is because EC_a is very dependent on the soil water content [11, 12, 14]; Hoefer et al. [45] found good correlations between PR and EC_a measured with EM38, and they concluded that EM38 survey can be used to detect subplots with an extreme compaction or noncompaction state. According to Ehlers et al. [39] PR is much more influenced by soil water content than by soil bulk density. The electrical conductivity and PR data obtained with Veris P3000 showed negative significant correlation, which matches the negative correlations between EC_a and PR. According to Drummond et al. [24] although there are various equipment available for measuring soil resistance to penetration and soil electrical conductivity, the joint measurement of PR and EC_{veris} would allow to characterize the soil not only along the landscape but also in depth. This could contribute not only to the understanding of the spatial distribution of PR and EC_a, but also to assessing density, texture, and water content in the soil.

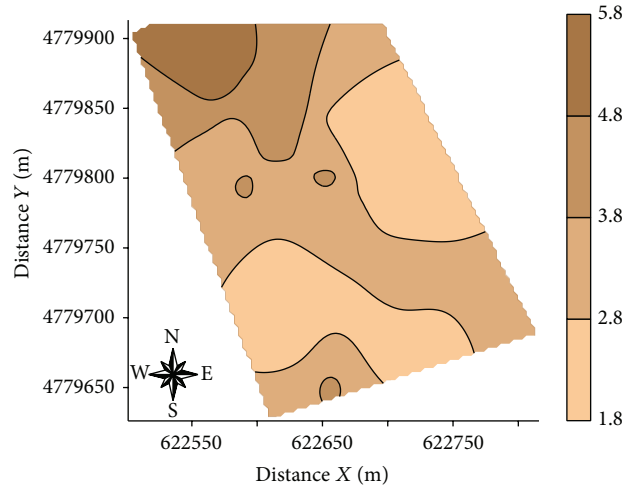

FIGURE 5: Map of $EC_{veris\ average\ 0.4–0.9}$ ($mS{\cdot}m^{-1}$) obtained by universal cokriging.

Table 5 shows the type of variogram models fitted to the experimental data and the parameters of these models. $EC_{veris\ 0.0\text{-}0.1}$, $EC_{veris\ 0.1\text{-}0.2}$, $EC_{veris\ 0.2\text{-}0.3}$, $EC_{veris\ 0.3\text{-}0.4}$, $EC_{veris\ 0.4\text{-}0.5}$, $EC_{veris\ 0.5\text{-}0.6}$, $EC_{veris\ 0.5\text{-}0.6}$, $EC_{veris\ 0.7\text{-}0.8}$, $EC_{veris\ 0.8\text{-}0.9}$, $EC_{veris\ average\ 0.0–0.4}$ $PR_{0.5\text{-}0.6}$, $PR_{0.6\text{-}0.7}$, $PR_{0.7\text{-}0.8}$, and $PR_{0.8\text{-}0.9}$ showed pure nugget effect. This might indicate that the spacing used between samples was not adequate to detect the spatial variability but may also reflect the small number of points used in the analysis process. The values of the degree of spatial dependence showed that all variables studied had a high value of this parameter, following the accredited criteria of Cambardella et al. [46]. Spherical models were fitted to the experimental variograms of most studied variables (EC_a-V, EC_a-H, $EC_{veris\ average\ 0.4–0.9}$, $PR_{0.0\text{-}0.1}$, $PR_{0.1\text{-}0.2}$, $PR_{0.2\text{-}0.3}$, $PR_{0.3\text{-}0.4}$, $PR_{0.4\text{-}0.5}$, $PR_{average\ 0.0–0.4}$, and $PR_{average\ 0.4–0.9}$). The lower range value (a) corresponds to Log $EC_{veris\ average\ 0.4–0.9}$ (50 m), whereas the highest value was found for Log $PR_{average\ 0\text{-}0.4}$ (130 m). Jabro et al. [47] studied the spatial variability of the EC_a ($mS\,m^{-1}$) and PR (MPa) with the Veris penetrometer described values of range for both parameters of 161 m; the values of range in this study were for Veris penetrometer approximately 50 m for $EC_{veris\ average\ 0.4–0.9}$ and 130 m and 70 m for the $PR_{0.0–0.4}$ and $PR_{average\ 0.4–0.9}$, respectively. Figures 5, 6, and 7, respectively, show the maps for EC_a-V, EC_a-H, $EC_{veris\ average\ 0.4–0.9}$, and PR ($PR_{0.0\text{-}0.1}$, $PR_{0.1\text{-}0.2}$, $PR_{0.2\text{-}0.3}$, $PR_{0.3\text{-}0.4}$, $PR_{0.4\text{-}0.5}$, $PR_{average\ 0.0–0.4}$, and $PR_{average\ 0.4–0.9}$).

The map of the $EC_{veris\ average\ 0.4–0.9}$ (Figure 6) has a similar spatial pattern to EC_a-V and EC_a-H (Figure 5), exhibiting varying EC in specific areas, in the eastern part of the area

Table 2: Pearson's coefficients of correlation matrix between the variables measured by EM38 and VERIS P3000 (**significant for $P < 0.05$; *significant for $P < 0.1$).

	EC_a-V	EC_a-H	$PR_{0.0\text{-}0.1}$	$PR_{0.1\text{-}0.2}$	$PR_{0.2\text{-}0.3}$	$PR_{0.3\text{-}0.4}$	$PR_{0.4\text{-}0.5}$	$PR_{0.5\text{-}0.6}$	$PR_{0.6\text{-}0.7}$	$PR_{0.7\text{-}0.8}$	$PR_{0.8\text{-}0.9}$	$PR_{\text{average } 0.0\text{–}0.4}$	$PR_{\text{average } 0.4\text{–}0.9}$
EC_a-V	1												
EC_a-H	0.75^{**}	1											
$PR_{0.0\text{-}0.1}$	-0.36^{*}	-0.44^{**}	1										
$PR_{0.1\text{-}0.2}$	-0.5^{**}	-0.56^{**}	0.66^{**}	1									
$PR_{0.2\text{-}0.3}$	-0.6^{**}	-0.59^{**}	0.41^{**}	0.85^{**}	1								
$PR_{0.3\text{-}0.4}$	-0.7^{**}	-0.53^{**}		0.74^{**}	0.79^{**}	1							
$PR_{0.4\text{-}0.5}$	-0.45^{**}			0.74^{**}	0.74^{**}	0.73^{**}	1						
$PR_{0.5\text{-}0.6}$	-0.52^{**}	-0.44^{*}		0.51^{**}		0.47^{*}	0.63^{**}	1					
$PR_{0.6\text{-}0.7}$				0.61^{**}				0.78^{**}	1				
$PR_{0.7\text{-}0.8}$	-0.49^{*}			0.48^{*}					0.84^{**}	1			
$PR_{0.8\text{-}0.9}$	-0.67^{**}	-0.62^{**}	0.57^{*}	0.68^{**}					0.79^{**}	0.89^{**}	1		
$PR_{\text{average } 0.0\text{–}0.4}$	-0.65^{**}	-0.62^{**}	0.64^{**}	0.95^{**}	0.91^{**}	0.87^{**}	0.74^{**}	0.48^{*}	0.46^{*}		0.58^{**}	1	
$PR_{\text{average } 0.4\text{–}0.9}$	-0.41^{*}			0.71^{**}	0.6^{**}	0.63^{**}	0.86^{**}	0.81^{**}	0.95^{**}	0.92^{**}	0.87^{**}	0.65^{**}	1
$EC_{a\ 0.0\text{-}0.1}$	0.51^{**}	0.35^{*}			-0.37^{*}				-0.56^{**}	-0.56^{*}	-0.55^{*}		-0.44^{**}
$EC_{a\ 0.1\text{-}0.2}$	0.54^{**}	0.51^{**}	-0.35^{*}	-0.41^{**}	-0.53^{**}			-0.53^{**}	-0.64^{**}	-0.67^{**}	-0.67^{**}	-0.43^{**}	-0.46^{**}
$EC_{a\ 0.2\text{-}0.3}$	0.71^{**}	0.72^{**}			-0.42^{**}			-0.63^{**}	-0.63^{**}		-0.68^{**}	-0.39^{*}	
$EC_{a\ 0.3\text{-}0.4}$	0.75^{**}	0.78^{**}			-0.47^{**}	-0.4^{*}		-0.57^{**}	-0.5^{*}		-0.66^{**}	-0.43^{**}	
$EC_{a\ 0.4\text{-}0.5}$	0.54^{**}	0.52^{**}		-0.46^{**}	-0.64^{**}	-0.49^{**}	-0.55^{**}					-0.51^{**}	-0.5^{**}
$EC_{a\ 0.5\text{-}0.6}$	0.51^{**}	0.57^{**}		-0.46^{*}	-0.57^{**}	-0.49^{**}	-0.64^{**}	-0.6^{**}			-0.52^{*}	-0.5^{**}	-0.54^{**}
$EC_{a\ 0.6\text{-}0.7}$		0.45^{*}		-0.54^{**}					-0.5^{*}		-0.79^{**}		-0.55^{**}
$EC_{a\ 0.7\text{-}0.8}$											-0.63^{**}		
$EC_{a\ 0.8\text{-}0.9}$													
$EC_{a\ \text{average } 0.0\text{–}0.4}$	0.67^{**}	0.61^{**}		-0.38^{*}	-0.53^{**}			-0.58^{**}	-0.69^{**}	-0.68^{**}	-0.72^{**}	-0.43^{**}	-0.44^{**}
$EC_{a\ \text{average } 0.4\text{–}0.9}$	0.57^{**}	0.53^{**}		-0.46^{**}	-0.57^{**}	-0.5^{**}	-0.61^{**}	-0.53^{**}			-0.7^{**}	-0.49^{**}	-0.59^{**}

	$EC_{veris\ 0.0\text{-}0.1}$	$EC_{veris\ 0.1\text{-}0.2}$	$EC_{veris\ 0.2\text{-}0.3}$	$EC_{veris\ 0.3\text{-}0.4}$	$EC_{veris\ 0.4\text{-}0.5}$	$EC_{veris\ 0.5\text{-}0.6}$	$EC_{veris\ 0.6\text{-}0.7}$	$EC_{veris\ 0.7\text{-}0.8}$	$EC_{veris\ 0.8\text{-}0.9}$	$EC_{veris\ \text{average } 0.0\text{–}0.4}$	$EC_{veris\ \text{average } 0.4\text{–}0.9}$		
EC_a-V													
EC_a-H													
$PR_{0.0\text{-}0.1}$													
$PR_{0.1\text{-}0.2}$													
$PR_{0.2\text{-}0.3}$													
$PR_{0.3\text{-}0.4}$													
$PR_{0.4\text{-}0.5}$													
$PR_{0.5\text{-}0.6}$													
$PR_{0.6\text{-}0.7}$													
$PR_{0.7\text{-}0.8}$													
$PR_{0.8\text{-}0.9}$													
$PR_{\text{average } 0.0\text{–}0.4}$													
$PR_{\text{average } 0.4\text{–}0.9}$													
$EC_{a\ 0.0\text{-}0.1}$	1												
$EC_{a\ 0.1\text{-}0.2}$	0.69^{**}	1											
$EC_{a\ 0.2\text{-}0.3}$	0.6^{**}	0.71^{**}	1										
$EC_{a\ 0.3\text{-}0.4}$	0.53^{**}	0.69^{**}	0.95^{**}	1									
$EC_{a\ 0.4\text{-}0.5}$		0.62^{**}	0.55^{**}	0.7^{**}	1								
$EC_{a\ 0.5\text{-}0.6}$		0.53^{**}	0.66^{**}	0.77^{**}	0.85^{**}	1							
$EC_{a\ 0.6\text{-}0.7}$		0.56^{**}	0.53^{**}	0.52^{**}	0.59^{**}	0.75^{**}	1						
$EC_{a\ 0.7\text{-}0.8}$		0.49^{*}			0.55^{*}	0.68^{**}	0.93^{**}	1					
$EC_{a\ 0.8\text{-}0.9}$	0.62^{*}	0.65^{*}					0.71^{**}	0.87^{**}	1				
$EC_{a\ \text{average } 0.0\text{–}0.4}$	0.83^{**}	0.94^{**}	0.86^{**}	0.83^{**}	0.61^{**}	0.57^{**}	0.56^{**}		0.66^{*}	1			
$EC_{a\ \text{average } 0.4\text{–}0.9}$		0.53^{**}	0.47^{**}	0.61^{**}	0.89^{**}	0.96^{**}	0.9^{**}	0.9^{**}	0.72^{**}	0.55^{**}	1		

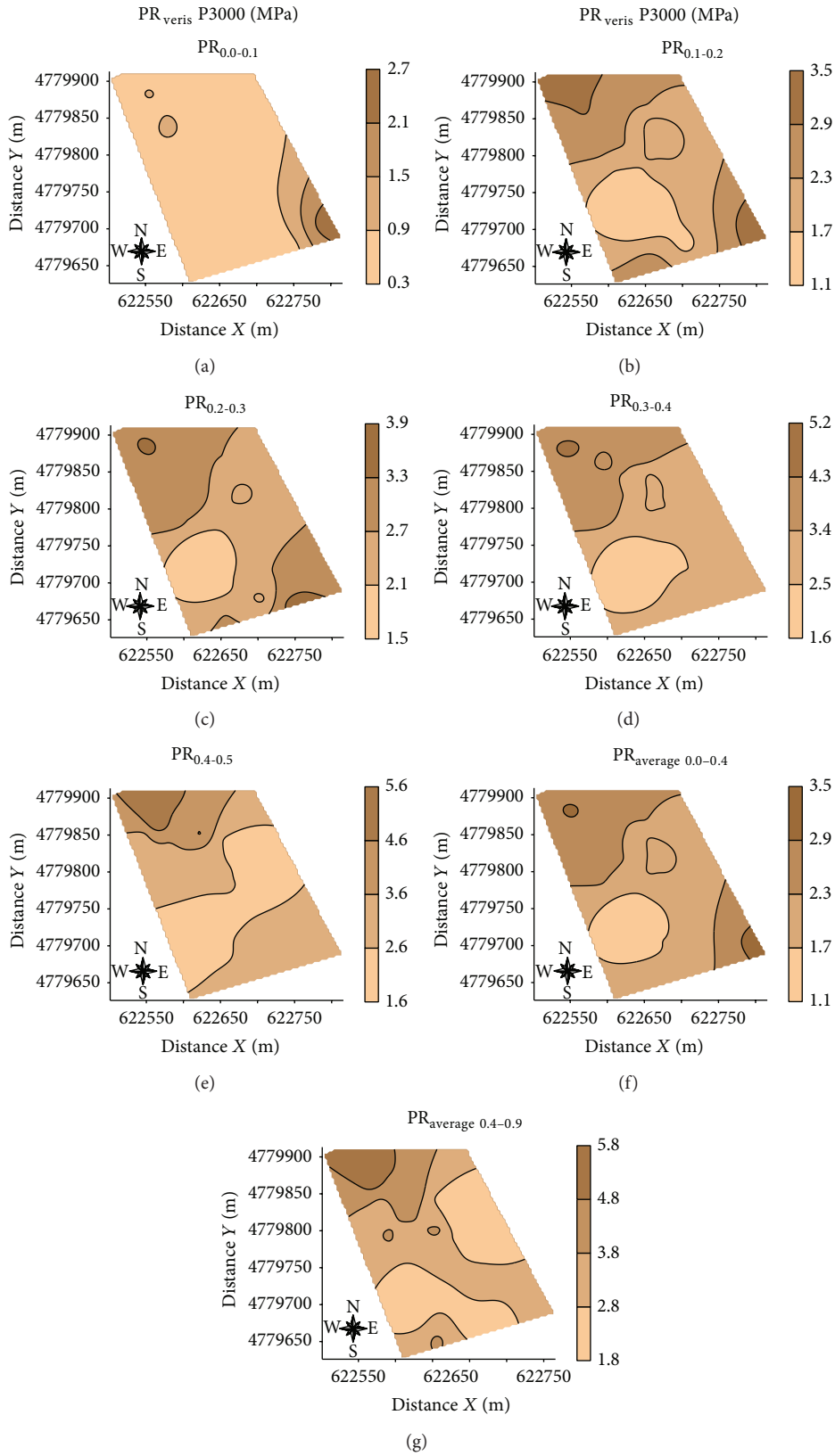

Figure 6: Maps of soil resistance to penetration measured with the penetrometer Veris ($PR_{0.0\text{-}0.1}$, $PR_{0.1\text{-}0.2}$, $PR_{0.2\text{-}0.3}$, $PR_{0.3\text{-}0.4}$, $PR_{0.4\text{-}0.5}$, $PR_{0.0\text{–}0.4\ average}$, and $PR_{average\ 0.4\text{–}0.9}$) obtained by universal kriging.

Table 3: Fitted models and variogram parameters for all the variables measured by EM38 and VERIS P3000.

Variable	Geostatistical analysis	Model	C_0	C_1	a (m)
$\log EC_a$-V	Universal kriging	Spherical	0.001	0.01	130.00
$\log EC_a$-H	Universal kriging	Spherical	0.001	0.005	130.00
$\log EC_{a\ 0.0\text{-}0.1}$	Universal kriging	Pure nugget effect			
$\log EC_{a\ 0.1\text{-}0.2}$	Universal kriging	Pure nugget effect			
$\log EC_{a\ 0.2\text{-}0.3}$	Universal kriging	Pure nugget effect			
$\log EC_{a\ 0.3\text{-}0.4}$	Universal kriging	Pure nugget effect			
$\log EC_{a\ 0.4\text{-}0.5}$	Universal kriging	Pure nugget effect			
$\log EC_{a\ 0.5\text{-}0.6}$	Universal kriging	Pure nugget effect			
$\log EC_{a\ 0.6\text{-}0.7}$	Universal kriging	Pure nugget effect			
$\log EC_{a\ 0.7\text{-}0.8}$	Universal kriging	Pure nugget effect			
$\log EC_{a\ 0.8\text{-}0.9}$	Universal kriging	Pure nugget effect			
$\log EC_{a\ average\ 0.0\text{–}0.4}$	Universal kriging	Pure nugget effect			
$\log EC_{a\ average\ 0.4\text{–}0.9}$	Universal kriging	Spherical	0.01	0.10	50.00
$\log PR_{0.0\text{-}0.1}$	Universal kriging	Spherical	0.00	0.045	90.00
$\log PR_{0.1\text{-}0.2}$	Universal kriging	Spherical	0.00	0.014	125.00
$\log PR_{0.2\text{-}0.3}$	Universal kriging	Spherical	0.00	0.011	120.00
$\log PR_{0.3\text{-}0.4}$	Universal kriging	Spherical	0.00	0.011	90.00
$\log PR_{0.4\text{-}0.5}$	Universal kriging	Spherical	0.00	0.017	100.00
$\log PR_{0.5\text{-}0.6}$	Universal kriging	Pure nugget effect			
$\log PR_{0.6\text{-}0.7}$	Universal kriging	Pure nugget effect			
$\log PR_{0.7\text{-}0.8}$	Universal kriging	Pure nugget effect			
$\log PR_{0.8\text{-}0.9}$	Universal kriging	Pure nugget effect			
$\log PR_{average\ 0.0\text{–}0.4}$	Universal kriging	Spherical	0.00	0.015	130.00
$\log PR_{average\ 0.4\text{–}0.9}$	Universal kriging	Spherical	0.00	0.0095	70.00

C_0: pure nugget effect; C_1: structural variance; a: range.

Table 4: Fitted models and parameters of the cross-variograms between PR and EC_a.

Variable	Geostatistical Analysis	Model	C_0	C_1	a (m)
$\log PR_{average\ 0.0\text{–}0.4} \times \log EC_a$-V	Universal cokriging	Spherical	0.00	0.0095	130.00
$\log PR_{average\ 0.0\text{–}0.4} \times \log EC_a$-H	Universal cokriging	Spherical	0.00	0.0065	130.00
$\log PR_{average\ 0.4\text{–}0.9} \times \log EC_a$-V	Universal cokriging	Spherical	0.00	0.0100	130.00
$\log PR_{average\ 0.4\text{–}0.9} \times \log EC_a$-H	Universal cokriging	Spherical	0.00	0.0075	130.00

C_0: Pure nugget effect; C_1: structural variance; a: range.

Table 5: Correlation coefficient (r) between measured and estimated data by kriging and cokriging for selected variables.

Universal Kriging		Universal Cokriging	
$\log PR_{average\ 0.0\text{–}0.4}$	0.644	$\log PR_{average\ 0.0\text{–}0.4} \times \log EC_a$-V	0.676
		$\log PR_{average\ 0.0\text{–}0.4} \times \log EC_a$-H	0.696
$\log PR_{average\ 0.4\text{–}0.9}$	0.339	$\log PR_{average\ 0.4\text{–}0.9} \times \log EC_a$-V	0.392
		$\log PR_{average\ 0.4\text{–}0.9} \times \log EC_a$-H	0.415

that exhibits low EC values in both maps. $EC_{veris\ average\ 0.4\text{–}0.9}$ map exhibits areas with higher EC_a data, especially in the right center area, this difference in depth of the EC measured with the penetrometer Veris is probably related to the greater water content in depth or with areas where the clay content is increased [11, 12, 14, 19, 47]. We emphasize that the EM38-DD gives a value of EC_a it is a measure of the interactions of electromagnetic pulse with a specific volume of soil (water content, density, porosity, clay content, organic matter, etc.) [14] and the penetrometer Veris measures EC in a comparatively small soil volume, providing a better description of the characteristics of the soil in depth, according to what is described by Drummond et al. [24], Sudduth et al. [33], and Jabro et al. [47].

The matrix of linear correlation between the measured data with the EM38-DD equipment (EC_a-V and EC_a-H) with EC measured with the penetrometer Veris ($EC_{a\ 0.0\text{-}0.1}$, $EC_{a\ 0.1\text{-}0.2}$, $EC_{a\ 0.2\text{-}0.3}$, $EC_{a\ 0.3\text{-}0.4}$, $EC_{a\ 0.4\text{-}0.5}$, $EC_{a\ 0.5\text{-}0.6}$, $EC_{a\ 0.6\text{-}0.7}$, $EC_{a\ 0.7\text{-}0.8}$, $EC_{a\ 0.8\text{-}0.9}$, $EC_{a\ average\ 0.0\text{–}0.4}$, and $EC_{a\ average\ 0.4\text{–}0.9}$) (Table 2) confirms the relationship between measures of the EC_a.

The maps of spatial variability of soil penetration resistance (Figure 7) show that the highest values of PR are located mainly in the northwestern part of the area ($PR_{0.1\text{-}0.2}$, $PR_{0.2\text{-}0.3}$,

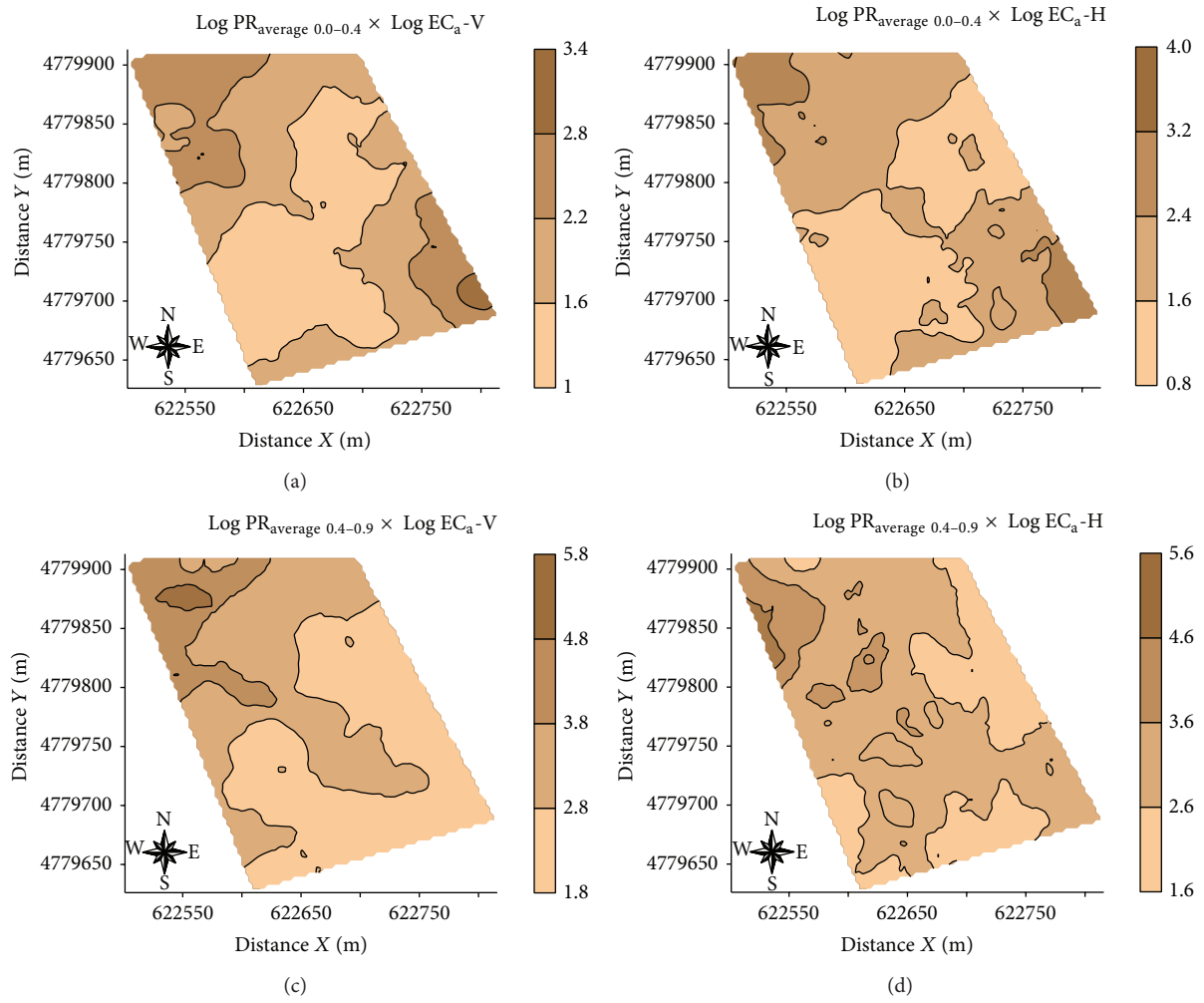

FIGURE 7: Maps of soil resistance to penetration at the layers 0.0–0.4 m (PR$_{average\ 0.0–0.4}$) and 0.4–0.9 m (PR$_{average\ 0.4–0.9}$) obtained by universal cokriging using EC$_a$-V and EC$_a$-H as secondary variables.

PR$_{0.3\text{-}0.4}$, PR$_{0.4\text{-}0.5}$, PR$_{average\ 0.0–0.4}$, and PR$_{average\ 0.4–0.9}$). Maps of PR show the opposite behavior to EC$_{veris\ average\ 0.4–0.9}$ confirming the negative correlation (Figures 5 and 6), where areas with higher EC$_a$ showed lower values of PR, corroborating the hypothesis that EC data measured with Veris penetrometer can be used as indicator of soil water content. According to Canarache [6] PR values can be classified according to the degree of constraint on the growth of roots <1.1 MPa very low without limitation for crops; low 1.1–2.5 MPa with little limitation for crops; medium 2.6–5.0 MPa with some limitations for crops; 5.1–10.0 MPa high with severe limitations for crops; 10.1 to 15.0 MPa very high where the roots do not grow virtually; >15.0 MPa extremely high the roots do not grow. In general, the study area is not a problem for root growth, since rarely exceeds the value of 5 MPa PR (PR$_{0.4\text{-}0.5}$, PR$_{0.5\text{-}0.6}$, and PR$_{0.6\text{-}0.7}$) (Table 1) indicating that the study area has medium PR with few limitations for cultivation and some areas with low PR, according to the classification of Canarache [6].

Table 5 shows the fitted parameters of cross variogram models between Log PR$_{average\ 0.0–0.4}$× Log EC$_a$-V, Log PR$_{average\ 0.0–0.4}$× Log EC$_a$-H, Log PR$_{average\ 0.4–0.9}$× Log EC$_a$-V, and Log PR$_{average\ 0.4–0.9}$× Log EC$_a$-H, since these were the only attributes that showed an improvement in the coefficient of correlation between the measured and estimated values obtained using kriging and cokriging (Table 5).

PR maps made by universal cokriging (Figure 7) are less smooth when compared with PR maps made by ordinary kriging (Figure 6), although the improvement obtained with the use of the estimate cokriging PR has been small.

4. Conclusions

The data sets EC$_{veris}$ and PR showed low values of coefficient of variation (CV, %), except for PR at 0.0-0.1 m layer that has a high value of CV (60.30%). The spherical model was fitted to the data of soil resistance penetration (PR$_{0.0\text{-}0.1}$, PR$_{0.1\text{-}0.2}$, PR$_{0.2\text{-}0.3}$, PR$_{0.3\text{-}0.4}$, and PR$_{0.4\text{-}0.5}$) at the top soil layers. The presence of pure nugget effect for soil penetration resistance at the bottom (PR$_{0.5\text{-}0.6}$, PR$_{0.6\text{-}0.7}$, PR$_{0.7\text{-}0.8}$, and PR$_{0.8\text{-}0.9}$) may be caused by the limited number of data available for these layers, since the recorded PR values were

often not useful, as they were higher than the maximum value measured by the penetrometer (5.5 MPa). Apparent soil electrical conductivity data (EC_a) were used to determine the optimized sampling scheme where PR was measured, and this methodology has proved to be efficient and capable for representing the spatial pattern of PR. EC_a and PR data show significant negative correlation coefficients, once both properties are related to the soil water content. The use of EC_a as secondary variable improved slightly the estimation of PR using universal cokriging with respect to kriging.

Acronyms

EC_a: Apparent soil electrical conductivity
EC_{veris}: Soil electrical conductivity measured with penetrometer Veris P3000
PR: Soil resistance to penetration
EC_a-H: Apparent soil electrical conductivity in horizontal dipole
EC_a-V: Apparent soil electrical conductivity in vertical dipole
CV: Coefficient of variation.

Conflict of Interests

The authors declare that there is no conflict of interests regarding the publication of this paper. The referencing brands of commercial products in the paper do not imply that the authors recommend the equipment utilized this study. The support funds presented by the Development Agencies do not show conflict of interests regarding the publication of this paper.

Acknowledgments

The authors are grateful to the Ministerio de Asuntos Exteriores y de Cooperación (MAEC-AECID) from Spain for the granting of scholarships for Ph.D. studies. This work has been funded by Ministerio de Educación y Ciencia, within the framework of research Projects CGL2005-08219-C02-02 and CGL2009-13700-C02-02, co-funded by Xunta de Galicia, within the framework of research project PGIDIT06PXIC291062PN and by the European Regional Development Fund (ERDF). The authors would like to thank FACEPE and CNPq (Brazil) for the scholarship DCR granted to the first author. Thanks are due to FAPEMA financial support for publication.

References

[1] A. W. Warrick and D. R. Nielsen, "Spatial variability of soil physical properties in the field," in *Applications of Soil Physics*, D. Hillel, Ed., pp. 319–344, Academic Press, New York, NY, USA, 1980.

[2] A. Utset and G. Cid, "Soil penetrometer resistance spatial variability in a Ferralsol at several soil moisture conditions," *Soil & Tillage Research*, vol. 61, no. 3-4, pp. 193–202, 2001.

[3] C. J. Gerard, H. C. Mehth, and F. Hinojosa, "Root growth in a clay soil," *Soil Science*, vol. 114, pp. 37–49, 1972.

[4] H. H. Becher, "Resistances to penetration of aggregates from loess-derived topsoils at different soil water tensions," *Soil & Tillage Research*, vol. 47, no. 1-2, pp. 73–81, 1998.

[5] A. G. Benghough, D. J. Campbell, and M. F. O'Sullivan, "Penetrometer techniques in relation to soil compaction and root growth," in *Soil and Environmental Analysis: Physical Methods*, K. A. Smith and C. E. Mullins, Eds., pp. 377–404, Marcel Decker, New York, NY, USA, 2001.

[6] A. P. Canarache, "PENETR—a generalized semi-empirical model estimating soil resistance to penetration," *Soil & Tillage Research*, vol. 16, no. 1-2, pp. 51–70, 1990.

[7] A. Merotto and C. M. Mundstock, "Wheat root growth as affected by soil strength," *Revista Brasileira de Ciencias do Solo*, vol. 23, pp. 197–202, 1999.

[8] M. A. Arshad, B. Lowery, and B. Grossman, "Physical tests for monitoring soil quality," in *Methods for Assessing Soil Quality, SSSA Special Publication*, J. W. Doran and A. J. Jones, Eds., vol. 49, pp. 123–141, Soil Science Society of America, Madison, Wis, USA, 1996.

[9] R. L. Hill and M. Meza-Montalvo, "Long-term wheel traffic effects on soil physical properties under different tillage systems," *Soil Science Society of America Journal*, vol. 54, no. 3, pp. 865–870, 1990.

[10] A. B. McBratney and M. J. Pringle, "Spatial variability in soil, implications for precision agriculture," in *Spatial Variability in Soil and Crop*, J. V. Satafford, Ed., vol. 1 of *Precision Agriculture '97*, pp. 3–31, Bios Scientific Publishers, Warwick, UK, 1997.

[11] J. D. Rhoades, P. C. A. Raats, and R. J. Prather, "Effects of liquid-phase electrical conductivity, water content, and surface conductivity on bulk soil electrical conductivity," *Soil Science Society of American Journal*, vol. 40, no. 5, pp. 651–655, 1976.

[12] A. Nadler, "Estimating the soil water dependence of the electrical conductivity soil solution/electrical conductivity bulk soil ratio.," *Soil Science Society of America Journal*, vol. 46, no. 4, pp. 722–726, 1982.

[13] J. D. McNeill, "Electrical conductivity of soils and rocks," Tech. Rep. TN-5, Geonics Ltda, Ontario, Canada, 1990.

[14] N. R. Kitchen, K. A. Sudduth, and S. T. Drummond, "Mapping of sand deposition from 1993 midwest floods with electromagnetic induction measurements," *Journal of Soil and Water Conservation*, vol. 51, no. 4, pp. 336–340, 1996.

[15] E. C. Brevik and T. E. Fenton, "Soil sensing techniques as soil survey tools in lacustre-derived soils, central Iowa (CD)," in *International Econference on Precision Agriculture*, vol. 5, ASA-CSSA-SSSA, Bloomington, Ind, USA, 2000.

[16] N. J. Harstock, T. G. Mueller, G. W. Thomas, R. I. Barnhisel, and K. L. Wells, "Soil electrical conductivity variability (Cd)," in *Proceedings of the 5th International Conference on Precision Agriculture and Other Resource Management, Bloomington, MN. 16–19 July 2000*, ASA-CSSA-SSSA, Madison, Wis, USA, 2000.

[17] R. G. Kachanoski, E. de Jong, and I. J. van Wesenbeeck, "Field scale patterns of soil water storage from non-contacting measurements of bulk electrical conductivity," *Canadian Journal of Soil Science*, vol. 70, no. 3, pp. 537–541, 1990.

[18] P. G. Cook and G. R. Walker, "Depth profiles of electrical conductivity from linear combinations of electromagnetic induction measurements," *Soil Science Society of America Journal*, vol. 56, no. 4, pp. 1015–1022, 1992.

[19] K. R. Sheets and J. M. H. Hendrickx, "Noninvasive soil water content measurement using electromagnetic induction," *Water Resources Research*, vol. 31, no. 10, pp. 2401–2409, 1995.

[20] J. D. Rhoades, "Electrical conductivity methods for measuring and mapping soil salinity," *Advances in Agronomy*, vol. 49, pp. 201–251, 1993.

[21] FAO-ISRIC, *World Reference Base for Soil Resources*, FAO, Rome, Italy; ISRIC, Wageningen, The Netherlands, 1994.

[22] G. M. Siqueira, J. Dafonte, M. Valcárcel-Armesto, and F. F. de França e Silva, "Using multivariate geostatistics to assess patterns of spatial dependence of apparent soil electrical conductivity and selected soil properties," *The Scientific World Journal*, 2014.

[23] S. M. Lesch, J. D. Rhoades, and D. L. Corwin, *The ESAP Version 2.01r User Manual and Tutorial Guide*, Research Report vol. 146, George E. Brown Jr., Salinity Laboratory, Riverside, Calif, USA, 2000, http://www.ussl.ars.usda.gov/lcrsan/esap95.pdf.

[24] P. E. Drummond, C. D. Christy, and E. D. Lund, "Using an automatic penetrometer and soil EC_a probe to characterize the rooting zone," in *Proceedings of the 5th International Conference on Precision Agriculture*, ASA-CSSA-SSSA, Bloominghton, Minn, USA, July 2000.

[25] F. E. Harrell Jr., *Hmisc: Harrell Miscellaneous R Package version 3.14-5*, 2014, http://cran.r-project.org/web/packages/Hmisc/index.html.

[26] E. J. Pebesma and B. Graeler, *Package Gstat*, 2013, http://cran.r-project.org/web/packages/gstat/gstat.pdf.

[27] P. Goovaerts, *Geostatistics for Natural Resources Evaluation*, Oxford University Press, New York, NY, USA, 1997.

[28] P. Goovaerts, "Geostatistics in soil science: State-of-the-art and perspectives," *Geoderma*, vol. 89, no. 1-2, pp. 1–45, 1999.

[29] C. V. Deutsch and A. G. Journel, *GSLIB—Geostatistical Software Library and User's Guide*, Oxford University Press, New York, NY, USA, 2nd edition, 1998.

[30] C. K. Johnson, J. W. Doran, H. R. Duke, B. J. Wienhold, K. M. Eskridge, and J. F. Shanahan, "Field-scale electrical conductivity mapping for delineating soil condition," *Soil Science Society of America Journal*, vol. 65, no. 6, pp. 1829–1837, 2001.

[31] P. P. Motavalli, S. H. Anderson, P. Pengthamkeerati, and C. J. Gantzer, "Use of soil cone penetrometers to detect the effects of compaction and organic amendments in claypan soils," *Soil & Tillage Research*, vol. 74, no. 2, pp. 103–114, 2003.

[32] K. A. Sudduth, J. W. Hummel, N. R. Kitchen, and S. T. Drummond, "Evaluation of a soil conductivity sensing penetrometer," in *Proceedings of the American Society of Agricultural Engineers Annual International Meeting*, Paper No. 001043, American Society of Agricultural Engineers, St. Joseph, Mich, USA, July 2000.

[33] K. A. Sudduth, J. W. Hummel, and S. T. Drummond, "Comparison of the veris profiler 3000 to an ASAE-standard penetrometer," *Applied Engineering in Agriculture*, vol. 20, no. 5, pp. 535–541, 2004.

[34] X. X. Neira, *Development of Water Management Methods for Rational Water Use in Irrigation*, Universidade de Santiago de Compostela, Escola Politécnica Superior, 1993, (Spanish).

[35] D. S. Nesmith, D. E. Radcliffe, W. L. Hargrove, R. L. Clark, and E. W. Tollner, "Soil compaction in double-cropped wheat and soybeans on an Ultissol," *Soil Science Society of America Journal*, vol. 51, no. 1, pp. 183–186, 1987.

[36] M. Yasin, R. D. Grisso, L. L. Bashford, A. J. Jones, and L. N. Mielke, "Normalizing cone resistance values by covariance analysis," *Transactions of the American Society of Agricultural Engineers*, vol. 36, no. 5, pp. 1267–1270, 1993.

[37] H. M. Taylor and H. R. Gardner, "Penetration of cotton seedling taproots as influenced by bulk density and, moisture content, and strength of soil," *Soil Science*, vol. 96, no. 3, pp. 153–156, 1963.

[38] H. M. Taylor and E. Burnett, "Influence of soil strength on the root-growth habits of plants," *Soil Science*, vol. 98, pp. 174–180, 1964.

[39] W. Ehlers, U. Köpke, F. Hesse, and W. Böhm, "Penetration resistance and root growth of oats in tilled and untilled loess soil," *Soil and Tillage Research*, vol. 3, no. 3, pp. 261–275, 1983.

[40] J. Letey, "Relationship between soil physical properties and crop production," *Advances in Soil Science*, vol. 1, pp. 277–294, 1985.

[41] J. Bueno, C. Amiama, J. L. H. Hernanz, and J. M. Pereira, "Penetration resistance, soil water content, and workability of grasslands soils under two tillage systems," *Transactions of the American Society of Agricultural and Biological Engineers*, vol. 49, no. 4, pp. 875–882, 2006.

[42] A. T. P. Bennie, "Growth and mechanical impedance," in *Plant Roots the Hidden Half*, pp. 393–414, Marcel Dekker, New York, NY, USA, 1991.

[43] J. Bueno, *Forrage maize under no-tillage in wet conditions, comparison with traditional tillage in soil response, yield and energy budget [Ph.D. thesis]*, Universidad Politécnica de Madrid, 1997 (Spanish).

[44] C. Amiama, *Italian Raygrass under no-tillage, influence of residues from last crop and comparison with traditional tillage of physical soil properties, yield and economic aspects [Ph.D. dissertation]*, Universidad de Santiago de Compostela, 2003, (Spanish).

[45] G. Hoefer, J. Bachmann, and K. H. Hartge, "Can the EM38 probe detect spatial patterns of subsoil compaction?" in *Proximal Soil Sensing*, R. A. V. Rossel, A. B. McBratney, and B. Minasny, Eds., vol. 1 of *Progress in Soil Science*, pp. 265–273, Springer Science, Dordrecht, The Netherlands, 2010.

[46] C. A. Cambardella, T. B. Moorman, J. M. Novak et al., "Field scale variability of soil properties in central Iowa soils," *Soil Science Society of America Journal*, vol. 58, no. 5, pp. 1501–1511, 1994.

[47] J. D. Jabro, R. G. Evans, Y. Kim, W. B. Stevens, and W. M. Iversen, "Characterization of spatial variability of soil electrical conductivity and cone index using coulter and penetrometer-type sensors," *Soil Science*, vol. 171, no. 8, pp. 627–637, 2006.

Hindawi Publishing Corporation
The Scientific World Journal
Volume 2014, Article ID 407049, 11 pages
http://dx.doi.org/10.1155/2014/407049

Research Article

Applications of Organic and Inorganic Amendments Induce Changes in the Mobility of Mercury and Macro- and Micronutrients of Soils

Mercedes García-Sánchez, Adéla Šípková, Jiřina Száková, Lukáš Kaplan, Pavla Ochecová, and Pavel Tlustoš

Department of Agro-Environmental Chemistry and Plant Nutrition, Faculty of Agrobiology, Food and Natural Resources, Czech University of Life Sciences, Suchdol, 16521 Prague 6, Czech Republic

Correspondence should be addressed to Jiřina Száková; szakova@af.czu.cz

Received 11 June 2014; Revised 3 September 2014; Accepted 24 September 2014; Published 23 October 2014

Academic Editor: Antonio Paz González

Both soil organic matter and sulfur (S) can reduce or even suppress mercury (Hg) mobility and bioavailability in soil. A batch incubation experiment was conducted with a Chernozem and a Luvisol artificially contaminated by 440 $mg \cdot kg^{-1}$ Hg showing wide differences in their physicochemical properties and available nutrients. The individual treatments were (i) digestate from the anaerobic fermentation of biowaste; (ii) fly ash from wood chip combustion; and (iii) ammonium sulfate, and every treatment was added with the same amount of S. The mobile Hg portion in Chernozem was highly reduced by adding digestate, even after 1 day of incubation, compared to control. Meanwhile, the outcome of these treatments was a decrease of mobile Hg forms as a function of incubation time whereas the contents of magnesium (Mg), potassium (K), iron (Fe), manganese (Mn), copper (Cu), zinc (Zn), and phosphorus (P) were stimulated by the addition of digestate in both soils. The available calcium (Ca) contents were not affected by the digestate addition. The experiment proved digestate application as the efficient measure for fast reduction of mobile Hg at extremely contaminated soils. Moreover, the decrease of the mobile mercury portion was followed by improvement of the nutrient status of the soils.

1. Introduction

Industrial activities have increased the proportion of Hg in the atmosphere and oceans and have contaminated a number of local environments [1]. From the ecotoxicological point of view, critical limits of Hg (given as soil element contents above which unacceptable effects are expected) are substantially lower than values derived for other metals such as Cd, Cu, Ni, Pb, and Zn [2]. Li et al. [3] compared the mobility and plant-availability of risk elements from industrially contaminated soil where the soil-to-plant transfer coefficients were in the order of Cd > Zn > Cu > Hg > As > Pb, confirming the relatively low availability of soil Hg for various vegetables. Rodrigues et al. [4] observed the water-soluble contents of Hg in highly contaminated sediment and soil samples (total Hg contents even higher than 3000 $mg \cdot kg^{-1}$) to be less than 1.2% of the total Hg content. Boszke et al. [5] classified the divalent and elemental Hg bounds to humic matter/organic matter as the "semimobile" element portion and observed low portions of the water-soluble Hg species as well.

Luo et al. [6] suggested that soil organic matter and nitrogen were the important sinks for Hg in the soils. The good capacity of Hg for adsorption and complexation in the solid media resulted in limited bioaccessibility of this element, which was reported by Hassen et al. [7]. Distribution coefficients for Hg^{2+} binding by humic acids were determined by Khwaja et al. [8], confirming that the calculated concentration of free Hg^{2+} at equilibrium is very low. Also, Heeraman et al. [9] observed decreasing Hg mobility and plant-availability in the organic matter-treated soil. The importance of soil organic matter for Hg mobility and bioavailability in soil samples is known and well described [5, 10]. As observed by Yao et al. [11], the addition of humus can either suppress or promote Hg bioavailability depending on the soil composition. In

this context, the effect of a particular humus fraction on Hg bioavailability is related to its ability to convert Hg bound by solid phases into soluble complexes, as well as the stability of the released complexes. On the contrary, the presence of dissolved organic matter (DOM) can significantly reduce maximum Hg adsorption capacity and even promote Hg desorption from the soils [12].

Zagury et al. [13] evaluated the potential mobility and plant-availability of Hg in the highly contaminated soils by chlor-alkali plants, where the total Hg contents in soil reached up to 11500 mg·kg^{-1}. Although the water extractable Hg portion was relatively low with regard to the high total content, it represented significant concentrations correlating with Hg uptake by experimental plants.

Reis et al. [14] observed that the presence of Hg in the mobile phase could be related to Mn and aluminum (Al) soil contents. A positive relation between Hg in the semimobile fraction and the Al content was also observed. On the contrary, organic matter and S contents contributed to Hg retention in the soil matrix, reducing the mobility of the metal. Sulfide minerals are known to be effective adsorbents for Hg(II) being the primary sink for Hg in the environment [15]. In this context, Hesterberg et al. [16] demonstrated the preferential binding of Hg(II) to reduced organic S sites. Subsequently, similar observations were provided and described in soils as mentioned by Remy et al. [17]. Concentration of MeHg is negatively correlated with soil total organic matter and total S and is influenced by the soil total Hg concentration [17]. Åkerblom et al. [18] highlighted that long-term chronic SO_4^{2-} deposition at rates similar to those found in polluted areas of Europe and North America increase the capacity of peatlands to methylate Hg and store MeHg. Competitive relationships between Hg and other metals in soil were observed by Jing et al. [19], where desorption of adsorbed Hg increased with elevated concentrations of added Cu or Zn.

In our investigation, a laboratory batch incubation experiment was conducted with Chernozem and Luvisol differing in their physicochemical parameters and the available nutrient contents. Digestate, the bio-waste originating from biogas production plants, was applied as a S-rich source of organic matter. Alternatively, wood ash from biomass combustion plants was applied as a different source of S and other macro- and micronutrients. As proven by Ochecová et al. [20], the plant-availability of the risk elements in the contaminated soil decreased after ash application, whereas the nutrient contents tended to increase. To separate the effect of organic matter and S in the soil, inorganic source of S, ammonium sulfate, $(NH_4)_2SO_4$, was applied, as well. The main objectives of the study were as follows: (i) to assess the ability of the individual treatments to immobilize Hg in the artificially contaminated soil and (ii) to evaluate the potential interactions between Hg sorption in the experimental soil and the mobility of the essential macro- and microelements in these soils.

2. Materials and Methods

2.1. Soils and Ameliorative Materials. The following two soils, differing in their physicochemical characteristics, were selected for the experiment: (i) uncontaminated Chernozem with a cation exchange capacity (CEC) of 230 mmol kg^{-1}, a pH level of 7.5, and an oxidizable carbon content (Cox) of 2.6%, and (ii) uncontaminated Luvisol with a CEC of 145 mmol kg^{-1}, a pH level of 6.5, and a Cox of 1.7%. Nutrient contents and other characteristics in both soil samples are summarized in Table 1. Soils were sampled from a depth of 20 cm, immediately after which they were homogenized, sieved through a 5 mm diameter mesh, and kept at room temperature. For the experimental incubation soils, samples were sieved again using a 2 mm mesh and kept at 4°C until use. The fly ash (pH 12.1) was produced by the combustion of wood ash produced in two reactors (1.8 MW and 0.6 MW). The digestate sample (pH 8.2) originated from a biogas station (1732 kW/h), where the digested material consisted of sugar beet pulp (50%), marc of fruit (42%), and silage maize (8%). The macro- and micronutrient contents in both ameliorative materials are summarized in Table 2. As an inorganic amendment, solid particles of $(NH_4)_2SO_4$ were used (Reagent from Fisher Scientific).

Table 1: Main physicochemical characteristics of the experimental soils.

Soil type	Luvisol	Chernozem
NRSC Soil Texture	Silt loam	Silt loam
Clay (<0.002 mm) [%]	5.38	2.18
Silt (0.002–0.05 mm) [%]	68.14	71.80
Sand (0.05–2 mm) [%]	26.48	26.03
Location	50°4′22″N, 14°10′19″E	50°7′40″N, 14°22′33″E
Altitude (m a.s.l.)	410	286
P Mehlich III* (mg kg^{-1})	100	91
K Mehlich III* (mg kg^{-1})	80	230
Mg Mehlich III* (mg kg^{-1})	110	240
Ca Mehlich III* (mg kg^{-1})	3600	9000

*Šípková et al. [23].

2.2. Experimental Design. For the experimental incubation soils, 100 g of Chernozem and Luvisol soils were placed into polypropylene bottles and immediately after were brought to 60% moisture saturation. Then, half of the soil samples were artificially contaminated with Hg by adding 60 mg of $HgCl_2$ to reach a concentration of 440 mg·kg^{-1} of Hg. Subsequently, organic and inorganic amendments: (1) ash, (2) digestate, and (3) $(NH_4)_2SO_4$, were applied both to contaminated and noncontaminated soils. The rate of amendment was calculated for 600 mg S per kg of soil as follows: (1) ash: 1.5 g, (2) digestate: 10 g, and (3) NH_4SO_4: 0.25 g per bottle.

Soils that were contaminated and noncontaminated with Hg were thoroughly mixed and incubated at 28°C for 21 days. To evaluate the mobility of Hg in both soils and interactions with macro- and micronutrients as well, soil samples were collected after 1, 2, 3, 4, 7, 14, and 21 days of incubation. Three replicates were set up per treatment.

Table 2: Nutrient contents in the dry matter of ameliorative materials.

Element	Fly-ash	Digestate
P (%)	1.29 ± 0.01	1.20 ± 0.01
K (%)	7.74 ± 0.02	2.12 ± 0.01
Mg (%)	1.44 ± 0.02	0.49 ± 0.02
Ca (%)	13.4 ± 0.1	3.15 ± 0.01
S (%)	4.07 ± 0.01	0.60 ± 0.01
Cu (%)	0.020 ± 0.001	0.004 ± 0.001
Fe (%)	2.79 ± 0.01	0.18 ± 0.01
Mn (%)	1.29 ± 0.01	0.02 ± 0.00
Zn (%)	3.58 ± 0.08	0.03 ± 0.00

2.3. Extraction of Soluble Portions of Hg and Macro- and Micronutrients. For the determination of bioavailable element portions in soils during the experiment, 0.5 g of each sample was added to 10 mL of 0.11 mol L^{-1} solution of CH_3COOH and shaken overnight [21]. Each extraction was carried out in three replicates. For the centrifugation of extracts, a Hettich Universal 30 RF (Germany) instrument was used. The reaction mixture was centrifuged at 3000 rpm (i.e., 460 g) for 10 minutes at the end of each extraction procedure, and the supernatants were kept at 6°C prior to measurements. Prior to the analysis, extracts were acidified with a mixture of acids (HNO_3 : HCl = 3 : 1). For the determination of nutrient status in the experimental soils before the experiment, the Mehlich III extraction procedure (0.2 mol L^{-1} of CH_3COOH + 0.25 mol L^{-1} of NH_4NO_3 + 0.013 mol L^{-1} of HNO_3 + 0.015 mol L^{-1} of NH_4F + 0.001 mol L^{-1} of EDTA) at the ratio of 1 g of soil per 10 mL of the extraction mixture for 10 min [22] was applied.

2.4. Determination of Hg. Hg content in the extracts was measured by inductively coupled plasma mass spectrometry (ICP-MS, Agilent 7700x, Agilent Technologies Inc., USA). The auto-sampler ASX-500, a three-channel peristaltic pump, and MicroMist nebulizer equipped the ICP-MS. Calibration solutions were prepared in diluted single element ICP-MS standards as 0.1–100 μg L^{-1} for Hg and the isotope Hg(202) was measured. As an internal standard, Pt(195) was used at the concentration of 100 μg L^{-1}.

2.5. Determination of Macro- and Micronutrients. Inductively coupled plasma-atomic emission spectrometry (ICP-OES, Agilent 720, Agilent Technologies Inc., USA) equipped with a two-channel peristaltic pump, a Struman-Masters spray chamber, and a V-groove pneumatic nebulizer made of inert material was applied for the determination of Cu, Fe, Mn, Zn, P, and S in the extracts (the experimental conditions were as follows: power of 1.2 kW, plasma flow of 15.0 L·min^{-1}, auxiliary flow of 0.75 L·min^{-1}, nebulizer flow of 0.9 L·min^{-1}), whereas flame atomic absorption spectrometry (F-AAS, Varian 280FS, Varian, Australia; air flow of 13.5 L·min^{-1}, acetylene flow of 2.2 L·min^{-1}, burner height of 13.5 mL, nebulizer uptake rate of 5 mL·min^{-1}) was used for Ca, Mg, and K determination in the extracts.

2.6. Determination of Total Nutrient Contents in the Ameliorative Materials. For determination of total element contents in the ash, nondestructive X-ray fluorescence (XRF) spectrometry (Spectro IQ, Kleve, Germany) was used; the target material was palladium and the target angle from the central ray was 90°. The focal point was a 1 mm × 1 mm square, and the maximum anode dissipation was 50 W with 10 cfm forced-air cooling. The instrument was equipped with the Barkla crystal HOPG. The tested samples were pressed into pellets; this involved mixing 4.0 g of ash (particle size 15–20 μm) with 0.9 g of the binding additive (HWC Hoechst wax, Germany) for 10 min with a pressing power of 80 kN. The determination was performed in the Institute of Rock Structure and Mechanics, Academy of Sciences of the Czech Republic.

The digestate sample was decomposed by pressurized wet ashing as follows: aliquots (~0.5 g) of air-dried samples were decomposed in a digestion vessel with 10 mL of *Aqua regia* (i.e., nitric and hydrochloric acid mixture in the ratio 1 : 3). The mixture was heated in an Ethos 1 (MLS, Germany) microwave assisted wet digestion system for 33 min at 210°C. ICP-OES and F-AAS were then applied as described in the previous subchapter.

2.7. Statistics. The data obtained were subjected to Dixon's test for the identification of outliers (significance level α = 0.05) using Microsoft Office Excel 2007 (Microsoft Corporation, USA). Subsequently, one-way analysis of variance was used at the significance level α = 0.05 using the Statistica 12 program (StatSoft, USA).

3. Results and Discussion

3.1. Changes in Hg Mobility in the Treated Soils. The mobile Hg contents affected by the individual treatments and their variability during the incubation experiment are summarized in Figure 1. In the treatments without artificial Hg application, the mobile Hg contents were under the detection limit of ICP-MS. Similarly to our previous observations [23], Ruggiero et al. [24] also documented that most of the Hg in the long-term polluted soils was scarcely mobile and available. The Hg contents in digestates and fly ash are usually low as well [25, 26] and did not affect the mobile portions of Hg in our experiment. The extractable Hg contents differed according to the physicochemical parameters of the used soils and to the individual treatments. In Chernozem, the extractable Hg contents were low regardless of the treatment at the beginning and end of incubation. Within the 3rd and 7th day of incubation, the mobile Hg portions increased in all treatments (including control) except for the digestate. Similar course of Hg mobility changes were observed by Bower et al. [27] in the experiments studying the mercury adsorption onto pyrite indicating the formation of nonmobile sulfides over time. In the Luvisol, the mobile Hg portions decreased during the incubation, whereas they dropped to the levels reached in Chernozem by the end of the experiment. As stated by Müller et al. [28] soil Hg contamination can cause reduced microbial biomass at the contaminated sites.

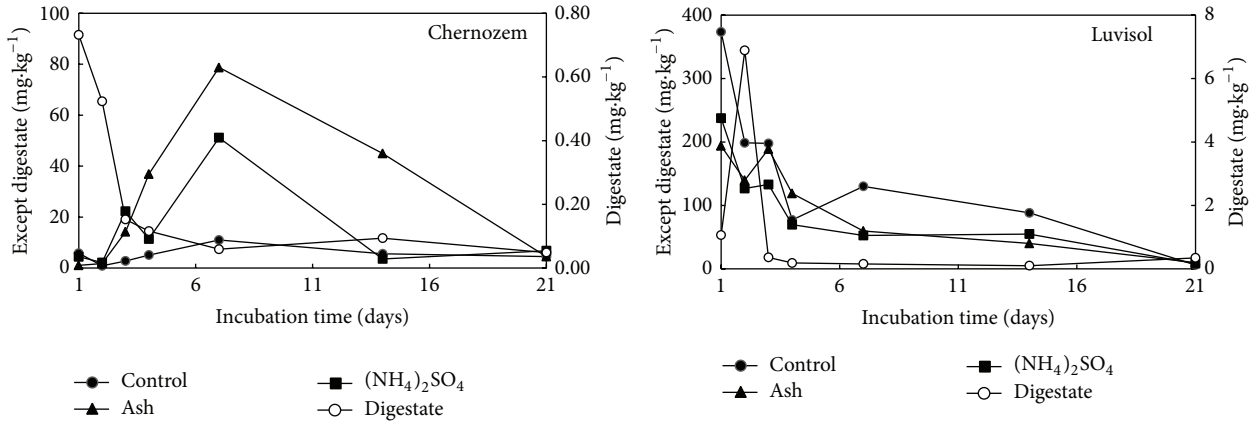

Figure 1: The concentrations of Hg extractable with 0.11 mol L^{-1} acetic acid within the incubation experiment (mg·kg^{-1}) according to the individual treatments.

However, some microorganisms have developed mechanisms to adapt to Hg, that is, Hg-resistant bacteria. Thus, the changes in Hg mobility observed throughout the experiment could be partially attributed to different communities of soil microorganism present in both Chernozem and Luvisol.

Therefore, among the individual treatments, digestate was shown to be the most effective Hg immobilizing agent, whereas fly ash seemed to be less effective, and no significant difference was reported comparing the ammonium sulfate treatment and untreated control except the faster increase of mobile Hg content in 3rd and 4th days of the incubation indicating potential role of increased portion of mobile sulfur as mentioned below. The effectiveness of individual treatments as well as the temporal changes in mobile Hg portions were also affected predominantly by the soil where higher sorption capacity and organic matter content in Chernozem resulted in lower mobile portions of Hg in all the treatments except increased mobility of Hg after ash application in 7th and 14th day of the incubation. These results also indicated that S content in the ameliorative materials was not the main factor controlling the Hg mobility in the soils. Luo et al. [6] reported a low relationship between S and Hg contents in soils with low total organic carbon (~2%), as in our case, where the carbon content was not increased by the addition of ammonium sulfate and ash. In the opposite, the Hg behaviour in soils strongly differed if digestate with high content of both S and total carbon content was applied.

Higher organic carbon content in the soil can enhance both soil microbial activities and the retention of total Hg and MeHg in soil [29]. Soil microorganisms need essential metals for their metabolism, which are often required in low concentrations and act as enzyme cofactors [30]. Therefore, high contents of macro- and micronutrients in both ash and digestate (Table 2) can be beneficial for the enhancement of the microbial activity in soils. Limited Hg mobility *via* complexation with soil organic matter was already described [9]. Ravichandran [31] reviewed the formation of extremely strong ionic bonds between Hg and reduced S sites in soil organic matter supporting the importance of the mutual role of S and organic matter in Hg immobilization in soil. Therefore, the Hg desorption increased with elevating concentrations of dissolved organic matter [10]. In our case, the dissolved organic matter after 1 day of incubation varied between 71.9 mg·kg^{-1} (control) and 1070 mg·kg^{-1} (digestate) in Chernozem and between 21.2 mg·kg^{-1} (control) and 56.4 mg·kg^{-1} (digestate) in Luvisol. After 7 days of incubation, the DOM contents increased even 22-fold in the digestate-treated Luvisol, whereas the maximum 1.5-fold increase was observed in Chernozem. Therefore, our results indicate that more complex factors can change the Hg mobility in soil than solely the content and solubility of organic carbon in soil. For example, the affinity of Hg to bind to metal oxides should be taken into account [32]. Also, the role of some soil bacteria which are able to degrade Hg compounds into metallic Hg by the action of specific enzymes encoded by the *mer* genes and then be released into the surrounding environment should be considered [33]. Thus, the decrease of mobile Hg in soil could be partially figured in the volatilization of this element during incubation. This assumption remains to be verified in further research. In our investigation, the experiments were concerned on the description of potential decrease of mobile Hg content without exact resolution between immobilization/volatilization ratios after the individual treatments.

3.2. The Effect of Hg and/or Ameliorative Materials on Mobile Contents of Macro- and Micronutrients in the Soil. The mobile macro- and microelement contents affected by the individual treatments and/or duration of incubation are summarized in Tables 3, 4, 5, 6, 7, 8, 9, 10, and 11. The presence of digestate showed a predominant effect on the mobile portions of most of the elements among all the treatments. The mobile element contents significantly increased after digestate application for most of the determined nutrients, except Ca and Cu in Chernozem (because of its low availability in the ameliorative materials). More apparent increase of mobile element contents after application of digestate was observed for Luvisol compared to Chernozem due to higher sorption capacity of Chernozem in accordance with their higher CEC level. For example, Table 4 shows 5-fold increase of mobile Mg

Table 3: The concentrations of Ca extractable with 0.11 mol L^{-1} acetic acid within the incubation experiment (mg·kg^{-1}); the averages marked by the same letter did not significantly differ at $P < 0.05$ within individual columns; data are presented as mean ± standard deviation ($n = 3$).

Chernozem	Day 1	Day 2	Day 3	Day 4	Day 7	Day 14	Day 21
Control	7555 ± 331^{a}	7655 ± 183^{a}	8390 ± a213^{a}	9674 ± 219^{a}	9034 ± 238^{ab}	9856 ± 1191^{ab}	6040 ± 270^{a}
Control + Hg	8074 ± 260^{a}	7694 ± 359^{a}	7467 ± a677^{a}	9607 ± 193^{a}	8891 ± 702^{a}	8951 ± 236^{ab}	7865 ± 983^{abc}
Digestate	8282 ± 735^{a}	8094 ± 155^{a}	8049 ± a687^{a}	10122 ± 206^{a}	8886 ± 362^{a}	11004 ± 926^{b}	12402 ± 2330^{bc}
Digestate + Hg	8108 ± 232^{a}	9656 ± 282^{a}	7824 ± a454^{a}	11360 ± 1521^{a}	10104 ± 205^{b}	10232 ± 499^{ab}	11286 ± 1243^{c}
Ash	8448 ± 548^{a}	8246 ± a282^{a}	8746 ± a272^{a}	9898 ± 213^{a}	9661 ± 466^{ab}	9633 ± 203^{ab}	9835 ± 2134^{abc}
Ash + Hg	8164 ± 921^{a}	8072 ± a511^{a}	8717 ± a611^{a}	10910 ± 898^{a}	9862 ± 300^{ab}	10599 ± 387^{ab}	9359 ± 1118^{abc}
$(NH_4)_2SO_4$	7330 ± 57^{a}	7409 ± a201^{a}	8037 ± a311^{a}	10134 ± 1290^{a}	8942 ± 307^{a}	8893 ± 990^{a}	10045 ± 2115^{abc}
$(NH_4)_2SO_4$ + Hg	8041 ± 796^{a}	7393 ± a359^{a}	8350 ± 1151^{a}	9820 ± 207^{a}	8991 ± 382^{ab}	10238 ± 790^{ab}	7031 ± 3008^{abc}
Luvisol	Day 1	Day 2	Day 3	Day 4	Day 7	Day 14	Day 21
Control	1404 ± 96^{a}	1401 ± 73^{a}	1372 ± 56^{a}	1691 ± 51^{ab}	1671 ± 90^{a}	1764 ± 223^{a}	1273 ± 125^{a}
Control + Hg	1450 ± 93^{a}	1407 ± 38^{a}	1396 ± 45^{a}	1635 ± 52^{a}	1575 ± 107^{a}	1655 ± 89^{a}	1274 ± 283^{a}
Digestate	3558 ± 121^{b}	2593 ± 574^{b}	2733 ± 492^{b}	4086 ± 116^{d}	3776 ± 264^{c}	3294 ± 380^{b}	3757 ± 428^{ab}
Digestate + Hg	3455 ± 569^{b}	3190 ± 282^{b}	3139 ± 328^{b}	3804 ± 613^{d}	4462 ± 644^{c}	3975 ± 206^{c}	4758 ± 327^{b}
Ash	2335 ± 433^{a}	2382 ± 197^{a}	2281 ± 321^{a}	2540 ± 234^{bc}	2917 ± 164^{b}	2686 ± 281^{b}	2121 ± 286a^{b}
Ash + Hg	1981 ± 254^{a}	1908 ± 149^{a}	2044 ± 161^{a}	2574 ± 512^{c}	2717 ± 117^{b}	3092 ± 190^{b}	2784 ± 467^{ab}
$(NH_4)_2SO_4$	1514 ± 57^{a}	1356 ± 36^{a}	1411 ± 102^{a}	1651 ± 69^{a}	1597 ± 79^{a}	1684 ± 135^{a}	1663 ± 92^{ab}
$(NH_4)_2SO_4$ + Hg	1655 ± 54^{a}	1577 ± 246^{a}	1431 ± 59^{a}	1742 ± 108^{abc}	1616 ± 32^{a}	1666 ± 124^{a}	1690 ± 107^{ab}

Table 4: The concentrations of Mg extractable with 0.11 mol L^{-1} acetic acid within the incubation experiment (mg·kg^{-1}); the averages marked by the same letter did not significantly differ at $P < 0.05$ within individual columns; data are presented as mean ± standard deviation ($n = 3$).

Chernozem	Day 1	Day 2	Day 3	Day 4	Day 7	Day 14	Day 21
Control	389 ± 20^{a}	401 ± 2^{ab}	483 ± 8^{a}	562 ± 18^{a}	503 ± 48^{a}	546 ± 23^{a}	371 ± 50^{a}
Control + Hg	347 ± 111^{a}	406 ± 20^{abc}	442 ± 32^{a}	556 ± 16^{a}	502 ± 69^{a}	505 ± 34^{a}	533 ± 135^{ab}
Digestate	544 ± 50^{c}	544 ± 30^{d}	603 ± 65^{b}	753 ± 52^{bc}	656 ± 76^{ab}	781 ± 54^{c}	963 ± 155^{c}
Digestate + Hg	519 ± 37^{c}	603 ± 24^{e}	610 ± 45^{b}	809 ± 44^{d}	734 ± 73^{b}	742 ± 22^{bc}	859 ± 77^{bc}
Ash	442 ± 24^{ab}	458 ± 27^{c}	522 ± 22^{ab}	612 ± 22^{ac}	566 ± 56^{a}	574 ± 66^{a}	636 ± 147^{abc}
Ash + Hg	432 ± 57^{ab}	447 ± 9^{bc}	518 ± 35^{ab}	681 ± 72^{ab}	555 ± 31^{a}	626 ± 62^{ab}	585 ± 122^{ab}
$(NH_4)_2SO_4$	374 ± 3^{a}	394 ± 16^{ab}	461 ± 13^{a}	572 ± 72^{a}	506 ± 59^{a}	494 ± 71^{a}	626 ± 171^{abc}
$(NH_4)_2SO_4$ + Hg	406 ± 30^{ab}	390 ± 10^{a}	468 ± 32^{a}	566 ± 10^{a}	505 ± 45^{a}	553 ± 39^{a}	489 ± 119^{a}
Luvisol	Day 1	Day 2	Day 3	Day 4	Day 7	Day 14	Day 21
Control	65 ± 5^{a}	72 ± 5^{a}	71 ± 2^{a}	89 ± 3^{a}	120 ± 47^{a}	129 ± 61^{a}	89 ± 19^{a}
Control + Hg	70 ± 4^{a}	72 ± 2^{a}	73 ± 1^{a}	86 ± 3^{a}	108 ± 43^{a}	115 ± 45^{a}	82 ± 11^{a}
Digestate	362 ± 27^{c}	259 ± 70^{c}	325 ± 52^{b}	446 ± 5^{c}	408 ± 40^{b}	391 ± 51^{b}	423 ± 11^{c}
Digestate + Hg	364 ± 89^{c}	336 ± 38^{c}	363 ± 92^{b}	460 ± 54^{c}	476 ± 28^{b}	416 ± 33^{b}	366 ± 90^{c}
Ash	144 ± 32^{b}	156 ± 19^{b}	162 ± 34^{ab}	176 ± 21^{b}	231 ± 51^{a}	214 ± 66^{a}	174 ± 40^{ab}
Ash + Hg	116 ± 19^{b}	121 ± 14^{ab}	140 ± 21^{ab}	178 ± 47^{b}	214 ± 52^{a}	243 ± 31^{a}	240 ± 33^{b}
$(NH_4)_2SO_4$	73 ± 0^{a}	68 ± 0^{a}	72 ± 5^{a}	85 ± 1^{a}	120 ± 49^{a}	114 ± 43^{a}	120 ± 33^{a}
$(NH_4)_2SO_4$ + Hg	85 ± 9^{a}	74 ± 5^{ab}	76 ± 2^{ab}	92 ± 7^{a}	115 ± 46^{a}	119 ± 50^{a}	117 ± 38^{a}

contents in the digestate treated Luvisol compared to up to 40% increase of mobile Mg in Chernozem.

Möller and Müller [34] reviewed recent research about nutrient availability after the field application of digestate and stated that there is no available information concerning the availability of S, although digestate seems to be a good source of S in soil; this was also observed in our case (Table 2) where the S content in the digestate sample reached up to 0.6%. Similarly, they stated that there were many published studies describing the effect of anaerobic digestion on micronutrient distribution and bioavailability in sewage sludge, but rarely any concerning digestates. Moreover, the availability of micronutrients in the digestate can be affected by the wide complex of various factors such as precipitation as sulfide, carbonate, phosphates, and hydroxides, sorption to the solid fraction, either biomass or inert suspended matter, and the formation of complexes in solution with intermediates and compounds produced during anaerobic digestion [34]. The application of digestate results in an improvement of crop yields compared to inorganic fertilizer. Moreover, analysis of soil solution showed that there was less potential for the loss of nutrients *via* leaching [35] in the digestate treated soil.

Table 5: The concentrations of K extractable with 0.11 mol L^{-1} acetic acid within the incubation experiment (mg·kg^{-1}); the averages marked by the same letter did not significantly differ at $P < 0.05$ within individual columns; data are presented as mean ± standard deviation ($n = 3$).

Chernozem	Day 1	Day 2	Day 3	Day 4	Day 7	Day 14	Day 21
Control	68 ± 5^{a}	78 ± 4^{a}	78 ± 2^{a}	84 ± 2^{a}	92 ± 4^{a}	95 ± 0^{a}	53 ± 3^{a}
Control + Hg	83 ± 17^{a}	76 ± 4^{a}	77 ± 10^{a}	87 ± 3^{a}	90 ± 6^{a}	94 ± 3^{a}	76 ± 12^{a}
Digestate	2882 ± 906^{b}	2931 ± 491^{b}	3026 ± 304^{b}	3547 ± 163^{b}	3615 ± 177^{c}	3842 ± 277^{c}	4408 ± 506^{b}
Digestate + Hg	2461 ± 510^{b}	3163 ± 128^{b}	2961 ± 261^{b}	3915 ± 370^{b}	3780 ± 164^{d}	3697 ± 191^{c}	4283 ± 367^{b}
Ash	269 ± 66^{a}	284 ± 40^{a}	294 ± 59^{a}	317 ± 78^{a}	374 ± 35^{cd}	362 ± 18^{ab}	406 ± 146^{a}
Ash + Hg	260 ± 61^{a}	305 ± 77^{a}	310 ± 47^{a}	467 ± 101^{a}	362 ± 25^{bc}	446 ± 63^{b}	359 ± 82^{a}
$(NH_4)_2SO_4$	97 ± 5^{a}	119 ± 11^{a}	107 ± 6^{a}	130 ± 13^{a}	126 ± 6^{ab}	117 ± 13^{ab}	109 ± 6^{a}
$(NH_4)_2SO_4$ + Hg	105 ± 6^{a}	109 ± 4^{a}	112 ± 6^{a}	135 ± 2^{a}	130 ± 5^{abc}	145 ± 10^{ab}	1568 ± 207^{a}
Luvisol	Day 1	Day 2	Day 3	Day 4	Day 7	Day 14	Day 21
Control	117 ± 7^{a}	126 ± 7^{a}	117 ± 3^{a}	140 ± 4^{a}	138 ± 2^{a}	147 ± 9^{a}	111 ± 12^{a}
Control + Hg	122 ± 6^{a}	130 ± 6^{a}	125 ± 4^{a}	139 ± 4^{a}	138 ± 5^{a}	146 ± 3^{a}	122 ± 21^{a}
Digestate	3324 ± 201^{b}	2684 ± 425^{b}	3173 ± 54^{b}	3857 ± 252^{b}	3936 ± 37^{c}	3665 ± 83^{c}	4063 ± 418^{c}
Digestate + Hg	3728 ± 541^{b}	3306 ± 214^{b}	3351 ± 540^{b}	4065 ± 150^{b}	3927 ± 308^{c}	3655 ± 64^{c}	3304 ± 180^{b}
Ash	431 ± 146^{a}	487 ± 78^{a}	431 ± 111^{a}	419 ± 70^{a}	548 ± 66^{b}	446 ± 71^{b}	387 ± 18^{a}
Ash + Hg	316 ± 70^{a}	343 ± 41^{a}	370 ± 39^{a}	454 ± 102^{a}	489 ± 15^{b}	546 ± 66^{b}	553 ± 118^{a}
$(NH_4)_2SO_4$	152 ± 3^{a}	145 ± 5^{a}	143 ± 11^{a}	162 ± 1^{a}	161 ± 5^{a}	167 ± 9^{a}	166 ± 17^{a}
$(NH_4)_2SO_4$ + Hg	159 ± 6^{a}	158 ± 9^{a}	152 ± 4^{a}	176 ± 9^{a}	169 ± 4^{a}	162 ± 4^{a}	170 ± 14^{a}

Table 6: The concentrations of Cu extractable with 0.11 mol L^{-1} acetic acid within the incubation experiment (mg·kg^{-1}); the averages marked by the same letter did not significantly differ at $P < 0.05$ within individual columns; data are presented as mean ± standard deviation ($n = 3$).

Chernozem	Day 1	Day 2	Day 3	Day 4	Day 7	Day 14	Day 21
Control	0.045 ± 0.007^{a}	0.039 ± 0.008^{a}	0.015 ± 0.003^{a}	0.025 ± 0.003^{a}	0.162 ± 0.018^{abc}	0.064 ± 0.013^{a}	0.017 ± 0.008^{a}
Control + Hg	0.047 ± 0.012^{a}	0.017 ± 0.001^{a}	0.017 ± 0.004^{a}	0.023 ± 0.003^{a}	0.039 ± 0.019^{a}	0.098 ± 0.025^{a}	0.034 ± 0.015^{a}
Digestate	0.224 ± 0.092^{b}	0.230 ± 0.098^{b}	0.187 ± 0.037^{c}	0.299 ± 0.010^{c}	0.362 ± 0.051^{c}	0.517 ± 0.089^{c}	0.911 ± 0.141^{b}
Digestate + Hg	0.120 ± 0.010^{a}	0.094 ± 0.026^{a}	0.089 ± 0.028^{b}	0.166 ± 0.038^{b}	0.264 ± 0.031^{bc}	0.334 ± 0.031^{b}	0.763 ± 0.065^{b}
Ash	0.053 ± 0.019^{a}	0.059 ± 0.014^{a}	0.032 ± 0.007^{a}	0.054 ± 0.012^{a}	0.065 ± 0.042^{ab}	0.073 ± 0.043^{a}	0.148 ± 0.029^{a}
Ash + Hg	0.079 ± 0.011^{a}	0.042 ± 0.003^{a}	0.026 ± 0.005^{a}	0.060 ± 0.013^{a}	0.055 ± 0.035^{a}	0.095 ± 0.027^{a}	0.141 ± 0.069^{a}
$(NH_4)_2SO_4$	0.047 ± 0.035^{a}	0.048 ± 0.013^{a}	0.018 ± 0.006^{a}	0.022 ± 0.006^{a}	0.081 ± 0.031^{ab}	0.091 ± 0.038^{a}	0.090 ± 0.060^{a}
$(NH_4)_2SO_4$ + Hg	0.038 ± 0.020^{a}	0.029 ± 0.007^{a}	0.008 ± 0.008^{a}	0.029 ± 0.002^{a}	0.029 ± 0.013^{a}	0.066 ± 0.048^{a}	0.379 ± 0.093^{ab}
Luvisol	Day 1	Day 2	Day 3	Day 4	Day 7	Day 14	Day 21
Control	0.095 ± 0.003^{a}	0.084 ± 0.019^{a}	0.061 ± 0.007^{a}	0.134 ± 0.021^{a}	0.142 ± 0.042^{a}	0.226 ± 0.008^{a}	0.252 ± 0.055^{a}
Control + Hg	0.128 ± 0.020^{a}	0.118 ± 0.021^{ab}	0.098 ± 0.011^{a}	0.156 ± 0.024^{ab}	0.164 ± 0.062^{a}	0.357 ± 0.021^{ab}	0.230 ± 0.062^{a}
Digestate	0.284 ± 0.085^{a}	0.268 ± 0.022^{b}	0.316 ± 0.051^{b}	0.553 ± 0.087^{c}	0.534 ± 0.136^{b}	0.785 ± 0.032^{d}	1.200 ± 0.142^{c}
Digestate + Hg	0.166 ± 0.122^{a}	0.095 ± 0.012^{a}	0.120 ± 0.055^{a}	0.131 ± 0.092^{a}	0.119 ± 0.015^{a}	0.594 ± 0.137^{cd}	0.678 ± 0.164^{ab}
Ash	0.196 ± 0.026^{a}	0.161 ± 0.036^{ab}	0.145 ± 0.023^{ab}	0.269 ± 0.051^{ab}	0.220 ± 0.045^{a}	0.542 ± 0.046^{bc}	0.493 ± 0.081^{ab}
Ash + Hg	0.225 ± 0.048^{ab}	0.261 ± 0.024^{b}	0.193 ± 0.016^{ab}	0.298 ± 0.045^{b}	0.266 ± 0.040^{a}	0.578 ± 0.058^{c}	0.900 ± 0.042^{bc}
$(NH_4)_2SO_4$	0.101 ± 0.022^{a}	0.191 ± 0.048^{ab}	0.078 ± 0.004^{a}	0.184 ± 0.018^{ab}	0.161 ± 0.024^{a}	0.308 ± 0.051^{a}	0.658 ± 0.103^{ab}
$(NH_4)_2SO_4$ + Hg	0.140 ± 0.027^{a}	0.138 ± 0.028^{ab}	0.121 ± 0.014^{a}	0.247 ± 0.068^{ab}	0.193 ± 0.050^{a}	0.422 ± 0.101^{abc}	0.555 ± 0.062^{ab}

Also, Frøseth et al. [36] observed that the field application of digestate contributed to higher soil aggregate stability. According to Fernández-Delgado Juarez et al. [37], amending soils with digestate resulted in a higher nutrient content as well as more efficient soil microbial community relative to the variants treated with farmyard manure. Therefore, the application of digestate seemed to be the effective measure for immobilization of Hg in soil together with increase of mobile nutrients in these soils.

The application of wood fly ash as a potential source of available nutrients in the soil is widely discussed in the literature [38, 39]. The benefits on the growth of the plants as the result of an increase in available P, Ca, Mg, K, and B and a decrease in Al toxicity was described [38]. Steenari et al. [40] tested the release of macro- and microelements from various ash samples, whereas low leaching rates were observed for the important plant nutrients P and Mg, as well as for Fe, Mn, Cu, and Zn, up to 50% of total K was released during the batch leaching test. In our case, the extractable element contents in the ash amended samples differed according to the experimental soil, where Ca, Fe, and Cu levels remained unchanged compared to the control.

Table 7: The concentrations of Fe extractable with 0.11 mol L^{-1} acetic acidwithin the incubation experiment (mg·kg^{-1}); The averages marked by the same letter did not significantly differ at $P < 0.05$ within individual columns; data are presented as mean ± standard deviation ($n = 3$).

Chernozem	Day 1	Day 2	Day 3	Day 4	Day 7	Day 14	Day 21
Control	1.54 ± 0.38^{a}	20.47 ± 6.26^{a}	8.49 ± 0.70^{a}	0.28 ± 0.02^{a}	0.48 ± 0.11^{a}	4.52 ± 0.24^{a}	0.25 ± 0.06^{a}
Control + Hg	1.40 ± 0.09^{a}	8.20 ± 2.34^{a}	10.76 ± 8.02^{a}	0.18 ± 0.03^{a}	0.20 ± 0.03^{a}	2.90 ± 1.05^{a}	0.24 ± 0.04^{a}
Digestate	49.3 ± 9.4^{c}	95.4 ± 17.2^{c}	105.9 ± 2.6^{b}	142.5 ± 11.7^{c}	102.4 ± 2.7^{c}	32.4 ± 5.3^{b}	48.7 ± 6.4^{b}
Digestate + Hg	27.0 ± 4.2^{b}	61.9 ± 15.2^{b}	77.1 ± 28.8^{b}	73.1 ± 10.7^{b}	69.4 ± 5.5^{b}	48.0 ± 14.2^{c}	48.3 ± 9.6^{b}
Ash	1.31 ± 0.16^{a}	28.78 ± 5.86^{a}	6.87 ± 1.97^{a}	0.26 ± 0.10^{a}	0.35 ± 0.11^{a}	1.53 ± 0.17^{a}	0.90 ± 0.24^{a}
Ash + Hg	1.16 ± 0.46^{a}	8.17 ± 2.01^{a}	7.58 ± 4.58^{a}	0.30 ± 0.11^{a}	0.28 ± 0.04^{a}	1.07 ± 0.10^{a}	0.06 ± 0.03^{a}
$(NH_4)_2SO_4$	1.29 ± 0.15^{a}	17.20 ± 5.83^{a}	5.53 ± 1.19^{a}	0.35 ± 0.17^{a}	0.26 ± 0.06^{a}	3.91 ± 1.32^{a}	0.15 ± 0.12^{a}
$(NH_4)_2SO_4$ + Hg	1.13 ± 0.28^{a}	10.53 ± 3.15^{a}	7.21 ± 2.97^{a}	0.14 ± 0.09^{a}	0.23 ± 0.03^{a}	1.53 ± 0.19^{a}	2.37 ± 0.36^{a}
Luvisol	Day 1	Day 2	Day 3	Day 4	Day 7	Day 14	Day 21
Control	3.88 ± 2.13^{a}	20.08 ± 6.85^{a}	7.35 ± 1.27^{a}	1.31 ± 0.18^{a}	1.04 ± 0.14^{a}	7.17 ± 2.64^{a}	1.13 ± 0.66^{a}
Control + Hg	2.21 ± 0.27^{a}	10.02 ± 4.27^{a}	12.24 ± 2.19^{a}	1.38 ± 0.31^{a}	0.91 ± 0.08^{a}	5.99 ± 0.76^{a}	0.67 ± 0.47^{a}
Digestate	100.8 ± 33.1^{b}	51.9 ± 25.4^{b}	67.6 ± 40.6^{ab}	44.7 ± 14.3^{b}	77.4 ± 14.5^{b}	42.5 ± 13.0^{a}	173.5 ± 71.0^{b}
Digestate + Hg	108.0 ± 38.7^{b}	340.9 ± 82.3^{b}	329.4 ± 70.4^{b}	413.7 ± 52.8^{c}	484.7 ± 97.2^{c}	396.9 ± 54.1^{b}	315.4 ± 63.8^{c}
Ash	2.80 ± 0.70^{a}	16.71 ± 3.74^{a}	15.41 ± 3.44^{a}	1.82 ± 0.59^{a}	1.58 ± 0.77^{a}	7.44 ± 2.02^{a}	2.86 ± 1.43^{a}
Ash + Hg	2.56 ± 0.27^{a}	15.88 ± 9.53^{a}	11.24 ± 4.10^{a}	1.21 ± 0.44^{a}	0.99 ± 0.18^{a}	2.94 ± 1.18^{a}	0.59 ± 0.05^{a}
$(NH_4)_2SO_4$	3.07 ± 0.09^{a}	8.82 ± 0.53^{a}	7.06 ± 2.55^{a}	1.61 ± 0.21^{a}	1.28 ± 0.07^{a}	5.68 ± 1.15^{a}	1.64 ± 0.30^{a}
$(NH_4)_2SO_4$ + Hg	3.01 ± 0.32^{a}	10.36 ± 2.32^{a}	14.56 ± 2.55^{a}	1.59 ± 0.21^{a}	1.39 ± 0.24^{a}	2.47 ± 0.42^{a}	1.02 ± 0.23^{a}

Table 8: The concentrations of Mn extractable with 0.11 mol L^{-1} acetic acid within the incubation experiment (mg·kg^{-1}); the averages marked by the same letter did not significantly differ at $P < 0.05$ within individual columns; data are presented as mean ± standard deviation ($n = 3$).

Chernozem	Day 1	Day 2	Day 3	Day 4	Day 7	Day 14	Day 21
Control	19.5 ± 1.2^{a}	19.9 ± 0.7^{a}	22.2 ± 1.1^{a}	35.0 ± 6.1^{a}	33.9 ± 0.9^{a}	46.7 ± 16.0^{a}	34.7 ± 8.7^{a}
Control + Hg	21.4 ± 4.4^{a}	22.1 ± 3.4^{ab}	20.7 ± 3.9^{a}	36.2 ± 4.8^{a}	36.6 ± 0.3^{a}	37.3 ± 5.0^{c}	37.8 ± 11.6^{a}
Digestate	168 ± 22^{c}	168 ± 12^{c}	177 ± 10^{c}	232 ± 4^{d}	204 ± 4^{c}	218 ± 11^{a}	301 ± 68^{d}
Digestate + Hg	152 ± 4^{c}	181 ± 6^{c}	168 ± 4^{c}	229 ± 23^{d}	204 ± 5^{c}	208 ± 3^{c}	266 ± 30^{cd}
Ash	42.4 ± 7.3^{b}	38.7 ± 9.8^{ab}	57.5 ± 21.7^{b}	70.2 ± 8.5^{bc}	66.3 ± 10.6^{b}	66.9 ± 14.0^{a}	101.5 ± 53.7^{ab}
Ash + Hg	38.5 ± 9.2^{b}	40.0 ± 4.4^{b}	46.1 ± 7.0a^{b}	96.8 ± 18.0^{c}	73.9 ± 6.5^{b}	93.1 ± 15.5^{ab}	83.0 ± 32.3^{ab}
$(NH_4)_2SO_4$	23.8 ± 1.5^{a}	24.1 ± 1.6^{ab}	27.0 ± 0.7^{a}	46.7 ± 5.0^{ab}	69.7 ± 16.6^{b}	143.1 ± 19.7^{b}	125.6 ± 36.1^{bc}
$(NH_4)_2SO_4$ + Hg	26.4 ± 8.5^{a}	28.0 ± 7.4^{ab}	30.3 ± 9.3^{ab}	39.2 ± 5.5^{ab}	40.7 ± 9.8^{a}	56.5 ± 13.9^{a}	70.8 ± 33.6^{ab}
Luvisol	Day 1	Day 2	Day 3	Day 4	Day 7	Day 14	Day 21
Control	27.0 ± 1.0^{a}	30.3 ± 1.0^{a}	33.6 ± 3.6^{a}	55.9 ± 1.0^{a}	50.8 ± 9.3^{a}	64.2 ± 14.0^{a}	34.7 ± 7.8^{a}
Control + Hg	43.6 ± 0.8^{abc}	43.3 ± 10.1^{ab}	45.1 ± 7.0^{abc}	67.4 ± 5.1^{ab}	61.5 ± 6.7^{a}	77.4 ± 8.5^{ab}	37.8 ± 7.1^{a}
Digestate	161 ± 9^{d}	142 ± 23^{d}	169 ± 8^{d}	191 ± 2^{c}	198 ± 25^{c}	189 ± 19^{c}	301 ± 30^{c}
Digestate + Hg	148 ± 9^{d}	176 ± 2^{e}	180 ± 5^{d}	222 ± 10^{d}	223 ± 11^{c}	229 ± 11^{d}	266 ± 81^{c}
Ash	54.9 ± 10.4^{c}	59.4 ± 8.8^{b}	53.2 ± 9.0^{bc}	87.0 ± 14.2^{b}	131.4 ± 42.3^{b}	114.0 ± 23.8^{b}	101.5 ± 34.1^{b}
Ash + Hg	54.4 ± 7.2^{c}	58.6 ± 2.4^{b}	58.9 ± 4.8^{c}	86.0 ± 12.1^{b}	81.9 ± 5.8^{ab}	108.9 ± 0.8^{b}	83.0 ± 69.1^{a}
$(NH_4)_2SO_4$	27.9 ± 0.5^{ab}	28.5 ± 1.5^{a}	29.0 ± 1.7^{a}	50.3 ± 8.3^{a}	42.8 ± 6.6^{a}	60.9 ± 12.4^{a}	125.6 ± 3.2^{b}
$(NH_4)_2SO_4$ + Hg	46.5 ± 4.6^{bc}	46.9 ± 5.2^{ab}	42.6 ± 3.2^{ab}	62.4 ± 12.4^{ab}	65.9 ± 6.0^{a}	63.6 ± 2.9^{a}	70.8 ± 5.2^{a}

On the contrary, the extremely high Zn level in the ash (Table 2) resulted in the significant increase in the extractable Zn portion of the ash-treated soil regardless of the soil type (Table 11). A similar pattern was reported for Mg, where the increase in the extractable Mg portion was more apparent in Luvisol (Table 4). Whereas in the Luvisol the mobile Mg contents increased twice after ash application, the mobile portion of Mg in Chernozem rised only by 10–15%. The low mobility of micronutrients in various ash samples was also confirmed by Száková et al. [41]. The K, Mn, and P extractable levels tended to increase compared to controls (significance of the differences at $P < 0.05$ was unambiguously proved only in the case of Mn, see Table 8) but were significantly lower compared to digestate application, not confirming the high K leachability from ash samples observed by Steenari et al. [40]. Although the total S contents added *via* the individual treatments were comparable, the mobile portions of ash-derived S were lower compared to those after the application of digestate and ammonium sulfate. Ochecová et al. [20] observed increasing mobile portions of Ca, P, K, Mg, and Mn in the fly ash-treated soil after a 3-year model pot experiment. However, the effects were significant for the 3–6 fold higher

Table 9: The concentrations of P extractable with 0.11 mol L^{-1} acetic acid within the incubation experiment (mg·kg^{-1}); the averages marked by the same letter did not significantly differ at $P < 0.05$ within individual columns; data are presented as mean ± standard deviation ($n = 3$).

Chernozem	Day 1	Day 2	Day 3	Day 4	Day 7	Day 14	Day 21
Control	90.9 ± 6.3^{a}	88.9 ± 24.9^{a}	112.3 ± 33.3^{a}	109.3 ± 7.0^{a}	93.6 ± 7.9^{a}	88.8 ± 11.7^{a}	55.9 ± 6.5^{a}
Control + Hg	85.0 ± 17.9^{a}	88.1 ± 1.9^{a}	108.4 ± 19.0^{a}	127.8 ± 14.3^{a}	91.2 ± 4.7^{a}	98.1 ± 14.1^{a}	79.3 ± 13.9^{a}
Digestate	259.0 ± 50.0^{b}	269.0 ± 49.5^{b}	235.2 ± 63.2^{b}	320.9 ± 60.5^{b}	189.1 ± 23.5^{b}	278.6 ± 30.5^{b}	246.0 ± 59.9^{b}
Digestate + Hg	250.9 ± 62.4^{b}	285.6 ± 28.3^{b}	261.6 ± 40.4^{b}	361.0 ± 14.2^{b}	293.6 ± 12.5^{c}	274.5 ± 51.7^{b}	253.5 ± 51.8^{b}
Ash	107.1 ± 6.2^{a}	102.1 ± 17.1^{a}	101.7 ± 2.9^{a}	130.0 ± 18.1^{a}	115.4 ± 17.5^{a}	98.9 ± 9.2^{a}	123.3 ± 30.4^{a}
Ash + Hg	104.2 ± 7.5^{a}	101.6 ± 5.7^{a}	105.5 ± 6.4^{a}	138.3 ± 11.9^{a}	118.4 ± 28.0^{a}	115.3 ± 6.0^{a}	96.6 ± 19.6^{a}
$(NH_4)_2SO_4$	96.9 ± 10.0^{a}	91.3 ± 1.7^{a}	93.4 ± 13.1^{a}	110.4 ± 4.8^{a}	94.4 ± 1.2^{a}	102.2 ± 12.6^{a}	116.8 ± 15.6^{a}
$(NH_4)_2SO_4$ + Hg	84.3 ± 4.7^{a}	90.2 ± 4.3^{a}	117.9 ± 22.3^{a}	118.7 ± 17.1^{a}	95.4 ± 3.1^{a}	91.8 ± 7.9^{a}	106.5 ± 37.4^{a}
Luvisol	Day 1	Day 2	Day 3	Day 4	Day 7	Day 14	Day 21
Control	62.9 ± 5.8^{a}	61.9 ± 6.3^{a}	61.2 ± 11.1^{a}	70.8 ± 0.6^{a}	65.8 ± 16.3^{a}	56.62.7 ±^{a}	38.9 ± 3.8^{a}
Control + Hg	66.8 ± 9.6^{a}	63.4 ± 0.5^{a}	65.6 ± 10.4^{a}	71.5 ± 8.6^{a}	62.3 ± 1.7^{a}	67.4 ± 5.7^{a}	43.7 ± 12.0^{a}
Digestate	323.7 ± 26.2^{b}	210.2 ± 67.6^{b}	203.4 ± 58.7^{b}	323.4 ± 14.3^{b}	290.3 ± 30.1^{b}	245.8 ± 56.8^{b}	254.0 ± 24.0^{c}
Digestate + Hg	329.6 ± 82.9^{b}	286.5 ± 40.6^{b}	246.3 ± 77.2^{b}	350.0 ± 44.8^{b}	348.6 ± 90.4^{b}	262.2 ± 28.7^{b}	130.7 ± 48.9^{b}
Ash	85.0 ± 5.3^{a}	84.4 ± 8.8^{a}	80.5 ± 13.1^{a}	90.6 ± 14.1^{a}	92.6 ± 7.4^{a}	78.3 ± 4.8^{a}	55.6 ± 6.0^{a}
Ash + Hg	76.4 ± 6.3^{a}	73.7 ± 4.7^{a}	75.8 ± 3.6^{a}	90.7 ± 12.4^{a}	81.4 ± 2.5^{a}	86.5 ± 4.0^{a}	68.7 ± 1.6^{a}
$(NH_4)_2SO_4$	61.3 ± 1.1^{a}	58.3 ± 3.6^{a}	57.3 ± 4.0^{a}	69.1 ± 8.2^{a}	59.4 ± 4.8^{a}	59.3 ± 4.2^{a}	60.6 ± 9.2 ^{a}
$(NH_4)_2SO_4$ + Hg	60.4 ± 1.6^{a}	72.9 ± 13.7^{a}	59.6 ± 2.8^{a}	69.5 ± 1.2^{a}	63.3 ± 4.1^{a}	58.8 ± 2.5^{a}	58.7 ± 0.6^{a}

Table 10: The concentrations of S extractable with 0.11 mol L^{-1} acetic acid within the incubation experiment (mg·kg^{-1}); the averages marked by the same letter did not significantly differ at $P < 0.05$ within individual columns; data are presented as mean ± standard deviation ($n = 3$).

Chernozem	Day 1	Day 2	Day 3	Day 4	Day 7	Day 14	Day 21
Control	8.8 ± 1.0^{a}	9.7 ± 0.9^{a}	12.3 ± 5.6^{a}	14.9 ± 5.0^{a}	17.7 ± 2.1^{a}	16.1 ± 4.1^{a}	10.0 ± 2.7^{a}
Control + Hg	9.3 ± 0.6^{a}	9.6 ± 0.6^{a}	9.6 ± 1.5^{a}	13.0 ± 2.4^{a}	15.1 ± 4.3^{a}	15.2 ± 3.7^{a}	15.5 ± 4.6^{a}
Digestate	255.0 ± 114.1^{bc}	199.5 ± 54.8^{b}	129.0 ± 31.7^{b}	89.7 ± 21.3^{ab}	66.1 ± 3.5^{ab}	132.2 ± 52.9^{ab}	211.3 ± 93.9^{bc}
Digestate + Hg	141.4 ± 30.4^{b}	221.6 ± 29.6^{b}	162.7 ± 46.2^{b}	198.1 ± 63.6^{ab}	91.6 ± 6.7^{ab}	136.4 ± 49.1^{ab}	307.6 ± 110.8^{cd}
Ash	138.1 ± 37.6^{b}	140.8 ± 32.9^{b}	143.9 ± 33.0^{b}	153.8 ± 37.3^{ab}	168.1 ± 12.0^{b}	165.4 ± 16.1^{ab}	201.9 ± 62.7^{bc}
Ash + Hg	138.2 ± 20.2^{b}	158.9 ± 7.5^{b}	155.2 ± 21.9^{b}	243.6 ± 41.8^{ab}	192.6 ± 3.3^{b}	205.0 ± 28.7^{b}	202.5 ± 54.7^{bc}
$(NH_4)_2SO_4$	344.0 ± 82.0^{c}	494.3 ± 153.6^{c}	454.5 ± 79.6^{c}	602.6 ± 145.5^{c}	483.6 ± 55.2^{c}	528.4 ± 91.7^{c}	519.6 ± 104.6^{e}
$(NH_4)_2SO_4$ + Hg	366.3 ± 66.7^{c}	445.8 ± 94.6^{c}	386.7 ± 13.1^{c}	660.6 ± 189.3^{c}	483.2 ± 162.3^{c}	766.5 ± 78.7^{d}	429.7 ± 123.6^{de}
Luvisol	Day 1	Day 2	Day 3	Day 4	Day 7	Day 14	Day 21
Control	4.6 ± 1.0^{a}	4.9 ± 1.0^{a}	5.3 ± 1.1^{a}	8.6 ± 2.3^{a}	11.1 ± 3.6^{a}	11.8 ± 6.3^{a}	9.2 ± 3.3^{a}
Control + Hg	5.0 ± 1.0^{a}	4.7 ± 0.3^{a}	5.7 ± 0.4^{a}	9.8 ± 6.1^{a}	11.4 ± 5.5^{a}	10.2 ± 4.9^{a}	7.0 ± 0.6^{a}
Digestate	296.4 ± 27.4^{bc}	221.6 ± 27.5^{bc}	275.5 ± 32.2^{bc}	420.5 ± 122.4^{cd}	329.1 ± 62.0^{cd}	220.3 ± 121.1^{b}	264.9 ± 101.4^{b}
Digestate + Hg	273.2 ± 55.6^{bc}	205.9 ± 19.7^{bc}	234.2 ± 46.2^{bc}	229.7 ± 48.9^{bc}	80.3 ± 26.6^{ab}	94.9 ± 11.1a^{b}	362.5 ± 93.2^{b}
Ash	183.2 ± 75.2^{b}	183.2 ± 20.0^{b}	214.5 ± 64.0^{b}	208.2 ± 15.6^{b}	223.6 ± 13.8^{bc}	198.3 ± 14.0^{b}	151.0 ± 27.1^{b}
Ash + Hg	134.5 ± 21.6^{b}	131.6 ± 11.8^{b}	152.8 ± 21.2^{b}	219.1 ± 27.2^{bc}	233.4 ± 34.5^{bc}	228.7 ± 40.6^{b}	203.4 ± 36.8^{b}
$(NH_4)_2SO_4$	443.5 ± 96.3^{c}	403.0 ± 96.0^{c}	466.6 ± 87.8^{c}	590.4 ± 130.9^{d}	430.3 ± 97.5^{d}	505.2 ± 108.6^{c}	570.8 ± 118.5^{c}
$(NH_4)_2SO_4$ + Hg	536.1 ± 61.6^{c}	564.1 ± 30.2^{c}	541.0 ± 78.0^{c}	687.8 ± 87.9^{e}	560.1 ± 24.8^{e}	564.4 ± 72.6^{c}	701.8 ± 31.8^{c}

ash rate compared to our experiment. Thus, the increase of mobile nutrient contents in soils will manifest at higher ash rates compared to our experiment.

The interrelationships between soil Hg and other soil element contents described by Reis et al. [14] indicate that the presence of Hg in the mobile phase could be related to Mn and Al soil contents. Furthermore, an antagonistic effect of Mn against Hg is suggested. Our data tended to increase of mobile Mn contents during the incubation (Table 8) as related to decreasing mobile Hg (Figure 1). Similarly, Sierra et al. [42] observed negative significant correlation between the available Mn in the rhizosphere and Hg content in plants. On the contrary, S content contributed to Hg retention in the soil matrix, reducing the mobility of the metal [14]. In our case, the changes of Hg mobility in soils (Figure 1) did not reflect the changes in mobile portion of S during the incubation experiment (Table 10). In contrast, the presence of sulfates seems to favor Hg uptake by the plant. There was a positive significant correlation between the sulfate concentration in the rhizosphere and the Hg within the

Table 11: The concentrations of Zn extractable with 0.11 mol L^{-1} acetic acid within the incubation experiment (mg·kg^{-1}); the averages marked by the same letter did not significantly differ at $P < 0.05$ within individual columns; data are presented as mean ± standard deviation ($n = 3$).

Chernozem	Day 1	Day 2	Day 3	Day 4	Day 7	Day 14	Day 21
Control	1.34 ± 0.07[a]	1.37 ± 0.08[a]	0.87 ± 0.03[a]	1.57 ± 0.19[a]	1.42 ± 0.40[a]	1.32 ± 0.26[a]	0.59 ± 0.02[a]
Control + Hg	1.43 ± 0.29[a]	1.27 ± 0.06[a]	0.88 ± 0.15[a]	1.36 ± 0.19[a]	1.28 ± 0.08[a]	1.28 ± 0.16[a]	0.97 ± 0.33[a]
Digestate	6.56 ± 0.81[a]	6.69 ± 1.21[a]	6.02 ± 1.11[a]	9.02 ± 0.93[a]	7.44 ± 0.26[a]	11.06 ± 1.22[a]	12.51 ± 1.37[a]
Digestate + Hg	5.23 ± 1.36[a]	5.74 ± 0.82[a]	5.21 ± 0.84[a]	7.76 ± 0.34[a]	6.69 ± 0.26[a]	7.89 ± 0.17[a]	9.98 ± 1.51[a]
Ash	109.3 ± 23.2[b]	52.1 ± 20.0[b]	85.8 ± 21.8[b]	93.9 ± 23.7[b]	102.9 ± 12.2[b]	77.2 ± 17.3[b]	126.6 ± 32.9[b]
Ash + Hg	52.6 ± 25.8[b]	47.1 ± 10.4[b]	81.5 ± 21.4[b]	153.8 ± 25.7[c]	108.5 ± 31.6[b]	137.6 ± 22.4[c]	154.3 ± 28.8[b]
$(NH_4)_2SO_4$	1.57 ± 0.29[a]	1.55 ± 0.15[a]	1.12 ± 0.09[a]	1.67 ± 0.07[a]	1.66 ± 0.20[a]	2.29 ± 0.27[a]	2.27 ± 0.32[a]
$(NH_4)_2SO_4$ + Hg	1.65 ± 0.26[a]	1.39 ± 0.08[a]	1.15 ± 0.18[a]	1.44 ± 0.13[a]	1.45 ± 0.13[a]	1.56 ± 0.06[a]	5.02 ± 0.35[a]
Luvisol	Day 1	Day 2	Day 3	Day 4	Day 7	Day 14	Day 21
Control	2.66 ± 0.10[a]	2.92 ± 0.19[a]	2.46 ± 0.21[a]	3.45 ± 0.19[a]	3.21 ± 0.12[a]	3.15 ± 0.10[a]	2.02 ± 0.39[a]
Control + Hg	2.94 ± 0.06[a]	2.99 ± 0.30[a]	2.64 ± 0.15[a]	4.84 ± 2.17[a]	3.05 ± 0.04[a]	3.26 ± 0.06[a]	2.41 ± 0.89[a]
Digestate	11.58 ± 0.67[a]	8.13 ± 2.02[a]	8.53 ± 1.57[a]	14.04 ± 0.43[a]	13.07 ± 0.99[a]	12.49 ± 1.14[a]	14.68 ± 1.98[a]
Digestate + Hg	9.02 ± 1.29[a]	8.33 ± 1.04[a]	7.86 ± 0.69[a]	10.24 ± 0.52[a]	9.98 ± 0.73[a]	11.85 ± 1.90[a]	6.81 ± 4.38[a]
Ash	181.6 ± 30.7[b]	172.9 ± 28.8[b]	161.4 ± 32.8[b]	164.6 ± 31.0[b]	214.2 ± 24.5[c]	155.6 ± 25.8[b]	115.8 ± 23.0[b]
Ash + Hg	112.4 ± 31.8[b]	92.2 ± 12.3[b]	121.1 ± 23.3[b]	165.8 ± 34.6[b]	162.6 ± 4.6[b]	201.9 ± 35.7[b]	230.9 ± 38.7[c]
$(NH_4)_2SO_4$	3.05 ± 0.18[a]	3.16 ± 0.73[a]	2.65 ± 0.04[a]	3.74 ± 0.21[a]	3.38 ± 0.13[a]	3.98 ± 0.50[a]	4.39 ± 1.42[a]
$(NH_4)_2SO_4$ + Hg	3.37 ± 0.24[a]	3.17 ± 0.28[a]	2.95 ± 0.24[a]	4.18 ± 0.08[a]	3.18 ± 0.31[a]	3.44 ± 0.07[a]	3.46 ± 0.35[a]

aerial and root parts of plants [42]. However, only total S extracted with the 0.11 mol L^{-1} solution of CH_3COOH was determined by the ICP-OES and a portion of mobile sulfates in the extract was not determined in our case and requires further research. The competition between Hg and Cu and Hg and Zn in soils described by Jing et al. [19] was not confirmed in our case. For Fe, Mehrotra and Sedlak [43] and Rhoton and Bennett [44] highlighted Hg immobilization *via* sorption and/or the complexation of Hg with Fe compounds in soil. This statement seems to be confirmed for Chernozem, whereas the opposite pattern was observed in Luvisol. In Chernozem, the mobile portions of Fe decreased significantly after digestate application on the Hg amended samples compared to the unamended ones. In Luvisol, the mobile Fe contents increased in the Hg + digestate amended samples since 2nd day of incubation with maximum at 7th day suggesting competitive relationships of Fe and Hg in this case. The complexity of Hg sorption on Fe/Mn oxides was documented by Liang et al. [45], where the role of amorphous/crystalline Fe and Mn hydroxides, humic acids content, and also chlorine concentrations were mentioned. Šípková et al. [46] observed a negative correlation between Hg content bound to the humic acids and the content of Mg, Mn, and Fe. Therefore, the more detailed information concerning soil components, humic acid portions in the digestate, as well as the importance of the application of $HgCl_2$ compared to the other Hg compounds remains to be elucidated in further research.

4. Conclusions

Although the response of Hg contaminated soils in different ameliorative materials was affected by the individual parameters of the soils, especially by the different soil sorption capacity and organic matter contents in these soils, digestate proved to be the most effective for the immobilization of Hg in soil. Contrary to the other S-bearing measures such as wood fly ash and ammonium sulfate, in the case of digestate, the Hg immobilizing effectiveness resulted from the cooperation of various factors such as S and organic matter content. Moreover, the digestate application can result in an improvement in the macro- and micronutrient status of the soil, where mobile and theoretically plant-available portions of these elements increased in particular. Thus, the field application of organic matter-rich biowaste such as digestate seems to be reasonable for the disposal of this type of material, leading to a decreased environmental risk of Hg contamination in soil.

Conflict of Interests

The authors declared that there is no conflict of interests.

Acknowledgments

Authors are thankful for financial support of the GAČR Project P503/12/0682, ESF and MŠMT Project no. CZ.1.07/2.3.00/30.0040, and Czech University of Life Science Project no. 21140/1313/3130; correction and improvement of language was provided by Proof-Reading-Service.com Ltd., Devonshire Business Centre, Works Road, Letchworth Garden City SG6 1GJ, United Kingdom.

References

[1] EPA, *Mercury Study Report to Congress*, vol. 1 of *Executive Summary, EPA-452/R-97-003*, GPO, Washington, DC, USA, 1997.

[2] E. Tipping, S. Lofts, H. Hooper, B. Frey, D. Spurgeon, and C. Svendsen, "Critical Limits for Hg(II) in soils, derived from chronic toxicity data," *Environmental Pollution*, vol. 158, no. 7, pp. 2465–2471, 2010.

[3] J. Li, Y. Lu, H. Shim et al., "Use of the BCR sequential extraction procedure for the study of metal availability to plants," *Journal of Environmental Monitoring*, vol. 12, no. 2, pp. 466–471, 2010.

[4] S. M. Rodrigues, B. Henriques, J. Coimbra, E. F. da Silva, M. E. Pereira, and A. C. Duarte, "Water-soluble fraction of mercury, arsenic and other potentially toxic elements in highly contaminated sediments and soils," *Chemosphere*, vol. 78, no. 11, pp. 1301–1312, 2010.

[5] L. Boszke, A. Kowalski, A. Astel, A. Barański, B. Gworek, and J. Siepak, "Mercury mobility and bioavailability in soil from contaminated area," *Environmental Geology*, vol. 55, no. 5, pp. 1075–1087, 2008.

[6] W. Luo, Y. Lu, B. Wang et al., "Distribution and sources of mercury in soils from former industrialized urban areas of Beijing, China," *Environmental Monitoring and Assessment*, vol. 158, no. 1–4, pp. 507–517, 2009.

[7] A. Hassen, N. Saidi, M. Cherif, and A. Boudabous, "Resistance of environmental bacteria to heavy metals," *Bioresource Technology*, vol. 64, no. 1, pp. 7–15, 1998.

[8] A. R. Khwaja, P. R. Bloom, and P. L. Brezonik, "Binding constants of divalent mercury (Hg^{2+}) in soil humic acids and soil organic matter," *Environmental Science & Technology*, vol. 40, no. 3, pp. 844–849, 2006.

[9] D. A. Heeraman, V. P. Claassen, and R. J. Zasoski, "Interaction of lime, organic matter and fertilizer on growth and uptake of arsenic and mercury by Zorro fescue (*Vulpia myuros* L.)," *Plant and Soil*, vol. 234, no. 2, pp. 215–231, 2001.

[10] M. Linde, I. Öborn, and J. P. Gustafsson, "Effects of changed soil conditions on the mobility of trace metals in moderately contaminated urban soils," *Water, Air, and Soil Pollution*, vol. 183, no. 1–4, pp. 69–83, 2007.

[11] A. Yao, R. Qiu, C. Qing, S. Mu, and E. J. Reardon, "Effects of humus on the environmental activity of mineral-bound Hg: influence on Hg plant uptake," *Journal of Soils and Sediments*, vol. 11, no. 6, pp. 959–967, 2011.

[12] Y. Yang, L. Liang, and D. Wang, "Effect of dissolved organic matter on adsorption and desorption of mercury by soils," *Journal of Environmental Sciences*, vol. 20, no. 9, pp. 1097–1102, 2008.

[13] G. J. Zagury, C.-M. Neculita, C. Bastien, and L. Deschênes, "Mercury fractionation, bioavailability, and ecotoxicity in highly contaminated soils from chlor-alkali plants," *Environmental Toxicology and Chemistry*, vol. 25, no. 4, pp. 1138–1147, 2006.

[14] A. T. Reis, S. M. Rodrigues, C. M. Davidson, E. Pereira, and A. C. Duarte, "Extractability and mobility of mercury from agricultural soils surrounding industrial and mining contaminated areas," *Chemosphere*, vol. 81, no. 11, pp. 1369–1377, 2010.

[15] M. O. Barnett, L. A. Harris, R. R. Turner et al., "Formation of mercuric sulfide in soil," *Environmental Science & Technology*, vol. 31, no. 11, pp. 3037–3043, 1997.

[16] D. Hesterberg, J. W. Chou, K. J. Hutchison, and D. E. Sayers, "Bonding of HG(II) to reduced organic sulfur in humic acid as affected by S/Hg ratio," *Environmental Science and Technology*, vol. 35, no. 13, pp. 2741–2745, 2001.

[17] S. Remy, P. Prudent, and J.-L. Probst, "Mercury speciation in soils of the industrialised Thur River catchment (Alsace, France)," *Applied Geochemistry*, vol. 21, no. 11, pp. 1855–1867, 2006.

[18] S. Åkerblom, K. Bishop, E. Björn, L. Lambertsson, T. Eriksson, and M. B. Nilsson, "Significant interaction effects from sulfate deposition and climate on sulfur concentrations constitute major controls on methylmercury production in peatlands," *Geochimica et Cosmochimica Acta*, vol. 102, pp. 1–11, 2013.

[19] Y. D. Jing, Z. L. He, and X. E. Yang, "Effects of pH, organic acids, and competitive cations on mercury desorption in soils," *Chemosphere*, vol. 69, no. 10, pp. 1662–1669, 2007.

[20] P. Ochecová, P. Tlustoš, and J. Száková, "Wheat and soil response to wood fly ash application in contaminated soils," *Agronomy Journal*, vol. 106, no. 3, pp. 995–1002, 2014.

[21] P. Quevauviller, A. Ure, H. Muntau, and B. Griepink, "Improvement of analytical measurements within the BCR-program—single and sequential extraction procedures applied to soil and sediment analysis," *International Journal of Environmental Analytical Chemistry*, vol. 51, pp. 129–134, 1993.

[22] A. Mehlich, "Mehlich 3 soil test extractant: a modification of Mehlich 2 extractant," *Communications in Soil Science & Plant Analysis*, vol. 15, no. 12, pp. 1409–1416, 1984.

[23] A. Šípková, J. Száková, P. Coufalík, O. Zvěřina, L. Kacálková, and P. Tlustoš, "Mercury distribution and mobility in contaminated soils from vicinity of waste incineration plant," *Plant, Soil and Environment*, vol. 60, no. 2, pp. 87–92, 2014.

[24] P. Ruggiero, R. Terzano, M. Spagnuolo et al., "Hg bioavailability and impact on bacterial communities in a long-term polluted soil," *Journal of Environmental Monitoring*, vol. 13, no. 1, pp. 145–156, 2011.

[25] B. Demirel, N. P. Göl, and T. T. Onay, "Evaluation of heavy metal content in digestate from batch anaerobic co-digestion of sunflower hulls and poultry manure," *Journal of Material Cycles and Waste Management*, vol. 15, no. 2, pp. 242–246, 2013.

[26] R. Pöykiö, H. Nurmesniemi, and R. L. Keiski, "Total and size fractionated concentrations of metals in combustion ash from forest residues and peat," *Proceedings of the Estonian Academy of Sciences*, vol. 58, no. 4, pp. 247–254, 2009.

[27] J. Bower, K. S. Savage, B. Weinman, M. O. Barnett, W. P. Hamilton, and W. F. Harper, "Immobilization of mercury by pyrite (FeS_2)," *Environmental Pollution*, vol. 156, no. 2, pp. 504–514, 2008.

[28] A. K. Müller, K. Westergaard, S. Christensen, and S. J. Sørensen, "The effect of long-term mercury pollution on the soil microbial community," *FEMS Microbiology Ecology*, vol. 36, no. 1, pp. 11–19, 2001.

[29] P. Pant and Ć. M. Allen, "Interaction of soil and mercury as a function of soil organic carbon: some field evidence," *Bulletin of Environmental Contamination and Toxicology*, vol. 78, no. 6, pp. 539–542, 2007.

[30] F. A. O. Camargo, F. M. Bento, and R. J. S. Jacques, "Uso de microrganismos para remediação de metais," in *Tópicos em Ciência do Solo*, C. A. Ceretta, L. S. Silva, and J. M. Reichert, Eds., pp. 468–496, Sociedade Brasileira de Ciência do Solo, Minas Gerais, Brazil, 2007.

[31] M. Ravichandran, "Interactions between mercury and dissolved organic matter—a review," *Chemosphere*, vol. 55, no. 3, pp. 319–331, 2004.

[32] A. Kabata-Pendias, *Trace Elements in Soils and Plants*, CRC Press LLC, Boca Raton, Fla, USA, 3rd edition, 2001.

[33] V. B. Mathema, B. C. Thakuri, and M. Sillanpää, "Bacterial mer operon-mediated detoxification of mercurial compounds: a short review," *Archives of Microbiology*, vol. 193, no. 12, pp. 837–844, 2011.

[34] K. Möller and T. Müller, "Effects of anaerobic digestion on digestate nutrient availability and crop growth: a review," *Engineering in Life Sciences*, vol. 12, no. 3, pp. 242–257, 2012.

[35] J. J. Walsh, D. L. Jones, G. Edwards-Jones, and A. P. Williams, "Replacing inorganic fertilizer with anaerobic digestate may maintain agricultural productivity at less environmental cost," *Journal of Plant Nutrition and Soil Science*, vol. 175, no. 6, pp. 840–845, 2012.

[36] R. B. Frøseth, A. K. Bakken, M. A. Bleken et al., "Effects of green manure herbage management and its digestate from biogas production on barley yield, N recovery, soil structure and earthworm populations," *European Journal of Agronomy*, vol. 52, pp. 90–102, 2014.

[37] M. Fernández-Delgado Juarez, S. Waldhuber, A. Knapp, C. Partl, M. Gómez-Brandón, and H. Insam, "Wood ash effects on chemical and microbiological properties of digestate- and manure-amended soils," *Biology and Fertility of Soils*, vol. 49, no. 5, pp. 575–585, 2013.

[38] A. Demeyer, J. C. Voundi Nkana, and M. G. Verloo, "Characteristics of wood ash and influence on soil properties and nutrient uptake: an overview," *Bioresource Technology*, vol. 77, no. 3, pp. 287–295, 2001.

[39] R. M. Pitman, "Wood ash use in forestry—a review of the environmental impacts," *Forestry*, vol. 79, no. 5, pp. 563–588, 2006.

[40] B.-M. Steenari, L. G. Karlsson, and O. Lindqvist, "Evaluation of the leaching characteristics of wood ash and the influence of ash agglomeration," *Biomass and Bioenergy*, vol. 16, no. 2, pp. 119–136, 1999.

[41] J. Száková, P. Ochecová, T. Hanzlíček, I. Perná, and P. Tlustoš, "Variability of total and mobile element contents in ash derived from biomass combustion," *Chemical Papers*, vol. 67, no. 11, pp. 1376–1385, 2013.

[42] M. J. Sierra, J. Rodríguez-Alonso, and R. Millán, "Impact of the lavender rhizosphere on the mercury uptake in field conditions," *Chemosphere*, vol. 89, no. 11, pp. 1457–1466, 2012.

[43] A. S. Mehrotra and D. L. Sedlak, "Decrease in net mercury methylation rates following iron amendment to anoxic wetland sediment slurries," *Environmental Science and Technology*, vol. 39, no. 8, pp. 2564–2570, 2005.

[44] F. E. Rhoton and S. J. Bennett, "Soil and sediment properties affecting the accumulation of mercury in a flood control reservoir," *Catena*, vol. 79, no. 1, pp. 39–48, 2009.

[45] P. Liang, Y.-C. Li, C. Zhang et al., "Effects of salinity and humic acid on the sorption of Hg on Fe and Mn hydroxides," *Journal of Hazardous Materials*, vol. 244-245, pp. 322–328, 2013.

[46] A. Šípková, J. Száková, and P. Tlustoš, "Affinity of selected elements to individual fractions of soil organic matter," *Water, Air, & Soil Pollution*, vol. 225, no. 1, article 1802, 2014.

Hindawi Publishing Corporation
The Scientific World Journal
Volume 2014, Article ID 487563, 9 pages
http://dx.doi.org/10.1155/2014/487563

Research Article

Connecting Soil Organic Carbon and Root Biomass with Land-Use and Vegetation in Temperate Grassland

Devan Allen McGranahan,[1] Aaron L. Daigh,[1] Jessica J. Veenstra,[2] David M. Engle,[3] James R. Miller,[4] and Diane M. Debinski[5]

[1] *School of Natural Resource Sciences Range Science Program, North Dakota State University, Fargo, ND 58108-6050, USA*
[2] *Natural Sciences, Flagler College, St. Augustine, FL 32085-1027, USA*
[3] *Department of Natural Resource Ecology and Management, Oklahoma State University, Stillwater, OK 74078-6013, USA*
[4] *Natural Resources and Environmental Sciences, University of Illinois, Urbana, IL 61801, USA*
[5] *Department of Ecology, Evolution, and Organismal Ecology, Iowa State University, Ames, IA 50011, USA*

Correspondence should be addressed to Devan Allen McGranahan; devan.mcgranahan@ndsu.edu

Received 19 July 2014; Revised 15 September 2014; Accepted 16 September 2014; Published 20 October 2014

Academic Editor: Antonio Paz González

Soils contain much of Earth's terrestrial organic carbon but are sensitive to land-use. Rangelands are important to carbon dynamics and are among ecosystems most widely impacted by land-use. While common practices like grazing, fire, and tillage affect soil properties directly related to soil carbon dynamics, their magnitude and direction of change vary among ecosystems and with intensity of disturbance. We describe variability in soil organic carbon (SOC) and root biomass—sampled from 0–170 cm and 0–100 cm, respectively—in terms of soil properties, land-use history, current management, and plant community composition using linear regression and multivariate ordination. Despite consistency in average values of SOC and root biomass between our data and data from rangelands worldwide, broad ranges in root biomass and SOC in our data suggest these variables are affected by other site-specific factors. Pastures with a recent history of severe grazing had reduced root biomass and greater bulk density. Ordination suggests greater exotic species richness is associated with lower root biomass but the relationship was not apparent when an invasive species of management concern was specifically tested. We discuss how unexplained variability in belowground properties can complicate measurement and prediction of ecosystem processes such as carbon sequestration.

1. Introduction

Soils constitute the greatest stock of terrestrial organic carbon [1] and soil properties can be affected by land-use and management [2, 3]. Globally, approximately one-quarter of the potential carbon sequestration in soils occurs in rangelands [4]. Rangelands are also one of the most widespread human-impacted biomes on Earth [5], making their role in carbon sequestration sensitive to land-use and climate change [6, 7].

The effects of grazing and fire, specifically, can be varied and opposing. In rangeland, grazing can increase bulk density [8, 9] and has a neutral or negative effect on soil organic carbon (SOC) [10–12]. Likewise, grazing can either increase or decrease root production [13, 14]. Fire increases root growth in tallgrass prairie [13, 15], but across fire-adapted ecosystems the effect of fire on soil carbon varies with severity and temporal scale [16–19]. Temporal scale is especially important to SOC because although SOC can decline over just a few years, SOC accumulation occurs on the scale of decades [20, 21].

Vegetation affects soil carbon stocks by depositing organic matter in the soil. Two major pathways of organic matter input—root tissue and exudates—directly involve plants [22]. Roots contribute to SOC pools through rhizodeposition [23] and the longer residence time of carbon from root tissue than shoot tissue [24]. Abiotic factors can also affect root growth and SOC. Soil clay content has been associated with greater SOC in many soils [25–27]. Bulk density can limit root growth and decrease SOC [28, 29].

Vegetation changes that affect organic matter input deep in the soil profile have an important impact on carbon dynamics. For instance, invasive deep-rooted, warm-season (C_4) grasses can increase carbon sequestration by increasing organic matter deposition deep in the soil profile [30]. Conversely, the invasion of shallow-rooted, cool-season (C_3) grasses might reduce soil carbon because cool-season grasses contribute less root tissue than native warm-season grasses deep in the soil profile [31, 32] despite greater root biomass near the soil surface [33].

Carbon dynamics deep in the soil profile are especially important but infrequently studied. Increasing the considered depth from 100 cm to 300 cm increases the global SOC budget by 56% [34]. Carbon deeper in the soil profile is subject to different soil structure, chemistry, and biotic activity, which might contribute to greater carbon sequestration [35].

We studied the effect of grazing history, prescribed fire, and the invasion of an exotic C_3 grass on root biomass and SOC in rangeland managed with fire and grazing in the tallgrass prairie region of central North America. We describe variability in SOC and root biomass—sampled from 0–170 cm and 0–100 cm, respectively—in terms of soil properties, land-use history, current management, and plant community composition using linear regression and multivariate ordination methods. We expected pastures with a recent history of severe grazing to have less root biomass and lower SOC. We also expected plots with greater abundance of exotic C_3 invasive species to have less root biomass. Finally, we expected to associate belowground properties with variation in aboveground plant community composition.

2. Methods

2.1. Study Location and Site History. Our research was conducted in conjunction with ongoing research in the Grand River Grasslands, a 30,000 ha working landscape in Ringgold County, IA, and Harrison County, MO [36]. Study tracts were initially identified as having medium to high potential for prairie conservation and restoration, based on the observed presence of native species indicating parcels of remnant prairie (The Nature Conservancy, unpublished data). When the Grand River Grasslands research project began in 2006, a pretreatment vegetation survey of potentially-remnant tracts confirmed a high incidence of native plant species as well as a range of invasion by nonnative plants [37].

Tracts were identified by historical grazing management. Grazing histories were reconstructed through interviews with current and former managers; four of the tracts were reported ungrazed for at least six years prior to the beginning of the study while five had been grazed by cattle (*Bos taurus*) at high stocking rates (ca. 15 animal unit months/ha) (Table 1) [37, 38]. At the time of this study, tracts were assigned to treatments for the purposes of a fire and grazing experiment that divided the tracts into moderately grazed and ungrazed [39]. We did not expect these recent changes in management to affect belowground soil and root properties (although the effect was tested as part of multivariate analyses, see below). However, because fire has been shown to reduce belowground biomass in tallgrass prairie, for example [15], we did record time-since-fire for each patch for inclusion in our analyses.

2.2. Sample Collection and Analysis. As part of ongoing research in these tracts, six modified Whittaker plots per pasture were located with respect to soil series as described by McGranahan et al. [37, 40]. All study tracts were classified to the Gara-Armstrong-Pershing association [41]. Two soil series—Gara loam and Armstrong loam (Fine-loamy, mixed, superactive, mesic Mollic Hapludalf, parent material: glacial till; and Fine, smectitic, mesic Aquertic Hapludalf, parent material: loess over palesol formed in glacial till, respectively [41])—dominated the study tracts, and within each tract three plots were located within each soil series. Slopes spanned three classifications (C, D, and E) and ranged from 8 to 35%.

In June 2010, we located 31, 500 m^2 modified Whittaker plots (permanently-located vegetation survey plots established in 2006 for estimation of canopy cover [37, 42]) across six tracts in the Grand River Grasslands. Although each tract has six permanent plots, some plots were not accessible by the heavy equipment required for soil sampling. At each plot, we sampled the abundance of tall fescue by recording canopy coverage from 10, 0.5 m^2 quadrats according to the Daubenmire [43] canopy cover index. We used the mean canopy cover of these 10 quadrats to represent tall fescue abundance in our analyses.

We extracted four adjacent 7.5 cm diameter soil cores from the approximate center of each vegetation plot with a vehicle-mounted hydraulic Giddings probe. Three, 100 cm cores were analyzed for root biomass at 20 cm intervals to determine rooting depth. Twenty-centimeter sections of each core were soaked overnight in a 1% solution of sodium hexametaphosphate (Calgon) [14]. We separated root tissue from soil particles with a sieve and bucket arrangement similar to Lauenroth and Whitman [44]: water was flushed through each soaked core section in a 10 mesh sieve mounted atop a 19L bucket. Mineral material sank in the bucket while root tissue that passed through the 10 mesh sieve floated and was collected in a 40 mesh sieve. Root tissue was collected with tweezers from remaining particles in the sieve and dried for 48 hours at 45°C, with root biomass expressed as mass per unit area [31, 32].

The fourth soil core was sampled to 170 cm and analyzed for soil organic carbon (SOC) at varying depth intervals: 10 cm intervals, 0–60 cm; 20 cm intervals, 60–140 cm, and a 30 cm interval from 140 to 170 cm. To standardize depth intervals when making comparisons with root biomass—which was sampled 0–100 cm in 20 cm increments—we summed 10 cm incremental SOC data from the top 0–60 cm into 20 cm increments. These cores were air-dried and stored unsealed.

Prior to laboratory analysis, the fourth core from each plot was also analyzed for variables that might affect root penetration, including clay content and bulk density in 20 cm increments, depth to argillic and gleyed horizons (which indicate clay accumulation and anoxic conditions, resp.), and depth to an observable plow layer. Based on previous experience with these similar soil series, A. Daigh identified potentially root-limiting thresholds for clay content (27%)

Table 1: Summary of historical (2000–2006) and 2010 grazing management information and tall fescue abundance (as percent canopy cover) for six pastures in the Grand River Grasslands of Ringgold County, IA, and Harrison County, MO, USA. Severe grazing refers to approximately 15 animal unit months/ha [37].

Pasture	Grazing		Tall fescue canopy cover (%)		
	Historical	Current	Minimum	Mean (±se)	Maximum
Lee Trail	Not recently grazed	Moderately grazed	13	35 (±8)	61
Pawnee	Not recently grazed	Ungrazed	0	<1	<1
Pyland North	Recently severely grazed	Moderately grazed	38	59 (±7)	75
Pyland South	Recently severely grazed	Moderately grazed	20	37 (±5)	53
Pyland West	Recently severely grazed	Moderately grazed	17	50 (±8)	63
Ringgold North	Not recently grazed	Ungrazed	0	<1	1

and bulk density (1.4 g/cm^3) and for each core determined the depth at which the root-limiting layer was first observed.

Because our study considered only organic carbon, we tested for and eliminated any inorganic carbon fraction from soil samples. Total carbon and inorganic carbon was determined by the Iowa State University Plant and Soil Analysis Lab, Ames, IA, USA, using the dry combustion and modified pressure calcimeter methods. pH was determined with a glass electrode in a 1 : 1 soil to water suspension. Composite samples from each depth interval were analyzed for total carbon and pH. For samples <7.0 pH, total carbon was assumed to equal organic carbon. Samples ≥7.0 pH were reanalyzed for inorganic carbon, which, when subtracted from total carbon, gives the organic carbon fraction. Prior to submission to the lab, we determined soil bulk density via the soil core method to calculate soil organic carbon on a volumetric rather than gravimetric basis, the standard for reporting and comparing soil carbon data globally, for example [34].

2.3. Data Analysis

2.3.1. Belowground Properties and Land-Use. To determine the relationship between soil variables (root mass, SOC, and bulk density) and land-use variables (grazing history, time-since-fire, and tall fescue cover) we constructed linear mixed effect regression (LME) models with the lmer function in the lme4 package (version 1.0-5) for the *R* statistical environment (version 3.0.2) [45, 46]. Response variables included both whole core root biomass (0–100 cm) and surface biomass (0–20 cm); whole core SOC (0–170 cm), surface SOC (0–20 cm), and surface percent SOC (0–10 cm); and surface bulk density (0–20 cm). We also compared total SOC, percent SOC, and root mass in the top 0–20 cm against clay content and bulk density (0–20 cm) and tested for a correlation between bulk density and clay content.

In lieu of *P* values as a measure of statistical significance, we estimated 95% confidence intervals for grazing history and tall fescue cover using the simulation method developed by Nakagawa and Cuthill [47], which compares 1000 simulations of the LME model to empirical response variable data. To test the goodness-of-fit of the mixed-effect regression model we calculated a coefficient of determination (R^2) with a custom rsquared.lme function following Nakagawa and Schielzeth [48]. The rsquared.lme function extracts variance components from the lme model and calculates marginal R^2 values that represent the goodness-of-fit for the fixed-effect term.

2.3.2. Multivariate Analysis of Soil, Root, and Vegetation Data. We used ordination to identify patterns among root mass, SOC, and soil properties data. We performed a Principal Components Analysis (PCA) with an unconstrained model using the rda function in the vegan package (version 2.0-7) for the *R* statistical environment [49]. We tested several physical and management-related factors against the ordination using the envfit function in vegan; these variables included tall grazing history, tall fescue cover, current grazing treatment, soil series, and slope of sampled plot.

We also used ordination to test for association between plant community composition and variation in soil and root properties. First, we extracted the principal components (PCs) from the PCA of soil and root data. Together, the PCs represent composite variables that each account for a proportion of variation in the root/soil dataset; as PCs are added the proportion of variation explained by the composite variables accumulates. We sought to include as many PCs as necessary to account for at least 70% of variation in the soil/root data.

Second, we set the PCs as constraints in a Constrained Analysis of Proximities (function capscale in vegan), which performs a constrained ordination based on a user-defined distance metric and is similar to the unconstrained ordination Multi-Dimensional Scaling. For plant community data we used the 2006 pretreatment vegetation survey [37] and used the Canberra distance metric. As applied here, the constrained ordination first describes variation in plant community composition along defined axes—in this case, the composite variables of soil/root data represented by the PCs—then proceeds to explain remaining variation via unconstrained ordination. To determine how useful the soil/root composite variables were in describing variation in plant community composition, we compared an unconstrained ordination of the vegetation data to the constrained ordination model using the anova function.

3. Results and Discussion

3.1. Relationship between Belowground Properties and Depth. Root biomass and SOC decreased rapidly with depth (Figure 1). Bulk density generally increased with depth; wide variation in samples from the 60 to 80 cm increment

Table 2: Descriptive statistics for soil organic carbon (SOC) and root biomass from 31 vegetation plots across five study tracts in the Grand River Grasslands of Ringgold County, IA, and Harrison County, MO, USA.

Variable	Minimum	Mean	Maximum
Total SOC in 170 cm profile (kg/m^2)	11.4	16.8	27.4
Percent of total SOC in top 20 cm	21.5%	37.2%	51.4%
Percent of total SOC in top 40 cm	28.8%	56.9%	71.5%
Percent of total SOC in top 100 cm	38.0%	81.9%	96.9%
Total root biomass in 100 cm profile (mg/cm^2)	53.6	102.0	212.4
Percent of total root biomass in top 20 cm	33.1%	69.8%	96.5%
Percent of total root biomass in top 40 cm	52.8%	80.5%	98.0%

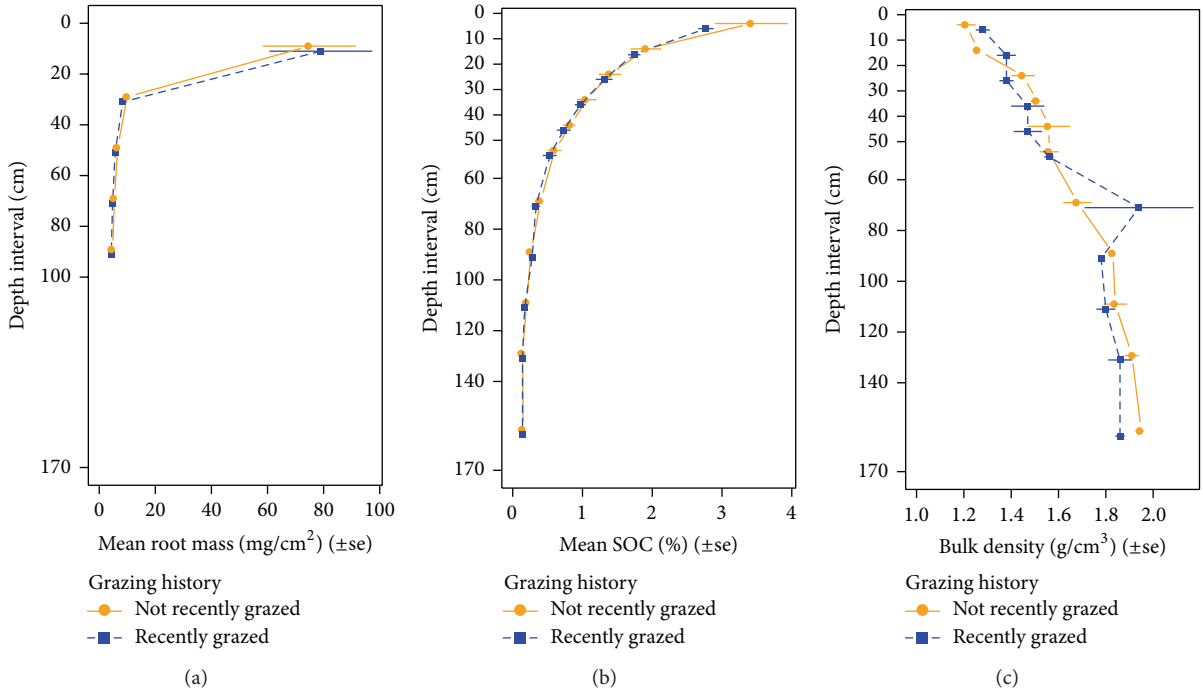

Figure 1: Root biomass, soil organic carbon (SOC), and bulk density for six tallgrass prairie pastures in the Grand River Grasslands of Ringgold County, IA, and Harrison County, MO, USA, plotted by depth (0–170 cm) and grazing history. See Methods for sampling procedures including depth intervals.

(Figure 1(c)) reflects a low-density sand lens (likely an isolated/local variation in the glacial till) in a subset of samples. Across all plots, the 0–20 cm increment of the soil profile contained the greatest root biomass and SOC (Table 2). In these soils, sampling to 100 cm increased SOC stock and root biomass by an average of 45% and 40%, respectively, when compared to amounts contained in the top 20 cm of the profile. For SOC, extending the sampling depth to 170 cm increased the estimate of SOC stock in the profile by an average of 63%. Deep sampling clearly increases the amount of organic carbon and root biomass accounted for under these grasslands.

In terms of vertical distribution, root biomass and SOC tended to be concentrated in the upper portion of the soil profile, a pattern consistent with other work. On average, we found 81% of root biomass in the top 40 cm of the soil profile (Table 1), similar to the 83% average for the top 30 cm of temperate grassland worldwide [50]. In another global review, Jobbágy and Jackson [34] report 70% of root biomass concentrated in the 0–20 cm increment and an additional 17% in the 20–40 cm increment, which is congruous with our mean values of 70% and 11%, respectively. Regarding SOC, Jobbágy and Jackson [34] report an average total of 16 kg/m^2 for the top 200 cm in temperate grasslands worldwide, very near the 17 kg/m^2 mean reported here. Broken down by depth increments, Jobbágy and Jackson [34] report an average of 42% of SOC distributed in the 0–20 cm increment and 23% in the 20–40 cm increment, again consistent with our values of 37% and 20%, respectively.

3.2. Land-Use versus Natural Variation in Belowground Properties. Our data indicate that previous grazing management has affected both belowground and aboveground properties of these grasslands. Pastures with a recent history of severe

Table 3: Results of six multiple linear mixed effect regression models each comparing response variables against tall fescue abundance and grazing history as independent variables (fixed effects). Lower and upper bounds define simulated 95% confidence intervals while R^2 reports goodness-of-fit for multiple fixed effects.

Response variable	Tall fescue		Grazing history		R^2
	Lower	Upper	Lower	Upper	
Soil organic carbon					
0–20 cm	−2.9	20.6	−927	316	0.07
0–100 cm	−58	115	−5339	3307	0.01
% 0–10 cm	−0.02	0.02	−1.68	0.51	0.10
Root mass					
0–20 cm	−0.01	0.06	−4.1	−0.9	0.24
0–100 cm	−0.01	0.18	−13.7	−3.6	0.28
Bulk density					
0–20 cm	−0.002	0.002	0.02	0.2	0.22

Table 4: Results of four multiple linear mixed effect regression models each comparing response variables against bulk density and clay content as independent variables (fixed effects). Lower and upper bounds define simulated 95% confidence intervals while R^2 reports goodness-of-fit for multiple fixed effects.

Response variable	Bulk density		Clay content		R^2
	Lower	Upper	Lower	Upper	
Soil organic carbon					
SOC 0–20 cm	−2052	1857	−33.5	15.5	0.01
% 0–10 cm	−4.8	0.7	−0.03	0.04	0.07
Root mass (0–20 cm)	−10.8	2.2	−0.09	0.06	0.06
Bulk density (0–20 cm)			−0.006	0.002	0.03

grazing had lower root biomass in both the top 20 cm and the entire 100 cm profile than other pastures, and greater bulk density (Table 3). These results indicate both biotic and abiotic effects of soil compaction associated with intensive livestock management [11, 13, 51]. That these effects persist at least five years following the cessation of severe grazing highlights the influence of land-use legacies on biophysical properties and ecological pattern and process [52, 53]. Likewise, these recently severely-grazed pastures have different plant community composition, including lower native species richness and a greater abundance of tall fescue [37, 40]. But tall fescue abundance was associated with neither SOC nor root biomass (Table 3). Likewise, current management showed no effect on belowground properties. Specifically, prescribed fire had no association with root biomass or SOC in the top 20 cm of the soil profile (95% CI = −2.6–0.7, R^2 = 0.05 and 95% CI = −1407–225, R^2 = 0.06, resp.).

We observed several properties in the upper portion of the soil column that could physically impair root penetration. The average depth of the shallowest root-limiting layer was 12 (±2) cm, and it appears to have an association with reduced root biomass in the top 20 cm of the soil profile (95% CI = 0.01–0.11, R^2 = 0.13), but not percent SOC (95% CI = −0.02–0.04, R^2 = 0.01). There was no correlation between bulk density and clay content in the top 20 cm, and neither had an association with SOC or root biomass at the same depth (Table 4), contrary to predictions [29].

Nine plots on four of the six pastures showed evidence of a plow layer, observed at an average depth of 7.7 (±1.5) cm. These data suggest that cultivation had occurred at some point since European settlement of the area in the late 19th century, contrary to our previous efforts to document agricultural histories (interviews with managers and searches through local US Department of Agriculture records) that presented no evidence of tillage. While historical cultivation is not surprising and is in fact expected, it is clear that even land-use activity that occurred long ago and/or briefly in time can leave a long-lasting imprint on soil. But the long-term impact of such activity is less clear: the presence of a plow layer was not associated with differences in bulk density (95% CI = −0.12–0.07, R^2 = 0.01) or amount of SOC (95% CI = −284–1005, R^2 = 0.03) in the top 20 cm of soil profiles. For these pastures, it is possible that tillage occurred so long ago that soil has since recovered [20].

3.3. Multivariate Analyses of Belowground Properties and Vegetation. Although the ordination of soil and root data highlighted several patterns among belowground properties, we did not observe patterns that indicate associations between belowground properties, land-use, and vegetation. The PCA revealed three general trends in variation within the soil and root data along which correlated variables clustered (Figure 2): one following root biomass, another SOC, and

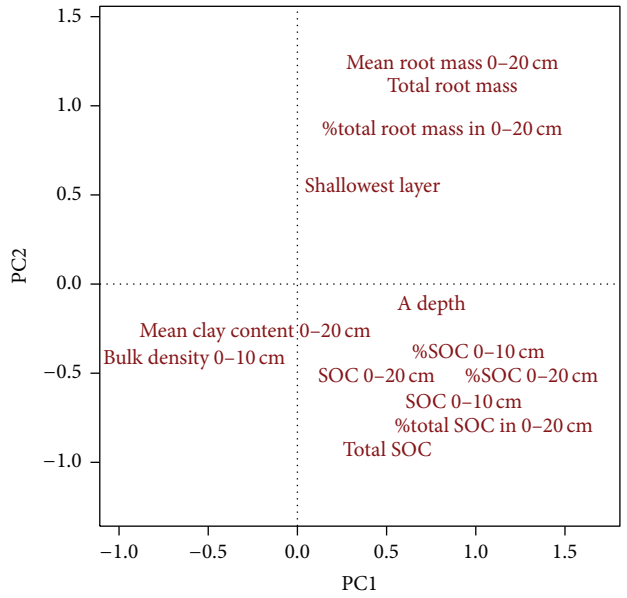

Figure 2: Relationships among 13 belowground properties with respect to first two Principal Components from Principal Components Analysis. For description of plotted text codes and quantified loadings for each variable, see Table 4.

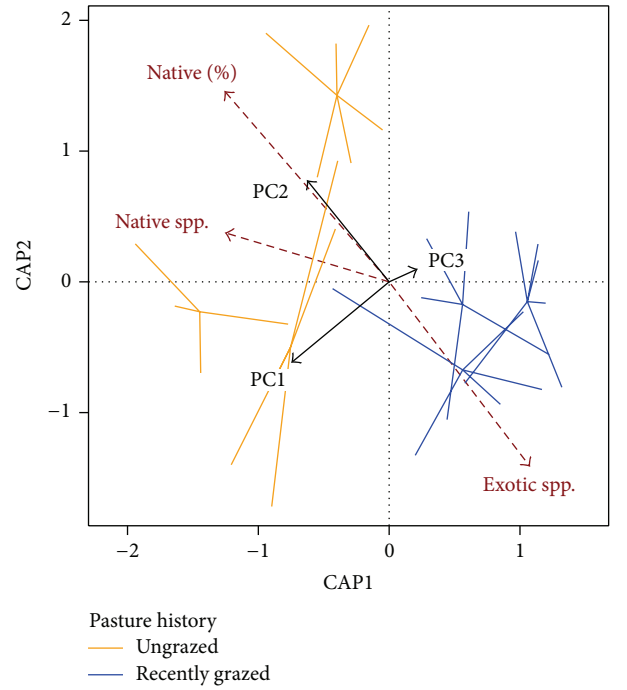

Figure 3: Results of a constrained ordination of plant community composition using composite variables of belowground properties created from soil and root PCA. Spiderplots group sampled modified Whittaker plots by grazing history, thick black arrows show constraining variables, and thin red arrows overlay plant community metadata fitted to the ordination ("Native (%)" = proportion of native species in community, "Native spp." = native species richness, and "Exotic spp." = exotic species richness).

a third combining clay content and bulk density. Variables related to SOC loaded most heavily along PC1 while variables related to root biomass contributed in greater proportion to PC2 (Table 5). The first three axes of the PCA accounted for 72% of the variation in belowground properties, but there was no association between the PCA and factors that might explain variation in belowground properties, including historical and current grazing, tall fescue abundance, soil series, and slope ($P > 0.1$). We did not expect current management to affect either root biomass or SOC given the low severity and brief time span of the experimental disturbance regime [18, 54].

Not surprisingly—given the concentration of root biomass and SOC near the soil surface (Table 2)—total root biomass (0–100 cm) and total SOC (0–170 cm) each clustered with their respective shallow measures (0–20 cm). These results suggest that unless a complete accounting of the carbon budget is required, shallow sampling is sufficient to characterize root and SOC dynamics through much of the soil column.

An unexpected result of the multivariate analysis is the relationship between root biomass and SOC. Whereas we expected a direct, linear correlation between these two variables, they in fact occur orthogonal to each other in ordination space (Figure 2). Both root biomass and SOC variables appear to have a negative relationship with clay content and bulk density, although no associations were indicated by linear regression models (Table 4). The ordination supports above evidence that deeper root-limiting layers are associated with greater root biomass and suggests that deeper topsoil (A horizon) might tend to have greater root biomass and SOC.

There is evidence that plant community composition is associated with variation in belowground properties. PC1 and PC2—composite variables from the PCA ordination of multivariate soil and root data most influenced by 0–10 cm SOC and 0–20 cm root biomass, respectively (Table 5)—were significant terms in the constrained ordination of plant community composition (PC1: $P = 0.01$, PC2: $P = 0.04$). Likewise, the first axis of the constrained ordination was significantly associated with variation in plant community composition (CAP1: $P = 0.005$). There appears to be an association between PC2 and exotic species richness in ordination space (Figure 3); although PC2 is the axis of secondary variation in the PCA, it is also the axis most influenced by root biomass. Thus, these data might suggest a connection between greater exotic species richness and reduced root biomass, which supports a pattern seen elsewhere in tallgrass prairie documenting greater root biomass among native species versus exotic species [32]. But the three constraining axes explained just 13% of variation in the ordination of vegetation data, leaving substantial amount of variation in plant community composition unexplained by belowground properties. As shown elsewhere, grazing history, tall fescue abundance, and the ratio of native to exotic species strongly influence plant community composition in these grasslands [37, 39].

Table 5: Loadings along first three Principal Components (PC1, PC2, and PC3) for 13 belowground properties measured from six pastures in the Grand River Grasslands of Ringgold County, IA, and Harrison County, MO, USA. Plotting code refers to plotted text in Figure 2.

Variable type	Plotting code	Meaning	PC1	PC 2	PC3
Soil organic carbon (SOC)	Total SOC	Total mass of SOC in 0–100 cm column	0.76	−0.54	−0.5
	SOC 0–10 cm	SOC mass in 0–10 cm	0.98	−0.33	0.63
	SOC 0–20 cm	SOC mass in 0–20 cm	0.79	−0.37	−0.68
	% total SOC 0–10 cm	Proportion of total SOC mass in 0–10 cm	0.98	−0.31	0.63
	% total SOC 0–20 cm	Proportion of total SOC mass in 0–20 cm	1.13	−0.43	0.13
	% SOC 0–20 cm	% SOC, 0–20 cm	1.12	−0.35	0.12
Root mass	Total root mass	Total root biomass in 0–100 cm column	0.73	0.9	0.07
	Mean root mass 20 cm	Root biomass in 0–20 cm	0.77	0.91	0.07
	% total root mass in 0–20 cm	Proportion of total root biomass in 0–20 cm	0.7	0.81	0.13
Root limitations	Mean clay content 0–20 cm	Average clay content of 0–10 and 11–20 cm intervals	−0.11	−0.22	0.51
	Bulk density 0–10 cm	Bulk density 0–10 cm	−0.43	−0.34	0.21
	Shallowest layer	Shallowest depth (cm) of a soil property expected to limit root penetration[1]	0.38	0.47	−0.29
	A depth	Depth of a horizon (topsoil)	0.81	−0.09	−0.66

[1] Variables used to determine limitation to rooting depth: clay content = 27%, bulk density = 1.4, observation of argillic or gleyed horizon, or a plow layer.

3.4. Land-Use, Variability, and Ecosystem Processes. Given that sampling deeper in the soil profile makes important contributions to the global carbon cycle [34], we sampled soil organic carbon (SOC) and root biomass to 170 cm and 100 cm, respectively, in temperate rangeland soils. Although on one hand such deep sampling did increase the amount of soil organic carbon we can account for in this system, on the other hand our ability to relate these data to ecosystem-level processes like carbon sequestration is limited by (i) the high degree of variability we observed in belowground properties at shallow soil layers and (ii) the lack of pattern between variability in belowground properties and known land-uses and plant composition.

Most relevant to carbon budgets, we did not observe any relationship between vegetation and SOC or root biomass at any level of the soil profile, let alone at depth. Although the majority of organic matter is found in the upper strata of the soil, carbon deep in the soil profile might have a disproportionately greater influence on the long-term carbon cycle if deep carbon has a longer residence time than carbon higher in the profile, for example [55]. Other studies indicate exotic plants can affect the vertical distribution of root biomass in native communities [30–32], but greater root biomass in native grass versus tall fescue stands does not necessarily lead to increased SOC [56]. Likewise, our results do not suggest that tall fescue, specifically, affects root biomass or SOC in these rangelands at either the fine or broad temporal scales considered here, despite indications of a community-level association between exotic species richness and reduced root biomass (Figure 3). If one were to consider the gradient of invasion/floristic degradation across the study tracts as a space-for-time substitution, for example [57], one could draw two conclusions: either invasive species might not reduce the carbon sequestration potential of these rangelands or the restoration of native plant dominance does not seem likely to increase carbon sequestration potential of invaded/degraded rangeland in the foreseeable future.

4. Conclusion

Although sampling deep into the soil profile substantially increased estimated stocks of SOC and root biomass in these rangelands, observed dynamics between soil properties, management, and plant communities appear restricted to the upper 20 cm of the soil profile. These results corroborate two important themes in soil carbon research. First, increasing the sampling depth contributes to substantially greater soil organic carbon (SOC) stocks in temperate grassland soils. Second, vegetation, land-use management, and soil properties interact to affect soil carbon and root biomass stocks, but this relationship is not necessarily straightforward. Together, these results support the claim that rangeland soils are important carbon pools but also suggest it is unlikely that rangeland plant communities can be effectively categorized by their

carbon sequestration potential without considering biotic and abiotic factors, even within climate zones and regions.

Conflict of Interests

The authors declare that there is no conflict of interests regarding the publication of this paper.

Acknowledgments

The authors thank the Leopold Center for Sustainable Agriculture at Iowa State University, Ames, Iowa, and the US Environmental Protection Agency's P3 Award for funding data collection. Analysis was supported by the Iowa State and Oklahoma State Agriculture Experiment Stations. The authors appreciate the logistical contributions of R. Harr, R. Limb, and M. Kirkwood.

References

[1] N. H. Batjes, "Total carbon and nitrogen in the soils of the world," *European Journal of Soil Science*, vol. 47, no. 2, pp. 151–163, 1996.

[2] A. P. da Silva, B. D. Kay, and E. Perfect, "Management versus inherent soil properties effects on bulk density and relative compaction," *Soil and Tillage Research*, vol. 44, no. 1-2, pp. 81–93, 1997.

[3] R. L. McCulley, I. C. Burke, J. A. Nelson, W. K. Lauenroth, A. K. Knapp, and E. F. Kelly, "Regional patterns in carbon cycling across the Great Plains of North America," *Ecosystems*, vol. 8, no. 1, pp. 106–121, 2005.

[4] R. F. Follett and D. A. Reed, "Soil carbon sequestration in grazing lands: societal benefits and policy implications," *Rangeland Ecology and Management*, vol. 63, no. 1, pp. 4–15, 2010.

[5] E. C. Ellis and N. Ramankutty, "Putting people in the map: anthropogenic biomes of the world," *Frontiers in Ecology and the Environment*, vol. 6, no. 8, pp. 439–447, 2008.

[6] R. T. Conant and K. Paustian, "Potential soil carbon sequestration in overgrazed grassland ecosystems," *Global Biogeochemical Cycles*, vol. 16, no. 4, pp. 90-1–90-9, 2002.

[7] C. Dean, G. W. Wardell-Johnson, and R. J. Harper, "Carbon management of commercial rangelands in Australia: major pools and fluxes," *Agriculture, Ecosystems & Environment*, vol. 148, pp. 44–64, 2012.

[8] J. T. Manley, G. E. Schuman, J. D. Reeder, and R. H. Hart, "Rangeland soil carbon and nitrogen responses to grazing," *Journal of Soil and Water Conservation*, vol. 50, no. 3, pp. 294–298, 1995.

[9] G. Pineiro, J. M. Paruelo, M. Oesterheld, and E. G. Jobbágy, "Pathways of grazing effects on soil organic carbon and nitrogen," *Rangeland Ecology and Management*, vol. 63, no. 1, pp. 109–119, 2010.

[10] S. Bagchi and M. E. Ritchie, "Introduced grazers can restrict potential soil carbon sequestration through impacts on plant community composition," *Ecology Letters*, vol. 13, no. 8, pp. 959–968, 2010.

[11] N. P. He, Y. H. Zhang, Q. Yu et al., "Grazing intensity impacts soil carbon and nitrogen storage of continental steppe," *Ecosphere*, vol. 2, no. 1, article 8, 2011.

[12] E. Medina-Roldán, J. Paz-Ferreiro, and R. D. Bardgett, "Grazing exclusion affects soil and plant communities, but has no impact on soil carbon storage in an upland grassland," *Agriculture, Ecosystems and Environment*, vol. 149, pp. 118–123, 2012.

[13] L. C. Johnson and J. R. Matchett, "Fire and grazing regulate belowground processes in tallgrass prairie," *Ecology*, vol. 82, no. 12, pp. 3377–3389, 2001.

[14] E. Pucheta, I. Bonamici, M. Cabido, and S. Díaz, "Below-ground biomass and productivity of a grazed site and a neighbouring ungrazed exclosure in a grassland in central Argentina," *Austral Ecology*, vol. 29, no. 2, pp. 201–208, 2004.

[15] R. F. Limb, S. D. Fuhlendorf, D. M. Engle, and J. D. Kerby, "Growing-season disturbance in tallgrass prairie: evaluating fire and grazing on Schizachyrium scoparium," *Rangeland Ecology and Management*, vol. 64, no. 1, pp. 28–36, 2011.

[16] D. G. Neary, C. C. Klopatek, L. F. DeBano, and P. F. Ffolliott, "Fire effects on belowground sustainability: a review and synthesis," *Forest Ecology and Management*, vol. 122, no. 1-2, pp. 51–71, 1999.

[17] M. I. Bird, E. M. Veenendaal, C. Moyo, J. Lloyd, and P. Frost, "Effect of fire and soil texture on soil carbon in a sub-humid savanna (Matopos, Zimbabwe)," *Geoderma*, vol. 94, no. 1, pp. 71–90, 2000.

[18] R. W. S. Fynn, R. J. Haynes, and T. G. O'Connor, "Burning causes long-term changes in soil organic matter content of a South African grassland," *Soil Biology and Biochemistry*, vol. 35, no. 5, pp. 677–687, 2003.

[19] H. Knicker, "How does fire affect the nature and stability of soil organic nitrogen and carbon? A review," *Biogeochemistry*, vol. 85, no. 1, pp. 91–118, 2007.

[20] S. G. Baer, D. J. Kitchen, J. M. Blair, and C. W. Rice, "Changes in ecosystem structure and function along a chronosequence of restored grasslands," *Ecological Applications*, vol. 12, no. 6, pp. 1688–1701, 2002.

[21] S. G. Baer, C. K. Meyer, E. M. Bach, R. P. Klopf, and J. Six, "Contrasting ecosystem recovery on two soil textures: implications for carbon mitigation and grassland conservation," *Ecosphere*, vol. 1, no. 1, article 5, 2010.

[22] C. Rumpel and I. Kögel-Knabner, "Deep soil organic matter—a key but poorly understood component of terrestrial C cycle," *Plant and Soil*, vol. 338, no. 1-2, pp. 143–158, 2011.

[23] A. R. Wilts, D. C. Reicosky, R. R. Allmaras, and C. E. Clapp, "Long-term corn residue effects: harvest alternatives, soil carbon turnover, and root-derived carbon," *Soil Science Society of America Journal*, vol. 68, no. 4, pp. 1342–1351, 2004.

[24] D. P. Rasse, C. Rumpel, and M.-F. Dignac, "Is soil carbon mostly root carbon? Mechanisms for a specific stabilisation," *Plant and Soil*, vol. 269, no. 1-2, pp. 341–356, 2005.

[25] P. Sollins, P. Homann, and B. A. Caldwell, "Stabilization and destabilization of soil organic matter: mechanisms and controls," *Geoderma*, vol. 74, no. 1-2, pp. 65–105, 1996.

[26] R. Alvarez and R. S. Lavado, "Climate, organic matter and clay content relationships in the Pampa and Chaco soils, Argentina," *Geoderma*, vol. 83, no. 1-2, pp. 127–141, 1998.

[27] J. Leifeld, S. Bassin, and J. Fuhrer, "Carbon stocks in Swiss agricultural soils predicted by land-use, soil characteristics, and altitude," *Agriculture, Ecosystems and Environment*, vol. 105, no. 1-2, pp. 255–266, 2005.

[28] R. Lal and J. M. Kimble, "Importance of soil bulk density and methods of its importance," in *Assessment Methods for Soil Carbon*, Lewis, Boca Raton, Fla, USA, 2001.

[29] K. R. Brye, C. P. West, and E. E. Gbur, "Soil quality differences under native tallgrass prairie across a climosequence in Arkansas," *The American Midland Naturalist*, vol. 152, no. 2, pp. 214–230, 2004.

[30] M. J. Fisher, I. M. Rao, M. A. Ayarza et al., "Carbon storage by introduced deep-rooted grasses in the South American savannas," *Nature*, vol. 371, no. 6494, pp. 236–238, 1994.

[31] A. Tufekcioglu, J. W. Raich, T. M. Isenhart, and R. C. Schultz, "Fine root dynamics, coarse root biomass, root distribution, and soil respiration in a multispecies riparian buffer in Central Iowa, USA," *Agroforestry Systems*, vol. 44, no. 2-3, pp. 163–174, 1998.

[32] B. J. Wilsey and H. W. Polley, "Aboveground productivity and root-shoot allocation differ between native and introduced grass species," *Oecologia*, vol. 150, no. 2, pp. 300–309, 2006.

[33] K. A. Fink and S. D. Wilson, "Bromus inermis invasion of a native grassland: diversity and resource reduction," *Botany*, vol. 89, no. 3, pp. 157–164, 2011.

[34] E. G. Jobbágy and R. B. Jackson, "The vertical distribution of soil organic carbon and its relation to climate and vegetation," *Ecological Applications*, vol. 10, no. 2, pp. 423–436, 2000.

[35] H. Blanco-Canqui and R. Lal, "Mechanisms of carbon sequestration in soil aggregates," *Critical Reviews in Plant Sciences*, vol. 23, no. 6, pp. 481–504, 2004.

[36] J. R. Miller, L. W. Morton, D. M. Engle, D. M. Debinski, and R. N. Harr, "Nature reserves as catalysts for landscape change," *Frontiers in Ecology and the Environment*, vol. 10, no. 3, pp. 144–152, 2012.

[37] D. McGranahan, D. Engle, S. Fuhlendorf, J. Miller, and D. Debinski, "Multivariate analysis of rangeland vegetation and soil organic carbon describes degradation, informs restoration and conservation," *Land*, vol. 2, no. 3, pp. 328–350, 2013.

[38] D. A. Mcgranahan, D. M. Engle, S. D. Fuhlendorf, S. J. Winter, J. R. Miller, and D. M. Debinski, "Spatial heterogeneity across five rangelands managed with pyric-herbivory," *Journal of Applied Ecology*, vol. 49, no. 4, pp. 903–910, 2012.

[39] R. A. Moranz, D. M. Debinski, D. A. McGranahan, D. M. Engle, and J. R. Miller, "Untangling the effects of fire, grazing, and land-use legacies on grassland butterfly communities," *Biodiversity and Conservation*, vol. 21, no. 11, pp. 2719–2746, 2012.

[40] D. A. McGranahan, D. M. Engle, B. J. Wilsey, S. D. Fuhlendorf, J. R. Miller, and D. M. Debinski, "Grazing and an invasive grass confound spatial pattern of exotic and native grassland plant species richness," *Basic and Applied Ecology*, vol. 13, no. 8, pp. 654–662, 2012.

[41] USDA-NRCS, "Web Soil Survey data for Ringgold County, Iowa. Natural Resource Conservation Service, United States Department of Agriculture," 2010, http://websoilsurvey.nrcs.usda.gov.

[42] T. J. Stohlgren, K. A. Bull, and Y. Otsuki, "Comparison of rangeland vegetation sampling techniques in the Central Grasslands," *Journal of Range Management*, vol. 51, no. 2, pp. 164–172, 1998.

[43] R. Daubenmire, "A canopy-coverage method of vegetational analysis," *Northwest Science*, vol. 33, no. 1, pp. 43–64, 1959.

[44] W. K. Lauenroth and W. C. Whitman, "A rapid method for washing roots," *Journal of Range Management*, pp. 308–309, 1971.

[45] D. Bates, M. Maechler, B. Bolker, and S. Walker, "lme4: Linear mixed-effects models using Eigen and S4," 2013, http://cran.r-project.org/web/packages/lme4/index.html.

[46] R Development Core Team, *R: A Language and Environment for Statistical Computing*, R Foundation for Statistical Computing, Vienna, Austria, 2013.

[47] S. Nakagawa and I. C. Cuthill, "Effect size, confidence interval and statistical significance: a practical guide for biologists," *Biological Reviews*, vol. 82, no. 4, pp. 591–605, 2007.

[48] S. Nakagawa and H. Schielzeth, "A general and simple method for obtaining R^2 from generalized linear mixed-effects models," *Methods in Ecology and Evolution*, vol. 4, no. 2, pp. 133–142, 2013.

[49] J. Oksanen, F. G. Blanchet, R. Kindt et al., "vegan: Community ecology package," 2013, http://cran.r-project.org/web/packages/vegan/index.html.

[50] R. B. Jackson, J. Canadell, J. R. Ehleringer, H. A. Mooney, O. E. Sala, and E. D. Schulze, "A global analysis of root distributions for terrestrial biomes," *Oecologia*, vol. 108, no. 3, pp. 389–411, 1996.

[51] P. Savadogo, L. Sawadogo, and D. Tiveau, "Effects of grazing intensity and prescribed fire on soil physical and hydrological properties and pasture yield in the savanna woodlands of Burkina Faso," *Agriculture, Ecosystems and Environment*, vol. 118, no. 1–4, pp. 80–92, 2007.

[52] D. Foster, F. Swanson, J. Aber et al., "The importance of land-use legacies to ecology and conservation," *BioScience*, vol. 53, no. 1, pp. 77–88, 2003.

[53] K. W. Davies, T. J. Svejcar, and J. D. Bates, "Interaction of historical and nonhistorical disturbances maintains native plant communities," *Ecological Applications*, vol. 19, no. 6, pp. 1536–1545, 2009.

[54] D. A. McGranahan, D. M. Engle, S. D. Fuhlendorf, J. R. Miller, and D. M. Debinski, "An invasive cool-season grass complicates prescribed fire management in a native warm-season grassland," *Natural Areas Journal*, vol. 32, no. 2, pp. 208–214, 2012.

[55] S. Trumbore, "Age of soil organic matter and soil respiration: radiocarbon constraints on belowground C dynamics," *Ecological Applications*, vol. 10, no. 2, pp. 399–411, 2000.

[56] C. T. Garten Jr. and S. D. Wullschleger, "Soil carbon inventories under a bioenergy crop (Switchgrass): measurement limitations," *Journal of Environmental Quality*, vol. 28, no. 4, pp. 1359–1365, 1999.

[57] S. T. Pickett, "Space-for-time substitution as an alternative to long-term studies," in *Long-Term Studies in Ecology: Approaches and Alternatives*, pp. 110–135, Springer, New York, NY, USA, 1989.

Hindawi Publishing Corporation
The Scientific World Journal
Volume 2014, Article ID 625856, 7 pages
http://dx.doi.org/10.1155/2014/625856

Research Article

Land Use Intensification Effects in Soil Arthropod Community of an Entisol in Pernambuco State, Brazil

G. M. Siqueira,[1] E. F. F. Silva,[2] and J. Paz-Ferreiro[3]

[1] *Center of Agricultural and Environmental Sciences, Federal University of Maranhão, BR-222, KM 04, Boa Vista, s/n, 65500-000 Chapadinha, MA, Brazil*
[2] *Department of Rural Technology, Federal Rural University of Pernambuco, Dom Manoel de Medeiros, s/n, 52171-900 Recife, PE, Brazil*
[3] *Faculty of Sciences, University of Coruña, Campus A Zapateira, 15008 Coruña, Spain*

Correspondence should be addressed to J. Paz-Ferreiro; jpaz@udc.es

Received 17 July 2014; Revised 17 September 2014; Accepted 18 September 2014; Published 20 October 2014

Academic Editor: Antonio Paz González

The interactions between soil invertebrates and land use and management are fundamental for soil quality assessment but remain largely unaddressed. The aim of this study was to evaluate the changes in soil arthropod community of an entisol brought about by different land use systems under semiarid climate in Pernambuco State, Brazil. The soil invertebrate community was sampled using pitfall traps from areas with eight vegetation types by the end of the austral winter. The land uses studied were native thorn forest plus seven agricultural fields planted with elephant grass, apple guava, passion fruit, carrot, maize, tomato, and green pepper. Native vegetation was considered as a reference, whereas the agricultural fields showed a range of soil use intensities. The abundance of organisms, the total and average richness, Shannon's diversity index, and the Pielou uniformity index were determined, and all of these were affected by several crop and soil management practices such as residue cover, weed control, and pesticide application. Our study found differences in community assemblages and composition under different land use systems, but no single taxa could be used as indicator of soil use intensity.

1. Introduction

Soil fauna include a large number of species that play a central role in many essential ecosystem processes [1, 2]. When a natural system is shifted by human activities for agricultural or forestry purposes, major changes occur in the soil environment and in the fauna populations and community. The intensity of the modifications induced by land use changes compared with the original ecosystem and the ability of the various soil organisms to adapt to these changes will determine the ultimate community present after the perturbation [3].

Agricultural practices can have a dramatic effect upon soil invertebrate community. Practices generally considered as beneficial for the soil fauna include the management of organic matter, particularly the control of the quality or quantity of plant residues and the absence of soil tillage. Also crop rotation, fertilization, and liming may also play an important role in increasing the diversity of soil biota. The main practices generally considered as having negative effects on soil biota comprise the use of pesticides, frequent and deep tillage, inadequate soil cover and poor management of organic residues, physical degradation, contamination, and pollution [3, 4].

There is a current interest in improving both soil quality and sustainable land management systems [5, 6]. Intensive land use can lead to negative impacts on soil quality. While physical and chemical properties have been demonstrated to respond slower to changes in soil use and management, it is widely accepted that soil biological and biochemical properties and also soil organisms are suitable indicators of soil quality [4–9].

Macrofaunal organisms have been widely accepted as indicators of soil quality. This is due to the important role of fauna regulating processes such as the formation and stability of soil aggregates, nutrient cycling, and soil aeration. Soil fauna provides top-down regulation of microbial responses to soil quality alterations via the regulation of the bacterial

and fungal food webs in the soil. Other physical processes such as erosion and filtering can also be affected by soil fauna [1, 4, 7]. In addition, soil fauna measurements provide some advantages compared to other biological methods to measure soil quality as they rely on identifying and quantifying species living in the soil rather than on nonstandardized chemical analyses.

In particular, soil arthropods have been used as indicators of soil quality in soils and to compare different management systems, as they are regulated by anthropogenic impacts. Frequently, these studies have been done using single taxon groups, including Acari, Isopoda, Coleoptera, Araneae, or Collembola [8–10] or integrative quality indices [11, 12].

The interior region of northeastern Brazil is covered by xeric shrubland and thorn forest, locally referred to as "Caatinga," unlike the Atlantic rain forest, which borders the Atlantic see. The "Caatinga" biome, located between 3°S 45°W and 17°S 35°W, incorporates about 900,000 km^2. This native vegetation typically consists of small, thorny trees; herbaceous vegetation only starts growing in the rainy season. Due to the high demographic density (20–30 inhabitants per km^2) this is one of the most densely populated semiarid regions of the world. Therefore, there is a pressure to cultivate as much land as possible. Moreover, agricultural land use involves a large number of small properties with contrasting management systems, including irrigated, high input systems and rainfed, low input systems [13].

Intensive agricultural systems can produce negative impacts on soils, including a loss of soil quality and biodiversity. These aspects should be evaluated as soil fauna is sensitive to several soil management practices, including fertilizer use and tillage [14] or land use changes [15, 16]. Soil fauna is also sensitive to land degradation [17].

In spite of the essential role of arthropods in soil functioning, there is not enough knowledge about how they are affected by extensive and/or intensive agricultural systems. In particular, the arthropod community along intensification gradients has not been studied at the Brazilian Caatinga. Thus, in this work, we used soil arthropods as a mean to evaluate the effects of agricultural intensification on soil quality.

2. Material and Methods

2.1. Study Site, Climate, Soil Type, and Land Use. The study area was located in Fazenda Nossa Senhora do Rosário, Pesqueira municipality (Pernambuco, Brazil), at 8°34′17″S and 37°1′20″W. The average altitude is 610 m. The climate in the region is hot, semiarid, with dry austral summers and more rainy winters (BShw according to Köppen). Average annual temperature is 27°C and average annual rainfall is 600 mm. Usually, the rainy season starts in December or January.

Fazenda Nossa Senhora do Rosário is located on an alluvial valley (Figure 1). The soils of the studied fields were entisols, and they were classified as Fluvent and Orthent at the suborder level, following the Soil Survey Staff [18]. Fluvent and Orthent are equivalent to "Neossoo flúvico" and

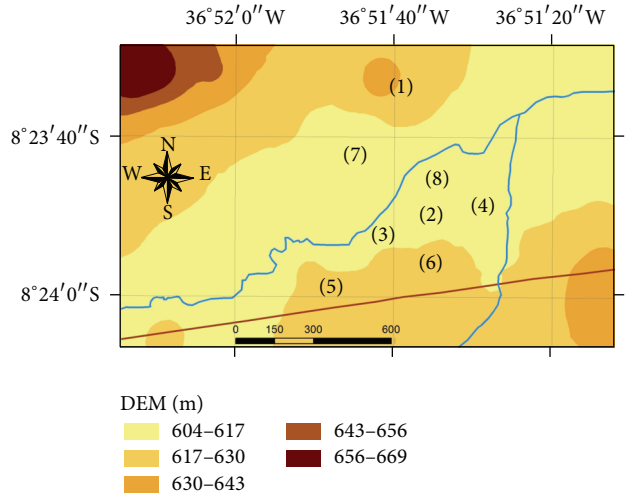

Figure 1: Localization of the studied stands (scale = meters).

"Neossolo Regolítico," respectively, in the Brazilian Soil Classification System [19]. General properties of these two soil types are listed in Tables 1 and 2. Both Fluvent and Orthent were sandy loam textured. Soil pH at the surface horizon (0–20 cm) was slightly acid, thus in the desired range for agricultural soils. Cation exchange capacity (CEC) was low, as expected for tropical soils, with values of 8,2 $Cmol_+ kg^{-1}$ and 6,6 $Cmol_+ kg^{-1}$ for Fluvent and Orthent, respectively. Organic matter content, however, was much higher for Orthent than for Fluvent.

In this area, production is carried out by small scale farmers, owning plots along the river valley. Some fields are used as forage for cattle, while most fields are subject to cultivation. The invertebrate community was evaluated in 8 plots, located within a thorn forest (which was taken as a reference) and in 7 agricultural fields with different cultivation systems and vegetation cover. Details about soil type, land use and soil and crop management of the sites studied are summarized in Table 3. A soil use intensity index for each of the studied stands was elaborated based on local expert knowledge and is also listed in Table 3.

The native forest (Caatinga) is a xeric or even hyperxeric vegetation with thorny tress as dominant species. In winter periods the small thorny trees lose their leaves and the understory merely consists of cacti, thick-stemmed plants, and arid-adapted grasses, limiting the litter available for soil biota. During the brief rainy season, however, many annual plants grow, flower, and produce much more abundant litter debris.

The agricultural fields studied were cropped with different plant species, including elephant grass (*Pennisetum purpureum*, Schumach), apple guava (*Psidium guajava*, L.), passion fruit (*Passiflora edulis,* Sims), carrot (*Daucus carota*, L.), maize (*Zea mays*, Mill.), tomato (*Solanum lycopersicum*, Mill.), and green pepper (*Capsicum annuum*, L.).

2.2. Sampling and Analysis of Active Fauna. Soil fauna was sampled using the pitfall trap method during a seven-day

Table 1: Granulometric analysis as a function of depth of the soils studied.

Fluvent (Neossolo Flúvico)				Orthent (Neossolo Regolítico)			
Depth (cm)	Sand (%)	Silt (%)	Clay (%)	Depth (cm)	Sand (%)	Silt (%)	Clay (%)
0–20	64.69	19.78	15.44	0–15	65.68	18.00	16.32
20–40	64.29	18.41	17.30	15–35	60.24	20.56	19.20
40–60	68.39	15.65	15.97	35–70	63.52	15.28	21.20

Table 2: General chemical properties of the soils studied.

Fluvent (Neossolo Flúvico)										
Depth (cm)	pH H_2O	P mg/dm^3	Na	K	Mg	Ca	H	CEC	OC	OM
					cmolc/dm^3				g/kg	
0–20	6.2	100	0.14	0.25	1.7	2.8	3.31	8.20	0.24	0.42
Orthent (Neossolo Regolítico)										
Depth (cm)	pH H_2O	P mg/dm^3	Na	K	Mg	Ca	H	CEC	CO	MO
					cmolc/dm^3				g/kg	
0–20	6.5	41	0.09	0.28	0.85	1.85	3.51	6.58	4.36	7.52

(CEC = cation exchange capacity; OC = organic carbon; OM = organic matter).

Table 3: Location, soil type, and soil and crop management of the studied natural and agricultural stands.

Coordinates	Altitude	Soil type (SSA)	Soil type (BSCS)	Vegetation	Tillage and soil cover	Weeds at sampling	Irrigation	Pesticides	Soil use intensity
8°23′38.84″S 36°51′34.52″W	634 m	Fluvent	Neossolo Flúvico	Natural vegetation (*Caatinga Biome*)	Uncultivated, soil 100% covered	—	No	No	0
8°23′47.26″S 36°51′35.56″W	611 m	Fluvent	Neossolo Flúvico	Elephant grass (*Pennisetum purpureum*)	Established 2 years ago, periodic grass mow	—	No	No	1
8°23′52.93″S 36°51′39.19″W	612 m	Fluvent	Neossolo Flúvico	Apple guava (*Psidium guajava*)	Established 3 years ago, soil 100% covered	Yes	No	No	1
8°23′46.59″S 36°51′33.15″W	613 m	Fluvent	Neossolo Flúvico	Passion fruit (*Passiflora edulis*)	Six months fallow, between lines coverage	No	Drip	No	2
8°23′58.23″S 36°51′39.06″W	621 m	Orthent	Neossolo Regolítico	*Carrot* (*Daucus carota*)	Plowing and disk harrow, soil partially covered	Yes	Drip	Yes	3
8°23′54.43″S 36°51′37.35″W	615 m	Orthent	Neossolo Regolítico	*Maize (Zea mays)*	Plowing and disk harrow, soil partially covered	No	Aspersion	Yes	3.5
8°23′41.19″S 36°51′37.54″W	610 m	Fluvent	Neossolo Flúvico	Tomato (*Solanum lycopersicum*)	Plowing and disk harrow, uncovered between lines	No	Drip	Yes	5
8°23′45.61″S 36°51′35.89″W	610 m	Fluvent	Neossolo Flúvico	Green Pepper (*Capsicum annuum*)	Plowing and disk harrow, uncovered between lines	Yes	Drip	Yes	5

(SSA = Soil Survey Staff; BSCS = Brazilian Soil Classification System).

period, from 22 to 29 August, 2013. Average temperature during the sampling period was 21.5°C (average maxima 28.2°C and average minima 16.0°C). Due to high evaporation rates the soil was dry, even if two significant rainfall events were recorded before starting field fauna sampling; these events occurred on 1 August (20 mm) and on 19 August (10 mm). Pitfall traps were made of plastic (9 cm height × 8 cm diameter) [20]. Five traps were installed per land use. Each trap remained active for a week. The glass was set flush with the soil surface and contained 200 mL of formaldehyde (4%). The content of each glass was emptied afterwards in the field into a container, which was completed with 70% alcohol for preservation of the specimens.

Each sample was processed in the laboratory, separating and classifying the arthropods. All the adult and juvenile specimens were classified to the order level using a binocular microscope and taxonomic keys, with some exceptions. Within the order Hemiptera, the suborder Heteroptera was

separated from the suborders Auchenorrhyncha and Sternorrhyncha. Acari was considered as an order. The total number of individuals were first counted per pitfall and taxa studied.

The data were also converted into number of individuals per trap per day. This parameter indicates the fauna abundance and was calculated for each taxonomic group and for the total arthropod community sampled. Aside from abundance, diversity of soil fauna was evaluated using the following ecological indices: mean richness (mean number of taxa trapped per pitfall and land use), total richness (total number of taxa trapped per land use, regardless of trap), Shannon diversity index and Pielou equitability (or evenness) index.

The Shannon-Weaner index was obtained as

$$H = -\sum pi \cdot \log 2 \cdot pi, \quad (1)$$

where pi: ni/N; ni is number of individuals per trap per day for each of the orders studied (Ind·arm·dia^{-1}), and N is sum of individuals per trap per day. This index describes the diversity as a weighted geometric mean of the relative distribution of abundance of the individuals between the groups sampled.

The Pielou evenness index is indicative of the uniformity of soil fauna for each land use and is calculated as follows:

$$U = \frac{H}{\log 2S}, \quad (2)$$

where H is Shannon index and S is remaining groups present in treatments.

This index quantifies how equal the community is numerically. Close relative abundance of the studied taxa is indicated by high values of Pielou index.

The Kolmogorov-Smirnov test was applied to assess the normality of the distribution of the data sets. Data were log-transformed to meet the requirements for parametric statistical tests. Only those arthropod groups that met the statistical assumptions were analyzed. Thus, the groups analyzed were available in high numbers. Moreover, most of the taxa were not assessed adequately with pitfall traps and were excluded from further analyses. As an example, flying organisms are trapped with different techniques depending on their behavior (e.g., stick and pheromone traps).

We used a one-way ANOVA to investigate the effects of land use intensification on the densities of soil surface-active arthropods. Differences between groups were assessed using the Tukey test.

3. Results and Discussion

All together, 6340 specimens were collected by pitfalls during the sampling period of seven days. They were grouper per land use and taxonomic group (Table 4). The total number of individuals trapped per land use showed wide differences. The largest arthropod community was found under apple guava (3224 individuals), but carrot (959 individuals) and green pepper (974 individuals) also showed much larger fauna recovery than other land uses. The smallest arthropod communities were collected under maize (59 individuals) and tomato (95 individuals). Under native forests 286 individuals were trapped, which is mostly comparable to elephant grass (330 individuals) and passion fruit (213 individuals). Entomobryomorpha was the dominant taxonomic group under apple guava (3080 individuals) and green pepper (780 individuals), whereas Poduromorpha prevailed under carrot (716 individuals).

Several factors may influence the soil invertebrate community, particularly season, microclimate, soil, and crop management, and resource availability [16, 17, 21]. With regard to the season, indeed rainfall might contribute to a more favorable environment for fauna activity at the semiarid region of northeast Brazil. In the studied area, however, water provided by irrigation has to be taken into account. Therefore, nonirrigated (elephant grass, apple guava, and passion fruit) and irrigated (passion fruit, carrot, maize, tomato, and green pepper) stands will show contrasting soil water content and microclimatic conditions that may influence arthropod density. Tillage system and soil cover are factor affecting the organic matter and litter production in agricultural fields and therefore the food availability for soil fauna. Thus, a higher litter production is expected under native forest, apple guava, and passion fruit, because plant residues are left on the soil surface; the more the litter production, the higher food availability for soil fauna.

Mainly two crop protection practices are expected to affect the soil fauna activity: weed control and pesticide application. At the sampling date weeds had been strictly excluded from passion fruit and tomato fields, because these crops were in the main fruiting phase. However, under apple guava, carrot, and green pepper the presence of weeds was not a challenge, because when sampling was performed, the crop production was out. As herbivores, Entomobryomorpha and Poduromorpha are enhanced by the presence of weeds. Thus, it is highly possible that the large number of Entomobryomorpha under apple guava and green pepper (followed by important figures for carrot) and also the dominance of Poduromorpha under carrot was related to the increased food availability, due to no restriction of weed growth.

Pesticides have been applied to carrot, maize, tomato, and green pepper. The low number of individuals collected under maize and tomato may be related to the use of pesticides together with the scarce or even absent soil cover and strict weed control. Carrot and green pepper also received pesticide treatment; however, these crops were near the end of the vegetative growth period and weeds provided food availability for certain specialized arthropod groups. Therefore, in these stands, Entomobryomorpha and Poduromorpha found a favorable environment, even after pesticide application.

The arthropods extracted from all the land uses belong to 18 taxa, with a minimum of 9 at carrot, maize, and tomato, and a maximum of 16 at passion fruit and the native forest (Table 5). The fauna richness therefore was lower in stands treated with pesticides (carrot, maize, tomato, and green pepper) than in stands without pesticide application (elephant grass, apple guava, and passion fruit) and in the native forest. The taxa exhibiting the greatest number of specimens were Entomobryomorpha, Poduromorpha, Formicidae, Diptera, Auchenorrhyncha, Araneae, Hymenoptera,

Table 4: Total number of individuals collected by 5 pitfall traps during a week for the taxonomic groups studied.

Taxonomic group	Native forest	Elephant grass	Apple guava	Passion fruit	Carrot	Maize	Tomato	Green pepper
Acari	8	5	18	2	3		1	1
Araneae	19	5	13	1		3		17
Auchenorryncha	1	4	2	24		1	25	43
Coleóptera	18	9	6	13	5	11	6	11
Diplura				1				
Diptera	51	18	22	38	9	13	13	24
Entomobryomorpha	67	251	3080	53	188	21	21	780
Formicidae	90	14	70	29	19	4	7	36
Heteroptera			1					
Hymenoptera	19	6	10	11			15	2
Isoptera	1	3	13		1			
Larva Coleoptera	1			1				4
Orthoptera	1	2	3	4		3		
Poduromorpha	2	1	2	1	716		4	
Psocoptera				2				
Sternorryncha	5	8		1	5	1		5
Thysanoptera	3	4	1	32	13	2	3	51
Tricoptera			1					
Total	**286**	**330**	**3424**	**213**	**959**	**59**	**95**	**974**

Table 5: Parameters and indices used to assess arthropod communities under native forest and the different agricultural land uses studied.

	Abundance ± std (Ind·pitfall·day^{-1})	CV	Shannon index	Pielou index	Mean richness	Total richness
Native forest	8.17 ± 2.83	34.7	2.709	0.712	8.4	14
Elephant grass	9.43 ± 3.56	37.8	1.641	0.444	8.4	13
Apple guava	92.63 ± 64.42	69.5	0.439	0.115	8.2	14
Passion fruit	6.09 ± 0.91	15.0	2.983	0.764	8.6	15
Carrot	27.40 ± 12.54	45.8	1.150	0.363	6	9
Maize	1.69 ± 0.51	30.2	2.562	0.808	4.4	9
Tomato	2.71 ± 0.49	18.2	2.749	0.867	7	9
Green pepper	27.83 ± 5.81	20.9	1.267	0.366	8	11

and Thysanoptera, accounting for approximately 95% of the collected organisms.

In general, we found very strong effects of land use on the arthropod abundance. Several taxonomic groups showed higher abundance under specific crops. Entomobryomorpha were higher in plots under green pepper and apple guava ($F = 4.58$, $P < 0.010$). Poduromorpha were much higher in the plots under carrot than in any other treatment ($F = 33.21$, $P < 0.001$). Higher amounts of Auchenorrhyncha were found in the traps located in passion fruit, tomato, and green pepper plots ($F = 15.20$, $P < 0.001$). Thysanoptera was higher in soils under carrot and maize ($F = 15.08$, $P < 0.001$). Other taxa, like Coleoptera were ubiquitous; their abundance was similar in all the investigated land uses, but they were less abundant than other taxa. On the other hand, Formicidae were higher in the reference stand, under native vegetation, and in the stand under apple guava than in other cultivated stands ($F = 7.01$, $P < 0.001$). Also Hymenoptera were higher in the soil under native than in soils cropped with maize or tomato ($F = 4.03$, $P < 0.010$).

The pitfall trap is thought to be a sampling method most adequate for Araneae, Coleoptera, Formicidae, and Orthoptera, whereas other soil taxa should be investigated using other different methods [17]. The communities of Formicidae collected were significantly lower in all the cultivated stands than in the native forest stand, and this is irrespective of soil and crop management system. Therefore, this taxonomic group show promise as an indicator of soil quality in the Brazilian semiarid, because it exhibits the most pronounced decrease in cultivated plots compared to native forest. Assessment of this taxonomic group may be useful to evaluate the biological status of the cultivated stands.

The abundances of soil arthropods (individuals/pitfall/day) were lowest for maize (1.69 ± 0.51) and tomato (2.71 ± 0.49) and highest for apple guava (92.63 ± 64.42), followed by green pepper (27.83 ± 5.81) and passion fruit (27.40 ± 12.54), as shown in Table 5. Again, high pesticide application rates and weed control at sampling date were responsible for the small arthropod abundance under maize and tomato. On the other hand, the highest abundance of arthropods

under apple guava and the relatively high abundance under passion fruit and green pepper was due to the effect of weed population, which dramatically increased the presence of specialized herbivores, as before mentioned.

Under native Caatinga, the abundance of arthropods was 8.17 ± 2.83 individuals/pitfall/day, intermediate in comparison with the various agricultural land uses. As expected, the fauna abundance under this biome was lower than in other tropical soils. For example, under secondary Atlantic forest the figures obtained using also pitfall traps ranged from 80.13 to 111.37 individuals/pitfall/day [21], depending on the sampling season, rainy or dry, respectively.

The Shannon index suggested that diversity was highest not only at the reference stand (native forest) but also at tomato and passion fruit; it was lowest at apple guava, followed by carrot and green pepper. Thus, this index ranked as passion fruit > tomato > native forest > maize > elephant grass > green pepper > carrot > apple guava. The Pielou index showed the highest evenness or equality at tomato and maize and the lowest at apple guava. It ranked as tomato > maize > passion fruit > native forest > green pepper > carrot > apple guava. The arthropod communities under tomato and maize exhibited a high diversity and evenness (high Shannon and Pielou indices), and this is in spite of pesticide application and weed control. Therefore, such crop management practices affected fauna abundance, but not biodiversity and evenness. On the other hand, the presence of weeds dramatically increased the abundance of some taxa and this lead to a lower diversity and a lower equitability under apple guava, carrot, and green pepper.

Surprisingly, agricultural intensification does not seem to cause always a decrease of arthropod diversity and evenness. Moreover, high taxa richness could be a consequence of a shift in community composition towards a high number of taxa better adapted to the conditions in these soils. It should be also taken into account that diversity indices are known to be sensitive to various factors, such as the sampling unit size which limits their predictive capability [22].

The soils under different land uses widely differed in invertebrate density, whereas they differed more slightly in taxa richness. Therefore, we can hypothesize that individual abundance and density are affected by different soil management factors than taxa richness. It appeared that in agricultural land uses abundance was mainly related to the presence of weeds, while richness was associated to pesticide application. This is a result consistent with previous studies [22, 23].

On the other hand, the soil use intensity index (Table 5) showed no significant correlation with the studied biodiversity indices or with single taxa abundance. This may be simple due to the semiquantitative nature of the soil use intensity index.

The community composition did greatly differ among the studied land uses, which would have severe implications for soil functionality [23]. As an example, several arthropods, including mites and termites, are involved in organic matter decomposition and nutrient cycling. In addition, ants and other arthropods create channels, aggregates, and mounds that deeply affect the fluxes of gases and water in soil. This physical alteration will also modify the microhabitats for other soil organisms.

The high relative abundance of Auchenorrhyncha, Entomobryomorpha, Hymenoptera, Poduromorpha, Formicidae, and Thysanoptera suggests that these taxa are tolerant to a wide range of soil properties. This would limit their use as indicators of soil conditions and, thus, soil quality [23]. These taxa, however, showed variations in individual abundance among the different management systems, which may be due to high food availability when sampling. As an example, Entomobryomorpha had a 100-fold higher abundance in the soil under apple guava than in the soils under tomato or maize. Again Formicidae among the ubiquitous taxa appears to be the most sensitive to changes in land use and soil management.

Other taxa such as Acari, Araneae, Auchenorrhyncha, Hymenoptera, Isoptera, Orthoptera, Poduromorpha, and Sternorrhyncha were absent in some treatments, which may suggest a good potential as indicators of soil quality. In particular, Acari was absent under maize and almost absent under tomato and green pepper, while Poduromorpha were absent under maize and green pepper. This would indicate that these taxa are very sensitive to specific practices of intensification in soil and crop management. This is supported by the fact that Acari numbers and traits may change due to an intensification of soil use [24].

Overall, the highly variable density of microarthropods in this agricultural landscape seems to be dependent on several variables. Appropriate statistical analyses are required to identify those variables. Further research could be useful to better assess the sensitivity and the role of single species, since many species belonging to the same taxa and exhibiting different traits can adopt different strategies in the landscape. It is important to highlight that our study demonstrates there are differences in invertebrate communities between land uses, even at taxa levels, that can be attributed to intensive agricultural management. This leads to significant differences that are indicated by the presence or absence of arthropod taxa.

4. Conclusions

The abundance of arthropods under native forest in the Brazilian semiarid has been found to be much lower than under other native biomes, such as the Atlantic forest.

Under agricultural land use several variables related with soil and crop management influence the highly variable density of arthropods. Abundance has been shown to be related with food availability provided by weeds, which dramatically increased the presence of specialized herbivores, such as Entomobryomorpha and Poduromorpha. Richness was mainly associated with pesticide application.

Agricultural land use strongly decreased the abundance of Formicidae compared to native forest, which suggest this taxonomic group responds sensitively to agricultural land use. Several other taxonomic groups showed significantly higher abundances under specific crops, but this effect may

be due to distinct soil and crop management practices at the sampling date. However, no single taxa could be used as indicator of soil use intensity.

Conflict of Interests

The authors declare that there is no conflict of interests regarding the publication of this paper.

Acknowledgments

The authors thank CNPq (Conselho Nacional de Desenvolvimento Cientifico e Tecnológico) and FACEPE (Fundação de Amparo à Ciência e Tecnologia do Estado de Pernambuco) for their support through a DCR (Desenvolvimento Cientifico Regional) grant. Also thanks are given to FAPEMA, Maranhão State, Brazil, for funding the publication of this paper.

References

[1] V. Wolters, "Biodiversity of soil animals and its function," *European Journal of Soil Biology*, vol. 37, no. 4, pp. 221–227, 2001.

[2] J. D. Majer, K. E. C. Brennan, and M. L. Moir, "Invertebrates and the restoration of a forest ecosystem: 30 years of research following bauxite mining in Western Australia," *Restoration Ecology*, vol. 15, pp. 104–115, 2007.

[3] P. F. Hendrix, R. W. Parmelee, D. A. Crossley Jr., D. C. Coleman, E. P. Odum, and P. M. Groffman, "Detritus food webs in conventional and no-tillage agroecosystems," *Bioscience*, vol. 36, no. 6, pp. 374–380, 1986.

[4] P. Lavelle, E. Barros, E. Blanchart et al., "SOM management in the tropics: why feeding the soil macrofauna?" *Nutrient Cycling in Agroecosystems*, vol. 61, no. 1-2, pp. 53–61, 2001.

[5] J. Paz-Ferreiro and S. Fu, "Biological indices for soil quality evaluation: perspectives and limitations," *Land Degradation and Development*, 2013.

[6] J. Paz-Ferreiro, C. Trasar-Cepeda, M. C. Leirós, S. Seoane, and F. Gil-Sotres, "Effect of management and climate on biochemical properties of grassland soils from Galicia (NW Spain)," *European Journal of Soil Biology*, vol. 46, no. 2, pp. 136–143, 2010.

[7] A. Cerdà and M. F. Jurgensen, "Ant mounds as a source of sediment on citrus orchard plantations in eastern Spain. A three-scale rainfall simulation approach," *Catena*, vol. 85, no. 3, pp. 231–236, 2011.

[8] J. M. Holland and C. J. M. Reynolds, "The impact of soil cultivation on arthropod (Coleoptera and Araneae) emergence on arable land," *Pedobiologia*, vol. 47, no. 2, pp. 181–191, 2003.

[9] L. Santorufo, C. A. M. van Gestel, A. Rocco, and G. Maisto, "Soil invertebrates as bioindicators of urban soil quality," *Environmental Pollution*, vol. 161, pp. 57–63, 2012.

[10] D. Cluzeau, M. Guernion, R. Chaussod et al., "Integration of biodiversity in soil quality monitoring: baselines for microbial and soil fauna parameters for different land-use types," *European Journal of Soil Biology*, vol. 49, pp. 63–72, 2012.

[11] G. P. Aspetti, R. Boccelli, D. Ampollini, A. A. M. Del Re, and E. Capri, "Assessment of soil-quality index based on microarthropods in corn cultivation in Northern Italy," *Ecological Indicators*, vol. 10, no. 2, pp. 129–135, 2010.

[12] V. Parisi, C. Menta, C. Gardi, C. Jacomini, and E. Mozzanica, "Microarthropod communities as a tool to assess soil quality and biodiversity: a new approach in Italy," *Agriculture, Ecosystems and Environment*, vol. 105, no. 1-2, pp. 323–333, 2005.

[13] R. S. C. Menezes, E. V. S. B. Sampaio, V. Giongo, and A. M. Pérez-Marin, "Biogeochemical cycling in terrestrial ecosystems of the Caatinga biome," *Brazilian Journal of Biology*, vol. 72, no. 3, pp. 643–653, 2012.

[14] T. Brévault, S. Bikay, J. M. Maldès, and K. Naudin, "Impact of a no-till with mulch soil management strategy on soil macrofauna communities in a cotton cropping system," *Soil and Tillage Research*, vol. 97, no. 2, pp. 140–149, 2007.

[15] J. F. Ponge, S. Gillet, F. Dubs et al., "Collembolan communities as bioindicators of land use intensification," *Soil Biology and Biochemistry*, vol. 35, no. 6, pp. 813–826, 2003.

[16] M. K. da Silva Moço, E. F. da Gama-Rodrigues, A. C. da Gama-Rodrigues, R. C. R. MacHado, and V. C. Baligar, "Soil and litter fauna of cacao agroforestry systems in Bahia, Brazil," *Agroforestry Systems*, vol. 76, no. 1, pp. 127–138, 2009.

[17] A. S. F. De Araújo, N. Eisenhauer, L. A. P. L. Nunes, L. F. C. Leite, and S. Cesarz, "Soil surface-active fauna in degraded and restored lands of northeast brazil," *Land Degradation and Development*, 2013.

[18] Soil Survey Staff, *Key to Soil Taxonomy*, USDA-NRCS, Washington, DC, USA, 12th edition, 2014.

[19] EMBRAPA (Brazilian Agricultural Research Corporation), *Brazilian System of Soil Classification (in Portuguese)*, Brasilia, Brazil, 2006.

[20] M. E. F. Correia and L. C. M. Oliveira, *Soil Fauna: General and Methodological Aspects*, Embrapa Agrobiologia, Seropédica, Brazil, 2000, (Portuguese).

[21] F. V. D. C. Neto, M. E. F. Correia, G. H. A. Pereira, M. G. Pereira, and P. S. D. S. Leles, "Soil fauna as an indicator of soil quality in forest stands, pasture and secondary forest," *Revista Brasileira de Ciencia do Solo*, vol. 36, no. 5, pp. 1407–1417, 2012.

[22] J. Nahmani and P. Lavelle, "Effects of heavy metal pollution on soil macrofauna in a grassland of Northern France," *European Journal of Soil Biology*, vol. 38, no. 3-4, pp. 297–300, 2002.

[23] N. E. McIntyre, J. Rango, W. F. Fagan, and S. H. Faeth, "Ground arthropod community structure in a heterogeneous urban environment," *Landscape and Urban Planning*, vol. 52, no. 4, pp. 257–274, 2001.

[24] J. Farská, K. Prejzková, and J. Rusek, "Management intensity affects traits of soil microarthropod community in montane spruce forest," *Applied Soil Ecology*, vol. 75, pp. 71–79, 2014.

Hindawi Publishing Corporation
The Scientific World Journal
Volume 2014, Article ID 845460, 8 pages
http://dx.doi.org/10.1155/2014/845460

Research Article

Mapping Soil Surface Macropores Using Infrared Thermography: An Exploratory Laboratory Study

João L. M. P. de Lima,[1,2] João R. C. B. Abrantes,[1,2] Valdemir P. Silva Jr.,[3] M. Isabel P. de Lima,[1,2] and Abelardo A. A. Montenegro[3]

[1] *Department of Civil Engineering, Faculty of Science and Technology of the University of Coimbra (FCTUC), Rua Luís Reis Santos, Campus II, University of Coimbra, 3030-788 Coimbra, Portugal*
[2] *Institute of Marine Research, IMAR/MARE, Coimbra, Portugal*
[3] *Department of Agricultural Engineering, Rural Federal University of Pernambuco, 52171-900 Recife, PE, Brazil*

Correspondence should be addressed to João L. M. P. de Lima; plima@dec.uc.pt

Received 24 June 2014; Revised 28 August 2014; Accepted 29 August 2014; Published 14 October 2014

Academic Editor: Antonio Paz González

Macropores and water flow in soils and substrates are complex and are related to topics like preferential flow, nonequilibrium flow, and dual-continuum. Hence, the quantification of the number of macropores and the determination of their geometry are expected to provide a better understanding on the effects of pores on the soil's physical and hydraulic properties. This exploratory study aimed at evaluating the potential of using infrared thermography for mapping macroporosity at the soil surface and estimating the number and size of such macropores. The presented technique was applied to a small scale study (laboratory soil flume).

1. Introduction

Macropores and water flow in soils and substrates are complex, are related to topics like preferential flow, nonequilibrium flow, and dual-continuum, and have been addressed by many studies in the last decades (e.g., the reviews by Beven and Germann in 1982 [1] and, most recently, 30 years later, in 2013 [2]). Since macropores affect soil permeability, they directly influence other hydrological processes (e.g., surface runoff and associated transport processes).

The water movement and the fertilizers, pesticides, and other pollutants transporting in the soil through macropores have significant impact on hydrological response and water quality (e.g., [3]). These structures convey water to greater depths with higher speed, thus influencing water infiltration into the soil and solute transport. The macropores also directly affect the air flow into the soil, the plants root growth, and biological activity (e.g., [4–6]). Therefore, a high macroporosity enhances air and water movement in the soil, promoting also infiltration and root penetration.

Recently, infrared thermography has been successfully applied as a tool for high resolution imaging in different hydrological studies, conducted at quite different spatial scales. Thermographic techniques are based on records of bodies' temperatures, which are taken at certain instants or over time and at a given space scale; this technology is allowing for a nonconventional acquisition of data and analysis of different processes and their time and space dynamics.

The use of portable infrared cameras or thermal imaging cameras has gained popularity due to their easy handling and adjustment of the vision field to a specific study area. Mejías et al. [7] and Danielescu et al. [8] used infrared cameras mounted in aircrafts for mapping groundwater discharge in shallow estuaries, provided that there is a thermal contrast between groundwater and the receiving surface waters. Cardenas et al. [9] characterized the thermal heterogeneity in a small stream during different flow conditions. Pfister et al. [10] used ground-based thermal imagery as a simple, practical tool, for mapping saturated area connectivity and dynamics. It was possible to discriminate between areas with snow cover, snow melt, soil seepage, and stream water. It was possible to detect when and where variably saturated areas were active and when connectivity existed between

the hillslope-riparian-stream systems. This was a simple and inexpensive technology for sequential mapping and characterisation of surface saturated areas and a useful complement to conventional tracer techniques. Schuetz et al. [11] used infrared thermal imaging combined with the injection of heated water as an artificial tracer technique to characterize the spatial distribution of flow paths and to assess transport properties in a 65 m^2 experimentally constructed wetland with water depths between 0.1 and 0.2 m. For the studied conditions, the authors observed that heated water can be used as a conservative artificial tracer for plot scale experiments.

Infrared thermographic techniques studied in laboratory conditions were used to assess different surface hydrological processes. A technique to estimate soil surface microrelief and rill morphology using infrared thermography is presented in de Lima and Abrantes [12]. The authors were able to generate 3D models of soil surface elevation for both bare soil and soil covered with organic residue. In de Lima and Abrantes [13] the authors estimated very shallow flow velocities (overland and rill flow), by injecting a thermal tracer (e.g., heated water) into very shallow flows and visualizing the leading edge of the tracer by means of infrared video. Soil flume laboratory experiments have been conducted for many years aiming at studying specific processes and interactions in controlled conditions allowing for repetitions in a short period of time (e.g., [14–19]).

In situ small scale infiltration tests (e.g., profile or plot scale), under saturated or unsaturated soil conditions, normally have difficulty to cope with macropores. The quantification of the number of macropores, which are drivers of water, and the determination of their geometry will provide a better understanding of the effects of pores on the physical and hydraulic properties of the soil (e.g., [20]). Thus, this exploratory study aimed at evaluating the potential of using infrared thermography for mapping macroporosity at the soil surface and estimating the number and size of such macropores. The presented technique was applied to a small laboratory scale study (i.e., soil flume). Thus, upscaling results to field, hillslope, and even plot scales will require further investigation, which is beyond the scope of the presented analysis.

2. Material and Methods

2.1. Laboratory Setup. A schematic representation of the used exploratory laboratory setup is shown in Figure 1. The experiments were carried out using a 3.00 m long, 0.30 m wide, and 0.12 m deep free drainage soil flume, set at a 10% slope (round number also used in many other works). A feeder box installed at the upslope end of the flume allowed the application of a defined volume of hot water uniformly over the soil surface. A rectangular measuring area (0.50 × 0.30 m^2) with macropores was defined at the flume soil surface, approximately 0.5 m downstream of the hot water feeder box.

The experiments were carried out using a loamy-sand soil collected from the River Mondego banks (Coimbra, Portugal). The soil presented 6% clay, 11% silt, 82% sand, and a 1750 kg/m^3 bulk density. Saturated hydraulic conductivity was ~4.51×10^{-6} m/s, for the macropores-free soil.

Thermal videos of the soil surface were recorded with an Optris PI-160 portable infrared video camera (Optris GmbH, Germany) with an optical resolution of 160 × 120 pixels, a thermal resolution of 0.1°C, an accuracy of ±2%, a frame rate of 100 Hz, and a lens with a view field of 23° × 17° and focal length of 10 mm. The camera was attached to a metal support structure 0.75 m above the flume soil surface with the focal length direction perpendicular to the soil surface (Figure 1).

2.2. Soil Surface Macropores. Soil surface vertical macropores with three different rectangular cross section areas were artificially created to test the proposed thermographic technique: (i) large macropores with an area of 256 mm^2 (16 × 16 mm^2); (ii) medium macropores with an area of 120 mm^2 (12 × 10 mm^2); and (iii) small macropores with an area of 36 mm^2 (6 × 6 mm^2). The tests were conducted for four different macropores spatial arrangement's scenarios; these scenarios are shown in Figure 2: (a) 9 large macropores (Scenario A); (b) 9 medium macropores (Scenario B); (c) 9 small macropores (Scenario C); and (d) a combination of 3 large, 3 medium, and 3 small macropores (Scenario D). It should be noted that field conditions are quite different from a uniform plane surface, clean of stones, debris, and vegetation, with homogeneous colours and macropores with well-defined shapes, used in this exploratory study.

2.3. Experimental Procedure. Air dried presieved soil was manually spread over the flume and gently tapped to obtain a soil layer with a uniform thickness of 0.10 m with a bulk density of ~1750 kg/m^3. A sharp straight-edged blade was used to produce a smooth plane soil surface. The soil was saturated and left to dry, aiming to obtain a consistency that allowed the artificial creation of vertical macropores at the soil surface; this was carried out by perforating the soil layer, throughout its 0.10 m thickness, with rectangular cross-section metal rods that were described in Section 2.2. After the creation of the macropores, the soil was again saturated.

The technique starts by applying approximately 1.5 L of heated water over the soil surface, at a temperature around 80–85°C. The water was manually released using the feeder box located upslope of the flume (Figure 1). It was applied with the lowest possible discharge in order to guarantee flow depth uniformity over the measuring area, minimum soil surface disturbance, and the unaltered structure of the macropores by the flowing water. The volume of hot water used (and applied discharge) should be adjusted to the test's conditions (e.g., dimension of the measuring area, slope, water temperature, soil permeability, and dimension of macropores).

The hot water created a wave that covered uniformly the soil surface; along the flume, part of the water flows to the macropores, part infiltrates into the soil, and part flows out of the flume through the downslope outlet, as overland flow. The hot water briefly accumulates inside the macropores before exiting freely the soil layer due to the

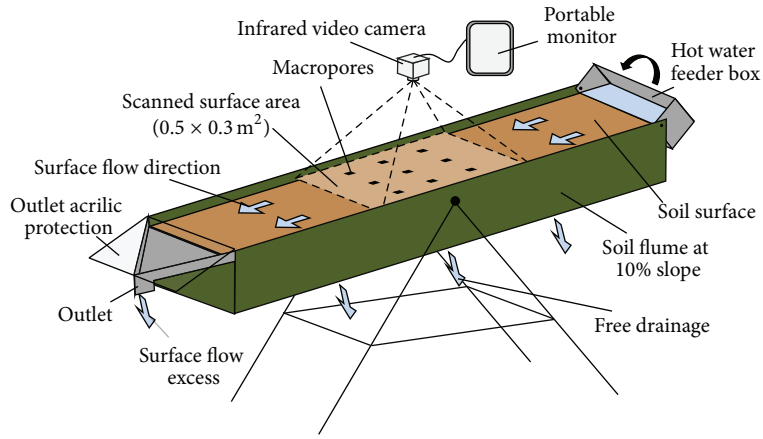

Figure 1: Sketch of the laboratory setup using a soil flume and an infrared video camera.

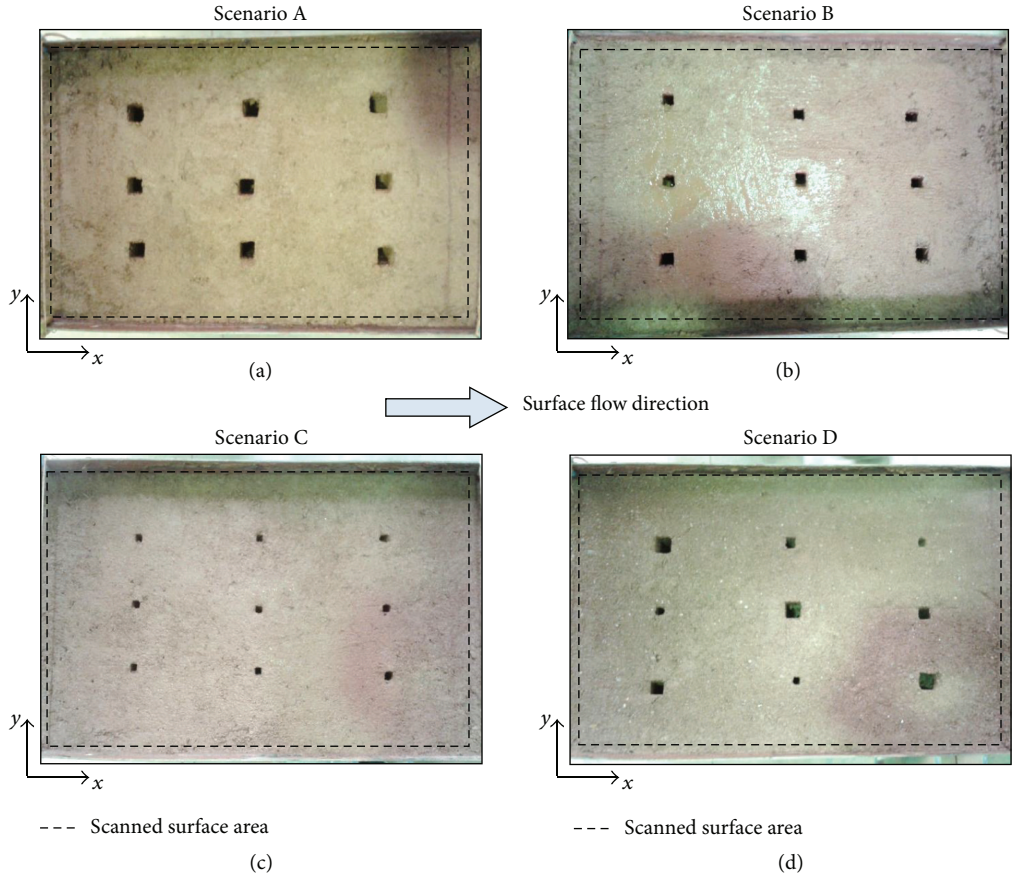

Figure 2: Top view (photographs) of the flume soil surface showing macropores of different sizes scattered in accordance with the four scenarios described in the text: (a) Scenario A; (b) Scenario B; (c) Scenario C; and (d) Scenario D. The x-axis represents the downslope distance along the length of the flume and the y-axis represents the distance across the width of the flume (the dashed line defines the measuring area with $0.50 \times 0.30\ m^2$). See Figure 1.

flume free drainage (Figure 1). Since macropores were filled with flowing hot water, they present higher temperatures in the thermal videos, recorded with the infrared video camera, which allowed the mapping of their spatial location and the estimation of their approximate area. Because the soil was close to the field capacity at the beginning of the experiments, the percentage of water infiltrated into the soil was very low compared to the percentage flowing into the macropores.

Soil surface thermal videos were recorded with the infrared camera throughout the experiments. However, thermograms of the surface of the overland flow layer did not provide any spatial variability of temperature. Therefore, for

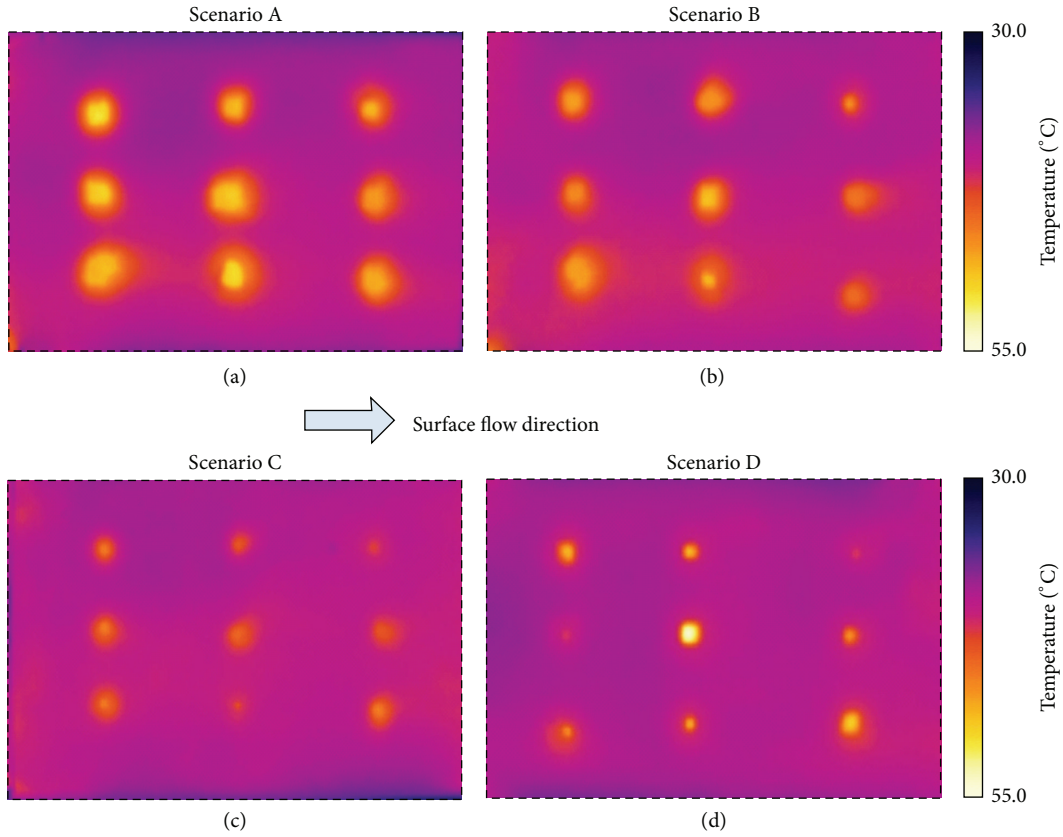

Figure 3: Thermograms of the soil surface for the four scenarios: (a) Scenario A; (b) Scenario B; (c) Scenario C; and (d) Scenario D. The dashed line defines the measuring area with $0.50 \times 0.30\ m^2$. See also Figure 2.

each scenario (Figure 2), a thermogram of the soil surface was selected, corresponding to an instant just after (approximately 30 s) the passage of the wave of hot water through the scanned area; thermogram is a graphic record of temperature variations, and it represents radiation in the infrared range of the electromagnetic spectrum, providing identification of pixels associated with different surface temperatures. Because, in general, macropores present higher temperatures, a threshold temperature (τ) can be selected, which allows identifying the pixels associated with the macropores (i.e., pixels with temperature values above a given threshold temperature), thus distinguishing them from the remaining pixels that cover the soil surface scanned area (i.e., pixels with temperature values below the temperature threshold). The percentage of pixels that have temperature above the threshold temperature was called threshold percentage of pixels (α).

The number of macropores detected with this technique, as well as their position and area, depends upon the selected threshold temperature (τ). Higher threshold temperatures will lead to a detection of a lower number of macropores with smaller cross-section area (and, correspondingly, lower temperatures identified by the thermal images). On the contrary, lower threshold temperatures will lead to a detection of a higher number of macropores with bigger cross-section area. The lower-limit temperature from which all macropores are detected was called critical threshold temperature (τ_c). Selected threshold temperatures below τ_c will only lead to an increase of the macropores' area, since the maximum number and position of macropores were already detected since the location of every pixel is known.

3. Results and Discussion

Thermograms for the four scenarios defined in Section 2.2 are presented in Figure 3. In the thermograms, it is possible to identify the location of the different macropores, perceptible by the presence of groups of pixels exhibiting a brighter colour. These thermal marks are the result of the higher temperatures produced by the accumulation of flowing hot water in the macropores. Despite the rectangular shape of the macropores, the thermal marks identified visually in the thermograms are of approximate circular shapes. Also, the thermal marks are, in general, larger than the actual area of the macropores. This temperature smearing around the macropores is caused by thermal diffusion, by the higher infiltration of hot water around the macropores, and by the relatively low resolution of the camera.

In general, larger macropores led to larger thermal marks, exhibiting higher temperatures at the centre caused by the accumulation of hot water. Thermograms of Scenarios A, B, and C, of Figures 3(a) to 3(c), clearly show thermal marks with different areas, which are in accordance with the different

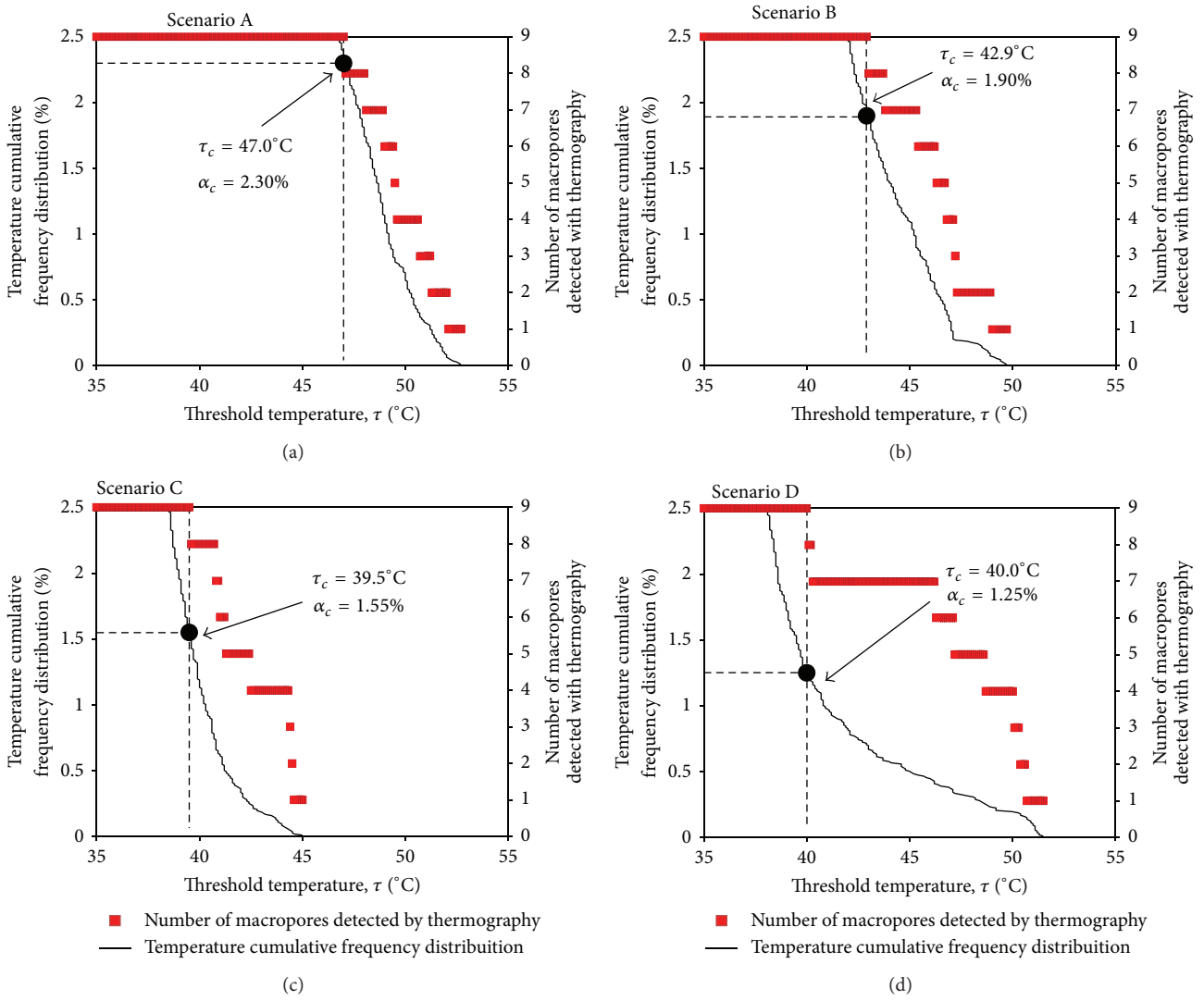

FIGURE 4: Relation between threshold temperature (τ) and the number of macropores detected with thermography, for the four scenarios: (a) Scenario A; (b) Scenario B; (c) Scenario C; and (d) Scenario D. Temperature cumulative frequency distribution curves are also plotted, up to 2.5%. Critical threshold temperature (τ_c) and corresponding critical threshold percentage of pixels (α_c) are identified.

areas of the macropores of each scenario. In the thermogram of Scenario D, in Figure 3(d), it is also possible to distinguish the macropores of different areas in the same thermogram. Macropores concentrate water which flows into these hollows and are, therefore, in contact with more hot water than the surrounding soil. This is why macropores have a different temperature than the soil surface.

The relation between the threshold temperature (τ) and the number of macropores detected using thermography is shown in Figure 4 (right axis). The same graph shows the temperature cumulative frequency distribution of the pixels' temperature (T), corresponding to the four thermograms in Figure 3, up to 2.5% (left axis). For each scenario, the critical threshold temperature (τ_c) and corresponding critical threshold percentage of pixels (α_c) are identified in the figure. We highlight that both τ_c and α_c depend on the area of the thermal marks in the thermograms; For example, Scenario A, with only large macropores, leads to the highest τ_c and α_c. The threshold τ_c depends also on the temperature of the hot water applied, the initial surface temperature, and the macropores present at the soil surface. Therefore, it is not possible to specify single τ_c or α_c values, representative of all scenarios. Nevertheless, such values are essential for processing the data and mapping existing soil surface macropores. Therefore, bearing in mind the results obtained in our experiment for all the tests (Figure 4), we have further adopted a threshold percentage of pixels (α) of 2.5% for all scenarios, since in our tests we found always $\alpha_c < 2.5\%$. For each scenario, the corresponding temperature frequency distribution curve (Figure 4) yields a specific value of the threshold temperature (τ) for $\alpha = 2.5\%$, which we have used to study the area and location of the macropores, using thermography.

Soil surface macropores were identified by applying to the temperature data the threshold temperature (τ) corresponding to $\alpha = 2.5\%$; the selected τ were subtracted to all temperature values from the thermograms; positive values,

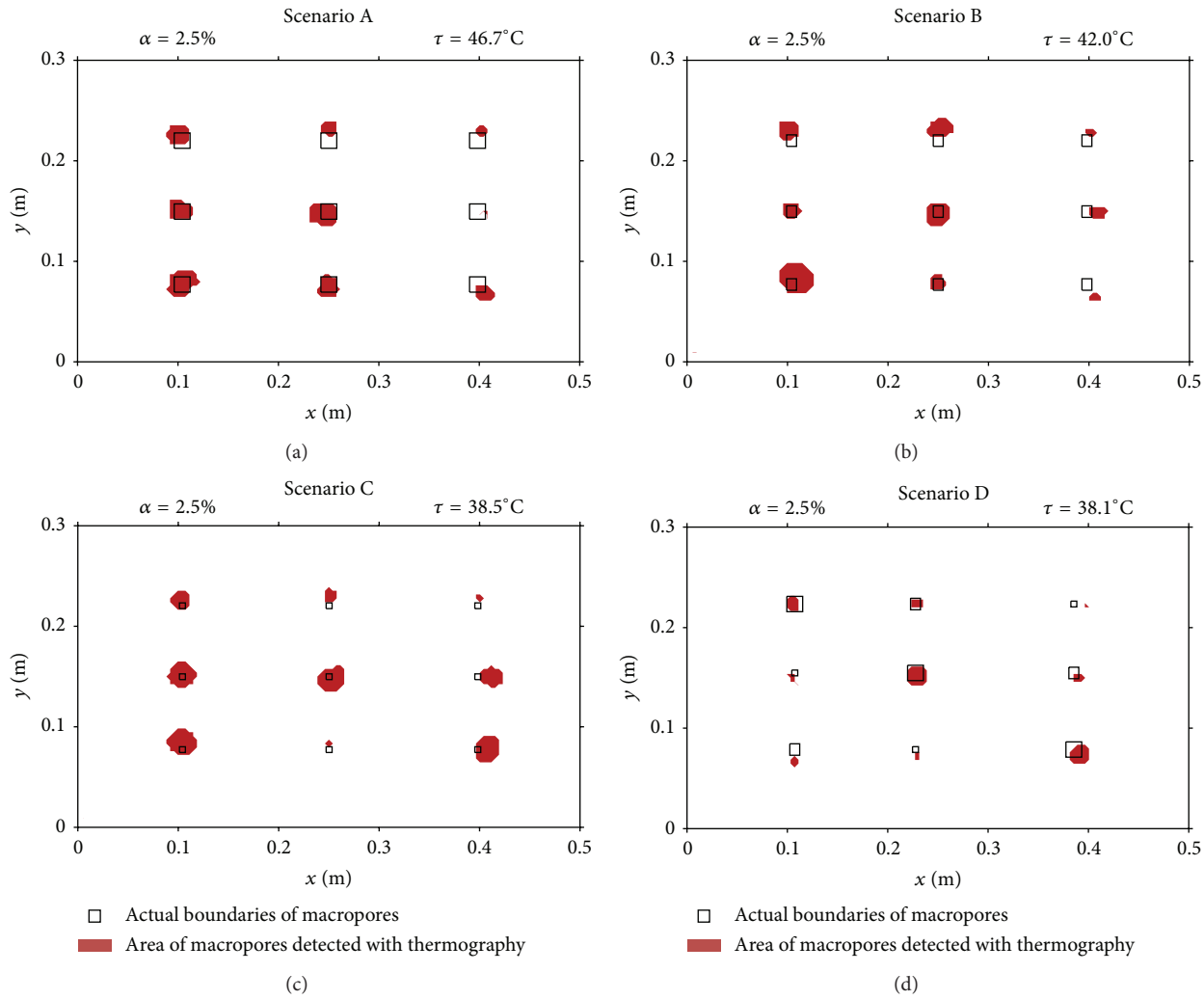

FIGURE 5: Comparison between the boundaries of the actual macropores and the area detected with thermography, for the four scenarios. Across the area scanned by the thermographic camera, the macropores are located using (x, y) coordinates. The x-axis represents the downslope distance along the length of the flume (0.5 m) and the y-axis represents the distance across the width of the flume (0.3 m). See also Figures 2 and 3.

which correspond to pixels with temperature values above τ, are associated with the macropores. The comparison between the boundaries of the actual macropores and the macropores' area detected with thermography is shown in Figure 5 (top view - 2D). The macropores' area detected with thermography was, in general, larger than their actual area. Therefore, the technique did not accurately estimate the actual area of the macropores, especially for the smaller ones. It is possible to observe in Figure 5(d) that the proposed technique can be used to distinguish macropores with different sizes (i.e., cross-section area), since larger macropores were detected with thermography as having also larger areas. This has already been suggested by visual observation of the thermal marks in the thermograms in Figure 3.

Figure 6 shows the comparison between the position of the actual geometric centre of the macropores and their geometric centre detected using thermography. In general, the proposed technique allowed the correct estimation of the macropores' location. Although the technique did not assess accurately the actual area of macropores, it clearly allowed mapping the macropores and identifying their spatial distribution and position across the studied soil surface area.

4. Conclusion

A novel technique to detect and characterize soil surface macropores based on infrared thermography was presented and discussed, based on exploratory laboratory soil flume experiments. For our laboratory conditions, the thermographic technique was successful in identifying the presence of macropores at the soil surface, providing a low cost and fast methodology to map soil surface macropores. Although uncertainties arise during the analysis about the macropores boundaries at the soil surface, which therefore restricts the quantification of their shape and size, the technique

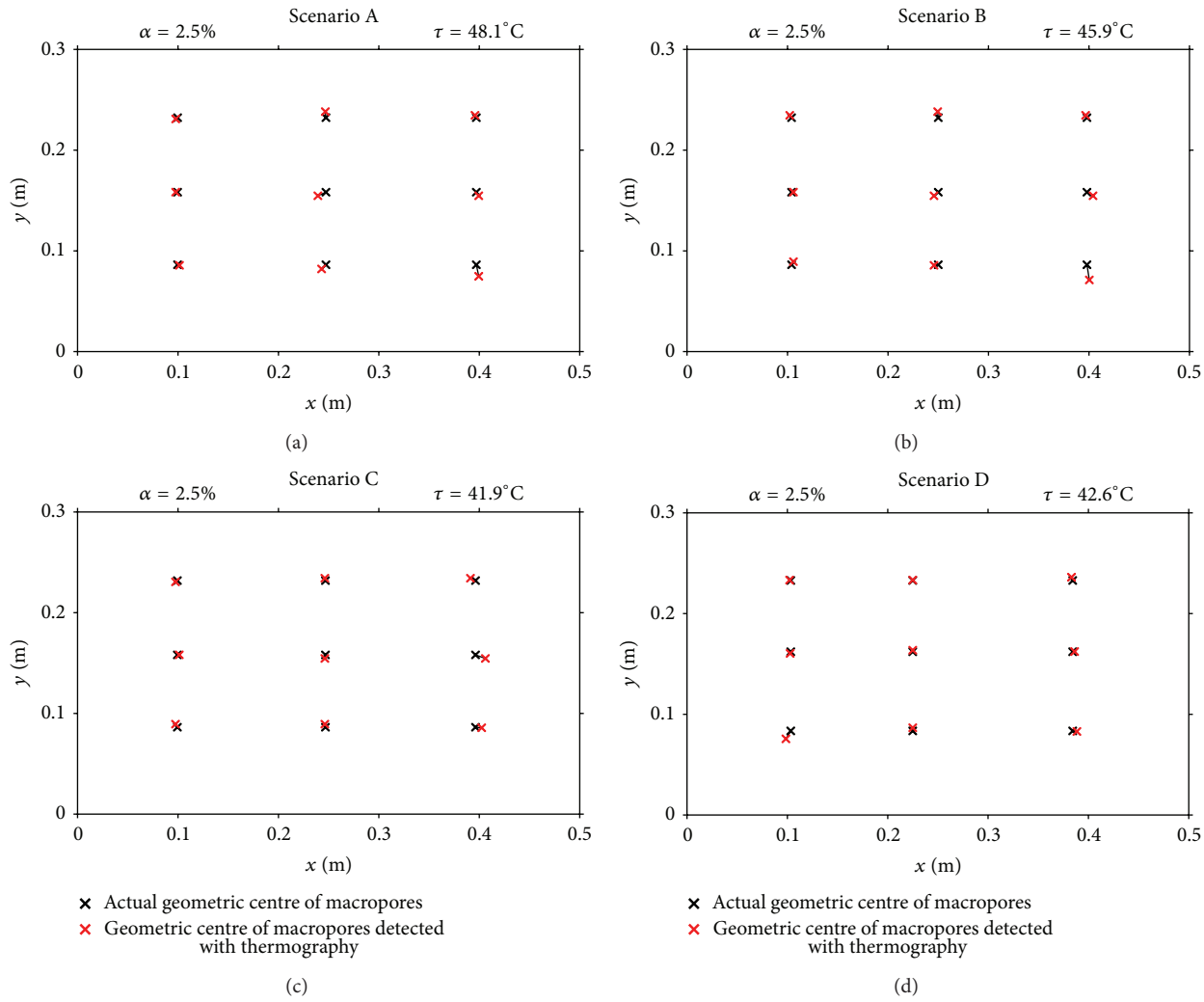

Figure 6: Comparison between the actual geometric centre of the macropores and their geometric centre detected using thermography, for the four scenarios. See Figure 5.

seems promising and able to identify macropores' spatial distribution with satisfactory accuracy.

Only extensive field work can, in fact, reveal the relevance of the technique in real (field) conditions. Future work has to be carried out to verify the applicability of the proposed technique under different field conditions, such as soil type, dimensions of scanned area, surface microrelief and roughness, presence of vegetation, stones, and other obstructions, which is beyond the scope of the presented analysis.

Conflict of Interests

The authors declare that there is no conflict of interests regarding the publication of this paper.

Acknowledgments

The laboratory experiments described in this study were conducted at the Laboratory of Hydraulics, Water Resources and Environment of the Department of Civil Engineering of the Faculty of Science and Technology, University of Coimbra, Portugal. This research was supported by the scholarship program for Special Visiting Researcher of the Brazilian scientific mobility program Science without Borders, funded by CNPq/MCT, of the first author. The second author acknowledges FCT, Portugal, for the doctoral Grant SFRH/BD/92816/2013 and the third author acknowledges CAPES, Brazil, for the doctoral Grant 11526/13-0.

References

[1] K. Beven and P. Germann, "Macropores and water flow in soils.," *Water Resources Research*, vol. 18, no. 5, pp. 1311–1325, 1982.

[2] K. J. Beven and P. F. Germann, "Macropores and water flow in soils revisited," *Water Resources Research*, vol. 49, no. 6, pp. 3071–3092, 2013.

[3] K. Beven, D. Zhang, and A. Mermoud, "On the value of local measurements for prediction of pesticide transport at the field scale," *Vadose Zone Journal*, vol. 5, no. 1, pp. 222–233, 2006.

[4] J. Perret, S. O. Prasher, A. Kantzas, and C. Langford, "Three-dimensional quantification of macropore networks in undisturbed soil cores," *Soil Science Society of America Journal*, vol. 63, no. 6, pp. 1530–1543, 1999.

[5] N. J. Jarvis, "A review of non-equilibrium water flow and solute transport in soil macropores: principles, controlling factors and consequences for water quality," *European Journal of Soil Science*, vol. 58, no. 3, pp. 523–546, 2007.

[6] L. Luo, H. Lin, and S. Li, "Quantification of 3-D soil macropore networks in different soil types and land uses using computed tomography," *Journal of Hydrology*, vol. 393, no. 1-2, pp. 53–64, 2010.

[7] M. Mejías, B. J. Ballesteros, C. Antón-Pacheco et al., "Methodological study of submarine groundwater discharge from a karstic aquifer in the Western Mediterranean Sea," *Journal of Hydrology*, vol. 464-465, pp. 27–40, 2012.

[8] S. Danielescu, K. T. B. MacQuarrie, and R. N. Faux, "The integration of thermal infrared imaging, discharge measurements and numerical simulation to quantify the relative contributions of freshwater inflows to small estuaries in Atlantic Canada," *Hydrological Processes*, vol. 23, no. 20, pp. 2847–2859, 2009.

[9] M. B. Cardenas, J. W. Harvey, A. I. Packman, and D. T. Scott, "Ground-based thermography of fluvial systems at low and high discharge reveals potential complex thermal heterogeneity driven by flow variation and bioroughness," *Hydrological Processes*, vol. 22, no. 7, pp. 980–986, 2008.

[10] L. Pfister, J. J. McDonnell, C. Hissler, and L. Hoffmann, "Ground-based thermal imagery as a simple, practical tool for mapping saturated area connectivity and dynamics," *Hydrological Processes*, vol. 24, no. 21, pp. 3123–3132, 2010.

[11] T. Schuetz, M. Weiler, J. Lange, and M. Stoelzle, "Two-dimensional assessment of solute transport in shallow waters with thermal imaging and heated water," *Advances in Water Resources*, vol. 43, pp. 67–75, 2012.

[12] J. L. M. P. de Lima and J. R. C. B. Abrantes, "Can infrared thermography be used to estimate soil surface microrelief and rill morphology?" *Catena*, vol. 113, pp. 314–322, 2014.

[13] J. L. M. P. de Lima and J. R. C. B. Abrantes, "Using a thermal tracer to estimate overland and rill flow velocities," *Earth Surface Processes and Landforms*, vol. 39, no. 10, pp. 1293–1300, 2014.

[14] J. L. M. P. de Lima, V. P. Singh, and M. I. P. de Lima, "The influence of storm movement on water erosion: storm direction and velocity effects," *Catena*, vol. 52, no. 1, pp. 39–56, 2003.

[15] J. L. M. P. de Lima, M. I. P. de Lima, and V. P. Singh, "The importance of the direction, speed, intensity and length of moving storms on water erosion," *Advances in GeoEcology*, vol. 36, pp. 163–176, 2005.

[16] J. L. M. P. de Lima, P. A. Dinis, C. S. Souza et al., "Patterns of grain-size temporal variation of sediment transported by overland flow associated with moving storms: interpreting soil flume experiments," *Natural Hazards and Earth System Science*, vol. 11, no. 9, pp. 2605–2615, 2011.

[17] J. L. M. P. de Lima, S. C. P. Carvalho, and M. I. P. de Lima, "Rainfall simulator experiments on the importance of when rainfall burst occurs during storm events on runoff and soil loss," *Zeitschrift für Geomorphologie*, vol. 57, no. 1, pp. 91–109, 2013.

[18] A. A. A. Montenegro, J. R. C. B. Abrantes, J. L. M. P. de Lima, V. P. Singh, and T. E. M. Santos, "Impact of mulching on soil and water dynamics under intermittent simulated rainfall," *Catena*, vol. 109, pp. 139–149, 2013.

[19] A. A. A. Montenegro, J. L. M. P. de Lima, J. R. C. B. O. Abrantes, and T. E. M. Santos, "Impact of mulching on soil and water conservation in semiarid catchment: simulated rainfall in the field and in the laboratory," *Die Bodenkultur*, vol. 64, no. 3-4, pp. 79–85, 2013.

[20] C. G. Soracco, L. A. Lozano, R. Balbuena, J. M. Ressia, and R. R. Filgueira, "Contribution of macroporosity to water flux of a soil under different tillage systems," *Revista Brasileira de Ciencia do Solo*, vol. 36, no. 4, pp. 1149–1156, 2012.

Hindawi Publishing Corporation
The Scientific World Journal
Volume 2014, Article ID 626732, 6 pages
http://dx.doi.org/10.1155/2014/626732

Research Article

Carbon Dioxide Emissions as Affected by Alternative Long-Term Irrigation and Tillage Management Practices in the Lower Mississippi River Valley

S. F. Smith and K. R. Brye

Department of Crop, Soil, and Environmental Sciences, University of Arkansas, Fayetteville, AR 72701, USA

Correspondence should be addressed to K. R. Brye; kbrye@uark.edu

Received 18 July 2014; Revised 25 August 2014; Accepted 28 August 2014; Published 13 October 2014

Academic Editor: Antonio Paz González

Ensuring the sustainability of cultivated soils is an ever-increasing priority for producers in the Lower Mississippi River Valley (LMRV). As groundwater sources become depleted and environmental regulations become more strict, producers will look to alternative management practices that will ensure the sustainability and cost-effectiveness of their production systems. This study was conducted to assess the long-term (>7 years) effects of irrigation (i.e., irrigated and dryland production) and tillage (conventional and no-tillage) on estimated carbon dioxide (CO_2) emissions from soil respiration during two soybean (*Glycine max* L.) growing seasons from a wheat- (*Triticum aestivum* L.-) soybean, double-cropped production system in the LMRV region of eastern Arkansas. Soil surface CO_2 fluxes were measured approximately every two weeks during two soybean growing seasons. Estimated season-long CO_2 emissions were unaffected by irrigation in 2011 ($P > 0.05$); however, during the unusually dry 2012 growing season, season-long CO_2 emissions were 87.6% greater ($P = 0.044$) under irrigated (21.9 Mg CO_2 ha^{-1}) than under dryland management (11.7 Mg CO_2 ha^{-1}). Contrary to what was expected, there was no interactive effect of irrigation and tillage on estimated season-long CO_2 emissions. Understanding how long-term agricultural management practices affect soil respiration can help improve policies for soil and environmental sustainability.

1. Introduction

Soybean (*Glycine max* L.) is a major crop grown in the Lower Mississippi River Valley (LMRV). Arkansas produces the greatest amount of soybean of the three states that generally constitute the LMRV (i.e., Arkansas, Louisiana, and Mississippi) and is ranked eighth nationally for total economic gain from soybean production [1]. The Alluvial Aquifer, which is the southeastern portion of the Mississippi embayment, is the major source of groundwater used for irrigation in this dense, agriculturally productive region. The Alluvial Aquifer is ranked third in the nation for total annual withdrawals [2], and most of the water is used for irrigated crop production, particularly rice (*Oryza sativa* L.) and soybean [3]. However, increased withdrawal rates from the Alluvial Aquifer, due in part to increasing areas of irrigated rice and soybean production and shifting rainfall patterns during the growing season, have led to substantial decreases in groundwater levels throughout eastern Arkansas and the neighboring states [4].

In order to assure adequate soybean yields, most producers irrigate during the growing season on an as-needed basis [5, 6]. Alternatively, when water is unavailable or the implementation of irrigation is too costly, producers will practice dryland production, in which the sole source of water to the crop is rainfall. Recently, 20% of soybean produced in eastern Arkansas was grown in a dryland cropping system [7]. However, irrigation can be absolutely essential to producing optimal yields to meet economic demands, especially in a wheat-soybean, double-crop system where soybean is planted in late spring. During warm weather, the lack of available water in a dryland cropping system can result in yield loss

[6]. Consequently, it is important for producers to choose management options that can help conserve soil water and protect the crop from water stress.

Conventional tillage (CT) is the most common soil management practice in the LMRV region of eastern Arkansas. Conventional tillage prior to a soybean growing season in the region generally consists of several passes with a disk to manipulate a soil depth of 5 to 10 cm, followed by smoothing with a soil conditioner to break up soil clods. However, CT breaks up the soil's natural structure and leaves the soil surface nearly bare and vulnerable to wind and water erosion at times [8]. Following CT, weakened soil structural stability near the surface can increase the risk of the formation of a surface crust or seal, which can further reduce water infiltration and the soil's water-holding capacity [9]. It has been documented that the long history of cultivated agriculture in the LMRV region of eastern Arkansas has severely impacted infiltration-runoff partitioning [10]. The impacts have been so drastic that the recharge area for the Alluvial Aquifer has been condensed and shifted to the point where annual recharge of the Alluvial Aquifer is only a small fraction of the annual withdrawals for irrigation [10].

As an alternative to CT, producers can practice no-tillage (NT) in order to maximize water conservation and improve many soil-quality-related characteristics [9, 11]. When NT is used, maintaining surface residue can improve soil water retention by reducing runoff and by acting as a protective and evaporative barrier for the soil surface. As water becomes increasingly limited, improving soil-quality-related characteristics and using management practices that promote water conservation will likely become increasingly necessary to ensure sustained yields.

A good indicator of the soil's ability to support plant life is soil respiration, which is the combined production of carbon dioxide (CO_2) from soil organisms and plant roots. Soil respiration is closely correlated with soil organic matter content, root respiration, microbial activity, and decomposition rates [12]. Soil respiration can be influenced by many environmental conditions, such as moisture and temperature [13]. Generally, optimal conditions for soil respiration occur when the soil is warm and the soil water content is near field capacity.

Environmental factors affecting soil respiration can be manipulated by residue- and water-management practices in agroecosystems. In general, management practices that promote plant biomass formation (e.g., adequate soil fertility), increase the bioavailability of carbon (C) sources (e.g., tillage), and maintain optimal soil moisture for soil microbial activity (e.g., irrigation) will increase soil respiration rates [13]. Inferences about nutrient cycling can also be made using soil respiration rates. Excessive respiration can indicate that a soil is losing nutrients or is in a state of flux following a disturbance, such as tillage. In contrast, decreased soil organic matter, poor soil structure, and limited nutrient availability may inhibit soil respiration and indicate poor soil quality. Root respiration can account for up to 80% of total soil CO_2 emissions [12]; therefore, plant biomass production and productivity that has been limited from water-stressed conditions can result in greatly reduced soil respiration rates and seasonal CO_2 emissions.

Since CO_2 is a greenhouse gas of concern and atmospheric concentrations have increased dramatically in the past half century or so [14], there is a growing worldwide interest to identify ways to reduce CO_2 emissions, sequester C, and remove CO_2 from the atmosphere. Optimizing agroecosystem management practices for soil sustainability can also help store C from the atmosphere in a semipermanent state [15]. Furthermore, there are few studies that have examined the impacts of long-term (>5 years) agricultural management practices on soil respiration, especially in the midsouthern United States. Therefore, the objective of this study was to evaluate the effects of irrigation (irrigated and dryland), tillage (conventional tillage (CT) and no-tillage (NT)), and residue level (high and low) on season-long CO_2 emissions from soil respiration after more than seven years of consistent management in a wheat-soybean, double-crop production system in the LMRV region of eastern Arkansas. It was hypothesized that irrigation would increase CO_2 emissions by reducing the occurrence of water-stressed conditions, especially during warm and dry periods. It was also hypothesized that irrigation would mask any differential effects of tillage on CO_2 emissions and that differential effects of tillage on CO_2 emissions would be greater in dryland production.

2. Materials and Methods

2.1. Site Description. This long-term study was initiated in fall 2001 at the University of Arkansas' Lon Mann Cotton Research Station (N 34°, 44′, 2.26″ and W 90°, 45′, 51.56″), which is located in east-central Arkansas, near Marianna in Lee County [16]. The study was conducted on a Calloway silt loam (fine-silty, mixed, active, thermic Aquic Fraglossudalf) [17].

The 30-year mean monthly air temperatures for the soybean growing season for the region are 25.4, 27.3, 26.3, 22.7, and 16.8°C for June, July, August, September, and October, respectively [18]. The 30-year monthly rainfall amounts for the soybean growing season for the region are 11.1, 9.7, 6.9, 8.0, and 9.6 cm for June, July, August, September, and October, respectively [18]. The 30-year mean annual air temperature in the region is 15.9°C and the mean annual precipitation is 133.7 cm [18].

2.2. Treatments and Experimental Design. A randomized complete block design, consisting of burning, tillage, and fertility treatments, with three replications was established in 2001 [16]. Two replications of the burning treatment were arranged as a randomized complete block (RCB). Three replications of tillage were also arranged as a RCB but were stripped across the burning block. The fertility treatments were split into each burn-tillage combination. The whole field was split in half in 2005 in order to incorporate the irrigation treatment. Due to practical limitations, the irrigation treatment was necessarily placed in the experimental design with a similar blocking structure as the burning treatment.

This resulted in three replications for each of the 16 possible treatment combinations. The irrigation treatment consisted of either irrigating the field on an as-needed basis (irrigated) or no irrigation applied during the soybean growing season (dryland). The tillage treatment was a strip within the irrigation treatment and consisted of CT or direct sowing of soybean after harvest with no residue incorporation (i.e., NT). A nitrogen (N) fertility treatment, used to produce differing amounts of wheat residue into which the subsequent soybean crop would be planted, was established as a split plot within the tillage treatment. The study site consisted of 48 plots, each 3 m wide and 6 m long [16].

2.3. Field Management. Following the application of the tillage treatment each year, a glyphosate-resistant soybean variety of maturity group 5.3 to 5.4 was planted with a 19-cm row spacing throughout the study site in early-to-mid-June. Soybean grown within the irrigated treatment was irrigated on an as-needed basis [6], while the dryland soybean was only rain fed. Soybean harvest generally occurred between late October and the middle of November each year. Following soybean harvest, wheat was drill-seeded with 19-cm row spacing [19]. Since 2005, wheat grown within the high-fertility treatment was fertilized with a split application of urea (i.e., 56 kg N ha^{-1} applied in early March and 56 kg N ha^{-1} in late March), while a low-fertility treatment received no N applications. In early-to-mid-June each year, wheat was harvested and the remaining stubble was mowed with a rotary mower to create a uniform layer of residue. After mowing and prior to tillage, a residue burning treatment was imposed each year [20]. Additional details regarding the history of the study site and past management are summarized in Brye et al. [19], Cordell et al. [16], and Smith et al. [20].

2.4. Soil Respiration Measurements. During the 2011 and 2012 soybean growing seasons (i.e., June to October), soil respiration was measured approximately every two weeks in the morning between 0600 and 1100 hours. There were a total of 124 and 151 days in the 2011 and 2012 soybean growing seasons, respectively. Respiration measurements were conducted nine times in 2011 and 11 times in 2012. At least one day prior to measurements, 10-cm diameter PVC collars, with a beveled edge on the bottom, were placed in each plot to facilitate soil respiration measurements, similar to the procedures used in a previous study [19]. A portable infrared gas analyzer (LI-6400, LI-COR, Inc., Lincoln, NE) with a soil chamber attachment (LI-6400-09, LI-COR) was used as per manufacturer's recommendations and as used previously [19].

2.5. Soybean Yields. In late October each year, soybean from the middle 1.5 m of each plot was harvested with a plot combine. The harvest area was 1.5-m wide and 6-m long. Grain was air-dried for approximately three weeks before weighing. A subsample from each plot was oven dried for 48 hr at 70°C and weighed to adjust reported yields to a 13% moisture content.

2.6. Data Analyses. Growing-season-long CO_2 emissions were estimated using linear interpolation between measurement dates and the trapezoid method was used for area-under-the-curve calculations [21, 22]. Since irrigation was superimposed into the experimental design with a similar blocking structure as the burning treatment, the two treatments were confounded. Therefore, irrigation and burning treatments could not be analyzed together. For this reason, two separate three-factor analyses of variance (ANOVAs) were conducted based on a strip-split-plot design, each excluding one of the confounding factors. The PROC GLM procedure in SAS (version 9.2 SAS Institute, Inc., Cary, NC) was used to evaluate the effects of burning or irrigation, tillage, fertility, year, and their interactions on season-long CO_2 emissions. This study was focused on the effects of irrigation and any interactions containing irrigation on soil respiration. For the results concerning the effects of burning and interactions containing burning, see Smith et al. [20]. Where appropriate, means were separated by least significant difference (LSD) at the 0.05 level.

3. Results and Discussion

3.1. Growing-Season Weather Conditions. The growing-season weather conditions the soybean crop experienced differed somewhat between 2011 and 2012 and differed somewhat from the 30-year mean conditions. The 30-year mean monthly air temperature in eastern Arkansas near Marianna peaks at 27.3°C in July decreases thereafter to 16.8°C in October and averages 23.7°C throughout the typical 5-month soybean growing season [18]. The 30-year monthly rainfall in eastern Arkansas ranges from 6.9 cm in August to 11.1 cm in June and totals 45.3 cm throughout the 5-month soybean growing season [18]. Actual mean air temperatures measured on-site in 2011 (24.3°C) and 2012 (24.2°C) throughout the 5-month growing season were only slightly greater than the 30-year mean air temperature for the same 5-month period. However, for both 2011 (38.5 cm) and 2012 (35.4 cm), rainfall amounts measured on-site were at least 15% lower than the 30-year mean rainfall total (45.3 cm) [18] over the 5-month soybean growing season. Furthermore, eastern Arkansas experienced a drought in 2012 relative to previous years. Though total rainfall during the 5-month soybean growing season was only 8% lower in 2012 than in 2011, total rainfall in June, July, and August, the critical early period of the soybean crop, in 2012 (11.6 cm) was less than 43% of that in 2011 (27.2 cm) and less than 42% of the 30-year mean total rainfall (27.7 cm) [18]. Based on differences in growing-season rainfall, both seasonal CO_2 emissions and soybean yields were expected to differ between 2011 and 2012.

3.2. Seasonal CO_2 Emissions. Estimated season-long CO_2 emissions from soil respiration, measured 20 times throughout the 2011 and 2012 soybean growing seasons in eastern Arkansas, differed between irrigation treatments across years ($P = 0.044$) and differed between tillage treatments ($P = 0.020$; Table 1). Season-long CO_2 emissions averaged 22.3 Mg CO_2 ha^{-1} in 2011 and were unaffected by

Table 1: Analysis of variance summary of the effects of irrigation, tillage, residue level (residue), year, and their interactions on estimated season-long CO_2 emissions at the University of Arkansas' Lon Mann Cotton Research Station near Marianna, AR, on a silt-loam soil. Interactions and main effects that are considered significant are indicated by bolded text ($P < 0.05$). This analysis ignores the burning treatment in the design.

Treatment effect	Season-long CO_2 emissions
Irrigation	0.243
Tillage	**0.020**
Irrigation ∗ tillage	0.383
Residue	0.512
Irrigation ∗ residue	0.097
Tillage ∗ residue	0.699
Irrigation ∗ tillage ∗ residue	0.759
Year	**<0.001**
Irrigation ∗ year	**0.044**
Tillage ∗ year	0.366
Residue ∗ year	0.689
Irrigation ∗ tillage ∗ year	0.277
Irrigation ∗ residue ∗ year	0.926
Tillage ∗ residue ∗ year	0.455
Irrigation ∗ tillage ∗ residue ∗ year	0.838

the irrigation treatments (irrigated (22.4 Mg CO_2 ha^{-1}) and dryland (22.2 Mg CO_2 ha^{-1}). However, estimated season-long CO_2 emissions were 87.6% greater under irrigated (21.9 Mg CO_2 ha^{-1}) compared to under dryland management (11.7 Mg CO_2 ha^{-1}) in the drought year of 2012.

Total season-long emissions were closely tied with soybean yields. During the more favorable 2011 growing season, soybean yields were 3.2 and 1.7 Mg ha^{-1} for the irrigated and dryland treatments, respectively. However, only 0.15 Mg ha^{-1} of soybean was harvested from the dryland treatment during the drier 2012 year, which was 6% of the soybean yield from the irrigated treatment (2.5 Mg ha^{-1}).

Although season-long CO_2 emissions may be limited by water-stressed conditions, a substantial pulse of CO_2 from the soil can follow a precipitation or irrigation event when soil microbial activity is stimulated after a long dry period [23]. Peak respiratory pulses on the order of 60 to 80 times the baseline respiration rate were reported following rainfall events in an annual grassland and a nearby oak-(*Quercus douglasii*-) grass savanna on a rocky silt-loam soil in California [23]. Sainju et al. [24] concluded that antecedent soil water content and water retention were the two greatest determinants for soil CO_2 pulse intensities and duration following rainfall or irrigation in a North Dakota barley-(*Hordeum vulgare* L.-) pea (*Pisum sativum* L.) rotation. Although many others have described similar soil CO_2 pulses after irrigation and rainfall events [25–27], the intensities and durations have been extremely variable, even within the same study area [28].

Irrigation can have a direct effect on soil respiration by regulating available soil water for microbial and plant activity. Optimal soil moisture for plant and microbial function is generally around field moisture capacity, where micropores (i.e., <0.08 mm diameter) in the soil are still mostly filled with water and macropores (i.e., >0.08 mm diameter) are mostly air-filled, which facilitates oxygen diffusion [12]. Below field moisture capacity, water and nutrients can become limiting for plants and microorganisms. When biological consumption of soil organic matter is limited, soil C can build up in the soil. Although plant productivity may be limited in dry years, dryland agriculture can have both economic and environmental benefits [29].

Mean annual declines in the Alluvial Aquifer's water levels between 1982 and 2006 have been reported to be around 16.8 cm yr^{-1} for Lee County, Arkansas [4]. By using the recharge rate and rate of withdrawal in 1997, Scott et al. [30] estimated that the Alluvial Aquifer's water available for irrigation would be depleted by 2050. Since water is becoming more limited and since some agricultural production is on land that is difficult to irrigate, some producers choose to rely only on rainfall to water their soybean crop. During favorable years, dryland management can save producers the cost of installation of the irrigation system and water-pumping costs throughout the season. Although this is a bit of a gamble with natural precipitation being hard to predict, dryland soybean production can work in the producer's favor. Parsch et al. [31] reported that nonirrigated soybean grown in eastern Arkansas generally provided a larger net economic return for the producer than irrigated soybean. Verkler et al. [29] also demonstrated that, during a favorable rainfall year, dryland soybean production was equally profitable as irrigated soybean production in eastern Arkansas. However, not surprisingly, during growing seasons of less-than-optimal rainfall, dryland production was much less profitable than irrigated soybean production. Results of this study indicate that dryland soybean production may be more environmentally sustainable due to the lower water consumption and generally lower seasonal CO_2 emissions.

Beyond the potential economic value that can be associated with dryland cropping, there are numerous environmental benefits. In addition to preserving groundwater, dryland cropping can favor the accumulation of soil organic matter by reducing erosion of topsoil and/or by decreasing soil respiration. Depending on the irrigation system implemented, soil erosion can occur due to the sudden inundation of fragile soil aggregates, which can disintegrate upon submersion, raindrop impact from sprinkler systems, and/or surface erosion caused by runoff in surface irrigation systems [32]. Churchman and Tate [33] reported a decrease in total water-stable aggregates and soil C stocks after >25 years of annual irrigation of a seasonally dry, silt-loam soil in New Zealand, which was likely due to increased microbial decomposition compared to dryland production. The sudden inundation of the soil by water from furrow irrigation, the most common soybean irrigation technique in eastern Arkansas, can also cause slaking to occur and unstable aggregates to disintegrate. The most unstable, larger aggregates are more affected by slaking due to irrigation than the aggregates that are smaller in diameter [34]. In addition, near-surface soil aggregates, many of which protect soil organic matter and C, are greatly impacted by mechanical disturbances, such as tillage [34].

Although many others have noted a short-term increase in soil respiration following tillage [21, 34–37], we expected these fluctuations to remain short in duration and likely not persist throughout an entire growing season. Wander and Bidart [11] reported greater CO_2 fluxes following tillage; however, the increased rates of soil surface CO_2 evolution only lasted approximately 24 hours. No-tillage, which has been shown to improve soil water conservation [38], increase soil organic matter and C contents [11], and improve soil structure [39], was expected to produce greater season-long CO_2 than CT, especially within the dryland treatment. However, in contrast to that hypothesized, CT produced greater season-long CO_2 than NT, regardless of irrigation scheme. When averaged over all other field treatments and years, estimated season-long CO_2 emissions were 21.0 Mg CO_2 ha^{-1} yr^{-1} under CT, compared to only 18.1 Mg CO_2 ha^{-1} yr^{-1} under NT ($P = 0.020$; Table 1). Although production of CO_2 may indicate a healthy soil with high microbial activity, some soils that have historically low concentrations of organic matter to sustain microbial activity may benefit from lower decomposition rates. Since the study area is in a region with generally low soil organic matter concentrations (~2.1% by loss-on-ignition; [40]) due to a long history of highly productive, cultivated agriculture, producers may benefit from using NT management practices that reduce the amount of C emitted to the atmosphere via soil respiration in both irrigated and dryland cropping systems.

4. Conclusions

The impact of irrigation on seasonal CO_2 emissions differed between years. As was expected, irrigation only affected estimated season-long CO_2 emissions during water-stressed conditions by supplementing adequate soil moisture for soybean growth and soil microbial respiration. Contrary to that hypothesized, the tillage effect on total CO_2 emissions was not dependent on the irrigation scheme used. No-tillage management reduced seasonal CO_2 emissions during both soybean growing seasons.

Conflict of Interests

The authors declare that there is no conflict of interests regarding the publication of this paper.

Acknowledgments

This research was partially funded by the Arkansas Soybean Promotion Board. Field and laboratory assistance from Michelle Helton, Wanda Holifield, Jill Motschenbacher, Richard McMullen, Taylor Adams, Matt Gregory, Bill Apple, and Claude Kennedy are gratefully acknowledged.

References

[1] USDA-ERS, "State fact sheets: arkansas," United States Department of Agriculture—Economic Research Service, 2013, http://www.ers.usda.gov/data-products/state-fact-sheets.aspx.

[2] M. A. Maupin and N. L. Barber, *Estimated Withdrawals from Principal Aquifers in the United States, 2000*, US Department of the Interior, US Geological Survey, 2005.

[3] B. R. Clark, R. M. Hart, and J. J. Gurdak, *Groundwater Availability of the Mississippi Embayment*, US Geological Survey, 2011.

[4] T. P. Schrader, *Water Levels and Selected Water-quality Conditions in the Mississippi River Valley Alluvial Aquifer in Eastern Arkansas, 2006*, US Geological Survey, 2008.

[5] S. Bajaj, P. Chen, D. E. Longer et al., "Irrigation and planting date effects on seed yield and agronomic traits of early-maturing soybean," *Journal of Crop Improvement*, vol. 22, no. 1, pp. 47–65, 2008.

[6] UACES, *Arkansas Soybean Handbook*, University of Arkansas Cooperative Extension Service, Little Rock, Ark, USA, 2000.

[7] USDA-NASS, "Statistics by state: arkansas," United States Department of Agriculture—National Agricultural Statistics Service, 2012, http://www.nass.usda.gov/Statistics_by_State/Arkansas/index.asp.

[8] J. Six, E. T. Elliott, and K. Paustian, "Soil macroaggregate turnover and microaggregate formation: a mechanism for C sequestration under no-tillage agriculture," *Soil Biology and Biochemistry*, vol. 32, no. 14, pp. 2099–2103, 2000.

[9] J. L. Pikul Jnr and J. F. Zuzel, "Soil crusting and water infiltration affected by long-term tillage and residue management," *Soil Science Society of America Journal*, vol. 58, no. 5, pp. 1524–1530, 1994.

[10] T. W. Harper, K. R. Brye, T. C. Daniel, N. A. Slaton, and B. E. Haggard, "Land use effects on runoff and water quality on an Eastern Arkansas soil under simulated rainfall," *Journal of Sustainable Agriculture*, vol. 32, no. 2, pp. 231–253, 2008.

[11] M. M. Wander and M. G. Bidart, "Tillage practice influences on the physical protection, bioavailability and composition of particulate organic matter," *Biology and Fertility of Soils*, vol. 32, no. 5, pp. 360–367, 2000.

[12] Y. Luo and X. Zhou, *Soil Respiration and the Environment*, Academic Press, Elsevier, San Diego, Calif, USA, 2010.

[13] A. J. Franzluebbers, F. M. Hons, and D. A. Zuberer, "Tillage and crop effects on seasonal soil carbon and nitrogen dynamics," *Soil Science Society of America Journal*, vol. 59, no. 6, pp. 1618–1624, 1995.

[14] N. Jones, "Troubling milestone for CO_2," *Nature Geoscience*, vol. 6, no. 8, article 589, 2013.

[15] M. U. F. Kirschbaum, "Will changes in soil organic carbon act as a positive or negative feedback on global warming?" *Biogeochemistry*, vol. 48, no. 1, pp. 21–51, 2000.

[16] M. L. Cordell, K. R. Brye, D. E. Longer, and E. E. Gbur, "Residue management practice effects on soybean establishment and growth in a young wheat-soybean double-cropping system," *Journal of Sustainable Agriculture*, vol. 29, no. 2, pp. 97–120, 2007.

[17] NRCS, "Web Soil Survey. Natural Resources Conservation Service," 2013, http://websoilsurvey.sc.egov.usda.gov/App/HomePage.htm.

[18] NOAA, *Climatography of the United States No. 81, Monthly Station Normals of Temperature, Precipitation, and Heating and Cooling Degrees Days 1971–2000: Arkansas*, National Oceanic and Atmospheric Admi Nistration, Ashville, NC, USA, 2002.

[19] K. R. Brye, D. E. Longer, and E. E. Gbur, "Impact of tillage and residue burning on carbon dioxide flux in a wheat-soybean production system," *Soil Science Society of America Journal*, vol. 70, no. 4, pp. 1145–1154, 2006.

[20] F. Smith, K. R. Brye, E. E. Gbur, P. Chen, and K. Korth, "Long-term residue management effects on soil respiration in a wheat-soybean double-crop system," *Soil Science*, vol. 179, pp. 118–129, 2014.

[21] D. C. Reicosky, "Tillage-induced CO_2 emission from soil," *Nutrient Cycling in Agroecosystems*, vol. 49, no. 1–3, pp. 273–285, 1997.

[22] F. J. Morell, C. Cantero-Martínez, J. Lampurlanés, D. Plaza-Bonilla, and J. Álvaro-Fuentes, "Soil carbon dioxide flux and organic carbon content: Effects of tillage and nitrogen fertilization," *Soil Science Society of America Journal*, vol. 75, no. 5, pp. 1874–1884, 2011.

[23] L. Xu, D. D. Baldocchi, and J. Tang, "How soil moisture, rain pulses, and growth alter the response of ecosystem respiration to temperature," *Global Biogeochemical Cycles*, vol. 18, no. 4, pp. 1–10, 2004.

[24] U. M. Sainju, J. D. Jabro, and W. B. Stevens, "Soil carbon dioxide emission and carbon content as affected by irrigation, tillage, cropping system, and nitrogen fertilization," *Journal of Environmental Quality*, vol. 37, no. 1, pp. 98–106, 2008.

[25] S. B. Verma, A. Dobermann, K. G. Cassman et al., "Annual carbon dioxide exchange in irrigated and rainfed maize-based agroecosystems," *Agricultural and Forest Meteorology*, vol. 131, no. 1-2, pp. 77–96, 2005.

[26] J. D. Jabro, U. Sainju, W. B. Stevens, and R. G. Evans, "Carbon dioxide flux as affected by tillage and irrigation in soil converted from perennial forages to annual crops," *Journal of Environmental Management*, vol. 88, no. 4, pp. 1478–1484, 2008.

[27] J. Bauder and R. Schneider, "Nitrate-nitrogen leaching following urea fertilization and irrigation," *Soil Science Society of America Journal*, vol. 43, pp. 348–352, 1979.

[28] P. Rochette, R. L. Desjardins, and E. Pattey, "Spatial and temporal variability of soil respiration in agricultural fields," *Canadian Journal of Soil Science*, vol. 71, no. 2, pp. 189–196, 1991.

[29] T. L. Verkler, K. R. Brye, J. H. Popp, E. E. Gbur, P. Chen, and N. Amuri, "Soil properties, soybean response, and economic return as affected by residue and water management practices," *Journal of Sustainable Agriculture*, vol. 33, no. 7, pp. 716–744, 2009.

[30] H. D. Scott, J. A. Ferguson, L. Hanson, T. Fugitt, and E. Smith, *Agricultural Water Management in the Mississippi Delta Region of Arkansas*, Arkansas Agricultural Experiment Station, Division of Agriculture, University o f Arkansas, Fayetteville, Ark, USA, 1998.

[31] L. D. Parsch, T. C. Keisling, P. A. Sauer, L. R. Oliver, and N. S. Crabtree, "Economic analysis of conservation and conventional tillage cropping systems on clayey soil in eastern Arkansas," *Agronomy Journal*, vol. 93, no. 6, pp. 1296–1304, 2001.

[32] G. Lehrsch, D. Bjorneberg, and R. Sojka, "Erosion: irrigation-induced," *Encyclopedia of Soils in the Environment*, vol. 1, pp. 456–463, 2005.

[33] G. Churchman and K. Tate, "Effect of slaughterhouse effluent and water irrigation upon aggregation in seasonally dry New Zealand soil under pasture," *Soil and Tillage Research*, vol. 24, pp. 505–516, 1986.

[34] J. Six, K. Paustian, E. T. Elliott, and C. Combrink, "Soil structure and organic matter I. Distribution of aggregate-size classes and aggregate-associated carbon," *Soil Science Society of America Journal*, vol. 64, no. 2, pp. 681–689, 2000.

[35] R. W. Gesch, D. C. Reicosky, R. A. Gilbert, and D. R. Morris, "Influence of tillage and plant residue management on respiration of a Florida Everglades Histosol," *Soil & Tillage Research*, vol. 92, no. 1-2, pp. 156–166, 2007.

[36] W. Dong, C. Hu, S. Chen, and Y. Zhang, "Tillage and residue management effects on soil carbon and CO_2 emission in a wheat-corn double-cropping system," *Nutrient Cycling in Agroecosystems*, vol. 83, no. 1, pp. 27–37, 2009.

[37] B. H. Ellert and H. H. Janzen, "Short-term influence of tillage on CO_2 fluxes from a semi-arid soil on the Canadian Prairies," *Soil and Tillage Research*, vol. 50, no. 1, pp. 21–32, 1999.

[38] S. M. Dabney, "Cover crop impacts on watershed hydrology," *Journal of Soil and Water Conservation*, vol. 53, no. 3, pp. 207–213, 1998.

[39] M. Kasper, G. D. Buchan, A. Mentler, and W. E. H. Blum, "Influence of soil tillage systems on aggregate stability and the distribution of C and N in different aggregate fractions," *Soil and Tillage Research*, vol. 105, no. 2, pp. 192–199, 2009.

[40] R. DeLong, N. Slaton, K. Brye, N. Wolf, and M. Mosaffari, "Relationships between organic carbon and other chemical properties in Arkansas soils," in *Proceedings of the American Society of Agronomy Annual Meeting*, Denver, Colo, USA, 2003.

Hindawi Publishing Corporation
The Scientific World Journal
Volume 2014, Article ID 617408, 9 pages
http://dx.doi.org/10.1155/2014/617408

Research Article

Image Analysis to Estimate Mulch Residue in Soil

Carmen Moreno,[1] Ignacio Mancebo,[1] Antonio Saa,[2,3] and Marta M. Moreno[1]

[1] *Universidad de Castilla-La Mancha/Escuela de Ingenieros Agrónomos, Ronda de Calatrava 7, 13071 Ciudad Real, Spain*
[2] *Departamento de Edafología y Climatología, ETSI Agrónomos, Universidad Politécnica de Madrid, Ciudad Universitaria sn, 28040 Madrid, Spain*
[3] *CEIGRAM, Universidad Politécnica de Madrid, Ciudad Universitaria sn, 28040 Madrid, Spain*

Correspondence should be addressed to Carmen Moreno; carmen.moreno@uclm.es

Received 18 June 2014; Accepted 31 July 2014; Published 17 September 2014

Academic Editor: Ana Maria Tarquis

Mulching is used to improve the condition of agricultural soils by covering the soil with different materials, mainly black polyethylene (PE). However, problems derived from its use are how to remove it from the field and, in the case of it remaining in the soil, the possible effects on it. One possible solution is to use biodegradable plastic (BD) or paper (PP), as mulch, which could present an alternative, reducing nonrecyclable waste and decreasing the environmental pollution associated with it. Determination of mulch residues in the ground is one of the basic requirements to estimate the potential of each material to degrade. This study has the goal of evaluating the residue of several mulch materials over a crop campaign in Central Spain through image analysis. Color images were acquired under similar lighting conditions at the experimental field. Different thresholding methods were applied to binarize the histogram values of the image saturation plane in order to show the best contrast between soil and mulch. Then the percentage of white pixels (i.e., soil area) was used to calculate the mulch deterioration. A comparison of thresholding methods and the different mulch materials based on percentage of bare soil area obtained is shown.

1. Introduction

Mulching is a method of improving the condition of agricultural soils by covering the soil surface with different kinds of materials. For this purpose, black polyethylene (PE), a petroleum-based plastic, is the most used due to its low price and the positive effects on crop yields [1, 2]. However, a major problem derived from its use is how to remove it from the field and how it can be completely done [2], because the useful life of plastic materials exceeds the duration of crop cycles, and they are usually left in the soil afterward. Although the part exposed to the light undergoes photodegradation and favors the plastic decomposition, the rest of the material is broken into pieces by ploughing labors, some pieces being buried or remaining on the soil surface. The buried pieces are more difficult to decompose since they are less affected by light and heat, creating serious soil problems whose environmental repercussion has not been fully evaluated [3]. Feuilloley et al. [4] found that it is difficult to foresee the accumulative effects of PE fragments and the impact of the repeated use of these PE films on the environment. In this context, the microfragments derived from the buried pieces are electrically charged and their impact, if accumulated, on the argilo-humic complex is unknown. With the aim of accelerating the PE fragmentation in the soil, special prooxidant additives are used. These substances contain different complexes of transition metals, particularly Fe, Co, and Mn [5], with the environmental risk associated with soil heavy metal accumulation.

One possible solution to these environmental problems is to use biodegradable plastic or paper, as mulch, which could present an alternative to polyethylene in reducing nonrecyclable waste and decreasing the environmental pollution associated with it [6–8]. On the other hand, it is essential to control the functionality of these materials in the soil. This can be done at the laboratory, such as by measuring the transmittance of the materials [9], which would be quite complex, or at field level, by determining the level of deterioration of materials. In the latter case, it is very common

to use qualitative scales to measure the degree of disrepair, for example, 9 or no deterioration (material practically intact) down to 1 or totally degraded, as indicated by Martin-Closas et al. [10], accompanied by photographic monitoring, apart from visual inspection, which is largely subjective.

Determination of mulch residues on the ground is one of the basic requirements to estimate the potential of each material to degrade. Determining the extent of mulch residue in the field is an exhausting job and there is not a distinct and accurate criterion for its measurement, as reported in detail in the review by Cowan [11]. There are several indices to estimate the residue covers but most of them are not only laborious and time consuming but also greatly affected by human errors. Human vision is fast and accurate enough in this case but the problem is that the magnitude must be stated numerically to be reported and to be used for comparison between different mulches or mulches at different times. Interpretation of the extent perceived by vision into figures is possible by a simulation of the human vision system.

Machine vision comprising image processing systems can perform these tasks. Lately, recent developments in robotics, computer vision, and hardware have helped to solve several problems in agriculture. Thus, the information provided by digital imaging has been used extensively in ground classification cover [12], leaf area index estimation in forest ecosystems [13], identifying eroded areas [14], mechanical properties of horticultural products [15], crop classification [16], and weed recognition [17]. In these latter cases, it is important to have efficient and automatic image segmentation to distinguish vegetation from the ground (Guijarro et al. [18] and references therein).

However, these images in field conditions, with soil and mulch, are quite complex, especially because of the small contrast between them. Meanwhile the initial appearance of most of the mulches is a kind of black PE and at the end of the crop campaign the materials appeared somewhat discolored and soil and/or crop residue was impregnated making it very difficult to completely remove them (Figure 1(a) as an example).

This work has a double objective: first, to determine an image analysis method, reliable and accurate, in order to evaluate the residue of the mulch materials at the end of the crop season, and based on it, their deterioration level; and second, to determine and to compare the mulch residual of alternative materials to polyethylene. In order to achieve this, four thresholding methods were applied to binarize the images of four different mulch materials. Then a simple matrix calculation automatically determined the soil area as a measure of mulch deterioration. The results are compared with an area obtained by an expert user of imaging software. A preliminary idea of this work can be consulted in Moreno et al. [19].

2. Material and Methods

2.1. Mulch Materials and Image Acquisition. The mulch materials used were two black biodegradable plastics (BD) composed of corn starch (mulch 1: 15 μm, Novamont; mulch 2: 17 μm, Barbier), standard black polyethylene (PE) (mulch 3: 15 μm, Siberline), and one black paper (PP) (mulch 4: 85 g m^{-2}, Mimcord).

Images were taken 100 days after the mulch was implanted in the ground to determine the deterioration, in August 2009. During the experimental period, meteorological data such as mean, mean maximum, and mean minimum temperatures, rainfall, and solar radiation were 22.8°C, 31.8°C, 12.3°C, 83.0 mm, and 27.1 MJ m^{-2}, respectively. The corresponding mean values for the previous 9-year historical series (2000–2008) were 19.6°C, 27.2°C, 10.9°C, 49.0 mm, and 25.9 MJ m^{-2}, respectively. Irrigation was applied, so the soil had moisture conditions similar to those reached with summer vegetable crops. Also the time spent on the ground was adjusted to the duration of a horticulture crop cycle (e.g., tomatoes and peppers). The test was carried out in the experimental farm "El Chaparrillo" (3°56′W–39°0′N, altitude 640 m), property of the Junta de Comunidades de Castilla-La Mancha, in Ciudad Real (Central Spain).

A digital camera (Canon PowerShot A80-35 mm) was used to acquire color digital images (JPG format) under similar lighting conditions (sunny day and at noon) at the experimental field. A total of 24 photographs, 6 per mulch, were taken according to a randomized block design. Images were captured accurately covering a 1 × 0.5 meter frame which yielded images cropped to be 2400 × 1200 pixels. The images were processed with the Image Processing Toolbox from Matlab R2009a [20] belonging to The Mathworks, Inc. (Natick, MA, USA).

2.2. RGB and HSV Color Space Histograms. "Color" refers to the human brain's subjective interpretation of combinations of a narrow band of wavelengths of light. González and Wood [21] define the "color space" transformations as various specifications of a three-dimensional coordinate system where each color is represented by a single point. The RGB model (red, green, and blue) is based on a system of Cartesian coordinates where each point is described by its primary red, green, and blue spectral components. RGB image color consists of three independent image planes, one for each primary color. Another color space is HSV, where each point is defined by hue (H), saturation (S), and value (V) coordinates.

The HSV color space has a better capability of representing the colors of human perception than the RGB color space does. The H and S components are closely related to the human eye color perception. The third component (V) is related to image brightness [21]. The transformation equations from RGB to HSV space are commonly used and can be consulted in the work of Chun-Ming Tsai [22]. The use of different color spaces is applied in agriculture, especially in plant detection, to discern the plant from the background [23, 24].

Both spaces (RGB and HSV) have been taken into consideration to study the image histograms derived from them and to see which one was better to binarize the image.

2.3. Image Segmentation. The segmentation process partitions the digital image into disjoint regions [25], the automated segmentation being, in general, one of the most difficult tasks in the image analysis [26]. There are many color segmentation techniques reported in the literature, such as texture analysis, edge detection, region split and merging, feature analysis and histogram thresholding or clustering, the last being the most commonly used, as indicated by Du et al. [27].

Image segmentation by the thresholding technique involves the assumption that the objects and the background have distinct level distributions and so the histogram contains two—or more—distinct peaks and the threshold value separating them can be obtained. If the histogram is bimodal, the image can be segmented into two classes or regions: the object with value levels above the threshold (t) and background with values below the threshold, or vice versa [21, 28]. Then, usually, a binary (black and white) thresholded $B(x, y)$ image is obtained from the corresponding histogram image $f(x, y)$: a value of 1 is assigned to the pixels of the object, and 0 to the background pixels. A survey on threshold selection techniques can be consulted at Sahoo et al. [28]. This study identified the soil as foreground and mulch as background.

When the threshold depends only on $f(x, y)$, the threshold is called global, while if it also depends on local properties of each point (x, y), the threshold is called local. In this study we have two global methods and one local method. The global Otsu [29] (OT) and Ridler-Calvard [30] (RC) thresholds have been chosen because they are widely used thresholding techniques which have proven their effectiveness in various fields [31]. Furthermore, the OT method is implemented as the default approach to image thresholding in some free or commercial software such as Matlab. The local entropy-based thresholding method (LE) is a local thresholding method that has been shown to be promising and effective in image thresholding [27, 32]. Below we briefly explain each method.

Otsu's method (OT) [29] has shown great success in image segmentation. Several improved versions of Otsu's method have been proposed, such as a recursive Otsu's method by Cheriet et al. [33] or the version of the method given by Xu et al. [34].

OT finds the threshold (t) that maximizes the between-class variance (background and foreground), σ_b^2, in the image histogram. Equivalently, OT finds the threshold (t) that minimizes the within-class variance, σ_w^2.

The principle of the RC method [30, 35] is to evaluate the threshold (t) for any image with a bimodal histogram by assuming t to be $t = (m_1 + m_2)/2$, where m_1 and m_2 are the means of each of the two components of the histogram separated by the threshold. For this, an initial threshold is selected, and a new threshold is obtained by averaging the means of the two classes. The process continues until the value of the threshold converges. When the iterative algorithm stops, the threshold calculated is the average of the mean levels of the two classes [34, 36].

LE thresholding is based on the maximization of the information measure between two classes, foreground and background. Therefore, the optimal t maximizes the addition of foreground and background entropy [37–39]. A survey and comparative analysis of entropy and relative entropy thresholding techniques can be consulted in Chang et al. [40].

Entropy refers to the amount of information that can be obtained from a set of messages and was first introduced into information theory by Shannon [41]. The entropy of an image can be defined as $H = -\sum_{i=1}^{i=L} p_i \log_2 p_i$, where p_i is the probability that the gray-value i appears in the image, and L is the maximum gray-value.

Additionally, threshold setting by the user, partly subjective, in the image histogram is quite frequently applied and therefore also incorporated into the study named as manual thresholding (MT).

2.4. Performance to Obtain Binary Images and Percentage of Bare Soil Area. The thresholding methods tested (Otsu, Ridler-Calvard, local entropy, and manual thresholding) were applied to the histograms corresponding to each independent plane (red, blue, and green at RGB color space and hue, saturation, and value at HSV color space).

Otsu's method was applied directly using Matlab commands; Ridler-Calvard method was implemented automatically using the iterative Isodata algorithm [20], and the development of the local entropy method is based on Du et al. [27] and Du [32] works.

The result of segmentation using the proposed methods is a binary image (B') with white pixels representing bare soil and black pixels representing the mulch. A last step consisted of applying to each B' binary image a morphological operation to reduce the noise regions with an area smaller than $m \times n/100$. Removing small objects (both in foreground and background) was carried out by opening the binary areas (in both binary image B' and its complement) with an 8-connectivity. Then all small objects were removed to obtain the final binary image (B). This operation was performed using a specific Matlab function.

The area estimated was the percentage of bare soil and it is determined by dividing the number of white pixels by that of all pixels of the image.

Manual thresholding was based on the image histogram. Most image processing software programmes, including Matlab or Photoshop, have an interactive contrast and brightness adjustment tool that can be associated with a grayscale image. Then the thresholds were adjusted in the histograms to achieve the best discrimination between soil and mulch.

The reference areas (A_R) were obtained from the color images to use them as the optimum classification. They were obtained by an expert user of Adobe Photoshop CS 3 software who used a zoom of 800 to discriminate soil and mulch.

2.5. Statistical Analysis. A paired 2-tailed Student's t-test was performed to determine the variability in the metrics for each pair of areas: area of reference A_R (obtained by the expert of Adobe Photoshop CS 3) and area using a threshold method. A paired 2-tailed Wilcoxon nonparametric test was used in case of no normality (tested by Shapiro-Wilk's test).

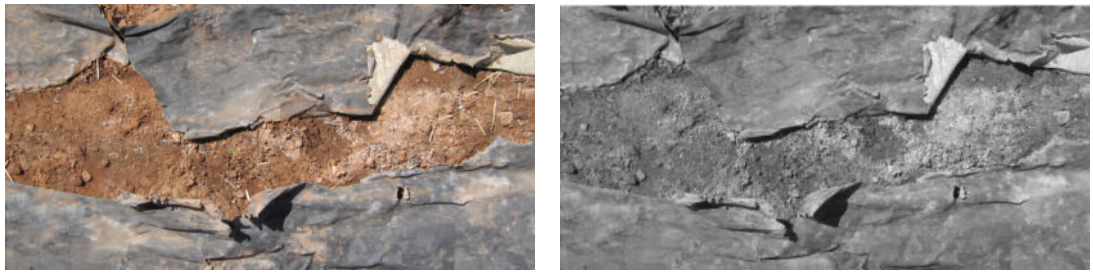

(a) (b)

Figure 1: Image with mulch and soil 100 days after field implementation. (a) Original image in RGB color space; (b) grayscale image.

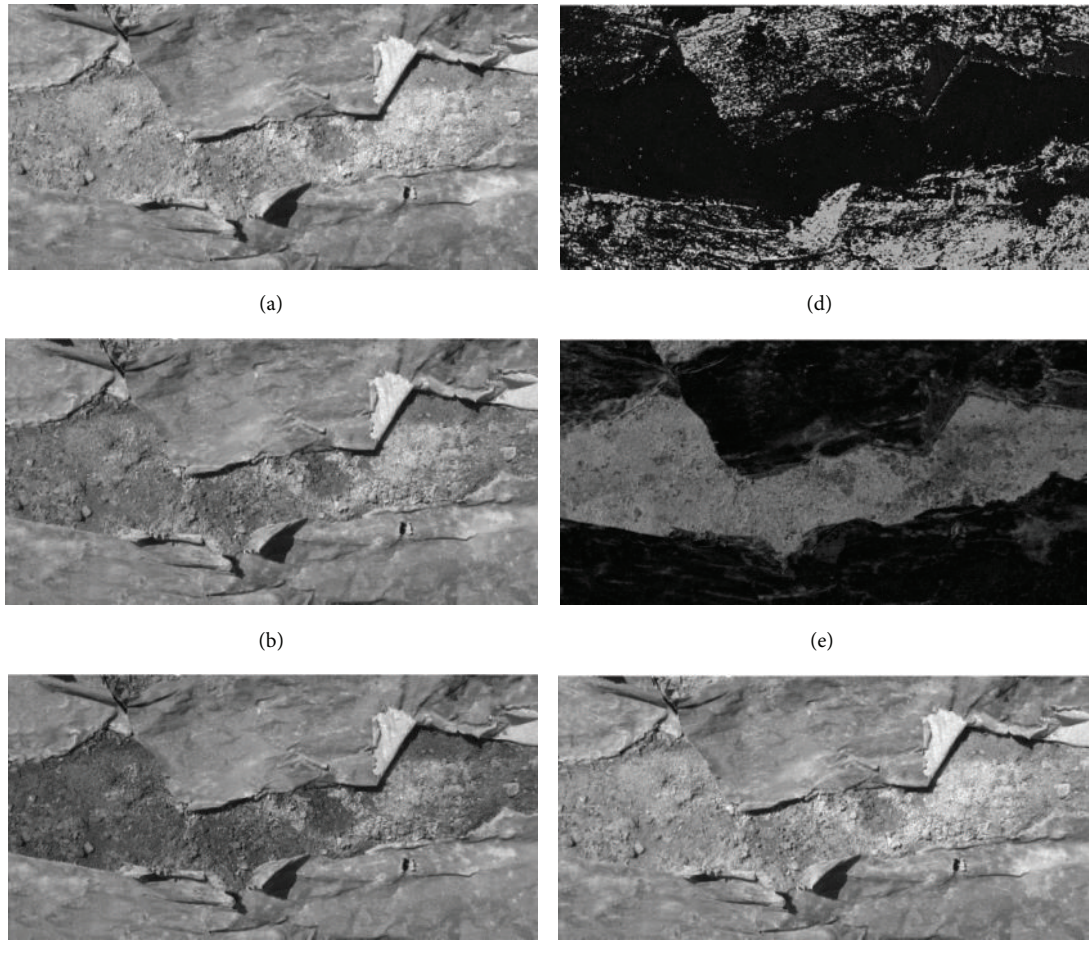

(a) (d)

(b) (e)

(c) (f)

Figure 2: Representation of the original image shown in Figure 1 in the RGB system (left column) and in the HSV system (right column). (a) Red plane, (b) green plane, (c) blue plane, (d) hue plane, (e) saturation plane, and (f) value plane.

An analysis of variance (ANOVA) was applied to compare the degradation among the mulch materials, by comparing the percentage of soil area estimated by each thresholding method.

3. Results and Discussion

3.1. Histograms Selected. The original RGB images used in this work had the problem of presenting a very low reflectance difference between soil and mulch, with low contrast also in each of the three separate color planes (Figures 2(a), 2(b), and 2(c)).

The histograms of the grayscale image corresponding to the original RGB color images were practically unimodal (Figure 1(b) and its histogram in Figure 3(a)); that is, soil and mulch looked confused to each other. Neither of the images of R, G, and B obtained from the separate RGB color planes showed good contrast levels (Figures 2(a), 2(b), and 2(c)).

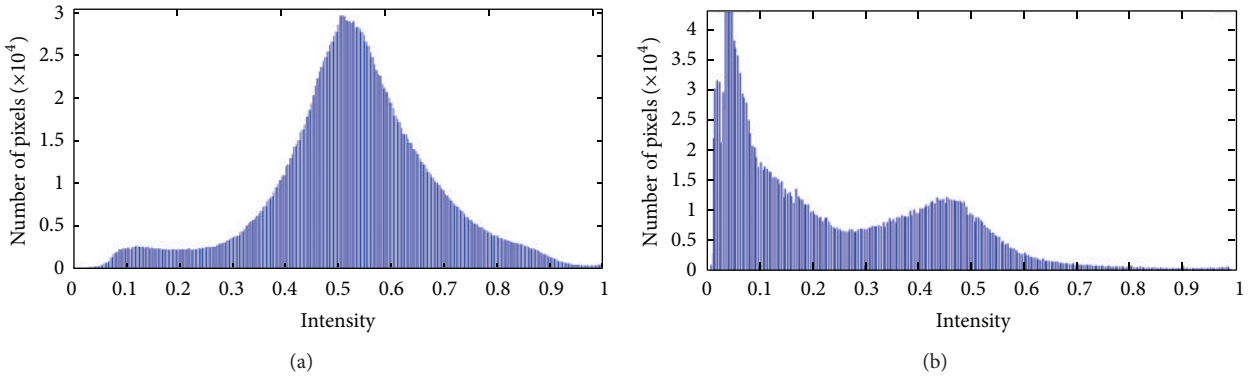

Figure 3: Histograms corresponding to color image of Figure 1 in (a) grayscale image and (b) saturation plane.

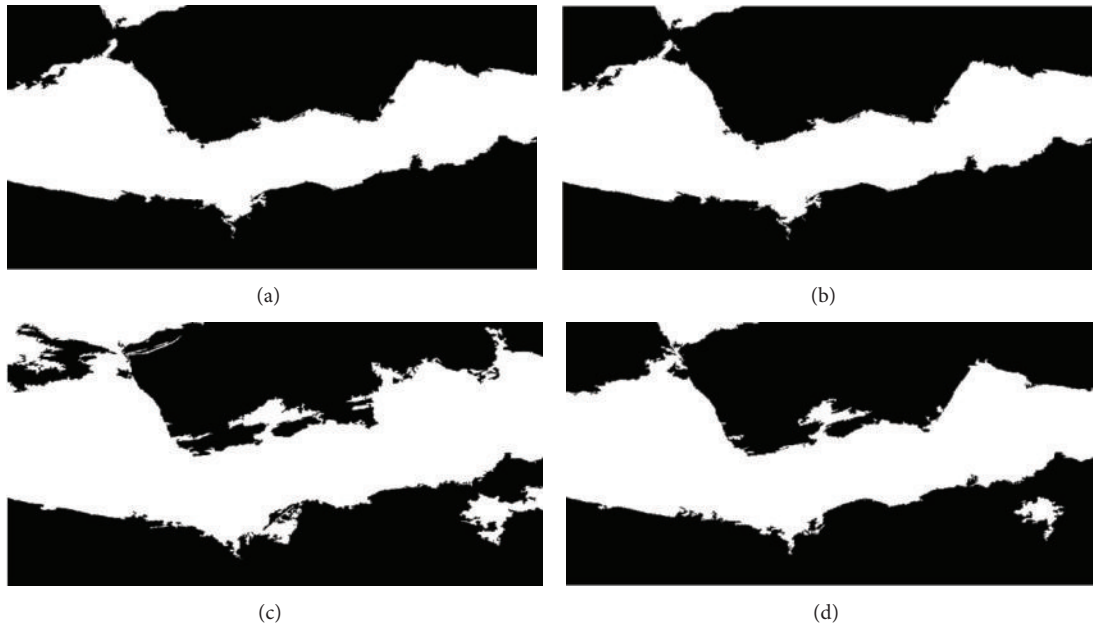

Figure 4: Binary images from saturation plane (HSV color system), obtained from the original image showed in Figure 1, applying different thresholding methods: (a) Otsu ($t_{OT} = 0.2745$; $A_{OT} = 36.43$); (b) Ridler-Calvard ($t_{RC} = 0.2677$; $A_{RC} = 35.72$); (c) local entropy ($t_{LE} = 0.1412$; $A_{LE} = 57.57$); (d) manual thresholding ($t_{MT} = 0.2499$; $A_{MT} = 38.24$). Black pixels represent mulch and white pixels represent bare soil.

For this reason we carried out the conversion of images from the RGB color space to HSV space and the three independent planes (Figures 2(d), 2(e), and 2(f)) were examined.

All images corresponding to saturation plane provided a good contrast between soil and mulch (Figure 2(e)) and the histograms appeared bimodal (Figure 3(b)). So these histograms were chosen to give the corresponding binary images by applying the four thresholding methods.

3.2. Comparison of Thresholding Methods and Computational Time. In all images it was fulfilled that the relationship between the Ridler-Calvard and the Otsu thresholds was $t_{RC} < t_{OT}$ (Table 1). Therefore, in the binary images obtained initially (prior to performing morphological operations), the relationship between the values corresponding to the bare soil (white) obtained through these thresholds was the opposite: $A_{OT} < A_{RC}$. Additionally, in most of the images the following was satisfied: $t_{MT} < t_{RC} < t_{OT}$, and therefore the ratio of initial areas (data not shown) was $A_{OT} < A_{RC} < A_{MT}$ for all of them. In these cases, the area corresponding to bare soil was overestimated by the t_{MT} threshold, especially when compared with t_{OT}. Guijarro et al. [18] also observed that the threshold obtained by Otsu's method tended to produce an undersegmentation of white pixels, corresponding to barley and corn crops, because it provided a relatively high value in the histogram.

For example, the thresholds corresponding to Figure 1 were $t_{MT} = 0.2499$, $t_{RC} = 0.2677$, and $t_{OT} = 0.2745$, and the corresponding bare soil areas, prior to performing morphological operations (expressed as a percentage), were 39.16, 36.41 and 35.78, respectively.

The maximum difference between the $t_{OT} - t_{RC}$ thresholds was 0.0191, while the maximum differences between $\text{abs}(t_{OT} - t_{MT})$ and $\text{abs}(t_{RC} - t_{MT})$ were higher (0.2350 and 0.2541,

Table 1: Thresholds and areas obtained after eliminating small objects. Thresholds: Otsu (t_{OT}), Ridler-Calvard (t_{RC}), manual thresholding (t_{MT}), and local entropy (t_{LE}). Soil areas by Otsu (A_{OT}), Ridler-Calvard (A_{RC}), manual thresholding (A_{MT}), local entropy (A_{LE}), and reference area (A_R).

Image	Mulch*	Block	Threshold				Area				
			t_{OT}	t_{RC}	t_{MT}	t_{LE}	A_{OT}	A_{RC}	A_{MT}	A_{LE}	A_R
1	1	1	0.2902	0.2874	0.2468	0.5059	50.9052	49.4967	52.9680	39.8214	49.0100
2	1	2	0.2745	0.2717	0.2297	0.4667	46.5797	45.5628	50.4214	38.7190	55.7600
3	1	3	0.3451	0.3425	0.2158	0.5529	70.6396	70.8865	82.7414	61.2655	86.7600
4	1	4	0.2706	0.2677	0.2494	0.5098	46.4310	45.7977	47.7424	27.5502	39.7300
5	1	5	0.2353	0.2283	0.2390	0.4667	45.2831	46.4100	44.8275	9.6671	29.0600
6	1	6	0.2824	0.2795	0.2430	0.1804	43.7783	43.8106	45.0526	67.6796	45.0500
7	2	1	0.3255	0.3228	0.2691	0.5843	64.9501	63.4503	68.4051	43.6728	59.9000
8	2	2	0.2784	0.2756	0.2483	0.1922	46.8627	44.7348	47.8013	65.0698	45.5200
9	2	3	0.2745	0.2677	0.2499	0.1412	36.4270	35.7161	38.2370	57.5681	33.7800
10	2	4	0.3216	0.3189	0.2599	0.5608	68.6014	68.0766	71.7309	52.9240	71.0700
11	2	5	0.3137	0.3189	0.2897	0.3490	49.5972	50.1565	51.2083	52.3749	52.0200
12	2	6	0.3255	0.3228	0.2819	0.5529	61.5203	62.4738	66.2118	38.5616	54.2500
13	3	1	0.2588	0.2559	0.2616	0.0902	24.5614	24.6451	24.4695	45.8991	22.2100
14	3	2	0.2745	0.2677	0.2406	0.1804	31.0725	31.3840	32.8444	44.1760	23.8300
15	3	3	0.2667	0.2598	0.2400	0.1176	19.3475	18.8066	19.6754	45.0813	23.3600
16	3	4	0.2392	0.2362	0.2332	0.1412	28.6458	28.8813	29.0930	46.7529	29.2300
17	3	5	0.1569	0.1378	0.3919	0.9961	1.6047	1.9750	0.6406	0.0000	2.7600
18	3	6	0.2118	0.2047	0.4327	0.1529	12.4904	7.4138	0.8420	44.7230	4.5300
19	4	1	0.2353	0.2323	0.2297	0.4706	47.0578	47.1434	47.3097	6.9027	26.3000
20	4	2	0.3098	0.3071	0.2517	0.1333	42.9258	43.0054	45.3668	60.3160	42.6000
21	4	3	0.2980	0.2953	0.2773	0.1569	47.2435	46.5150	47.6497	66.6117	48.9300
22	4	4	0.2980	0.2953	0.2662	0.1608	46.5599	46.6459	47.7724	63.7267	47.6600
23	4	5	0.3059	0.2992	0.2622	0.2275	45.0941	45.9767	49.0865	59.3983	42.4800
24	4	6	0.2902	0.2874	0.2439	0.1490	40.0192	35.5562	41.6854	59.2816	40.7600

*Mulch 1: biodegradable (BD). Mulch 2: biodegradable (BD). Mulch 3: polyethylene (PE). Mulch 4: paper (PP).

Table 2: Computational time (in minutes) for the calculation of soil area in binary images obtained by several thresholding methods: Otsu (OT), Ridler-Calvard (RC), local entropy (LE), manual thresholding (MT), and reference area (R). This time has been estimated based on a set of 24 color images. The ratio has been calculated with respect to MT method.

	OT	RC	LE	MT	R
Time (minutes)	10.5	9	18	230	3200
Ratio (%)	4.5	3.9	7.8	100	1391

Table 3: Comparison of the soil area percentage values obtained by thresholding methods (Otsu (OT), Ridler-Calvard (RC), manual threshold (MT), and local entropy (LE)) with the reference area (A_R). The comparison was analyzed with a paired 2-tailed Student's t-test and a paired 2-tailed Wilcoxon nonparametric test in case of LE.

Groups		Average			S.D. (Dif.)	t	P bilateral*
G1	G2	Dif.	G1	G2			
A_R	A_{OT}	−1.73	40.69	42.42	7.42	−1.15	0.2637
A_R	A_{RC}	−1.17	40.69	41.86	7.61	−0.75	0.4611
A_R	**A_{MT}**	−3.22	40.69	43.91	6.53	−2.42	**0.0241**
A_R	A_{LE}	−5.05	40.69	45.73	19.23		0.0540

*In bold the pair of methods that present significant differences in the areas at level $\alpha = 0.05$. S.D. (Dif.): standard deviation of the mean difference.

resp.). The averages of the differences among abs($t_{OT} - t_{RC}$), abs($t_{OT} - t_{MT}$), and abs($t_{RC} - t_{MT}$) were 0.0046, 0.0530, and 0.0515, respectively. All this proves the close proximity existing between the t_{OT} and t_{RC} thresholds and the greater difference they show in relation to the manual threshold.

Xu et al. [34] proved that the optimal Otsu (t) threshold is equal to the average value of the mean levels of two classes partitioned by this threshold. This result revealed the Ridler-Calvard method as an iterative version of Otsu's method, and therefore both approaches to image thresholding would be very close [31]. However, the slight right shift of the t_{OT} threshold observed in the histograms would indicate, according to the studies by Xu et al. [34] and Xue et al. [31], that the class with pixels of bare soil (foreground) has larger variance than the class with pixels of mulch (background). According to these studies, t_{OT} tends to balance the two classes, deviating from the intersection point of the two classes toward the class with larger variance. Also, t_{OT} shifts to the bigger size class when the size difference between background and object is very significant. This occurs in pictures 17 and 18 (Table 1), in which the size of the foreground class is much smaller

Table 4: Comparison of mulch deterioration by percentage of bare soil area (% of white pixels) ± standard error in binary images obtained by thresholding methods: Otsu (OT), Ridler-Calvard (RC), and local entropy (LE). The areas obtained based on the reference images (A_R) are shown in the first column. Mulch materials: biodegradable (BD), polyethylene (PE), and paper (PP).

Mulch*,**	A_R	A_{OT}	A_{RC}	A_{LE}***
1	50.90 ± 8.06[a]	50.60 ± 4.12[a]	50.33 ± 4.18[a]	40.78 ± 8.74[a]
2	52.76 ± 5.17[a]	54.66 ± 5.05[a]	54.10 ± 5.14[a]	51.70 ± 3.88[a]
3	17.65 ± 4.54[b]	19.62 ± 4.52[b]	18.85 ± 4.85[b]	37.77 ± 7.56[a]
4	41.46 ± 3.30[a]	44.82 ± 1.16[a]	44.14 ± 1.82[a]	52.71 ± 9.24[a]
P-value	0.0019	0.0001	0.0002	0.3715

*Mulch 1: biodegradable (BD). Mulch 2: biodegradable (BD). Mulch 3: polyethylene (PE). Mulch 4: paper (PP).
**100 days after mulch laying. ANOVA and Duncan test, $\alpha = 0.05$. Different letters in the same column indicate significant differences between soil areas.
***x^2 transformation.

than the background class, so t_{OT} would shift left from the histogram valley. These findings [31, 34] could explain the infrasegmentation concerning the identification of green obtained by Guijarro et al. [18] with the Otsu threshold.

The thresholds obtained by the LE method did not follow a pattern of behavior similar to the thresholds obtained by the other methods. The t_{LE} thresholds were very different from the t_{OT} and t_{RC}. Du et al. [27] also obtained OT and LE thresholds very different from each other in the R, G, and B color domains. However, when comparing four gray level thresholding methods (Otsu, Pal and Pal's local entropy, joint entropy, and the joint relative entropy methods), no conclusions could be drawn on which thresholding method performed better than the others. In this context, Glasbey [42], when comparing bimodal histograms for 11 thresholding methods including Otsu, Ridler-Calvard, and other methods based on entropy, found that the entropy method generated the widest spread of thresholds.

The initial binary images obtained from OT, RC, and MT thresholding methods differed little from the final binary images (after eliminating the small objects), both visually and in terms of the value of the area. For example, the respective areas before and after eliminating the small objects in the image presented in Figure 1 were 39.1596 and 38.2370 for MT, 36.4105 and 35.7161 for RC, and 35.7760 and 36.4270 for OT thresholding methods. In the case of the binary images obtained by the LE method, there were higher visual differences before and after performing morphological operations (for the cited image, the areas were 51.7199 and 57.5681, resp.).

In general, the binary images derived from the OT and RC thresholds gave a better visual fit to reality than those derived from both the manual and the LE thresholds (Figure 4 as an example).

Moreover, the time spent in obtaining areas using a manual threshold was higher than the automatic thresholding methods, as expected (Table 2). Among the automatic methods, LE gave a longer computational time, in fact double the time of the RC. Calculating the ratio with respect to the MT method, the automatic methods from faster to slower are RC, OT, and LE (Table 2). In accordance with Glasbey [42], RC is slightly less computationally intensive than Otsu.

3.3. Comparison among Bare Soil Areas. The comparison of the areas obtained from each method with the reference area (A_R) is shown in Table 3. There we can see the results of the paired 2-tailed Student's t-test between the A_R and the area obtained by the OT, RC, and MT thresholding methods (A_{OT}, A_{RC}, and A_{MT}, resp.). In the comparison of the area provided by LE (A_{LE}) and A_R, due to the lack of normality (shown by the Shapiro-Wilk's test) in the differences of the corresponding pairs of areas, the Wilcoxon test (for paired data) was performed. Statistically significant differences ($P < 0.05$) between A_R and A_{MT} were obtained; however, the visual appearance of both images was quite similar.

Despite the dubious significance of the paired 2-tailed Wilcoxon test for A_R and A_{LE} areas, the differences between these values became important (Table 1), with max abs($A_R - A_{LE}$) = 40.1930. In these cases, visual differences between both types of binary image were perceived. The average of these differences, in absolute value, was 18.01, while this value was 5.13 for the OT method.

However, in some cases the use of entropies for image thresholding has provided better results than even Otsu's method [43, 44].

3.4. Mulch Residue Analysis. The comparison of bare soil (where the mulch was gone) provided by each of the statistically reliable methods for the four types of mulches considered is shown in Table 4. These methods were OT, RC, and LE (Section 3.3, Table 3). ANOVA tables of the reference areas are also included to compare the results.

Table 4 is a comparison of mulch deterioration in actual field conditions, as measured by the percentage of bare soil area, by using different image thresholding methods. Data shown in Table 4 for the OT and RC methods in comparison with those obtained by ideal images are very similar, because ANOVA was significant in the three cases, and also because the mean values obtained in the deterioration of mulches by each method were quite similar. However, with the LE method, no significant differences between treatments ($P > 0.05$) were observed; the area of bare soil for mulch 3 was much overestimated (37.77% versus 17.65% for the reference image) and also altered the behavior of mulches 2 and 4 with respect to the reference image (Table 4). Therefore, we discard

LE as an accurate thresholding method for soil and mulch image segmentation. As a result, we choose the automatic OT and RC methods as the best thresholding methods with very similar results to each other and also with respect to the reference images. In general terms, both are simple and well-known methods. The RC method has a slightly lower computational cost while the OT method has the advantage of being included in specialized software.

The mean values of rate of deterioration (% bare soil area) obtained by expert user (A_R) and by the accurate thresholding methods (A_{OT}, A_{RC}) were, respectively, 50.90%, 50.60%, and 50.33% for mulch 1; 52.76%, 54.66%, and 54.10% for mulch 2; 17.65%, 19.62%, and 18.85% for mulch 3; 41.46%, 44.82 %, and 44.14 % for mulch 4.

The best thresholding methods obtained (OT and RC) indicate that mulch 3 (polyethylene) differs significantly from the others by presenting much less deterioration (a lower percentage of bare soil) than the biodegradable materials. As expected, these results highlight the low degradability of polyethylene in the soil and warn of the environmental problems this may cause.

4. Conclusions

The results obtained by four thresholding methods from color images containing soil and mulch were compared: Otsu (OT), Ridler-Calvard (RC), local entropy (LE) and manual thresholding (MT). Furthermore, deterioration of four mulch materials (polyethylene, two biodegradable plastics, and paper) was analyzed 100 days after implantation in the soil, through computation of the area of bare soil.

The following conclusions were reached.

(i) The problem of low-contrast color images in the field, with soil and mulch, can be solved by converting RGB to HSV color space and using the saturation plane histogram.

(ii) Among the thresholding methods studied to obtain binary images, the most accurate ones with regard to the respective reference areas are Otsu and Ridler-Calvard.

(iii) The percentage of missing mulch (soil area) has been automatically computed using binarized images.

(iv) A hundred days after its implementation on the ground, biodegradable materials have deteriorated around 50%, well above the deterioration of polyethylene (below 20%).

The rate of deterioration of a mulch material, measured reliably and quickly in field conditions as we propose, is an important fact. It could help to better understand the overall behavior of the materials used as mulch. Therefore, the methods to obtain such data, as proposed in this study, will be useful to mulch manufacturers and farmers.

Acronyms

t_{MT}: Threshold obtained by manual thresholding
t_{OT}: Threshold obtained by Otsu's method
t_{RC}: Threshold obtained by Ridler-Calvard's method
t_{LE}: Threshold obtained by local entropy method
A_R: Reference area
A_{MT}: Area obtained by manual thresholding
A_{OT}: Area obtained by Otsu's method
A_{RC}: Area obtained by Ridler-Calvard's method
A_{LE}: Area obtained by local entropy method.

Conflict of Interests

The authors declare that there is no conflict of interests regarding the publication of this paper.

Acknowledgments

This work was funded by the Project INIA RTA2005-00189-C05-04, Spain. Materials were generously provided by Novamont S.p.A., Mimcord S.A., and Barbier S.A. companies. The authors thank Javier Casanova, Jaime Villena, and Ramón Meco for their assistance over the study period.

References

[1] M. M. Moreno, A. Moreno, and I. Mancebo, "Comparison of different mulch materials in a tomato (*Solanum lycopersicum* L.) crop," *Spanish Journal of Agricultural Research*, vol. 7, no. 2, pp. 454–464, 2009.

[2] T. Haapala, P. Palonen, A. Korpela, and J. Ahokas, "Feasibility of paper mulches in crop production: a review," *Agricultural and Food Science*, vol. 23, pp. 60–79, 2014.

[3] S. Kasirajan and M. Ngouajio, "Polyethylene and biodegradable mulches for agricultural applications: a review," *Agronomy for Sustainable Development*, vol. 32, no. 2, pp. 501–529, 2012.

[4] P. Feuilloley, G. César, L. Benguigui et al., "Degradation of polyethylene designed for agricultural purposes," *Journal of Polymers and the Environment*, vol. 13, no. 4, pp. 349–355, 2005.

[5] M. Koutny, J. Lemaire, and A. Delort, "Biodegradation of polyethylene films with prooxidant additives," *Chemosphere*, vol. 64, no. 8, pp. 1243–1252, 2006.

[6] L. Martín-Closas and A. M. Pelacho, "Agronomic potential of biopolymer films," in *New Materials for Sustainable Films and Coating. Biopolymers*, D. Plackett, Ed., pp. 277–299, Wiley, New York, NY, USA, 2011.

[7] A. Cirujeda, J. Aibar, A. Anzalone et al., "Biodegradable mulch instead of polyethylene for weed control of processing tomato production," *Agronomy for Sustainable Development*, vol. 32, no. 4, pp. 889–897, 2012.

[8] M. M. Moreno, C. Moreno, and A. M. Tarquis, "Mulch materials in processing tomato: a multivariate approach," *Scientia Agricola*, vol. 70, no. 4, pp. 250–256, 2013.

[9] E. Schettini, F. R. de Salvador, G. Scarascia-Mugnozza, and G. Vox, "Radiometric properties of photoselective and photoluminescent greenhouse plastic films and their effects on peach and cherry tree growth," *Journal of Horticultural Science and Biotechnology*, vol. 86, no. 1, pp. 79–83, 2011.

[10] L. Martin-Closas, A. M. Pelacho, P. Picuno, and D. Rodríguez, "Properties of new biodegradable plastics for mulching, and characterization of their degradation in the laboratory and in the field," *Acta Horticulturae*, vol. 801, pp. 275–282, 2008.

[11] J. S. Cowan, *The use of biodegradable mulch for tomato and broccoli production: crop yield and quality, mulch deterioration, and growers' perceptions [Ph.D. dissertation]*, Washington State University, Washington, DC, USA, 2013.

[12] J. D. Luscier, W. L. Thompson, J. M. Wilson, B. E. Gorham, and L. D. Dragut, "Using digital photographs and object-based image analysis to estimate percent ground cover in vegetation plots," *Frontiers in Ecology and the Environment*, vol. 4, no. 8, pp. 408–413, 2006.

[13] S. Fuentes, A. R. Palmer, D. Taylor, M. Zeppel, R. Whitley, and D. Eamus, "An automated procedure for estimating the leaf area index (LAI) of woodland ecosystems using digital imagery, MATLAB programming and its application to an examination of the relationship between remotely sensed and field measurements of LAI," *Functional Plant Biology*, vol. 35, no. 10, pp. 1070–1079, 2008.

[14] A. Trueba-Espinosa, J. L. Oropeza-Mota, C. A. Ortiz-Solorio, A. Martínez-Alcántara, and G. Ruelas-Ángeles, "Identification of eroded zones with digital images using artificial neural networks," *Agrociencia*, vol. 38, no. 6, pp. 573–581, 2004.

[15] K. Mollazade, M. Omid, F. Akhlaghian Tab, Y. R. Kalaj, S. S. Mohtasebi, and M. Zude, "Analysis of texture-based features for predicting mechanical properties of horticultural products by laser light backscattering imaging," *Computers and Electronics in Agriculture*, vol. 98, pp. 34–45, 2013.

[16] M. R. Golzarian and R. A. Frick, "Classification of images of wheat, ryegrass and brome grass species at early growth stages using principal component analysis," *Plant Methods*, vol. 7, no. 1, article no. 28, 2011.

[17] T. F. Burks, S. A. Shearer, and F. A. Payne, "Classification of weed species using color texture features and discriminant analysis," *Transactions of the American Society of Agricultural Engineers*, vol. 43, no. 2, pp. 441–448, 2000.

[18] M. Guijarro, G. Pajares, I. Riomoros, P. J. Herrera, X. P. Burgos-Artizzu, and A. Ribeiro, "Automatic segmentation of relevant textures in agricultural images," *Computers and Electronics in Agriculture*, vol. 75, no. 1, pp. 75–83, 2011.

[19] C. Moreno, M. M. Moreno, and A. M. Tarquis, "Image analysis to estimate mulch residual on soil," *Geophisysical Research Abstracts*, vol. 16, Article ID 16801, 2014.

[20] The Mathworks, 2010, http://www.mathworks.com/.

[21] R. C. González and R. E. Woods, *Digital Image Processing*, Prentice-Hall, Upper Saddle River, NJ, USA, 2008.

[22] C. Tsai and H. Lee, "Binarization of color document images via luminance and saturation color features," *IEEE Transactions on Image Processing*, vol. 11, no. 4, pp. 434–451, 2002.

[23] I. Philipp and T. Rath, "Improving plant discrimination in image processing by use of different colour space transformations," *Computers and Electronics in Agriculture*, vol. 35, no. 1, pp. 1–15, 2002.

[24] X. D. Bai, Z. G. Cao, Y. Wanga, Z. H. Yua, X. F. Zhang, and C. N. Li, "Crop segmentation from images by morphology modeling in the CIE $L^*a^*b^*$ color space," *Computers and Electronics in Agriculture*, vol. 99, pp. 21–34, 2013.

[25] K. R. Castleman, *Digita Image Processing*, Prentice Hall, Upper Saddle River, NJ, USA, 1996.

[26] R. Gonzalez and O. Wintz, *Digital Image Processing*, Addison-Wesley, Massachusetts, Mass, USA, 3rd edition, 1991.

[27] Y. Du, C. Chang, and P. D. Thouin, "Unsupervised approach to color video thresholding," *Optical Engineering*, vol. 43, no. 2, pp. 282–289, 2004.

[28] P. K. Sahoo, S. Soltani, and A. K. C. Wong, "A survey of thresholding techniques," *Computer Vision, Graphics and Image Processing*, vol. 41, no. 2, pp. 233–260, 1988.

[29] N. Otsu, "A threshold selection method from gray-level histograms systems," *IEEE Transactions on Systems, Man, and Cybernetics*, vol. 9, no. 1, pp. 62–66, 1979.

[30] T. W. Ridler and S. Calvard, "Picture thresholding using iterative selection method," *IEEE Transactions on Systems, Man and Cybernetics*, vol. 8, no. 8, pp. 630–632, 1978.

[31] J. H. Xue and Y. J. Zhang, "Ridler and Calvard's, Kittler and Illingworth's and Otsu's methods for image thresholding," *Pattern Reccognition Letters*, vol. 33, pp. 793–797, 2012.

[32] Y. Du, *Text detection and restoration of color video image [Ph.D. thesis]*, University of Maryland, Baltimore, Md, USA, 2003.

[33] M. Cheriet, J. N. Said, and C. Y. Suen, "A recursive thresholding technique for image segmentation," *IEEE Transactions on Image Processing*, vol. 7, no. 6, pp. 918–921, 1998.

[34] X. Xu, S. Xu, L. Jin, and E. Song, "Characteristic analysis of Otsu threshold and its applications," *Pattern Recognition Letters*, vol. 32, no. 7, pp. 956–961, 2011.

[35] H. J. Trussell, "Comments on "picture thresholding using iterative selection method" by T. W. Ridler and E. S. Calvard," *IEEE Transactions on Systems, Man and Cybernetics*, vol. 9, no. 5, p. 311, 1979.

[36] A. Magid, S. R. Rotman, and A. M. Weiss, "Comments on "Picture thresholding using an iterative selection method" by T. W. Ridler and E. S. Calvard," *IEEE Transactions on Systems, Man and Cybernetics*, vol. 20, no. 5, pp. 1238–1239, 1990.

[37] T. Pun, "A new method for grey-level picture thresholding using the entropy of the histogram," *Signal Processing*, vol. 2, no. 3, pp. 223–237, 1980.

[38] T. Pun, "Entropic thresholding, a new approach," *Computer Graphics and Image Processing*, vol. 16, no. 3, pp. 210–239, 1981.

[39] N. R. Pal and S. K. Pal, "Entropic thresholding," *Signal Processing*, vol. 16, no. 2, pp. 97–108, 1989.

[40] C. Chang, Y. Du, J. Wang, S. Guo, and P. D. Thouin, "Survey and comparative analysis of entropy and relative entropy thresholding techniques," *IEE Proceedings: Vision, Image and Signal Processing*, vol. 153, no. 6, pp. 837–850, 2006.

[41] C. E. Shannon, "A mathematical theory of communication," *The Bell System Technical Journal*, vol. 27, pp. 379–423, 1948.

[42] C. A. Glasbey, "An analysis of histogram-based thresholding algorithms," *Graphical Models and Image Processing*, vol. 55, no. 6, pp. 532–537, 1993.

[43] C. A. Cattaneo, L. I. Larcher, A. I. Ruggeri, A. C. Herrera, and E. M. Biasoni, "Métodos de umbralización basados en la entropía de Shannon y otros," *Asociación Argentina de Mecánica Computacional*, vol. 30, pp. 2785–2805, 2010.

[44] C. A. Cattaneo, L. I. Larcher, A. I. Ruggeri, A. C. Herrear, E. M. Biasoni, and M. Escañuelas, "Segmentación de imágenes digitales mediante umbralizado adaptativo en imágenes de color," *Asociación Argentina de Mecánica Computacional*, vol. 29, pp. 6177–6193, 2011.

Hindawi Publishing Corporation
The Scientific World Journal
Volume 2014, Article ID 276892, 13 pages
http://dx.doi.org/10.1155/2014/276892

Research Article

Fragipan Horizon Fragmentation in Slaking Experiments with Amendment Materials and Ryegrass Root Tissue Extracts

A. D. Karathanasis, L. W. Murdock, C. J. Matocha, J. Grove, and Y. L. Thompson

Department of Plant & Soil Sciences, University of Kentucky, Lexington, KY 40546, USA

Correspondence should be addressed to A. D. Karathanasis; akaratha@uky.edu

Received 5 June 2014; Revised 6 August 2014; Accepted 7 August 2014; Published 2 September 2014

Academic Editor: Ana Maria Tarquis

Slaking experiments were conducted of fragipan clods immersed in solutions of poultry manure, aerobically digested biosolid waste (ADB), fluidized bed combustion byproduct (FBC), D-H_2O, $CaCO_3$, NaF, Na-hexa-metaphosphate, and ryegrass root biomass. The fragipan clods were sampled from the Btx horizon of an Oxyaquic Fragiudalf in Kentucky. Wet sieving aggregate analysis showed significantly better fragmentation in the NaF, Na-hexa-metaphosphate, and ryegrass root solutions with a mean weight diameter range of 15.5–18.8 mm compared to the 44.2–47.9 mm of the poultry manure, ADB, and FBC treatments. Dissolved Si, Al, Fe, and Mn levels released in solution were ambiguous. The poor efficiency of the poultry manure, ADB, and FBC treatments was attributed to their high ionic strength, while the high efficiency of the NaF, Na-hexa-metaphosphate, and rye grass root solutions to their high sodium soluble ratio (SSR). A slaking mechanism is proposed suggesting that aqueous solutions with high SSR penetrate faster into the fragipan capillaries and generate the critical swelling pressure and shearing stress required to rupture the fragipan into several fragments. Additional fragmentation occurs in a followup stage during which potential Si, Al, Fe, and Mn binding agents may be released into solution. Field experiments testing these findings are in progress.

1. Introduction

Fragipans are naturally causing restrictive layers occurring in about 53,000 km^2 of Kentucky soils and more than 970,000 km^2 in the US [1, 2]. They usually form as a result of weathering of primary minerals (mainly feldspars) in relatively acidic environments. Upon dissolution, these minerals release high levels of Si, Al, and other cations (Fe, Mn), which, under dry conditions, form Si-enriched amorphous gels that harden into a cement-type material that binds the soil particles into large masses of impermeable prism-like structures [3–5]. The fragipan, which usually occurs at depths between 45 and 60 cm from the soil surface, greatly restricts water movement and root growth [6]. Therefore, it reduces the water holding potential in these soils to about one-half of that of many other crop producing soils [7]. It also causes saturated soil conditions in the winter and spring that result in adverse conditions to crops growing during this time [8, 9]. By far the biggest production problem for corn and soybeans grown on these soils is limited water holding capacity, which may reduce yields by at least 20–25% [10, 11].

Field evidence suggests that fragipan horizons occurring in landscape positions with high hydraulic loads show signs of considerable degradation, particularly in their upper part which is in contact with the developing perched water table [4, 5, 12]. However, these weathering effects are the result of hundreds or thousands of years with no practical significance. In laboratory experiments, slaking (breakdown of soil clods into smaller fragments on rapid wetting) of soil clods obtained from Btx horizons of two Fragiudalfs in the southern Mississippi Valley Silty Uplands occurred at significantly lower rates than clods obtained from Bt horizons of a Hapludalf [13]. However, the extent and severity of slaking were independent of particle size distribution and extractable Si or Fe. Aggregate stability tests by wet sieving of fragipan and nonfragipan soil materials obtained from two Fragiudalfs in Italy indicated a protective effect of organic matter and a correlation of aggregate destabilization with

particle arrangement and porosity rather than particle size distribution [14].

Surprisingly, not many studies have explored alternative feasible management options that could accelerate fragipan degradation and remediate the problem. Physical treatments, including mechanical disturbance in combination with 2% organic matter application, somewhat lowered the bulk density of some fragipans but only for a limited time of 5 years [15]. Application of lime, sawdust, and fertilizer to back-filled trenches excavated into fragipan horizons also lowered their bulk density and significantly increased water storage capacity and crop yields for a duration of 16 years compared to similar untreated soils [16]. Other agricultural and industrial solid waste amendments have been used extensively in fragipan soils but mainly as alternative nutrient sources or structural stability contributors rather than fragipan remediation products [7, 17–20].

Most researchers have attributed loessial fragipan cementation to excess Si, Al, and Fe hydroxide precipitates binding soil particles and sealing a significant part of the fragipan pore system [4, 21–25]. Since the restrictive nature of fragipans has been attributed to Si-enriched amorphous binding agents, high pH amendments in the presence of dispersive materials (Na or Mg based) at low concentrations may facilitate their dissolution and reduce fragipan rigidity [26], thus allowing greater soil depths of rooting and water storage capacity. Rhoton et al. [27] evaluated under laboratory conditions a fluidized bed combustion byproduct (FBC) of pH 12 as a potential amendment to dissolve the cementing agents and decrease fragipan strength. Although different application rates did not significantly reduce fragipan strength below that of natural unamended samples, it was found that higher application rates slightly lowered fragipan strength apparently due to the dispersive effect of high Mg levels present in the FBC. It was also suggested that the true potential of fly ash as a fragipan weathering amendment may have been hindered by reprecipitation of poorly crystalline Mg-silicate phases in the closed laboratory system, while it may be more effective under natural field conditions, where dissolution products may be readily leached from the soil.

The use of cover crops has grown in popularity as means to control erosion and improve nutrient and water storage capacity, particularly in soils with limitations like fragipans [28–32]. Ryegrass (*Lolium perenne* L.), winter wheat (*Triticum aestivum* L.), hairy vetch (*Vicia villosa*), and other cover crops are most commonly used, but their effect on fragipan weathering is little understood [31–33]. Field trials by the University of Illinois suggested greater root penetration into the upper part of the fragipan by annual ryegrass plants and formation of root channels (macropores) that the succeeding spring crop can utilize to reach moisture within the cemented layer that normally is not available [34]. Planting annual ryegrass for two years allowed for 10–15 cm root penetration into the pan and improved moisture accessibility, something that corn and soybean roots cannot do by themselves. Whether this effect is exclusively physical/mechanical or it is facilitated by biochemical interactions through biomass accumulation and/or exudate excretion is unknown [20, 35–37].

The objectives of this study were to evaluate under laboratory conditions a number of amendment type materials and cover crop biomass extracts in hopes of finding effective means to accelerate the degradation of fragipan soil materials. The ultimate goal of the research findings is to test some of the most promising amendment materials and cover crops on field trials with fragipan soils.

2. Materials and Methods

The fragipan resistance to degradation was evaluated with slaking experiments of undisturbed fragipan clods immersed in solution extracts from amendment or cover crop biomass materials. The fragipan samples were collected from a Zanesville silt loam soil (fine-silty, mixed, active mesic, and Oxyaquic Fragiudalfs) at field moisture capacity (~ −10 kPa matric potential). The undisturbed samples were sealed in plastic bags and stored under refrigeration until used. The fragipan samples were treated with solutions/extracts from the following materials: deionized water (D-H_2O), reagent grade $CaCO_3$ at solubility strength, 0.005 M NaF, 0.005 M Na-hexa-meta-phosphate, an aerobically digested biosolid waste (ADB) collected from a waste water treatment plant in Jessamine County, KY, a fluidized bed combustion byproduct (FBC) from a coal power facility, broiler litter collected from a poultry facility, and ryegrass root biomass collected from a field where it was grown as a cover crop. Poultry litter, FBC, ADB, and ryegrass root solution extracts were generated using 1 : 1 solid dry weight to D-H_2O ratio. The ryegrass root biomass solution was extracted by 30-min boiling with D-H_2O and cooled down to room temperature (~20°C). All solutions and extracts were filtered before interacting with the fragipan materials.

The rationale for selection of the treatments was based on the following criteria. The D-H_2O treatment was mainly used as control. Poultry litter, $CaCO_3$, and other biosolid wastes are extensively used as amendments in soils, including many with fragipan horizons. Fly ash materials have been tested before in fragipan slaking experiments with some potential benefits. Na-hexa-metaphosphate is a primary dispersing agent used in particle size analysis while NaF could serve as a dispersant and Al complexing agent. Finally, the ryegrass is widely used as a cover crop, with some recent evidence suggesting that its roots can penetrate into the upper part of the fragipan horizon.

Sections of undisturbed fragipan samples representing prism interiors from the Btx_1 horizon were trimmed to potato shaped clods at field moisture state, approximately 8 × 5 cm in size, weighing about 140 g, and placed in 1 liter wide mouth glass jars. Each fragipan clod was immersed in 500 mL of solution extract representing the eight amendment materials using five replicates from each treatment. The jars were left undisturbed except for being subjected to a 2 min sonication treatment twice a week to accelerate degradation. Ten mL aliquots from the solutions/extracts in contact with the fragipan clods were collected the day after sonication and analyzed for pH, EC, Si, Al, Fe, and Mn [38]. Fragipan resistance to slaking was visually evaluated at every sampling

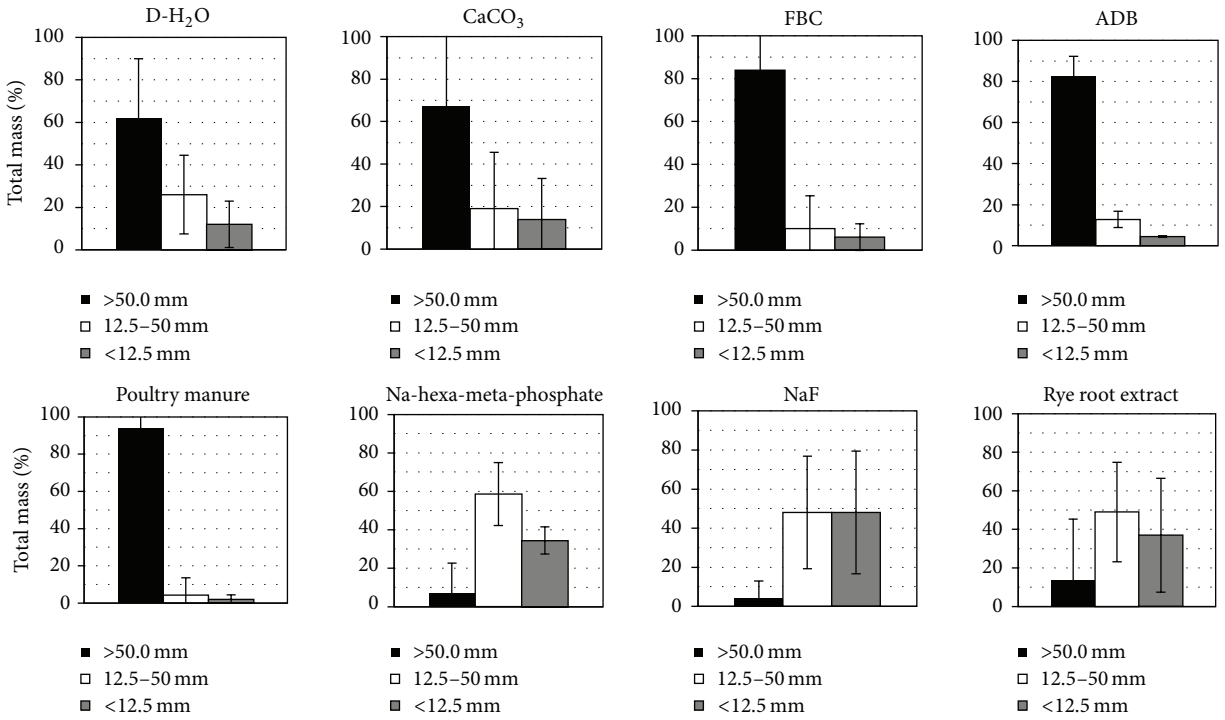

Figure 1: Wet aggregate size distribution of fragipan fragments in slaking experiments with D-H_2O, $CaCO_3$, FBC, ADB, poultry manure, 0.05 M Na-hexa-metaphosphate, 0.05 M NaF, and rye root extracts.

for four weeks and at the end of the experiment through wet aggregate sieving analysis using the following sieve sizes: 50 mm, 22.4 mm, 15.9 mm, 12.5 mm, 7.9 mm, 6.4 mm, 4.0 mm, and 2.00 mm [39, 40]. The % contribution of each aggregate size fraction was used to calculate the aggregate MWD. Fragipan subsamples were processed for particle size distribution, pH, exchangeable cations, CEC, organic matter, and mineralogical composition [38]. Particle size distribution, selected chemical, and mineralogical characterization data for the soil studied are shown in Table 1. Statistical comparisons of treatments were performed using ANOVA (Fisher's protected least significant difference test and Duncan's test) in SAS 9.3 with $\alpha < 0.05$ probability levels. Significant statistical relationships between slaking solution variables and aggregate MWD were determined with single and multiple regression analysis in SAS 9.3 with $\alpha < 0.05$ (*) and $\alpha < 0.01$ (**) probability levels.

3. Results and Discussion

3.1. Aggregate Stability Measurements. Wet sieving analysis of aggregate size distribution following completion of the experiment indicated considerable variability between and within treatments (Figure 1). Three aggregate size ranges were selected for comparison purposes including the >50 mm, the 50–12.5 mm, and the <12.5 mm fraction. The poultry manure, FBC, and ADB treatments contained the highest overall % of fragments in the >50 mm fraction with mean values of 93.8 ± 10.7, 84.0 ± 20.4, and 82.8 ± 18.2%, respectively (Figure 1). Several of these samples remained intact without any signs of alteration by the end of the experiment, while the remaining clods experienced very little degradation. Mean % values for the 50–12.5 mm size fraction for the same amendments ranged from 4.2 to 12.8 and for the <12.5 mm fraction 2.0 to 4.0. Fragipan clods exhibited intermediate resistance to D-H_2O and $CaCO_3$ treatments, with mean % values of fragments in the >50 mm size fraction of 62.0 ± 28.0 and 67.0 ± 47.2, respectively (Figure 1). In these treatments, significant fragipan degradation signs were observed only after the second week of the experiment with high standard error (SE) within treatments. Mean % values for the 50–12.5 mm size fraction ranged from 19.0 ± 26.6 for the $CaCO_3$ to 26.0 ± 18.5 for the D-H_2O treatments, and for the <12.5 mm fraction 14.0 ± 19.2 and 12.0 ± 11.0, respectively. The NaF, Na-hexa-metaphosphate, and ryegrass root treatments were the most effective in causing significant slaking in the fragipan clods (Figure 1). The degradation effects were evident before the end of the first week of the experiments. Only one replicate of five in each one of these treatments contained aggregates in the >50 mm size fraction and in all cases the original clod was fragmented. Mean % values for the >50 mm size fraction ranged from 4.0 ± 8.9 for the NaF to 14.0 ± 31.9 for the ryegrass root treatments (Figure 1). The respective values for the 50–12.5 mm size fraction were between 48.8 ± 28.5 and 58.6 ± 13.3, while for the <12.5 mm size fraction 34.4 ± 7.1 and 48.0 ± 31.3. The highest values of the smallest aggregate size fraction were observed with the NaF and the lowest with the Na-hexa-meta-phosphate treatment.

Mean weight diameter (MWD) estimates for the eight treatments are shown in Figure 2. Statistical analysis of mean

Table 1: Selected physical, chemical, and mineralogical properties of the Zanesville soil used in the study.

Horizon	Depth (cm)	Sand (%)	Silt (%)	Clay (%)	Texture	pH (1 : 1 H_2O)	Ca	Mg	K	Na	CEC	O M (%)	Clay mineralogy[†]
							meq/100 g						
Ap	0–20	8.7	70.1	21.2	Silt loam	7.52	4.98	1.07	0.13	0.05	9.0	3.94	V/HIV44 K26 Mi9 Q10 Gi8 F3
Bt_1	20–42	5.3	75.4	19.3	Silt loam	5.05	3.12	1.58	0.16	0.08	12.7	2.10	V/HIV52 K23 Mi9 Q9 Gi3 F4
Bt_2	42–65	4.2	72.4	23.4	Silt loam	4.52	1.42	2.38	0.17	0.15	13.0	0.33	Sm23 V/HIV31 K24 Mil1Q7 F4
Btx_1	65–127	10.5	65.3	24.2	Silt loam	4.28	0.80	2.96	0.13	0.18	11.8	0.19	Sm23 V/HIV40 K28 Q5 F4
Btx_2	127–140+	13.9	55.4	30.7	Silty clay loam	4.23	1.05	4.21	0.10	0.30	13.3	0.19	Sm23 V/HIV18 K39 Q9 Gi4 F3 Go4

[†]Sm: smectite; V/HIV: hydroxy-interlayered vermiculite; K: kaolinite; Mi: mica; Q: quartz; Gi: gibbsite; F: feldspar; Go: goethite.

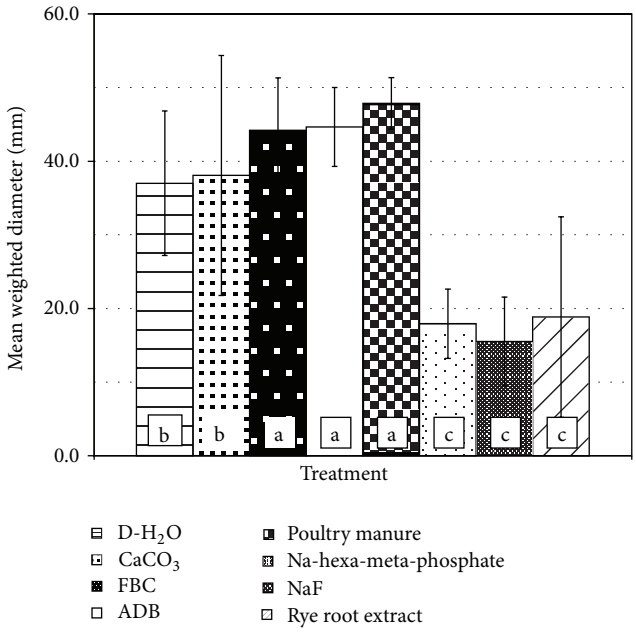

Figure 2: Mean weighted diameter (MWD) ± SE of fragipan fragments following 30-day slaking experiments with eight different amendment solutions/extracts (different letters designate significant differences in MWD based on Duncan's and LSD tests at $\alpha < 0.05$).

comparisons using the LSD and Duncan's tests confirmed significant differences ($\alpha < 0.05$) between treatment groups, consistent with the trends observed in aggregate size distribution patterns shown in Figure 1. The most effective fragipan slaking treatments appeared to be those with NaF, Na-hexa-meta-phosphate, and ryegrass root solutions/extracts as shown by the smallest overall MWD size range ($\alpha < 0.05$). The respective values ranged from 15.5 ± 6.0 for NaF to 18.8 ± 13.6 mm for the ryegrass root extract treatment. The poultry manure, ADB, and FBC treatments were the least effective in slaking the fragipan materials with MWD of 47.9 ± 3.5, 44.7 ± 5.4, and 44.2 ± 7.1 mm, respectively. These treatments also consistently showed the lowest overall variability within replicates. Fragipan clods in the presence of D-H_2O and $CaCO_3$ solutions exhibited intermediate but only slightly lower resistance to slaking compared to the poultry manure, ADB, and FBC treatments ($\alpha < 0.05$), with MWD ranging from 37.0 ± 9.8 to 38.1 ± 16.3 mm, respectively.

3.2. Solution Compositions. Concentrations of selected soluble components in contact with the fragipan clods over the length of the experiments are shown in Figures 3–8. The plotted values represent the initial, final, and middle time compositions unless a maximum or minimum occurred during the experiment. Solution mean pH values ranged from 3.8 in the ADB to 7.2 in the poultry manure treatments (Figure 3). Statistically significant trends ($\alpha < 0.05$) of mean solution pH levels over the length of the experiment among treatments followed the sequence PM > $CaCO_3$ > NaF = rye root extract = D-H_2O = Na-hexa-meta-phosphate > FBC > ADB. The pH values remained relatively constant throughout the experiment between 5.2 and 5.8 in the D-H_2O, $CaCO_3$, and NaF treatments. The more drastic changes occurred in the FBC and Na-hexa-metaphosphate treatments, where solution pH dropped from around 6.0 at the beginning of the experiment to 4.0 and 4.8, respectively, indicating significant hydrolysis effects, probably from Al released into solution. The rest of the solutions experienced only minor changes over time, with slight increases in the poultry manure and ryegrass treatments or a slight decrease in the ADB treatment. Even though the poultry manure had the highest solution pH, it showed the lowest overall fragipan slaking potential among the treatments, suggesting that the higher pH was not enough to induce greater dispersion.

Mean solution EC values differed drastically among treatments, being lowest (<70 μS/cm) in the ryegrass root, D-H_2O, and $CaCO_3$ solutions and highest (4,000–22,000 μS/cm) in the ADB and poultry manure treatments (Figure 4). Statistically significant trends ($\alpha < 0.05$) of mean EC solution values among treatments over the length of the experiment followed the sequence PM > ADB > Na-hexa-meta-phosphate = FBC > NaF > $CaCO_3$ > D-H_2O = rye root extract. Even though EC values decreased slightly over time, they likely contributed to fragipan resistance to slaking by inhibiting dispersibility [40]. A similar inhibition may have occurred in the FBC solution where EC values ranged from around 1000 to 840 μS/cm and the pH dropped to 4.0 during the experiment. Mean solution EC values reached maxima at or before the midpoint of the experiment in the D-H_2O and the $CaCO_3$ treatments before reaching the lowest level at the end of the experiment, probably representing a release stage of soluble components followed by a resorption or reprecipitation stage. Decreasing trends in solution EC values were also exhibited by the Na-hexa-meta-phosphate, NaF, and ryegrass root treatments, suggesting a partial reprecipitation or resorption of earlier solubilized fragipan constituents by the relatively large amount of finer aggregates/particles produced during the slaking process.

Mean concentrations of soluble Si released in solution for the different treatments over the course of the experiment are shown in Figure 5. Since Si is assumed to be a main contributor in the cementation of fragipan, higher Si releases were expected to correspond with greater slaking efficiency trends. However, since each amendment solution used had different inherent soluble Si levels at the beginning of the experiment, comparisons accounted only for differences between initial and final or initial and maximum concentrations. Statistically significant trends ($\alpha \leq 0.05$) of mean Si concentrations in solution among treatments for the duration of the experiment followed the sequence ADB > FBC > $CaCO_3$ = D-H_2O = rye root extract > NaF > Na-hexa-meta-phosphate. The highest amounts of Si released into solution (8–10 mg/L) during the slaking experiments were associated with the D-H_2O, $CaCO_3$, FBC, and ADB treatments (Figure 5). These concentrations increased regularly over time for the D-H_2O, and ADB treatments, reaching maximum levels at the conclusion of the experiment, showed a decreasing trend with time in the $CaCO_3$ and FCB treatments, apparently due to reprecipitation. An increasing Si concentration trend with time was also observed with the NaF treatment, but

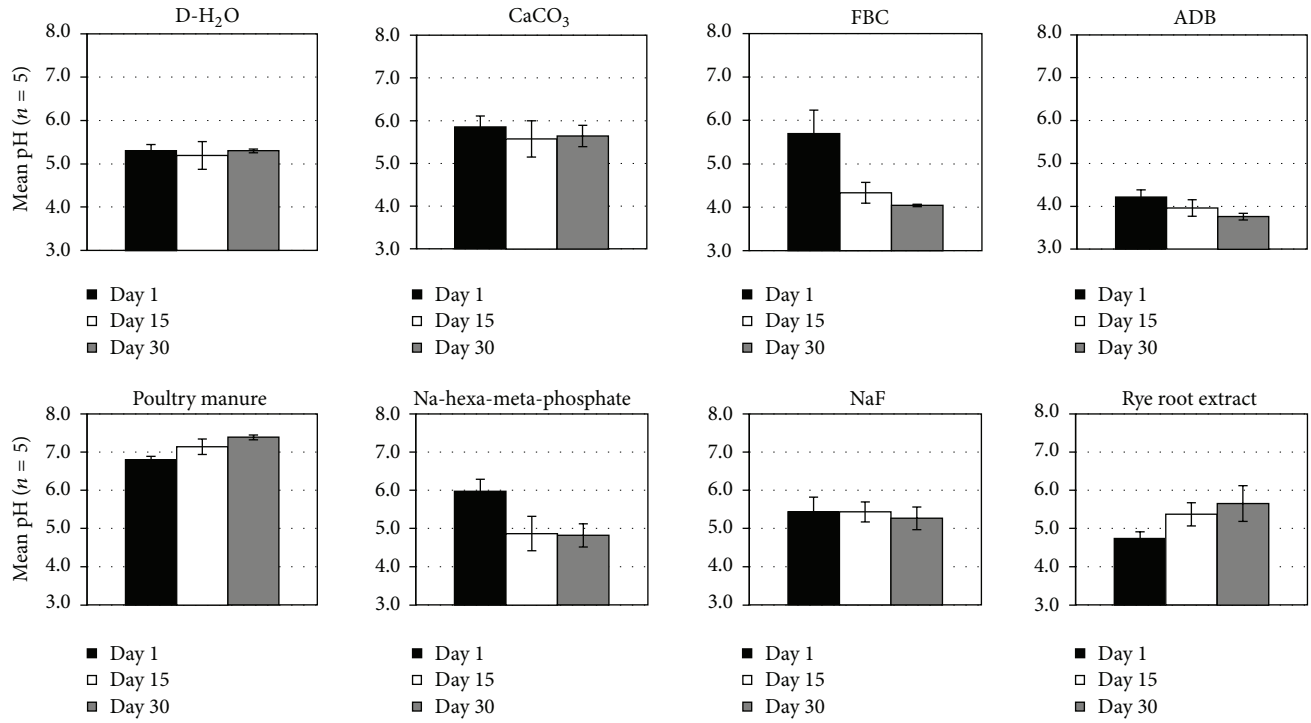

Figure 3: Mean ± SE solution pH levels at the beginning, the end, and the midpoint of the fragipan slaking experiments with the eight amendment treatments.

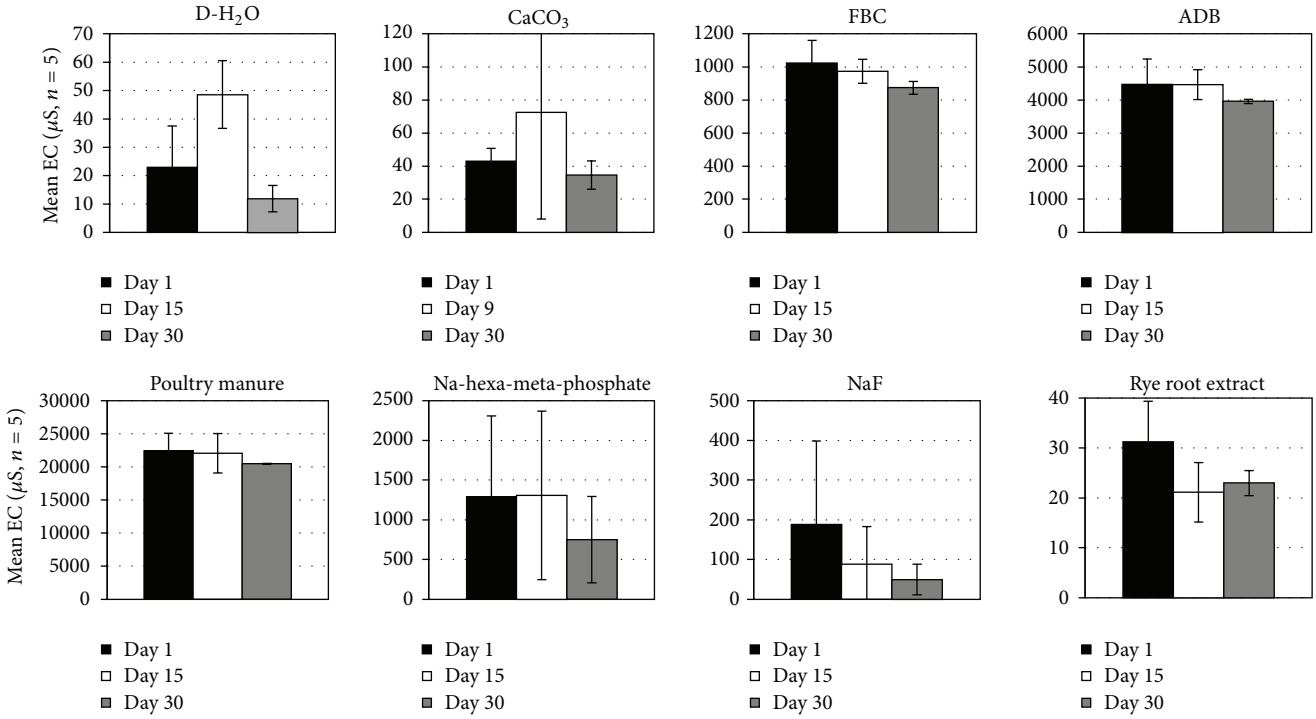

Figure 4: Mean ± SE solution EC levels at the beginning, the end, and the midpoint (or time of maximum level attained) of the fragipan slaking experiments with the eight amendment treatments.

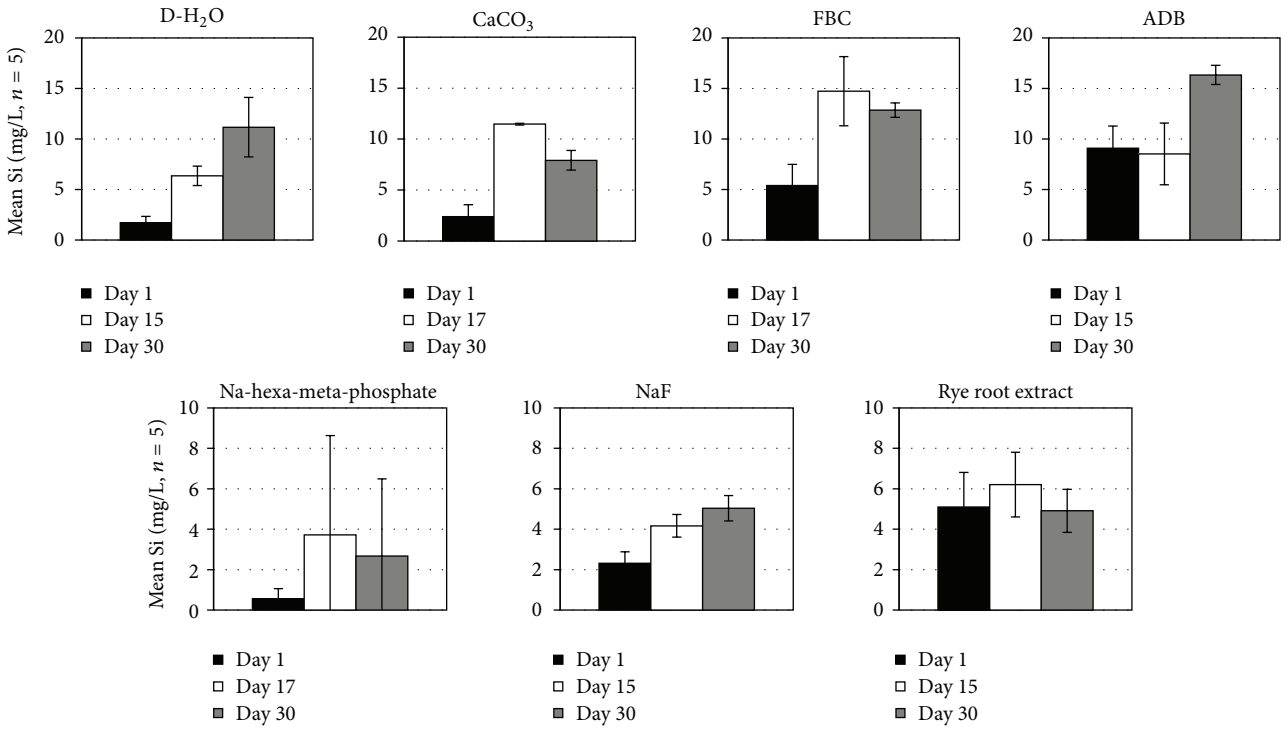

Figure 5: Mean ± SE solution Si concentrations at the beginning, the end, and the midpoint (or time of maximum level attained) of the fragipan slaking experiments with the eight amendment treatments.

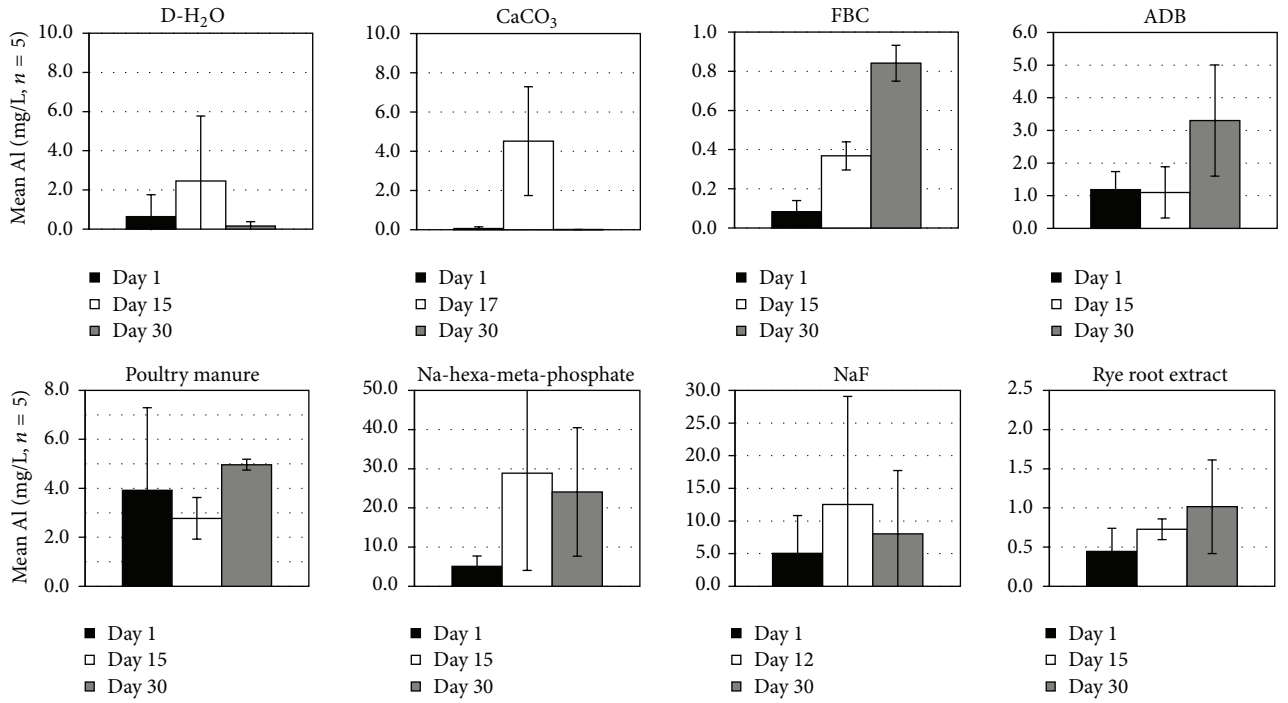

Figure 6: Mean ± SE solution Al concentrations at the beginning, the end, and the midpoint (or time of maximum level attained) of the fragipan slaking experiments with the eight amendment treatments.

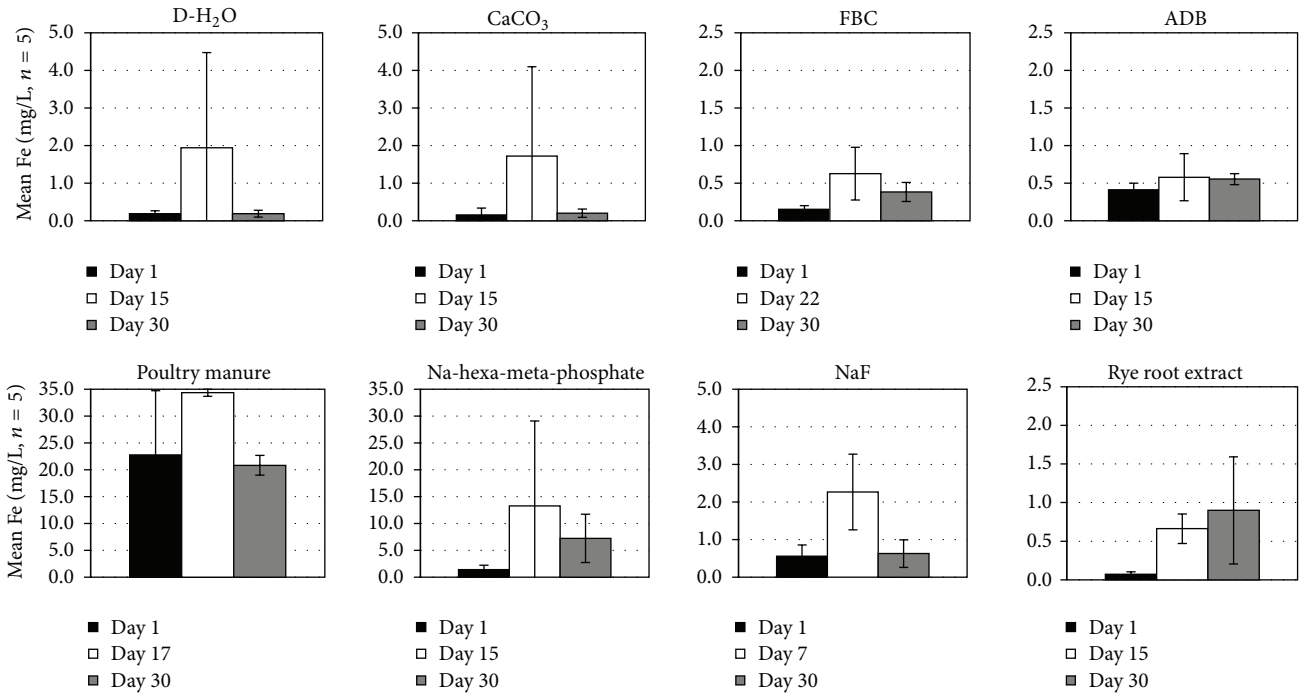

Figure 7: Mean ± SE solution Fe concentrations at the beginning, the end, and the midpoint (or time of maximum level attained) of the fragipan slaking experiments with the eight amendment treatments.

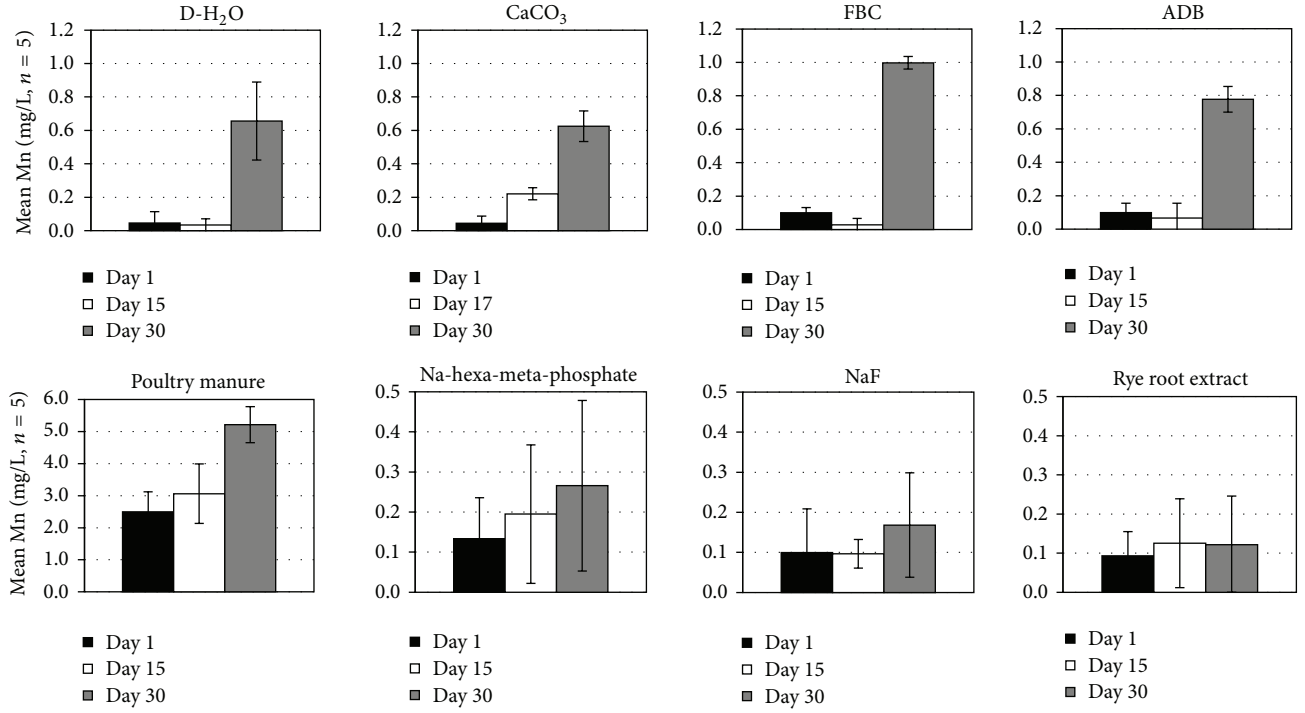

Figure 8: Mean ± SE solution Mn concentrations at the beginning, the end, and the midpoint (or time of maximum level attained) of the fragipan slaking experiments with the eight amendment treatments.

Table 2: Mean ± SE solution concentrations of Ca, Mg, K, Na, and SSR in the fragipan slaking experiments with the eight amendment treatments over the 30-day experimental period.

Treatment	Ca	K	Mg	Na	SSR
			mg L^{-1}		
D-H_2O	0.16 ± 0.08	0.17 ± 0.16	0.01 ± 0.01	0.52 ± 0.17	0.603
$CaCO_3$	0.13 ± 0.05	0.16 ± 0.18	0.01 ± 0.02	1.77 ± 0.88	0.851
FBC	49.95 ± 5.52	0.63 ± 0.10	17.63 ± 2.10	4.94 ± 0.08	0.068
ADB	276.25 ± 7.55	12.75 ± 0.42	76.95 ± 2.55	39.33 ± 3.28	0.097
Poultry manure	73.33 ± 1.89	1852.66 ± 18.27	37.76 ± 1.08	493.0 ± 7.21	0.201
Na-hexa-meta-phosphate	2.16 ± 1.99	0.38 ± 0.02	9.41 ± 8.63	881.90 ± 6.73	0.987
NaF	0.10 ± 0.06	0.15 ± 0.07	0.08 ± 0.03	1055.77 ± 8.40	0.999
Rye root extract	0.67 ± 0.63	3.61 ± 3.08	0.57 ± 0.55	8.03 ± 7.33	0.623

the total amount of Si released was <3 mg/L. The Na-hexa-meta-phosphate and ryegrass root treatments showed Si release maxima around the midpoint of the experiment in the range of 1–3 mg/L before a final drop at the end of the experiment. Soluble Si release was not measured in the poultry manure treatment due to interference with the dissolved organic matter. Surprisingly, the three most effective fragipan slaking treatments (NaF, Na-hexa-metaphosphate, and ryegrass root) as documented by the wet aggregate analysis measurements released the lowest levels of soluble Si levels, suggesting that additional mechanisms may be involved in promoting the slaking of fragipan materials [14].

Mean concentrations of Al, which is another component that along with Si presumably contributes to fragipan rigidity, ranged from <1 to about 25 mg/L, with the highest levels associated with the Na-hexa-meta-phosphate and NaF treatments (Figure 6). Ryegrass root, FBC, and poultry manure treatments had the lowest amounts of Al release. Statistically significant trends ($\alpha < 0.05$) among treatments of mean Al concentrations in solution for the duration of the experiment followed the sequence Na-hexa-meta-phosphate > NaF > PM = ADB = D-H_2O = $CaCO_3$ = rye root extract = FBC. The D-H_2O and $CaCO_3$ treatments showed moderate concentrations that peaked around the midpoint and dropped sharply to near 0 at the end of the experiment, suggesting reprecipitation or resorption processes. Comparing both Si and Al release among treatments, it appears that NaF and Na-hexa-meta-phosphate treatments were most consistent in maintaining moderate to high soluble levels of both by the end of the experiment even though some of the released Al may have been sequestered by formation of AlF complexes or Al-phosphates [41].

Mean soluble Fe levels released during the slaking experiments ranged from <1 to about 12 mg/L (Figure 7). The highest values were observed in the Na-hexa-meta-phosphate and poultry manure solutions and the lowest with the ADB, FBC, and ryegrass root treatments. Statistically significant trends ($\alpha < 0.05$) among treatments of mean Fe concentrations in solution for the length of the experiment followed the sequence PM > Na-hexa-meta-phosphate > $CaCO_3$ = D-H_2O = NaF = rye root extract =ADB = FBC. In most cases (except for the ryegrass root and the ADB treatments) maximum levels of Fe release occurred before the end of the experiment, suggesting the occurrence of resorption or reprecipitation reactions in later stages of treatment. The high levels of Fe released in the poultry solution were more likely the result of anoxic Fe dissolution from organic particles or the surface of the fragipan clods, since very little or no slaking occurred during the treatment [42, 43]. Mean Mn concentrations released in solution were generally low compared to other solution components (<1 to 2.5 mg/L), reaching maximum or near maximum values in the end of the experiment (Figure 8). Significantly higher ($\alpha < 0.05$) Mn concentrations occurred in the poultry manure solution than in the other treatments, where anoxic conditions were more prevalent [43]. Since no or minimum fragipan slaking occurred with poultry manure treatments, most of the Mn released was probably associated with organic particulate material or the surface of the fragipan clods, thus minimizing its potential contribution as a binding component.

Mean concentrations of soluble Ca, Mg, K, and Na in the end of the experiment are shown in Table 2. The ADB, poultry manure, and FBC treatments had significantly higher ($\alpha < 0.05$) Ca (50–276 mg/L) and Mg (17–77 mg/L) levels in solution. The rest of the treatments averaged <2 mg/L Ca and <10 mg/L Mg, with values near 0 for D-H_2O, $CaCO_3$, and NaF solutions. The poultry manure had by far the highest ($\alpha < 0.05$) soluble K levels (1853 mg/L), while the D-H_2O, $CaCO_3$, and NaF solutions the lowest (<0.5 mg/L). The highest Na concentrations ($\alpha < 0.05$) were observed in the NaF, Na-hexa-metaphosphate, and poultry manure solutions (493–1056 mg/L) and the lowest with the D-H_2O and $CaCO_3$ treatments (<1.8 mg/L). A soluble sodium ratio (SSR) function equal to soluble Na/soluble (Ca + Mg + K) was also estimated to further explore the dispersive characteristics of Na relative to other ions since the three weakest slaking treatments (poultry manure, ADB, and FBC) showed the lowest overall ($\alpha < 0.05$) SSR values (Table 2).

3.3. Statistical Relationships. There was no significant relationship between final solution pH and MWD whether considering the entire population of samples used in all treatments or after grouping the samples by treatments showing statistically similar MWD trends. Apparently, either the pH range used in the experiment was not broad enough to significantly impact aggregate size and stability or the effect was

counterbalanced by opposite trends within the same MWD group. A significant relationship ($R^2 = 0.25^*$) was observed between EC and MWD with a tendency for less slaking and larger aggregate size with increasing EC. This is consistent with literature findings that suggest increasing trends of aggregate stabilization at high electrolyte concentrations [44, 45]. This relationship was probably enhanced by the high EC values of the poultry manure, ADB, and FBC solutions which produced the least slaking and the largest size aggregates. A significant relationship was also observed between MWD and Si released in solution ($R^2 = 0.37^{**}$). However, the positive trend between these two variables suggesting higher soluble Si concentrations being associated with lower slaking effects is somewhat surprising. Assuming that the amount of Si released is the result of fragipan degradation, a negative correlation would have been more fitting. However, it is not possible to distinguish between Si released as a result of fragipan matrix breakdown or dissolution from the surface of still intact fragipan clods. Apparently, most of the Si released in the least effective slaking treatments (FBC, ADB, and poultry manure) was associated with the fragipan clod surfaces rather than the interior binding agents and may have been induced by interaction with soluble organics. Indeed, the presence of organic acids has been documented to significantly increase the solubility of siliceous materials through formation of organic complexes [46]. Although this association may have obscured the soluble Si-MWD relationship in the most effective slaking treatments that released low to moderate Si levels, additional slaking mechanisms should not be discounted.

Weak positive trends were also present between MWD and soluble Al ($R^2 = 0.15^*$) and Mn ($R^2 = 0.13^*$), but this relationship was also skewed by the high levels of dissolved organic carbon in treatments with low slaking efficiency that caused increased soluble Mn release from the surface of the clods. Soluble Fe released in solution during the experiment did not show significant correlations with MWD of the fragipan aggregates, implying that its role as a binding agent affecting fragipan resistance to slaking in these experiments was limited or the effect was overshadowed by fragipan surface clod solubility reactions induced by soluble organics. Considering that none of the hypothesized binding agents (Si, Al, Fe, and Mn) have shown the expected statistical trends, it is likely that the slaking of the fragipan clods has been induced by alternative mechanisms not necessarily depending on the dissolution of these components.

The positive correlations of Ca ($R^2 = 0.22^*$), Mg ($R^2 = 0.23^*$), and K ($R^2 = 0.13^*$) in solution with MWD suggested that their role in the slaking process was mostly inhibitive rather than conducive with increasing concentrations [47]. Therefore, low levels of these components in solution and low ionic strength (low EC values) are important for generating a dispersive environment that could weaken fragipan resistance to slaking [48]. Indeed, the treatments showing moderate to high slaking efficiency had low solution EC levels, while the least effective treatments had some of the highest. The importance of a dispersive environment in enhancing the slaking process was demonstrated by the overall negative relationship between MWD and soluble Na ($R^2 = 0.20^*$), which was improved to $R^2 = 0.40^{**}$ when using the SSR function. This underscores the role of Na in excess of other ions in creating an environment conducive to weakening fragipan resistance regardless of the slaking mechanism involved [48]. A multiple regression analysis model including soluble Si and SSR with opposing trends accounted for 52% of the variation ($\alpha < 0.05$) in the MWD of the slaked fragments. Only the addition of soluble K significantly improved the predictability of the model ($R^2 = 70$, $\alpha < 0.05$). Potassium has been reported to exhibit dispersive properties in association with Na in low ionic strength environments [49, 50].

Assuming that the role of binding agents (Si, Al, Fe, and Mn) through dissolution reactions in the slaking process is ambiguous in these experiments, the involvement of Na may be more significant than originally perceived. Soil hydration reactions proceed at a much faster rate in the presence of dilute electrolytes than at higher concentrations. Therefore, the high ionic strength of poultry manure, ADB, and FBC solutions considerably slowed the hydration of fragipan clods. Elevated electrolyte concentrations usually cause increases in the surface tension of water molecules and larger contact angles with the solid surface [44, 49, 51]. Some of these contact angles may have even increased further by organic films coating the surface of fragipan clods in treatments with high levels of dissolved organics (poultry manure, ADB), thus forming a less hydrophilic surface for water penetration [47, 52, 53]. Water infiltration into soil micropores is enhanced when the contact angle of the hydrated ions is relatively small. The contact angle of hydrated Na ions in relatively low ionic strength but high SSR solutions being smaller than that of Ca and Mg will expedite fragipan micropore penetration and increase capillary rise [51, 54]. That can generate a swelling pressure inside the capillaries which causes the entrapped air to implode the fragipan clod along planes of weakness [45, 55, 56]. This is supported by the very small fraction of aggregates below the 2 mm size range, indicating limited dispersion of the fragipan material. Hydrated Ca and Mg ions as well as high electrolyte concentration solutions with low SSR having slower penetration within the capillary space of the fragipan clod allow more time for air diffusion in the water, which reduces the pressure on the matrix and allows it to maintain its original cohesiveness. Similar effects on soil aggregate stability by Na and Ca electrolytes of different strength and SAR values were observed by Abu-Sharar et al. [48] and were attributed to repulsion forces developed within the capillaries that allowed increased shearing stresses to break down the aggregates without significant clay dispersion. Cass and Sumner [57] also reported a random breakdown of soil aggregates along planes of weakness within the matrix of the aggregate rather than at the periphery prior to clay dispersion from the rupturing effect of internal swelling pressure or from shearing stresses in the presence of Na electrolytes.

3.4. Proposed Slaking Mechanism. Based on this evidence, it is likely that the slaking mechanism of the fragipan clods in our experiments may involve at least two steps. During

the first step, fragipan fragmentation occurs with the dispersive action of Na in high SSR solutions, increased capillary rise within the clod matrix, and a swelling pressure build-up that increases shearing stress and causes the rupture of the clod into several fragments [44, 45, 58]. Presence of entrapped air bubbles within the capillaries may accentuate the fragmentation process by building extra pressure and inducing implosion of the clods [53, 56, 58, 59]. The initial fragmentation stage appears to be mainly physical but it may be followed by additional fragmentation steps into smaller aggregates during which physical and possibly chemical dissolution reactions may be involved. During this stage a small number of binding agents (Si, Al, Fe, and Mn) exposed on the surface of broken fragments may be released into solution and accelerate the degradation. Given the low solubility and the slow dissolution kinetics of these agents, a certain amount of the solubilized fraction may reprecipitate or resorb as polymers on the exposed surfaces if the degradation products are not flushed out of the system. In an open soil environment, leaching of these dissolved components away from the fragipan matrix will likely promote further dissolution and expedite fragipan fragmentation. In solutions of high electrolyte concentration with an abundance of Ca or Mg ions, the first stage of fragmentation is inhibited due to less and slower capillary penetration and lower swelling pressure that does not build the critical shearing stress needed to cause meaningful fragipan fragmentation [45]. The slower pace of water movement within the capillaries also allows enough time for the entrapped air to diffuse in the water thus eliminating the build-up of additional pressure on the capillary walls. Since minimal or no fragmentation occurs in these treatments, most of the Si, Al, Fe, or Mn released during the experiments was dissolved from the periphery of the fragipan clods and not from the interior of the fragments. This release may be enhanced by dissolved organic carbon (DOC) in solutions of organic amendments but organic coatings of fragipan surfaces may also inhibit water penetration in the capillaries by creating a semihydrophobic barrier.

4. Conclusions

The findings of these experiments suggested that amendment materials producing solutions with relatively low ionic strength and elevated SSR (NaF, Na-hexa-meta-phosphate, and ryegrass root) create an environment more conducive to fragipan slaking than that of high electrolyte concentrations, Ca, Mg, or DOC enriched solutions (poultry manure, ADB, and FBC). The facilitation of water entry into fragipan capillaries in the presence of Na ions generates the critical swelling pressure and shearing stress to cause fragipan fragmentation. Additional fragmentation with minimal clay dispersion occurs in a follow-up stage during which a moderate number of potential binding agents (Si, Al, Fe, and Mn) are released in solution. These dissolved constituents may polymerize in situ and resorb on the surfaces of the broken fragments if not flushed out of the system. The results suggest that selecting an amendment with low salt content and elevated SSR may produce favorable conditions for fragipan degradation. Currently, we are exploring the potential effects of other Na-based amendments on fragipan slaking before testing these findings under field conditions, which will be the next phase of this project. A potential incorporation of a wetting agent (surfactant) in the applied amendment may facilitate the fragipan fragmentation process.

Conflict of Interests

The authors declare that there is no conflict of interests regarding the publication of this paper.

Acknowledgments

The authors express sincere appreciation to the Kentucky Soybean Association and the Kentucky Small Grain Growers Association for providing funding for this project.

References

[1] J. E. Witty and E. G. Knox, "Identification, role in soil taxonomy and worldwide distribution of fragipans," in *Fragipans: Their Occurrence, Classification and Genesis*, N. E. Smeck and E. J. Ciolkosz, Eds., SSSA Special Publication 24, pp. 1–9, SSSA, Madison, Wis, USA, 1989.

[2] J. G. Bockheim and A. E. Hartemink, "Soils with fragipans in the USA," *Catena*, vol. 104, pp. 233–242, 2013.

[3] D. P. Franzmeier, L. D. Norton, and G. C. Steinhardt, "Fragipan formation in loess of the Midwestern United States," in *Fragipans: Their Occurrence, Classification and Genesis*, N. E. Smeck and E. J. Ciolkosz, Eds., SSSA Special Publication, 24, pp. 69–97, SSSA, Madison, Wis, USA, 1989.

[4] A. D. Karathanasis, "Solution chemistry of fragipans-thermodynamic approach to understanding fragipan formation," in *Fragipans: Their Occurrence, Classification and Genesis*, vol. 24 of *SSSA Special Publication*, pp. 113–139, Soil Science Society of America, Madison, Wis, USA, 1989.

[5] D. L. Lindbo, F. E. Rhoton, W. H. Hudnall, N. E. Smeck, J. M. Bigham, and D. D. Tyler, "Fragipan degradation and nodule formation in glossic fragiudalfs of the lower Mississippi River Valley," *Soil Science Society of America Journal*, vol. 64, no. 5, pp. 1713–1722, 2000.

[6] W. W. Frye, L. W. Murdock, and R. L. Blevins, "Corn yield-fragipan depth relations on a Zanesville soil," *Soil Science Society of America Journal*, vol. 47, no. 5, pp. 1043–1045, 1983.

[7] F. E. Rhoton, "Soybean yield response to various depths of erosion on a fragipan soil," *Soil Science Society of America Journal*, vol. 54, no. 4, pp. 1073–1079, 1990.

[8] M. A. Fairchild, M. S. Coyne, J. H. Grove, and W. O. Thom, "Denitrifying bacteria stratify above fragipans," *Soil Science*, vol. 164, no. 3, pp. 190–196, 1999.

[9] P. A. McDaniel, M. P. Regan, E. Brooks et al., "Linking fragipans, perched water tables, and catchment-scale hydrological processes," *Catena*, vol. 73, no. 2, pp. 166–173, 2008.

[10] J. G. Graveel, D. D. Tyler, J. R. Jones, and W. W. McFee, "Crop yield and rooting as affected by fragipan depth in loess soils in the southeast USA," *Soil and Tillage Research*, vol. 68, no. 2, pp. 153–161, 2002.

[11] R. F. Cullum, "Influence of tillage on maize yield in soil with shallow fragipan," *Soil and Tillage Research*, vol. 119, pp. 1–6, 2012.

[12] W. Szymański, M. Skiba, and S. Skiba, "Fragipan horizon degradation and bleached tongues formation in Albeluvisols of the Carpathian Foothills, Poland," *Geoderma*, vol. 167-168, pp. 340–350, 2011.

[13] D. L. Lindbo and F. E. Rhoton, "Slaking in fragipan and argillic horizons," *Soil Science Society of America Journal*, vol. 60, no. 2, pp. 552–554, 1996.

[14] G. Falsone and E. Bonifacio, "Destabilization of aggregates in some typic Fragiudalfs," *Soil Science*, vol. 171, no. 3, pp. 272–281, 2006.

[15] D. D. Fritton, F. N. Swader, and K. Hoddinott, "Profile modification persistence in a fragipan soil," *Soil Science*, vol. 136, no. 2, pp. 124–130, 1983.

[16] J. M. Bradford and R. W. Blanchar, "The effect of profile modification of a fragiudalf on water extraction and growth by grain sorghum," *Soil Science Society of America Journal*, vol. 44, pp. 374–378, 1980.

[17] J. T. Sims and D. C. Wolf, "Poultry waste management: agricultural and environmental issues," *Advances in Agronomy*, vol. 52, pp. 1–83, 1994.

[18] A. A. Isse, A. F. MacKenzie, K. Stewart, D. C. Cloutier, and D. L. Smith, "Cover crops and nutrient retention for subsequent sweet corn production," *Agronomy Journal*, vol. 91, no. 6, pp. 934–939, 1999.

[19] S. Brown, R. L. Chaney, M. Sprenger, and H. Compton, "Soil remediation using biosolids," *BioCycle*, vol. 43, no. 6, pp. 41–44, 2002.

[20] A. Liu, B. L. Ma, and A. A. Bomke, "Effects of cover crops on soil aggregate stability, total organic carbon, and polysaccharides," *Soil Science Society of America Journal*, vol. 69, no. 6, pp. 2041–2048, 2005.

[21] C. T. Hallmark and N. E. Smeck, "The effect of extractable aluminum, iron, and silicon on strength and bonding of fragipans of northeastern Ohio," *Soil Science Society of America Journal*, vol. 43, pp. 145–150, 1979.

[22] L. D. Norton, G. F. Hall, N. E. Smeck, and J. M. Bigham, "Fragipan bonding in a late-Wisconsinan loess-derived soil in East- Central Ohio," *Soil Science Society of America Journal*, vol. 48, no. 6, pp. 1360–1366, 1984.

[23] M. M. Duncan and D. P. Franzmeier, "Role of free silicon, aluminum, and iron in fragipan formation," *Soil Science Society of America Journal*, vol. 63, no. 4, pp. 923–929, 1999.

[24] M. A. Wilson, S. J. Indorante, B. D. Lee et al., "Location and expression of fragic soil properties in a loess-covered landscape, Southern Illinois, USA," *Geoderma*, vol. 154, no. 3-4, pp. 529–543, 2010.

[25] W. Szymański, M. Skiba, and S. Skiba, "Origin of reversible cementation and brittleness of the fragipan horizon in Albeluvisols of the Carpathian Foothills, Poland," *Catena*, vol. 99, pp. 66–74, 2012.

[26] M. L. Norfleet and A. D. Karathanasis, "Some physical and chemical factors contributing to fragipan strength in Kentucky soils," *Geoderma*, vol. 71, no. 3-4, pp. 289–301, 1996.

[27] F. E. Rhoton, J. H. Edwards, and L. D. Norton, "Physical and chemical properties of fragipan horizon materials amended with fluidized bed combustion ash," *Soil Science*, vol. 166, no. 7, pp. 465–474, 2001.

[28] B. Hermawan and A. A. Bomke, "Effects of winter cover crops and successive spring tillage on soil aggregation," *Soil and Tillage Research*, vol. 44, no. 1-2, pp. 109–120, 1997.

[29] S. M. Dabney, "Cover crop impacts on watershed hydrology," *Journal of Soil and Water Conservation*, vol. 53, no. 3, pp. 207–213, 1998.

[30] P. W. Unger and M. F. Vigil, "Cover crop effects on soil water relationships," *Journal of Soil and Water Conservation*, vol. 53, no. 3, pp. 200–207, 1998.

[31] J. W. Singer and K. A. Kohler, "Rye cover crop management affects grain yield in a soybean-corn rotation," 2005.

[32] G. W. Feyereisen, B. N. Wilson, G. R. Sands, J. S. Strock, and P. M. Porter, "Potential for a rye cover crop to reduce nitrate loss in Southwestern Minnesota," *Agronomy Journal*, vol. 98, no. 6, pp. 1416–1426, 2006.

[33] M. Plumer, *Effect of Tillage and Annual Ryegrass Cover Crop on Corn Yield*, University of Illinois Extension, 2008.

[34] M. Plumer, *Annual Ryegrass Variety Report*, University of Illinois Extension, 2012.

[35] J. R. Crush, L. Ouyang, J. P. J. Eerens, and A. V. Stewart, "The growth of roots of perennial, Italian, hybrid and annual ryegrasses through a high-strength root medium," *Grass and Forage Science*, vol. 57, no. 4, pp. 322–328, 2002.

[36] J. R. Hirth, B. M. McKenzie, and J. M. Tisdall, "Ability of seedling roots of *Lolium perenne* L. to penetrate soil from artificial biopores is modified by soil bulk density, biopore angle and biopore relief," *Plant and Soil*, vol. 272, no. 1-2, pp. 327–336, 2005.

[37] Z. C. Zhou and Z. P. Shangguan, "The effects of ryegrass roots and shoots on loess erosion under simulated rainfall," *Catena*, vol. 70, no. 3, pp. 350–355, 2007.

[38] NRCS, "Soil Survey Laboratory Methods Manual," Soil Survey Investment Report 42, Version 3.0. USDA, National Soil Survey Center, Lincoln, Neb, USA, 1996.

[39] W. D. Kemper and R. C. Rosenau, "Aggregate stability and size distribution," in *Methods of Soil Analysis, Part 1: Physical Methods*, A. Klute, Ed., SSSA Book Series No. 9, pp. 425–442, SSSA, Madison, Wis, USA, 2nd edition, 1986.

[40] J. R. Nimmo and K. S. Perkins, "Aggregate stability and size distribution," in *Methods of Soil Analysis, Part 4—Physical Methods*, J. H. Dane and G. C. Topp, Eds., pp. 317–328, Soil Science Society of America, Madison, Wis, USA, 2002.

[41] W. L. Lindsay, *Chemical Equilibria in Soils*, John Wiley & Sons, New York, NY, USA, 1979.

[42] J. G. McColl and A. A. Pohlman, "Soluble organic acids and their chelating influence on A1 and other metal dissolution from forest soils," *Water, Air, and Soil Pollution*, vol. 31, no. 3-4, pp. 917–927, 1986.

[43] N. S. Bolan, A. A. Szogi, T. Chuasavathi, B. Seshadri, M. J. Rothrock, and P. Panneerselvam, "Uses and management of poultry litter," *World's Poultry Science Journal*, vol. 66, no. 4, pp. 673–698, 2010.

[44] G. J. Levy, A. I. Mamedov, and D. Goldstein, "Sodicity and water quality effects on slaking of aggregates from semi-arid soils," *Soil Science*, vol. 168, no. 8, pp. 552–562, 2003.

[45] M. N. Wuddivira, E. I. Ekwue, and R. J. Stone, "Modelling slaking sensitivity to assess the degradation potential of humid tropic soils under intense rainfall," *Land Degradation and Development*, vol. 21, no. 1, pp. 48–57, 2010.

[46] P. Bennett and D. I. Siegel, "Increased solubility of quartz in water due to complexing by organic compounds," *Nature*, vol. 326, no. 6114, pp. 684–686, 1987.

[47] A. Solé, F. Plana, F. Gallart, R. Josa, G. Pardini, and R. Aringhieri, "How mudrock and soil physical properties influence badland formation at Vallcebre (Pre-Pyrenees, NE Spain)," *Catena*, vol. 19, no. 3-4, pp. 287–300, 1992.

[48] T. M. Abu-Sharar, F. T. Bingham, and J. D. Rhoades, "Stability of soil aggregates as affected by electrolyte concentration and composition," *Soil Science Society of America Journal*, vol. 51, no. 2, pp. 309–314, 1987.

[49] P. Leroy, A. Lassin, M. Azaroual, and L. André, "Predicting the surface tension of aqueous 1:1 electrolyte solutions at high salinity," *Geochimica et Cosmochimica Acta*, vol. 74, no. 19, pp. 5427–5442, 2010.

[50] J. Shang, M. Flury, J. B. Harsh, and R. L. Zollars, "Contact angles of aluminosilicate clays as affected by relative humidity and exchangeable cations," *Colloids and Surfaces A: Physicochemical and Engineering Aspects*, vol. 353, no. 1, pp. 1–9, 2010.

[51] M. Goebel, S. K. Woche, and J. Bachmann, "Quantitative analysis of liquid penetration kinetics and slaking of aggregates as related to solid-liquid interfacial properties," *Journal of Hydrology*, vol. 442-443, pp. 63–74, 2012.

[52] J. C. Van Dam, J. H. M. Wösten, and A. Nemes, "Unsaturated soil water movement in hysteretic and water repellent field soils," *Journal of Hydrology*, vol. 184, no. 3-4, pp. 153–173, 1996.

[53] H. Zaher and J. Caron, "Aggregate slaking during rapid wetting: hydrophobicity and pore occlusion," *Canadian Journal of Soil Science*, vol. 88, no. 1, pp. 85–97, 2007.

[54] A. Marmur, "Penetration of a small drop into a capillary," *Journal of Colloid And Interface Science*, vol. 122, no. 1, pp. 209–219, 1988.

[55] W. D. Kemper, R. Rosenau, and S. Nelson, "Gas displacement and aggregate stability of soils," *Soil Science Society of America Journal*, vol. 49, no. 1, pp. 25–28, 1985.

[56] H. Zaher, J. Caron, and B. Ouaki, "Modeling aggregate internal pressure evolution following immersion to quantify mechanisms of structural stability," *Soil Science Society of America Journal*, vol. 69, no. 1, pp. 1–12, 2005.

[57] A. Cass and M. E. Sumner, "Soil pore structural stability and irrigation water quality: i. Empirical sodium stability model," *Soil Science Society of America Journal*, vol. 46, no. 3, pp. 503–506, 1982.

[58] W. W. Emerson, "Aggregate slaking and dispersion class, bulk properties of soil," *Australian Journal of Soil Research*, vol. 32, no. 2, pp. 173–184, 1994.

[59] Y. Le Bissonnais, "Aggregate stability and assessment of soil crustability and erodibility: I. Theory and methodology," *European Journal of Soil Science*, vol. 47, no. 4, pp. 425–437, 1996.

Hindawi Publishing Corporation
The Scientific World Journal
Volume 2014, Article ID 913852, 12 pages
http://dx.doi.org/10.1155/2014/913852

Research Article

Soil Diversity as Affected by Land Use in China: Consequences for Soil Protection

Wei Shangguan,[1] Peng Gong,[2,3,4] Lu Liang,[2] YongJiu Dai,[1,4] and Keli Zhang[5]

[1] *State Key Laboratory of Earth Surface Processes and Resource Ecology, College of Global Change and Earth System Science, Beijing Normal University, Beijing 100875, China*
[2] *Ministry of Education Key Laboratory for Earth System Modeling, Center for Earth System Science, Tsinghua University, Beijing 100084, China*
[3] *Department of Environmental Science, Policy and Management, University of California, Berkeley, CA 94720, USA*
[4] *Joint Center for Global Change Studies, Beijing 100875, China*
[5] *School of Geography, Beijing Normal University, Beijing 100875, China*

Correspondence should be addressed to Wei Shangguan; shanggv@bnu.edu.cn

Received 21 April 2014; Revised 17 July 2014; Accepted 5 August 2014; Published 27 August 2014

Academic Editor: Antonio Paz González

Rapid land-use change in recent decades in China and its impact on terrestrial biodiversity have been widely studied, particularly at local and regional scales. However, the effect of land-use change on the diversity of soils that support the terrestrial biological system has rarely been studied. Here, we report the first effort to assess the impact of land-use change on soil diversity for the entire nation of China. Soil diversity and land-use effects were analyzed spatially in grids and provinces. The land-use effects on different soils were uneven. Anthropogenic soils occupied approximately 12% of the total soil area, which had already replaced the original natural soils. About 7.5% of the natural soil classes in China were in danger of substantial loss, due to the disturbance of agriculture and construction. More than 80% of the endangered soils were unprotected due to the overlook of soil diversity. The protection of soil diversity should be integrated into future conservation activities.

1. Introduction

As human impacts on environment reach farther and deeper into relatively undisturbed areas of the world, we begin to protect or conserve various components of the earth that we have valued from ancient times [1]. In the last several decades, the concern over the fate of biological diversity has led to more efforts devoted to the monitoring and protection of the complete variety of genes, species, and ecosystems [2]. It has been widely recognized that one of the major consequences of land use is the loss of biodiversity [3]. However, soils, as the foundation of the terrestrial ecosystems, are rarely given careful consideration in the development of biodiversity and geodiversity planning. Amundson et al. [4] conducted the first comprehensive assessment of the human impact on soil diversity in the USA by defining four types of rare or uncommon soils. Papa et al. [5] found that land-use change was a cause of loss of pedodiversity in Sicily. The possible use of the concept of pedodiversity to select and delineate natural soil reserves has been discussed, and the damage of urbanization to top quality soils has been widely recognized [6–10]. China, as the most populated country in the world, has experienced tremendous land-use change in the past few decades. The pressure on soil resources in China has been widely recognized [11, 12]. However, a comprehensive study on the effect of land use on soil diversity in rapidly developing countries, such as China, does not exist. Such a study is urgently needed before rare natural soil heritages are ruined without even being noticed.

Here, we investigated the abundance and rarity of soils at the national scale of China. Then, we assessed land-use effects on soil diversity and mapped the distribution of endangered soils in China due to agricultural expansion and urbanization. Finally, we assessed the extent of protection of endangered soils by nature reserves.

Table 1: Number of taxa or map units at taxonomic levels in China.

Taxonomic level	Number of taxa in GSCC[a]	Number of map units[b]	Number of taxa in soil profiles[c]
Order	12	—	—
Suborder	29	—	—
Great group	61	22	17
Subgroup	231	215	129
Family	909	688	199
Specie	—	—	7477

[a]GSCC, Genetic Soil Classification of China.
[b]Map units in the 1 : 1,000,000 soil map of China.
[c]This is according to the most detailed taxonomic information of a soil profile.

2. Materials and Methods

2.1. Definition of Soil Diversity. In this study, soil diversity was quantified using both a soil map and a soil profile data set (described in the next section), which have been developed within the framework of the Genetic Soil Classification of China (GSCC) [14]. The GSCC contains six hierarchical levels including order, suborder, great group, subgroup, family, and species. Table 1 shows the summary of the current number of taxa at different taxonomic levels of the GSCC. Table 2 shows the distribution patterns and major distinguishing characteristics of the 11 soil orders.

We used two simple numerical measurements to quantify soil diversity [4]: (a) "taxon density": number of taxa/area by region and (b) "taxon abundance": total area of each soil class in a region. In the following sections, "soil classes" only include soil taxa at the great group, subgroup, and family levels if not specified otherwise. We defined rare and uncommon soils based on the number of taxa at a soil taxonomic level because the rarity of the soils depends on the soil taxonomic level (high level soil classes have fewer taxa than low level ones and occupy more area), so that the rarity of different taxonomic levels is comparable and it can be made better by the use of the taxonomic information of the soil map. Thus, the taxonomic level of the soil map (Figure 1) should be referenced when the soil diversity is analyzed.

The definitions of rare and uncommon soils are as follows: (a) rare soils: less than 200, 600, and 2,000 km^2 at the family, subgroup, and great group levels, respectively; (b) unique soils: existing in only one province; (c) rare-unique soils: occurring in only one province, whose total area is less than 2,000, 6,000, and 20,000 km^2 at the family, subgroup, and great group levels, respectively. Finally, for those natural soils (anthropogenic soils were excluded), we defined (d) endangered soils as (1) those rare or rare-unique soils that have lost more than 50% of their area due to various land disturbance by agriculture and construction, (2) those soils (regardless of whether they are rare) that have lost more than 50% of their area to land disturbance and that have less than 100, 300, and 1,000 km^2 of undisturbed area at the family, subgroup, and great group levels, respectively, or (3) those unique soils that have lost more than 50% of their area to land disturbance and that have less than 1,000, 3,000, and 10,000 km^2 of undisturbed area at the family, subgroup, and great group levels, respectively. The second and third types of endangered soils have similar undisturbed areas of the first type, which is a logical extension of the definition of Amundson et al. [4]. Soils with 90–100% of their total area disturbed are defined as extinct.

2.2. Data Acquisition and Analysis. The two soil datasets that have been used in this study were the 1 : 1,000,000 soil map of China [13] (Figure 1) and the 8,979 soil profiles [15] (Figure 2) classified by GSCC, both of which were compiled from the Second National Soil Survey of China conducted in the 1980s. The soil map was based on field sampling (including the soil profiles used in this paper), remotely sensed data, and expert knowledge. This soil map was used to calculate the area of different soils. Each of the 925 soil map units in the soil map contains only one soil class, which are at the great group, subgroup, or family levels (Table 1 and Figure 1).The concept of soil map unit was demonstrated in our previous paper [16]. There are a number of soil polygons belonging to a soil map unit in the soil map. There are fewer classes at each soil taxonomic level in the soil map than the GSCC system, because some soils were not considered in the process of map generalization. The area of soil map polygons (overall 94303 polygons) was tabulated to obtain the total area of a soil class in China. There are 7822 different soil classes of soil profiles, and 7477 of them are at the soil species level (Table 1). However, we only used the soil taxonomic information at the family or higher taxonomic levels to assess soil diversity for the convenience of comparing with the soil map.

Soil disturbance in China was determined using the 1 km Grid China Land Use Data (GCLU) of 2005 [17]. To obtain the number and location of the endangered soils, the cultivated land and construction land layers were overlaid with the soil map. In the soil map, the rare and rare-unique soils were identified according to their definition. Then, we analyzed soil diversity by provinces and equal-area grids. Various grid sizes were tested, and finally the 100 km × 100 km grid size was chosen because it can show enough spatial details with a moderate number of grids. In addition, the 1 km GCLU data derived for late 1980s, 1995, and 2000 were also used in our analysis using the same procedure. As a result, the land-use effect on the soils over time could be assessed. The above spatial analyses were done using the ArcGIS software.

The endangered status of soil profiles was determined according to the results of the analysis based on the soil map. If a soil class on the soil map was endangered, the soil profiles belonging to this class were also considered endangered, or vice versa.

3. Results

3.1. Soil Diversity. Grids with a high quantity of soil orders were located in the northwest, northeast, and southwest of China (Figure 3(a)). The distributions of soil diversity at the soil suborder, great group, and subgroup levels had similar spatial patterns with those at the order level but they have been demonstrated to be less abundant in the northeast. The spatial pattern of the number of taxonomic classes at lower

Table 2: Distribution and brief description of characteristics of the soil orders in China.

Order	Distribution	Characteristics
Alfisols	Humid region	Calcium carbonate leached well, acid or neutral, clay-enriched B horizons
Semi-Alfisols	Semihumid region	Weak leaching, neutral to slight alkaline, calcium carbonate illuviated, argillation of different degree
Pedocals	Semiarid and arid regions	Horizons with off-white lime
Aridisols	Arid region	Arid A horizons and any other subhorizons
Desert soils	Most arid region	Hydromica as major clay mineral, crust with vesicles and platy horizon, horizon with rich gypsum and salt
Amorphic soils	Azonal	Week pedogenesis, characteristics of parent material
Semiaqueous soils	Intrazonal	Groundwater invasion or temporarily stagnant water, soil humification surface horizon and rust horizon of oxidation-reduction
Aqueous soils	Intrazonal	Surface water or groundwater near the surface, crude humification or peat surface layer, gley horizon
Alkaline-saline soils	Intrazonal	Soil property and profile change caused by soil salt or alkalization, no crops
Anthrosols	Nonzonal	Characters caused by long period of cultivation
Alpine soils	Plateau and alpine area	Week humification, freezing-thawing morphology, low soil depth, coarse soil texture, low mineral chemical decomposition
Ferralsols	Warm-wet climate zone	Desilication, Fe and Al enriched, bioaccumulation

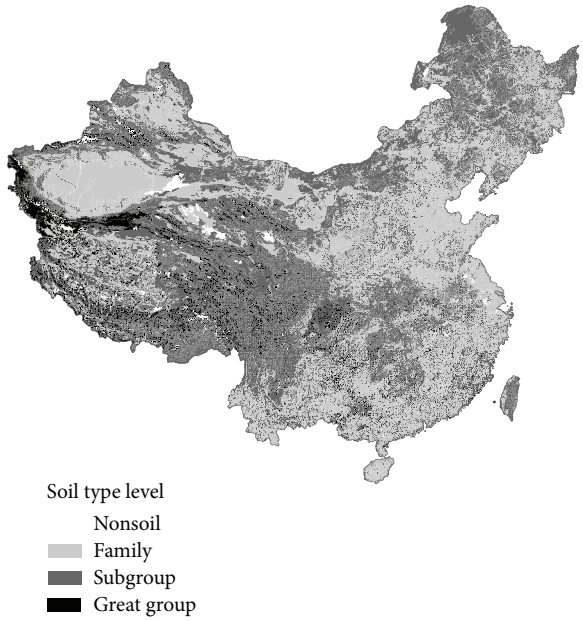

Figure 1: Soil taxonomic level of the 1 : 1,000,000 soil map of China [13].

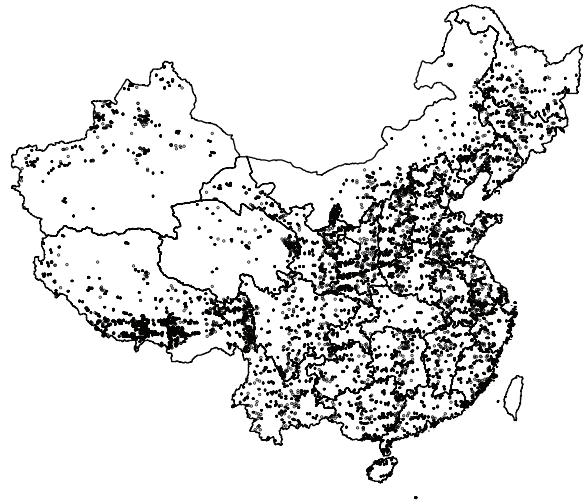

Figure 2: Location of soil profiles of China [15].

hierarchical levels per grid was quite different (Figure 3(b)). Grids with higher numbers of soil classes were located in the northwest, the north, the southern part of the southwest, and the northern part of the southeast. Areas with either low or high temperature or rainfall had low pedodiversity, as climate becomes the major limiting factor to soil formation [18]. The soil diversity at high levels (subgroup and above) was mainly a reflection of bioclimate (for zonal soils) and hydrologic (for intrazonal soils) factors. As the GSCC takes the local variation of soil-forming factors into account at the soil family level, soil diversity was mainly a reflection of the difference in parent material, topography, and hydrologic conditions. However, due to the incomplete information at the soil family level in the soil map of China some families were absent from the maps of soil diversity distribution, particularly in the south, northeast, and the northern part of southwest (Figure 1), where the presence of more soil families was expected due to the diversity of soil-forming factors in these areas.

The distributions of soil diversity based on the soil profiles were quite different from that based on the soil map (Figure 3). This was due to the distinct sampling density of

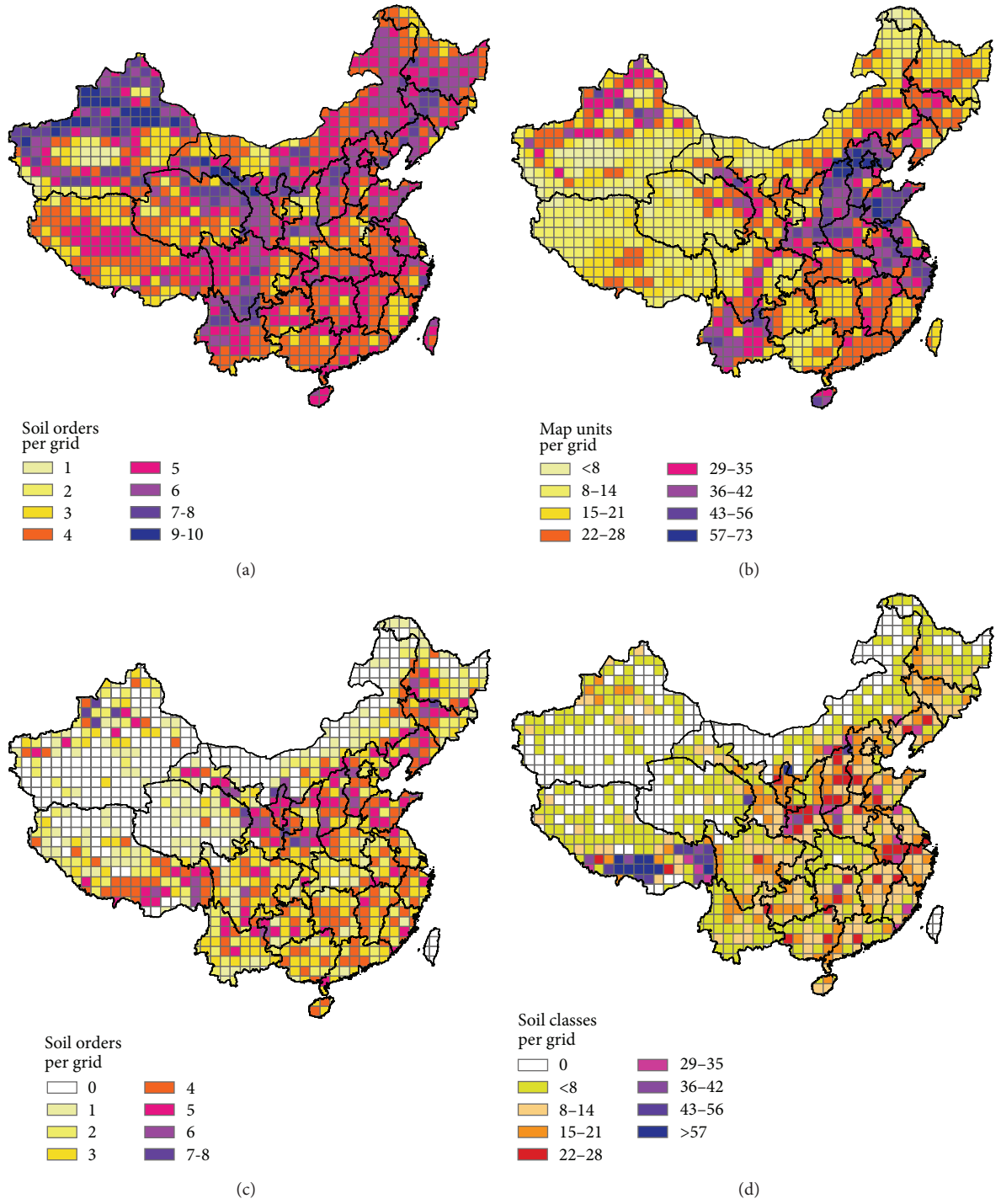

Figure 3: Soil orders (a) and soil map units at lower taxonomic levels (b) per grid in China based on soil map and soil orders (c) and soil classes at lower taxonomic levels (d) per grid in China based on soil profiles. Each grid is 100 km × 100 km in area. (The taxonomic level of the soil map is shown in Figure 1.)

the soil profiles in different areas. Most of the provinces had fewer soil orders based on the soil profiles than based on the soil map, which indicated that the taxonomic coverage of the soil profiles was not good at the soil order level. On the other hand, most provinces had more soil classes based on the soil profiles than those based on the soil map, particularly Tibet, which had a much more detailed soil profile database. As a result, the current soil map did not represent all the soil classes in the soil profiles and there should be more soil classes. Due to the above analysis, the actual soil diversity in China is expected to be much higher than the diversity shown by the available data.

Soil diversity was also analyzed by province (Table 3). Gansu, Inner Mongolia, Qinghai, Shanxi, and Xinjiang had soils belonging to 11 different orders. The first four provinces are located in the transition zone of the semihumid to semiarid and arid climates, while Xinjiang has a wide range and vertical soil zones on the mountains. With the exception of Ferralsols, all of the remaining soil orders existed in these provinces because of their diversified soil-forming conditions. On the contrary, the diversity of the soil orders was not high in the tropic and subtropical provinces, where only one kind of zonal soils (i.e., Ferralsols) existed. In terms of the number of soil map units at the great group, subgroup, or family levels, Hebei had the greatest number (235), followed by Xinjiang (218), Inner Mongolia (207), and Henan (168). For the number of soil taxa per 10,000 km^2, Hainan had the highest density (21.79), followed by Jiangsu (13.9), Ningxia (12.76), and Taiwan (12.32), while Tibet (0.88) and Xinjiang (1.33) had the lowest.

3.2. Land Use and Soil Diversity. There are 231 anthropogenic soils on the soil map of China, which occupy approximately 12% of the nation's total soil area. These anthropogenic soils developed under long periods of cultivation [19], and their properties are quite different from their natural counterparts. As anthropogenic soils have already replaced the original natural soils, they were excluded when assessing land-use effects in the recent 3 decades on soil diversity.

Two types of land-use effects (i.e., construction and cultivation) were assessed in this study. Soils become exposed to big changes due to the intensive human disturbance. They are not likely to remain the same as their natural counterparts. Mankind can be as a soil forming factor, and it may create new soils such as anthropogenic soils. However, the original natural soils do not exist anymore even if the pedodiversity increased, and this may cause threats to some soils or even lead to soil extinction. Although construction land occupies only 0.18 million km^2 (approximately 1.98%), rapid urbanization in China was considered a great threat to soil protection and food security [12]. Figure 4 shows 359 soils in the soil map which had 50% or more of their area impacted by cultivation and construction, regardless of their total extent. Overall, 52% of the profiles are highly impacted by construction or cultivation.

At the soil order and great group levels, certain soils are more heavily affected by construction and cultivation than others as a result of uneven development of construction and cultivation activities (Table 4). All of the anthropogenic soils had high percentages of impacted area (approximately 60% or more). With the exception of Anthrosols, the four soil orders with the greatest areas of disturbance were: semiaqueous soils (62%), semi-Alfisols (45%), Pedocal (24%), and Ferralsols (20%). For natural soils at the great group level, the impact of land use was not equal. Black soils, which are distributed in the plains of northeast China, were most heavily disturbed (80%) due to their high content of organic matter, which benefits crop growth. Other soils that were highly devoted to agricultural land include yellow-cinnamon soils (67%), albic soils (52%), dark loessial soils (49%), purplish soils (45%), castano-cinnamon soils (44%), red clay soils (44%), and cinnamon soils (42%). With the exception of cold brown calcic soils, all of the soils in the Alpine soil order were nearly undisturbed. Although amorphic soils are immature soils, most great groups of this order were relatively heavily disturbed (over 40% of their area).

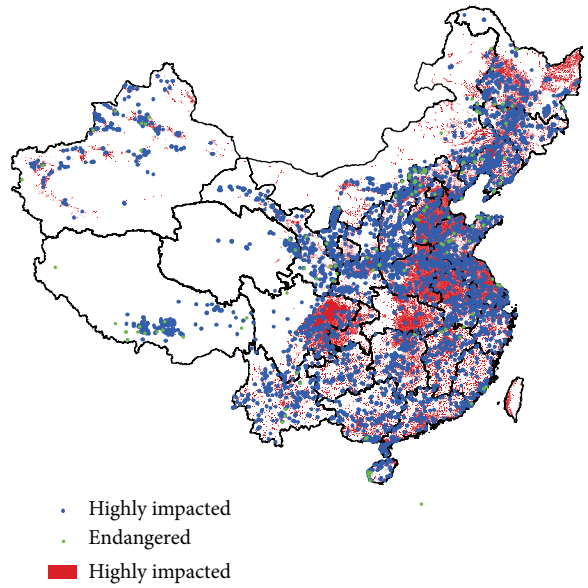

Figure 4: Soils that have 50% or more of their area impacted by construction and cultivation (the taxonomic level of the soil map is shown in Figure 1).

3.3. Unique, Rare, and Rare-Unique Soils. "Soil endemism" refers to soils occupying very small areas in a geographical distribution [20]. Most soils existed in five or fewer provinces (approximately 81% of the total), and only 71 soils appeared in more than ten provinces. 302 soils were identified as unique soils in China. Xinjiang has the greatest number of unique soils (75), followed by Tibet (30), Hebei (29), Qinghai (22), and Yunnan (22).

We found 332 rare or rare-unique soils, occupying 1.3% of China's land area. Figure 5 shows that the rare or rare-unique soils were distributed mainly in the north, east, southwest, and northwest of China. Table 4 shows the number of rare or rare-unique soils in each province. Xinjiang had the greatest number of rare or rare-unique soils (64), followed by Hebei (54), Shanxi (27), Qinghai (26), and Tibet (24). In terms of rare or rare-unique soil density, Hainan led the nation (3.6 soil cs per 10,000 km^2), followed by Hebei (2.5), Shanxi (1.7), Jiangsu (1.6), and Zhejiang (1.6).

3.4. Endangered Soils. A total of 88 endangered soils with a total area of 19.2 thousand km^2 were found in China, occupying approximately 0.2% of China's land area (Table 4, Figure 6(a)). Most endangered soils were located in the north of China. Hebei had the greatest number of endangered soils (37), followed by Shanxi (19), Shandong (14), and Henan (11). With respect to endangered soil density, these provinces also

Table 3: (a) Soil diversity and rarity, by province, for China based on the 1,000,000 soil map of China [13]. (b) Number of endangered soils caused by cultivation and construction.

(a)

Province[a]	Order	Number				Ratio of endangered soil to rare soil[d]	Number/10,000 km^2		
		Map units[b]	Rare plus rare-unique	Endangered	Extinct[c]		Map units	Rare plus rare-unique	Endangered
Anhui	8	130	12	2	1	0.17	9.28	0.86	0.14
Fujian	6	48	1	0	0	0.00	3.96	0.08	0.00
Gansu	11	157	10	1	0	0.10	3.88	0.25	0.02
Guang-dong	6	68	3	1	0	0.33	3.83	0.17	0.06
Guangxi	6	75	10	2	1	0.20	3.17	0.42	0.08
Guizhou	5	51	1	0	0	0.00	2.90	0.06	0.00
Hainan	6	73	12	3	0	0.25	21.79	3.58	0.90
Hebei	8	235	54	37	6	0.69	10.92	2.51	2.04
Henan	8	168	23	11	5	0.48	10.14	1.39	0.66
Heilong-jiang	9	76	11	2	1	0.18	1.68	0.24	0.04
Hubei	6	96	5	1	0	0.20	5.17	0.27	0.05
Hunan	6	58	1	0	0	0.00	2.74	0.05	0.00
Jilin	9	92	12	6	1	0.50	4.82	0.63	0.31
Jiangsu	8	149	17	3	2	0.18	13.90	1.59	0.28
Jiangxi	5	67	4	0	0	0.00	4.01	0.24	0.00
Liaoning	8	101	9	3	0	0.33	6.97	0.62	0.21
Inner Mongolia	11	207	20	9	0	0.45	1.80	0.17	0.08
Ningxia	10	66	6	0	0	0.00	12.76	1.16	0.00
Qinghai	11	130	26	2	0	0.08	1.81	0.36	0.03
Shandong	7	148	19	14	3	0.74	9.59	1.23	0.91
Shanxi	9	149	27	19	3	0.70	9.51	1.72	1.21
Shaanxi	11	133	11	0	0	0.00	6.46	0.53	0.00
Sichuan	8	114	10	2	0	0.20	2.35	0.21	0.04
Taiwan	6	44	4	1	0	0.25	12.32	1.12	0.28
Tibet	9	106	24	1	0	0.04	0.88	0.20	0.01
Xinjiang	11	218	64	3	0	0.05	1.33	0.39	0.02
Yunnan	9	148	22	1	0	0.05	3.87	0.57	0.03
Zhejiang	7	117	16	3	1	0.19	11.37	1.56	0.29
Chong-qing	5	43	1	0	0	0.00	5.21	0.12	0.00

[a]Some small administration districts were merged into adjacent provinces. Hong Kong and Macao were merged into Guangdong, Beijing and Tianjin were merged into Hebei, and Shanghai was merged into Jiangsu.

[b]The map units are at the great group, subgroup, or family levels.

[c]The endangered soils in China and the percentage of their area that has been disturbed by cultivation and construction are given in Table 3(b).

[d]Number of endangered soils can be bigger than the rare plus rare-unique soils because some endangered soils are not rare plus rare-unique soils.

(b)

Percent of disturbed area	Cultivation/construction[a]	Construction (>20)[b]
50–60	21	1
60–70	19	0
70–80	13	0
80–90	18	1
90–100	17	4
Total	88	6

[a]Number of endangered soils in China with percentage of land (as defined in column 1) devoted to combined cultivation and construction use.

[b]Number of endangered soils in China with more than 20% land devoted to construction use.

Table 4: Percentage of soil order and great group affected by development in China.

Order	%			En[c]	Great group	%			En[c]
	Con[a]	Cul[b]	Total			Con[a]	Cul[b]	Total	
Alfisols	1.49	18.21	19.70	6	Brown coniferous forest soils	0.04	0.21	0.25	
					Brown earths	0.00	0.00	0.00	
					Yellow-brown earths	0.37	16.82	17.20	
					Yellow-cinnamon soils	8.84	67.10	75.94	
					Brown earths	2.86	22.59	25.45	6
					Dark-brown earths	0.43	10.15	10.58	
					Albic soils	2.74	51.74	54.48	
Semi-Alfisols	4.94	39.62	44.57	24	Torrid red soils	1.70	28.97	30.67	2
					Cinnamon soils	6.43	42.49	48.92	22
					Gray-cinnamon soils	0.79	9.91	10.70	
					Black soils	5.37	74.76	80.12	
					Gray forest soils	0.18	4.66	4.84	
Pedocal	1.67	22.79	24.45	23	Chernozems	2.34	33.42	35.75	3
					Castanozems	1.21	15.28	16.49	12
					Castano-cinnamon soils	2.85	43.56	46.42	8
					Dark loessial soils	3.25	48.85	52.11	
Aridisols	0.58	6.69	7.27	1	Brown Pedocals	0.38	3.12	3.50	
					Sierozems	1.73	26.68	28.41	1
Desert soils	0.30	2.00	2.30	1	Gray desert soils	1.22	10.46	11.69	1
					Gray-brown desert soils	0.18	0.66	0.84	
					Brown desert soils	0.18	1.27	1.45	
Amorphic soils	0.81	18.51	19.32	9	Cultivated loessial soils	1.44	41.22	42.66	
					Red clay soils	3.59	44.42	48.01	
					Alluvial soils	4.67	38.46	43.14	5
					Takyr	0.50	2.48	2.98	
					Aeolian soils	0.31	3.75	4.06	1
					Limestone soils	0.71	24.28	25.00	
					Volcanic soils	3.31	35.29	38.60	
					Purplish soils	0.87	45.23	46.10	
					Litho soils	0.30	2.96	3.26	1
					Skeletol soils	1.21	18.45	19.66	2
Semi-Aqueous soils	8.31	53.54	61.85	7	Meadow soils	3.14	34.86	38.01	7
					Lime concretion black soils	14.03	83.97	97.99	
					Mountain meadow soils	0.15	4.25	4.40	
					Shrubby meadow soils	0.34	7.54	7.89	
					Fluvo-aquic soils	13.00	70.41	83.41	
Aqueous soils	0.72	12.20	12.92	8	Bog soils	0.72	12.21	12.94	8
					Peat soils	0.60	11.93	12.54	
Alkaline-saline soils	2.98	12.52	15.50	6	Saline soils	1.15	12.98	14.13	1
					Desert solonchaks	0.12	2.65	2.77	
					Coastal solonchaks	25.42	32.51	57.93	5
					Sulphate soils	13.09	13.55	26.64	
					Frigid plateau solonchaks	0.00	0.00	0.00	
					Solonetzs	1.90	26.50	28.40	
Anthrosols	7.86	59.70	67.56		Paddy soils	7.91	59.51	67.42	
					Cumulated irrigated soils	7.82	63.91	71.74	
					Irrigated desert soils	5.92	59.68	65.59	

Table 4: Continued.

Order	Con[a]	% Cul[b]	Total	En[c]	Great group	Con[a]	% Cul[b]	Total	En[c]
					Felty soils	0.01	0.06	0.07	
					Dark felty soils	0.05	0.95	1.01	
					Frigid calcic soils	0.00	0.01	0.01	
Alpine soils	0.02	0.27	0.28		Cold calcic soils	0.04	0.79	0.84	
					Cold brown calcic soils	1.01	14.65	15.66	
					Frigid desert soils	0.00	0.00	0.00	
					Cold desert soils	0.00	0.00	0.00	
					Frigid frozen soils	0.00	0.01	0.02	
					Humid-thermo ferralitic	3.51	29.58	33.10	1
Ferralsols	1.20	19.01	20.22	3	Latosolic red earths	2.48	19.61	22.09	1
					Red earths	1.00	17.78	18.78	1
					Yellow earths	0.26	19.89	20.14	

[a]Land for construction.
[b]Land for cultivation.
[c]Number of endangered soils.

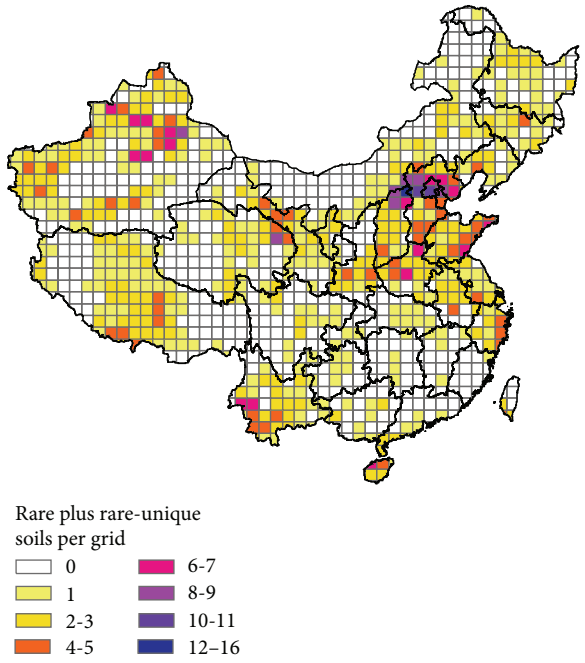

Figure 5: Rare plus rare-unique soils per grid in China (the taxonomic level of the soil map is shown in Figure 1).

led the nation. These provinces are adjacent and located in the North China Plain and the Loess Plateau. Although Xinjiang, Qinghai, and Tibet had large numbers of rare or rare-unique soils, the number of endangered soils in these provinces was small because land-use activities are less intensive. The endangered soils belonged to 10 soil orders and 19 soil great groups (Table 4). More than half of the endangered soils were in the Semi-Alfisols (24) and Pedocal (23) orders. Cinnamon soils had the greatest number of endangered soils (22), followed by castanozems (12), castano-cinnamon soils (8), bog soils (8), and meadow soils (7). In China, 17 soils might be considered "extinct" (90–100% land conversion) (Table 3), which were located in the intensively disturbed area of the north (Shanxi, Henan, Anhui, and Shandong). Most of the conversion was caused by cultivation. Only 6 soils had more than 20% of their area converted by construction land use. Four provinces had a ratio of endangered soils to rare soils that was greater than 0.5, that is, Shandong (0.74), Shanxi (0.70), Hebei (0.69), and Jilin (0.50). High ratios of endangered soils to rare soils indicate intensive land disturbance. It is even worse in these places, as their endemic soils (more importantly if they are China's endemic soils) are under pressure. According to the Harmonized World Soil Database [21], 17 soils were unique in China (but not endangered), which include Gelic Leptosols (14), Albic Lixisols (1), Fimic Anthrosols (1), and Gypsic Solonetz (1), based on FAO-90 (Food and Agriculture Organization of the United Nations) soil classification [22]. However, the FAO-90 classification, which has only 155 soil units, is not detailed enough to determine all of the soil endemism.

Overall 133 soil profiles belonged to the endangered soils, accounting for 1.5% of the total number of soil profiles (Figures 4 and 6(b)). Approximately one quarter of the endangered soil profiles were not occupied by cultivation or construction yet, particularly for those on the Tibet Plateau. The distributions of endangered soil profiles and soil map units were quite different (Figure 6). This is partly because the sampling of profiles is based mainly on the availability of legacy data and not on an area-weighted method, and partly because the soil map has missed some of the soils. The analysis of the soil profiles can offer some complementary information on endangered soils.

The soil map of China was compiled based on a survey from 1979 to 1994 and almost all of the field survey took place during the 1980s, and it reflects the state of soils in

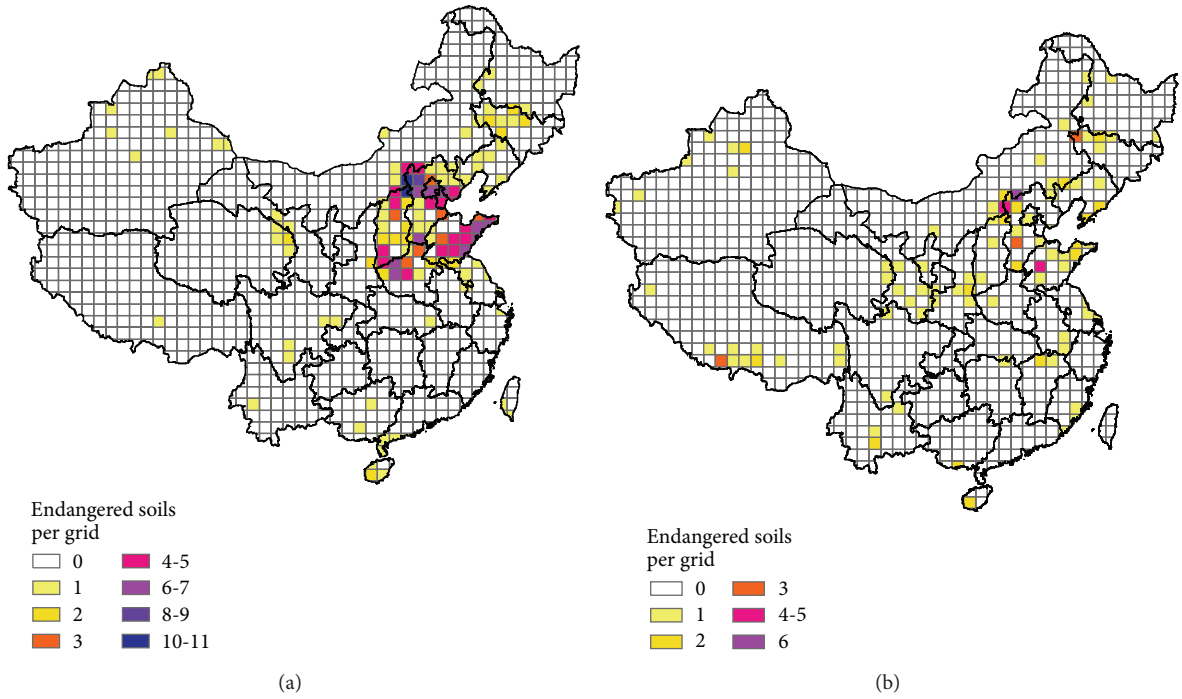

Figure 6: Endangered soils per grid based on soil map (a) and based on soil profiles (b) in China (the taxonomic level of the soil map is shown in Figure 1).

Table 5: Land use stress on soil over time.

Number	1980s[a]	1995	2000	2005	Any[b]	Persistent[c]
Endangered soils	78	72	80	88	94	66
Extinct soils	16	14	17	17	23	10

[a]Late 1980s.
[b]Soils disturbed in any years.
[c]Soils disturbed all the time.

the 1980s. During the past 30 years, the stress on the soil has changed over time (Table 5). The number of endangered soils increased, while the number of extinct soils seemed to be stable. 94 soils were identified as endangered during this period. However, only 70% of endangered soils were always disturbed by cultivation and construction. Other endangered soils were either newly severely occupied by construction and cultivation or occupied at once but were later changed into other land categories, such as forest and grassland. The soils that were once disturbed were not likely to resume, as the current land use now may not likely be the same before the soils were disturbed.

3.5. The Protection Status of Soils. Although the planning of ecological functions has taken soil erosion and desertification into account [23], soil diversity has not been considered as a priority in soil conservation practices in countries around the world. In China, many endangered soils (84% in area and 89% in number of soil profiles) are outside nature reserves (Figure 7). Protection of such soils should be a high priority in the creation of future nature reserves.

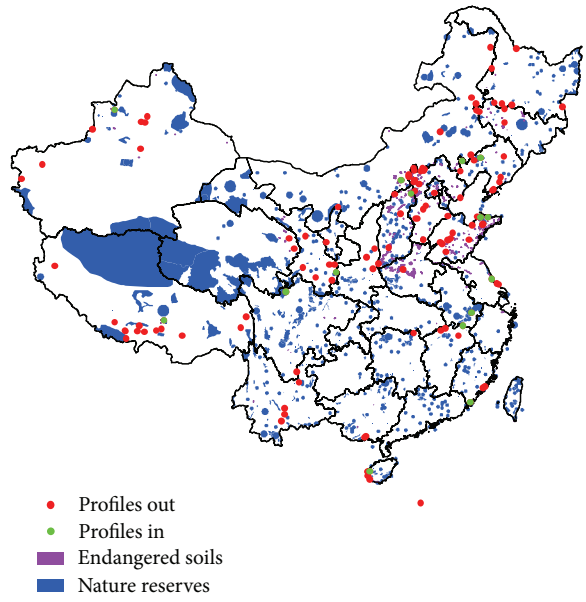

Figure 7: Endangered soils and nature reserves. The symbol of endangered soils is emphasized. "Profiles in" are endangered soil profiles in the nature reserves, and "profiles out" are endangered soil profiles out of the nature reserves.

4. Discussion

In the past 300 years, as population growth led to increasing amount of agriculture and construction land use in China,

human impacts on the natural environment have become more intensive and have been expanding [24]. Although agricultural soils have been highly treasured by farmers in China, there is a lack of recognition of soil diversity and why natural soils as a whole, or specific natural soils individually, are important to the society [4]. For the first time, through this study, a clear knowledge on the rare and threatened soils in China is obtained. Our findings will have significant implications for future soil protection planning in China.

The soil extinction seemed to have stopped in southern China (Figure 6) but was prevalent in northern China. However, the extinction may be underestimated in Hunan and Hubei due to the lack of taxonomic information at the family level. Anthropogenic soils, which have replaced their natural soil counterparts under the GSCC classification system, may imply that some soils have already been extinct. In this sense, "extinction" had already happened in the most populated regions of China. However, the GSCC does not reflect all of the aspects of human impacts on soils, even for some significant changes in soil properties. For example, the black soil in northeast China has been cultivated intensively since 1949 when the People's Republic of China was funded, and the organic matter in these black soils has decreased dramatically accompanied by noticeable soil erosion. However, none of the four map units of black soil in the soil map was considered endangered soils due to the effects of land use.

The list of endangered soils in this study was identified by considering only the rarity and the land disturbance, but the importance of soils in their economic, ecosystem, scientific, and historical/cultural value is quite different [25] and should be studied in the future. From a purely economic perspective, the endangered soils in the amorphic soils, alkaline-saline soils, desert soils, and Aridisols orders have little economic value and thus may not need to be preserved. However, the so-called "precautionary principle" [26] in habitat conservation planning requires that the diversity of natural soils be maintained because we lack the scientific understanding of their full values and functions [4].

Different soils, with their unique physical and chemical properties and biological functions, are related to the diversity of soil biota, which is an uprising field of scientific research [27]. Almost all of the processes in the soils are related to soil biota, which has the greatest number of species in the terrestrial ecosystem. Pedodiversity was found to be strongly correlated to biodiversity at the global level [28]. Many threatened and endangered plants have specific soil property requirements, which can be used to predict rare plant habitats [29]. The loss of a soil may change the whole soil ecosystem and cause a loss of its corresponding soil organisms [30]. Overall, the loss of some soils represents a substantial loss of biodiversity below ground and above ground in the corresponding biological communities [31].

The inherent uncertainty brought by the soil data is greatly outweighed by the insights that the results provide, and it is very likely that the assessment of endangered soils in our study is an underestimate for several reasons as discussed elsewhere [4]. The soil map of China that was used in this study does not give information at the soil species level; therefore the analysis omitted many endangered soils. Furthermore, parts of the soil map were mapped at the soil subgroup or great group level. This may be an important reason for the few endangered soils that were found at coarsely mapped areas, particularly in south China in this study. Each map unit in the soil map of China has only one soil class, and the purity of the soil map of China is less than 50% to 65% [32], which means that other soil classes in a map unit were not presented in our analysis. In addition, the soils that were disturbed once but not persistently are actually gone, as their nature has already been altered (Table 5). We do not have precise land-use data before the 1980s nor do we have high temporal frequency land-use data to fully assess land-use stress on the soils. All of the above factors combined increase the level of underestimation of the land-use effects on soil diversity in China.

Because of soil endemism [20], pedodiversity conservation should be considered an important aspect in international cooperation. If a unique soil in a country disappears, it will be a loss of soil diversity for the whole world. It is difficult to determine China's endemic soils due to the lack of a detailed soil map of the world using the same classification system [16]. The World Reference Base for Soil Resources (WRB) [33] provides opportunities to compare soils worldwide, although a truly universal classification system does not yet exist [34]. At the working scale included in this study, it is suggested to use enough qualifiers (4) attached to the main groups that can provide enough details to differentiate soils. This will require a large amount of resources and well-coordinated international collaboration [35]. In addition, a more comprehensive soil survey is needed in order to have a clearer picture of the soil diversity at a finer level of soil classification.

The loss of soil diversity caused by land-use change and other changes, such as climate change, desertification, and soil pollution, is not fully accounted for in this study. For example, irrational and intensive land use on a fragile Karst geoecological environment is causing serious soil erosion and rocky desertification in southwest of China [36]; urban and agriculture soils are suffering from heavy metal pollution [37, 38], and global warming is thawing frozen soils on the Tibetan Plateau [39].

5. Conclusions

Although there were some limitations due to the lack of detailed data, this study was the first attempt to give some insights about the effects of land use on pedodiversity at the national scale. First, agriculture and construction land use have significant influence on pedodiversity. Second, the distribution of endangered soils was uneven across the country. Third, most of the endangered soils remain unprotected out of natural reserves. More attention should be paid to soil diversity in conservation activities.

Conflict of Interests

The authors declare that there is no conflict of interests regarding the publication of this paper.

Acknowledgments

This research was supported by MOST 2010CB951802, the NSFC under Grant 41205037, and the Fundamental Research Funds for the Central Universities. The authors thank the reviewers for their careful and helpful comments.

References

[1] C. Glacken, *Traces on the Rhodian Shore*, University of California Press, Berkeley, Calif, USA, 1967.

[2] S. H. M. Butchart, M. Walpole, B. Collen et al., "Global biodiversity: indicators of recent declines," *Science*, vol. 328, no. 5982, pp. 1164–1168, 2010.

[3] J. A. Foley, R. DeFries, G. P. Asner et al., "Global consequences of land use," *Science*, vol. 309, no. 5734, pp. 570–574, 2005.

[4] R. Amundson, Y. Guo, and P. Gong, "Soil diversity and land use in the United States," *Ecosystems*, vol. 6, no. 5, pp. 470–482, 2003.

[5] G. L. Papa, V. Palermo, and C. Dazzi, "Is land-use change a cause of loss of pedodiversity? The case of the Mazzarrone study area, Sicily," *Geomorphology*, vol. 135, no. 3-4, pp. 332–342, 2011.

[6] A. B. McBratney, "On variation, uncertainty and informatics in environmental soil management," *Australian Journal of Soil Research*, vol. 30, no. 6, pp. 913–935, 1992.

[7] J. J. Ibáñez, S. de-Alba, and J. Boixadera, "The pedodiversty concept and its measurement: application to soil information systems," in *European Land Information Systems for Agro-Environmental Monitoring*, D. King, R. J. A. Jones, and A. J. Thomasson, Eds., pp. 181–195, EU-JRC, 1995.

[8] J. J. Ibáñez, S. De-Alba, A. Lobo, and V. Zucarello, "Pedodiversity and global soil patterns at coarse scales (with discussion)," *Geoderma*, vol. 83, no. 3-4, pp. 171–214, 1998.

[9] A. B. McBratney, "Pedodiversity," *Pedometron*, vol. 3, pp. 1–3, 1995.

[10] J. J. Ibáñez, P. V. Krasilnikov, and A. Saldaña, "Archive and refugia of soil organisms: applying a pedodiversity framework for the conservation of biological and non-biological heritages," *Journal of Applied Ecology*, vol. 49, no. 6, pp. 1267–1277, 2012.

[11] X. Zhang, J. Chen, M. Tan, and Y. Sun, "Assessing the impact of urban sprawl on soil resources of Nanjing city using satellite images and digital soil databases," *Catena*, vol. 69, no. 1, pp. 16–30, 2007.

[12] J. Chen, "Rapid urbanization in China: a real challenge to soil protection and food security," *Catena*, vol. 69, no. 1, pp. 1–15, 2007.

[13] X. Shi, D. Yu, E. D. Warner et al., "Soil database of 1:1,000,000 digital soil survey and reference system of the Chinese Genetic Soil Classification System," *Soil Survey Horizons*, vol. 45, pp. 129–136, 2004.

[14] C. F. Xi, *Soils of China*, China Agriculture Press, Beijing, China, 1998, (Chinese).

[15] W. Shangguan, Y. Dai, B. Liu et al., "A China data set of soil properties for land surface modeling," *Journal of Advances in Modeling Earth Systems*, vol. 5, no. 2, pp. 212–224, 2013.

[16] W. Shangguan, Y. Dai, Q. Duan, B. Liu, and H. Yuan, "A global soil data set for earth system modeling," *Journal of Advances in Modeling Earth Systems*, vol. 6, no. 1, pp. 249–263, 2014.

[17] J. Liu, M. Liu, X. Deng, D. Zhuang, Z. Zhang, and D. Luo, "The land use and land cover change database and its relative studies in China," *Journal of Geographical Sciences*, vol. 12, no. 3, pp. 275–282, 2002.

[18] B. Minasny, A. B. McBratney, and A. E. Hartemink, "Global pedodiversity, taxonomic distance, and the world reference base," *Geoderma*, vol. 155, no. 3-4, pp. 132–139, 2010.

[19] J. M. Diamond, *Guns, Germs, and Steel: The Fates of Human Societies*, Norton Company, New York, NY, USA, 1999.

[20] J. J. Ibáñez, R. Pérez-Gómez, and F. M. San José, "The spatial distribution of soils across Europe: a fractal approach," *Ecological Complexity*, vol. 6, no. 3, pp. 294–301, 2009.

[21] FAO/IIASA/ISRIC/ISS-CAS/JRC, *Harmonized World Soil Database (version1.1)*, FAO, Rome, Italy, IIASA, Laxenburg, Austria, 2009.

[22] FAO/UNESCO/ISRIC, "Revised legend of the Soil Map of the World," World Soil Resources Report, FAO, Rome, Italy, 1990.

[23] MEP and CAS, "National ecological function zoning," Beijing, China, 2008.

[24] Q. Ge, J. Dai, and F. He, *Land Use Changes and Terrestrial Carbon Budgets in China during the Last 300 Years*, Science Press, Beijing, China, 2008.

[25] P. J. Drohan and T. J. Farnham, "Protecting life's foundation: a proposal for recognizing rare and threatened soils," *Soil Science Society of America Journal*, vol. 70, no. 6, pp. 2086–2096, 2006.

[26] K. S. Shrader-Frechette and E. D. McCoy, *Method in Ecology: Strategies for Conservation*, Cambridge Univeristy Press, Cambridge, Mass, USA, 1993.

[27] J. L. Kirk, L. A. Beaudette, M. Hart et al., "Methods of studying soil microbial diversity," *Journal of Microbiological Methods*, vol. 58, no. 2, pp. 169–188, 2004.

[28] J. J. Ibáñez and E. Feoli, "Global relationships of pedodiversity and biodiversity," *Vadose Zone Journal*, vol. 12, no. 3, 2013.

[29] J. L. Boettinger, S. Kienast-Brown, C. W. Brungard, B. B. Fonnesberck, J. B. Baker, and J. D. Armentrout, "GlobalSoilMap data to inform ecological management of arid lands," in *Proceedings of the GlobalSoilMap Conference*, French National Institute for Agricultural Research, Orleans, France, 2013.

[30] D. A. Wardle, R. D. Bardgett, J. N. Klironomos, H. Setälä, W. H. Van Der Putten, and D. H. Wall, "Ecological linkages between aboveground and belowground biota," *Science*, vol. 304, no. 5677, pp. 1629–1633, 2004.

[31] Z. A. Sylvain and D. H. Wall, "Linking soil biodiversity and vegetation: Implications for a changing planet," *The American Journal of Botany*, vol. 98, no. 3, pp. 517–527, 2011.

[32] W. Shangguan, Y. Dai, B. Liu, A. Ye, and H. Yuan, "A soil particle-size distribution dataset for regional land and climate modelling in China," *Geoderma*, vol. 171-172, pp. 85–91, 2012.

[33] X. Z. Shi, D. S. Yu, S. X. Xu et al., "Cross-reference for relating Genetic Soil Classification of China with WRB at different scales," *Geoderma*, vol. 155, no. 3-4, pp. 344–350, 2010.

[34] P. R. Owens, J. Hempe, E. Micheli, and A. McBratney, "Advancing towards a universal soil classification system," in *Proceedings of the EGU General Assembly*, vol. 16, Vienna, Austria, U16432, 2014.

[35] P. A. Sanchez, S. Ahamed, F. Carré et al., "Digital soil map of the world," *Science*, vol. 325, no. 5941, pp. 680–681, 2009.

[36] S.-J. Wang, Q.-M. Liu, and D.-F. Zhang, "Karst rocky desertification in southwestern China: geomorphology, landuse, impact and rehabilitation," *Land Degradation and Development*, vol. 15, no. 2, pp. 115–121, 2004.

[37] B. Wei and L. Yang, "A review of heavy metal contaminations in urban soils, urban road dusts and agricultural soils from China," *Microchemical Journal*, vol. 94, no. 2, pp. 99–107, 2010.

[38] M. Qu, W. Li, C. Zhang, B. Huang, and Y. Zhao, "Estimating the pollution risk of cadmium in soil using a composite soil environmental quality standard," *The Scientific World Journal*, vol. 2014, Article ID 750879, 9 pages, 2014.

[39] L. Zhao, C.-L. Ping, D. Yang, G. Cheng, Y. Ding, and S. Liu, "Changes of climate and seasonally frozen ground over the past 30 years in Qinghai-Xizang (Tibetan) Plateau, China," *Global and Planetary Change*, vol. 43, no. 1-2, pp. 19–31, 2004.

Hindawi Publishing Corporation
The Scientific World Journal
Volume 2014, Article ID 906021, 9 pages
http://dx.doi.org/10.1155/2014/906021

Research Article

Partitioning Carbon Dioxide Emission and Assessing Dissolved Organic Carbon Leaching of a Drained Peatland Cultivated with Pineapple at Saratok, Malaysia

Liza Nuriati Lim Kim Choo[1,2] and Osumanu Haruna Ahmed[1]

[1] *Department of Crop Science, Faculty of Agriculture and Food Science, Universiti Putra Malaysia (UPM), Bintulu Campus, P.O. Box 396,97008 Bintulu, Sarawak, Malaysia*
[2] *Soil and Water Management Programme, Strategic Resource Research Centre, Malaysian Agricultural Research and Development Institute (MARDI), P.O. Box 59, Roban, 95300 Saratok, Sarawak, Malaysia*

Correspondence should be addressed to Osumanu Haruna Ahmed; osumanu@upm.edu.my

Received 31 May 2014; Revised 8 July 2014; Accepted 28 July 2014; Published 19 August 2014

Academic Editor: Antonio Paz González

Pineapples (*Ananas comosus* (L.) Merr.) cultivation on drained peats could affect the release of carbon dioxide (CO_2) into the atmosphere and also the leaching of dissolved organic carbon (DOC). Carbon dioxide emission needs to be partitioned before deciding on whether cultivated peat is net sink or net source of carbon. Partitioning of CO_2 emission into root respiration, microbial respiration, and oxidative peat decomposition was achieved using a lysimeter experiment with three treatments: peat soil cultivated with pineapple, bare peat soil, and bare peat soil fumigated with chloroform. Drainage water leached from cultivated peat and bare peat soil was also analyzed for DOC. On a yearly basis, CO_2 emissions were higher under bare peat (218.8 t CO_2 ha/yr) than under bare peat treated with chloroform (205 t CO_2 ha/yr), and they were the lowest (179.6 t CO_2 ha/yr) under cultivated peat. Decreasing CO_2 emissions under pineapple were attributed to the positive effects of photosynthesis and soil autotrophic activities. An average 235.7 mg/L loss of DOC under bare peat suggests rapid decline of peat organic carbon through heterotrophic respiration and peat decomposition. Soil CO_2 emission depended on moderate temperature fluctuations, but it was not affected by soil moisture.

1. Introduction

Tropical peat soils are generally defined as soils formed by the accumulation of partially decayed woody plant materials under waterlogged condition. Tropical peatlands cover 27.1 million hectares in Southeast Asia [1] and about 2.6 million hectares in Malaysia [2]. Peats of the tropics are increasingly being cultivated. Although they store large amount of organic carbon, peat soils drained for agriculture in particular accelerate their decomposition rates. Rapid decomposition of peats leads to increase in CO_2 release into the atmosphere [3, 4]. Carbon dioxide may be emitted from peatland through burning by wildfires, microbial respiration, root respiration, and physical oxidation [5, 6]. Carbon dioxide emissions are related to water table depth [7], soil temperature [8, 9], fertilization [10], land use type [11], and peat type [12]. Moreover, carbon in the form of DOC is lost through leaching due to microbial metabolism [13]. Carbon losses through emission and leaching may shift the peatland carbon balance from sink to source [14].

In Malaysia, approximately 600,000 hectares of peatland are cultivated with oil palm, pineapple, rubber, and sago [15]. Presently, there is scarce information on soil CO_2 emission from pineapple cultivation on drained peat soils. The understanding of the contribution of pineapple cultivation on peats to the greenhouse gas emission is important, as 90% of pineapples are grown on peat soils of Malaysia [16]. Although attempts have been made to measure CO_2 emission from cultivated tropical peats, such studies are limited to a few measurements. The recent measurements only account for total soil CO_2 emission as they do not partition soil respiration into root respiration, microbial respiration, and oxidative

peat decomposition [10, 17]. With the growing concern about the effects of greenhouse gases on the environmental quality coupled with the need to achieve sustainable agriculture, it is essential to partition CO_2 emission before deciding on whether cultivated or degraded soils are net sinks or net sources of atmospheric greenhouse gases [5]. Accounting for CO_2 emission from cultivated peats is needed to evaluate future rates of increase in atmospheric greenhouse gases and their effect on the global environmental change processes [18, 19].

Based on the above rationale, the general objective of this study was to quantify CO_2 emission and also carbon loss from a drained tropical peat grown with pineapple. The first specific objective was to partition soil CO_2 emission from a cultivated peat into root respiration, microbial respiration, and oxidative peat decomposition. The second specific objective was to estimate DOC in water drained from lysimeters with peat soil. The third specific objective was to assess the effects of soil temperature and soil moisture on soil CO_2 emission.

In this study, it was hypothesized that microbial respiration and peat decomposition will cause higher loss of CO_2 and DOC from the bare peat soil than from the peat soil cultivated with pineapple. This hypothesis is based on the assumption that CO_2 emission of drained and uncultivated peats is mainly controlled by heterotrophic respiration. However, CO_2 and DOC release in the presence of root respiration (cultivated peats) is expected to be lower as both processes are regulated by autotrophic respiration and photosynthesis. Information obtained from partitioning respiration components could be used to control CO_2 and DOC losses from drained tropical peats that are cultivated with pineapples and other related crops.

2. Materials and Methods

2.1. Site Description. The study was carried out at the Malaysian Agricultural Research and Development Institute (MARDI) Peat Research Station at Saratok, Sarawak, Malaysia. The research station has a total area of 387 hectares located on a logged-over forest with a flat topography of 5 to 6 m above mean sea level. Based on the Von Post Scale of H7 to H9, the peat soil is classified as well decomposed dark brown to almost dark coloured sapric peat with a strong smell. The thickness of the peat soil ranges from 0.5 to 3.0 m.

The mean temperature of the peat area ranges from 22.1 to 31.7°C. The relative humidity of the area ranges from 61 to 98%. The annual mean rainfall of the area is 3749 mm. In the wet season (November to January), the monthly rainfall is more than 400 mm whereas in the dry season, particularly in July, the mean rainfall is 189 mm.

2.2. Soil Chemical and Physical Analysis. Before setting up the lysimeter experiment, peat samples were collected at a peat excavation site (0.5 hectares) located at MARDI Peat Research Station. The experimental area was planted with *Moris* pineapple from 2004 to 2005, after which it was abandoned to lie fallow for six years. Samplings were performed at depths of 0–20 cm, 20–40 cm, and 40–, 60 cm systematically in 12 points located over a 20 m × 12.5 m grid. The soil samples were analyzed for pH, conductivity, ammonium-N, nitrate-N, organic carbon, total nitrogen, and cation exchange capacity (CEC). Soil pH and conductivity were measured based on a 1 : 5 soil to water suspension [20]. Ammonium-N and nitrate-N were determined using the steam distillation method [21]. Soil organic carbon was determined using the Walkley and Black method [22] whereas total nitrogen was determined using the Kjeldahl method [23]. Cation exchange capacity was determined using the Harada and Inoko method [24]. Bulk density was determined using the core method [25], and soil water holding capacity was determined using the method of Dugan et al. [26].

2.3. Characteristics of the Lysimeters. Twelve cylindrical field lysimeters made from high density polyethylene, measuring 1.43 m in diameter and 1.58 m in height, were set up in April 2012 to mimic the natural condition of drained tropical peats. The size of the lysimeters used in this study was designed to ensure satisfactory growth and development of the pineapples for sixteen months. The twelve lysimeters were used for three peat soil treatments (Section 2.4). The lysimeters were equipped with water spillage opening which was attached to clear tubes mounted on the outside of the vessel to regulate and monitor water level.

Each lysimeter was filled with peat soil up to 120 cm depth. Water loss from the soil was replenished by showering each lysimeter with 34.5 litres of rainwater. The amount of rainwater added was based on the volume of the fabricated lysimeter and the mean annual rainfall at Saratok, Sarawak, Malaysia. The lysimeters with the peat soil were left in the open for five months to ensure that the peat soil had settled before beginning this study. The length of this initial phase was based on weekly determination of the peat subsidence. The equilibrium state was achieved in September 2012 before carrying out the CO_2 measurement. Water table of the peat was maintained at 50 to 60 cm from the soil surface throughout the duration of the experiment.

2.4. Peat Soil Treatments. The three treatments involved in this lysimeter experiment were peat soil cultivated with pineapple (A), bare peat soil (B), and bare peat soil treated with chloroform (C). Each treatment had four replications. The treatments were arranged in completely randomized design.

Treatment A represents total amount of CO_2 emitted from root respiration, microbial respiration, and peat decomposition. Three *Moris* pineapple suckers were planted in the lysimeters at a distance of 30 cm. Treatment B represents CO_2 emitted by microbial respiration and peat decomposition. Weed sprouting on the soil surface was controlled when necessary. Treatment C represents CO_2 emitted by oxidative peat decomposition. For this treatment, concentrated chloroform was applied evenly on the peat soil surface to eliminate microbial respiration, and 64.6 litres of concentrated chloroform was used. This volume was based on the peat soil's water holding capacity. After the chloroform application, the soil was covered with cling film and canvas to produce

Table 1: Physical and chemical properties of a drained peat soil sampled at different depths.

Variable	Mean (0 to 10 cm)	Results per soil depth (cm)			Reported standard range
		0 to 20 cm	20 to 40 cm	40 to 60 cm	
Physical properties					
Bulk density (g/cm^3)	0.14				0.09–0.12 [31]
Water holding capacity (%)	40.2				275–322 [31]
Moisture (%)		80.9^c	84.9^b	88.8^a	90–95 [32]
Chemical properties					
pH		3.8^a ± 0.1	3.9^a ± 0.1	3.9^a ± 0.1	3.0–4.5 [31]
Conductivity (μS/cm)		178.5^a ± 4.6	175.4^a ± 4.3	172.7^a ± 2.4	<200 [33]
Cation exchange capacity (cmol$_{(+)}$/kg)		146.4^a ± 20.1	137.6^a ± 13.7	175.6^a ± 34.9	200 [31] 145 [33]
Total organic carbon (%)		40.0^a ± 0.8	39.8^a ± 1.4	36.5^a ± 1.1	12–60 [31] 20.4–38.4 [34]
Total nitrogen (%)		1.33^a ± 0.03	1.18^b ± 0.04	1.12^b ± 0.03	1.10–1.67 [32]
Ammonium-Nitrogen (mg/L)		138.5^a ± 16.2	100.0^b ± 4.2	94.8^b ± 7.7	n.a.
Nitrate-Nitrogen (mg/L)		72.0^a ± 5.4	48.8^b ± 6.3	65.8^{ab} ± 3.0	n.a.

Values (mean ± standard error) with different letters across the column are significantly different at $P \leq 0.05$.
(Note: n.a.: not available).

a vacuum-like condition in the lysimeters to minimize chloroform volatilization. The soil microbial population before and after the chloroform application was determined using the culture method. With this method, bacteria, fungi, and actinomycetes were enumerated as colony forming units (CFU) per gram of fresh soil on nutrient agar, Rose Bengal, and actinomycetes isolation agar, respectively [27]. The concentrated chloroform was used to fumigate the peat soil one week before the soil CO_2 measurement was commenced (optimum time interval achieved for the biocidal effect on soil microorganisms).

2.5. Soil CO_2 Emission Measurements. Carbon dioxide emissions from the field lysimeters were measured using the closed chamber method [28]. Extracted gas samples from the chamber were analyzed for CO_2 using gas chromatography (Agilent 7890A) equipped with thermal conductivity detector (TCD). The CO_2 results were based on the measured CO_2 from treatments A, B, and C in the wet and dry seasons. The values were averaged and converted into units of t/ha/yr. The gas flux was calculated from the increase in the chamber concentration over time using the chamber volume and soil area covered, using the following equation [28–30]:

$$\text{Flux} = \left[\frac{d\left(\text{CO}_2\right)}{dt}\right] \times \frac{PV}{ART}, \quad (1)$$

where $d(CO_2)/(dt)$ is the evolution rate of CO_2 within the chamber headspace at a given time after putting the chamber into the soil, P is the atmospheric pressure, V is the volume headspace gas within the chamber, A is the area of soil enclosed by the chamber, R is the gas constant, and T is the air temperature.

The gas flux was measured in the early morning (2.40 a.m. to 5.55 a.m.), morning (7.15 a.m. to 10.30 a.m.), mid-morning to afternoon (10.35 a.m. to 1.50 p.m.), afternoon (1.55 p.m. to 5.10 p.m.), evening (8.00 p.m. to 11.15 p.m.), and night (11.20 p.m. to 2.35 a.m.) to obtain a 24 hour CO_2 emission. The flux measurements were carried out in September 2012, November 2012, and January 2013 to represent the concentrations of CO_2 in the wet season whereas April 2013 and July 2013 flux measurements represent the concentrations of CO_2 in the dry season. Soil temperature and moisture were measured using Eijkelkamp IP68 and ML3 sensors, respectively. Rainfall, temperature, and air humidity data were also recorded using a portable weather station (WatchDog 2900) installed at the experimental site.

2.6. Measurement of DOC. Water draining through the openings of the lysimeters of treatments A and B was collected for determinations of DOC concentration. The water samples were chilled at 10°C before being analyzed. The samples were filtered to pass a 0.45 μm cellulose nitrate membrane filter and the contents of DOC were determined using total carbon analyzer (Shimadzu TOC). The DOC from treatment C was not measured because of the high residual chloroform in the peat water.

2.7. Statistical Analysis. Treatment effects were tested using analysis of variance (ANOVA) and means of treatments were compared using Duncan's New Multiple Range Test at $P \leq 0.05$. The relationships between gas flux, soil temperature, and soil moisture were analyzed using Pearson correlation analysis. The statistical software used for this analysis was the Statistical Analysis System (SAS) Version 9.3.

3. Results and Discussion

3.1. Peat Physical Properties. Results of peat soil properties are compared with the previously reported ranges (Table 1)

for tropical peats in Southeast Asia [31] and Malaysia [31–33]. The bulk density of the sampled peat soil is within the reported range [31] whereas the water holding capacity and moisture content of the soil are lower than the reported range [31, 32]. The bulk density at 10 cm ranged from 0.09 to 0.18 g/cm^3, which is typical of a sapric peat. The bulk density was determined at 10 cm due to the saturated condition of the excavation site. The water holding capacity of the peat (40.2%) was below the reported range [31] because the water holding capacity determination was based on oven-dry weight method [31]. The increasing moisture content with increasing peat soil depth is related to the high water table at the excavation site during soil sampling. However, the soil moisture is lower than the reported range [32]. Removal of trees and debris after land clearing may have accelerated oxidative peat decomposition and therefore soil moisture content is lower.

3.2. Peat Chemical Properties. Values of pH, conductivity, CEC, total organic carbon, and total nitrogen of the peat soil studied here are within the reported range [31–34] for the peat soil at MARDI Peat Research Station (Table 1). The soil chemical properties showed no significant difference with depth except for total nitrogen, ammonium-N, and nitrate-N. The pH of the peat soil was low, suggesting a need for liming before being cultivated. The low conductivity of the peat soil also indicates that the soil is not saline as the research station is drained by two large tidal rivers (Sebelak River and Nyabor River). However, intrusion of salt water at the station is prevented by a tidal gate constructed at the main outlet drain leading to Nyabor River. The CEC of the peat soil is high because of lignin-derivatives formed during decomposition. Ion exchange in peats relates to carboxyl and phenolic radicals of humic substances and hemicelluloses [31]. However, the CEC obtained is higher than the reported range [33]. This may be attributed to the past liming activities at the excavation site as this area was cultivated with pineapples from 2004 to 2005. The total organic carbon of the soil is within the reported range [31, 34]. The high organic carbon content can be associated with the botanical origin (woody) of the sapric peat used in this study [31, 32]. The total nitrogen of the soil was high and it was mostly in organic form. The total nitrogen ranged from 1.1 to 1.3%. Ammonium-N ranged from 94.8 to 138.5 mg/L whereas nitrate-N ranged from 48.8 to 72.0 mg/L at the three soil depths. Total nitrogen, ammonium-N, and nitrate-N contents decreased with increasing soil depth (from 0–20 cm to 20–40 cm depths) because decomposition of peats generally decreases (low oxidation with increasing water content) down the soil profile [31].

3.3. Soil CO_2 Emission. The CO_2 emissions under treatments A, B, and C varied in the wet and dry seasons (Figure 1). In the wet season, the CO_2 emission under treatment A was significantly lower than under treatments B and C. However, in the dry season, the CO_2 emission under treatment C was significantly lower than under treatments A and B. The CO_2 emission under treatment A was affected by root development and growth of the pineapple plants. Differences in day and night temperatures in the wet and dry seasons (Table 2) may have also impeded photosynthetic activity of the pineapple plants [35]. Furthermore, heterotrophic respiration and decomposition of root exudates in the rhizosphere [5, 36] may have contributed to the CO_2 emission under treatment A.

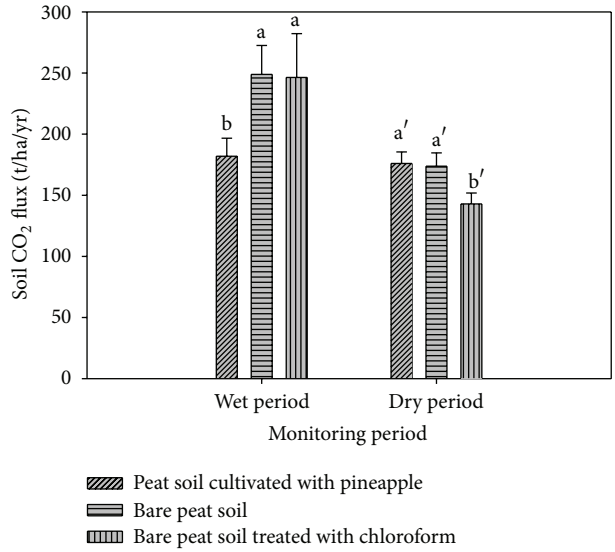

Figure 1: Carbon dioxide emission (wet and dry seasons) from peat soil cultivated with pineapple, bare peat soil, and chloroform fumigated peat soil. (Error bars represent standard error and soil mean fluxes with different letters are significantly different at $P \leq 0.05$.)

The CO_2 emission under treatment B is related to the microbial population of the peat soil and the availability of adequate substrate for microbial metabolism, but not to plant root activities [5, 12]. The CO_2 emission under treatment B was also regulated by moderate temperature fluctuation (Table 2), which is in agreement with previous studies in peat soils [9, 12]. The effect of soil temperature on CO_2 emission from peat soils has been also recently studied by Jauhiainen et al. [8] and Paz-Ferreiro et al. [37], showing that the rate of organic material decomposition increased with increasing temperature of peat soils.

The CO_2 emission under treatment C was mainly due to oxidative peat decomposition (shrinkage and consolidation) as the fumigant (chloroform) used inhibited microbial respiration. Bacteria and actinomycetes populations before and after fumigation were statistically similar. Fungi were not detected in this present study. These findings are in agreement with most previous findings, which demonstrate that chloroform can effectively kill (94% to 99%) microorganisms [38–42]. The effectiveness of the fumigation is supported by the decrease in the mean soil microbial biomass carbon (Table 3). This result also corroborates previous work by Zelles et al. [43] who reported 80% reduction in microbial biomass carbon after fumigating a soil with chloroform. The fact that the subsidence rates of the peat soil in treatments A, B, and C were statistically similar suggests that the chloroform used

Table 2: Day and night temperatures of the experimental site (Saratok, Malaysia).

Variable	Wet season			Dry season	
	September 2012	November 2012	January 2013	April 2013	July 2013
Mean day time temperature (°C)	26.7	29.2	29.6	26.3	27.0
Mean night time temperature (°C)	23.6	24.9	24.5	24.6	24.7
Mean day and night time temperature differences (°C)	3.1	4.3	5.1	1.7	2.3
Mean soil temperature (°C)					
Early morning	29.8^{a}	30.0^{bc}	28.2^{bc}	30.1^{a}	28.7^{b}
Morning	30.8^{a}	32.1^{ab}	29.8^{a}	30.5^{a}	29.5^{b}
Mid-morning to afternoon	30.9^{a}	32.8^{a}	30.7^{a}	30.5^{a}	30.6^{b}
Afternoon	29.7^{a}	31.1^{abc}	30.5^{a}	29.3^{ab}	32.6^{a}
Evening	29.5^{a}	30.1^{bc}	29.4^{ab}	28.7^{ab}	29.2^{b}
Night	29.0^{a}	29.2^{c}	27.9^{c}	27.7^{b}	28.7^{b}

Mean values with different letters within the same column are significantly different at $P \leq 0.05$.

Table 3: Effect of fumigating drained peat soil with chloroform on soil microbial biomass carbon.

Monitoring cycle	Mean soil microbial biomass carbon (μg C/g soil)
Initial before chloroform application	94.7^{a}
September 2012	29.6^{f}
November 2012	73.4^{b}
January 2013	56.0^{d}
April 2013	67.2^{c}
July 2013	46.0^{e}

Mean values with different letters are significantly different at $P \leq 0.05$.

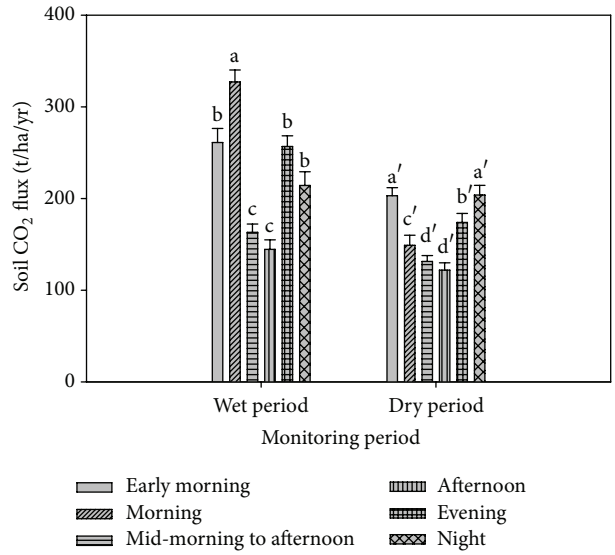

Figure 2: Carbon dioxide emission (at different times of the day and different seasons) from peat soil cultivated with pineapple. (Error bars represent standard error and soil mean fluxes with different letters are significantly different at $P \leq 0.05$.)

did not affect CO_2 emission due to oxidative peat decomposition. This observation corroborates that of Toyota et al. [40] who also found no significant effect of chloroform fumigation on soil bulk density and compaction. The higher CO_2 emission under treatment C in the wet season was due to the decomposition of dead microorganisms [42]. In contrast, the decrease in the CO_2 emission under treatment C in the dry season was because of the adaptation of the microorganisms towards the biocidal effect of chloroform. Again, it must be stressed that the CO_2 emission was mainly because of oxidative peat decomposition [1, 6]. The oxidative peat decomposition (shrinkage and consolidation) was due to the loss of water in the aerobic layer of the peat. Oxidative peat decomposition is a continuous process and it takes several years to achieve the equilibrium state of peat subsidence.

The CO_2 emission was also affected by time of sampling (Figure 2). In the wet season, the CO_2 emission decreased from morning to mid-morning to afternoon followed by an increase in the evening. In the dry season, the CO_2 emission decreased from the early morning to mid-morning to afternoon followed by an increase in the evening and night. These observations are consistent with the significant negative correlation between soil CO_2 emission and soil temperature (Table 4). These findings also suggest that the CO_2 emission increased with decreasing temperature. Although the CO_2 emission was negatively correlated with soil temperature, the overall data (wet and dry seasons) showed no correlation between CO_2 emission and soil temperature (Table 4). This indicates that although soil temperature regulates soil CO_2 emission, the differences in the CO_2 emissions under treatments A, B, and C across time rather depends on the moderate fluctuation in soil temperature (0.2 and 1.6°C) of the tropics. There was no correlation between CO_2 emission and soil moisture (Table 4) because the water table in the lysimeters was maintained at 50 and 60 cm. This finding is further supported by the fact that the soil moisture was not significantly affected by time of sampling (Table 5). In a related study, Kechavarzi et al. [12] found that soil moisture had no effect on CO_2 emission in humified peat surface but higher soil moisture which constrained oxygen diffusion affected soil respiration.

Table 4: The relationship between soil CO_2 emission, soil temperature, and soil moisture in dry and wet seasons.

Weather season	Monitoring period	Variable	Soil temperature	Soil moisture
Wet season	September 2012	Soil CO_2 emission	$r = 0.2253$ $P = 0.1464$	$r = 0.1955$ $P = 0.2091$
	November 2012		$r = -0.5169$ $P = 0.0001$	$r = 0.1127$ $P = 0.4264$
Dry season	January 2013		$r = -0.4829$ $P = 0.0004$	$r = 0.2290$ $P = 0.1135$
	April 2013		$r = -0.7431$ $P = 0.0001$	$r = -0.0776$ $P = 0.5558$
	July 2013		$r = -0.5992$ $P = 0.0001$	$r = -0.2299$ $P = 0.0854$
Pooling data throughout the wet and dry seasons			$r = -0.1119$ $P = 0.0710$	$r = 0.1027$ $P = 0.0980$

Note: top values represent Pearson's correlation coefficient (r) while bottom values represent probability level at 0.05 ($n = 72$ for each monitoring period, $n = 360$ for pooling data throughout wet and dry seasons).

Table 5: Soil moisture during CO_2 measurement at different times of the day in dry and wet seasons.

Time	Wet season			Dry season	
	September 2012	November 2012	January 2013	April 2013	July 2013
	Mean soil moisture (%)				
Early morning	77.7[a]	76.7[a]	77.7[a]	77.3[a]	75.1[a]
Morning	80.4[a]	77.4[a]	78.7[a]	77.9[a]	75.5[a]
Mid-morning to afternoon	77.2[a]	78.3[a]	78.3[a]	78.0[a]	75.1[a]
Afternoon	76.2[a]	79.7[a]	77.5[a]	77.5[a]	76.7[a]
Evening	78.5[a]	77.6[a]	77.0[a]	78.4[a]	73.6[a]
Night	76.3[a]	77.9[a]	76.3[a]	78.1[a]	76.1[a]

Mean values with same letter within the same column are not significantly different at $P \geq 0.05$.

In summary, the CO_2 emission was estimated at about 218.8 t CO_2 ha/yr under bare peat soil (B), followed by 205 t CO_2 ha/yr under bare peat soil treated with chloroform (C), and 179.6 t CO_2 ha/yr under peat soil cultivated with pineapple (A). The higher CO_2 emission from treatment B suggests that it is controlled by heterotrophic respiration whereas the lower CO_2 emission from treatment A suggests that it is regulated by autotrophic respiration (through photosynthetic activity and respiration in the rhizosphere). The CO_2 emission in this study was higher than that reported by Jauhiainen et al. [8], who found that microbial respiration contributed with 80 t CO_2 ha/yr whereas root respiration contributed with 21% of the total respiration. The CO_2 emission rate reported in this study is not consistent with that of Jauhiainen et al. [8] because the present study was carried out on sapric peat whereas that reported by Jauhiainen et al. [8] was on fibric to hemic peat.

3.4. Dissolved Organic Carbon. The DOC under the bare peat soil (B) (235.7 mg/L) was significantly higher than under peat soil cultivated with pineapple (A) (194.6 mg/L) (Figure 3) because of the greater decomposition of organic substrate by heterotrophs. One of the byproducts of heterotrophs is DOC [13]. The lower DOC under treatment A is related to the consumption of carbon, nitrogen, and root exudates by microbes at the rhizosphere [5, 44]. The DOC under treatment B is in accordance with the results of our field monitoring as the mean CO_2 under treatment B (218.8 t CO_2 ha/yr) was higher than under treatment A (179.6 t CO_2 ha/yr).

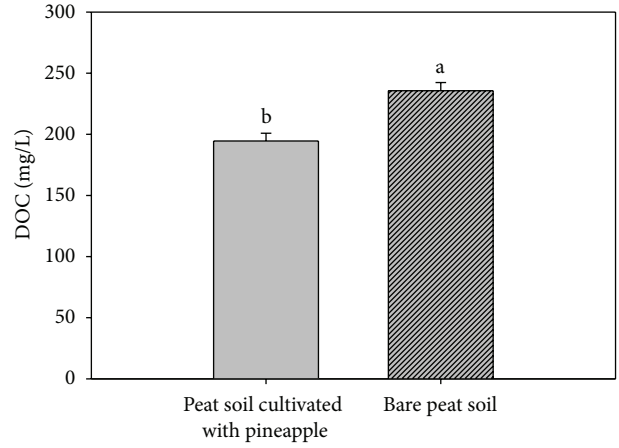

Figure 3: Dissolved organic carbon (DOC) leaching losses under peat soil cultivated with pineapple and bare peat soil. (Error bars represent standard error, and mean DOC with different letters are significantly different at $P \leq 0.05$.)

The DOC was statistically similar irrespective of the monitoring period (Figure 4). This result was expected as

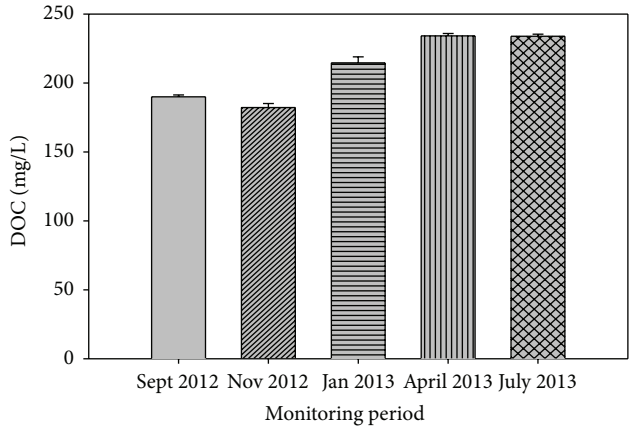

Figure 4: Dissolved organic carbon from peat soil cultivated with pineapple in the wet and dry seasons. (Error bars represent standard error and mean DOC are not significantly different at $P \geq 0.05$.)

the peat water table was controlled to fluctuate between 50 and 60 cm in the lysimeters, so as to minimize oxygen availability for carbon decomposition in the aerobic zone. Furthermore, the restriction of soil water movement in the lysimeter may have contributed to the similarity of the DOC content. This finding is also consistent with the fact that wet and dry seasons have no significant effect on DOC production in drained peats.

The higher DOC in this study than the initial concentration (64.3 mg/L) suggests that draining peat soils accelerates their chemical oxidation. This buttresses the fact that carbon is not only lost as CO_2 but also lost through DOC. Loss of DOC is an important indicator for carbon release, because when it is leached from the peat soils into rivers it poses environmental pollution risk. This is because DOC can react with chlorine to form trihalomethane and haloacetic acids. Although these chemicals are carcinogenic, they are not completely removed from treated water [45, 46].

4. Conclusion

Peat soils drained for agriculture released 218.8 t CO_2 ha/yr under bare conditions, followed by bare peat soil treated with chloroform (205 t CO_2 ha/yr), and peat soil cultivated with pineapple (179.6 t CO_2 ha/yr). The lower CO_2 emission from the peat soil cultivated with pineapple was due to the regulation by pineapple photosynthetic activity, heterotrophic respiration, and decomposition of root exudates at the rhizosphere whereas the CO_2 emission from the bare peat fumigated with chloroform was mainly due to shrinkage and consolidation of the soil. Soil CO_2 emission was neither affected by soil temperature nor by soil moisture but the emission seemed to be controlled by moderate soil temperature fluctuation in the wet and dry seasons. Draining peat soil affected leaching of DOC. An average 235.7 mg/L loss of DOC under bare conditions, arisen principally from microbial respiration and oxidative peat decomposition, suggests rapid decline of peat organic matter through heterotrophic microbial activities. Identification of beneficial microorganisms that reduce peat decomposition may help to minimize carbon dioxide emission from cultivated peats. Further research is needed to assess partitioning of soil CO_2 emission at the rhizosphere, as CO_2 emission from drained peats seems to be influenced by heterotrophic and autotrophic respiration processes.

Conflict of Interests

The authors declare that there is no conflict of interests regarding the publication of this paper.

Acknowledgments

The authors acknowledge the financial support of the Ministry of Education Malaysia through Universiti Putra Malaysia. This research was funded through Research University Grants Scheme (RUGS). The facilities provided by the Malaysian Agricultural Research and Development Institute at MARDI Saratok Peat Research Station for this study are appreciated.

References

[1] A. Hooijer, S. Page, J. G. Canadell et al., "Current and future CO_2 emissions from drained peatlands in Southeast Asia," *Biogeosciences*, vol. 7, no. 5, pp. 1505–1514, 2010.

[2] A. B. Ismail and J. Jamaludin, "Land clearing techniques employed at MARDI Peat Research Station, Sessang, Sarawak, and their immediate impacts," in *A Case Study at MARDI Peat Research Station Sessang, Sarawak, Malaysia*, A.B. Ismail, H.K. Ong, M.J. Mohamad Hanif, and M.S. Umi Kalsom, Eds., pp. 1–8, MARDI, Sarawak, Malaysia, 2007.

[3] M. Maljanen, V. M. Komulainen, J. Hytönen, P. J. Martikainen, and J. Laine, "Carbon dioxide, nitrous oxide and methane dynamics in boreal organic agricultural soils with different soil characteristics," *Soil Biology and Biochemistry*, vol. 36, no. 11, pp. 1801–1808, 2004.

[4] B. Kløve, T. E. Sveistrup, and A. Hauge, "Leaching of nutrients and emission of greenhouse gases from peatland cultivation at Bodin, Northern Norway," *Geoderma*, vol. 154, no. 3-4, pp. 219–232, 2010.

[5] Y. Kuzyakov, "Sources of CO_2 efflux from soil and review of partitioning methods," *Soil Biology and Biochemistry*, vol. 38, no. 3, pp. 425–448, 2006.

[6] Å. Kasimir-Klemedtsson, L. Klemedtsson, K. Berglund, P. Martikainen, J. Silvola, and O. Oenema, "Greenhouse gas emissions from farmed organic soils: a review," *Soil Use and Management*, vol. 13, no. 4, pp. 245–250, 1997.

[7] Ö. Berglund and K. Berglund, "Influence of water table level and soil properties on emissions of greenhouse gases from cultivated peat soil," *Soil Biology and Biochemistry*, vol. 43, no. 5, pp. 923–931, 2011.

[8] J. Jauhiainen, A. Hooijer, and S. E. Page, "Carbon dioxide emissions from an *Acacia* plantation on peatland in Sumatra, Indonesia," *Biogeosciences*, vol. 9, no. 2, pp. 617–630, 2012.

[9] Ö. Berglund, K. Berglund, and L. Klemedtsson, "A lysimeter study on the effect of temperature on CO_2 emission from cultivated peat soils," *Geoderma*, vol. 154, no. 3-4, pp. 211–218, 2010.

[10] A. Hadi, K. Inubushi, Y. Furukawa, E. Purnomo, M. Rasmadi, and H. Tsuruta, "Greenhouse gas emissions from tropical peatlands of Kalimantan, Indonesia," *Nutrient Cycling in Agroecosystems*, vol. 71, no. 1, pp. 73–80, 2005.

[11] A. B. Ismail, "Farm management practices for mitigation of carbon dioxide emission in peatland agrosystems," in *Proceedings of the International Conference on Balanced Nutrient Management for Tropical Agriculture*, pp. 72–76, Pahang, Malaysia, August 2010.

[12] C. Kechavarzi, Q. Dawson, M. Bartlett, and P. B. Leeds-Harrison, "The role of soil moisture, temperature and nutrient amendment on CO_2 efflux from agricultural peat soil microcosms," *Geoderma*, vol. 154, no. 3-4, pp. 203–210, 2010.

[13] N. Fenner, N. J. Ostle, N. McNamara et al., "Elevated CO_2 effects on peatland plant community carbon dynamics and DOC production," *Ecosystems*, vol. 10, no. 4, pp. 635–647, 2007.

[14] H. Vasander and J. Jauhiainen, "Land use change in tropical peatlands and current uncertainties in greenhouse gas emissions," in *Proceedings of the International Symposium and Workshop on Tropical Peatland: Peatland Development—Wise Use and Impact Management*, pp. 143–148, Sarawak, Malaysia, August 2008.

[15] A. B. Ismail, "Towards wise use of tropical peatland: from agriculture perspective," in *Proceedings of the International Symposium and Workshop on Tropical Peatland*, pp. 129–141, Sarawak, Malaysia, August 2008.

[16] M. L. Raziah and A. R. Alam, "Status and impact of pineapple technology on mineral soil," *Economic and Technology Management Review*, vol. 5, pp. 11–19, 2010.

[17] K. Inubushi, Y. Furukawa, A. Hadi, E. Purnomo, and H. Tsuruta, "Seasonal changes of CO_2, CH_4 and N_2O fluxes in relation to land-use change in tropical peatlands located in coastal area of South Kalimantan," *Chemosphere*, vol. 52, no. 3, pp. 603–608, 2003.

[18] S. E. Page, C. J. Rieley, and J. O. Rieley, "Tropical peatlands: distribution, extent and carbon storage—uncertainties and knowledge gaps," in *Proceedings of the International Symposium and Workshop on Tropical Peatland*, Yogyakarta, Indonesia, August 2007.

[19] O. H. Ahmed, M. H. Ahmad Husni, A. B. Anuar, and M. M. Hanafi, *Sustainable Production of Pineapples on Tropical Peat Soils*, Universiti Putra Malaysia Press, Selangor, Malaysia, 2013.

[20] A. B. Ismail, J. Asing, and M. Zulkefli, "Residual impact of various land clearing techniques on peat chemical characteristics," in *A Case Study at MARDI Peat Research Station Sessang, Sarawak, Malaysia*, A. B. Ismail, H. K. Ong, M. J. Mohamad Hanif, and M. S. Umi Kalsom, Eds., pp. 33–61, MARDI, Sarawak, Malaysia, 2007.

[21] J. M. Bremner and D. R. Keeney, "Determination and isotope-ratio analysis of different forms of nitrogen in soils. Part 3. Exchangeable ammonium, nitrate and nitrite by extraction-distillation method," *Soil Science Society of America Journal*, vol. 35, no. 5, pp. 577–582, 1966.

[22] D. W. Nelson and L. E. Sommers, "Total carbon, organic carbon and organic matter," in *Methods of Soil Analysis, Chemical and Microbiological Properties, Part 2*, A. L. Page, R. H. Miller, and D.R. Keeney, Eds., pp. 570–571, Soil Science Society of America, Wisconsin, Wis, USA, 1982.

[23] J. M. Bremner, "Nitrogen-total," in *Methods of Soil Analysis, Part 3: Chemical Methods*, D. L. Sparks, A. L. Page, P. A. Helmke et al., Eds., pp. 1085–1121, Soil Science Society of America, Madison, Wis, USA, 1960.

[24] Y. Harada and A. Inoko, "The measurement of the cation-exchange capacity of composts for the estimation of the degree of maturity," *Soil Science and Plant Nutrition*, vol. 26, no. 1, pp. 127–134, 1980.

[25] E. T. Lim, "Physical analysis: determination of bulk density," in *Peat Soils of Sarawak and the Analytical Methods*, pp. 27–28, Department of Agriculture, Sarawak, Malaysia, 1991.

[26] E. Dugan, A. Verhoef, S. Robinson, and S. Saran, "Bio-char from sawdust, maize stover and charcoal: impact on water holding capacities (WHC) of three soils from Ghana," in *Proceedings of the 19th World Congress of Soil Science: Soil Solutions for a Changing World*, pp. 9–12, Brisbane, Australia, August 2010.

[27] M. Suhaimi, K. R. Emmyrafedziawati, M. S. Umi Kalsom, A. M. Sahilah, and A. B. Ismail, "Effect of land-clearing methods on distribution of microbial populations in peat ecosystem," in *A Case Study at MARDI Peat Research Station Sessang, Sarawak, Malaysia*, A. B. Ismail, H. K. Ong, M. J. Mohamad Hanif, and M. S. Umi Kalsom, Eds., pp. 81–87, MARDI, Selangor, Malaysia, 2007.

[28] IAEA, "Sampling techniques and sample handling," in *Manual on Measurement of Methane and Nitrous Oxide Emissions from Agriculture*, IAEA-TECDOC, pp. 45–67, IAEA, Vienna, Austria, 1992.

[29] M. Zulkefli, L. K. C. Liza Nuriati, and A. B. Ismail, "Soil CO_2 flux from tropical peatland under different land clearing techniques," *Journal of Tropical Agriculture and Food Science*, vol. 38, no. 1, pp. 131–137, 2010.

[30] B. Widén and A. Lindroth, "A calibration system for soil carbon dioxide-efflux measurement chambers: description and application," *Soil Science Society of America Journal*, vol. 67, no. 1, pp. 327–334, 2003.

[31] J. P. Andriesse, "The main characteristics of tropical peats," in *Nature and Management of Tropical Peat Soils*, FAO Soils Bulletin 59, FAO, Rome, Italy, 1988.

[32] M. Murtedza, E. Padmanabhan, B. L. H. Mei, and W. B. Siong, "The peat soils of Sarawak," Strapeat Status Report, 2002.

[33] MARDI, *Master Plan for Malaysian Agricultural Research and Development Institute Sessang Peat Research Station*, MARDI, Selangor, Malaysia, 1996.

[34] STRAPEAT-UNIMAS-NREB, "Physico-chemical characteristics," in *Handbook for Environmental Impact Assessment (EIA) of Development on Peatlands*, pp. 3–7, UNIMAS, Sarawak, Malaysia, 2004.

[35] M. M. Selamat, "Biologi tanaman dan keperluan persekitaran," in *Penanaman Nanas—Nanas Makan Segar dan Nanas Kaleng*, M. M. Selamat, Ed., pp. 7–16, MARDI, Selangor, Malaysia, 1996.

[36] P. Mäkiranta, K. Minkkinen, J. Hytönen, and J. Laine, "Factors causing temporal and spatial variation in heterotrophic and rhizospheric components of soil respiration in afforested organic soil croplands in Finland," *Soil Biology and Biochemistry*, vol. 40, no. 7, pp. 1592–1600, 2008.

[37] J. Paz-Ferreiro, E. Medina-Roldán, N. J. Ostle, N. P. McNamara, and R. D. Bardgett, "Grazing increases the temperature sensitivity of soil organic matter decomposition in a temperate grassland," *Environmental Research Letters*, vol. 7, Article ID 014027, pp. 1–5, 2012.

[38] H. E. Dickens and J. M. Anderson, "Manipulation of soil microbial community structure in bog and forest soils using chloroform fumigation," *Soil Biology and Biochemistry*, vol. 31, no. 14, pp. 2049–2058, 1999.

[39] S. Hu and A. H. C. Van Bruggen, "Efficiencies of chloroform fumigation in soil: effects of physiological states of bacteria," *Soil Biology and Biochemistry*, vol. 30, no. 13, pp. 1841–1844, 1998.

[40] K. Toyota, K. Ritz, and I. M. Young, "Survival of bacterial and fungal populations following chloroform-fumigation: effects of soil matric potential and bulk density," *Soil Biology and Biochemistry*, vol. 28, no. 10-11, pp. 1545–1547, 1996.

[41] E. R. Ingham and K. A. Horton, "Bacterial, fungal and protozoan responses to chloroform fumigation in stored soil," *Soil Biology and Biochemistry*, vol. 19, no. 5, pp. 545–550, 1987.

[42] D. S. Jenkinson and D. S. Powlson, "The effects of biocidal treatments on metabolism in soil-I. Fumigation with chloroform," *Soil Biology and Biochemistry*, vol. 8, no. 3, pp. 167–177, 1976.

[43] L. Zelles, A. Palojärvi, E. Kandeler, M. Von Lützow, K. Winter, and Q. Y. Bai, "Changes in soil microbial properties and phospholipid fatty acid fractions after chloroform fumigation," *Soil Biology and Biochemistry*, vol. 29, no. 9-10, pp. 1325–1336, 1997.

[44] S. Saggar, N. Jha, J. Deslippe et al., "Denitrification and N_2O:N_2 production in temperate grasslands: processes, measurements, modelling and mitigating negative impacts," *Science of the Total Environment*, vol. 465, pp. 173–195, 2013.

[45] A. R. Yallop and B. Clutterbuck, "Land management as a factor controlling dissolved organic carbon release from upland peat soils 1: spatial variation in DOC productivity," *Science of the Total Environment*, vol. 407, no. 12, pp. 3803–3813, 2009.

[46] F. Worrall, H. S. Gibson, and T. P. Burt, "Modelling the impact of drainage and drain-blocking on dissolved organic carbon release from peatlands," *Journal of Hydrology*, vol. 338, no. 1-2, pp. 15–27, 2007.

Hindawi Publishing Corporation
The Scientific World Journal
Volume 2014, Article ID 216071, 8 pages
http://dx.doi.org/10.1155/2014/216071

Research Article

Soil-Borne Microbial Functional Structure across Different Land Uses

Eiko E. Kuramae,[1] Jizhong Z. Zhou,[2] George A. Kowalchuk,[3] and Johannes A. van Veen[1,4]

[1] *Department of Microbial Ecology, Netherlands Institute of Ecology (NIOO-KNAW), 6708 PB Wageningen, The Netherlands*
[2] *Institute for Environmental Genomics, University of Oklahoma, Norman, OK 73019, USA*
[3] *Department of Biology, Utrecht University, 3512 JE Utrecht, The Netherlands*
[4] *Institute of Biology, Leiden University, 2311 EZ Leiden, The Netherlands*

Correspondence should be addressed to Eiko E. Kuramae; e.kuramae@nioo.knaw.nl

Received 29 May 2014; Revised 26 June 2014; Accepted 16 July 2014; Published 10 August 2014

Academic Editor: Antonio Paz González

Land use change alters the structure and composition of microbial communities. However, the links between environmental factors and microbial functions are not well understood. Here we interrogated the functional structure of soil microbial communities across different land uses. In a multivariate regression tree analysis of soil physicochemical properties and genes detected by functional microarrays, the main factor that explained the different microbial community functional structures was C : N ratio. C : N ratio showed a significant positive correlation with clay and soil pH. Fields with low C : N ratio had an overrepresentation of genes for carbon degradation, carbon fixation, metal reductase, and organic remediation categories, while fields with high C : N ratio had an overrepresentation of genes encoding dissimilatory sulfate reductase, methane oxidation, nitrification, and nitrogen fixation. The most abundant genes related to carbon degradation comprised bacterial and fungal cellulases; bacterial and fungal chitinases; fungal laccases; and bacterial, fungal, and oomycete polygalacturonases. The high number of genes related to organic remediation was probably driven by high phosphate content, while the high number of genes for nitrification was probably explained by high total nitrogen content. The functional gene diversity found in different soils did not group the sites accordingly to land management. Rather, the soil factors, C : N ratio, phosphate, and total N, were the main factors driving the differences in functional genes across the fields examined.

1. Introduction

Nutrient cycling within terrestrial ecosystems is mostly performed via the activities of soil-borne microorganisms [1]. With the advent of molecular biological methods, considerable amount of knowledge has been accumulated, concerning the diversity and distribution of microorganisms in soil environments [2–4]. Most of the studies related to the impact of land use change on microbes have focused on the phylogenetic composition of the soil microbial community. With respect to microbial functions in soils, most studies have traditionally been based on enzyme activity screening, with relatively little attention paid to functional marker gene screening [5]. The use of functional gene markers to monitor the presence and activity of genes responsible for key steps in terrestrial nutrient cycles may provide a much more directed approach to the analysis of the nutrient cycling properties of terrestrial ecosystems.

A large amount of knowledge is becoming available concerning the microbial enzymes responsible for the key steps of the major nutrient cycles in soil (i.e., carbon, nitrogen, sulphur, etc.). Recent studies have revealed a great diversity within the genes encoding these key enzymatic processes [6–10], providing an expanding database representing the known diversity of genes encoding key enzymatic steps involved in nutrient cycling. Microarray technologies have made it possible to represent the diversity of key enzyme functions as an array of probes, which can be interrogated with DNA or RNA extracted from the environment [11–13]. In this way, the total metagenome of an environmental sample can be examined for the presence, diversity, and activity of genes critical to the major nutrient cycles. Coupling such data with

nutrient flux measurements, enzyme activities, and other measures of soil quality (including phylogenetic microarray data) could potentially provide a quantum advance in our understanding of nutrient cycling in soil systems [14]. Although sequence databases are becoming rather extensive, we clearly have yet to detect the full expanse of the diversity of key enzyme functions, and such microarray-based analyses still necessarily fail to cover all gene families that may be critical to nutrient cycling. Thus, as our knowledge of gene diversity increases, so too will our ability to design probes to monitor a broader range of genes and activities, and such functional microarrays will continue to improve and become more complete as research progresses.

Anthropogenic perturbations (e.g., pollution, fertilizer deposition, and habitat destruction) are known to influence soil nutrient cycles, but little is known about the mechanistic aspects of such disturbances. This lack of knowledge inhibits our ability to assess the extent to which human activities disturb terrestrial nutrient cycling potential and thwarts efforts to predict future anthropogenic impacts. Before the influence of such perturbations can be established or predicted, one must characterize the natural variation and normal operating range with respect to the diversity and expression of key genes related to nutrient cycle functions. To establish such normal operating boundaries, the dynamics of the gene diversity and expression must be monitored across relevant spatial and temporal scales and in response to natural and imposed variability. Although this still remains technically challenging, with hurdles related to limits of signal detection and reproducibility [15, 16], functional microarray platforms provide a powerful, high throughput, tool for the detailed assessment of microbial nutrient cycling activities.

In the current study, we exploited the functional structure of microbial communities in soils under different land uses. First, we determined the soil parameters of each field. Next, we tracked the microbial functional communities across land uses. Lastly, we identified links between soil parameters and microbial functions. The main questions addressed in this study were how does the microbial community functional structure vary with different soil managements and what are the main drivers that are related to this variation. In order to answer these questions, we used functional gene arrays (FGA), focussing on crucial steps of key nutrient cycles (C, N, P, and S) across eight fields representing five generally representative forms of land use (conventional arable field, organic arable field, pasture, natural grassland, and pine forest) in The Netherlands. To our knowledge, this is one of few studies to apply functional microarray technique across a range of different land managements. In addition, this study is one of the first to include a suite of soil measurements to explore the environmental factors driving soil microbial functions under different land uses.

2. Material and Methods

2.1. Experimental Design, Sampling, and Soil Analyses. Eight fields subjected to five generally representative forms of land management in The Netherlands (pine forest, natural grasslands, pasture, conventional arable field, and organic arable field) were sampled (Figure S1, Supplementary Material available online at http://dx.doi.org/10.1155/2014/216071) in May 2007; see Table 1. The eight fields were selected from a previous study [17] on soil factors driving microbial community composition in 26 fields across The Netherlands under different land management. In each field, a central point was selected, and subsequently four sampling points at 20 m of the central point were chosen so as to obtain five samples per field (A, B, C, D, and E). Each sample (A, B, C, D, and E) was comprised of five subsamples (A1, A2, A3, A4, A5; B1, B2, B3, B4, B5, etc) from soil cores (8 cm diameter × 20 cm deep) taken randomly within a two-meter radius of each of the five sample points A, B, C, D, and E. Soil samples were sieved through a 4 mm mesh to remove stones, roots, and plant materials. Equal amounts of each of the five subsamples of a given sampling point were pooled, thereby yielding a replication of five composite samples per field. Each composite sample was divided into two parts. One part was stored at −80°C for DNA extraction and the other part kept at 4°C for physical and chemical analysis. For physical and chemical analysis, equal amounts of each of the five replicates per field were pooled.

Physicochemical characterization was performed by BLGG (Bedrijfslaboratorium voor Grond en Gewasonderzoek, Wageningen, The Netherlands, http://blgg.agroxpertus.nl/). Soil pH was measured in a 1 : 2.5 soil/water suspension, and soil moisture was determined gravimetrically (g/100 g). Soil organic matter content (% OM) was determined by loss on ignition (LOI) analysis. Soil texture was determined using a Bouyoucos densimeter after shaking the soil vigorously with NaOH 1 M as dispersant. Soil $CaCO_3$ was determined a by Scheibler's method. Phosphate (P) was determined as the amount extracted from a soil after addition of water at a shaking ratio of 1 : 60, a procedure typically used to determine the soil fertility status of arable fields in The Netherlands. Cr, Cu, Hg, As, Ni, Cd, Pb, and Zn were extracted by Mehlich 1 and determined by atomic absorption spectrometry.

2.2. DNA Extraction, Amplification, Labelling, and Hybridization. DNA extractions were performed separately on each of the five replicates per field using the MoBio Power Soil Extraction kit (MoBio, Carlsbad, CA, USA) with bead-beating (Restch MM301, Retsch GmbH, Germany) at 5.5 m s^{-1} for 10 min. Total DNA concentration was quantified on a ND-1000 spectrophotometer (Nanodrop Technology, Wilmington, DE, USA).

The DNAs from replicates of each sample were pooled. Because the amount of DNA extracted was in most cases insufficient for direct labeling and hybridization, 30 ng of DNA per sample was amplified by whole community rolling cycle amplification (WCRCA) using a TempliPhi kit (GE Healthcare, Piscataway, NJ). We used the GeoChip functional microarray platform, which contains more than 24,000 oligonucleotide (50-mer) probes targeting targeted approximately 10,000 genes involved in nitrogen, carbon, sulfur and phosphorus transformations and cycling, metal reduction

Table 1: Soil physical and chemical variables measured in eight samples with different land uses.

Field	Land use	Vegetation	pH	Moisture	Organic matter	Clay	Silt	Sand	$CaCO_3$	P	Total C	Total N	C : N ratio	Cr	Cu	Hg	As	Ni	Cd	Pb	Zn
						%				mg/L	g/100 g	mg/kg		mg/kg							
8F	Conventional arable field	Beans	5.8	17.15	3.5	0.6	10.9	88.4	0	69	2.1	1267	16.6	7.6	11	0.03	1.4	0	0.20	15	28
16F	Conventional arable field	Crops	7.3	15.57	1.7	11.6	27.2	61.2	0.2	146	1.1	1217	9.00	19	0	0.04	7.5	6.7	0.11	16	29
4F	Forest	Pine	3.7	16.91	6.4	0.3	4.3	95.4	0	24	3.8	1703	22.3	0	0	0.04	1.8	0	0.10	15	0
25F	Natural	Grassland	5.5	24.93	5.3	1.8	6.4	91.9	0	3	2.9	2029	14.3	7.2	6.2	0.06	3.4	3.5	0.24	9.2	12
10F	Organic arable field	Maize	5.8	13.14	3.6	1.8	10.2	88	0	121	2.0	1338	14.9	7.2	5.3	0.03	2.5	0	0.18	17	25
13F	Organic arable field	Crops	7.4	18.37	2.4	8.2	39.8	52	3.8	69	1.4	1440	9.7	26	8.2	0.04	13	10	0.20	15	40
1F	Pasture	Grassland	6.2	13.77	5.8	4.1	16.1	79.7	0.2	84	2.7	2142	12.6	5.5	21	0.05	26	0	0.32	37	43
19F	Pasture	Grassland	6.0	29.14	9.4	36.7	51.1	12.1	0.2	32	4.8	5489	8.7	52	27	0.08	14	33	0.49	32	130

Table 2: Total number and percentage of functional genes unique and overlapping in samples of different land uses.

% of genes	25F	19F	16F	13F	10F	8F	4F	1F
25F	*13 (6.9)*	132 (19.7)	136 (23.8)	145 (14.5)	119 (31.4)	61 (20.4)	123 (22.1)	72 (27.6)
19F		*113 (18.4)*	300 (36.0)	429 (37.6)	214 (30.1)	107 (15.7)	264 (31.3)	109 (16.7)
16F			*72 (13.8)*	381 (34.8)	206 (33.0)	110 (18.9)	251 (33.0)	116 (21.1)
13F				*319 (33.4)*	254 (25.1)	133 (13.3)	328 (29.3)	120 (12.2)
10F					*16 (5.1)*	100 (26.0)	186 (30.1)	94 (25.9)
8F						*16 (9.2)*	96 (16.8)	59 (22.7)
4F							*97 (19.7)*	120 (23.1)
1F								*4 (2.7)*
Total number of genes	187	614	520	956	311	173	493	146

Italic numbers represent unique genes in each soil sample.
The remaining numbers represent the numbers of genes and their percentage (in parenthesis) overlapping between two samples.

and resistance and organic xenobiotic degradation [18]. The number of technical replicates for microarray hybridization was four for samples of fields 1F, 4F, 10F, 13F, 16F, 19F, and 25F and three for field 8F. The amplified DNAs were labelled with a Cy5 fluorescent dye, purified, and then hybridized to the GeoChip functional array (FGA II) [18] in a Tecan hybridization station (Durham, NC) at 42°C for 10 hours. Arrays were washed, dried, and scanned using a ScanArray 5000. The signal intensity for each probe was determined digitally by Imagene software (Biodiscovery Inc., Los Angeles, CA).

2.3. Microarray Data Processing and Analysis. The data processing was according to He et al. [18]. Each array was cleaned by deleting flag 1.3 and SNR < 2 and normalized by mean of all spots in the same slide. The final table of all intensities of all samples were obtained by removing the outline spots more than 2 sigma, the maximal ratio between spots was 3 if certain genes had only 2 spots in the array, the spots with final spot numbers was 0.51 times less than the original number and the minimal spots number for a gene was 2.

2.4. Statistical Analysis. Pearson correlations were calculated between soil factors (total C, total N, C : N ratio, organic matter, soil pH, $CaCO_3$, Cr, Cu, P, Zn, soil texture, and soil moisture) using the "multtest" package in R (version 2.6.0, The R Foundation for Statistical Computing). P values were corrected for multiple testing, using the false discovery rate controlling procedure [19]. The probe intensities and soil physicochemical factors were used for multivariate regression tree (MRT) analysis by using the "mvpart" package in R, and the distance matrix was based on Bray-Curtis built by the function "gdist."

Microbial community functional structure was related to soil factors using canonical correspondence analyses (CCA) in Canoco 4.5 for Windows [20]. Probe intensities were used as "species" data, while soil data was included in the analysis as "environmental" variables. Variables having the most significant influence on the microbial community structure were chosen by forward selection with a $P < 0.01$ baseline. The variables selected this way were then included in a model whose significance was tested with 999 permutations. Gene functional category and land fields were added as extra variables but not involved in the calculations.

3. Results and Discussion

3.1. Soil Properties. In general, the pasture field 19F was very different from the other fields with highest cadmium, clay, chromium, copper, mercury, nickel, organic matter, silt, total carbon, total nitrogen, and zinc contents (Table 1). The pine forest 4F had higher C : N ratio, sand, and total C contents and lower cadmium, clay, chromium, pH, phosphate, and zinc contents than the other sites (Table 1). The highest percentage of $CaCO_3$ was found in organic arable field 13F. The soil moisture at the time of sampling varied among fields. The moisture contents of 19F and 25F fields were the highest, while moisture contents of 10F and 1F fields were the lowest (Table 1).

The correlation analyses showed significant correlation between several soil factors. Soil pH was negatively correlated with C : N ratio. C : N ratio was negatively correlated with silt and chromium and positively correlated with sand. Total N was positively correlated with total C, organic matter, clay, chromium, and zinc and negatively correlated with sand. Chromium and zinc were positively correlated (Table S1).

3.2. Microarray Analyses. A total of 1405 genes across all samples were detected. The pasture field 1F had the lowest numbers of genes (146) detected by the GeoChip followed by conventional arable field 8F (173 genes) and natural grassland field 25F (Table 2). The organic arable field 13F had the highest number of genes detected (956). The pasture field 1F with lower functional gene number had high overlap with communities of natural grassland 25F (27.6%) and organic arable field 10F (25.9%) (Table 2). The shared genes between two or more field-soils varied from 12.2 to 37.6%, and the numbers of unique genes identified in only one soil were relative very small, varying from 2.7 to 19.7%, except for organic arable field 13F (33.4%) (Table 2). Although there were large differences in the number of genes detected in each field, fields with similar soil characteristics, such as high total nitrogen in 1F, 25F, and 10F and low phosphate content

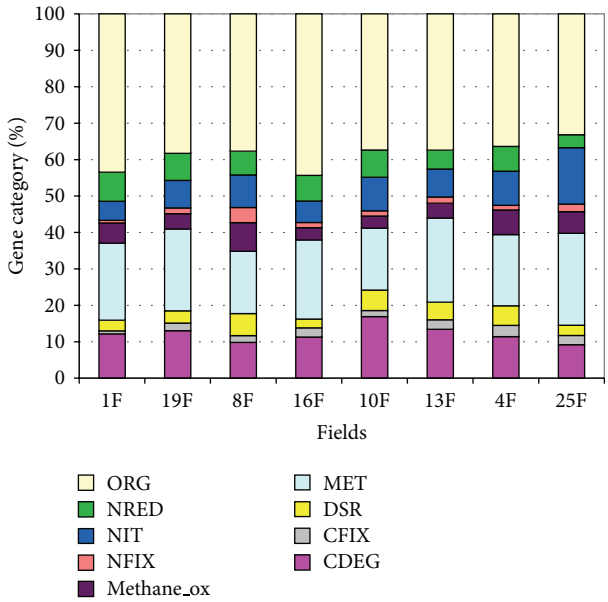

Figure 1: Percentage of gene categories given in the GeoChip present in soils from different land uses: pasture (1F, 19F), conventional arable field (8F, 16F), organic arable field (10F, 13F), forest (4F), and natural grassland (25F). CDEG: carbon degradation; CFIX: carbon fixation; DSR: dissimilatory sulfate reductase; MET: metal reductase; Methane_ox: methane oxidation NFIX: nitrogen fixation; NIT: nitrification; NRED: nitrogen reductase; ORG: organic remediation.

(Figure 2) in 13F and 19F showed the most overlap in detected genes.

In general, there were differences in microbial community functional structure among the study sites (Figure 1). The percentage of genes related to carbon degradation (17%) was highest in organic arable fields (10F) and lowest in natural grassland 25F. This low representation of carbon degradation genes in field 25F is somewhat expected, as this particular field represents a typical Dutch "Blauwgrasland" soil type, which is often inundated and therefore exposed to anaerobic conditions. Indeed, soil water content impacts oxygen diffusion what higher moisture content leads to decrease in organic matter decomposition due to low oxygen supply [21]. Genes detected for carbon fixation were generally similar across the soils examined, except for 10F and 1F fields, which both had a lower percentage of genes from this category. Interestingly, these two fields had the lowest soil moisture contents. Dissimilatory sulfate reductase genes were highest (5-6%) in soils from filed 4F, 8F, and 10F. Pine forest field 4F and conventional arable field 8F had higher percentages (6-7%) of genes of methane oxidation. The conventional arable field 8F had highest number of genes of nitrogen fixation (4%), while fields 16F and 1F had highest gene numbers for organic remediation (44%) (Figure 1).

In a multivariate regression tree (MRT) analysis, combining the measured soil factors (pH, total N, total C, C : N ratio, organic matter, phosphate, clay, silt, sand, $CaCO_3$, Cd, Cr, Cu, Ni, Pb, Zn, As, and Hg) and the intensities of the 1405 genes detected by the GeoChip, the main factor that explained the microbial community functional structure differences in the eight fields was C : N ratio (Figure 2). C : N ratio differentiated the fields into two main groups: (a) fields 16F (conventional arable field), 19F (pasture), and 13F (organic arable field) with C : N ratio lower than 11.15 and (b) fields 10F (organic arable field), 4F (pine forest), 25F (natural grassland), 1F (pasture), and 8F (conventional arable field) with C : N ratio higher than 11.15. The clustering of the three fields 13F, 16F, and 19F with C : N ratio lower than 11.16 also corresponds to less sand in the soil texture and higher soil pH as compared to the other fields, as C : N was significantly positively correlated with sand and soil pH.

The main differences between the two clusters A/B (fields 16F, 13F, and 19F) and C/D (fields 1F, 4F, 10F, 25F, and 8F) were that fields with C : N ratios lower than 11 had more genes for carbon degradation (CDEG), carbon fixation (CFIX), metal reductase (MET), and organic remediation (ORG) categories than the fields with C : N ratio higher than 11. C : N ratio is known to have a large influence on decomposition rates [22]. Fields 16F, 13F, and 19F had the lowest C : N ratios. It is expected that soils with lower C : N ratios will contain more easily decomposable organic matters as compared to soils with high C : N ratios [23]. Our results are consistent with this expectation, with higher numbers of carbon degradation genes in those sites with lowest C : N ratios. In addition, CO_2 is released into the environment during the organic material decomposition, and this may explain the high numbers of microbial carbon fixation genes [24] in fields 16F, 13F, and 19F. On the other hand, fields with a C : N ratio higher than 11 showed more genes from categories dissimilatory sulfate reductase (DSR), methane oxidation, nitrification (NIT), and nitrogen fixation (NFIX) than fields with C : N lower than 11 (Figure 2).

Among fields with C : N ratio lower than 11, field 16F had the highest number of genes of the organic remediation (ORG) category. This may be related to the high amount of phosphate in this soil—that is, greater than 107 mg/kg soil as calculated in MRT analysis and illustrated in the CCA plot (Figure 3). On the other hand, the high percentage of genes for CDEG and MET in fields 13F and 19F appeared to be explained by lower phosphate concentrations (less than 107 mg/kg; Figure 2). The higher phosphate contents in fields 13F, 16F, 19F and 16F may be related to the high clay content of these soils, as it is well known that phosphate availability strongly depends on clay quantity and quality [25].

The genes detected within the ORG category in 16F are related to a range of degradation activities (Table S2). In fact, phosphate has been shown to be an important nutrient factor required by bacterial biofilter for maximum methane elimination [26]. The field 16F is a conventional arable field that has been intensively cultivated with different crops. It has therefore been subjected to high inputs of inorganic fertilizers such as nitrogen, phosphate, and potassium. Phosphate was negatively correlated with total C and total C was positively correlated with organic matter content. In other words, the fields 13F and 19F had higher total carbon, higher organic matter and lower phosphate than field 16F, and these properties seem to be favourable for genes involved in carbon

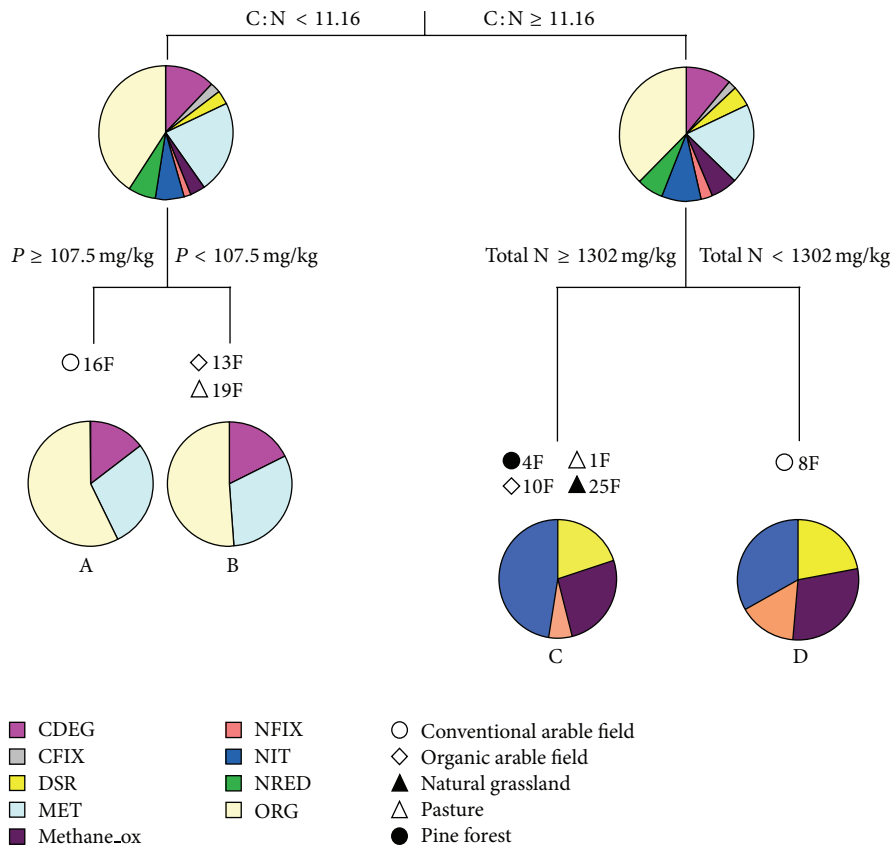

Figure 2: Multivariate regression tree (MRT) analysis of soil physicochemical properties and GeoChips intensities given by samples of fields 1F, 4F, 8F, 10F, 13F, 16F, 19F, and 25F. A, B, C, and D are clusters.

degradation (CDEG) and metal reductase (MET) activities (Figures 2 and 3). The CDEG genes overrepresented in samples 13F and 16F were related to bacterial and fungal cellulases; bacterial and fungal chitinases; fungal laccases; and bacterial, fungal, and oomycete polygalacturonases (Table S3). The MET genes overrepresented in these same fields 13F and 19F were genes encoding reductases of aluminium, arsenic, cadmium, chromium, cobalt, copper, cytochrome, lead, mercury, nickel, tellurium, and vanadium (Table S3), and some soil chemicals, that is, cadmium, chromium, copper, mercury, and nickel, were indeed highest in the pasture field 19F (Table 1).

Fields with a C : N ratio higher than 11 (1F, 4F, 10F, and 25F) had relatively high percentages of genes of nitrification (NIT), and high levels of total nitrogen (i.e., >1302 mg/kg) appeared to explain this result. The field 8F had the highest numbers of genes from categories for dissimilatory sulfate reductase, methane oxidation, and nitrogen fixation, and this pattern was explained by total N levels lower than 1302 mg/kg soil (Figure 2). The higher percentage of nitrogen fixation genes in field 8F than fields 1F, 4F, 10F, and 25F can be explained by the presence of nitrogen-fixing bacteria in this particular soil, probably related to the growth of legumes (beans) at this site. The nitrification-related genes abundant in fields 1F, 4F, 10F, and 25F were ureases, *amo*A, *pmo*A, and *ghd*. The DSR genes abundant in 8F were *dsr*A and *dsr*B; the methanol-oxidation category was dominated by *pmo*A and *mmo*A from methanotrophs and nitrogen fixation genes categorized as *nif*H from nitrogen-fixing bacteria (Table S4).

The nitrification genes found in fields 1F, 4F, 10F, and 25F were similar to uncultured ammonia-oxidizing *β-Proteobacteria amo*A genes. Ureases (E.C. 3.5.1.5) are complex metalloenzymes that catalyze the hydrolysis of urea to ammonia and carbon dioxide. This enzyme allows many soil bacteria to use urea as nitrogen source, and we detected several ureases in nitrogen-fixing bacteria such as *Mesorhizobium loti*, *Bradyrhizobium japonicus*, *Rhodopseudomonas palustris*, *Rhodobacter sphaeroides*, *Rhodobacter* (*α-Proteobacteria*), *Chromobacterium violaceum* (*β-Proteobacteria*), and *Nostoc* (*Cyanobacteria*) (Table S4). Urease is also an important virulence factor that improves survival of pathogenic bacteria in harsh conditions within the host and causes direct damage to the host due to ammonium, CO_2, or alkali production (for reviews see [27, 28]), and in our study we found ureases similar to those of plant pathogens such *Pseudomonas syringae*, *Klebsiella aerogenes*, (*γ-Proteobacteria*), *Mycobacterium* (*Actinobacteria*), and *Brucella melitensis* (*α-Proteobacteria*) (Table S4).

Fields 4F and 25F had distinct soil properties or conditions that would be expected to impact numerous microbial processes. However, we found no evidence for a sharp distinction in the functional gene repertoires of these communities.

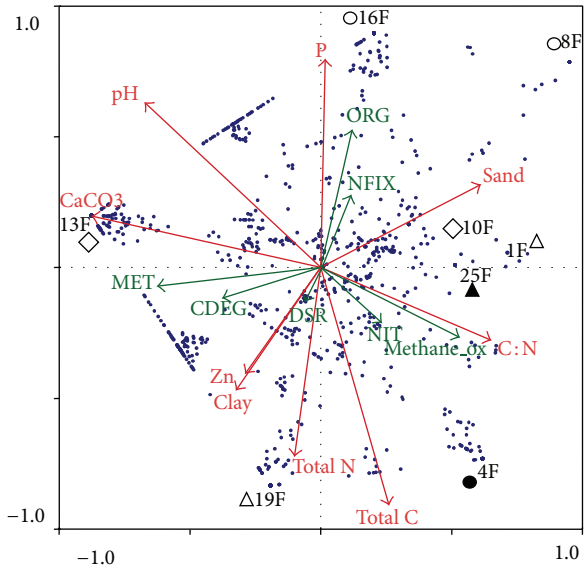

Figure 3: Canonical correspondence analysis (CCA) triplot of soil physicochemical properties (red arrows), GeoChips intensities (dots) with functional categories (green arrows), and eight fields with different land uses.

Field 4F was extremely acidic which distinguishes it from other natural and cultivated soils. In fact, in a previous study on microbial community composition across 26 fields under different land uses including the eight fields here studied, Kuramae et al. [17] found that field 4F had the most distinct microbial community composition. This difference was linked to low pH and high C : N ratio. However, in the present study, 4F and 25F have similar microbial function profiles, despite the differences in soil pH, C : N ratio, and moisture. Thus, it appears to be that soil microbial composition is more sensitive to changes in soil pH than the functional capability of the community. This may be due to the function redundancy present in soil communities. In addition, the soil factors that drive microbial composition are not the same as those driving microbial potential function structures.

4. Conclusion

The soil-borne microbial functional structure in the different fields in The Netherlands did not group the sites accordingly to land management. Although the number of fields examined here was limited to eight, the breadth of our study was sufficient to assess the differences in microbial functional genes in different systems of soil management, and specific soil factors could be identified that explained the differences observed in functional gene composition of the different soils examined.

Conflict of Interests

The authors declare that there is no conflict of interests regarding the publication of this paper.

Acknowledgments

The authors thank Dr. Z. He and Dr. Y. Deng (Institute of Environmental Genomics, The University of Oklahoma) for laboratory and bioinformatics assistance and thank Dr. Bart Pietersen (BDS-BioDetection System), Remy Hillekens (NIOO-KNAW), and Dr. Tjalf de Boer (Vrij University of Amsterdam) for assistance in soil sampling. Publication number 5639 of the Netherlands Institute of Ecology (NIOO-KNAW).

References

[1] J. I. Prosser, "Ecosystem processes and interactions in a morass of diversity," *FEMS Microbiology Ecology*, vol. 81, no. 3, pp. 507–519, 2012.

[2] V. Torsvik and L. Øvreås, "Microbial diversity and function in soil: from genes to ecosystems," *Current Opinion in Microbiology*, vol. 5, no. 3, pp. 240–245, 2002.

[3] E. A. Dinsdale, R. A. Edwards, D. Hall et al., "Functional metagenomic profiling of nine biomes," *Nature*, vol. 452, no. 7214, pp. 629–632, 2008.

[4] A. A. Navarrete, E. E. Kuramae, M. de Hollander, A. S. Pijl, J. A. van Veen, and S. M. Tsai, "Acidobacterial community responses to agricultural management of soybean in Amazon forest soils," *FEMS Microbiology Ecology*, vol. 83, no. 3, pp. 607–621, 2013.

[5] G. A. Kowalchuk, B. Drigo, E. Yergeau, and J. A. van Veen, "Molecular approaches to assess the structure of bacterial and fungal communities in soil—the use of rRNA and other gene markers," in *Nucleic Acids and Proteins in Soil*, P. Nannipieri and K. Smalla, Eds., pp. 159–188, Springer, Heidelberg, Germany, 2006.

[6] A. Priemé, G. Braker, and J. M. Tiedje, "Diversity of nitrite reductase (nirK and nirS) gene fragments in forested upland and wetland soils," *Applied and Environmental Microbiology*, vol. 68, no. 4, pp. 1893–1900, 2002.

[7] G. Braker and J. M. Tiedje, "Nitric oxide reductase (norB) genes from pure cultures and environmental samples," *Applied and Environmental Microbiology*, vol. 69, no. 6, pp. 3476–3483, 2003.

[8] T. Yan, M. W. Fields, L. Wu, Y. Zu, J. M. Tiedje, and J. Zhou, "Molecular diversity and characterization of nitrite reductase gene fragments (nirK and nirS) from nitrate- and uranium-contaminated groundwater," *Environmental Microbiology*, vol. 5, no. 1, pp. 13–24, 2003.

[9] X. D. Liu, S. M. Tiquia, G. Holguin et al., "Molecular diversity of denitrifying genes in continental margin sediments within the oxygen-deficient zone off the Pacific coast of Mexico," *Applied and Environmental Microbiology*, vol. 69, no. 6, pp. 3549–3560, 2003.

[10] S. W. Lee, J. Im, A. A. Dispirito, L. Bodrossy, M. J. Barcelona, and J. D. Semrau, "Effect of nutrient and selective inhibitor amendments on methane oxidation, nitrous oxide production, and key gene presence and expression in landfill cover soils: characterization of the role of methanotrophs, nitrifiers, and denitrifiers," *Applied Microbiology and Biotechnology*, vol. 85, no. 2, pp. 389–403, 2009.

[11] L. Wu, L. Kellogg, A. H. Devol, J. M. Tiedje, and J. Zhou, "Microarray-based characterization of microbial community functional structure and heterogeneity in marine sediments from the Gulf of Mexico," *Applied and Environmental Microbiology*, vol. 74, no. 14, pp. 4516–4529, 2008.

[12] Z. He, Y. Deng, J. D. van Nostrand et al., "GeoChip 3.0 as a high-throughput tool for analyzing microbial community composition, structure and functional activity," *ISME Journal*, vol. 7, no. 9, pp. 1167–1179, 2010.

[13] J. R. Reeve, C. W. Schadt, L. Carpenter-Boggs, S. Kang, J. Zhou, and J. P. Reganold, "Effects of soil type and farm management on soil ecological functional genes and microbial activities," *ISME Journal*, vol. 4, no. 9, pp. 1099–1107, 2010.

[14] E. M. H. Wellington, A. Berry, and M. Krsek, "Resolving functional diversity in relation to microbial community structure in soil: exploiting genomics and stable isotope probing," *Current Opinion in Microbiology*, vol. 6, no. 3, pp. 295–301, 2003.

[15] J. Zhou and D. K. Thompson, "Challenges in applying microarrays to environmental studies," *Current Opinion in Biotechnology*, vol. 13, no. 3, pp. 204–207, 2002.

[16] V. J. Denef, J. Park, J. L. M. Rodrigues, T. V. Tsoi, S. A. Hashsham, and J. M. Tiedje, "Validation of a more sensitive method for using spotted oligonucleotide DNA microarrays for functional genomics studies on bacterial communities," *Environmental Microbiology*, vol. 5, no. 10, pp. 933–943, 2003.

[17] E. E. Kuramae, E. Yergeau, L. C. Wong, A. S. Pijl, J. A. Van Veen, and G. A. Kowalchuk, "Soil characteristics more strongly influence soil bacterial communities than land-use type," *FEMS Microbiology Ecology*, vol. 79, no. 1, pp. 12–24, 2012.

[18] Z. He, T. J. Gentry, C. W. Schadt et al., "GeoChip: a comprehensive microarray for investigating biogeochemical, ecological and environmental processes," *ISME Journal*, vol. 1, no. 1, pp. 67–77, 2007.

[19] Y. Benjamini and Y. Hochberg, "Controlling the false discovery rate: a practical and powerful approach to multiple testing," *Journal of the Royal Statistical Society B: Methodological*, vol. 57, no. 1, pp. 289–300, 1995.

[20] C. J. F. ter Braak and P. Šmilauer, *CANOCO Reference Manual and CanoDraw for Windows User's Guide: Software for Canonical Community Ordination (Version 4.5)*, Microcomputer Power, Ithaca, NY, USA, 2002.

[21] K. Killham, M. Amato, and J. N. Ladd, "Effect of substrate location in soil and soil pore-water regime on carbon turnover," *Soil Biology and Biochemistry*, vol. 25, no. 1, pp. 57–62, 1993.

[22] S. Manzoni, R. B. Jackson, J. A. Trofymow, and A. Porporato, "The global stoichiometry of litter nitrogen mineralization," *Science*, vol. 321, no. 5889, pp. 684–686, 2008.

[23] M. W. I. Schmidt, M. S. Torn, S. Abiven et al., "Persistence of soil organic matter as an ecosystem property," *Nature*, vol. 478, no. 7367, pp. 49–56, 2011.

[24] X. H. Wu, T. D. Ge, H. Z. Yuan et al., "Changes in bacterial CO_2 fixation with depth in agricultural soils," *Appiedl Microbiology Biotechnology*, vol. 98, no. 5, pp. 2309–2319, 2014.

[25] J. K. Edzwald, D. C. Toensing, and M. C. Leung, "Phosphate adsorption reactions with clay minerals," *Environmental Science and Technology*, vol. 10, no. 5, pp. 485–490, 1976.

[26] J. Nikiema, R. Brzezinski, and M. Heitz, "Influence of phosphorus, potassium, and copper on methane biofiltration performance," *Canadian Journal of Civil Engineering*, vol. 37, no. 2, pp. 335–345, 2010.

[27] H. L. T. Mobley and R. P. Hausinger, "Microbial ureases: significance, regulation, and molecular characterization," *Microbiological Reviews*, vol. 53, no. 1, pp. 85–108, 1989.

[28] H. L. T. Mobley, M. D. Island, and R. P. Hausinger, "Molecular biology of microbial ureases," *Microbiological Reviews*, vol. 59, no. 3, pp. 451–480, 1995.

Hindawi Publishing Corporation
The Scientific World Journal
Volume 2014, Article ID 563038, 9 pages
http://dx.doi.org/10.1155/2014/563038

Research Article

Spatial Characterization of Landscapes through Multifractal Analysis of DEM

P. L. Aguado,[1] J. P. Del Monte,[1] R. Moratiel,[2,3] and A. M. Tarquis[3,4]

[1] *Departamento de Producción Vegetal, Botánica, E.T.S.I.A., UPM, 28040 Madrid, Spain*
[2] *Departamento de Producción Vegetal, Fitotecnia, E.T.S.I.A., UPM, 28040 Madrid, Spain*
[3] *CEIGRAM, E.T.S.I.A., UPM, 28040 Madrid, Spain*
[4] *Departamento de Matemática Aplicada, E.T.S.I.A., UPM, 28040 Madrid, Spain*

Correspondence should be addressed to P. L. Aguado; pl.aguado@upm.es

Received 30 April 2014; Accepted 18 July 2014; Published 6 August 2014

Academic Editor: Antonio Paz González

Landscape evolution is driven by abiotic, biotic, and anthropic factors. The interactions among these factors and their influence at different scales create a complex dynamic. Landscapes have been shown to exhibit numerous scaling laws, from Horton's laws to more sophisticated scaling of heights in topography and river network topology. This scaling and multiscaling analysis has the potential to characterise the landscape in terms of the statistical signature of the measure selected. The study zone is a matrix obtained from a digital elevation model (DEM) (map 10 × 10 m, and height 1 m) that corresponds to homogeneous region with respect to soil characteristics and climatology known as "*Monte El Pardo*" although the water level of a reservoir and the topography play a main role on its organization and evolution. We have investigated whether the multifractal analysis of a DEM shows common features that can be used to reveal the underlying patterns and information associated with the landscape of the DEM mapping and studied the influence of the water level of the reservoir on the applied analysis. The results show that the use of the multifractal approach with mean absolute gradient data is a useful tool for analysing the topography represented by the DEM.

1. Introduction

Each landscape unit is defined by primary physiographic characteristics. In the landscape, several abiotic and biotic factors, as well as anthropic factors, interact to generate a characteristic dynamic over time. The focus of this study is an alluvial surface of arkose resulting from the erosion of the granite of the Sierra del Guadarrama produced by the factors cited above. These factors, along with their interactions at different scales, produce a strong modelling effect through erosion. The universal equation of hydraulic erosion presented by Wischmeyer and Smith (1978) [1] can be used to evaluate the intensity of this process. This model incorporates abiotic factors such as soil type, soil erodibility as a function of composition and structure, topographic factors described by the slope and its length, rain erosivity as function of rain volume, and precipitation intensity. In addition, the vegetation cover produces a biotic effect. In certain cases, anthropic factors, such as soil management and conservation, dominate the evolution of the landscape.

A digital elevation model (DEM) provides the information basis used for many geographic applications, for example, topographic studies, geomorphologic studies, and landscape analysis with geographic information systems (GIS). The ability of a DEM to represent the earth's surface depends on the surface roughness and the resolution used [2, 3]. The information in each DEM pixel depends on the scale used and is characterised by two variables, the resolution and the extension of the area studied [4]. DEMs can vary in resolution and accuracy according to the method used to produce the model [5, 6], although there are statistical characteristics that remain constant or highly similar over a broad range of scales [7]. Based on this property, several techniques have been applied to characterise DEMs through multiscale analysis [8] directly related to fractal geometry. In this way, the complexity of natural landscapes can be revealed [9, 10].

In the general mathematical framework of fractal geometry, many analytical methods have been developed. For example, textural homogeneity has been characterised using the fractal dimension [11]. The fractal dimension has also been used as a spatial measure for describing the complexity of remote sensing imagery [12]. Changes in image complexity have been detected through the spectral range of hyperspectral images affecting the fractal dimension [13], dependence of fractal dimension on the spectral bands of Landsat TM imagery De Cola [14], Lam [15], and other authors [16]. The use of multifractal/wavelet techniques is becoming more widespread in the analysis of remote sensing images [2, 17]; it is not as popular in DEM analysis, although there are several studies characterising soil surface microrelief [18].

Motivated by the fractal geometry of sets [19, 20], the development of multifractal (MF) theory, introduced in the context of turbulence, has been applied in many areas such as earthquake distribution analysis [21], soil pore characterisation [22, 23], image analysis [24], and remote sensing [25–35]. Research into relationships between landscape pattern and process has been influenced by the introduction of fractal geometry and the advent of fractal analysis [36]. With the increasing availability of high-resolution digital elevation data from increasingly larger areas, together with advances in geocomputation and geomorphometry, fractals have become of increasing interest for local-level environmental applications [37].

The acquisition of remotely sensed multiple spectral images is thus a unique source of data for determining the scale-invariant characteristics of the radiant fields related to many factors such as the chemical composition of soil and bedrock, their moisture content, and their surface temperature [28–30, 38–42]. In the MF scheme used, the digital elevation data are considered to represent a singular measure. The analysis then proceeds through an MF spectrum, which gives either geometrical or probabilistic information about the height distribution having the same singularity. Gagnon et al. [43] demonstrated on purely statistical grounds that monofractals are not sufficient to describe topography and that multifractals are needed. A profound review on how this topic has advanced can be found in Gagnon et al. [44].

There are scientific debates over what is fractal. However, a surface does not need to be multifractal to admit a multifractal analysis (MFA). The most important issues are whether MFA is a reliable method for determining fractal parameters and how the results of the MFA are to be interpreted in a given context [35]. We want to remark that the approach does not depend on the assumption that topography is fractal. This observation leads us to the general aim of the paper, which is to use MFA to characterise the information contained in DEM based on the original elevation data and on the absolute gradient. At the same time, we have investigated how the map information is affected by analysing the area under differing conditions, that is, for various water levels in the reservoir.

2. Materials and Methods

2.1. Site Description. The study area is represented by a 1024 × 1024 data matrix obtained from a DEM with a resolution of 10 × 10 m at each point and a height resolution of 1 m, which correspond with a region known as "*Monte de El Pardo*" a property of Spanish national heritage (*patrimonio nacional Español*) of 15,820 Ha located at a short distance from Madrid city with altitude ranging from 576 to 900 m and UTM coordinates Huse 30, Hemisphere Northern, X: 444312.312 to 434542.312 and Y: 4494542.408 to 4484312.408. *Manzanares* River goes through this area from north to south as it can be observed in Figure 1(a). In the southern area, a reservoir is found with a capacity of 43 hm^3, with an altitude ranging from 576 m to 632 m when it is at the highest capacity as it is represented in Figure 1(b). In the middle of the reservoir, the minimum altitude of this area is achieved. Geologic characteristics of the area correspond to arkose deposits coming from granite and gneisses erosion, basis of the *Sierra de Guadarrama*. Several smooth slopes and a river network very few branched can be found with a surface ravaging. The potential vegetation is mainly of a Mediterranean occidental forest; *Q. ilex* L. is the climax specie with several shrub heliophilous vegetation and herbaceous (Gen. *Cistus*). There are some *Q. suber* L. isolated. Actually, this forest has been kept for hunting use.

The criteria of the selection of the study area were to delimit a homogeneous area with respect to soil characteristics and climatology, and then the topographic factor acquires a main role. Regarding vegetation cover, Mediterranean forest is present with some areas influenced by pasture characteristics as a consequence of historical use for hunting and a minimum soil management. With regard to anthropic factors, these have been much less than in the surrounding areas which have been cultivated, producing a high reduction in the original trees and shrubs of the area. However, in 1973, the construction of the reservoir on Manzanares River modified the water level equilibrium of some local streams at the same time than the main river in this area. A direct consequence was an alteration of the dynamic processes that shape this landscape.

2.2. Multifractal DEM Analysis. A multifractal analysis is basically the measurement of a statistic distribution and therefore gives useful information on a self-similar behaviour [45].

A monofractal object can be measured by counting the number N of δ size boxes needed to cover the object. The measure depends on the box size as

$$N(\delta) \propto \delta^{-D_0}, \tag{1}$$

where

$$D_0 = \lim_{\delta \to 0} \frac{\log N(\delta)}{\log(1/\delta)} \tag{2}$$

is the fractal dimension. D_0 is calculated from slope of a log-log plot.

There are several methods for implementing multifractal analysis; in this section, the selected moment method is explained [46]. This method uses mainly three functions: $\tau(q)$, known as the mass exponent function, α, the coarse

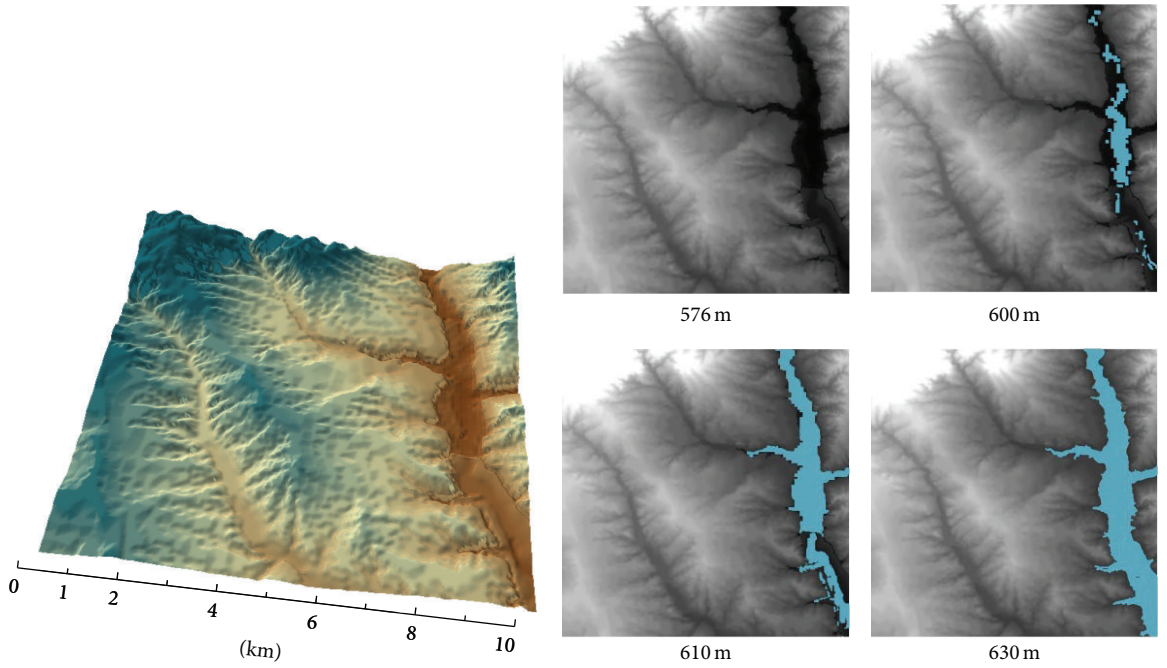

Figure 1: Visualization of DEM (1024 × 1024 data points) at the area studied (a) and the localization of the reservoir in the map at different filling levels (b) from emptiness (576 m) to full capacity (630 m).

Hölder exponent, and $f(\alpha)$, multifractal spectrum. A measure (or field), defined in two-dimensional data grid embedding space ($n \times n$ data points) and with values based on altitude (from 576 till 900 meters in this case), cannot be considered as a geometrical set and therefore cannot be characterized by a single fractal dimension.

Applying a nonoverlapping covering by boxes in an "upscaling" partitioning process, we obtain the partition function $\chi(q, \delta)$ [47] defined as

$$\chi(q,\delta) = \sum_{i=1}^{N(\delta)} \mu_i^q(\delta) = \sum_{i=1}^{N(\delta)} m_i^q, \tag{3}$$

where m is the mass of the measure, q is the statistical moments order, δ is the length size of the box, and $N(\delta)$ is the number of boxes in which $m_i > 0$. Based on this, the mass exponent function ($\tau(q)$) shows the moments of the measure scales with the box size,

$$\tau(q) = \lim_{\delta \to 0} \frac{\log \langle \chi(q,\delta) \rangle}{\log(\delta)} = \lim_{\delta \to 0} \frac{\log \left\langle \sum_{i=1}^{N(\delta)} m_i^q \right\rangle}{\log(\delta)}, \tag{4}$$

where $\langle\,\rangle$ represents statistical moment of the measure $\mu_i(\delta)$ defined on a group of nonoverlapping boxes of the same size partitioning the area studied. This method is known as the method of moments [48].

The singularity index (α) can be determined by the Legendre transformation of the $\tau(q)$ curve [46] as

$$\alpha(q) = \frac{d\tau(q)}{dq}. \tag{5}$$

The number of cells of size δ with the same α, $N_\alpha(\delta)$, is related to the cell size as $N_\alpha(\delta) \propto \delta^{-f(\alpha)}$, where $f(\alpha)$ is a scaling exponent of the cells with common α. Parameter $f(\alpha)$ can be calculated as

$$f(\alpha) = q\alpha(q) - \tau(q). \tag{6}$$

Multifractal spectrum (MFS), that is, a graph of α versus $f(\alpha)$, quantitatively characterizes variability of the measure studied with asymmetry to the right and left indicating domination of small and large values, respectively. The width of the MF spectrum indicates overall variability [23, 49].

Schertzer and Lovejoy [7, 50] proposed a multifractal model based on the codimension $c(\gamma)$. In this model, the scale ratio λ ($\lambda = n/\delta$) is used instead of δ itself being n the maximum length size considered (in this case is 1024 pixels). The measure or field (μ_λ) is characterized by its probability distribution or by the corresponding law for statistical moments [50]:

$$\begin{aligned} \Pr(\mu_\lambda \geq \lambda^\gamma) &\propto \lambda^{-C(\gamma)}, \\ \langle \mu_\lambda^q \rangle &\propto \lambda^{K(q)}, \end{aligned} \tag{7}$$

where $\langle\,\rangle$ represents the mathematical expectation of the statistical moment, $c(\gamma)$ is termed the codimension of a subset with field order greater than γ, and $K(q)$ is the moment scaling function. The relations between $K(q)$, $c(\gamma)$, and γ were derived as [7]

$$\begin{aligned} K(q) &= \max_\gamma (q\gamma - c(\gamma)), \\ c(\gamma) &= \max_q (q\gamma - K(q)). \end{aligned} \tag{8}$$

The characteristics of both functions have been discussed in detail by Schertzer and Lovejoy [7] who proposed a universal model for fitting $c(\gamma)$ based on three parameters: H, C_1, and A. From a statistical point of view, H defines the scaling on the mean field, C_1 measures the mean homogeneity of the field or measure the sparseness of the field, and A expresses the deviation from the mean of the field values or the "degree" of multifractality.

In the case that $H = 0$ the case studied is a conservative multifractal field, otherwise ($H > 0$) is not and then the analysis applying (4)–(6) to the original measure is insensitive to all the singularities below a critical value so that the ranges of α and $f(\alpha)$ are highly restricted.

In addition, the relationships between their model and the multifractal formalism based on $\tau(q)$, α, and $f(\alpha)$ are the following equations [43]:

$$\tau(q) = (q-1)E - K(q), \tag{9a}$$

or

$$K(q) = (q-1)E - \tau(q), \tag{9b}$$

$$\begin{aligned} f(\alpha) &= E - c(\gamma), \\ \alpha &= E - \gamma, \end{aligned} \tag{10}$$

where E is the Euclidean dimension where the measure is embedded.

According to numerous analyses of remote sensing images, the value of H is typically around 0.1-0.2 depending on the site and resolution [16, 29, 30, 33, 40, 43]. If $0 < H < 1$, then taking the absolute gradients (μ), instead of the original measure (m) of the field, is enough to be able to calculate the full range of singularities. It is therefore important to estimate H; in order to do this, a structure function method has been used [51], and based on a bilog plot of the correlation function ($M_2(\delta)$) and δ, this value was obtained as follows:

$$M_2(\delta) \equiv \left\langle \left|\Delta m_\delta(x,y)\right|^2 \right\rangle, \tag{11}$$

$$\begin{aligned} &\left|\Delta m_\delta(x,y)\right| \\ &\quad \approx \Big| m(x,y) \\ &\qquad - \Big(\big(m(x+\delta,y) + m(x,y+\delta) \\ &\qquad\quad + m(x-\delta,y) + m(x,y-\delta) \big) \times (4)^{-1} \Big) \Big|, \end{aligned} \tag{12}$$

where m refers to the original height value at the point (x, y) in the DEM.

Then, the original measure was replaced by $\mu(x, y) = |\Delta m_1(x, y)|$ and, based on this, absolute gradient Hölder exponents and MFS were calculated for each case based on (4)–(6), then $K(q)$ was estimated based on (9b).

3. Results and Discussion

3.1. Fractal Dimension at Different Threshold Height. First, a preliminary fractal analysis was performed to study how a change in the altitude threshold would affect the fractal dimension (D_0). The intuitive notion of the D_0 of a set of points is that the number of disjoint boxes of size δ ($N(\delta)$) needed to completely cover the set varies according to (1). Several altitude thresholds (altitude maxima) were applied to DEM data to extract the D_0 of the set of points with an altitude equal or less than a certain value. An increasing D_0 function was obtained by increasing the altitude maximum (see Figure 2).

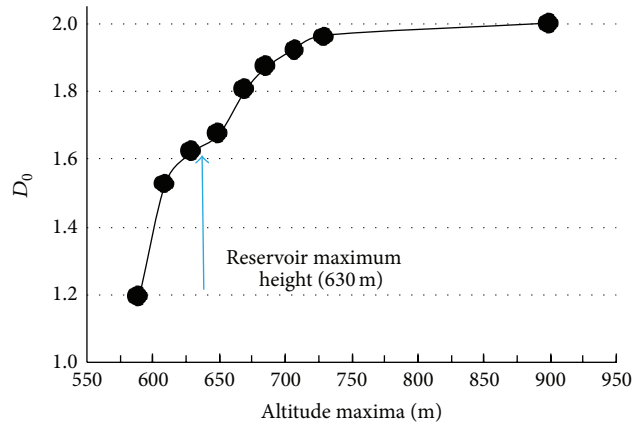

Figure 2: Box-counting dimension (D_0) including points with an altitude less or equal to x-axis value with the water reservoir empty. The blue arrow points out D_0 value when the reservoir is full.

As the threshold increased, the value of D_0 approached 2 as expected (see Figure 2). However, the function describing this tendency exhibits an inflection point if the maximum altitude considered is the height of the reservoir at its maximum capacity. As the threshold value increases from 630 m to 675 m, the spatial distribution of altitude in the area presents a different pattern from that observed for lower threshold values. The pattern continues to change with further increases in the threshold until 700 m is used as the maximum altitude.

3.2. Multifractal Spectrum of the Altitudes. The altitude frequencies for different water levels of the reservoir are shown in Figure 3(a). The only difference among these frequency distributions is the pattern of the lower values. As the water level increases, the minimum altitude increases along with its frequency. We will apply an MFA to each case in which the frequency and the position of the altitude values have a quantitative influence.

The original measure (altitude) was analysed by first calculating the mass exponent function ($\tau(q)$) for reservoir water levels of 576, 600, 610, 620, and 630 m. All of them show highly similar $\tau(q)$ behaviour, with a high degree of linearity expressing a low multifractal tendency (Figure 4(a)). The null value for τ ($q = 1$) confirms the conservative character of the measure.

The MF spectra for the five water levels analysed show that the differences among the five spectra with respect to altitude and frequency amplitude are almost null (see Table 1). The value of the Hölder exponent at the box dimension (α_0)

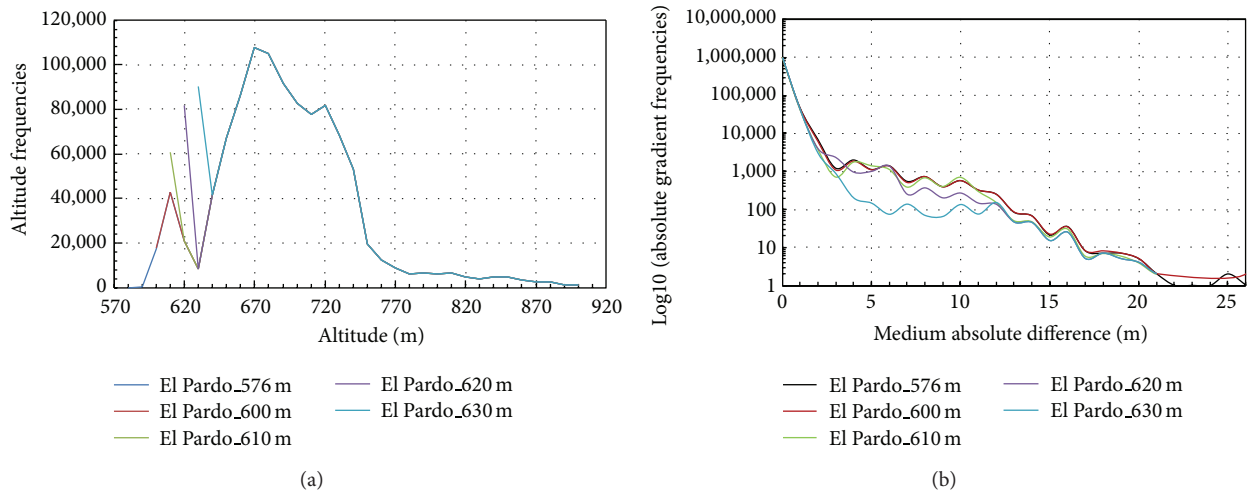

Figure 3: Frequencies distribution, with the water reservoir at different filling levels of (a) altitudes and (b) absolute gradient (frequency in logarithmic scale).

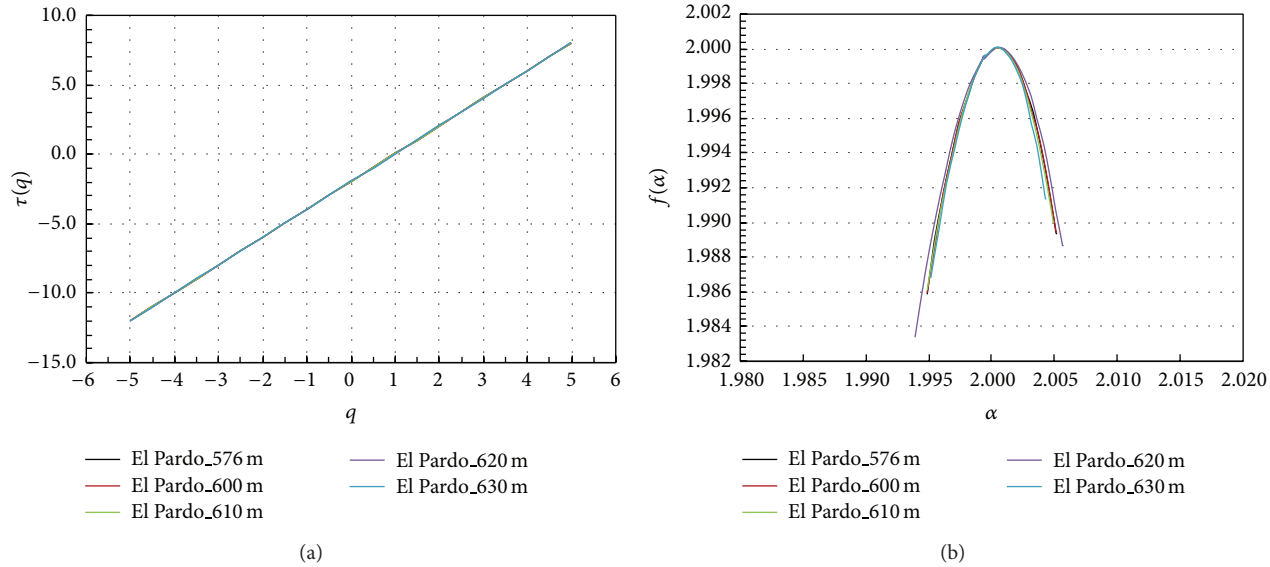

Figure 4: (a) Mass exponent function ($\tau(q)$ versus q) and (b) multifractal spectrum ($f(\alpha)$ versus α) based on the original measure (altitude). Each colour represents the water reservoir at different filling levels.

Table 1: Parameters extracted from the multifractal spectrum based on the original measure (altitude) with the water reservoir at different filling levels. Holder exponent at $q = -5$ (α_{max}), $q = 0$ (α_0), $q = 1$ (α_1), $q = +5$ (α_{min}), and $\alpha_{max} - \alpha_{min}$ ($\Delta\alpha$). Multifractal value at α_{max} ($f(\alpha_{max})$), α_{min} ($f(\alpha_{min})$), and $f(\alpha_{max}) - f(\alpha_{min})$ (Δf).

	α_{min}	α_0	α_1	α_{max}	$\Delta\alpha$	$f(\alpha_{min})$	$f(\alpha_{max})$	Δf
El Pardo_576	1.995	2.001	1.999	2.005	0.010	1.986	1.989	0.003
El Pardo_600	1.995	2.001	1.999	2.005	0.010	1.986	1.989	0.003
El Pardo_610	1.995	2.000	1.999	2.005	0.010	1.986	1.990	0.004
El Pardo_620	1.994	2.001	1.999	2.006	0.012	1.983	1.989	0.006
El Pardo_630	1.995	2.001	2.000	2.004	0.009	1.987	1.991	0.004

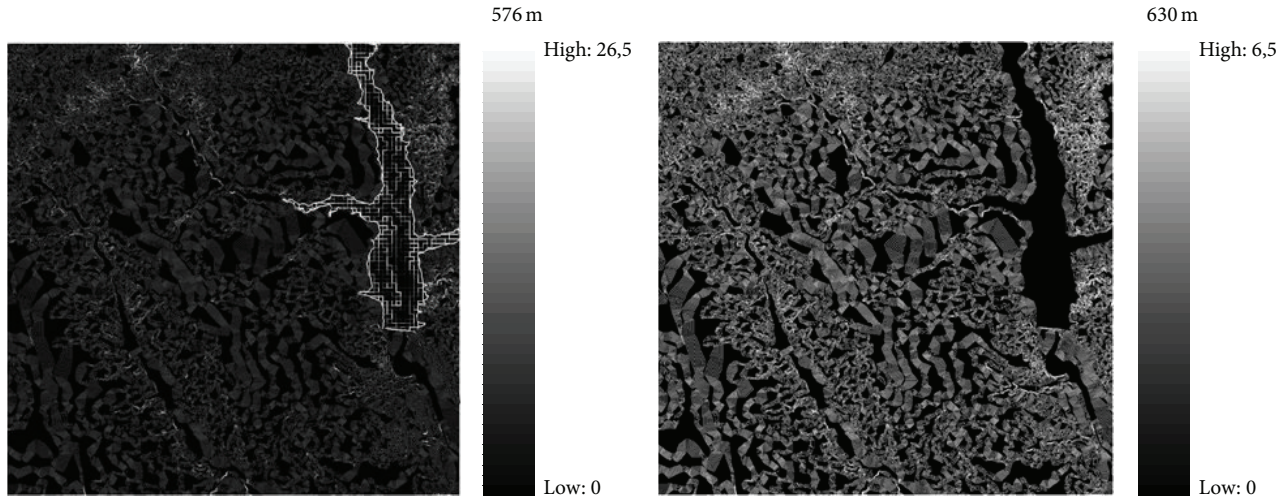

FIGURE 5: Absolute gradient, $|\Delta m_\delta(x, y)| \approx |m(x, y) - (m(x + \delta, y) + m(x, y + \delta) + m(x - \delta, y) + m(x, y - \delta))/4|$, where m refers to the original altitude value at the point (x, y) in DEM and $\delta = 1$. (a) With the water reservoir empty (minimum altitude 576 m). (b) With the water reservoir full (minimum altitude 630 m).

is approximately 2 and α_1 is 1.999 and constant in all cases. In contrast, the differences between $f(\alpha_{\min})$ and $f(\alpha_{\max})$ are approximately +0.004, indicating a stronger scaling at high values than at low values, with very tight symmetry in the spectrum (see Figure 4(b)). As the water level of the reservoir increases from 576 m to 610 m, the multifractal parameters are very similar (Table 1), changing slightly for water levels of 610 m and 620 m.

3.3. Multifractal Spectrum of the Absolute Gradient. The same type of analysis was applied after the data were transformed (see (12)) to an absolute gradient. The results of this transformation for the cases of an empty reservoir and a reservoir at maximum capacity are illustrated in Figures 5(a) and 5(b). A comparison of this figure with Figure 1(a) highlights the differences between the results of the analysis for the original measure and the transformed data. In the analysis of the absolute gradient, the points showing the greatest differences from the points surrounding them (edges) are the higher values. In contrast, the lower values of the absolute gradient show almost no differences from the surrounding points (darker colour in Figure 5).

These differences are even more pronounced if the frequencies of the absolute gradient are plotted for each case study (see Figure 3(b)). The distributions for the different case studies are similar. However, the cases considered show a pattern as the water level increases. As the water level of the reservoir increases to 630 m, the distribution becomes steepest. This tendency is a result of the increase in the area of the reservoir as the reservoir is filled. This process increases the frequency of 0 and 1 values of the absolute gradient. When the water level of the reservoir is 630 m, the distribution shows its greatest slope for absolute gradient values less than or equal to 5 m. The frequencies are lower ranging from 5 to 11 m. For values greater than 11 m, the behaviour for the water level of 630 m is similar to that for the other water levels. Although the differences shown in Figure 3(b) appear to be minimal, they have implications for the MFA, as we will show below.

The nonlinearity observed in $\tau(q)$ (Figure 6(a)) implies a scale dependence of the dimensionless moments and, therefore, a pronounced MF character versus the behaviour shown in the MFA of the original measure (Figure 4(a)). This richness in multiscaling behaviour is shown in Figure 5. The spatial distribution of the mean absolute gradient displays a more complex pattern, highlighting the points with a greater number of rough edges. At the next step, the MF spectrum shows different amplitudes for the different water levels of the reservoir (Figure 6(b)). This behaviour is clear from Table 2.

The value of the Hölder exponent at the box dimension (α_0) is slightly greater than 2. α_1 ranges from 1.93 to 1.98, with a tendency to increase as the water level increases. The values of altitude and frequency amplitude for the five cases studied are higher and more significant than in the MF analysis of the original measure (compare Tables 1 and 2). In general, $\Delta\alpha$ and Δf increase with the filling of the reservoir. However, there are exceptions to this pattern. At El Pardo_620, $\Delta\alpha$ shows a decrease to 1.218, and there is a singular value of −0.840 at El Pardo_610.

The general increase in $\Delta\alpha$ implies an increase in overall variability in space. As it is clear from Figure 5, the highest values are concentrated around the limits of the reservoir when the reservoir is empty. This tendency no longer holds when the reservoir is full, as a more complex structure with higher spatial variability develops. The differences in $f(\alpha_{\min})$ and $f(\alpha_{\max})$ are all negative, indicating a stronger scaling at low values than at high values, with no pattern of symmetry in the spectrum (see Figure 6(b)).

If we transform the multifractal spectrum into a moment scaling function ($K(q)$), we obtain a clear picture of the difference between the case of the full reservoir (El Pardo_630)

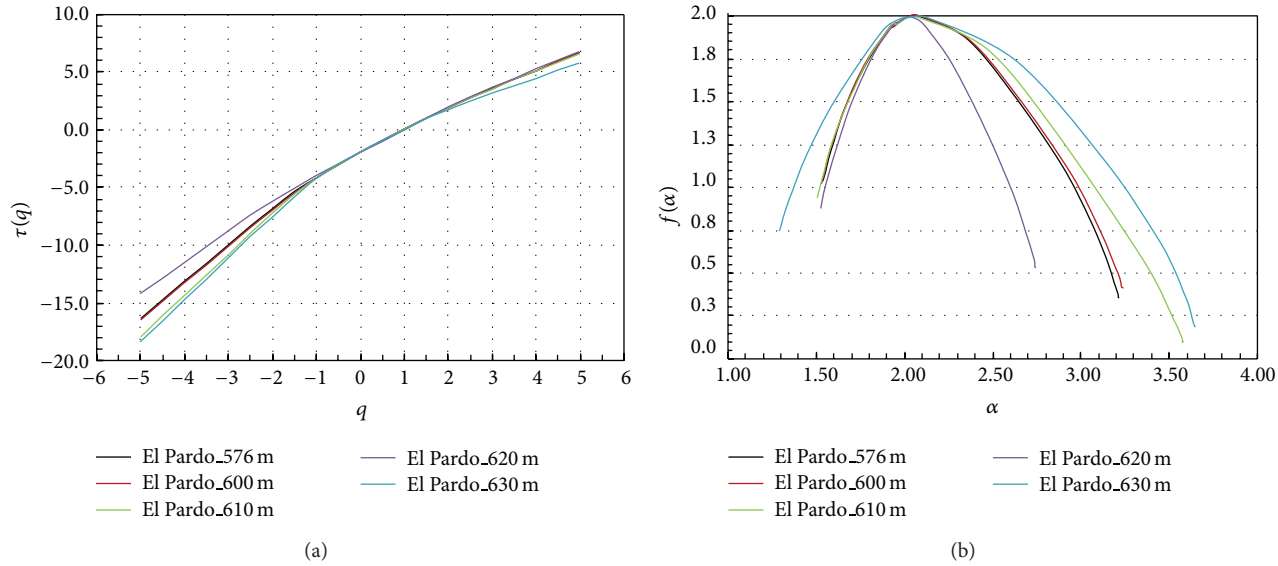

Figure 6: (a) Mass exponent function ($\tau(q)$ versus q) and (b) multifractal spectrum ($f(\alpha)$ versus α) based on absolute gradient. Each colour represents the water reservoir at different filling levels.

Table 2: Parameters extracted from the multifractal spectrum based on the average absolute differences of altitudes with the water reservoir at different filling levels. Holder exponent at $q = -5$ (α_{max}), $q = 0$ (α_0), $q = 1$ (α_1), $q = +5$ (α_{min}), and $\alpha_{max} - \alpha_{min}$ ($\Delta\alpha$). Multifractal value at α_{max} ($f(\alpha_{max})$), α_{min} ($f(\alpha_{min})$), and $f(\alpha_{max}) - f(\alpha_{min})$ (Δf).

	α_{min}	α_0	α_1	α_{max}	$\Delta\alpha$	$f(\alpha_{min})$	$f(\alpha_{max})$	Δf
El Pardo_576	1,539	2,094	1,930	3,213	1,674	1,033	0,357	−0,676
El Pardo_600	1,539	2,098	1,932	3,226	1,687	1,033	0,409	−0,624
El Pardo_610	1,509	2,092	1,950	3,580	2,071	0,098	0,938	−0,840
El Pardo_620	1,527	2,045	1,960	2,745	1,218	0,873	0,528	−0,345
El Pardo_630	1,294	2,124	1,980	3,645	2,351	0,744	0,186	−0,558

and the other water levels (see Figure 7). In all of the cases studied, the moment scaling functions are the same for $q \leq 1$. The differences are found for $q > 1$.

4. Conclusions

The goal of this study was to examine the multiscale statistical properties of the altitude and the absolute gradient in an area of homogeneous soil. In this area, the topography and the reservoir constructed on the river played a main role. Such characterisation is related to the spatial organisation of the landscape and could shed light on its evolution.

Several clear results have emerged from this analysis. First, topographic altitude exhibits a weak multiscale statistical structure and a negligible deviation from scale invariance or monoscaling when a multifractal spectrum is obtained. Second, if the original measure (altitude) is replaced by the mean absolute gradient (or mean absolute difference), the multiscale analysis reveals a higher degree of multifractality, allowing a more informative analysis of the influence of the water level of the reservoir.

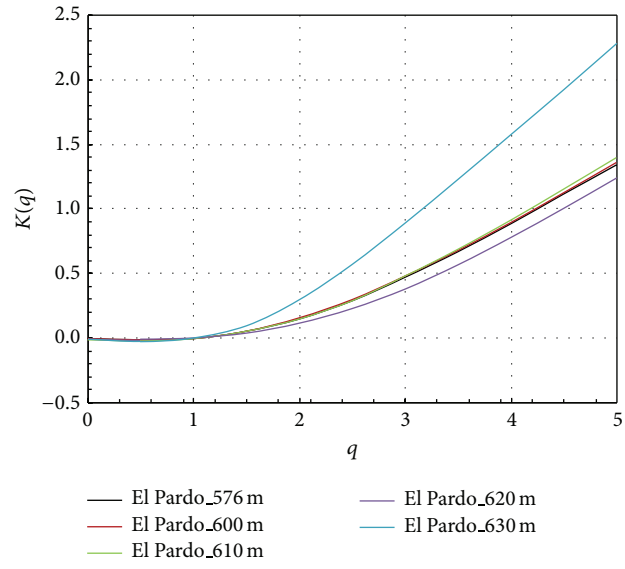

Figure 7: Moment scaling function ($k(q)$ versus q) based on the absolute gradient. Each colour represents the water reservoir at different filling levels.

By addressing the issues of structure and scale, the multifractal formalism, unlike classical geomorphometrical tools, provides scale-invariant attributes for characterising topography and landscapes. The results of this study show that the use of the multifractal approach with mean absolute gradient data is a useful tool for analysing the topography represented by the digital elevation model.

Conflict of Interests

The authors declare that there is no conflict of interests regarding the publication of this paper.

Acknowledgments

The data provided by Guadarrama Monitoring Network Initiative (GuMNet) through the Project of CEI Campus Moncloa is greatly appreciated.

References

[1] W. H. Wischmeyer and D. D. Smith, *Predicting Rainfall Erosion Losses. A Guide to Conservation Planning*, US. Dep. of Agriculture Handbook 357, Washington, DC, USA, 1978.

[2] J. Grazzini, A. Turiel, H. Yahia, and I. Herlin, "Edge-preserving smoothing of high-resolution images with a partial multifractal reconstruction scheme," in *Proceedings of the International Society for Photogrammetry and Remote Sensing*, pp. 1125–1129, 2004.

[3] J. Grazzini and N. Chrysoulakis, "Extraction of surface properties from a high accuracy DEM using multiscale remote sensing techniques," in *Proceedings of the 19th International Conference: Informatics for Environmental Protection (EnviroInfo '05)*, J. Hřebiček and J. Ráček, Eds., vol. 1, pp. 352–356, 2005.

[4] J. Wood, "Visualisation of scale dependencias in surface models," in *Proceedings of the 19th International Conference of Cartography (ICA/ACI '99)*, Ottawa, Canada, 1999.

[5] K. T. Chang, *Introduction to Geographic Informaition Systems*, McGraw-Hill, New York, NY, USA, 4th edition, 2006.

[6] K. T. Chang and B. W. Tsai, "The effect of DEM resolution on slope and aspect mapping," *Cartography & Geographic Information Systems*, vol. 18, no. 1, pp. 69–77, 1991.

[7] D. Schertzer and S. Lovejoy, *Non-Linear Variability in Geophysics*, Kluwer Academic Publishers, Dordrecht, The Netherlands, 1991.

[8] J. T. Bjøorke and S. Nilsen, "Wavelets applied to simplification of digital terrain models," *International Journal of Geographical Information Science*, vol. 17, no. 7, pp. 601–621, 2003.

[9] A. Leduc, Y. T. Prairie, and Y. Bergeron, "Fractal dimension estimates of a fragmented landscape: sources of variability," *Landscape Ecology*, vol. 9, no. 4, pp. 279–286, 1994.

[10] C. Gangodagamage, E. Barnes, and E. Foufoula-Georgiou, "Scaling in river corridor widths depicts organization in valley morphology," *Geomorphology*, vol. 91, no. 3-4, pp. 198–215, 2007.

[11] S. Fioravanti, "Multifractals: theory and application to image texture recognition," in *Proceedings of the Joint JRC/ EARSeL Expert Meeting*, Fractals in Geosciences and Remote Sensing, Ispra, Italy, 1994.

[12] N. S. Lam and L. de Cola, *Fractals in Geography*, Prentice Hall, Englewood Cliffs, NJ, USA, 1993.

[13] H. Qiu, N. S. Lam, D. A. Quattrochi, and J. A. Gamon, "Fractal characterization of hyperspectral imagery," *Photogrammetric Engineering and Remote Sensing*, vol. 65, no. 1, pp. 63–71, 1999.

[14] L. De Cola, "Fractal analysis of a classified Landsat scene," *Photogrammetric Engineering and Remote Sensing*, vol. 55, no. 5, pp. 601–610, 1989.

[15] N. S. Lam, "Description and measurement of Landsat TM images using fractals," *Photogrammetric Engineering & Remote Sensing*, vol. 56, no. 2, pp. 187–195, 1990.

[16] S. Lovejoy, A. M. Tarquis, H. Gaonac'h, and D. Schertzer, "Single- and multiscale remote sensing techniques, multifractals, and MODIS-derived vegetation and soil moisture," *Vadose Zone Journal*, vol. 7, no. 2, pp. 533–546, 2008.

[17] A. Turiel and N. Parga, "The multifractal structure of contrast changes in natural images: from sharp edges to textures," *Neural Computation*, vol. 12, no. 4, pp. 763–793, 2000.

[18] E. V. Vázquez, R. G. Moreno, J. G. V. Miranda et al., "Assessing soil surface roughness decay during simulated rainfall by multifractal analysis," *Nonlinear Processes in Geophysics*, vol. 15, no. 3, pp. 457–468, 2008.

[19] C. J. G. Evertsz and B. B. Mandelbrot, "Multifractal measures. Appendix B.," in *Chaos and Fractals: New Frontiers of Science*, H. O. Peitgen, H. Jurgens, and D. Saupe, Eds., Springer, New York, NY, USA, 1992.

[20] B. B. Mandelbrot, *The Fractal Geometry of Nature*, Freeman, San Francisco, Calif, USA, 1983.

[21] T. Hirata and M. Imoto, "Multifractal analysis of spatial distribution of microearthquakes in the Kanto region," *Geophysical Journal International*, vol. 107, no. 1, pp. 155–162, 1991.

[22] A. N. Kravchenko, C. W. Boast, and D. G. Bullock, "Multifractal analysis of soil spatial variability," *Agronomy Journal*, vol. 91, no. 6, pp. 1033–1041, 1999.

[23] A. M. Tarquis, D. Giménez, A. Saa, M. C. Díaz, and J. M. Gascó, "Scaling and multiscaling of soil pore systems determined by image analysis," in *Scaling Methods in Soil Physics*, Y. Pachepsky, D. E. Radcliffe, and H. Magdi Selim, Eds., CRC Press, 2003.

[24] A. Sánchez, R. Serna, F. Catalina, and C. N. Afonso, "Multifractal patterns formed by laser irradiation in GeAl thin multilayer films," *Physical Review B*, vol. 46, no. 1, pp. 487–490, 1992.

[25] Q. Cheng and F. P. Agterberg, "Multifractal modelling and spatial statistics," *Mathematical Geology*, vol. 28, no. 1, pp. 1–16, 1996.

[26] Q. Cheng, "Multifractality and spatial statistics," *Computers and Geosciences*, vol. 25, no. 9, pp. 949–961, 1999.

[27] G. Du and T. S. Yeo, "A novel multifractal estimation method and its application to remote image segmentation," *IEEE Transactions on Geoscience and Remote Sensing*, vol. 40, no. 4, pp. 980–982, 2002.

[28] D. C. Harvey, H. Gaonac'h, S. Lovejoy, J. Stix, and D. Schertzer, "Multifractal characterization of remotely sensed volcanic features: a case study from Kilauea Volcano, Hawaii," *Fractals*, vol. 10, no. 3, pp. 265–274, 2002.

[29] A. Laferrière and H. Gaonac'h, "Multifractal properties of visible reflectance fields from basaltic volcanoes," *Journal of Geophysical Research B: Solid Earth*, vol. 104, no. 3, pp. 5115–5126, 1999.

[30] S. Lovejoy, D. Schertzer, Y. Tessier, and H. Gaonach, "Multifractals and resolution-independent remote sensing algorithms: the example of ocean colour," *International Journal of Remote Sensing*, vol. 22, no. 7, pp. 1191–1234, 2001.

[31] T. Parrinello and R. A. Vaughan, "Multifractal analysis and feature extraction in satellite imagery," *International Journal of Remote Sensing*, vol. 23, no. 9, pp. 1799–1825, 2002.

[32] D. Schertzer and S. Lovejoy, "Physically based rain and cloud modelling by anisotropic, multiplicative turbulent cascades," *Journal of Geophysical Research*, vol. 92, pp. 9693–9714, 1987.

[33] F. Schmitt, D. Schertzer, S. Lovejoy, and P. Marchal, "Multifractal analysis of satellite images: towards an automatic segmentation," in *Fractals in Engineering*, pp. 103–109, Jules, Arcachon, France, 1997.

[34] Y. Tessier, S. Lovejoy, D. Schertzer, D. Lavallee, and B. Kerman, "Universal multifractal indices for the ocean surface at far red wavelengths," *Geophysical Research Letters*, vol. 20, no. 12, pp. 1167–1170, 1993.

[35] A. Turiel, J. Isern-Fontanet, E. Garcia-Ladona, and J. Font, "Multifractal method for the instantaneous evaluation of the stream function in geophysical flows," *Physical Review Letters*, vol. 95, no. 10, Article ID 104502, 2005.

[36] Q. Cheng, H. Russell, D. Sharpe, F. Kenny, and P. Qin, "GIS-based statistical and fractal/multifractal analysis of surface stream patterns in the Oak Ridges Moraine," *Computers and Geosciences*, vol. 27, no. 5, pp. 513–526, 2001.

[37] J. J. Roering, J. W. Kirchner, and W. E. Dietrich, "Evidence for nonlinear, diffusive sediment transport on hillslopes and implications for landscape morphology," *Water Resources Research*, vol. 35, no. 3, pp. 853–870, 1999.

[38] A. Beaulieu and H. Gaonac'h, "Scaling of differentially eroded surfaces in the drainage network of the Ethiopian Plateau," *Remote Sensing of Environment*, vol. 82, no. 1, pp. 111–122, 2002.

[39] Q. Cheng, "A new model for quantifying anisotropic scale invariance and for decomposition of mixing patterns," *Mathematical Geology*, vol. 36, no. 3, pp. 345–360, 2004.

[40] H. Gaonac'h, S. Lovejoy, and D. Schertzer, "Resolution dependence of infrared imagery of active thermal features at Kilauea Volcano," *International Journal of Remote Sensing*, vol. 24, no. 11, pp. 2323–2344, 2003.

[41] S. Lovejoy, S. Pecknold, and D. Schertzer, "Stratified multifractal magnetization and surface geomagnetic fields-I. Spectral analysis and modelling," *Geophysical Journal International*, vol. 145, no. 1, pp. 112–126, 2001.

[42] H. Maître and M. Pinciroli, "Fractal characterization of a hydrological basin using SAR satellite images," *IEEE Transactions on Geoscience and Remote Sensing*, vol. 37, no. 1, pp. 175–181, 1999.

[43] J.-S. Gagnon, S. Lovejoy, and D. Schertzer, "Multifractal surfaces and terrestrial topography," *Europhysics Letters*, vol. 62, no. 6, pp. 801–807, 2003.

[44] J. S. Gagnon, S. Lovejoy, and D. Schertzer, "Multifractal earth topography," *Nonlinear Processes in Geophysics*, vol. 13, no. 5, pp. 541–570, 2006.

[45] R. E. Plotnick, R. H. Gardner, W. W. Hargrove, K. Prestegaard, and M. Perlmutter, "Lacunarity analysis: a general technique for the analysis of spatial patterns," *Physical Review E*, vol. 53, no. 5, pp. 5461–5468, 1996.

[46] T. C. Halsey, M. H. Jensen, L. P. Kadanoff, I. Procaccia, and B. I. Shraiman, "Fractal measures and their singularities: the characterization of strange sets," *Physical Review A*, vol. 33, no. 2, pp. 1141–1151, 1986.

[47] J. Feder, *Fractals*, Plenum Press, New York, NY, USA, 1989.

[48] H. Peitgen, H. Jürgens, and D. Saupe, *Chaos and Fractal New Frontiers of Science (Appendix B. Multifractal Measures)*, Hamilton Printing, New York, NY, USA, 1992.

[49] A. M. Tarquis, J. C. Losada, R. M. Benito, and F. Borondo, "Multifractal analysis of tori destruction in a molecular Hamiltonian system," *Physical Review E*, vol. 65, no. 1, Article ID 016213, 2002.

[50] D. Schertzer and S. Lovejoy, "Standard and advanced multifractal techniques in remote sensing," in *Fractas in Geosciences and Remote Sensing and GIS*, G. Wilkingo, I. Kanellopoulos, and J. Megier, Eds., pp. 361–394, CRC Press, London, UK, 1994.

[51] J. W. Kantelhardt, S. A. Zschiegner, E. Koscielny-Bunde, S. Havlin, A. Bunde, and H. E. Stanley, "Multifractal detrended fluctuation analysis of nonstationary time series," *Physica A*, vol. 316, no. 1–4, pp. 87–114, 2002.

Hindawi Publishing Corporation
The Scientific World Journal
Volume 2014, Article ID 514183, 7 pages
http://dx.doi.org/10.1155/2014/514183

Research Article

Short-Term Effects of Tillage Practices on Soil Organic Carbon Turnover Assessed by $\delta^{13}C$ Abundance in Particle-Size Fractions of Black Soils from Northeast China

Aizhen Liang,[1] Shenglong Chen,[1,2] Xiaoping Zhang,[1] and Xuewen Chen[1]

[1] *Northeast Institute of Geography and Agroecology, Chinese Academy of Sciences, Changchun 130102, China*
[2] *University of Chinese Academy of Sciences, Beijing 100049, China*

Correspondence should be addressed to Aizhen Liang; liangaizhen@iga.ac.cn

Received 3 April 2014; Revised 25 June 2014; Accepted 18 July 2014; Published 5 August 2014

Academic Editor: Antonio Paz González

The combination of isotope trace technique and SOC fractionation allows a better understanding of SOC dynamics. A five-year tillage experiment consisting of no-tillage (NT) and mouldboard plough (MP) was used to study the changes in particle-size SOC fractions and corresponding $\delta^{13}C$ natural abundance to assess SOC turnover in the 0–20 cm layer of black soils under tillage practices. Compared to the initial level, total SOC tended to be stratified but showed a slight increase in the entire plough layer under short-term NT. MP had no significant impacts on SOC at any depth. Because of significant increases in coarse particulate organic carbon (POC) and decreases in fine POC, total POC did not remarkably decrease under NT and MP. A distinct increase in silt plus clay OC occurred in NT plots, but not in MP plots. However, the $\delta^{13}C$ abundances of both coarse and fine POC increased, while those of silt plus clay OC remained almost the same under NT. The C derived from C_3 plants was mainly associated with fine particles and much less with coarse particles. These results suggested that short-term NT and MP preferentially enhanced the turnover of POC, which was considerably faster than that of silt plus clay OC.

1. Introduction

In the past few years physical fractionation has played an important role in studying soil organic carbon (SOC) pool and its turnover under different land uses and management systems [1]. The stable C isotope trace technique is increasingly used to study the dynamics of SOC and the influences of agricultural managements on SOC turnover [2, 3]. However, SOC dynamics is so complex that it is hard to tell how SOC pool responds to changes in land uses and soil managements if only total SOC is measured. Thus, a combination of stable C isotope trace technique and SOC fractionation can be used to explore the mechanism of C dynamics and quantify the accumulation of newly added SOC in different SOC fractions [4]. Piao et al. [5] found that in forest soils, the $\delta^{13}C$ values of SOC in light fractions were significantly lower than in heavy fractions, indicating that crop residues were first incorporated into the light fractions. The SOC in the light fraction or coarse particles was labile and sensitive to changes of soil managements [5, 6]. However, Magid et al. [7] found that labile SOC fractions were distributed in all-sized or all-density particles. Yonekura et al. [8] also found that when forest was converted to grassland, all soil organic matter fractions in the surface layer exhibited fast turnover based on natural abundance of $\delta^{13}C$.

Long-term intensive agricultural management could greatly reduce SOC level [9]. Also, it is well documented that conservation tillage could enhance C protection, increase SOC levels [10–13], and convert agricultural soils from C sources to C sinks, thereby removing significant amounts of CO_2 from the atmosphere [14]. However, the effect of conservation tillage on SOC storage is sometimes contradictory [15, 16], especially for short-term (≤10 years) effect of conservation tillage. It varies with soil conditions, such as soil texture, climate, and biomass return, as well as management itself, and is difficult to be generalized [10, 17]. Hence, the studies on short-term impacts of tillage systems on SOC have to be verified in different soil conditions.

Northeast China is an important agriculture region, mainly due to the production of soybean and maize. Black soil (Typic Hapludoll, US Soil Taxonomy) dominates this region and mainly occurs in Liaoning, Jilin, and Heilongjiang provinces. Since 1940s and 1950s, large-scale cultivation and improper management have resulted in a significant decline of soil fertility, and present SOC content is less than one-half of the initial content before cultivation [18]. Hence, it is essential to find out an appropriate tillage system which can enhance the SOC level, while maintaining or improving local crop production. The objectives of this study were to analyze the dynamics of particle-size SOC fractions and to explore SOC turnover using δ^{13}C natural abundances under short-term tillage practices in black soils of Northeast China.

2. Materials and Methods

2.1. Study Site. The tillage study was started in the fall of 2011 at the Experimental Station (44° 12′ N, 125° 33′ E) of Northeast Institute of Geography and Agroecology, Chinese Academy of Sciences, in Dehui, Jilin Province, China. The study site is located in the North Temperate Zone with a continental monsoon climate. Mean annual temperature is 4.4°C, and mean annual precipitation is 520.3 mm, with more than 70% occurring from June to August [18]. The soil was classified as a black soil, following the Chinese Soil Classification System, equivalent to a Typic Hapludoll in the Soil Taxonomy. This soil was clay loam textured, with an average of 36% clay, 24% silt, and 40% sand. Before the experiment started, the soil bulk density was 1.24–1.38 g cm^{-3}. The total SOC and nitrogen (N) contents were 15.5 g kg^{-1} and 1.31 g kg^{-1}, respectively. The slope of the experimental plots is less than 1°. The land had been used for continuous corn production under conventional tillage for many years (≥20 years) prior to 2001 [19].

2.2. Tillage Experiment. A tillage experiment, consisting of two treatments, mouldboard plough (MP) and no tillage (NT), was established in a randomized complete block design with four replicates. Each tillage plot was split into two subplots (5.2 m × 20 m) which were under corn-soybean rotation with both crops present each year. The MP included fall mouldboard ploughing (about 20 cm deep) after corn harvest, spring disking (7.5 to 10 cm deep), and field cultivation. The NT soils had no soil disturbance except for crop planting using a KINZE-3000 NT planter (Williamsburg, Iowa). All the crop residues were returned to the soil surface. Each year, 100 kg ha^{-1} N was applied to corn as starter fertilizer and 50 kg ha^{-1} N as top dressing at the V-6 growth stage, respectively. In addition, 45.5 kg ha^{-1} P and 78 kg ha^{-1} K were also added to corn as starter fertilizers. For soybean, all fertilizers were applied as starter fertilizer, including 40 kg ha^{-1} N, 60 kg ha^{-1} P, and 80 kg ha^{-1} K. The starter fertilizers for all plots were applied concurrently during the planting phase.

2.3. Soil Sampling and Measurements. Composite soil samples (7 subsamples per plot) were collected down to a depth of 20 cm after harvest (corn phase) in 2001 and 2006. The samples were taken using a hand auger (2.64 cm diameter) which allowed separation of each soil core into three segments (0–5, 5–10, and 10–20 cm) without soil compaction. Soil samples were gently broken and air-dried. Visibly identifiable crop residues were manually removed for SOC and SOC fractions measurements.

The silt plus clay (<20 μm) SOC was measured as described by Liang et al. [20]. 25 g dry soil was placed in a 250 mL beaker and 125 mL distilled water was added. The soil suspension was mixed and allowed to settle at room temperature overnight. Then, the suspension was dispersed for 10 min with an ultrasonic probe (JY92 and 24 kHz, Xinzhi, Ningbo) with an energy input of 480 J mL^{-1}. The dispersed soil suspension was transferred to a 1 L glass cylinder, and the cylinder was capped and shaken end over end to thoroughly homogenize the soil water suspension. Silt plus clay fraction and clay fraction were collected by siphoning the suspension based on Stokes' law. The collected solid fractions were oven-dried at 60°C and then ground for SOC analysis. Silt OC content was calculated by the silt plus clay OC minus clay OC.

Soil particulate organic carbon (POC, 53–2000 μm) was measured according to the method of Carter et al. [21]. 20 g soil sample passing through 2 mm sieve was put into a plastic vial and 100 mL 5 g L^{-1} sodium hexametaphosphate solution was added. The sample was shaken for 2 h for dispersion. The dispersed suspension was passed through a set of 250 and 53 μm sieves from top to bottom. Distilled water was used to rinse soil particles on the sieves. Soil fractions retained on the sieves were collected and oven-dried at 60°C and then ground for SOC analysis. The POC in the >250 μm size was defined as coarse POC, and POC in the 53–250 μm size was fine POC.

All soil samples were free of carbonate, and hence SOC content was assumed to be equal to total C content. The total SOC and SOC fractions were determined using a FlashEA1112 elemental analyzer (ThermoFinnigan, Italy). Soil subsamples of 20–40 mg and plant samples (including natural plant and corn residues) were ground and passed through a 100-mesh sieve and then were used to measure the δ^{13}C abundances of SOC by an isotope ration mass spectrograph (MAT252, Finnigan, USA).

2.4. Data Analysis. The proportion of C derived from corn was calculated using [22]

$$f = \frac{(\delta - \delta_0)}{(\delta_1 - \delta_0)}, \quad (1)$$

where f stands for the proportion of corn-derived C in the sample, δ for the measured δ^{13}C values in corn fields, δ_0 for the δ^{13}C of the corresponding sample from corn field as C_3 reference soil, and δ_1 for the δ^{13}C values of corn plant (about −12‰).

Turnover time of SOC was calculated according to [22]

$$T = \frac{1}{k} = \frac{-(t - t_0)}{\ln(C_t/C_{t0})}, \quad (2)$$

where k stands for the rate constant of the first-order decay, t for the year of sampling (2006), t_0 for the year of vegetation

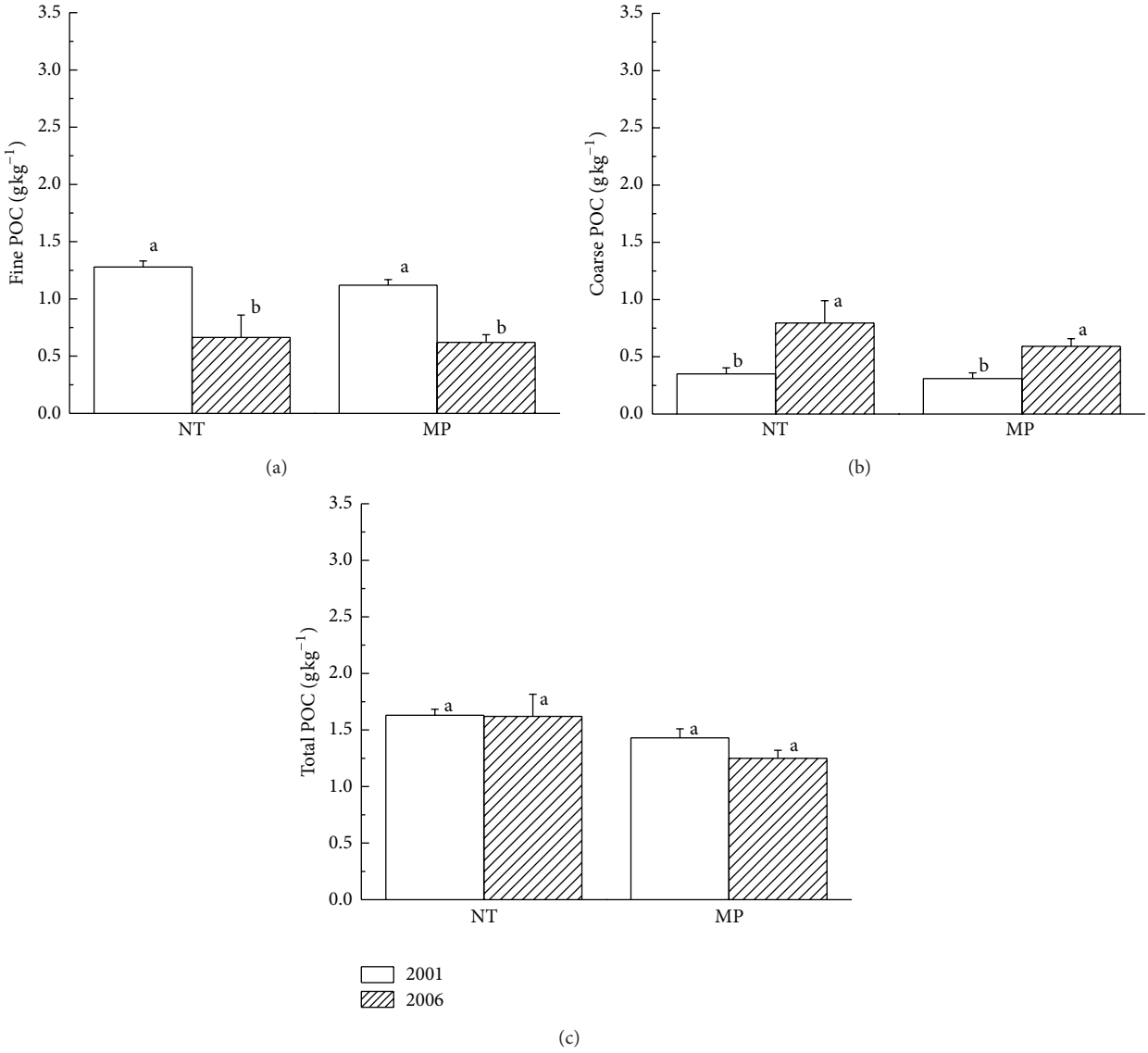

Figure 1: Particulate organic carbon (POC) in 0–20 cm layer of black soil under no tillage (NT) and mouldboard plough (MP). Bars indicate standard error. Different lowercase letters above the column indicate significant differences at $P = 0.05$.

change, C_t for the remaining proportion of C_3–C at the time of sampling (%), and C_{t0} for the proportion of C_3–C at t_0 (100%).

Least significant difference (LSD) between means was calculated to examine the effects of tillage practices on SOC in each fraction. The procedure was performed using SAS 9.1 (SAS Institute, Cary, NC, USA). Statistical significance was determined at $P < 0.05$.

3. Results and Discussion

3.1. Total and Particle-Size Soil Organic Carbon under NT and MP. Five-year NT resulted in no substantial changes (1.2%) in total SOC in top 0–20 cm soil compared to the initial level. However, there were significant increases (9.9%) in total SOC at 0–5 cm depth ($P < 0.05$), despite a lack of noticeable differences at 5–20 cm depths after 5-year NT. MP had no significant effects on total SOC contents in the entire plough layer ($P > 0.05$). This difference was likely not a result from the difference in biomass inputs [23], but rather it resulted from retention of carbon from crop residue on the soil surface of the NT plots whereas it was incorporated into the soil in the MP plots.

Over five years, NT and MP significantly affected both fine and coarse POC ($P < 0.05$, Figures 1(a) and 1(b)). Due to significant and opposite influences of tillage treatments on fine and coarse POC, total POC contents had no distinct changes (Figure 1(c)). There were significant increases in coarse POC under NT and MP ($P < 0.05$) which could be attributed to the annual input of organic materials. The NT decreased fine POC, which was different from the result of

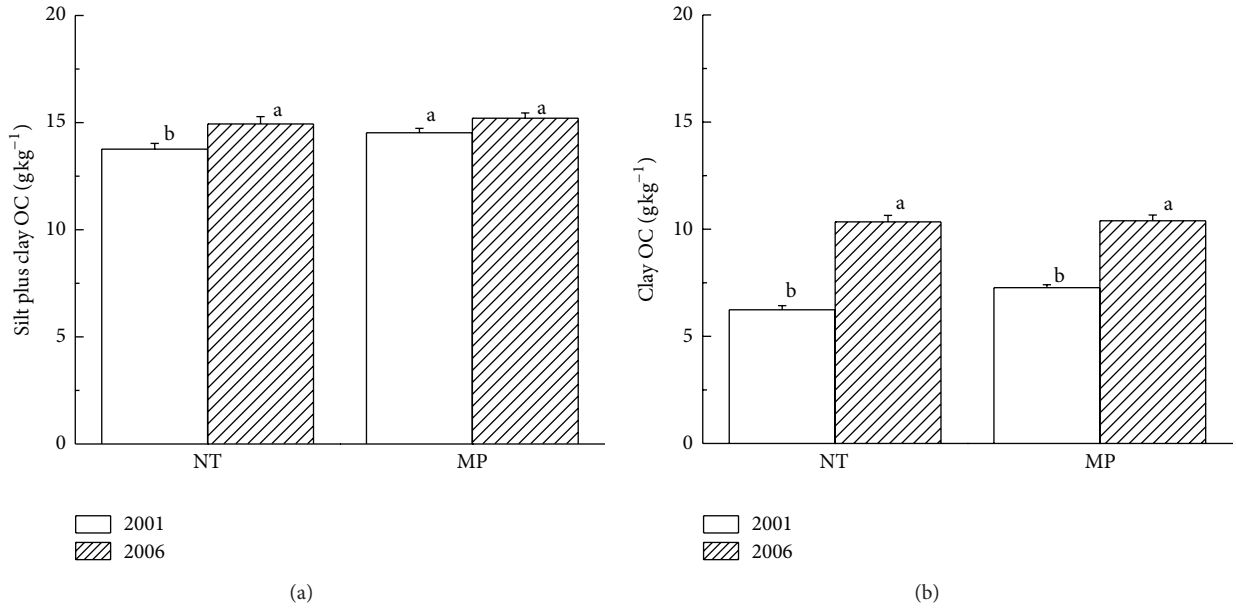

Figure 2: Soil organic carbon in <20 μm particles of the 0–20 cm layer under tillage practices.

Pikul et al. [24]. We considered that our experimental study was conducted for a short period (only five years) which was not sufficient for crop residue decomposition and subsequent C association with finer soil particles. Collectively, these results suggested that SOC in coarse particle was more sensitive to the conversion of tillage systems.

Under NT and MP treatments, silt plus clay OC and clay OC in the plough layers both showed an increasing trend over the five-year period (Figures 2(a) and 2(b)). Compared to data in 2001, the NT treatment significantly increased 7.9% and 39.7% SOC in these two size fractions ($P < 0.05$). These results indicated that short-term NT decreased silt OC, whereas clay OC played an important role in the total increase in silt plus clay OC. The reason was that the retention of crop residues above the soil surface and no disturbance under NT reduced the loss of silt plus clay OC. The MP only increased silt plus clay OC by 4.5% ($P > 0.05$). Similar to NT plots, there were significant increases in clay OC in the MP plots by 30.0% on average ($P < 0.05$). However, the concurrent decrease in silt OC and the increase in clay OC suggested that SOC in each fraction probably was translocated by splash erosion of rainfall or was transferred between fine and coarse particles [25]. The increase in silt plus clay OC under MP might be due to the breakdown of macroaggregates into microaggregates by tillage practice and incorporation of crop residues into soils which increased the input of organic materials. Also, undecomposed crop residues to some extent prevented soil from splash erosion. Hence, there were increases in silt plus clay OC in MP plots, but the increases were less than those in NT plots under greater protection of crop residues on the surface.

3.2. $\delta^{13}C$ Abundances in Organic Carbon Fractions under NT and MP. At 0–20 cm depths the $\delta^{13}C$ abundances (−19.9‰ and −21.1‰) of SOC in both fine and coarse fractions were lower than those of corn plants (−12.0‰) (Table 1). This was because the study site was conducted under corn-soybean rotation system; soybean residues (C_3) were returned into soils in addition to corn residues (C_4). Neither NT nor MP significantly affected the $\delta^{13}C$ values of SOC fractions (Table 1). Gregorich and Janzen [26] reported that the changes in $\delta^{13}C$ values of SOC with depths could approximately reflect the characters of SOC decomposition. In the present study, the $\delta^{13}C$ values of SOC in each size fraction decreased with depths under NT and MP treatments (Table 1), which could be related to the decreasing input of C_4 plants from top to subsurface soils. Average $\delta^{13}C$ values of POC in the coarse and fine fractions in 0–20 cm layers were −20.3‰ and −19.4‰ in the NT plots, respectively, slightly greater than that of silt plus clay OC (−21.0‰). Similar results were found in MP plots.

Factors affecting the $\delta^{13}C$ values include plant (plant types and water use efficiency of plant), soil (total SOC, SOC fractions, soil depths, and soil moisture), landform, and fertilization [27]. In this study, soil was the primary factor affecting $\delta^{13}C$ values at the experimental site because of the same plant, landform, and fertilization. In NT plots higher soil moisture [28, 29] resulted in lower $\delta^{13}C$ values of SOC in each fraction than in MP plots. It was due to the return of crop residues each year. Certainly the inputs and decomposition of organic materials were different between the NT and MP plots. Without fall ploughing, crop residues returned to the field significantly increased SOC concentration at 0–5 cm depth under NT [19]. We therefore hypothesized that in our present study $\delta^{13}C$ values of SOC in each fraction under NT were lower than under MP. However, the experimental result was not exactly consistent with the above hypothesis. Neither NT nor MP practice significantly affected $\delta^{13}C$ values of

Table 1: $\delta^{13}C$ abundances, C_3–C and C_4–C fractions in the plough layer of Black soil under no tillage (NT) and mouldboard plough (MP) in 2006.

	Treatments	$\delta^{13}C$ (‰)	f (%)	$1-f$ (%)	C_4–C (g kg^{-1})	C_3–C (g kg^{-1})
0–10 cm						
Coarse POC	NT	−19.8	32.2	67.8	0.48	0.83
	MP	−20.2	32.1	67.9	0.27	0.58
Fine POC	NT	−19.3	40.8	59.2	0.32	0.47
	MP	−19.2	41.2	58.8	0.43	0.60
Silt plus clay OC	NT	−21.1	27.4	72.6	4.00	10.6
	MP	−21.1	27.2	72.8	4.10	11.0
10–20 cm						
Coarse POC	NT	−20.8	25.3	74.7	0.10	0.29
	MP	−20.7	25.8	74.2	0.12	0.34
Fine POC	NT	−19.5	30.4	69.6	0.14	0.33
	MP	−19.8	27.3	72.7	0.26	0.63
Silt plus clay OC	NT	−21.1	16.1	83.9	2.34	12.1
	MP	−21.1	17.1	82.9	2.54	12.4

SOC fractions, despite the existence of differences (Table 1). In 0–20 cm layers, the $\delta^{13}C$ values of coarse and fine POC were both slightly greater in NT plots (−20.3‰ and −19.4‰) than in MP plots (−20.5‰ and −19.5‰), whereas the $\delta^{13}C$ values of silt plus clay OC were almost the same under two tillage treatments. Above results might be due to other soil conditions. Walley et al. [30] reported that NT increased soil water supplement and water use efficiency of plants. The higher the water use efficiency is, the higher the $\delta^{13}C$ values are [31]. In our case, crops with higher abundances of $\delta^{13}C$ were returned and then increased soil $\delta^{13}C$ values. Thus, the $\delta^{13}C$ values of coarse and fine POC at 0–20 cm depth were greater under NT than under MP. Additionally, the interactions among relevant factors might affect the $\delta^{13}C$ values. Collectively, the above results suggested that short-term impacts of tillage practices on SOC were shown in the coarse fractions, with no substantial changes in fine particles.

3.3. Plant Sources of Soil Organic Carbon under NT and MP. In NT soils C_3–C and C_4–C concentrations in coarse POC fraction significantly decreased ($P < 0.05$), and the former was greater than the latter (Table 1). The C_3–C and C_4–C concentrations in fine POC showed the same variation trend, though the changes were not significant ($P > 0.05$). In MP soils, C_3–C and C_4–C concentrations of POC in the fine and coarse fractions had no noticeable decreases at two depths. These different effects were attributed to the enrichment of organic materials on soil surface under NT treatment in contrast to the incorporation of returned crop residues into soils and thus even distribution of organic materials inputs in plough layers under MP.

There were no significant differences in C_3–C and C_4–C concentrations in each SOC fraction between the NT and MP treatments ($P > 0.05$) (Table 1). The NT only increased C_3–C and C_4–C concentrations in coarse POC at 0–10 cm depth. In other SOC fractions, both C_3–C and C_4–C concentrations were lower in NT soils than in MP soils, which could be attributed to the stratification of SOC in soil profiles under NT. In addition, the result indicated that the sensitive response of SOC to tillage conversion could be shown in the coarse fraction. There were no significant differences in the proportions of C_3–C and C_4–C between the NT and MP treatments ($P > 0.05$, Table 1). Short-term NT practice thus could not significantly affect the C source of SOC fractions, even POC. Regardless of the tillage practices (NT and MP), C derived from C_3 plants was mainly distributed in the fine-size fractions (Table 1). That is, the turnover of SOC was faster in the coarse-size fraction than in fine-size fraction, which is in agreement with studies of Yonekura et al. [8] and Yamashita et al. [22].

3.4. Turnover Rates of Soil Organic Carbon under NT and MP. The silt plus clay OC represented not only the majority of the total SOC, but also the SOC fraction with the longest apparent turnover time under NT and MP practices (Figure 3). The turnover time of POC in the NT and MP soils was more than 200 years, far longer than the results previously reported by Cambardella and Elliott [32] that the turnover time of POC ranged from 5 to 20 years in cultivated grassland soils. The reason might be that after cultivation of virgin black soils, soybean (C_3 crop) residues provided an extra source of organic matter input in addition to corn-derived C (C_4 crop). It might also be due to a certain amount of black C in POC [33]. The mean turnover time indicated faster turnover of SOC in coarse fraction than that in fine fraction. We suggested that short-term NT did not significantly affect the turnover time of SOC. The turnover time of SOC was even longer in MP plots because of the incorporation of returned crop residues into soils.

4. Conclusions

Five years of no tillage tended to stratify total SOC concentration in the plough layer (0–20 cm) on the studied clay loam

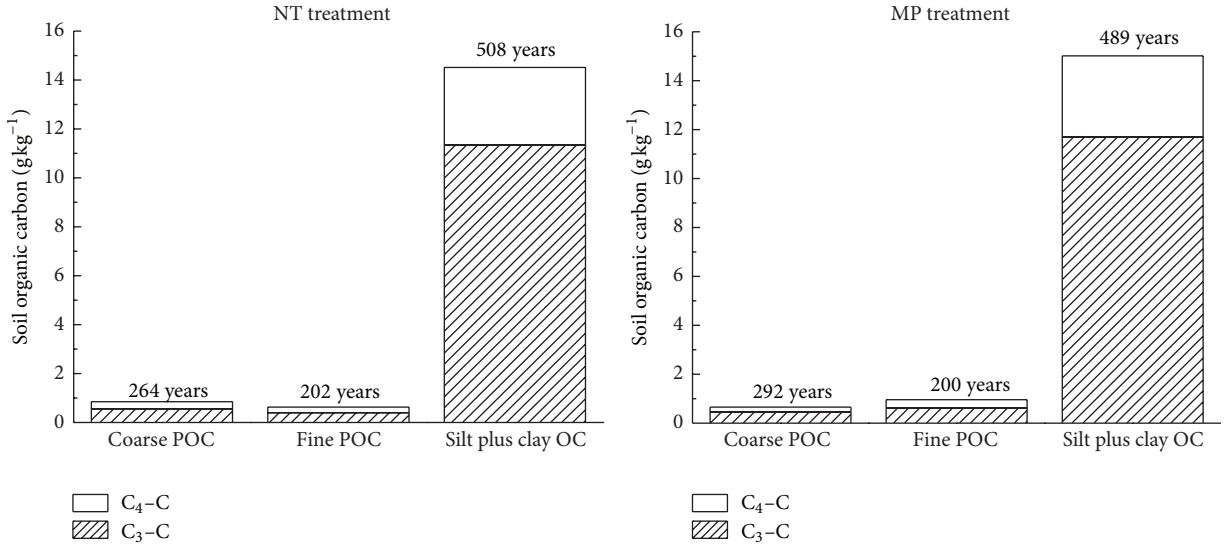

Figure 3: Concentrations of C_3–C and C_4–C in different fractions and the mean turnover time of C under tillage practices.

soil of Northeast China. Soil management using no tillage on this fine-textured and poor-drained black soil might not sequester more SOC than conventional tillage. No tillage had great impacts on fine and coarse POC, though the total POC did not significantly increase. Compared with mouldboard plough, no tillage remarkably increased silt plus clay OC in the plough layer. Both no tillage and mouldboard plough did not significantly affect $\delta^{13}C$ value in each SOC fraction, despite the occurrence of certain changes. The $\delta^{13}C$ values of coarse and fine POC under no tillage treatment were greater than those under mouldboard plough, but there were almost no changes in $\delta^{13}C$ values of silt plus clay OC between these two treatments. Thus, the short-term impact of no tillage was firstly shown in the coarse-size fractions (POC). The distribution of C_3–C mainly in fine particles (silt plus clay) indicated that the turnover of SOC in coarse-size fraction was faster under tillage practices. Further study is needed to verify the long-term effects of tillage practices on SOC turnover and distribution in different size fractions.

Conflict of Interests

The authors declare that there is no conflict of interests regarding the publication of this paper.

Acknowledgments

This research was supported by the Key Deployment Program of the Chinese Academy of Sciences (no. KZZD-EW-TZ-16-02), the National Natural Science Foundation of China (no. 31170483), and the Foundation of Excellent Young Talents in Northeast Institute of Geography and Agroecology, Chinese Academy of Sciences (no. DLSYQ12003).

References

[1] L. H. Zhang, Z. K. Xie, R. F. Zhao, and Y. J. Wang, "The impact of land use change on soil organic carbon and labile organic carbon stocks in the Longzhong region of Loess Plateau," *Journal of Arid Land*, vol. 4, no. 3, pp. 241–250, 2012.

[2] M. Fuentes, B. Govaerts, C. Hidalgo et al., "Organic carbon and stable 13C isotope in conservation agriculture and conventional systems," *Soil Biology and Biochemistry*, vol. 42, no. 4, pp. 551–557, 2010.

[3] M. D. Ampleman, K. M. Crawford, and D. A. Fike, "Differential soil organic carbon storage at forb-and grass-dominated plant communities, 33 years after tall grass prairie restoration," *Plant and Soil*, vol. 374, pp. 899–913, 2014.

[4] S. Dou, J. J. Zhang, E. Lichtfouse, and Y. C. Cao, "Study on dynamic change of soil organic matter during corn stalk decomposition by ^{13}C method," *Acta Pedologica Sinica*, vol. 40, no. 3, pp. 328–334, 2003 (Chinese).

[5] H. C. Piao, D. L. Yu, Q. M. Liu, J. H. Guo, and J. C. Ran, "Changes of natural ^{13}C abundance in light fraction in cleared Mallan Karst forest soils converted to maize cropping," *Soil and Environment Science*, vol. 9, no. 3, pp. 218–222, 2000 (Chinese).

[6] K. Y. Chan, D. P. Heenan, and A. Oates, "Soil carbon fractions and relationship to soil quality under different tillage and stubble management," *Soil and Tillage Research*, vol. 63, no. 3-4, pp. 133–139, 2002.

[7] J. Magid, A. Gorissen, and K. E. Giller, "In search of the elusive "active" fraction of soil organic matter: three size-density fractionation methods for tracing the fate of homogeneously ^{14}C-labelled plant materials," *Soil Biology and Biochemistry*, vol. 28, no. 1, pp. 89–99, 1996.

[8] Y. Yonekura, S. Ohta, Y. Kiyono et al., "Soil organic matter dynamics in density and particle-size fractions following destruction of tropical rainforest and the subsequent establishment of *Imperata* grassland in Indonesian Borneo using stable carbon isotopes," *Plant and Soil*, vol. 372, pp. 683–699, 2013.

[9] M. Wilson and J. Paz-Ferreiro, "Effect of soil use intensity on selected properties of Mollisols in Entre Ríos, Argentina,"

Communications in Soil Science and Plant Analysis, vol. 43, no. 1-2, pp. 71–80, 2012.

[10] K. Paustian, O. Andrén, H. H. Janzen et al., "Agricultural soils as a sink to mitigate CO_2 emissions," *Soil Use and Management*, vol. 13, no. 4, pp. 230–244, 1997.

[11] J. Antle, S. Capalbo, S. Mooney, E. T. Elliott, and K. H. Paustian, "Sensitivity of carbon sequestration costs to soil carbon rates," *Environmental Pollution*, vol. 116, no. 3, pp. 413–422, 2002.

[12] J. Six, S. M. Ogle, F. J. Breidt, R. T. Conant, A. R. Mosiers, and K. Paustian, "The potential to mitigate global warming with no-tillage management is only realized when practised in the long term," *Global Change Biology*, vol. 10, no. 2, pp. 155–160, 2004.

[13] R. López-Garrido, E. Madejón, J. M. Murillo, and F. Moreno, "Short and long-term distribution with depth of soil organic carbon and nutrients under traditional and conservation tillage in a Mediterranean environment (Southwest Spain)," *Soil Use and Management*, vol. 27, no. 2, pp. 177–185, 2011.

[14] T. Chevallier, T. Woignier, J. Toucet, and E. Blanchart, "Organic carbon stabilization in the fractal pore structure of Andosols," *Geoderma*, vol. 159, no. 1-2, pp. 182–188, 2010.

[15] A. J. VandenBygaart, E. G. Gregorich, and D. A. Angers, "Influence of agricultural management on soil organic carbon: a compendium and assessment of Canadian studies," *Canadian Journal of Soil Science*, vol. 83, no. 4, pp. 363–380, 2003.

[16] A. J. VandenBygaart, E. Bremer, B. G. McConkey et al., "Impact of sampling depth on differences in soil carbon stocks in long-term agroecosystem experiments," *Soil Science Society of America Journal*, vol. 75, no. 1, pp. 226–234, 2011.

[17] M. M. Al-Kaisi, X. Yin, and M. A. Licht, "Soil carbon and nitrogen changes as influenced by tillage and cropping systems in some Iowa soils," *Agriculture, Ecosystems and Environment*, vol. 105, no. 4, pp. 635–647, 2005.

[18] Jilin General Station of Soil and Fertilizer, *Soils of Jilin*, China Agriculture Press, Beijing, China, 1998, (Chinese).

[19] A. Liang, N. B. McLaughlin, X. Zhang, Y. Shen, X. Shi, and R. Fan, "Short-term effects of tillage practices on soil aggregate fractions in a Chinese Mollisol," *Acta Agriculturae Scandinavica B: Soil and Plant Science*, vol. 61, no. 6, pp. 535–542, 2011.

[20] A. Liang, X. Yang, X. Zhang, N. McLaughlin, Y. Shen, and W. Li, "Soil organic carbon changes in particle-size fractions following cultivation of Black soils in China," *Soil and Tillage Research*, vol. 105, no. 1, pp. 21–26, 2009.

[21] M. R. Carter, W. J. Parton, I. C. Rowland, J. E. Schultz, and G. R. Steed, "Simulation of soil organic carbon and nitrogen changes in cereal and pasture systems of Southern Australia," *Australian Journal of Soil Research*, vol. 31, no. 4, pp. 481–491, 1993.

[22] T. Yamashita, H. Flessa, B. John, M. Helfrich, and B. Ludwig, "Organic matter in density fractions of water-stable aggregates in silty soils: effect of land use," *Soil Biology and Biochemistry*, vol. 38, no. 11, pp. 3222–3234, 2006.

[23] R. Fan, X. Zhang, A. Liang et al., "Tillage and rotation effects on crop yield and profitability on a Black soil in northeast China," *Canadian Journal of Soil Science*, vol. 92, no. 3, pp. 463–470, 2012.

[24] J. L. Pikul, S. Osborne, M. Ellsbury, and W. Riedell, "Particulate organic matter and water-stable aggregation of soil under contrasting management," *Soil Science Society of America Journal*, vol. 71, no. 3, pp. 766–776, 2007.

[25] E. G. Gregorich, K. J. Greer, D. W. Anderson, and B. C. Liang, "Carbon distribution and losses: erosion and deposition effects," *Soil and Tillage Research*, vol. 47, no. 3-4, pp. 291–302, 1998.

[26] E. G. Gregorich and H. H. Janzen, "Storage of soil carbon in the light fraction and macroorganic matter," in *Structure and Organic Matter Storage in Agricultural Soils*, M. R. Carter and B. A. Stewart, Eds., pp. 167–190, CRC Press, Boca Raton, Fla, USA, 1996.

[27] J. J. Zhang and S. Dou, "Introduction of ^{13}C method for the study on soil organic matter," *Chinese Journal of Soil Science*, vol. 23, no. 2, pp. 64–67, 1999 (Chinese).

[28] X. P. Zhang, H. J. Fang, X. M. Yang, A. Z. Liang, and S. H. Wu, "Effects of no-tillage practices on temperature and moisture of a Black Soil in the spring and early summer," *Chinese Journal of Soil Science*, vol. 36, no. 3, pp. 313–316, 2005 (Chinese).

[29] P. I. Moraru and T. Rusu, "Effect of tillage systems on soil moisture, soil temperature, soil respiration and production of wheat, maize and soybean crops," *Journal of Food, Agriculture and Environment*, vol. 10, no. 2, pp. 445–448, 2012.

[30] F. L. Walley, G. P. Lafond, A. Matus, and C. van Kessel, "Water-use efficiency and carbon isotopic composition in reduced tillage systems," *Soil Science Society of America Journal*, vol. 63, no. 2, pp. 356–361, 1999.

[31] M. M. Iqbal, J. Akhter, W. Mohammad, S. M. Shah, H. Nawaz, and K. Mahmood, "Effect of tillage and fertilizer levels on wheat yield, nitrogen uptake and their correlation with carbon isotope discrimination under rainfed conditions in North-west Pakistan," *Soil and Tillage Research*, vol. 80, no. 1-2, pp. 47–57, 2005.

[32] C. A. Cambardella and E. T. Elliott, "Carbon and nitrogen dynamics of soil organic matter fractions from cultivated grassland soils," *Soil Science Society of America Journal*, vol. 58, no. 1, pp. 123–130, 1994.

[33] H. Knicker, A. Hilscher, F. J. González-Vila, J. A. González, and G. Almendros, "Transport of black carbon in fire-affected soils," *Geophysical Research Abstracts*, vol. 7, article 01529, 2005.

Hindawi Publishing Corporation
The Scientific World Journal
Volume 2014, Article ID 279895, 9 pages
http://dx.doi.org/10.1155/2014/279895

Research Article

Influence of Microsprinkler Irrigation Amount on Water, Soil, and pH Profiles in a Coastal Saline Soil

Linlin Chu,[1,2] Yaohu Kang,[2] and Shuqin Wan[2]

[1] *National Research Center of Pumps, Jiangsu University, Zhenjiang 212013, China*
[2] *Key Laboratory of Water Cycle and Related Land Surface Processes, Institute of Geographic Science and Natural Resources Research, Chinese Academy of Sciences, Beijing 100101, China*

Correspondence should be addressed to Yaohu Kang; kangyh@igsnrr.ac.cn

Received 13 March 2014; Revised 10 June 2014; Accepted 8 July 2014; Published 23 July 2014

Academic Editor: Antonio Paz González

Microsprinkler irrigation is a potential method to alleviate soil salinization. After conducting a homogeneous, highly saline, clayey, and coastal soil from the Bohai Gulf in northern China in a column experiment, the results show that the depth of the wetting front increased as the water amount applied increased, low-salinity and low-SAR enlarged after irrigation and water redistribution, and the soil pH increased with an increase in irrigation amount. We concluded that a water amount of 207 mm could be used to reclaim the coastal saline soil in northern China.

1. Introduction

The coastal land surrounding Bohai Gulf in northern China is a resource constrained by population growth, rapid industrialization, and agricultural production [1–3]. The soils developed from highly saline coastal mud flats consist of highly saline upper and lower soil horizons, with salinity similar to that of seawater [4]. The shallow groundwater system is also saline, with an electrical conductivity (ECe) between 4.9 and 20.5 dS/m [3, 5]. In addition, strong evaporation increases the rise of salts through the soil profile to the surface. These costal soils are characterized by heavy texture, high content of exchangeable sodium, poor structure, and low water permeability. As a result, the soil does not support vegetation, except for salt resistant halophytes. Therefore, urgent measures are required to alleviate soil salinization and to enable utilization of the saline land.

Several methods have been used to reclaim coastal saline soils including ponding irrigation, chemical amendment, biological reduction, and the replacement of the entire surface soil with nonsaline soil [4, 6–9]. However, these methods are not practical for the coastal land of Bohai Gulf due to the scarcity of freshwater resources and to the low hydraulic conductivities of the soil near saturation. Moreover, when saturated soil conditions persist, growth and production may be inhibited [10, 11]. Chemical amelioration is costly, and developing countries only provide marginal assistance to local farmers for soil amendments. Biological methods for the reduction of salts cannot ameliorate coastal saline soils for long periods of time, and this would be also the case if the entire soil surface would be replaced with a higher quality soil [12–14]. Therefore, there is a need for usable, cheap, and simple methods for combating soil salinization and reclaiming saline land.

Efficient irrigation methods such as drip irrigation, sprinkler irrigation, and microsprinkler irrigation allow precise quantification and positioning of water and chemicals within the soil profile. These methods are considered advantageous due to their high water-use efficiency and their ability to displace salt under unsaturated flow conditions. We have conducted several studies on the efficiency of different drip-irrigation rates for reclaiming coastal saline soils, and we succeeded in the design of adequate reclamation [3, 15].

Sprinkler irrigation, which has some similitude to natural rainfall, has been used to ameliorate saline soils under continuously unsaturated conditions [16, 17]. Nonetheless, the kinetic energy of sprinkler droplets can impact the soil surface, destroy soil aggregates, decrease infiltration rate, and

promote leaching. These effects are exacerbated by longer irrigation times and higher irrigation rates [18].

Microsprinkler irrigation has been demonstrated as beneficial for tree and vine crops, because it can promote growth, improve yields, decrease water, and decrease energy use compared to sprinkler or flood irrigation systems, and protects plants from adverse climatic conditions much more than drip irrigation [19]. Microsprinkler irrigation has been examined with a focus on water-use efficiency, crop growth, and system layout, but no studies have focused on the depth distributions of the soil water content (θ) and salinity. Drip irrigation is now considered a potential effective method to reclaim the coastal saline soils, but whether microsprinkler irrigation can more efficiently displace salt and more accurately deliver water volumes still remain open questions.

Based on the above rationale, the objectives of this research were to determine the depth distributions of soil water content (θ), electrical conductivity (ECe), sodium adsorption ratio (SAR), and pH of saturated soil extracts after application of different water amounts from microsprinklers.

2. Materials and Methods

2.1. Study Site, Soil Sampling, and Preparation. Soil samples were collected from the Caofeidian Development Zone (39°12′ N; 118°31′ E) in Tangshan Bay Eco-city, east of Hebei province and west of Bohai Gulf. The region has a semihumid marine climate, with a mean annual temperature of 11.4°C and a mean annual precipitation of 554.9 mm, with 74% of the precipitation occurring between June and September. Bulk density, ECe, and pH of the initial soil for each soil layer are shown in Table 1. The average ECe and pH were 29.6 dS/m and 7.4, respectively. In addition to the high ECe, the saturated hydraulic conductivity of the soil (0.0025 mm/d) was very low in fields irrigated with nonsaline water due to soil dispersion and clogging of soil pores.

Soil samples were collected from the A-horizon and were air-dried, crushed, passed through a 2 mm sieve, and characterized for general properties. The ECe, SAR, and pH of the homogenous soils were 27.8 dS/m, 59.7 $(\text{mmol/L})^{0.5}$, and 7.6, respectively. The study soil was classified as a Solonchak and it was silt loam textured, with 0.49% of particles less than 0.002 mm, 45.14% of particles between 0.002 and 0.02 mm, and 54.37% of particles larger than 0.02 mm.

2.2. Laboratory Experiment. Columns to contain the soil were made of acrylic glass with a diameter and height of 110 mm and 600 mm, respectively, and drainage holes at their base for percolating water (Figure 1(a)). Each soil column was filled with air-dried saline soil to attain 1.5 g/cm^3, the bulk density of the original soil at the experimental site. The initial soil water content of the experimental columns was 4 gr/100. The soil in the columns was homogeneous and assumed to have vertical water flow throughout the experiment. To reduce the impact of airflow and evaporation, the experiment was conducted in laboratory conditions.

The columns were irrigated using fresh water with an ECe of 0.4 dS/m and a pH of 8.6 via a small plastic swivel microsprinkler (RC-40, Luckrain Irrigation Company, Beijing, China) with a single nozzle, a height of 65 cm, and a wetting radius of 2.5 m. The nozzle operating pressure was maintained at 0.2 MPa using a hydraulic-pressure control valve. The soil columns were all arranged 2 mm apart in a concentric circle with a 2 m radius, and the microsprinkler was positioned at the center (Figure 1(b)). When a column received the designated quantity of water, it was covered immediately with plastic film. Five water amounts (55, 128, 185, 207, and 223 mm) were applied, and each irrigation treatment was repeated three times. The mean air temperature during irrigation was 25°C, and each treatment was irrigated at a rate of 1.2 mm/h.

Table 1: Bulk density, electrical conductivity of saturated paste extracts (ECe), and pH of the initial soil profile sampled at Caofeidian Eco-city, Hebei, China.

Depth (cm)	Bulk density (g/cm^3)	ECe (dS/m)	pH
0–10	1.32	30.6	7.2
10–20	1.51	29.4	7.3
20–30	1.58	28.8	7.6
30–40	1.71	28.6	7.7
40–60	1.62	28.9	7.5
60–80	1.79	29.6	7.3
80–100	1.62	30.9	7.1
100–120	1.62	30.1	7.1
Average	1.60	29.6	7.4

2.3. Measurements of Irrigation Dose and Soil Properties

2.3.1. Irrigation Amounts. The amount of water delivered by the microsprinkler was measured using a conical flask positioned at the same distance from the microsprinkler as the soil columns (Figure 1(c)). After each irrigation event, the quantity of water in each triangular flask was evaluated according to the following:

$$\text{IA} = \frac{m_2 - m_1}{\rho_w \times \pi \times r^2} \times 10, \quad (1)$$

where IA is the irrigation amount (mm); m_1 and m_1 are the quantities of water in the conical flask before and after irrigation was finished, respectively (g); ρ_w is the water density (g/cm^3); and r is the inlet radius of the triangular flask (cm).

2.3.2. Soil Water Content and Salinity. Soil samples for each treatment were extracted vertically from the soil column with an auger (3.0 cm diameter and 100 cm height). Samples were taken during the redistribution period at 0, 24, and 48 h after application of the prescribed water amount was finished (Figure 1(c)). The distance between adjacent vertical samples was set to 1.7 cm (Figure 1(d)). After a full vertical sample was obtained for each period, plastic cloth was placed over the hole to avoid a dehydrating influence of successive samplings. The sample depths were 0–5, 5–10, 10–15, 15–20, 20–25, 25–30,

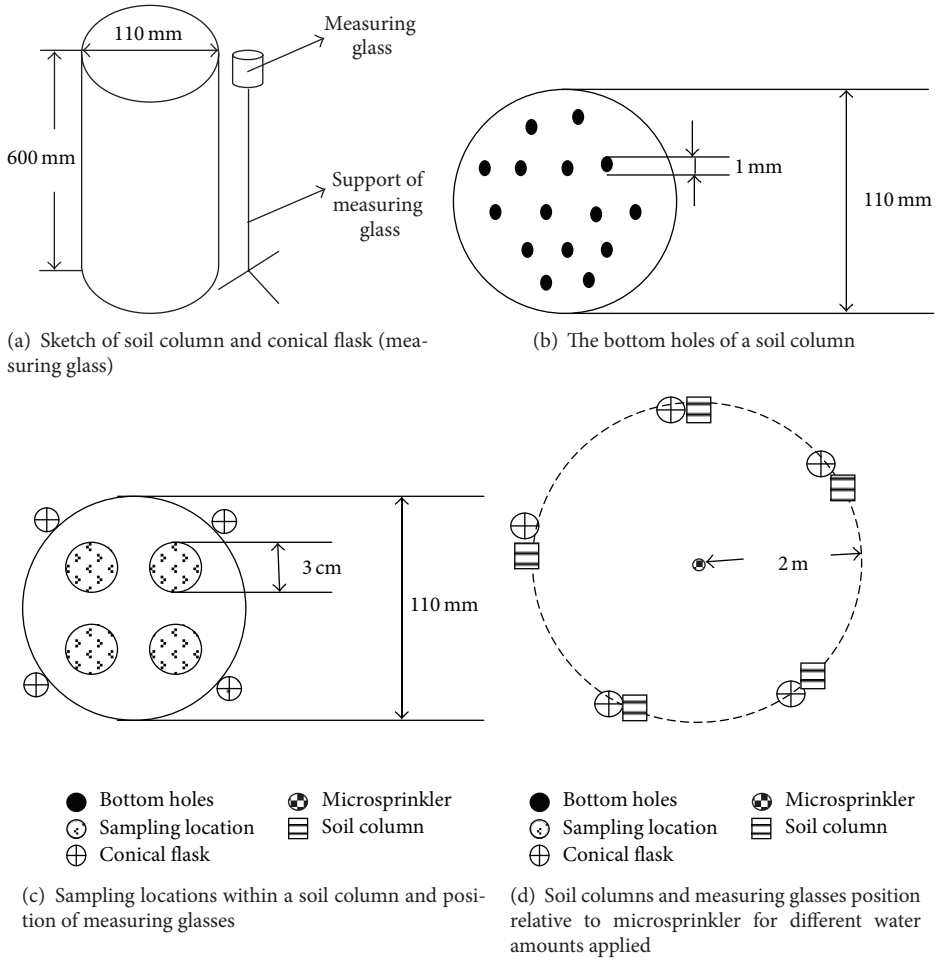

(a) Sketch of soil column and conical flask (measuring glass)

(b) The bottom holes of a soil column

(c) Sampling locations within a soil column and position of measuring glasses

(d) Soil columns and measuring glasses position relative to microsprinkler for different water amounts applied

Figure 1: Sketch of the experimental setup showing the location of microsprinkler, soil columns, and measuring glasses, with details of bottom holes and sampling location within a column.

30–35, 35–40, 40–45, 45–50, 50–55, and 55–60 cm. The water content (θ) was determined by oven-drying on a subsample.

For each sampling depth, the remaining soil samples were air-dried and sieved through a 2 mm sieve. A saturated soil paste was prepared via centrifugation (4000 rpm, 20 min) for chemical analysis. The soil ECe, soluble cations (Na^+, Ca^{2+}, and Mg^{2+}), and pH were determined in extracts of the saturated soil, and the results were determined using a conductivity meter (DDS-11, REX, Shanghai), inductively coupled plasma optical-emission spectrometer (Optima 5300DV, PerkinElmer, U.S.A), and a pH meter (PHS-3C, REX), respectively. The SAR of the saturated paste extract was calculated using the following:

$$\mathrm{SAR} = \frac{[\mathrm{Na}^+]}{\left([\mathrm{Ca}^{2+}] + [\mathrm{Mg}^{2+}]\right)^{0.5}} \quad (2)$$

where the concentration of each cation is in mmol/L.

The average θ, ECe, SAR, and pH of the wet zone were calculated as the weighted mean.

2.3.3. Statistical Analysis. Statistical analyses, including a one-way analysis of variance (ANOVA), were conducted to compare and rank the treatment means at the 5% probability level for θ, ECe, pH, and periods of soil water redistribution. Statistical analyses were performed using SPSS Version 16.0.

3. Results and Discussion

3.1. Wetting Front. When the irrigation time increased from 47 h to 189 h, the irrigation amount increased from 55 mm to 223 mm. This corresponded to a vertical wetting front, just after irrigation has been completed (at 0 h), of 15–20, 40–45, 55–60, 55–60, and 55–60 cm, for each successive irrigation amount. These results showed that as the irrigation amount increased, also the depth of the wetting front at 0 h increased (Table 2). Moreover, the vertical wetting front was not significantly different among 0, 24, and 48 h since irrigation has ceased.

3.2. Soil Water Content (θ). The depth distributions of θ at 0, 24, and 48 h since irrigation has finished under different irrigation amounts are presented in Figure 2. It is generally accepted that during infiltration θ will decrease with increasing soil depth and a relatively moist region forms in the upper

Table 2: Period of irrigation and depth of the wetting front at 0, 24, and 48 h during redistribution for each irrigation amount.

Irrigation amounts (mm)	Irrigation hours (h)	Depth of the wetting front (cm)		
		0 h of water redistribution	24 h of water redistribution	48 h of water redistribution
55	47	15–20	15–20	15–20
128	108	40–45	45–50	45–50
185	156	55–60	55–60	55–60
207	175	55–60	55–60	55–60
223	189	55–60	55–60	55–60

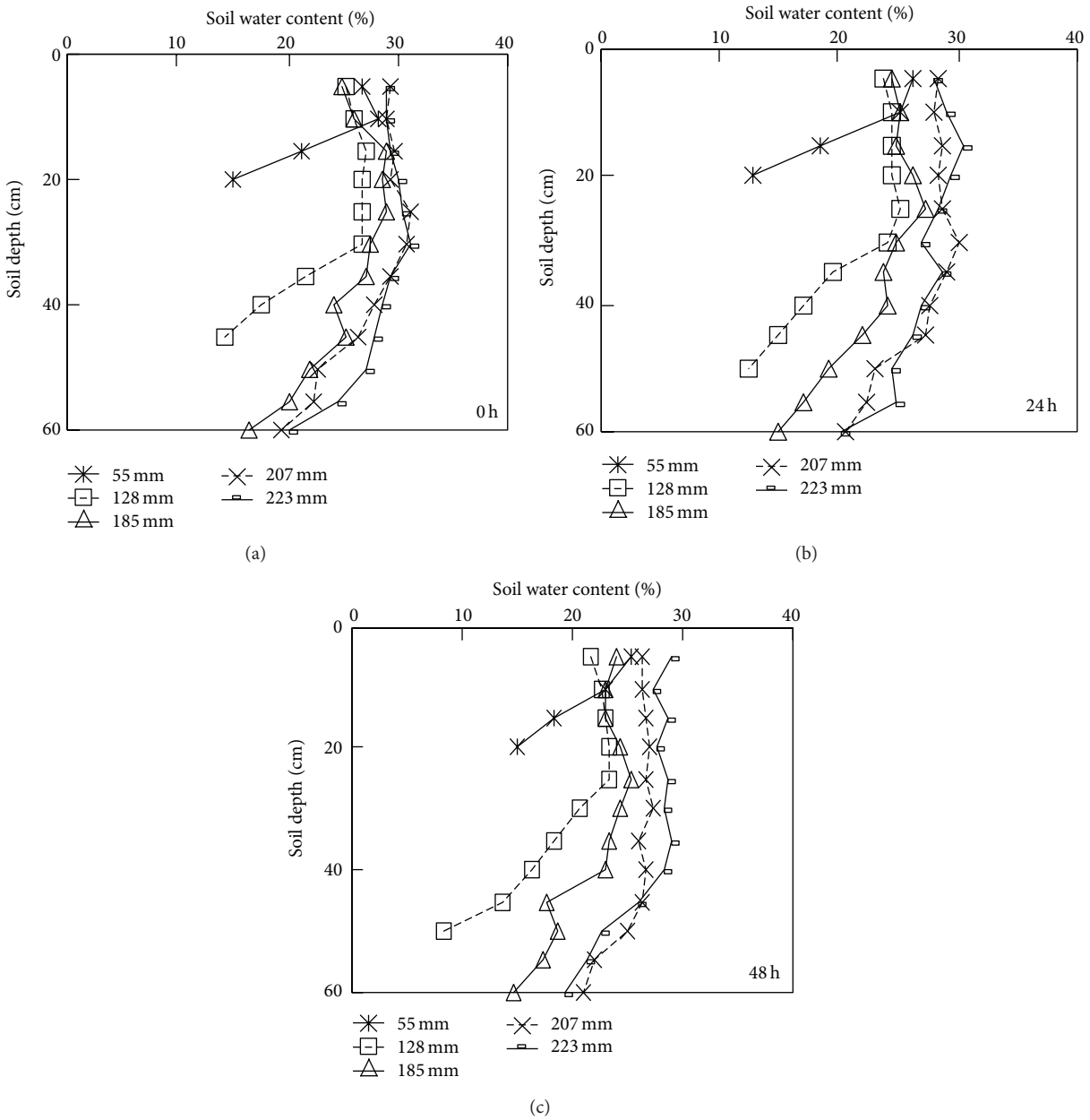

Figure 2: The depth distributions of soil water content at 0 hour (a), 24 hours (b), and 48 hours (c) during water redistribution under different water amounts applied.

layer, where in turn a saturated zone and a transmission zone may be recognized. In our experiment, only a small amount of soil water moved toward the deep layer of the soil column, due to the low hydraulic conductivity of the heavy textured soil studied. Therefore, just after irrigation (0 h), θ was greater at 0–20 cm depth than at 20–40 and 40–60 cm for all the studied treatments.

For all the treatments, the water content (θ) at the wet upper layer (involving saturation and transmission zones) was uniform and approached the maximum θ content. The maximum θ values for the irrigation amounts of 55, 128, 185, 207, and 223 mm were 28.3%, 26.9%, 28.8%, 31.1%, and 31.0%, respectively, and were measured at depths of 5–10, 10–15, 10–15, 20–25, and 25–30 cm, respectively. Therefore, as the total irrigation amount was the highest, the depth of the wet zone increased. Furthermore, the average θ value of the wet zone showed a trend to increase as the irrigation amount increased. For example, the average θ in the wet zone increased from 22.8% (55 mm) to 29.4% (223 mm), and the vertical extent of this zone also increased, which is in accordance with the results of Troiano et al. [20].

As expected, during the redistribution of soil moisture, the matric potential of the soil water showed a trend to approach equilibrium, and consequently the depth differences in θ decreased. Compared to the results obtained at 0 h, the water content (θ) measured at each depth decreased at 24 h and 48 h after irrigation has ceased. The mean θ values of the wet zones decreased by 10.9%, 19.0%, 13.5%, 5.9%, and 5.9% for the irrigation amount of 55, 128, 185, 207, and 223 mm, respectively. Overall, the observed reduction in θ decreased with an increase in irrigation amount. During soil-water redistribution events, the air in the soil pore space was replaced by water.

3.3. Soil Salinity

3.3.1. Depth Distributions of ECe. A consequence of the lateral and vertical movement of water, and the line-source nature of microsprinkler irrigation, is that salts and water are moving toward the subsoil forming a desalinized region at the saturated and transmission zones, and subsequently salts can accumulate near to the wetting front. The profiles of the ECe at 0, 24, and 48 h during water redistribution under different irrigation doses are shown in Figure 3. At 0 h, just after irrigation has ceased, as the irrigation amount increased, also the depth of the layer with low salinity (ECe < 4 dS/m) increased; this layer extended at 0–5, 0–10, 0–20, 0–20, and 0–25 cm for irrigation amounts of 55, 128, 185, 207, and 223 mm, respectively. Besides, the maximum ECe value of the column was significantly higher than the initial value, going up to 38.5, 38.6, 38.7, 30.2, and 32.1 dS/m for irrigation amounts of 55, 128, 185, 207, and 223 mm, respectively. Furthermore, the maximum ECe was observed at a depth of 15–20, 35–40, 50–55, 50–55, and 50–55 cm, for the successive irrigation doses applied. Thus, as the irrigation amount increased, the thickness of the desalinized upper layer increased, while the salt concentration reached a maximum at the middle and lower layers of the column.

During the water redistribution phase, at 48 h, for the irrigation amount of 55 mm, the average ECe decreased as water redistribution progressed, and a 33.8% reduction in ECe was measured at 0–20 cm depth at the 48 h sampling, during water redistribution. Reductions of average ECe for the other four irrigation amounts were not significant, but the desalinization rate of the irrigation amount of 55 mm was significantly lower than those of the other treatments.

3.3.2. Relationship between the Average ECe Value and Irrigation Amount. The relationships between average ECe values in the wetting zone, at successive times during redistribution, and the irrigation amount (IA) can be expressed by the following equation:

$$\begin{aligned}
&\text{average ECe}_0 \\
&= -0.0005(\text{IA})^2 + 0.0614\,(\text{IA}) + 20.489 \quad R^2 = 0.8853, \\
&\text{average ECe}_{24} \\
&= -0.0006(\text{IA})^2 + 0.101\,(\text{IA}) + 15.99 \quad R^2 = 0.9614, \\
&\text{average ECe}_{48} \\
&= -0.0005(\text{IA})^2 + 0.1103\,(\text{IA}) + 13.838 \quad R^2 = 0.9216.
\end{aligned} \tag{3}$$

The above relationships show that during redistribution, ECe and irrigation dose could be fitted by parabolic equations with high R^2 values (Figure 4). Compared to the initial results 0 h after water redistribution, the average ECe values for the wetting zones of irrigation amounts of 55, 128, 185, 207, and 223 mm were decreased by 17.6%, 31.9%, 32.8%, 52.4%, and 63.7%, respectively. When the irrigation amount increased from 55 to 223 mm, the average soil ECe in the wet zone decreased by 55.9% (from 22.9 to 10.1 dS/m).

As the irrigation amount decreased, the average ECe at a depth of 0–20 cm increased by 17.6%, 81.1%, 91.6%, 92.3%, and 94.4%, compared to the initial ECe value. All of the salts were leached down to deeper levels in each irrigation amount, especially for irrigation amounts of 207 and 223 mm. However, the observed differences in the profiles of soil moisture and ECe values among the irrigation amounts of 207 and 223 mm were low during water redistribution. Therefore, a significant change in the average ECe value was not observed as the irrigation amount increased from 207 mm to 223 mm. Meanwhile, the ANOVA results showed that the average ECe for all of the irrigation amounts were significant ($P < 0.05$).

3.4. Depth Distribution of SAR. The sodium adsorption ratio, SAR, is well known to be related to soil dispensability. In practice, SAR and electrical conductivity values of irrigation water allow assessment of its potential to promote soil dispersion. The depth distributions of SAR at 0 h after water application had ceased under the different irrigation amounts are shown in Figure 5. The observed changes in the SAR with successive irrigation doses were similar to those of the ECe values. At the end of the experiment, the SAR of all

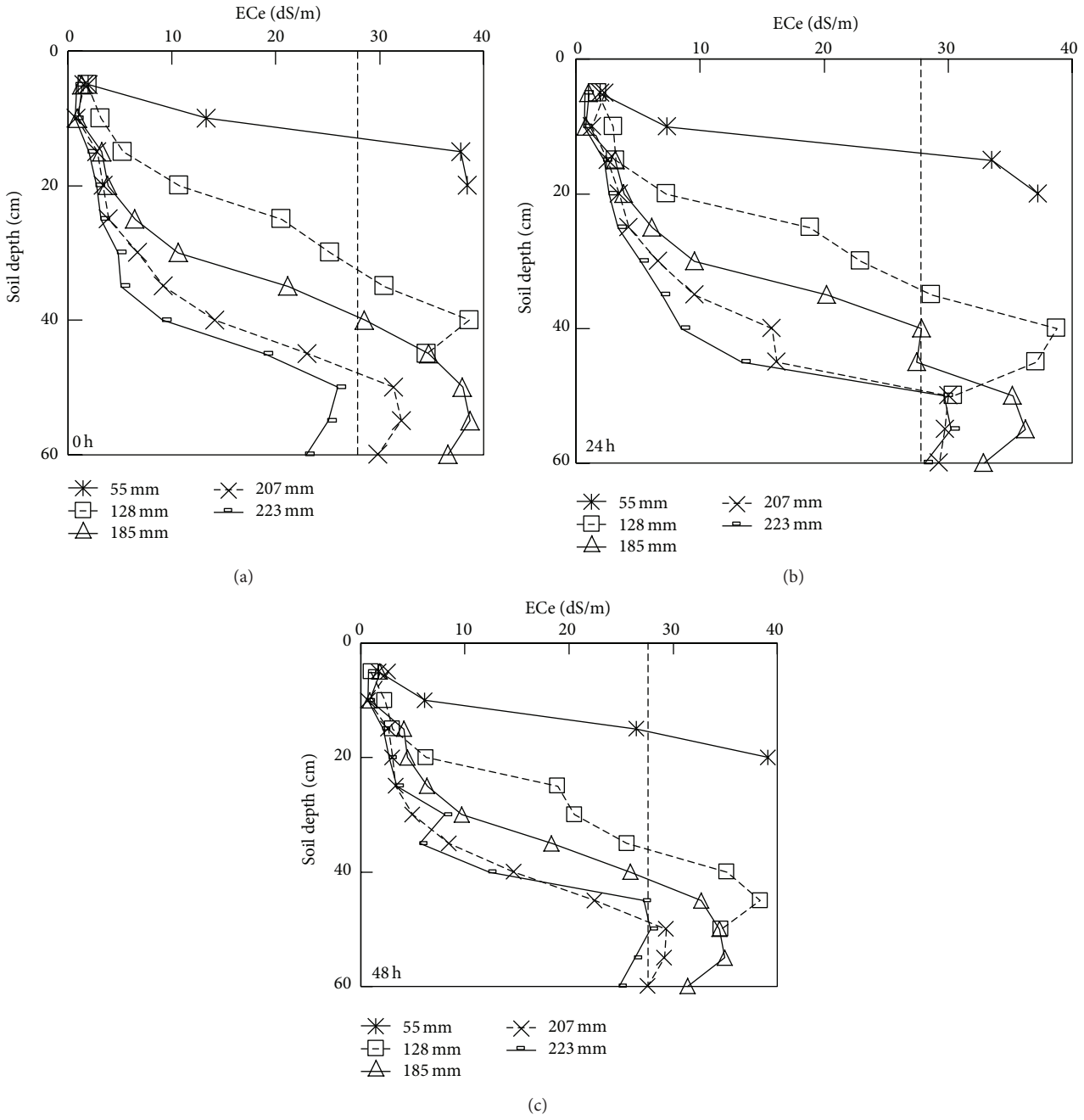

Figure 3: The depth distributions of ECe at 0 hour (a), 24 hours (b), and 48 hours (c) during water redistribution under different water amounts applied.

the treatments increased gradually with an increase in the soil depth.

As the irrigation amount increased, the depth of the highest SAR also increased. For the irrigation amounts of 55, 128, 185, 207, and 223 mm, the zone with the maximum SAR was located at a depth of 10–15, 35–40, 50–55, 50–55, and 55–60 cm, and the corresponding SAR was 387.2, 481.0, 532.6, 489.8, and 450.3 $(\text{mmol/L})^{0.5}$, respectively. However, except for the irrigation amount of 55 mm, a low SAR zone (SAR < 15 $\text{mmol/L})^{0.5}$ was observed at a depth of 0–5 cm. For the other four irrigation amounts, a low SAR zone also was observed at a depth of 0–10 cm. Meanwhile, as the irrigation amount increased, the SAR value of each depth increased, the amplitude of variation increased, and the depth increased, except for the irrigation amounts of 207 and 223 mm. The average soil SAR in the entire profile changed as the experiment progressed. For the irrigation amount of 55 mm, the average soil SAR at a depth of 0–20 cm increased by 272.1%, while that of the other irrigation amounts decreased. A significant reduction in the soil SAR occurred at a depth of 0–20 cm for the irrigation amounts of 128, 185, 207, and 223 mm. Compared to the initial levels,

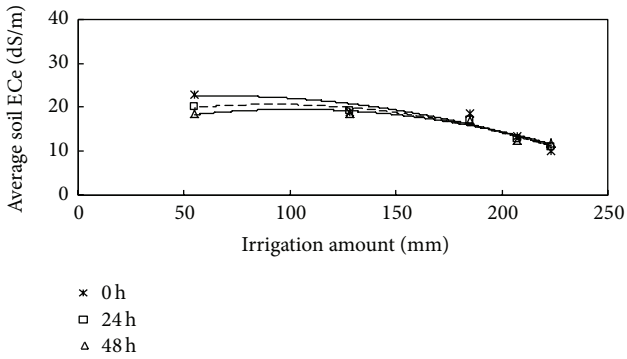

Figure 4: Relationships between average ECe in wetted zone and irrigation amount.

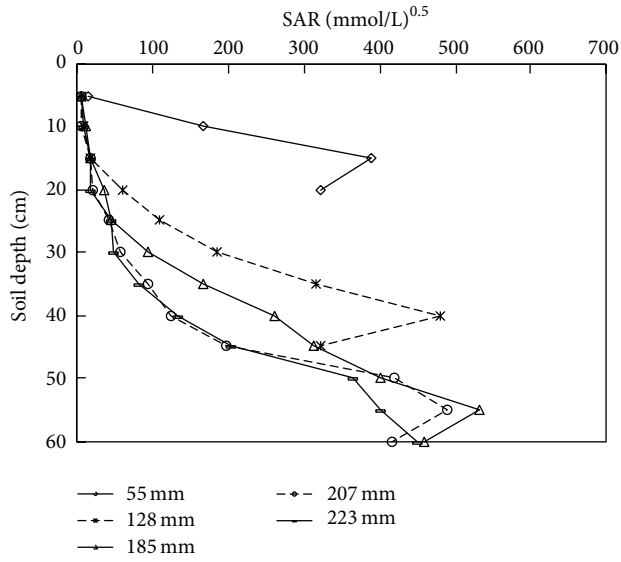

Figure 5: The depth distributions of SAR at 0 hour, just after irrigation has finished, under different water amounts applied.

the SAR at 0–20 cm was decreased by 61.3%, 70.4%, 79.2%, and 79.3%, respectively. However, the average SAR at 20–40 and 40–60 cm increased, and the greatest increase occurred at a depth of 40–60 cm. At this depth, the observed increase was more than two times greater than that of the initial value for all four irrigation amounts.

3.5. Depth Distribution of Soil pH. The depth distributions of pH at 0 h, 24 h, and 48 h during water redistribution are shown in Figures 6(a), 6(b), and 6(c), respectively. Changes in the soil pH associated to salt leaching were determined in each irrigation amount. Due to changes in the ECe depth distributions, the profiles of the soil pH in the experimental column changed concomitantly, but the amplitude of its variation was small. For all five irrigation amounts, high soil pH zones were primarily observed in the 0–10 cm layer at the end of irrigation. Moreover, the pH values of profiles obtained for irrigation amounts of 207 and 223 mm were higher than those for 55, 128, and 185 mm. Compared to the initial soil pH, the average pH values of the entire wet zone for the irrigation amounts of 55, 128, 185, 207, and 223 mm were increased by 2.9%, 6.2%, 5.7%, 6.3%, and 6.5%, respectively. Thus, as the irrigation amount increased, the average soil pH also increased, and the irrigation amount of 55 mm significantly differed from each of the other four irrigation amounts.

During soil water redistribution, the layer with high soil pH expanded for each water dose, but the observed differences among successive sampling times in the period of water redistribution were minor. These results indicated that the irrigation amount played an important role in the salt concentration of the soil but had a weaker effect on the average soil pH.

The study focused on the influence of irrigation amounts with microsprinkler irrigation on water, salt, and pH profiles in a coastal saline soil under laboratory conditions. Therefore the outcome of the experiment performed may be affected by some uncertainties. To adapt to the local conditions in northern China, further studies in field should be considered.

4. Conclusions

The irrigation amount, which ranged from 55 to 223 mm, had a significant effect on the depth distributions of θ, ECe, and SAR but had a relatively minor impact on the depth distributions of pH. Due to the characteristics of the studied soil, mainly the high clay content and low hydraulic conductivity, significant differences between the periods of water redistribution were not observed.

The differences among the depth distributions of θ were significant for the irrigation amounts of 55, 128, and 185, but not for those of 207 and 223 mm.

Except for the irrigation amount of 55 mm, salt was leached from the soil, and the low salinity zone enlarged as the irrigation amount increased. Parabolic relationship between the average ECe of the wetting front and the irrigation amounts was observed at 0, 24, and 48 h during water redistribution. Moreover, the reduction in the average ECe ranged from 17.6% for the irrigation amount of 55 mm to 63.7% for the 223 mm treatment.

The depth distributions of the SAR were similar to those of the ECe, but the observed reduction was smaller than that of the ECe.

Taking all of the above factors into consideration, irrigation amounts of 207 mm for 50–60 cm soil depth under microsprinkler irrigation appear to be the best option to reclaim highly saline coastal land surrounding Bohai Gulf in northern China.

Conflict of Interests

The authors declare that there is no conflict of interests regarding the publication of this paper.

Acknowledgments

This study was supported by the National High Technology R&D Program of China (Grant nos. 2013 BAC02B02 and

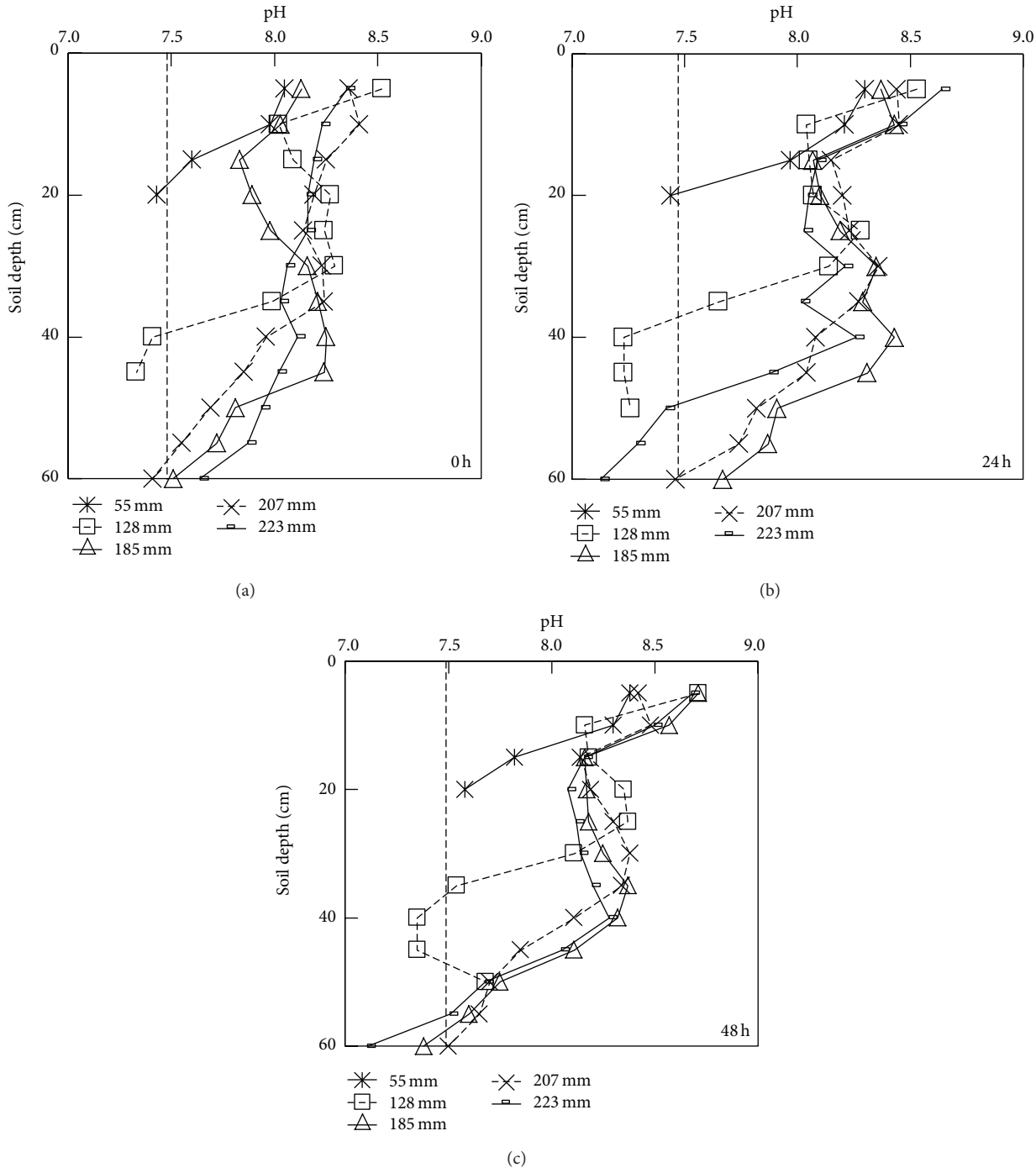

Figure 6: The depth distributions of pH at 0 hour (a), 24 hour (b), and 48 hours (c) during water redistribution under different water amounts applied.

2013BAC02B01), the Priority Academic Program Development of Jiangsu Higher Education Institutions (1033000001), the Research Foundation for Advanced Talents of Jiangsu University (1281440009), the Knowledge Innovation Program of the Chinese Academy of Sciences (Grant no. KZCX 2-YW-359), and the Action Plan for Development of Western China of Chinese Academy of Sciences (Grant no. KZCX 2-XB3-16).

References

[1] Z. Shi, Y. Li, R. C. Wang, and F. Makeschine, "Assessment of temporal and spatial variability of soil salinity in a coastal saline field," *Environmental Geology*, vol. 48, no. 2, pp. 171–178, 2005.

[2] X. Wang, Q. Zhao, Y. Hu et al., "An alternative water source and combined agronomic practices for cotton irrigation in coastal saline soils," *Irrigation Science*, vol. 30, no. 3, pp. 221–232, 2012.

[3] J. Sun, Y. Kang, S. Wan, W. Hu, S. Jiang, and T. Zhang, "Soil salinity management with drip irrigation and its effects on soil hydraulic properties in north China coastal saline soils," *Agricultural Water Management*, vol. 115, pp. 10–19, 2012.
[4] Z. Q. Wang, S. Q. Zhu, R. P. Yu et al., *China Saline and Sodic Soils*, Science Press, Beijing, China, 1993, edited by P.L. Chen.
[5] M. He, K. Sakurai, G. Q. Wang, Z. H. Chen, Y. Shu, and J. J. Xu, "Physico-chemical characteristics of the soils developed from alluvial deposits on Chongming Island in Shanghai, China," *Soil Science and Plant Nutrition*, vol. 49, no. 2, pp. 223–229, 2003.
[6] H. R. Khan, I. U. Ahmed, and H. P. Blume, "Effects of gypsum and Zn on uptake ratios of Na, K and growth-yield of rice grown on a coastal saline soil," *Zeitschrift fur Pflanzenernahrung und Bodenkunde*, vol. 159, no. 4, pp. 351–356, 1996.
[7] Z. Shi, M. X. Huang, and Y. Li, "Physico-chemical properties and laboratory hyperspectral reflectance of coastal saline soil in Shangyu City of Zhejiang Province, China," *Pedosphere*, vol. 13, no. 3, pp. 193–198, 2003.
[8] M. Singh, A. K. Bhattacharya, T. V. R. Nair, and A. K. Singh, "Ammonium losses through subsurface drainage effluent from rice fields of coastal saline sodic clay soils," *Water, Air, and Soil Pollution*, vol. 127, no. 1–4, pp. 1–14, 2001.
[9] A. Datta, J. B. Yeluripati, D. R. Nayak, K. R. Mahata, S. C. Santra, and T. K. Adhya, "Seasonal variation of methane flux from coastal saline rice field with the application of different organic manures," *Atmospheric Environment*, vol. 66, pp. 114–122, 2013.
[10] F. S. Davies and D. Wilcox, "Waterlogging of containerized rabbiteye blueberries in Florida," *Journal of the American Society for Horticultural Science*, vol. 109, pp. 520–524, 1984.
[11] D. R. Bryla and R. G. Linderman, "Implications of irrigation method and amount of water application on Phytophthora and Pythium infection and severity of root rot in highbush blueberry," *HortScience*, vol. 42, no. 6, pp. 1463–1467, 2007.
[12] A. Kumar and I. P. Abrol, "Studies on the reclaiming effect of Karnal-grass and para-grass grown in a highly sodic soil," *Indian Journal of Agricultural Sciences*, vol. 54, pp. 189–193, 1984.
[13] N. Ahmad, R. H. Qureshi, and M. Qadir, "Amelioration of a calcareous saline-sodic soil by gypsum and forage plants," *Land Degradation & Rehabilitation*, vol. 2, no. 4, pp. 277–284, 1990.
[14] T. Zhang, Y. Kang, and S. Wan, "Shallow sand-filled niches beneath drip emitters made reclamation of an impermeable saline-sodic soil possible while cropping with *Lycium barbarum* L.," *Agricultural Water Management*, vol. 119, pp. 54–64, 2013.
[15] J. X. Sun, Y. H. Kang, and S. Q. Wan, "Effects of an imbedded gravel-sand layer on reclamation of coastal saline soils under drip irrigation and on plant growth," *Agricultural Water Management*, vol. 123, pp. 12–19, 2013.
[16] D. Nielsen, J. W. Biggar, and J. N. Luthin, "Desalinization of soils under controlled unsaturated flow conditions," in *Proceedings of the 6th International Congress on Irrigation and Drainage*, pp. 15–19, New Delhi, India, 1966.
[17] J. D. Oster, L. S. Willardson, and G. J. Hoffman, "Sprinkling and ponding techniques for reclaiming saline soils," *Transactions of the American Society of Agricultural Engineers*, vol. 16, no. 1, pp. 89–91, 1973.
[18] S. Zeqiang, *Research on the Effect of Sprinkler Irrigation on Soil Structure and the Characteristic of Water and Nitrogen Distribution*, Graduate University of Chinese Academy of Sciences Press, Beijing, China, 2006.
[19] D. Reich, R. Godin, and I. Broner, *Micro-Sprinkler Irrigation for Orchards*, Colorado State University Extension, Crop Series, Irrigation, 2009, http://www.ext.colostate.edu/.
[20] I. Troiano, C. Garretson, C. Krauter, J. Brownell, and J. Huston, "Brownell influence of amount and method of irrigation water application on leaching of atraziue," *Hournal of Environmental Quality*, vol. 22, pp. 290–298, 1993.

Hindawi Publishing Corporation
The Scientific World Journal
Volume 2014, Article ID 198231, 9 pages
http://dx.doi.org/10.1155/2014/198231

Research Article

The Effects of Rape Residue Mulching on Net Global Warming Potential and Greenhouse Gas Intensity from No-Tillage Paddy Fields

Zhi-Sheng Zhang,[1,2] Cou-Gui Cao,[1,2] Li-Jin Guo,[1,2] and Cheng-Fang Li[1,2]

[1] *College of Plant Science and Technology, Huazhong Agricultural University, No. 1 Shizishan Street, Hongshan District, Wuhan, Hubei 430070, China*
[2] *Key Laboratory of Crop Ecophysiology and Farming System in the Middle Reaches of the Yangtze River, No. 1 Shizishan Street, Hongshan District, Wuhan, Hubei 430070, China*

Correspondence should be addressed to Cheng-Fang Li; lichengfang@126.com

Received 11 April 2014; Revised 29 June 2014; Accepted 5 July 2014; Published 22 July 2014

Academic Editor: Antonio Paz González

A field experiment was conducted to provide a complete greenhouse gas (GHG) accounting for global warming potential (GWP), net GWP, and greenhouse gas intensity (GHGI) from no-tillage (NT) paddy fields with different amounts of oilseed rape residue mulch (0, 3000, 4000, and 6000 kg dry matter (DM) ha^{-1}) during a rice-growing season after 3 years of oilseed rape-rice cultivation. Residue mulching treatments showed significantly more organic carbon (C) density for the 0–20 cm soil layer at harvesting than no residue treatment. During a rice-growing season, residue mulching treatments sequestered significantly more organic C from 687 kg C ha^{-1} $season^{-1}$ to 1654 kg C ha^{-1} $season^{-1}$ than no residue treatment. Residue mulching significantly increased emissions of CO_2 and N_2O but decreased CH_4 emissions. Residue mulching treatments significantly increased GWP by 9–30% but significantly decreased net GWP by 33–71% and GHGI by 35–72% relative to no residue treatment. These results suggest that agricultural economic viability and GHG mitigation can be achieved simultaneously by residue mulching on NT paddy fields in central China.

1. Introduction

China is the largest rice-producing country in the world, with a gross sown area of 29.6 million ha in 2009 [1]. CH_4 emissions from Chinese rice fields during the 2000 rice-growing season have been estimated to be 7.4 Tg, constituting approximately 29% of global CH_4 emissions from rice cultivation [2]. Annual N_2O emissions from rice fields in China have been estimated to be 91 Gg nitrogen (N), of which 50 Gg N is emitted during rice-growing seasons [3]. Furthermore, mean soil CO_2 fluxes from paddy fields of subtropical China have been estimated to be 178.5–259.9 mg m^{-2} h^{-1} [4], which are far more than mean fluxes of N_2O (6.0–74.3 μg m^{-2} h^{-1}) [5] and CH_4 from paddy fields in China (0.5–32.3 mg m^{-2} h^{-1}) [6]. In this way, mitigating GHG emissions from paddy fields in China is an important means of addressing the issue of climate change and developing sustainable agriculture.

China produces approximately 750 million tons of crop residues annually [1]. Farmers generally burn crop residues in their fields to reduce the time and expense of handling them, causing environmental pollution. For this reason, farmers are encouraged to return residues to their fields after harvesting, to stop burning them, and to improve the sustainability of agriculture. The soil C pool depends on the balance between C input and output. The use of crop residues can increase C input to soil and so improve soil C sequestration. However, this undoubtedly provides readily available C and N substrates, thus increasing GHG emissions [7]. Increases in GWP caused by increased GHG emissions from the use of crop residue application may significantly offset the mitigation benefits of soil C sequestration [8]. Effective measurement of crop residue returns and the resulting mitigation of climatic impacts requires a complete perspective of the impacts of returning crop residues on GHG emissions and soil C sequestration [9].

GWP is a simplified index based on radiative properties introduced to assess the potential impacts of GHG emissions on the climate system [10]. To estimate GWP, CO_2 is typically regarded as the reference gas, and an increase or decrease in CH_4 and N_2O emissions is converted into CO_2 equivalents through their GWP. A positive GWP represents a net source of CO_2 equivalents, and a negative value indicates a net sink of atmospheric GHGs. Net GWP reflects a complete understanding of agriculture's impact on radiative forcing and is calculated by the balance between SOC storage and N_2O and CH_4 emissions [10, 11]. In addition, GHGI relating agricultural practices to GWP is calculated by dividing GWP by crop yield. A positive GHGI value indicates a net source of CO_2 equivalents per kilogram of yield, whereas a negative value indicates a net sink of GHG in soil [9]. Although the effects of crop residue incorporation on GWP, net GWP, or GHGI from paddy fields or uplands have been reported [10, 11], little information is available on the effects of crop residue mulching on NT rice fields on GWP, net GWP, and GHGI.

NT rice cultivation has drawn increasing amounts of interest in China due to saving time and labor and preventing the soil erosion [12]. Central China is one of the country's major rice-producing regions, comprising 28% of the total area of cultivated rice in China [13]. Recently, NT practices have become increasingly popular in this region. This inevitably increases the amount of crop residue. So, the establishment of a government policy favors these crop residues returned to the field. However, crop residue mulching on the soil surface of NT rice fields may have different effects on GHG emissions than residue incorporation. Moreover, although a great amount of field measurements have focused on the effects of crop residue returning on GWP, or net GWPs or GHGI from paddy fields based on CO_2, CH_4, and N_2O flux data [14–16], to our knowledge, a few simultaneously investigated the effects of crop residue returning on these three indices from paddy fields, especially from NT paddy fields. In this way, the present study aims to (1) quantify GHG emissions under different oilseed rape residue mulching regimens in central China during the 2010 rice-growing season and (2) assess GWP, net GWP, and GHGI.

2. Materials and Methods

2.1. Site Description. This field trial was established in an experimental farm (Zhonggui Village, 29°55′ N, 115°30′ E, Wuxue City, Hubei, China), which belongs to Extend Service Center of Agricultural Technology of Wuxue Agricultural Bureau, Hubei. This experimental area has a humid mid-subtropical monsoon climate with an average annual temperature of 16.8°C and a mean annual precipitation of 1360.6 mm. For the 5 years prior to study initiation, most of the rainfall occurred between April and August. The soil in the experimental site is clay loam and is classified as anthrosol [17]. The main soil properties (0–20 cm depth) in the site sampled in October 2006 are as follows: pH (extracted by H_2O; soil : water = 1.0 : 2.5), 6.58; organic C, 17.9 g kg^{-1}; total N, 2.21 g kg^{-1}; NO_3^-–N, 3.78 mg kg^{-1}; NH_4^+–N, 13.15 mg kg^{-1}; total P, 0.53 g kg^{-1}; and soil bulk density, 1.26 g cm^{-3}.

2.2. Experimental Design. The experiment was designed as a randomized complete block with three replicates (45 m^2) and was established in October 2006, three years before the study began. The variety of mid-season rice planted was Liangyoupeijiu (*Oryza sativa* L.). The experimental site was cultivated with a rape-rice rotation for 30 years prior to October 2006, where rice was transplanted with conventional tillage (soil is commonly tilled to a 10 cm depth by hand and then moldboard plowed to a depth of 20 cm by animal power) from May to October each year and rape was planted with conventional tillage from October to May the following year. The experiment included four treatments: (1) no oilseed rape residue mulching (0 RRM), (2) 3000 kg DM ha^{-1} oilseed rape residue mulching (3000 RRM), (3) 4000 kg DM ha^{-1} oilseed rape residue mulching (4000 RRM), and (4) 6000 kg DM kg ha^{-1} oilseed rape residue mulching (6000 RRM) on the surface of the soil in NT rice fields. For the treatment of 0 RRM, oilseed rape residues were removed and not returned to the field. In the residue mulching treatments, dried oilseed rape residues were chopped to approximately 5–7 cm in length according to local conventional practice. The C/N ratio of the oilseed rape residue was 48.5.

Preemergent herbicides (20% paraquat) were used to control weeds on June 3, 2010. The experimental samples were then submerged. No soil disturbances appeared in any of the plots immediately after oilseed rape was harvested. Rice seeds were sown manually at a rate of 22.5 kg ha^{-1} on June 6, 2010 and harvested on October 17, 2010. Dried oilseed rape residues were mulched immediately on the rice fields on June 11, 2010. Commercial inorganic N-phosphorus-(P-) potassium (K) fertilizer (15% N, 15% P_2O_5, and 15% K_2O), urea (46% N), single superphosphate (16% P_2O_5), and potassium chloride (60% K_2O) were used to supply 210 kg N ha^{-1}, 135 kg P_2O_5 ha^{-1}, and 240 kg K_2O ha^{-1} during the rice-growing season. N fertilizers were supplied at a rate of 84 kg N ha^{-1} in the form of basal fertilizers immediately before crop residues were applied. The remaining N fertilizers were split into two doses of 63 kg N ha^{-1} on June 26 and July 21, 2010. P and K fertilizers were only used as basal fertilizers immediately after seeding. The plots were regularly irrigated based on local conventional irrigation-drainage practices during rice-growing seasons. Air temperature data in the experimental site were collected from the weather station in Wuxue city.

2.3. Soil Sampling and Analysis of SOC and Bulk Density. Paddy soil samples (0–20 cm depth) were collected to determine total organic C using a soil sampler with a diameter of 5 cm at five random positions in each plot 1 day before the preemergent herbicides were applied and immediately after rice was harvested. Total organic C in the 0–20 cm soil layer was determined by dichromate oxidation and titration with ferrous ammonium sulfate [18]. Soil bulk density for the 0–20 cm soil layer was determined by the method of Bao [18].

Soil samples were collected to measure bulk density using metallic cores (5.3 cm in diameter and 20 cm tall) with three replicates per plot. SOC density (kg C ha^{-1}) for the 0–20 cm soil layer was computed from the SOC concentration and the soil bulk density described by Lu et al. [19]. SOC sequestered during a rice-growing season can be calculated as the differences of SOC density between the end and beginning of the experiment.

2.4. Measurement of Rice Grain Yields. The rice grains harvested in 2010 were measured at three random positions in each plot using a 1 m × 1 m frame. Rice grains were weighed and adjusted to have 14% moisture content.

2.5. Measurement of CO_2, CH_4, and N_2O. In this study, soil CO_2 fluxes from paddy fields were monitored with a Li-6400 portable photosynthesis analyzer (LI-COR Biosciences, U.S.). Soil fluxes were measured over the course of 2 h between 9:00 and 11:00 (a representative time of day in this region, according to Lou et al. [20]). Soil CO_2 fluxes were measured at the same time as CH_4 and N_2O fluxes. Soil CO_2 flux was determined every 20 s for 180 s. Three measurements were performed for each plot on each sampling day. The soil CO_2 flux value considered in this study was the average of three individual measurements and is here expressed as mg m^{-2} h^{-1}.

Fluxes measurements of CH_4 and N_2O from all plots were conducted simultaneously by closed steel cylinders with a diameter of 58 cm and a height of 110 cm [21]. Each steel cylinder covered four hills of rice. Two permanent base rings were placed below the water level to create a seal in each plot. The steel cylinders were placed temporarily on these rings to measure gas fluxes. The installed equipment on the chambers was detailed by Li et al. [21]. The gases in the chamber were then drawn with a syringe and immediately transferred into a 25 mL vacuum glass container. Four gas samples were taken using 25 mL plastic syringes at intervals of 0, 8, 16, and 24 min after closing the chambers. The CH_4 and N_2O fluxes were measured between 9:00 and 11:00 am. The gas samples were collected 1 day after oilseed rape residue mulching was conducted until rice harvesting. The gas samples were collected 20 times during the rice-growing seasons based on climate conditions and N fertilization.

The concentrations of CH_4 and N_2O were analyzed with a gas chromatograph meter equipped with an electron capture detector for N_2O analysis and a flame ionization detector for CH_4 analysis, following the method described by Li et al. [21]. The CH_4 and N_2O fluxes were calculated based on changes in their concentrations throughout the sampling period, being estimated as the slope of linear regression between concentration and time [21].

Seasonal total GHG emissions were calculated for each plot by linearly interpolating gas emissions during the sampling days based on the assumption that the measured fluxes represented the average daily fluxes [21].

2.6. GWP, Net GWP, and GHGI. In the present study, CO_2 emission was based only on soil flux measured between rows of rice plants. Moreover, CO_2 emissions and consumption resulting from plant respiration and photosynthesis were not considered during the calculation of GWP. Under conventional rice-growing conditions, CO_2 emissions and consumption caused by plant respiration and photosynthesis are balanced [14]. In this way, CO_2 emissions from rice respiration are not considered when computing GWP from agriculture. Consequently, the GWPs (kg CO_2 equivalents ha^{-1}) of different treatments were calculated using

$$\mathrm{GWP} = \mathrm{CO_2} + \mathrm{CH_4} \times 25 + \mathrm{N_2O} \times 298. \quad (1)$$

Based on a 100-year time frame, the GWP coefficients of CH_4 and N_2O are 25 and 298, respectively, when the GWP value of CO_2 is assumed to be 1 [22].

Soil CO_2 is released by the decomposition of crop residues and soil organic C. It is affected by changes in agricultural management. Changes in soil organic C are the product of soil C sequestration and soil CO_2 emissions. In this way, CO_2 flux from soil is inherently accounted for in changes in soil organic C [23]. Robertson et al. [10] and Shang et al. [11] suggested that changes in soil organic C should be measured, thus accounting for the GWP of soil. Here, net GWP was calculated using [11]

$$\text{Net GWP} = \mathrm{CH_4} \times 25 + \mathrm{N_2O} \times 298 - \Delta\mathrm{TOCD} \times \frac{44}{12}. \quad (2)$$

Thereafter, GHGI (kg CO_2 equivalents kg^{-1} grain yield) was calculated by dividing net GWP by rice grain yield using [9, 11]

$$\mathrm{GHGI} = \frac{\text{Net GWP}}{\text{grain yield}}. \quad (3)$$

2.7. Data Analysis. SPSS 16.0 analytical software package (SPSS Inc., USA) was used for all statistical analyses. A one-way ANOVA of SPSS 16.0 was used to determine the effects of residue mulching on total organic C, organic C density, organic C sequestration, GHG emissions, GWP, and GHGI. Individual means were compared based on the least significant difference test. Only the means that were statistically different at $P \leq 0.05$ were considered different.

3. Results and Discussion

3.1. Total Organic C and Organic C Sequestration. Returning crop residues to the field is highly recommended as a means of increasing soil organic C concentration and storage in rice-based cropping systems [24]. Table 1 shows that residue mulching had significant effects on total organic C and organic C sequestration from NT paddy fields. Total organic C concentration and density at harvesting exhibited a tendency to increase as the amount of mulch used increased. Residue mulching treatments significantly increased total organic C concentrations at harvesting by 1.50 g kg^{-1} to 2.96 g kg^{-1}, equivalent to organic C density of 3780 g kg^{-1} to 7459 g kg^{-1}. During a rice-growing season, the treatments of 3000 RRM, 4000 RRM, and 6000 RRM significantly sequestered more organic C than no residue treatment, by 687 kg C ha^{-1} $season^{-1}$, 1257 kg C ha^{-1} $season^{-1}$,

Table 1: Differences in soil total organic C (g kg^{-1}), organic C density (kg C ha^{-1}), and sequestered organic C (kg C ha^{-1} season^{-1}) during a rice-growing season from NT paddy fields under different residue mulching treatments.

Treatments	Total organic C concentrations before direct seeding	Total organic C concentrations at harvesting	Organic C density before direct seeding	Organic C density at harvesting	Sequestered organic C
0 RRM	18.4 ± 0.5^{c}	18.5 ± 0.5^{d}	46166^{c}	46645^{c}	479^{d}
3000 RRM	19.5 ± 0.6^{b}	20.0 ± 0.5^{c}	49259^{b}	50425^{b}	1166^{c}
4000 RRM	20.2 ± 0.7^{a}	20.9 ± 1.76^{b}	51008^{a}	52744^{ab}	1736^{b}
6000 RRM	20.4 ± 1.1^{a}	21.5 ± 0.9^{a}	51476^{a}	54104^{a}	2629^{a}

Different letters in a column mean significant differences at the 5% level. Values are the means ± SD, $n = 3$.

and 1654 kg C ha^{-1} season^{-1}, respectively. The positive effects of residue mulching on soil organic C concentration and sequestration reflect considerable C supplementation to soil under these regimens. Similarly, a study performed in India showed that, in a single rice-growing season, the use of rice straw in a site that had been cultivated for 4 years significantly increased soil organic C concentration and sequestration [15]. The soil organic C sequestration caused by residue mulching in an NT rice system is attributed to the fact that the soil was flooded for 4 months and to the high biomass production of rice (Table 3). When the concentration of O_2 under submerged conditions is very low, even the moderate oxygen demands of microbial activity go unmet if large pores are filled with water, decreasing decomposition rates [15]. Sahrawat [25] found that flooded rice soil exhibited better accumulation of organic matter than aerobic soil because of incomplete decomposition of organic materials and decreased humification of organic matter under flooded conditions.

In the present study, soil organic C sequestration increased as the amount of mulching increased (Table 1), indicating that long-term cultivation of crop leads to deficits in soil organic C in central China. In this way, short-term residue application was found to promote accumulation of soil organic C.

3.2. Rice Grain Yield. In general, long-term application of organic residues and with chemical NPK fertilizers can increase crop yields of rice-based cropping systems because of improved soil fertility [26]. In the present study, residue mulching was found to have no significant effect on rice yields during a 4-year field experiment (Table 3). N fertilizers were applied at a rate of 210 kg N ha^{-1} during the rice-growing season. This is, on average, 28% higher than the recommended rates for Chinese cereal production (150–180 kg N ha^{-1}, Zhu and Chen [27]). Therefore, although residue mulching improved soil fertility, high N input could satisfy the N demands of rice, weakening the effects of residue mulching on rice yields [28]. Similarly, during a 3-year field experiment in Jiangsu province, China, Ma et al. [29] found no significant difference in rice grain yields between plots treated with residue and untreated plots. However, Ge et al. [30] found maize straw to have positive effects on rice yields during a 3-year field experiment. Further study on the short-term effects of crop residue application on rice yields is necessary.

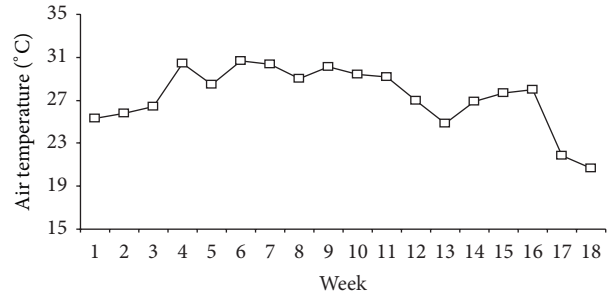

Figure 1: Changes in mean weekly air temperature during the rice-growing season.

3.3. GHG Emissions. The seasonal changes in soil CO_2, CH_4, and N_2O fluxes from NT paddy fields under different residue mulching treatments during the 2010 rice-growing season are shown in Figure 2. During the rice-growing season, the fluxes ranged from 70.9 mg m^{-2} d^{-1} to 401.1 mg m^{-2} h^{-1} for CO_2, from −7.38 mg m^{-2} h^{-1} to 41.4 mg m^{-2} h^{-1} for CH_4, and from −5.76 μg m^{-2} h^{-1} to 58.2 μg m^{-2} h^{-1} for N_2O from no residue mulching treatment. Moreover, the fluxes varied from 129.6 mg m^{-2} d^{-1} to 1066.6 mg m^{-2} h^{-1} for CO_2, from −11.6 mg m^{-2} h^{-1} to 9.42 mg m^{-2} h^{-1} for CH_4, and from −15.2 μg m^{-2} h^{-1} to 162.5 μg m^{-2} h^{-1} for N_2O from residue mulching treatments. In addition, peaks in soil CO_2 and CH_4 fluxes were found during the tillering stage and several peaks in N_2O fluxes were observed immediately after N fertilization. The peaks in soil CO_2 fluxes could be attributed to the increased availability of substrates from root exudation or microbial decomposition of leftover plant residues during this stage [21]. Moreover, high total CH_4 and CO_2 fluxes during this period could be related to high air temperature (Figure 1). The mean weekly air temperature ranged from 19.7°C to 32.5°C during the rice-growing season, and the air temperature ranged from 20°C to 33°C from mid-June to September (Figure 1). High air temperature is beneficial to CH_4 and CO_2 production. Increase in N_2O fluxes could be attributed to increased substrate availability from N fertilization [31].

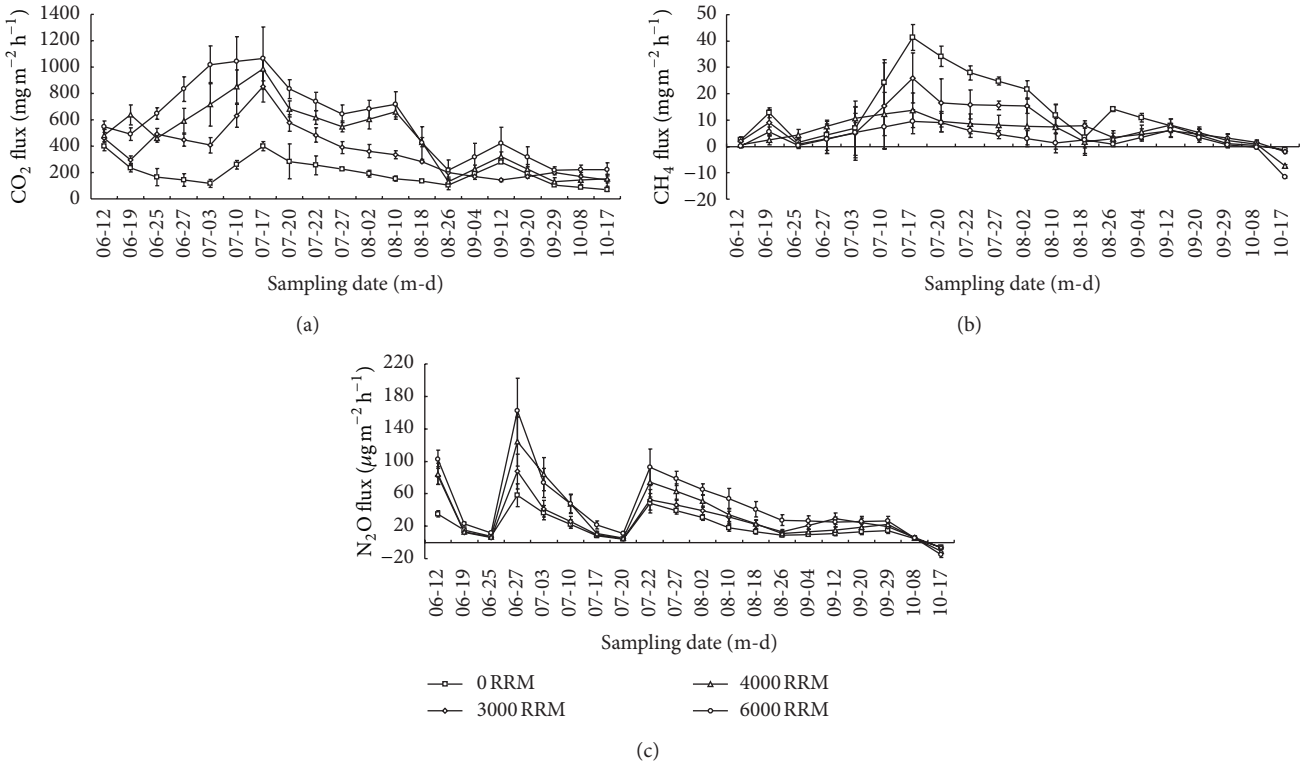

FIGURE 2: Changes in soil CO_2 (a), CH_4 (b), and N_2O (c) fluxes from NT paddy fields under different residue mulching treatments during the rice-growing season. The vertical bars are standard deviations of the mean, $n = 3$.

In the present study, residue mulching significantly affected seasonal total CO_2 emissions, in which the treatments of 3000 RRM, 4000 RRM, and 6000 RRM showed more total seasonal CO_2 emissions than untreated control, by 73%, 136%, and 186%, respectively (Table 2). Soil CO_2 fluxes are caused by complex interactions between climate and several biological, chemical, and physical properties of the soil [32]. Applying crop residues to cropland affects soil organic C pool, soil nutrients, and microbial environments and activities, thus influencing CO_2 emissions [33]. Significant positive effects of residue mulching on soil CO_2 emissions from NT paddy fields (Figure 2 and Table 3) indicate increased microbial activities resulting from high amounts of easily dissolved organic C from the decomposition of oilseed rape residues [34]. This expectation was confirmed in a previous, related study [35]. This previous study showed that CO_2 emissions from soil amended with rice straw were significantly related to dissolved organic C ($r = 0.95$) and microbial biomass C ($r = 0.94$). In a field study conducted on a paddy sandy clay loam soil in eastern India, Bhattacharyya et al. [15] showed that soil treated with rice straw and green manure could produce more CO_2 emissions than untreated soil. Bhattacharyya et al. [15] also found total organic C and microbial biomass C to be closely correlated with soil CO_2 emissions. Similar results have been observed by other researchers [14, 20, 34]. The average depth of the water layer in the present study was approximately 4-5 cm during the rice-growing season. In this way, the top of the mulched oilseed rape residue was exposed to the atmosphere, leading to the oxidation of a substantial amount of CO_2 produced by oilseed rape residue.

In this study, residue mulching had significant inhibiting effects on seasonal total CH_4 emissions and the treatments of 3000 RRM, 4000 RRM, and 6000 RRM decreased total seasonal total CH_4 emissions by 34%, 52%, and 75% compared with untreated control, respectively (Table 2). Previous studies have indicated that crop residue treatment does not only provide readily bioavailable organic C for CH_4 production but also stimulates soil reduction and creates a strict reductive condition for CH_4 production [36]. However, the present study showed residue mulching to inhibit CH_4 emissions (Table 2). This finding is different from those of previous reports, which state that crop residues considerably increase CH_4 emissions [8, 15, 37]. CH_4 flux is a net product of three simultaneous processes, the production, oxidation, and transport of CH_4. The position of crop residues directly influences CH_4 production and oxidation and eventually affects CH_4 emission from rice fields. Plots treated with residue mulching have greater dissolved organic C concentrations than untreated areas, possibly providing substrates for methanotrophic bacteria. However, residue mulch was exposed to more light, which suppressed methanogenesis. The subsequent growth of indigenous phototrophs was associated with the residue around the soil-floodwater interface [38]. The thin water layer (average 4-5 cm) observed during the rice-growing season caused the substantial CH_4 produced

Table 2: Seasonal total emissions of CO_2 (g m^{-2}), CH_4 (g m^{-2}), and N_2O (mg m^{-2}) from NT paddy fields under different residue mulching treatments.

Treatments	CO_2	CH_4	N_2O
0 RRM	570 ± 109^{d}	34.8 ± 2.6^{a}	54.8 ± 9.7^{d}
3000 RRM	986 ± 126^{c}	22.8 ± 3.3^{a}	79.2 ± 8.5^{c}
4000 RRM	1346 ± 239^{b}	16.6 ± 3.6^{c}	95.1 ± 10.0^{b}
6000 RRM	1632 ± 313^{a}	8.84 ± 3.1^{d}	125.1 ± 9.4^{a}

Different letters in a column mean significant differences at the 5% level. Values are the means ± SD, $n = 3$.

from soil and crop residues to be oxidized before escaping to the atmosphere. Furthermore, crop residues on the NT soil surface blocked CH_4 from the soil from entering the atmosphere. In this way, an elevation of O_2 partial pressure in the soil-floodwater interface, caused by the method of irrigation used in the present study, led to CH_4 oxidization. In this way, lower CH_4 emissions were found to be attributable to residue mulching treatments in the present study. Another study conducted in the same part of China showed that rice straw mulching on NT paddy soil did not increase CH_4 emissions from double rice cropping systems [16]. The present study indicated decreases in CH_4 emissions associated with increasing crop residue rates (Figure 2 and Table 2). This finding is inconsistent with that of Naser et al. [39] who found positive linear relationships between CH_4 emissions and the amount of straw used.

Nitrification and denitrification are two major microbial processes that are responsible for N_2O emissions from paddy soil. Although nitrification is aerobic and denitrification is anaerobic, both processes have been known to occur simultaneously in paddy soil. Crop residues can provide readily available C, N, and other nutrients. In addition, this measure can increase organic C input of soil [34–36]. This can influence nitrification and denitrification rates and N_2O emissions from the soil [34]. In the present study, the treatments of 3000 RRM, 4000 RRM, and 6000 RRM significantly increased total seasonal N_2O emissions by 45%, 74%, and 128% over untreated soil, respectively (Table 2). Similar results were reported by Shan and Yan [7], who indicated that N_2O emissions were higher when crop residues were mulched in paddy fields. Exposure of the mulching residue surface to the atmosphere led to high O_2 concentration in the mulch. High O_2 concentrations were found to stimulate nitrification and inhibit N_2O reduction to N_2 during denitrification [16, 29]. This increases N_2O production. Second, the area of the soil/air interface in the present study can be enlarged by partial or complete spreading of mulches onto the field surface, thus favoring N_2O production.

Soil N_2O emissions are affected by the use of crop residues. These emissions are complex and dependent on residue quality, the time of residue application, the use of fertilizer, and soil and environmental conditions [29, 37]. Among these factors, the C/N ratio of the crop residues appears to be the primary regulator [7]. In general, crop residues with low C/N ratios have been found to decompose faster than residues with high C/N ratios [7]. Heal et al. (1997) [40] indicated that plant residues with C/N ratios <20 decompose rapidly and NH_4^+ is released through mineralization. Plant residues with intermediate C/N ratios of 25 to 75 can also decompose rapidly, but N mineralization activity is typically decreased by increased microbial immobilization. Residues with high C/N ratios (>75) are typically more difficult to break down than residues with low C/N ratios, and they generally stimulate net immobilization of soil available N, thereby decreasing the amount of N substrate available for N_2O production [40]. In the present study, crop residues with high C/N ratios (48.5) were associated with temporary microbial immobilization of soil available N and with a decrease in N_2O emissions resulting from reduced nitrification and denitrification. However, this immobilization of soil N could be counteracted by adding N fertilizers (210 kg N ha^{-1}). In this way, higher N_2O emissions were observed from plots treated with residue mulching than from untreated plots.

3.4. GWP, Net GWP, and GHGI. Residue mulching significantly affected GWPs, net GWP, and GHGI but did not affect rice grain yields (Table 3). GWP increased as the amount of mulching increased, but net GWP and GHGI decreased as the amount of mulching increased. The treatments of 3000 RRM, 4000 RRM, and 6000 RRM showed significantly more GWP than the control, by 9%, 23%, and 30%, respectively, but they showed less net GWP, by 33%, 50%, and 71%, respectively, and less GHGI, by 35%, 56%, and 72%, respectively.

When CH_4 and N_2O emissions from paddy fields are expressed as CO_2 equivalents, the major contributor to GWP for the residue mulching treatments during the rice-growing season was clearly CO_2, and not CH_4, which only represented 12–36% of total GWP (Tables 2 and 3), thus indirectly reflecting the inhibitory effect of the residue mulching on CH_4 emissions. In the present study, although residue mulching inhibited CH_4 emissions from NT paddy fields, the stimulating effects of residue mulching on CO_2 and N_2O emissions, which overcame the reducing effects of residue mulching on CH_4 emissions, had positive effects on GWPs (Tables 2 and 3).

Although residue mulching increased GWP from NT paddy fields, soil organic C sequestration from residue mulching might partially offset this increase. In this way, determining the degree to which residue mulching mitigates climatic impact requires an integrated perspective of the effects of residue on soil organic C sequestration. In the present study, residue mulching was found to have a mitigating effect on net GWP and GHGI (Table 3). This suggested that the practice of crop residue mulching with NT may be

Table 3: GWP, net GWP, rice grain yield, and GHGI of different residue mulching treatments.

Treatments	GWP/ (kg CO_2 equivalents ha^{-1})	Net GWP/ (kg CO_2 equivalents ha^{-1})	Rice grain yield/ (kg ha^{-1})	GHGI/ (kg CO_2 equivalents kg^{-1} grain yield)
0 RRM	14560 ± 1259^{c}	8863 ± 1789^{a}	7764 ± 190^{a}	1.14^{a}
3000 RRM	15800 ± 1920^{b}	5936 ± 1264^{ab}	8062 ± 179^{a}	0.74^{b}
4000 RRM	17898 ± 1648^{ab}	4433 ± 477^{c}	8835 ± 224^{a}	0.50^{c}
6000 RRM	18904 ± 2789^{a}	2583 ± 436^{d}	8134 ± 150^{a}	0.32^{d}

Different letters in a column mean significant differences at the 5% level. Values are the means ± SD, $n = 3$.

a good way to mitigate GHG emissions in central China without sacrificing rice grain yield. The present results differ from those found by Yao et al. [37]. They found that the use of wheat residue with NT increased net GWP and GHGI from rice-wheat rotation farmland. This discrepancy could be because of the different methods of residue application used and different durations of NT. In the study by Yao et al. [37], residues were incorporated, and NT was only applied during the wheat-growing season. Liu et al. [41] also reported that incorporating oilseed rape straws enhanced net GWP and GHGI during a rice-growing season in oilseed rape-rice rotation farming.

Although the present results indicated that net GWP and GHGI increased as the amount of residue mulch used increased, Qu et al. [28] reviewed the effects of the use of crop residue on rice grain yields in China and found that rice grain yield could decrease when the amount of residue used exceeded 11,250 kg ha^{-1}. This is because increased concentrations of reducing matter from decomposition of large amounts of crop residue can inhibit rice growth. Accordingly, applying a rational amount of crop residue may mitigate GWP and maintain crop yield.

Although a field experiment conducted in Jurong of Jiangsu province, China, found that in-situ burning wheat straw decreased CH_4 emissions from paddy soils due to decreased organic C provided by straw ash as substrate for CH_4 production [36], the burning process also emitted a substantial amount of CH_4 into the atmosphere [42], thus bringing about various adverse effects on the environment. NT is a simple cultivation technology that has attracted considerable attention since the establishment of a government policy favors the adoption of NT farming. In China, the research and the application of NT have developed quickly since the 1970s; by the end of 2008, NT had been applied to approximately 1.33 million hectares of land [1]. Therefore, it is urgent to manage increased crop residue for reducing environmental pollution caused by in-situ burning residue. In this study, although residue mulching on NT paddy fields increased CO_2 and N_2O emissions and GWP, this measure decreased net GWP and GHGI without decreasing rice grain yield. Therefore, it is advisable to advocate mulching of crop residue as a way to achieve agricultural economic viability and GHG mitigation from NT paddy fields.

GHG emissions are highly variable in time and space because of soil heterogeneity and climate variability [43]. For this reason, the outcome of the present study, which addressed a complete GHG accounting of GWP and GHGI as affected by residue mulching only during a rice-growing season after 3 years of the conversion of conventional tillage to NT under an oilseed rape-rice cropping system, is somewhat uncertain. Further study should be considered to determine residue mulching effects on GHG emissions from integrated oilseed rape—fallow—rice seasons after the long-term conversion of conventional tillage to NT. C emitted from the manufacturing and use of agricultural input, such as the use of pesticides, irrigation, and farm machinery, may negate all or part of the increased C sequestered by soil [23]. In this way, C emissions associated with changes in practices should be incorporated comprehensively into analyses of C sequestration [23].

4. Conclusions

The present study provided an insight into a complete GHG accounting of GWP, net GWP, and GHGI from NT paddy fields as affected by residue mulching during a rice-growing season after 3 years of oilseed rape-rice cultivation. Residue mulching on NT paddy fields was found to significantly increase CO_2 and N_2O emissions but decrease CH_4 emissions. Residue mulching significantly increased GWP but decreased net GWP and GHGI due to increased soil organic C sequestration. Moreover, residue mulching did not decrease rice grain yields. Therefore, we conclude that residue mulching both limits GHG emissions and maintains rice grain yields if used with NT.

Conflict of Interests

The authors declare that there is no conflict of interests regarding the publication of this paper.

Acknowledgments

This work is funded by the National Technology Project for High Food Yield, China (2011BAD16B02), the National Natural Science Foundation of China (31100319), the Fundamental Research Funds for the Central Universities (2011PY148, 2013PY106), and the Program for Changjiang Scholars and Innovative Research Team in the University of China (IRT1247).

References

[1] Ministry of Agriculture of the People's Republic of China, *China Agriculture Yearbook 2010*, China Agriculture Press, Beijing, China, 2010.

[2] X. Yan, H. Akiyama, K. Yagi, and H. Akimoto, "Global estimations of the inventory and mitigation potential of methane emissions from rice cultivation conducted using the 2006 Intergovernmental Panel on Climate Change guidelines," *Global Biogeochemical Cycles*, vol. 23, no. 2, Article ID GB2002, 2009.

[3] X. H. Zheng, S. H. Han, Y. Huang, Y. S. Wang, and M. X. Wang, "Re-quantifying the emission factors based on field measurements and estimating the direct N_2O emission from Chinese croplands," *Global Biogeochemical Cycles*, vol. 18, no. 2, Article ID GB2018, 19 pages, 2004.

[4] X. Ren, Q. Wan, C. Tong et al., "Estimation of soil respiration from paddy fields of subtropical China," *Scientific Bulletin*, vol. 52, no. 13, pp. 1548–1553, 2007 (Chinese).

[5] Q. Liao, S. Wang, and X. Yan, "Estimation of N_2O emissions from paddy fields during rice growing season in China," *Journal of Agro-environment Science*, vol. 31, no. 1, pp. 212–218, 2012 (Chinese).

[6] X. Yan, Z. Cai, T. Ohara, and H. Akimoto, "Methane emission from rice fields in mainland China: amount and seasonal and spatial distribution," *Journal of Geophysical Research D: Atmospheres*, vol. 108, no. 16, p. 4505, 2003.

[7] J. Shan and X. Yan, "Effects of crop residue returning on nitrous oxide emissions in agricultural soils," *Atmospheric Environment*, vol. 71, pp. 170–175, 2013.

[8] F. Lu, X. K. Wang, B. Han, Z. Y. Ouyang, and H. Zheng, "Straw return to rice paddy: soil carbon sequestration and increased methane emission," *Chinese Journal of Applied Ecology*, vol. 21, no. 1, pp. 99–108, 2010 (Chinese).

[9] A. R. Mosier, A. D. Halvorson, C. A. Reule, and X. J. Liu, "Net global warming potential and greenhouse gas intensity in irrigated cropping systems in Northeastern Colorado," *Journal of Environmental Quality*, vol. 35, no. 4, pp. 1584–1598, 2006.

[10] G. P. Robertson, E. A. Paul, and R. R. Harwood, "Greenhouse gases in intensive agriculture: contributions of individual gases to the radiative forcing of the atmosphere," *Science*, vol. 289, no. 5486, pp. 1922–1925, 2000.

[11] Q. Y. Shang, X. X. Yang, C. M. Gao et al., "Net annual global warming potential and greenhouse gas intensity in Chinese double rice-cropping systems: a 3-year field measurement in long-term fertilizer experiments," *Global Change Biology*, vol. 17, no. 6, pp. 2196–2210, 2011.

[12] H. Harada, T. Ota, and S. Murakami, "Water conservation effect of puddle—elimination or reduction in depth of ponding water on pollutant loads before rice transplanting," in *Proceedings of the World Rice Research Conference*, p. 281, Tokyo, Japan, November 2004.

[13] M. Wang and J. Li, "CH_4 emission and oxidation in Chinese rice paddies," *Nutrient Cycling in Agroecosystems*, vol. 64, no. 1-2, pp. 43–55, 2002.

[14] A. Bhatia, H. Pathak, N. Jain, P. K. Singh, and A. K. Singh, "Global warming potential of manure amended soils under rice-wheat system in the Indo-Gangetic plains," *Atmospheric Environment*, vol. 39, no. 37, pp. 6976–6984, 2005.

[15] P. Bhattacharyya, K. S. Roy, S. Neogi, T. K. Adhya, K. S. Rao, and M. C. Manna, "Effects of rice straw and nitrogen fertilization on greenhouse gas emissions and carbon storage in tropical flooded soil planted with rice," *Soil & Tillage Research*, vol. 124, pp. 119–130, 2012.

[16] X. Qin, Y. Li, Y. Wan, S. Shi, Y. Liao, and Y. Liu, "Effects of straw mulching on greenhouse gas intensity under on-tillage conditions," *Transactions of the Chinese Society of Agricultural Engineering*, vol. 28, no. 6, pp. 210–216, 2012 (Chinese).

[17] "World Reference Base for Soil Resource," 2006, http://www.fao.org/ag/agl/agll/wrb/doc/wrb2006final.pdf.

[18] S. D. Bao, *Analytical Method for Soil and Agricultural Chemistry*, Chinese Agriculture Press, Beijing, China, 2000, (Chinese).

[19] F. Lu, X. K. Wang, B. Han et al., "Soil carbon sequestrations by nitrogen fertilizer application, straw return and no-tillage in China's cropland," *Global Change Biology*, vol. 15, no. 2, pp. 281–305, 2009.

[20] Y. S. Lou, Z. P. Li, and T. L. Zhang, "Carbon dioxide flux in a subtropical agricultural soil of China," *Water, Air, and Soil Pollution*, vol. 149, no. 1–4, pp. 281–293, 2003.

[21] C. F. Li, D. N. Zhou, Z. K. Kou et al., "Effects of tillage and nitrogen fertilizers on CH_4 and CO_2 emissions and soil organic carbon in paddy fields of central China," *PLoS ONE*, vol. 7, no. 5, Article ID e34642, 2012.

[22] IPCC, "Climate change 2007: the physical science basis," in *Contribution of Working Group I to the Fourth Assessment Report of the Intergovernmental Panel on Climate Change*, S. Solomon, D. Qin, M. Manning et al., Eds., Cambridge University Press, Cambridge, UK, 2007.

[23] T. O. West and G. Marland, "Net carbon flux from agricultural ecosystems: methodology for full carbon cycle analyses," *Environmental Pollution*, vol. 116, no. 3, pp. 439–444, 2002.

[24] D. K. Benbi, A. S. Toor, and S. Kumar, "Management of organic amendments in rice-wheat cropping system determines the pool where carbon is sequestered," *Plant and Soil*, vol. 360, no. 1-2, pp. 145–162, 2012.

[25] K. L. Sahrawat, "Organic matter accumulation in submerged soils," *Advances in Agronomy*, vol. 81, pp. 169–201, 2001.

[26] M. Liu, Z. Li, T. Zhang, C. Jiang, and Y. Che, "Discrepancy in response of rice yield and soil fertility to long-term chemical fertilization and organic amendments in paddy soils cultivated from infertile upland in subtropical China," *Agricultural Sciences in China*, vol. 10, no. 2, pp. 259–266, 2011.

[27] Z. L. Zhu and D. L. Chen, "Nitrogen fertilizer use in China—contributions to food production, impacts on the environment and best management strategies," *Nutrient Cycling in Agroecosystems*, vol. 63, no. 2-3, pp. 117–127, 2002.

[28] H. P. Qu, J. He, W. J. Ning, X. H. Liu, J. Huang, and M. H. Gu, "Reviews on effects of rice straw application on rice production," *Crops*, vol. 16, no. 6, pp. 9–11, 2007 (Chinese).

[29] J. Ma, X. L. Li, H. Xu, Y. Han, Z. C. Cai, and K. Yagi, "Effects of nitrogen fertiliser and wheat straw application on CH_4 and N_2O emissions from a paddy rice field," *Australian Journal of Soil Research*, vol. 45, no. 5, pp. 359–367, 2007.

[30] L. L. Ge, Y. H. Ma, J. L. Bian, Z. Q. Wang, J. C. Yang, and L. J. Liu, "Effects of returning maize straw to field and site-specific nitrogen management on grain yield and quality in rice," *Chinese Journal of Rice Science*, vol. 27, no. 2, pp. 153–160, 2013 (Chinese).

[31] D. A. N. Ussiri, R. Lal, and M. K. Jarecki, "Nitrous oxide and methane emissions from long-term tillage under a continuous corn cropping system in Ohio," *Soil & Tillage Research*, vol. 104, no. 2, pp. 247–255, 2009.

[32] K. Oorts, P. Garnier, A. Findeling, B. Mary, G. Richard, and B. Nicolardot, "Modeling soil carbon and nitrogen dynamics in no-till and conventional tillage using PASTIS model," *Soil Science Society of America Journal*, vol. 71, no. 2, pp. 336–346, 2007.

[33] Y. Huang, J. Zou, X. Zheng, Y. Wang, and X. Xu, "Nitrous oxide emissions as influenced by amendment of plant residues with different C:N ratios," *Soil Biology & Biochemistry*, vol. 36, no. 6, pp. 973–981, 2004.

[34] B. P. Singh, B. J. Hatton, A. L. Cowie, and A. Kathuria, "Influence of biochars on nitrous oxide emission and nitrogen leaching from two contrasting soils," *Journal of Environmental Quality*, vol. 39, no. 4, pp. 1224–1235, 2010.

[35] M. Ibrahim, C. G. Cao, M. Zhan, C. F. Li, and J. Iqbal, "Changes of CO_2 and labile organic carbon as influenced by rice straw and different water regimes," *International Journal of Environmental Science and Technology*, 2013.

[36] J. Ma, H. Xu, K. Yagi, and Z. Cai, "Methane emission from paddy soils as affected by wheat straw returning mode," *Plant and Soil*, vol. 313, no. 1-2, pp. 167–174, 2008.

[37] Z. S. Yao, X. H. Zheng, R. Wang, B. H. Xie, K. Butterbach-Bahl, and J. G. Zhu, "Nitrous oxide and methane fluxes from a rice-wheat crop rotation under wheat residue incorporation and no-tillage practices," *Atmospheric Environment*, vol. 79, pp. 641–649, 2013.

[38] N. Harada, S. Otsuka, M. Nishiyama, and S. Matsumoto, "Influences of indigenous phototrophs on methane emissions from a straw-amended paddy soil," *Biology and Fertility of Soils*, vol. 41, no. 1, pp. 46–51, 2005.

[39] H. M. Naser, O. Nagata, S. Tamura, and R. Hatano, "Methane emissions from five paddy fields with different amounts of rice straw application in central Hokkaido, Japan," *Soil Science and Plant Nutrition*, vol. 53, no. 1, pp. 95–101, 2007.

[40] O. W. Heal, J. M. Anderson, and M. J. Swift, "Plant litter quality and decomposition: an historical overview," in *Driven by Nature: Plant Litter Quality and Decomposition*, G. Cadisch and K. E. Giller, Eds., pp. 3–30, CAB International, Wallingford, Oxfordshire, UK, 1997.

[41] X. Y. Liu, Z. P. Li, G. X. Pan, and L. Q. Li, "Greenhouse gas emission and C intensity for a long-term fertilization rice paddy in Tai Lake Region, China," *Journal of Agro-Environmental Sciences*, vol. 30, no. 9, pp. 1783–1790, 2011 (Chinese).

[42] D. G. Streets, K. F. Yarber, J. H. Woo, and G. R. Carmichael, "Biomass burning in Asia: annual and seasonal estimates and atmospheric emissions," *Global Biogeochemical Cycles*, vol. 17, no. 4, article 1099, 2003.

[43] J. D. Wood, R. J. Gordon, and C. Wagner-Riddle, "Biases in discrete CH4 and N_2O sampling protocols associated with temporal variation of gas fluxes from manure storage systems," *Agricultural and Forest Meteorology*, vol. 171-172, pp. 295–305, 2013.

Hindawi Publishing Corporation
The Scientific World Journal
Volume 2014, Article ID 272684, 7 pages
http://dx.doi.org/10.1155/2014/272684

Research Article

Effects of Soil Temperature, Flooding, and Organic Matter Addition on N_2O Emissions from a Soil of Hongze Lake Wetland, China

Yan Lu[1,2] and Hongwen Xu[1]

[1] *School of Urban and Environmental Science, Huaiyin Normal University, Huai'an 223300, China*
[2] *Jiangsu Key Laboratory for Eco-Agricultural Biotechnology around Hongze Lake, Huai'an 223300, China*

Correspondence should be addressed to Hongwen Xu; hongwen_xu@163.com

Received 15 April 2014; Revised 15 June 2014; Accepted 4 July 2014; Published 14 July 2014

Academic Editor: Antonio Paz González

The objectives of this study were to test the effects of soil temperature, flooding, and raw organic matter input on N_2O emissions in a soil sampled at Hongze Lake wetland, Jiangsu Province, China. The treatments studied were—peat soil (I), peat soil under flooding (II), peat soil plus raw organic matter (III), and peat soil under flooding plus organic matter. These four treatments were incubated at 20°C and 35°C. The result showed that temperature increase could enhance N_2O emissions rate and cumulative emissions significantly; moreover, the flooded soil with external organic matter inputs showed the lowest cumulative rise in N_2O emissions due to temperature increment. Flooding might inhibit soil N_2O emissions, and the inhibition was more pronounced after organic matter addition to the original soil. Conversely, organic matter input explained lower cumulative N_2O emissions under flooding. Our results suggest that complex interactions between flooding and other environmental factors might appear in soil N_2O emissions. Further studies are needed to understand potential synergies or antagonisms between environmental factors that control N_2O emissions in wetland soils.

1. Introduction

Climate change has been a major issue within the twenty-first century. The main causes of global warming are the increase in carbon dioxide (CO_2), methane (CH_4), and nitrous oxide (N_2O). Concentrations of N_2O in the atmosphere are lower than those of either CH_4 or CO_2; however, on a per mole basis, N_2O has demonstrated a higher ability to disrupt the radiation balance than the other two gases aforementioned. Thus, N_2O has attracted much attention because it is a potent greenhouse gas with long atmospheric lifetimes, and it is involved in ozone depletion as well [1, 2]. Measurements of N_2O emissions have been increasing steadily. Until now, however, the vast majority of studies have focused on N_2O emissions from agroecosystem, as affected by temperature, soil type, crop growth, and management practices [3–5]. Therefore, there is much uncertainty surrounding the effect of flooding or the joint effects of several factors, for example, flooding and temperature changes.

Changes in land use patterns will cause alterations in the soil organic matter status and the soil nitrogen mineralization rates and therefore will also influence N_2O emissions. In addition, land use changes may also affect transfer and diffusion of N_2O in the soil through reorganization of the soil structure. Wetlands have been identified as major landforms regulating greenhouse gases dynamics [6]. CO_2 and CH_4 emissions from wetland system have been reported by numerous studies [7, 8]. However, research conducted on N_2O emission from the wetland soil has relatively fewer reports. The predominant factors affecting N_2O production and emission include soil temperature, soil moisture, exogenous organic matter inputs, and soil organic matter content [9–11]. They could have influence on microorganisms producing and consuming N_2O from wetland soils [12]. Soil temperature directly impacts production and consumption of N_2O though microorganism's activity, soil aeration, substrate availability, and redistribution. Soil moisture is a key determinant of the microbial processes [13]. Organic matter

Table 1: Basic physical and chemical properties of studied soils.

Total carbon ($g \cdot kg^{-1}$)	Total nitrogen ($g \cdot kg^{-1}$)	Ammonia nitrogen ($mg \cdot kg^{-1}$)	Nitrate nitrogen ($mg \cdot kg^{-1}$)	Available nitrogen ($mg \cdot kg^{-1}$)	Bulk density ($g \cdot cm^{-3}$)
62.11	3.96	26.68	6.55	382.81	0.87

fractions have been also found to enhance N_2O emissions as they supply substrates for nitrification and denitrification and augment microbial O_2 consumption [14].

The interactions among soil temperature, moisture, and raw organic matter addition on N_2O emissions are not well known and the gaps about the joint effects of these factors may increase the uncertainty in estimating global emissions budgets. Wetland soil from Hongze Lake was incubated under different temperature, moisture, and exogenous organic matter input. The objective was to analyze the interaction of soil temperature, flooding, and row organic matter inputs on N_2O losses. Knowledge about the nitrogen loss process of the wetland ecological system may provide the baseline data to undertake countermeasures allowing reductions of greenhouse gas emissions.

2. Material and Methods

2.1. Site and Soil Characteristics. Hongze Lake is located in the northwest region of Jiangsu Province (33°06′ N~33°40′ N, 118°10′ E~118°55′ E), and it is the fourth largest freshwater lake in China. The lake surface area covers 1597 km^2, the water level is 12.5 m, and the average depth is 1.9 m. The lake region has a monsoon climate with four distinct seasons. The average annual rainfall is 925.5 mm, mostly concentrated in the rainy season from June to September. The lake and the surrounding area are representative of inland wetlands in China. Wetlands are widely distributed around the lake; several wetland types have been described and the three most common are estuarine, floodplain, and out of the lake wetland.

Estuary wetlands located in the west coast of the Hongze Lake have been sampled in November 2012. Soil samples were collected at 0–20 cm depth using the multipoint hybrid method and taken to the laboratory in field-moist condition. Soil samples were divided into two subsamples, after manually removing visible plant roots and rocks. A subsample was put in the refrigerator (4°C) for incubation after sieving with 2 mm sieve, and the second subsample was dried and fine grinded for chemical analysis.

Basic physical and chemical properties of the tested soil are shown in Table 1. This soil was rich in organic matter with a total carbon content of 62.11 $g \cdot kg^{-1}$ and a total nitrogen content of 3.96 $g \cdot kg^{-1}$. Available nitrogen was as high as 382.81 $mg \cdot kg^{-1}$. Ammonia nitrogen (26.68 $mg \cdot kg^{-1}$) was approximately four times greater than nitrate nitrogen (6.55 $mg \cdot kg^{-1}$). Bulk density was 0.87 $g \cdot cm^{-3}$.

2.2. Incubation Experiment. An incubation experiment was setup to study NO_2 emissions under four treatments and each treatment was incubated at two different temperatures. Treatments were as follows: natural peat soil (I), peat soil under flooding (II), peat soil plus raw organic matter (III), and peat soil under flooding plus organic matter (IV). Three replications per treatments were analyzed. To assess the effect of temperature on N_2O treatments each replicate sample was incubated at 35°C (high temperature or treatment A) and at 20°C (room temperature or treatment B). At the same time, two blank tests were performed as a control treatment.

Soil sampled in the field was preincubated at room temperature for three days. Afterwards, 40 g of preincubated soil was enclosed in 1000 mL incubation bottles. Incubations were performed in 24 bottles (3 replicates × 4 different soil treatments × 2 temperatures). In the flooding treatment, 40 mL distilled water was added to the 40 g dry soil (soil was submerged by a 0.5 cm water column). In the treatment with exogenous organic matter addition, 1 g dried litter of *Phragmites communis* was grinded and mixed with the soil samples and added into each bottle. Bottles were sealed and maintained at constant temperatures of 20°C (treatment B) and 35°C (treatment A). Therefore, treatments incubated at high temperatures are labeled as AI, AII, AIII, and AIV, whereas labels for those incubated at low temperatures are BI, BII, BIII, and BIV.

2.3. N_2O Analysis. Measures of N_2O fluxes were a total of 12 times at the 2nd, 3rd, 5th, 7th, 9th, 11th, 13th, 16th, 19th, 22nd, 25th, and 28th days after incubation started. At each sampling date, 30 mL of gases was pumped from each incubation bottle. After then each bottle was open for half an hour to ensure that the gas in the bottle was equilibrated with that in the air and then the incubation bottles were again sealed. Gas chromatograph was used to measure the concentration of N_2O in the samples. Emission rates were expressed as $g \cdot kg^{-1} \cdot h^{-1}$ of N_2O.

2.4. Data Analysis. The data set was analyzed by one-way analysis of variance (ANOVA) followed by Duncan's test at 0.05 level to compare the mean of N_2O of each treatment. The SPSS 16.0 for Windows was used.

3. Results

3.1. Effect of Temperature on N_2O Emissions. It was found that all of the four treatments studied exhibited higher N_2O emissions rates at 35°C than at 20°C. The highest N_2O emissions rates occurred during the first periods of incubation and then gradually decreased (Figure 1). Moreover, complex changes of emission rates were noticed after organic matter was added to the wetland incubated at high temperature (Figure 1, AIV). Higher cumulative N_2O emissions were observed under high temperature as well (Figure 2, BIV).

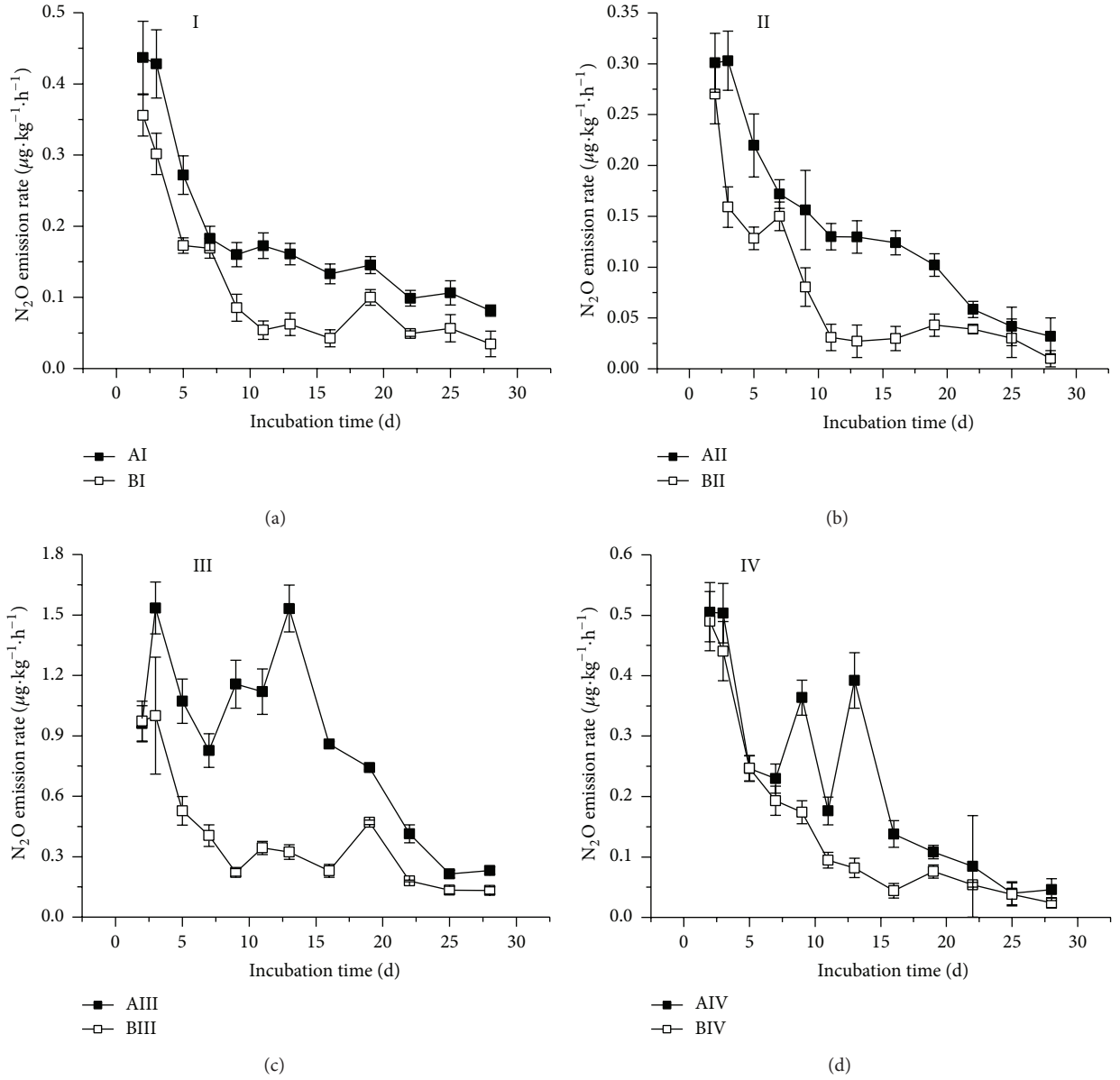

Figure 1: N_2O emission rate of the treatments studied. (Treatments notations are as follows: A: incubation at 35°C; B: incubation at 20°C; I: peat soil; II: peat soil under flooding; III: peat soil plus raw organic matter; IV: peat soil under flooding plus organic matter).

N_2O emission in treatment AI was 49.67% higher than in BI, AII was 54.78% higher than BII, AIII was 119.81% higher than BIII, and AIV was 42.33% higher than that of BIV. Moreover, highly significant differences were found between treatments AI and AIII (high temperature and peat soil versus peat soil plus exogenous organics matter) and also between BI and BIII (room temperature and peat soil plus exogenous organic matter) ($n = 3$, $P < 0.05$ or $P < 0.01$).

It could be deduced that increasing incubation temperature increased N_2O emissions. The maximum accumulative increase in N_2O emissions was for the peat soil added with raw organic matter, whereas the minimum accumulative was for the flooded peat soil added with raw organic matter.

3.2. Effect of Moisture Conditions on N_2O Emissions. Both N_2O emission rate and cumulative amount were lower in the flooding than in the unflooding treatment whether organic matter was added or no under high and room temperature conditions (Figures 1 and 2). N_2O emissions in AII were 20.72% lower than in AI; AIV emissions decreased by 72.23% with respect to AIII; meanwhile, BII was 23.34% lower than BI and BIV declined by 57.11% compared to BIII. Significant differences were found between AI and AII, AIII and AIV, BI and BII, and BIII and BIV ($n = 3$, $P < 0.05$). These results show that irrespective of incubation temperature, flooding inhibits soil N_2O emissions; moreover, the decline of N_2O emissions under flooding was more obvious in soils plus organic matter.

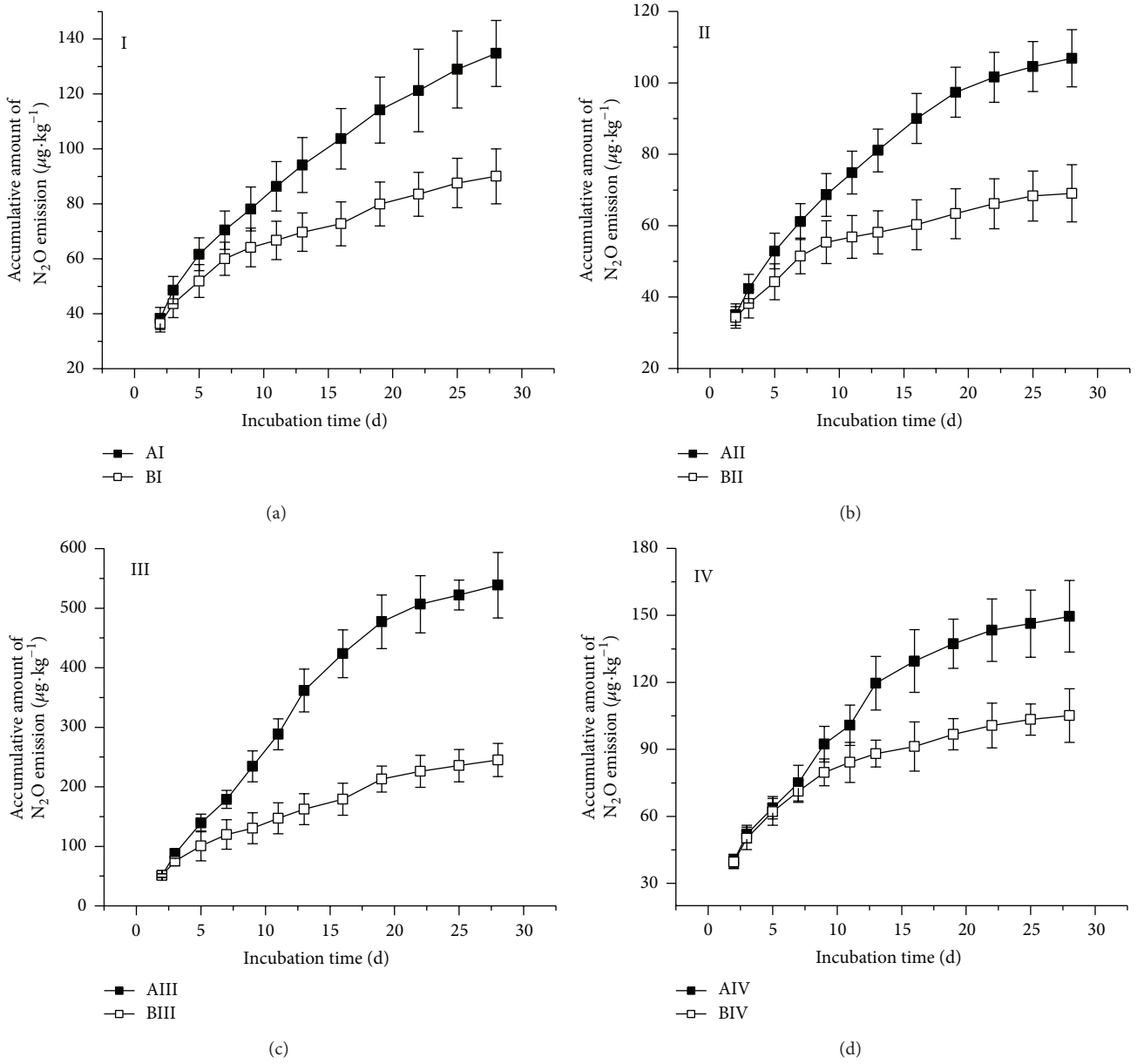

Figure 2: Cumulative amount of N_2O emission of the treatments studied. (Treatments notations are as follows: A: incubation at 35°C; B: incubation at 20°C; I: peat soil; II: peat soil under flooding; III: peat soil plus raw organic matter; IV: peat soil under flooding plus organic matter).

3.3. Effect of Organic Matter Input on N_2O Emissions. Further additions of organic matter to the studied peat soils increased soil N_2O emission rates in the flooded and the unflooded treatments at the two levels of temperature studied (Figure 1). Moreover, sharp fluctuations of soil N_2O emission along the incubation period occurred in soils added with organic matter under high temperature (AIII and AIV treatments). Organic matter additions clearly amplified cumulative amount of N_2O emissions (Figure 2). N_2O emissions in AIII were 299.62% higher than in AI, whereas those of AIV were 39.98% higher than those of AII. Also BIII emissions were 172.11% higher than in BI, and BIV were 52.23% higher than in BII. Very significant differences have been shown between AI and AIII (high temperature and peat soil versus peat soil plus organic matter), between AII and AII (high temperature and flooded soil versus flooded soil plus organic matter), and also between BI and BIII and BII and BIV ($n = 3$, $P < 0.01$). It was shown that the effect of exogenous organic matter input of increasing N_2O emissions was relatively much lower under flooding conditions, compared to normal unflooding conditions.

4. Discussion

Soil temperature has a great influence on N_2O formation through the biological processes of nitrification and

denitrification. Optimum temperatures for nitrifying bacterial activities are in the range from 15 to 35°C, and nitrification will be inhibited at below 5°C or above 40°C. Optimum temperatures for denitrifying microorganism are from 30 to 67°C [15]. Soil temperature was an important factor affecting N_2O emission as well. N_2O emission rate was shown to be nearly synchronized with surface soil temperature, and the temperature variation was the main driver of diurnal and seasonal changes in N_2O emissions [16]. In our wetland soil, N_2O emission increased with increasing temperature, which was consistent with previous reports on forest soils [10, 17]. This result could be ascribed to the fact that rates of enzymatic reactions would increase with temperature when other environmental factors are not restrictive [18]. Moreover, temperature might regulate soil denitrification both directly and indirectly, and it could promote the activity of soil nitrifying and denitrifying microorganism and hence enhance N_2O emission rate and cumulative emissions [19–22].

N_2O production and emission may be influenced by soil moisture, through its effects on soil aeration status, reduction-oxidation conditions, microbial activities, and N_2O diffusion into atmosphere. Feng and Yin [23] found that more N_2O was produced at 45%–75% water filled pore space. When it was below the saturated water content, soil N_2O emission increased with the increase of soil moisture, and nitrification was accredited as the basic source of N_2O. However, when it was above the saturated water content, the denitrification process was the main source of N_2O. With increasing soil moisture content above this threshold, the proportion of denitrifying N_2 increased gradually and N_2O emissions gradually weakened. Results from N_2O emission observed in the rice and wheat crop rotation system in east China showed that if soil moisture content was less than 415 $g \cdot kg^{-1}$, then soil N_2O emissions increased linearly with increasing soil moisture content; however, when the soil moisture content was more than 415 $g \cdot kg^{-1}$, N_2O emissions reduced with the increase of soil moisture content [24], indicating much higher N_2 loss under saturated soil water condition. Therefore, the production of N_2O was not positively related to soil moisture under high moisture condition. Soil moisture content was also a key determinant of soil microbial activity [25], and it had impact on the diffusion of N_2O produced during denitrification from microbial air into the surrounding environment [26]. Consequently, we deduced that both nitrifier-denitrifier microorganisms and coupled nitrification-denitrification processes contributed to the elevated N_2O emission in wetland soil [27].

Organic matter input was thought to be an important regulator of N_2O emissions, because organic matter on the soil surface could influence nitrification and denitrification reactions resulting from N mobilization and immobilization [28]. Toma and Hatano found huge N_2O emissions when accepting low C/N ratio residues, mainly because these residues tended to break up [29]. Liu et al. reported that wheat straw incorporation increased N_2O emissions, while the incorporation of maize straw had no impact on the emissions [30]. Millar et al. observed greater N_2O emissions in areas cultivated with corn-wheat due to high amount of N applied to the corn field [31]. Therefore similar to our study, other results have shown that organic matter input enhanced soil N_2O emission rate and cumulative emissions. The contribution of the organic matter could be mainly explained by the mineralization of litter which supplied substrates and thus promoted the production of N_2O. In opposite, results about the negative role of organic matter on N_2O emissions have also been reported [32]. Moreover, Tang et al. found that there were no significant impacts of organic matter on soil N_2O emissions in a subtropical and two tropical forests [33–35], which underlies the potential adverse effects of organic matter. Consequently, we hypothesize that the net integrated effect of organic matter on N_2O emission was the result of the counterbalance between the positive and negative feedbacks arising from interactions with other factors.

5. Conclusions

Both temperature rise and exogenous organic matter inputs increased N_2O emission rates and cumulative amount from a wetland soil. The flooded soil with external organic matter inputs showed the lowest cumulative rise in N_2O emissions as the temperature increased. Irregular changes of N_2O emission along the incubation period were found in soils added with organic matter under high temperature condition. Soil N_2O emissions could be inhibited by flooding; however, complex internal connections and cooperative or antagonistic actions between flooding and other environmental factors might appear in soil N_2O emissions. Thus, it is recommended to conduct further studies for assessing the way through which other environmental factors affect soil N_2O emissions of wetland ecosystem.

Conflict of Interests

The authors declare that there is no conflict of interests regarding the publication of this paper.

Acknowledgments

This work was supported by the National Natural Science Foundation of China (41201559; 41301314), the Natural Science Foundation of Jiangsu province (BK2011412), and the Natural Science Foundation of Universities in Jiangsu province area of China (10KJB170003).

References

[1] S. Nadeem, S. Hansen, M. Azzaroli Bleken, and P. Dörsch, "N_2O emission from organic barley cultivation as affected by green manure management," *Biogeosciences*, vol. 9, no. 7, pp. 2747–2759, 2012.

[2] A. R. Ravishankara, J. S. Daniel, and R. W. Portmann, "Nitrous oxide (N_2O): the dominant ozone-depleting substance emitted in the 21st century," *Science*, vol. 326, no. 5949, pp. 123–125, 2009.

[3] S. O. Petersen, P. Ambus, L. Elsgaard, P. Schjønning, and J. E. Olesen, "Long-term effects of cropping system on N_2O emission

potential," *Soil Biology and Biochemistry*, vol. 57, no. 1, pp. 706–712, 2013.

[4] D.-G. Kim, R. Vargas, B. Bond-Lamberty, and M. R. Turetsky, "Effects of soil rewetting and thawing on soil gas fluxes: a review of current literature and suggestions for future research," *Biogeosciences*, vol. 9, no. 7, pp. 2459–2483, 2012.

[5] T. Gomiero, D. Pimentel, and M. G. Paoletti, "Environmental impact of different agricultural management practices: conventional vs. organic agriculture," *Critical Reviews in Plant Sciences*, vol. 30, no. 1-2, pp. 95–124, 2011.

[6] L. Liengaard, L. P. Nielsen, N. P. Revsbech et al., "Extreme emission of N_2O from tropical wetland soil (Pantanal, South America)," *Frontiers in Microbiology*, vol. 3, no. 2, article 433, 2013.

[7] J. S. Yang, J. S. Liu, J. D. Wang, J. B. Yu, Z. G. Sun, and X. H. Li, "Emission rates of CH_4 and N_2O from a wetland in the Sanjiang Plain," *Journal of Plant Ecology*, vol. 30, no. 3, pp. 432–440, 2006.

[8] J. Paz-Ferreiro, E. Medina-Roldán, N. J. Ostle, N. P. McNamara, and R. D. Bardgett, "Grazing increases the temperature sensitivity of soil organic matter decomposition in a temperate grassland," *Environmental Research Letters*, vol. 7, no. 1, Article ID 014027, 2012.

[9] G. J. Luo, R. Kiese, B. Wolf, and K. Butterbach-Bahl, "Effects of soil temperature and moisture on methane uptake and nitrous oxide emissions across three different ecosystem types," *Biogeosciences*, vol. 10, no. 5, pp. 3205–3219, 2013.

[10] G. Schaufler, B. Kitzler, A. Schindlbacher, U. Skiba, M. A. Sutton, and S. Zechmeister-Boltenstern, "Greenhouse gas emissions from European soils under different land use: effects of soil moisture and temperature," *European Journal of Soil Science*, vol. 61, no. 5, pp. 683–696, 2010.

[11] X. Wu, Z. Yao, N. Brüggemann et al., "Effects of soil moisture and temperature on CO_2 and CH_4 soil-atmosphere exchange of various land use/cover types in a semi-arid grassland in Inner Mongolia, China," *Soil Biology and Biochemistry*, vol. 42, no. 5, pp. 773–787, 2010.

[12] N. Jäger, C. F. Stange, B. Ludwig, and H. Flessa, "Emission rates of N_2O and CO_2 from soils with different organic matter content from three long-term fertilization experiments-a laboratory study," *Biology and Fertility of Soils*, vol. 47, no. 5, pp. 483–494, 2011.

[13] X. Li, C. Y. Tang, Z. W. Han, J. Q. Piao, Y. J. Cao, and C. P. Zhang, "Spatial and seasonal variation of dissolved nitrous oxide in wetland groundwater," *Environment and Pollution*, vol. 3, no. 1, pp. 21–32, 2014.

[14] R. Markfoged, L. P. Nielsen, T. Nyord, L. D. M. Ottosen, and N. P. Revsbech, "Transient N_2O accumulation and emission caused by O_2 depletion in soil after liquid manure injection," *European Journal of Soil Science*, vol. 62, no. 4, pp. 541–550, 2011.

[15] M. Alexander, *Introduction to Soil Microbiology*, pp. 4–35, John Wiley and Sons, New York, NY, USA, 2nd edition, 1977.

[16] J. M. Bremner, S. G. Robbins, and A. M. Blackmer, "Seasonal variabity in emission of nitrous oxide from soil," *Geophysical Research Letters*, vol. 7, no. 9, pp. 641–644, 1980.

[17] Y. Cheng, J. Wang, S. Q. Wang, Z. C. Cai, and L. Wang, "Effects of temperature change and tree species composition on N_2O and NO emissions in acidic forest soils of subtropical China," *Journal of Environmental Sciences*, vol. 26, no. 3, pp. 617–625, 2014.

[18] F. X. Meixner and W. X. Yang, "Biogenic emissions of nitric oxide and nitrous oxide from arid and semi-arid land," in *Dryland Ecohydrology*, P. D'Odorico and A. Porporato, Eds., pp. 233–255, Springer, Dordrecht, Germany, 2006.

[19] Y. Lu, H. Xu, and C. Song, "Effects of plants on N_2O emission in freshwater marsh ecosystem," *Journal of Food, Agriculture and Environment*, vol. 10, no. 1, pp. 662–666, 2012.

[20] H. Tang, X. Xiao, W. Tang, and G. Yang, "Effects of straw recycling of winter covering crop on methane and nitrous oxide emissions in paddy field," *Acta Agronomica Sinica*, vol. 37, no. 9, pp. 1666–1675, 2011.

[21] A. Simojoki and A. Jaakkola, "Effect of nitrogen fertilization, cropping and irrigation on soil air composition and nitrous oxide emission in a loamy clay," *European Journal of Soil Science*, vol. 51, no. 3, pp. 413–424, 2000.

[22] X. J. Zhang, H. Xu, and G. X. Chen, "Important factors controlling rates of N_2O emission and CH_4 oxidation from forest soil," *Environmental Science*, vol. 23, no. 5, pp. 8–12, 2002.

[23] K. Feng and S. X. Yin, "Influence of soil properties on N_2O formation and emissions," *Progress in Soil Science*, vol. 23, no. 6, pp. 35–42, 1995.

[24] J. Gou, X. H. Zheng, and M. X. Wang, "A simulating of N_2O emission from a rice-wheat rotation ecosystem in southeast China," *Chinese Journal of Atmospheric Sciences*, vol. 24, no. 6, pp. 835–842, 2000.

[25] A. M. Weitz, E. Linder, S. Frolking, P. M. Crill, and M. Keller, "N_2O emissions from humid tropical agricultural soils: effects of soil moisture, texture and nitrogen availability," *Soil Biology and Biochemistry*, vol. 33, no. 7-8, pp. 1077–1093, 2001.

[26] J. H. Zeng and Z. P. Wang, "Research on production and emission of N_2O formation and emissions from agricultural soil," *Chinese Journal of Soil Science*, vol. 26, no. 3, pp. 132–134, 1995.

[27] X. J. Liu, A. R. Mosier, A. D. Halvorson, C. A. Reule, and F. S. Zhang, "Dinitrogen and N_2O emissions in arable soils: effect of tillage, N source and soil moisture," *Soil Biology and Biochemistry*, vol. 39, no. 9, pp. 2362–2370, 2007.

[28] D. Signor, C. E. P. Cerri, and R. Conant, "N_2O emissions due to nitrogen fertilizer applications in two regions of sugarcane cultivation in Brazil," *Environmental Research Letters*, vol. 8, no. 1, Article ID 015013, pp. 1–9, 2013.

[29] Y. Toma and R. Hatano, "Effect of crop residue C:N ratio on N_2O emissions from Gray Lowland soil in Mikasa, Hokkaido, Japan," *Soil Science and Plant Nutrition*, vol. 53, no. 2, pp. 198–205, 2007.

[30] C. Liu, K. Wang, S. X. Meng et al., "Effects of irrigation, fertilization and crop straw management on nitrous oxide and nitric oxide emissions from a wheat-maize rotation field in northern China," *Agriculture, Ecosystems and Environment*, vol. 140, no. 1-2, pp. 226–233, 2011.

[31] N. Millar, G. P. Robertson, P. R. Grace, R. J. Gehl, and J. P. Hoben, "Nitrogen fertilizer management for nitrous oxide (N_2O) mitigation in intensive corn (Maize) production: an emissions reduction protocol for US Midwest agriculture," *Mitigation and Adaptation Strategies for Global Change*, vol. 15, no. 2, pp. 185–204, 2010.

[32] Y. D. Wang, H. M. Wang, Z. L. Wang et al., "Effect of litter layer on soil-atmosphere N_2O flux of a subtropical pine plantation in China," *Atmospheric Environment*, vol. 82, no. 1-2, pp. 106–112, 2014.

[33] X. Tang, S. Liu, G. Zhou, D. Zhang, and C. Zhou, "Soil-atmospheric exchange of CO_2, CH_4, and N_2O in three subtropical forest ecosystems in southern China," *Global Change Biology*, vol. 12, no. 3, pp. 546–560, 2006.

[34] S. S. Vasconcelos, D. J. Zarin, M. Capanu et al., "Moisture and substrate availability constrain soil trace gas fluxes in an Eastern Amazonian regrowth forest," *Globle Biogeochemical Cycles*, vol. 18, no. 2, pp. 1–10, 2004.

[35] Y. Yan, L. Sha, M. Cao et al., "Fluxes of CH_4 and N_2O from soil under a tropical seasonal rain forest in Xishuangbanna, Southwest China," *Journal of Environmental Sciences*, vol. 20, no. 2, pp. 207–215, 2008.

Hindawi Publishing Corporation
The Scientific World Journal
Volume 2014, Article ID 212897, 13 pages
http://dx.doi.org/10.1155/2014/212897

Research Article

Fractal Analysis of Laplacian Pyramidal Filters Applied to Segmentation of Soil Images

J. de Castro,[1] F. Ballesteros,[1] A. Méndez,[2] and A. M. Tarquis[3]

[1] *Matemática Aplicada a las Tecnologías de la Información, E.T.S. de Ingenieros de Telecomunicación, Technical University of Madrid, Avenida Complutense 30, 28040 Madrid, Spain*
[2] *Matemática Aplicada a la Ingeniería Técnica de Telecomunicación, E.T.S. de Ingeniería y Sistemas de Telecomunicación, Technical University of Madrid, Carretera de Valencia km. 7, 28031 Madrid, Spain*
[3] *Matemática Aplicada a la Ingeniería Agronómica and CEIGRAM, E.T.S. de Ingenieros Agrónomos, Technical University of Madrid, Avenida Complutense 3, 28040 Madrid, Spain*

Correspondence should be addressed to F. Ballesteros; francisco.ballesteros@upm.es

Received 25 March 2014; Accepted 3 June 2014; Published 10 July 2014

Academic Editor: Antonio Paz González

The laplacian pyramid is a well-known technique for image processing in which local operators of many scales, but identical shape, serve as the basis functions. The required properties to the pyramidal filter produce a family of filters, which is unipara metrical in the case of the classical problem, when the length of the filter is 5. We pay attention to gaussian and fractal behaviour of these basis functions (or filters), and we determine the gaussian and fractal ranges in the case of single parameter a. These fractal filters loose less energy in every step of the laplacian pyramid, and we apply this property to get threshold values for segmenting soil images, and then evaluate their porosity. Also, we evaluate our results by comparing them with the Otsu algorithm threshold values, and conclude that our algorithm produce reliable test results.

1. Introduction

Image analysis involves many different tasks, such as identifying objects into images (segmentation), assigning labels to individual pixels by taking into account relevant information (classification), or extracting some meaning from the image as a whole (interpretation). The segmentation of soil images appears into Soil Science as a tool for the measurement of properties as well as for detecting and recognizing objects in soil [1–3].

Different methods have been used to segment soil images such as a simple binary threshold method [4] or multiple threshold method [5] and thresholds for typical and critical regions. Wang et al. [6] did a wide review of different segmentation methods applied in Geoscience. Other methods that appear to be most promising for soil applications are clustering methods and entropy-based methods [7–9].

Soil is not a continuous medium because soil is susceptible to changes from many influences: wetting, drying, compaction, plant growth, and so forth. So, the continuous soil models lead to approximate results only, and anomalous phenomena cannot be easily handled. It is known that pores in porous material are highly complex [10]. Their study and analysis have been usually avoided because of their difficulty.

Soil is formed from many constituents, and to represent it as a two-phase material, solid and pore, is often an oversimplification. The behaviour of water, gas, and organisms can affect it. A classification of pore models could be [11] (i) nonspatial, (ii) schematic, (iii) random set, (iv) fractal, and (v) other stochastic models. The fractal group has more models proposed and publications about.

Models of soil physical structure have been developed since the 1950s. Childs and Collisgeorge [12] introduced the cut-and-rejoin models of soil capillaries, which were modified by Marshall [13]. While many models of soil structure have been developed since then, most relate the structure to physical processes, generally ignoring heterogeneity, or assume simple pore-size distribution models.

More sophisticated approaches are [14] using a one-dimensional Markov chain model for horizontal soil, [15] proposing a two-dimensional fuzzy random model of soil pore structure, and [16] describing a network model to predict physical properties from topological parameters and fractal-based approaches like [17].

Our goal is to calculate the porosity of soil images. The proposed procedure for segmentation of soil micromorphological images is based on Laplacian pyramid algorithm [18], from which we compute a threshold that will binarize the original image, resulting with an image composed of continuous regions of pores (shown in black) and soil (shown in white). From this binarized soil image we compute an estimation to its porosity.

Another objective of this study is also to compare the results with those provided by the commonly used Otsu's algorithm [19] that is widely accepted as a good method to get an appropriate threshold.

2. Materials and Methods

2.1. Laplacian Pyramid. A multiresolution model consists of generating different versions of a given image by decreasing the initial resolution, which also means decreasing the initial size. This is achieved by a downsampling operator which must be associated with an appropriate filtering to avoid aliasing phenomena (downsampling theorem). Multiresolution approaches have been investigated for different purposes such as image segmentation and image compression [18]. In terms of image analysis, low resolution representations are convenient for global detection and recognition of image features while minute details can only be seen on high resolution images.

One usual property of images is that neighboring pixels are highly correlated. This property is inefficient to represent the complete image directly in terms of its pixel values, because most of the encoded information would be redundant. Burt and Adelson designed a technique, named Laplacian pyramid, for removing image correlation which combines characteristics of predictive and transform methods [18]. This technique is noncausal, and computations are relatively simple and local. The predicted value for each new pixel is computed as a local weighted average, using a unimodal weighting function centered on the pixel itself.

This pyramidal representation is useful for two important classes of computer graphics problems. The first class is composed of those tasks that involve analysis of existing images, such as merging images or interpolating to fill in missing data smoothly, become much more intuitive when we can manipulate easily visible local image features at several spatial resolutions. And the second, when we are synthesizing images, the pyramid becomes a multiresolution sketch pad. We can fill in the local spatial information at increasingly fine detail by specifying successive levels of a pyramid.

The first time that pyramidal structures were applied to multiresolution decompositions was at [18]. Later, the relationship to wavelets was realized shortly thereafter, because both decompositions are based on the idea of successive refinement: the image is obtained as a sum of an initial coarse version plus detail signals. One interesting thing to note about the pyramidal approach is that perfect reconstruction is possible; therefore it is a lossless data algorithm.

Pyramidal methods for multiresolution image analysis have been used since the 1970s. Early work in multiresolution image description was primarily motivated by a desire to reduce the computational cost of methods for image description and image matching. Later, multiresolution processing was generalized to computing multiple copies of an image by repeatedly summing nonoverlapping blocks of pixels and resampling until the image is reduced to a small number of pixels. Such a structure became known as a multiresolution pyramid [20].

Interest in multiresolution techniques for signal processing and analysis is increasing steadily [21]. An important instance of such a technique is the so-called pyramidal decomposition scheme. Our work uses a general axiomatic pyramidal decomposition scheme for soil image analysis. This scheme comprises the following ingredients.

(i) The pyramid consists of a finite number of levels such that the information content decreases towards higher levels.

(ii) Each step towards a higher level is constituted by an information-reducing analysis operator, whereas each step towards a lower level is modeled by an information-preserving synthesis operator. One basic assumption is necessary: synthesis followed by analysis yields the identity operator, meaning that no information is lost by these two consecutive steps.

2.2. Fractal Dimension. The techniques based on fractals show promising results in the field of image understanding and visualization of high complexity data.

The high complexity of some images demands new techniques for understanding and analyzing them. The similarity of fractals and real world objects has been observed and studied from the very beginning. The fractal geometry became a tool for computer graphics and data visualization in the simulation of the real world. In order to perform visual analysis and comparisons between natural and synthetic scenes several techniques have been developed. After a period of qualitative experiments, fractal geometry began to be used for objective and accurate purposes: modeling images, evaluating their characteristics, analyzing their textures, and so forth.

Nowadays, there are a lot of fields where fractals appear [22]. First of all, we present some of the elementary ideas necessary to understand applications of fractal geometry in geo-information processing [23].

Fractal geometry theory deals with the behaviors of sets of points S, in the n-dimensional space $\mathbb{R}^n$. Images, particularly soil images, are sets of points in $\mathbb{R}^2$.

Mandelbrot defined a fractal as a shape made of parts similar to the whole in some way [24]. That definition is qualitative but not ambiguous, as it looks at the first glance. The main behavior of a fractal is its self-similarity. A set is called self-similar if it can be expressed as a union of sets, each of which is a reduced copy of the full set. More generally a set

is said to be self-affine if it can be decomposed into subsets that can be linearly mapped into the full set. If the linear mapping is a rotation, translation, or isotropic dilatation the set is self-similar. The self-similar objects are particular cases of self-affine ones.

A fractal object is self-similar or self-affine at any scale. If the similarity is not described by deterministic laws stochastic resemblance criteria can be found. Such an object is said to be statistical self-similar. The natural fractal objects are statistically self-similar. A statistically self-similar fractal is by definition isotropic. To have a more precise, quantitative description of the fractal behavior of a set, a measure and a dimension are introduced. The rigorous mathematical description is done by Hausdorff's measure and dimension [25].

Let $S \subset \mathbb{R}^n$ and $r > 0$, and a δ-cover of S is a collection of sets $\{U_i : i \in I\}$ with diameter which is smaller than δ, such that

$$S \subset \bigcup_{i \in I} U_i \subset \mathbb{R}^n \quad \text{with } 0 < |U_i| < \delta, \tag{1}$$

where I is a finite or countable index set and $|\cdot|$ represents the diameter of the n-dimension set, defined as

$$|U| = \sup \{|x - y| : x, y \in U\}. \tag{2}$$

Also, let $\mathfrak{R}_\delta(S)$ be the collection of all δ-covers of S; we can define

$$H_\delta^r(S) = \inf_{\mathscr{R} \in \mathfrak{R}_\delta} \left\{ \sum_{i \in I} |U_i|^r : \mathscr{R} = \bigcup_{i \in I} U_i \right\}. \tag{3}$$

Now, if in (3) we let δ decrease to zero, we get the Hausdorff measure of the set S, $H^r(S)$:

$$H^r(S) = \lim_{\delta \to 0} H_\delta^r(S). \tag{4}$$

The Hausdorff measure generalizes the definition of length, area, volume, and so on. $H_\delta^r(S)$ gives the volume of a set S as measured with a ruler of δ units.

There is an interesting property of the Hausdorff measure: If the Hausdorff dimension of the set S is s, then

$$H^p(S) = \begin{cases} \infty & \text{if } p < s \\ 0 & \text{if } p > s. \end{cases} \tag{5}$$

So, the Hausdorff dimension of the set $S \subset \mathbb{R}^n$ could be defined as

$$\dim_H S = \sup \{r : H^r(S) = \infty\} = \inf \{r : H^r(S) = 0\} \tag{6}$$

as we can see in Figure 1.

Then, the value of the parameter r for which the r-dimensional Hausdorff measure of the set jumps from zero to infinite is said to be the Hausdorff dimension, $\dim_H$, of the set S.

A set is said to be fractal if its Hausdorff dimension strictly exceeds its topological dimension, $\dim_H S > n$.

Numerical evaluation of Hausdorff dimension is difficult because of the necessity to evaluate the infimum of the measure over all the coverings belongings to the set of interest. That is the reason to look for another definition for the dimension of a set. The box counting dimension allows the evaluation of the dimension of sets of points spread in an n-dimensional space and also gives possibilities for easy algorithmic implementation.

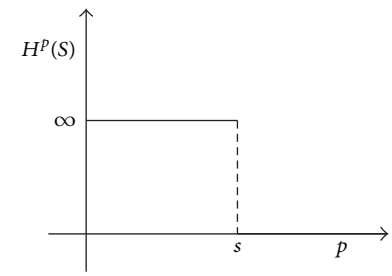

Figure 1: Hausdorff dimension of the set S.

Given a set of points S, in a n-dimensional space $\mathbb{R}^n$, and N_δ is the least number of sets of diameter at most δ that cover S, the box counting dimension, $\dim_B$, is defined as

$$\dim_B S = \lim_{\delta \to 0} \frac{\log N_\delta}{\log 1/\delta}. \tag{7}$$

Depending on the geometry of the box and the modality to cover the set, several box counting dimensions can be defined using closed balls, cubes, and so on [25].

The equivalence of these definitions was proved. Also it was proved that these dimensions are inferior bounded by the Hausdorff dimension [26].

Fractal geometry provides a mathematical model for many complex objects found in nature, such as coastlines, mountains, and clouds [22, 24]. These objects are too complex to possess characteristic sizes and to be described by traditional Euclidean geometry. Fractal dimension has been applied in texture analysis and segmentation [27, 28]. There are different methods that have been proposed to estimate the fractal dimension. The three major categories are the box-counting methods, the variance methods, and the spectral methods. The box-counting dimension is the most frequently used for measurements in various application fields. The reason for its dominance lies in its simplicity and automatic computability.

2.3. Segmentation of Soil Images. Image segmentation is the process of partitioning an image into several regions, in order to be easier to analyze and work with.

In image segmentation the level to which the subdivision of an image into its constituent regions or objects is carried depending on the problem being solved. In other words, when the object of focus is separated, image segmentation should stop [29]. The main goal of segmentation is to divide an image into parts having strong correlation with areas of interest in the image.

We study the simplest problem, dividing the image into just only two parts, foreground and background, or object pixels and background pixels. The intensity values, continuity

or discontinuity, color, texture, and other image characteristics are the origin of the different image segmentation techniques. Reference [9] is an exhaustive performance comparison of 40 selected methods put into groups according to histogram shape information, measurement space clustering, histogram entropy information, image attribute information, spatial information, and local characteristics.

So, some of the most important groups in image segmentation techniques are the threshold-based, the histogram-based, the edge-based, and the region based.

The threshold-based methods are based on pixels intensity values. The main goal here is to decide a threshold value λ to apply the rule:

$$g_{i+1}(x, y) = \begin{cases} 0 & \text{if } g_i(x, y) < \lambda \\ 255 & \text{if } g_i(x, y) \geq \lambda, \end{cases} \quad (8)$$

where $g_{i+1}(x, y)$ is the new pixel value and $g_i(x, y)$ is the old pixel value. In other words, after choosing a threshold, then every pixel in the image is compared with this threshold, and if the pixel lies above the threshold it will be marked as foreground, and if it is below the threshold it will be marked as background. The histogram-based methods are also based on pixels' intensity values. Here, histogram bars help to find the clusters of pixels values. One of the most famous threshold-based methods is Otsu's method [19].

The edge-based methods show boundaries in the image, determining different regions where we have to decide if they are foreground or background. The boundaries are calculated analyzing high contrasts in intensity, color, or texture. On the other hand, an opposed point of view are the region-based methods divide the image into regions, searching for same textures, colors, or intensity values.

In soil science the porosity of a porous medium is defined by the ratio of the void area and the total bulk area. Therefore, porosity is a fraction whose numerical value is between 0 and 1, typically ranging from 0.005 to 0.015 for solid granite to 0.2 to 0.35 for sand. It may also be represented in percent terms by multiplying the number by 100. Porosity is a dimensionless quantity and can be reported either as a decimal fraction or as a percentage.

The total porosity of a porous medium is the ratio of the pore volume to the total volume of a representative sample of the medium. Assuming that the soil system is composed of three phases—solid, liquid (water), and gas (air)—where V_s is the volume of the solid phase, V_l is the volume of the liquid phase, V_g is the volume of the gaseous phase, $V_p = V_l + V_g$ is the volume of the pores, and $V_t = V_s + V_l + V_g$ is the total volume of the sample, then the total porosity of the soil sample, p_t, is defined as follows:

$$p_t = \frac{V_p}{V_t} = \frac{V_l + V_g}{V_s + V_l + V_g}. \quad (9)$$

Table 1 lists representative porosity ranges for various geologic materials [30]. In general, porosity values for unconsolidated materials lie in the range of 0.25–0.7 (i.e., 25%–70%). Coarse-textured soil materials (such as gravel and sand) tend to have a lower total porosity than fine-textured soils (such as silts and clays). Porosity values in soils are not a constant quantity because the soil, particularly clayey soil, alternately swells, shrinks, compacts, and cracks. The porosity of our test image, shown in Figure 10(a), is 0.284.

Table 1: Range of porosity values.

Unconsolidated deposits	Porosity	Rocks	Porosity
Gravel	0.25–0.40	Fractured basalt	0.05–0.50
Sand	0.25–0.50	Karst limestone	0.05–0.50
Silt	0.35–0.50	Sandstone	0.05–0.30
Clay	0.40–0.70	Limestone, dolomite	0.00–0.20
		Shale	0.00–0.10
		Fractured crystalline rock	0.00–0.10
		Dense crystalline rock	0.00–0.05

Our work applies image segmentation techniques to calculate the porosity of soil images. Also, we have compared our results with the Otsu image segmentation algorithm.

3. Methodology

3.1. Laplacian Pyramid. The Laplacian pyramid representation expresses the original image as a sum of spatially band-passed images, while retaining local spatial information in each band. The Gaussian pyramid is created by low-pass-filtering an image G_0 with a two-dimensional compact filter. The filtered image is then subsampled by removing every other pixel and every other row to obtain a reduced image G_1. Graphical representations of these processes in one and two dimensions are given in Figures 2 and 3.

This process is repeated to form a Gaussian pyramid $G_0, G_1, G_2, \ldots, G_N$:

$$G_k(i, j) = \sum_m \sum_n G_{k-1}(2i + m, 2j + n) \quad k = 1, \ldots, N. \quad (10)$$

Expanding G_1 to the same size as G_0 and subtracting yields the band-passed image L_0, a Laplacian pyramid $L_0, L_1, \ldots, L_{n-1}$ can be built containing band-passed images of decreasing size and spatial frequency:

$$L_k = G_k - G_{k+1} \quad k = 0, \ldots, N - 1, \quad (11)$$

where the expanded image G_k is given by

$$G_k(i, j) = 4 \sum_m \sum_n w(m, n) G_{k-1}\left(\frac{2i + m}{2}, \frac{2j + n}{2}\right). \quad (12)$$

The original image can be reconstructed from the expanded bandpass images:

$$\begin{aligned} G_0 &= L_0 + G_1 \\ &= L_0 + L_1 + G_2 \\ &\vdots \\ &= L_0 + L_1 + L_2 + \cdots + L_{N-1} + G_N. \end{aligned} \quad (13)$$

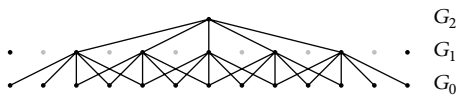

Figure 2: Representation of the one-dimensional Gaussian pyramid process.

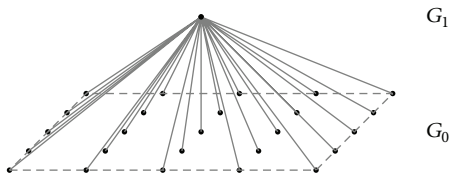

Figure 3: Representation of the two-dimensional Gaussian pyramid process.

The Gaussian pyramid contains low-passed versions of the original G_0 at progressively lower spatial frequencies, while the Laplacian pyramid consists of band-passed copies of the original image G_0. Each Laplacian level contains the edges of a certain size and spans approximately an octave in spatial frequency.

3.2. Fractal Dimension: Box-Counting Dimension. Fractal dimension is a useful feature for texture segmentation, shape classification, and graphic analysis in many fields. The box-counting approach is one of the frequently used techniques to estimate the fractal dimension of an image.

There are several methods available to estimate the dimension of fractal sets. The Hausdorff dimension is the principal definition of fractal dimension. However, there are other definitions, like box-counting or box dimension, that is popular due to its relative ease of mathematical calculation and empirical estimation. The main idea to most definitions of fractal dimension is the idea of measurement at scale δ. For each δ, we measure a set ignoring irregularities of size less than δ, and then we see how these measurements behave as $\delta \to 0$. For example, if F is a plane curve (one of our filters), then $N_\delta(F)$ might be the number of steps required by a pair of dividers set at length δ to traverse F. Then, the dimension of F is determined by the power law, if any exists, obeyed by $N_\delta(F)$ as $\delta \to 0$. So, we might say that F has dimension s if a constant s exists so that

$$\delta^s \cdot N_\delta(F) \simeq 1, \tag{14}$$

where taking logarithms and limits when δ tends to 0; we get (7).

These formulae are appealing for computational or experimental purposes, since s can be estimated as the gradient of a log-log graph plotted over a suitable range of δ.

3.3. Kolmogorov-Smirnov Normality Test. In order to determine the normality interval we use the Kolmogorov-Smirnov normality test [31, 32], which is the most usual empirical distribution function test for normality.

For a data set A of n we make the contrast of a distribution function F_n from a theoretical distribution function F, using the statistic D_n

$$D_n = D_n(F_n, F) = \max_{x \in A} \{|F_n(x) - F(x)|\} \tag{15}$$

that represents the distance between F_n and F.

For n large enough, the statistical distribution of D_n is close to the Kolmogorov-Smirnov distribution, $\mathcal{K}$, which is tabulated for some significant values. Obviously, the assumption of normality is rejected with significance level $1 - \alpha$, if $D_n > D_{n,\alpha}$, with $P(\mathcal{K} \leq D_{n,\alpha}) = \alpha$.

Let $D_{n,\alpha}$ be the K-S distribution percentiles. We reject at level $1 - \alpha$ because if n is big enough, $D_n = \mathcal{K}$ and $\alpha = 0.01$. Then, we reject small values of D_n, so if $|F_n - F|$ is smaller than the percentile α, we accept the hypothesis.

3.4. Otsu's Thresholding Method. The most common image segmentation methods are the histogram thresholding based, since thresholding is easy, fast, and economical in computation. For performing the image segmentation we need to calculate a threshold which will separate the objects and the background in our image. Since soil images are relatively simple when we just pay attention to void and bulk, so we are going to apply the global threshold technique, instead of more advanced variations (band thresholding, local thresholding, and multithresholding). The global thresholding technique consists of selecting one threshold value and applying it to the whole image.

The resultant image is a binary image where pixels that correspond to objects and background have values of 255 and 0, respectively. Quick and simple calculation is the main advantage of global thresholding.

Otsu's method searches for the threshold that minimizes the intraclass variance (or within class variance) $\sigma_W^2(t)$ defined as the weighted sum of variances of the two classes:

$$\sigma_w^2(t) = \omega_0(t)\,\sigma_0^2(t) + \omega_1(t)\,\sigma_1^2(t), \tag{16}$$

where ω_i are the probabilities of the two classes (foreground and background) separated by a threshold t and σ_i^2 are the variances of these both classes.

Otsu [19] proofed that minimizing the intraclass variance is the same as maximizing the interclass variance $\sigma_b^2(t)$ defined as follows:

$$\sigma_B^2(t) = \sigma^2 - \sigma_W^2(t) = \omega_0(t)\,\omega_1(t)\left[\mu_0(t) - \mu_1(t)\right]^2, \tag{17}$$

where ω_i are the class probabilities and μ_i the class means.

The class probabilities $\omega_0(t)$ and $\omega_1(t)$, and the class means $\mu_0(t)$ and $\mu_1(t)$, are computed as

$$\begin{aligned} \omega_0(t) &= \sum_0^t p(i) \qquad \omega_1(t) = \sum_{i>t} p(i) \\ \mu_0(t) &= \sum_0^t p(i)\,x(i) \qquad \mu_1(t) = \sum_{i>t} p(i)\,x(i), \end{aligned} \tag{18}$$

where $x(i)$ is the centered value of the ith histogram bin.

The class probabilities and class means can be computed iteratively. This idea yields an effective algorithm.

Otsu's algorithm assumes just only two sets of pixel intensities, the foreground and the background, or void and bulk for soil images. The main idea of the Otsu's method is to minimize the weighted sum of within-class variances of the foreground and background pixels to establish an optimum threshold. It can be formulated as

$$\lambda_{\text{Otsu}} = \arg\min \left\{ \omega_0(\lambda)\,\sigma_0^2(\lambda) + \omega_1(\lambda)\,\sigma_1^2(\lambda) \right\}, \tag{19}$$

where the weights $\omega_i(\lambda)$ are the probabilities of the two classes separated by the threshold λ and $\sigma_i^2(\lambda)$ are the corresponding variances of these classes. Otsu's method gives satisfactory results when the values of pixels in each class are close to each other, as in soil images.

Let the pixels of a given picture be represented in 256 gray levels: $0, 1, 2, \ldots, 255$. Let the number of pixels at level i be denoted by n_i and the total number of pixels by N. If we define p_i as $p_i = n_i/N$, then $p_i \geq 0$ and $\sum p_i = 1$. So, we have a probability distribution point of view.

The threshold at level k defines two classes: the foreground (C_0) and the background (C_1). Then, the probabilities of these classes and their means are

$$\begin{aligned}
\omega_0 &= \Pr(C_0) = \sum_{i=0}^{k} p_i = \omega(k), \\
\omega_1 &= \Pr(C_1) = \sum_{i=k+1}^{255} p_i = 1 - \omega(k), \\
\mu_0 &= \sum_{i=0}^{k} i \Pr(i \mid C_0) = \sum_{i=0}^{k} \frac{i p_i}{\omega_0} = \frac{\mu(k)}{\omega(k)}, \\
\mu_1 &= \sum_{i=k+1}^{255} i \Pr(i \mid C_1) = \sum_{i=k+1}^{255} \frac{i p_i}{\omega_1} = \frac{\mu_T - \mu(k)}{1 - \omega(k)},
\end{aligned} \tag{20}$$

where

$$\omega(k) = \sum_{i=0}^{k} p_i \qquad \mu(k) = \sum_{i=0}^{k} i p_i, \qquad \mu_T = \sum_{0}^{255} i p_i. \tag{21}$$

We can easily verify that, for any k, $\omega_0 + \omega_1 = 1$ and $\omega_0\mu_0 + \omega_1\mu_1 = \mu_T$. Now, we define the class variances as

$$\begin{aligned}
\sigma_0^2 &= \sum_{i=0}^{k} (i - \mu_0)^2 \Pr(i \mid C_0) = \sum_{i=0}^{k} \frac{(i - \mu_0)^2 p_i}{\omega_0}, \\
\sigma_1^2 &= \sum_{i=k+1}^{255} (i - \mu_1)^2 \Pr(i \mid C_1) = \sum_{i=k+1}^{255} \frac{(i - \mu_1)^2 p_i}{\omega_1}.
\end{aligned} \tag{22}$$

Now, we are going to apply the discriminant analysis to evaluate and quantify the threshold at level k, using the measures of class separability λ, κ, and η based on the within-class variance σ_W^2, the between-class variance σ_B^2, and the total variance σ_T^2, defined as

$$\begin{aligned}
\lambda = \frac{\sigma_B^2}{\sigma_W^2} \qquad \kappa = \frac{\sigma_T^2}{\sigma_W^2} \qquad \eta = \frac{\sigma_B^2}{\sigma_T^2}, \\
\sigma_W^2 = \omega_0\sigma_0^2 + \omega_1\sigma_1^2, \\
\sigma_B^2 = \omega_0(\mu_0 - \mu_T)^2 + \omega_1(\mu_1 - \mu_T)^2 = \omega_0\omega_1(\mu_1 - \mu_0)^2, \\
\sigma_T^2 = \sum_{i=0}^{255} (i - \mu_T)^2 p_i.
\end{aligned} \tag{23}$$

4. Results

4.1. Classification of 1D Filters. Our 1D filters are defined by the weighting function $w(m)$ and the pyramidal construction is equivalent to convolving repeatedly the original signal with this weighting functions. Some of these Gaussian-like weighting functions are shown in Figure 5.

Note that the functions double in width with each level. The convolution acts as a low-pass filter with the band limit reduced correspondingly by one octave with each level. Because of this resemblance to the Gaussian density function we refer to the pyramid of low-pass images as the Gaussian pyramid. Just as the value of each node in the Gaussian pyramid could have been obtained directly by convolving a Gaussian-like equivalent weighting function with the original image, each value of this bandpass pyramid could be obtained by convolving a difference of two Gaussians with the original image. These functions closely resemble the Laplacian operators commonly used in image processing. For this reason the bandpass pyramid is known as a Laplacian pyramid. An important property of the Laplacian pyramid is that it is a complete image representation: the steps used to construct the pyramid may be reversed to recover the original image exactly. The top pyramidal level, L_N, is first expanded and added to L_{N-1} to form G_{N-1}. Then this array is expanded and added to L_{N-2} to recover G_{N-2}, and so on.

The weighting function $w(m)$ is determined by these constraints

$$\begin{aligned}
&\text{Symmetry:} \quad w(m) = w(-m) \\
&\text{Normalization:} \quad \sum_{m=-2}^{2} w(m) = 1 \\
&\text{Equal contribution:} \quad \sum_{m\,\text{odd}} w(m) = \sum_{m\,\text{even}} w(m).
\end{aligned} \tag{24}$$

Normalization, symmetry, and equal contribution are satisfied when

$$\begin{aligned}
w(0) &= a, \\
w(1) = w(-1) &= \frac{1}{4}, \\
w(2) = w(-2) &= \frac{1}{4} - \frac{a}{2}.
\end{aligned} \tag{25}$$

If the size is 5, we have the filter w

$$(w_0[k]) = \left[\frac{1}{4} - \frac{a}{2}, \frac{1}{4}, a, \frac{1}{4}, \frac{1}{4} - \frac{a}{2}\right] \quad k = 1, \ldots, 5 \tag{26}$$

which represents a uniparametric family of weighting functions with parameter a. Observe that if the size is bigger than 5, constraints (24) generate a multiparametric family of weighting functions.

Convolution is a basic operation of most signal analysis systems. When the convolution and decimation operators are applied repeatedly n times, they generate a new equivalent filter w_n, whose length is

$$\begin{aligned} M_0 &= 5, \\ M_n &= 2M_{n-1} + 3 \quad n \geq 1, \end{aligned} \tag{27}$$

where M_0 is the length of the initial filter w_0.

Figure 4 shows an example of several iterations of the filter for $a = 0.4$. We can observe that there is a quick convergence to a stable shape. And, in this case, the shape of the plot of the limit filter is Gaussian.

We have tested different values a, from $a = 0.1$ to $a = 1.2$. The shape of the filter, the equivalent weighting function, depends on the choice of parameter a. There are several different shapes for different values of a: Gaussian-like and fractal-like. Figure 5 shows some examples of Gaussian and fractal shapes.

The first two filters are Gaussian-like, and the last two are fractal-like. It is possible to confirm these early conclusions. We have successfully applied normality tests to verify the normality of the filters obtained with the lowest a values. On the other hand, in fractal geometry, the box-counting dimension is a way of determining the fractal dimension of a set. To calculate the box-counting dimension for a set S, we draw an evenly-spaced grid over the set and count how many boxes are required to cover the set. The box-counting dimension is calculated by applying (7).

We can see the results of fractal dimension (FD) of filters 1D whose values are shown in Table 2 and Figure 9(a). From these results and this figure we can observe a fractal behaviour when $a < 0$ and when $a > 0.6$.

The generation of bidimensional filters $\widetilde{w}(m, n)$, also called generating kernels or mask filters, is based on the condition

$$\text{Separability:} \quad \widetilde{w}(m, n) = w(m)\, w(n). \tag{28}$$

So, a filter $\widetilde{w}(m, n)$ is called separable if it can be broken down into the convolution of two filters. This property is interesting because if we can separate a filter into two smaller filters, then usually it is computationally more efficient and quicker to apply both of them instead the original one. We work with 2D filters that can be separated into horizontal and vertical filters. 2D filters have been obtained by sequentially applying the same one-dimensional filter on rows and columns.

When we calculate the bidimensional filters, we obtain filters like Figure 6. These are obtained when $a = 0.4$ and $a = 0.8$.

Table 2: Fractal dimension of filters.

a	Fractal dimension
−0.2	1.578
−0.1	1.240
0.0	1.011
0.1	1.020
0.2	1.009
0.3	1.009
0.4	1.004
0.5	1.009
0.6	1.022
0.7	1.142
0.8	1.141
0.9	1.209
1.0	1.248
1.1	1.276
1.2	1.289

4.2. Normality Interval. There is a relevant result when we study the normality of filters: the Gaussian function is separable if variables are independent. Burt and Adelson show that if we choose $n = 5$ and $a = 0.4$, then the equivalent weight function is Gaussian [18]. Indeed, there is an interval for the parameter a where we can see the Gaussian behavior.

Once we have a chosen value for a and a pyramidal depth value k, we need to select the best normal distribution $N(\widehat{\mu}, \widehat{\sigma})$ that fits our weights. We estimate $\widehat{\mu}$ by the arithmetic mean and $\widehat{\sigma}$ by the minim of all D_n in an empirical confidence interval calculated as

$$\begin{aligned} &\text{CI}(\widehat{\sigma}) \\ &= \left(\max\left(\min\left(\widehat{\sigma}_1, \widehat{\sigma}_2\right) - 1, 0\right), \max\left(\min\left(\widehat{\sigma}_1, \widehat{\sigma}_2\right) + 1, 0\right)\right) \end{aligned} \tag{29}$$

with $\widehat{\sigma}_1$ and $\widehat{\sigma}_2$ two initial estimations of $\widehat{\sigma}$.

Because the symmetry property of the filter w, we have that the arithmetic mean is the central point, so

$$\widehat{\mu} = \frac{M_j + 1}{2} = 2^{j+1} - 1 \tag{30}$$

because the jth level is $M_j = 2^{j+2} - 3$, which is the solution of the linear recurrence relation (27).

Conditions to calculate $\widehat{\sigma}_1$ and $\widehat{\sigma}_2$ are the adjust to the histogram of the filter $\widetilde{w}$ and the normal distribution related to two known percentiles; specifically,

$$\begin{aligned} \Pr\left(N(\mu, \sigma) \leq \mu - z_1\sigma\right) &= \frac{1 - p_1}{2}, \\ \Pr\left(N(\mu, \sigma) \leq \mu - z_2\sigma\right) &= \frac{1 - p_2}{2} \end{aligned} \tag{31}$$

so we have the system of equations

$$\begin{aligned} \widehat{\sigma}_1 &= \widehat{\mu} - z_1 c_{p_1}, \\ \widehat{\sigma}_2 &= \frac{\widehat{\mu} - c_{p_2}}{z_2}, \end{aligned} \tag{32}$$

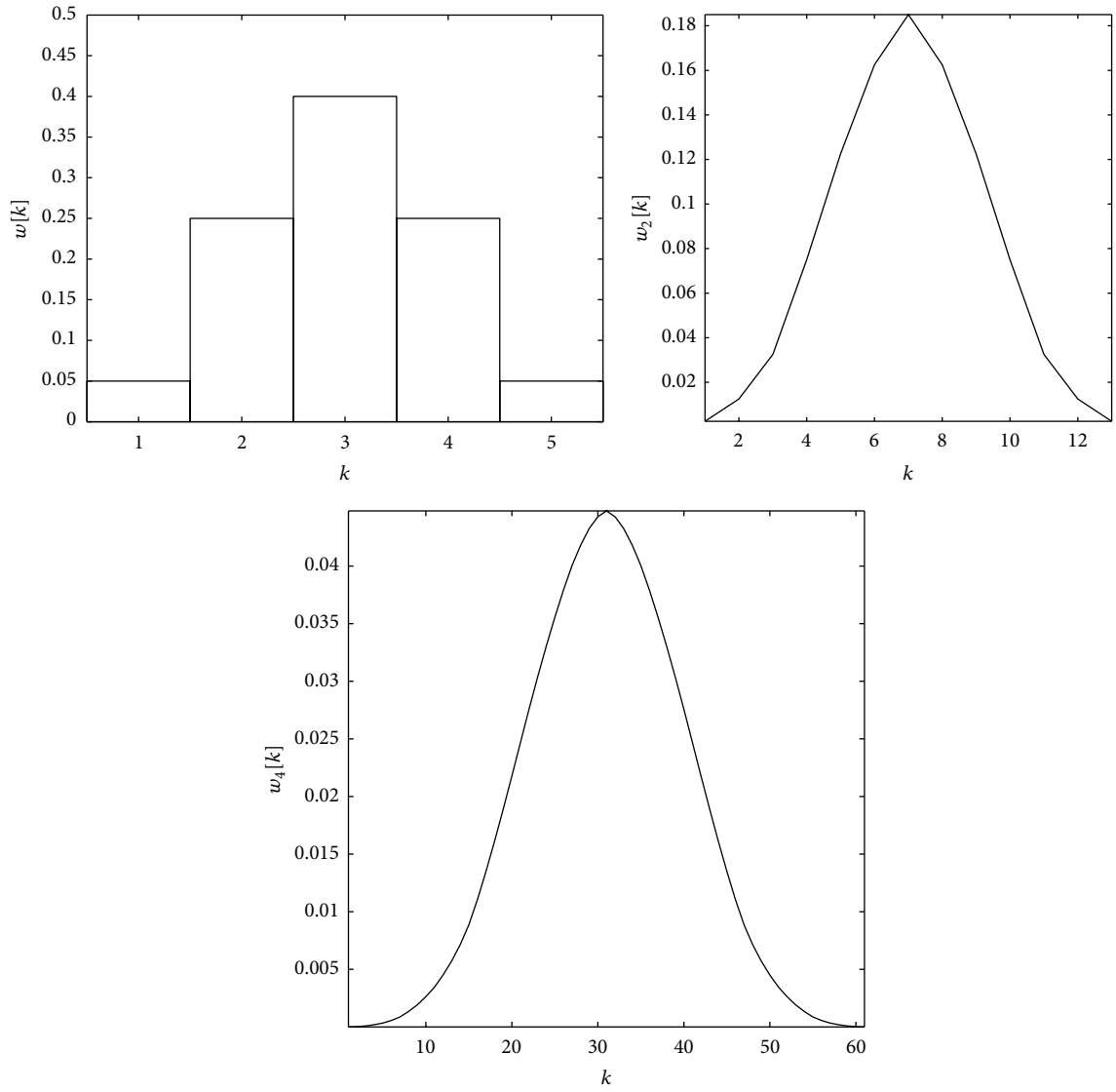

Figure 4: First, second, and fourth iteration of the filter 1D ($a = 0.4$).

where c_{p_1} and c_{p_2} are the corresponding abscissas to percentiles p_1 and p_2.

Specifically, the numerical simulation with $n = 5$, $p_1 = 0.682$, and $p_2 = 0.95$ (that correspond to the normalized abscissas $z_1 = 1$ and $z_2 = 1.96$) generates the normality intervals, which determinates the estimation for $\widehat{\sigma}$ of the normal distribution applied. Corresponding values for this case are shown in Figure 7(a). As we can see, $a = 0.39$ is the minimal value, and so it has the best adaptation to a normal distribution, as shown in Figure 7(b).

Figure 7(a) shows the value of the statistic D_n as a function of the parameter a and the normal threshold for a confidence level of 99%. For values of a in the interval $[-0.08, 0.57]$ the assumption of normality is not rejected. D_n attains the minimum for $a = 0.39$, corresponding to estimated Gaussian distribution, with mean 127 and standard deviation 36.74. Figure 7(b) shows the filter w_6 and the estimated density, where we can see the adjustment goodness.

4.3. Image Segmentation and Performance Evaluation. After these results, we have generated the Gaussian and Laplacian pyramids corresponding to one Gaussian value for a and another fractal value for a, applying the methodology previously shown, getting the corresponding Gaussian and Laplacian pyramids, and then we have compared the results obtained. Figure 8 shows pyramidal sets for $a = 0.4$ and $a = 1.2$, corresponding to a Gaussian and a fractal, respectively.

When we have applied our method to segment images with different values for the parameter a, we have obtained the threshold values shown in Figure 9(b) and results as shown in the Figure 10. We can compare these results with Otsu's method threshold value 0.259.

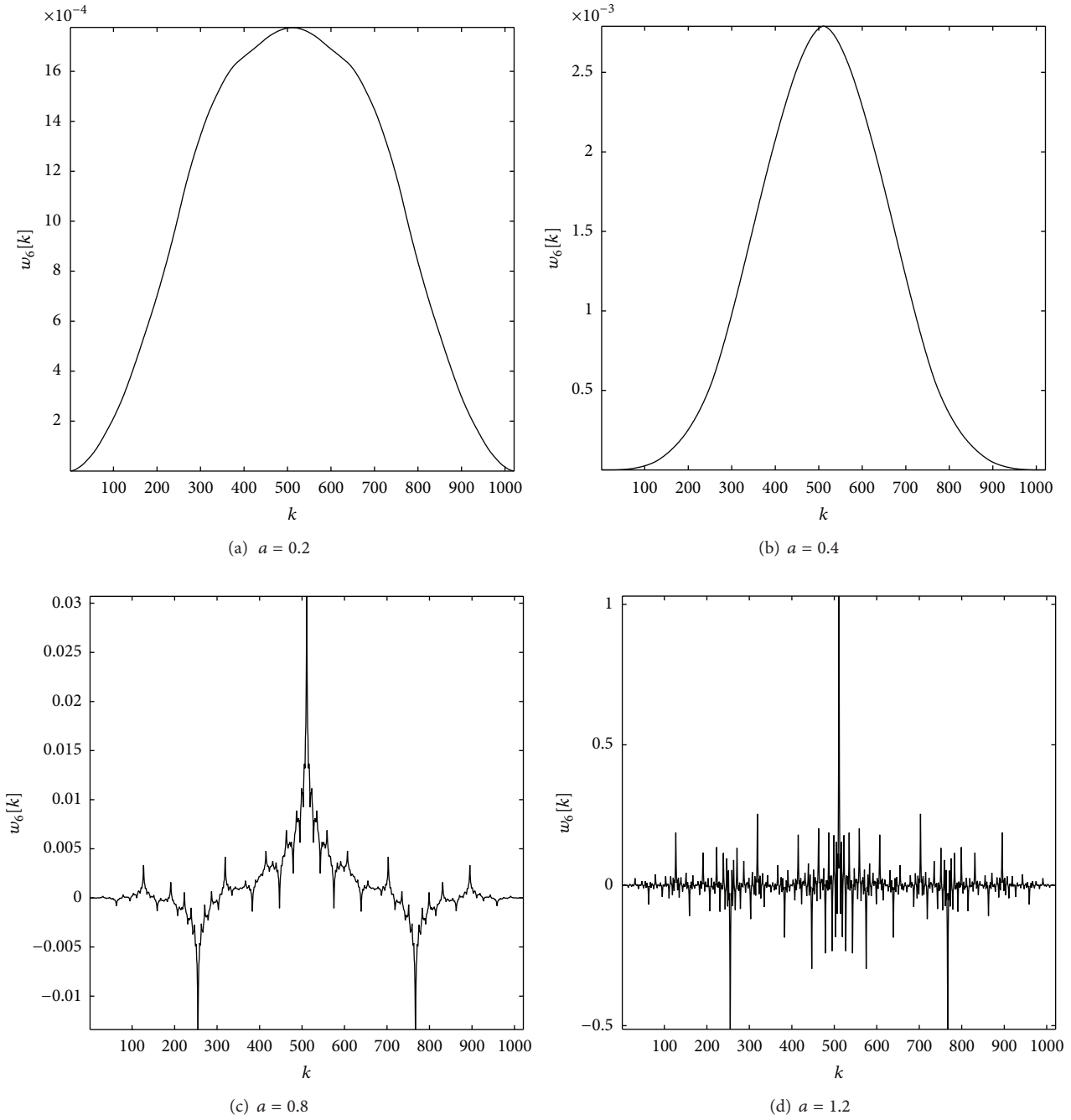

Figure 5: Sixth iteration of 1D Laplacian pyramid filters, $w_6[k]$, for different a values.

The application of our methods with different values a produces the results shown in Figure 10(b), together with Otsu's value. As we can see, our method obtains similar results for fractal threshold values.

4.4. Pore Size Distribution. We have presented threshold values obtained from Laplacian pyramid and the comparison with Otsu's values. On the other hand, if we compare the pore size frequency distribution obtained by Otsu's method and the threshold obtained based on Laplacian filter structure some difference is observed, as we can see in Figure 11. In the smallest size range, between 5 to 20 pixels, the former method presents higher porosity and the decrease in frequency is much smoother than with the latest method. Even the difference in porosity is not significant, Otsu's method gives 27.5% and this method estimates 31.1% the difference in sizes could affect several percolation models. These results are showed in Figure 11. Finally, the porosity obtained is this

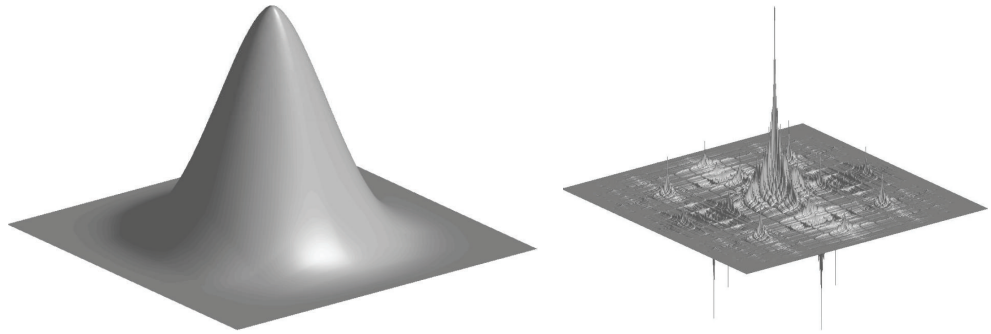

(a) (b)

Figure 6: Bidimensional filters corresponding to $a = 0.4$ (a) and $a = 0.8$ (b).

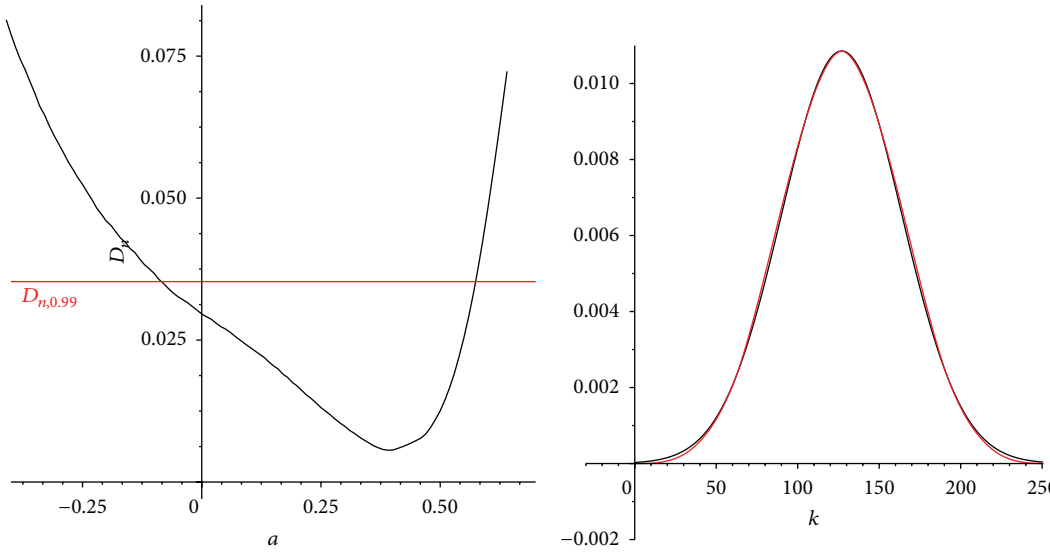

(a) D_n and $D_{n,0.99}$

(b) Density function of normal distribution (black) and weighting function for $a = 0.39$ (red)

Figure 7: Gaussian filter adjustment.

study approaches Otsu's result when a value increases from the range 0 till 1.2.

5. Conclusions

The field of fractals has been developed as an interdisciplinary area between branches of mathematics and physics and found applications in different sciences and engineering fields. In geo-information interpretation the applications developed from simple verifications of the fractal behavior of natural land structures, simulations of artificial landscapes, and classification based on the evaluation of the fractal dimension to advanced remotely sensed image analysis, scene understanding, and accurate geometric and radiometric modeling of land and land cover structures.

Referring to the computational effort, fractal analysis generally asks high complexity algorithms. Both wavelets and hierarchic representation allow now the implementation of fast algorithms or parallel ones. As a consequence a development of new experiments and operational applications is expected.

We have seen that the different choice of the parameter a gives two kinds of filters, the Gaussian-like and the fractal-like. This is demonstrated applying normality tests (Gaussian) and fractal dimension techniques (fractal), analytical and graphical in both cases.

The different shape of filters, Gaussian/fractal, has perceptible effects when we generate new levels of the Gaussian and Laplacian pyramids, getting blurred or accentuated new

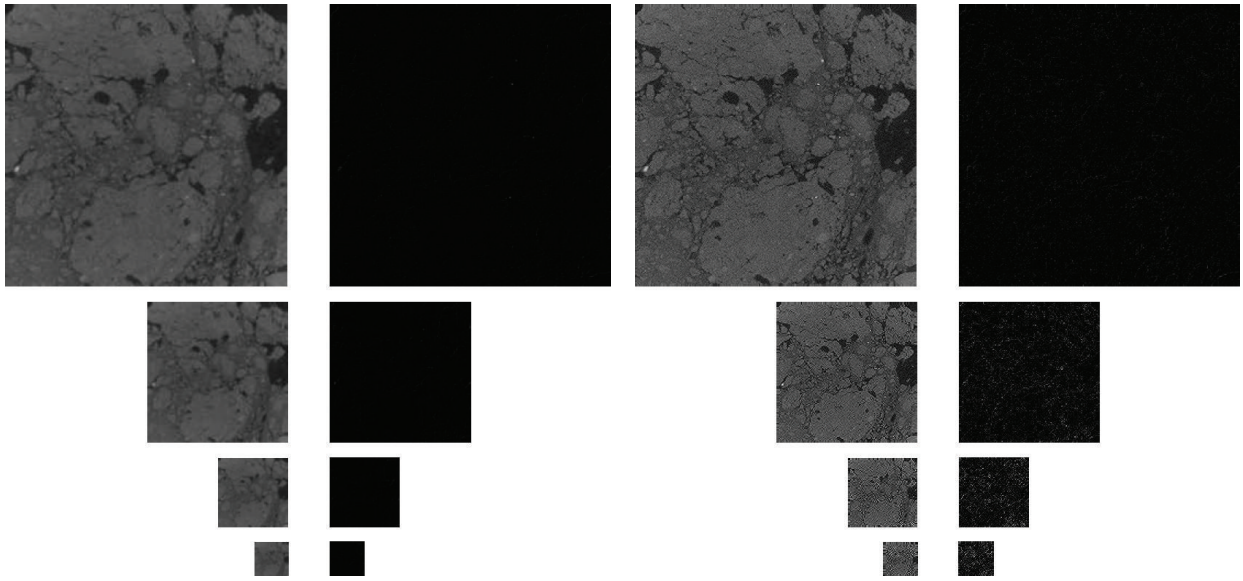

Figure 8: Gaussian and Laplacian pyramids of the soil image ((a) $a = 0.4$, (b) $a = 1.2$).

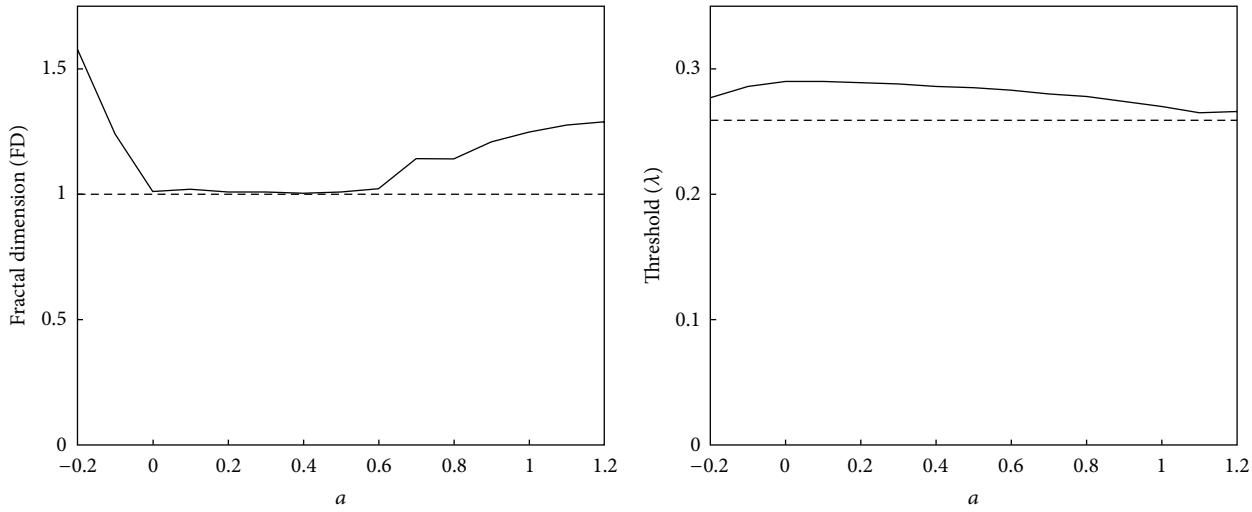

(a) Fractal dimension of filters 1D

(b) Threshold values from Laplacian pyramid filters and Otsu's technique

Figure 9: Fractal dimensions and threshold values.

images, at every new level. Filters generated with lowest a values produce blurred edges and images. On the other hand, filters obtained from highest a values generate new images with higher contrasts and sharp edges.

Also, there is a different behaviour of the energy of the different levels of the Laplacian pyramid if we choose different a values, that is, if we choose a Gaussian or fractal filter. The Gaussian-like filters always make a lower energy image. This fall is slow but there is always a fall. On the other hand, fractal-like filters also fall, but this happens after several iterations, and then, the fall is bigger than the fall of the Gaussian-like filters.

These filters can be applied to image segmentation of soil images, with a simple computation and good results, quite similar or even better to some famous techniques such as Otsu's method.

Moreover, results concerning porosity are similar but there are differences in pore size distribution that could improve percolation simulations. The implementation of this method in three dimensions is straightforward.

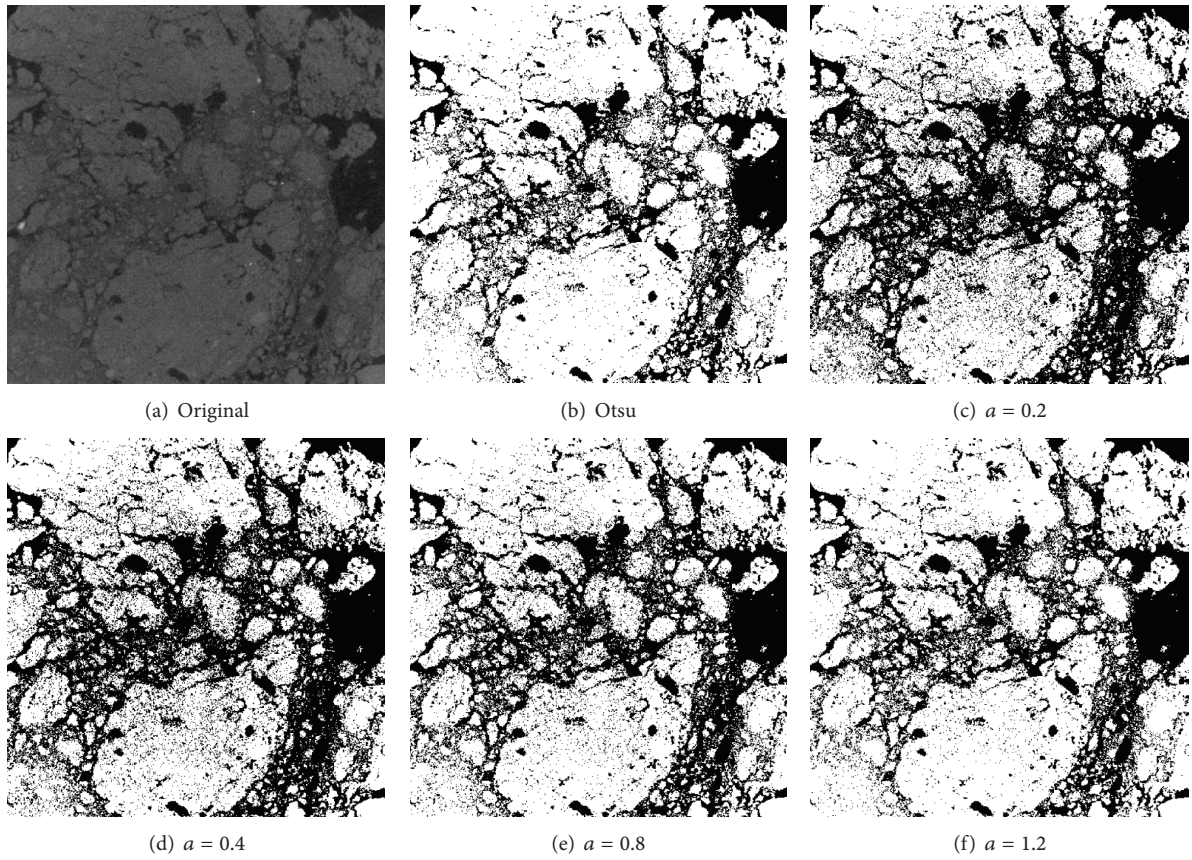

(a) Original (b) Otsu (c) $a = 0.2$

(d) $a = 0.4$ (e) $a = 0.8$ (f) $a = 1.2$

Figure 10: Soil image and several segmentations.

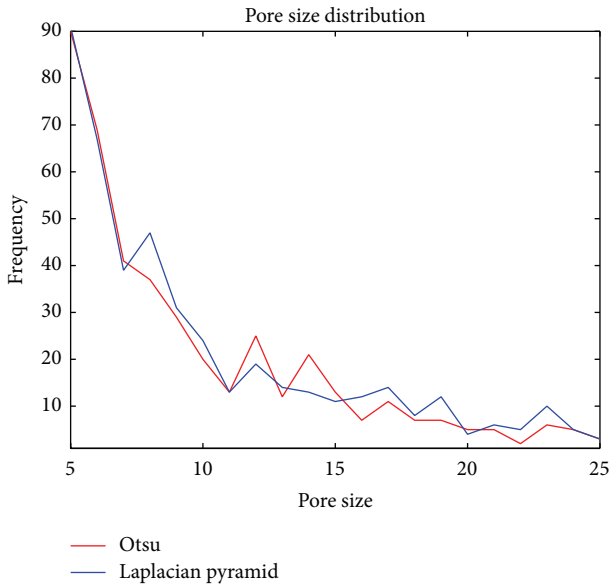

Figure 11: Pore size distribution.

Future work could add other image segmentation techniques and neural networks methods to select the optimal threshold values from information and characteristics of the image.

Conflict of Interests

The authors declare that there is no conflict of interests regarding the publication of this paper.

References

[1] P. C. Baveye, M. Laba, W. Otten et al., "Observer-dependent variability of the thresholding step in the quantitative analysis of soil images and X-ray microtomography data," *Geoderma*, vol. 157, no. 1-2, pp. 51–63, 2010.

[2] P. Lehmann, P. Wyss, A. Flisch et al., "Tomographical imaging and mathematical description of porous media used for the prediction of fluid distribution," *Vadose Zone Journal*, vol. 5, no. 1, pp. 80–97, 2006.

[3] H.-J. Vogel, U. Weller, and S. Schlüter, "Quantification of soil structure based on Minkowski functions," *Computers and Geosciences*, vol. 36, no. 10, pp. 1236–1245, 2010.

[4] J. S. Perret, S. O. Prasher, and A. R. Kacimov, "Mass fractal dimension of soil macropores using computed tomography: from the box-counting to the cube-counting algorithm," *European Journal of Soil Science*, vol. 54, no. 3, pp. 569–579, 2003.

[5] A. M. Tarquis, R. J. Heck, D. Andina, A. Alvarez, and J. M. Antón, "Pore network complexity and thresholding of 3D soil images," *Ecological Complexity*, vol. 6, no. 3, pp. 230–239, 2009.

[6] W. Wang, A. N. Kravchenko, A. J. M. Smucker, and M. L. Rivers, "Comparison of image segmentation methods in simulated

2D and 3D microtomographic images of soil aggregates," *Geoderma*, vol. 162, no. 3-4, pp. 231–241, 2011.

[7] P. Iassonov and M. Tuller, "Application of segmentation for correction of intensity bias in x-ray computed tomography images," *Vadose Zone Journal*, vol. 9, no. 1, pp. 187–191, 2010.

[8] P. Iassonov, T. Gebrenegus, and M. Tuller, "Segmentation of X-ray computed tomography images of porous materials: a crucial step for characterization and quantitative analysis of pore structures," *Water Resources Research*, vol. 45, no. 9, 2009.

[9] M. Sezgin and B. Sankur, "Survey over image thresholding techniques and quantitative performance evaluation," *Journal of Electronic Imaging*, vol. 13, no. 1, pp. 146–168, 2004.

[10] A. E. Scheidegger, *The Physics of Flow Through Porous Media*, University of Toronto Press, 1974.

[11] G. W. Horgan, *A Review of Soil Pore Models*, 1996.

[12] E. C. Childs and N. Collisgeorge, "The permeability of porous materials," *Proceedings of the Royal Society of London. Series A*, vol. 201, no. 1066, pp. 392–405, 1950.

[13] T. J. Marshall, "A relation between permeability and size distribution of pores," *Journal of Soil Science*, vol. 9, no. 1, pp. 1–8, 1958.

[14] A. R. Dexter, "Internal structure of tilled soil," *Journal of Soil Science*, vol. 27, no. 3, pp. 267–278, 1976.

[15] C. J. Moran and A. B. McBratney, "A two-dimensional fuzzy random model of soil pore structure," *Mathematical Geology*, vol. 29, no. 6, pp. 755–777, 1997.

[16] H. J. Vogel, "A numerical experiment on pore size, pore connectivity, water retention, permeability, and solute transport using network models," *European Journal of Soil Science*, vol. 51, no. 1, pp. 99–105, 2000.

[17] J. W. Crawford, N. Matsui, and I. M. Young, "The relation between the moisture-release curve and the structure of soil," *European Journal of Soil Science*, vol. 46, no. 3, pp. 369–375, 1995.

[18] P. J. Burt and E. H. Adelson, "The laplacian pyramid as a compact image code," *IEEE Transactions on Communications*, vol. 31, no. 4, pp. 532–540, 1983.

[19] N. Otsu, "A threshold selection method from gray-level histograms," *IEEE Transactions on Systems, Man and Cybernetics*, vol. 9, no. 1, pp. 62–66, 1979.

[20] S. Tanimoto and T. Pavlidis, "A hierarchical data structure for picture processing," *Computer Graphics and Image Processing*, vol. 4, no. 2, pp. 104–119, 1975.

[21] H. J. A. M. Heijmans and J. Goutsias, "Nonlinear multiresolution signal decomposition schemes. II. Morphological wavelets," *IEEE Transactions on Image Processing*, vol. 9, no. 11, pp. 1897–1913, 2000.

[22] H. O. Peitgen, H. Jürgens, and D. Saupe, *Chaos and Fractals: New Frontiers of Science*, Springer, 2004.

[23] D. L. Turcotte, *Fractals and Chaos in Geology and Geophysics*, Cambridge University Press, 1997.

[24] B. B. Mandelbrot, *The Fractal Geometry of Nature*, Henry Holt and Company, San Francisco, Calif, USA, 1982.

[25] K. J. Falconer, *Fractal Geometry: Mathematical Foundations and Applications*, John Wiley & Sons, 1990.

[26] J. Bélair and S. Dubuc, "Fractal geometry and analysis," in *Proceedings of the NATO Advanced Study Institute and Seminaire de Mathematiques Supérieures on Fractal Geometry and Analysis*, Kluwer Academic Publishers, Montreal, Canada, July 1989.

[27] B. B. Chaudhuri and N. Sarkar, "Texture segmentation using fractal dimension," *IEEE Transactions on Pattern Analysis and Machine Intelligence*, vol. 17, no. 1, pp. 72–77, 1995.

[28] T. Ida and Y. Sambonsugi, "Image segmentation and contour detection using fractal coding," *IEEE Transactions on Circuits and Systems for Video Technology*, vol. 8, no. 8, pp. 968–975, 1998.

[29] R. C. Gonzalez, R. E. Woods, and S. L. Eddins, *Matlab : Digital Image Processing Using MATLAB*, Publishing House of Electronics Industry, Beijing, China, 2009.

[30] R. A. Freeze and J. A. Cherry, *Groundwater*, Prentice-Hall, 1979.

[31] I. M. Chakravarti, R. G. Laha, and J. Roy, *Handbook of Methods of Applied Statistics*, John Wiley & Sons, 1967.

[32] J. R. Brown and M. E. Harvey, "Arbitrary precision mathematica functions to evaluate the one-sided one sample K-S cumulative sampling distribution," *Journal of Statistical Software*, vol. 26, no. 3, pp. 1–55, 2008.

Hindawi Publishing Corporation
The Scientific World Journal
Volume 2014, Article ID 565174, 8 pages
http://dx.doi.org/10.1155/2014/565174

Research Article

Risk of Leaching in Soils Amended by Compost and Digestate from Municipal Solid Waste

Marta García-Albacete,[1] Ana M. Tarquis,[2] and M. Carmen Cartagena[1]

[1] *Escuela Técnica Superior de Ingenieros Agrónomos, Universidad Politécnica de Madrid, Ciudad Universitaria sn, 28040 Madrid, Spain*
[2] *CEIGRAM, Campus Sur de Prácticas de la E.T.S. Ingenieros Agrónomos, Universidad Politécnica de Madrid, Ciudad Universitaria, 28040 Madrid, Spain*

Correspondence should be addressed to Marta García-Albacete; martagalba@gmail.com

Received 26 March 2014; Accepted 19 May 2014; Published 3 June 2014

Academic Editor: Antonio Paz González

New European directives have proposed the direct application of compost and digestate produced from municipal solid wastes as organic matter sources in agricultural soils. Therefore information about phosphorus leaching from these residues when they are applied to the soil is increasingly important. Leaching experiments were conducted to determine the P mobility in compost and digestate mixtures, supplying equivalent amounts to 100 kg P ha^{-1} to three different types of soils. The tests were performed in accordance with CEN/TS 14405:2004 analyzing the maximum dissolved reactive P and the kinetic rate in the leachate. P biowaste fractionation indicated that digestate has a higher level of available P than compost has. In contrast, P losses in leaching experiments with soil-compost mixtures were higher than in soil-digestate mixtures. For both wastes, there was no correlation between dissolved reactive P lost and the water soluble P. The interaction between soil and biowaste, the long experimentation time, and the volume of leachate obtained caused the waste's wettability to become an influential parameter in P leaching behavior. The overall conclusion is that kinetic data analysis provides valuable information concerning the sorption mechanism that can be used for predicting the large-scale behavior of soil systems.

1. Introduction

In the EU, between 118 and 138 million tons of biowaste are produced each year, approximately 88 million tons of which are municipal waste. This latter value is projected to increase by 10% by 2020. European standards encourage the recovery of the organic fraction of municipal solid waste (MSW) by composting, anaerobic digestion, or incineration [1], reducing the amount of waste sent to landfills in accordance with the Landfill Waste Directive [2]. In 2006, the EU was host to 124 plants performing anaerobic digestion of biowaste, with an overall treatment capacity of 3.9 million tons y^{-1} and a total annual compost production of 4.8 million tons.

The use of compost and digestate as soil fertilizer provides agronomic advantages, such as the improvement of several soil properties: structure, water infiltration, water-holding capacity, microorganism content (both amount and diversity), and nutrient content [3]. In particular, better phosphorus recycling may reduce the need for mineral fertilizers.

The most recent communication from the Commission to the Council and the European Parliament on future biowaste management steps in the European Union [1] proposed the recovery of both the digestate and compost from MSW anaerobic digestion as sources of stable degraded organic matter (approximately 45% of EU soils are characterized by low levels of humus [4], especially in southern Europe).

This new communication [1] promotes the digestate and the compost from MSW to be directly applied to the soil as valuable sources of organic matter and nutrients. Therefore, it is necessary to study the behavior and interaction of these biowastes with soils to evaluate their optimal use and potential environmental problems.

In many catchments around the world, agriculture is now the major contributor of P to surface waters [5]. The transport of P from agricultural soils to surface waters has been linked to eutrophication in fresh water and estuaries [6–8].

According to a recent document from the EU, "Sustainable phosphorus use" [9], 90% of the total phosphorus entering the food system (mineral fertilizer and organic manure) is lost before reaching the product, mostly via dissipation into the water system. Global losses from the soil to fresh water are estimated at 18.7 to 31.4 million tons per year [10]; in the EU-27, losses to leaching and runoff are estimated at 0.16 million tons per year [11].

Reuse of organic waste has been based on crop nitrogen (N) requirements and usually supplies P in excess of crop needs [12, 13]. Long-term phosphorus application to soils as fertilizer or manure can increase the potential for P loss to ground and surface waters.

These "excessive" soil P concentrations can be measured by environmental soil P-tests, such as water-soluble P (WSP) and FeO-P, which have been linked to P loss from agricultural land, or by agronomic soil tests, such as Mehlich-1 and Mehlich-3, which estimate the P available for crop growth [14–16]. The P source WSP test is a reliable mean for predicting the dissolved reactive P (DRP) concentrations in runoff from surface-applied manures and biosolids [17]. This phosphorus fraction should consist largely of the inorganic orthophosphate (PO_4^{3-}). The concentration of this fraction constitutes an index of the amount of phosphorus immediately available for algal growth. The WSP/TP ratio (the fraction of the total P that is water soluble) allows a more direct comparison of the environmentally relevant P in biosolids and manures with differing chemical and physical properties [18]. For leaching experiments, Sharpley and Moyer [19] found that the amount of P leached from six livestock manures and manure composts was significantly correlated with the water-extractable P in the materials (in the absence of soil). Other authors have suggested that the WSP of the P source materials is a good preliminary predictor for approximating the P leaching loss [20]; however, this may not account for continuous P release from added organic materials during continuous water infiltration.

Leaching and surface runoff experiments allow to evaluate the potential losses of soil P produced by the application of P sources to soils. Although P loss in runoff is considered to be the major contamination route, leaching also causes significant losses. Some authors have suggested that P leaching to groundwater is unimportant because the leaching is negligible [21]; however other authors report that the downward movement of P from organic wastes is potentially significant in areas with shallow groundwater and coarse soil with low P-absorption capacity [22, 23].

Laboratory leaching tests are common tools for assessing the long-term impact of contaminated materials on the soil-groundwater pathway by determining the source term as an expression of the release potential of water-soluble contaminants during the use or disposal of waste materials. These tests provide a flow-through pattern similar to that found in field conditions and permit the basic characterization of waste materials [24]. The release of soluble components upon contact with water is regarded as a main mechanism of release, and this result in a potential risk to the environment during the reuse or disposal of such materials.

Although the soil characteristics are not generally considered to be important in surface runoff tests [25], soil type is relevant in leaching tests due to its effects on the behavior of P, especially in applications by incorporation. The soil adsorption index of P (PSI) was analyzed for its relationship to the P source losses.

The evaluation of the P speciation in biowaste is very important when determining the suitability of biowastes for land application or the optimum application rate.

The physical properties of biowastes are also important. The wettability of biowastes is an important property in the leaching process in soil. Several authors have observed the influence of soil wettability in aggregate stability and the decomposition of soil organic matter [26, 27]. Although strong water repellency has been shown to have negative effects on hydrological process (e.g., soil erosion), a slight increase in water repellency may reduce the breakdown of aggregates and consequently reduce surface sealing, overland flow, and erosion. Hydrophobicity, as a measure of water repellency, caused by organic substances, favors the formation and protection of stable aggregates [28] which, in turn, stabilize the encapsulated organic substances against microbial degradation and mineralization [29, 30].

Wettability may have an important effect on the stabilization of SOM due to a reduction of liquid adsorption rates, accessibility for microorganisms, and restricted accessibility of water and nutrients. Hydrophobic SOM is more stable against microbial decomposition.

In soluble species in the waste that could be lost by leaching, water must pass through the soil profile, wet the waste, and dissolve these species. Soil water repellency has been extensively studied and is mainly caused by organic compounds of various origins and structures [31]. The wettability of soil particles increases with the charge density and fraction of polar groups on the surface [32, 33]. Sorption of organic matter with nonpolar functional groups promotes nonwettable surfaces [34], and long-chain amphiphilic organic compounds produced by a range of biota can induce hydrophobicity in soil [35]. When wetted, these compounds are usually hydrophilic, but drying can cause bonding of hydrophilic (polar) ends of amphiphilic molecules to each other or to particle surfaces, resulting in the exposure of hydrophobic (nonpolar) functional groups to the pore space [36]. This effect can be observed on biowastes after the application of various treatments.

The goals of this work were (a) to quantify the phosphorus leaching losses from organic waste generated in MSW treatment plants and (b) to evaluate the differences in the behaviors of digestate and compost on the potential mobility and P availability in three soil types. To that end, a first-order kinetic model was used to estimate digestate and compost wettability and leaching behavior.

2. Materials and Methods

2.1. P Source Samples. The biowastes applied as P sources were a compost and a digestate from an anaerobic MSW digestion plant, located in southern Madrid. Ten samples (5 kg each) were collected for the residues on different days and combined to produce a single homogenous sample representing each residue.

The digestate was obtained after the anaerobic digestion (21 d, 39°C, and constant agitation) of the organic fraction of MSW followed by dehydration with the addition of flocculants and centrifugation.

Compost was obtained by the composting in tunnels (14 d, 55°C, periodic watering and forced aeration) of a mixture of digestate of MSW and defibered plant matter, with a subsequent static stabilization period and sieving.

The digestate had a pasty texture, forming large clumps, whereas the compost was a powder with a much smaller particle size (<5 mm).

2.2. Chemical Analyses. The study was conducted with the surface horizon (0–20 cm) of three soils, from Madrid (40° 32′ N, 3° 17′ W), Guadalajara (40° 28′ N, 4° 0′ W), and Ciudad Real (39° 0′ N, 3° 56′ W) (Spain). All soil samples were collected in plots from agricultural research stations. These locations were chosen because their histories of P application are well known. The soils selected had not suffered applications of phosphorus in the last five years.

Soil organic matter (SOM) was determined by dry combustion at 540°C for 4 h. Soil pH was determined in a 1 : 5 (v/v) water extract. Soil Olsen-P was extracted with 0.5 M $NaHCO_3$, pH 8.5, for 30 min and analyzed using the Murphy and Riley [37] spectrophotometric method. Calcium (Ca) and iron (Fe) concentration in soil were determined by inductively coupled plasma atomic optical emission spectroscopy (ICP-OES) following USEPA Method 3050A [38] acid digestion (with additions of nitric acid and hydrogen peroxide). The adsorption index of P (PSI) of soils was determined using the method of Bache and Williams [39] as the amount of P adsorbed (X in mg kg^{-1}) after a single addition of a KH_2PO_4 solution containing 75 mg P L^{-1} divided by the logarithm of the P concentration in the equilibrium solution (Ce, mg L^{-1}). OM content, pH, Olsen-P, and calcium (Ca) and iron (Fe) concentrations in compost and digestate were determined with the method described for soils. Total P (TP) levels of compost and digestate were determined from the same extracts used for Ca and Fe sampling. The total solids (TS) contents of compost and digestate were determined by preweighing the subsamples and drying in an oven at 105°C for 24 h. Kjeldahl nitrogen of both materials was determined by acid digestion and distillation over a solution of sodium hydroxide, followed by a back titration. Electrical conductivity (EC) was determined in the same 1 : 5 (v/v) water extract used for pH determination. Soluble organic matter of compost and digestate was analyzed by permanganate oxidation and distillation.

The P chemistry of the materials was extensively characterized. The analysis included the inorganic (IP) and organic P (OP) [40] and the water-soluble P (WSP). IP was extracted with 1 mol L^{-1} HCl, shaken for 16 h, and centrifuged (2500 rpm). The supernatant was filtered (0.45 μm filters), and the extract was collected for IP determination. The previous residue was reused to determine OP, after calcination (450°C, 3 h), extraction with 3.5 mol L^{-1} HCl, shaking for 16 h, and centrifugation. The supernatant was filtered (0.45 μm filters), and the extract was collected for OP determination. WSP was extracted at a 1 : 250 solid-water ratio after 16 h of shaking (end-to-end shaking) followed by filtration (0.45 μm filters).

A modification of the fractionation method of Hedley et al. [41] and Sui et al. [42] described by Huang et al. [43] was employed to extract empirically defined pools of P. The P fractions were designated as WSP, membrane-P, $NaHCO_3$–P, NaOH–P, and HCl-P. Samples were sequentially extracted with deionized water (WSP), deionized water with an anion-exchangeable membrane (membrane-P), 0.5 mol L^{-1} $NaHCO_3$ (pH 8.5) ($NaHCO_3$-P), 1 mol L^{-1} NaOH (NaOH-P), and 1 mol L^{-1} HCl (HCl-P). Total P in filtrates of water, $NaHCO_3$, and NaOH extracts were determined by digesting aliquots of filtrates in an autoclave at 103.5 kPa with acidified $(NH_4)_2S_2O_8$ [44]. P in all the extracts was analyzed by inductively coupled plasma atomic emission spectroscopy (ICP-OES) following USEPA Method 3050A digestion. Labile P includes the sum of IP and OP from water, resin, and $NaHCO_3$ fractions, whereas refractory or unavailable P includes the remaining fractions. The procedure was performed in triplicate on each biowaste sample.

A Sigma force tensiometer and the Washburn technique for the wetting of porous solids were used to estimate the biowaste wettability, with the mass of adsorbed liquid (water, g) measured by weight difference every second for 20 minutes. Finally, biowaste particle size was determined by a granulometric analysis.

2.3. Column Leaching Experiment. The leaching tests were performed according to the European standard CEN 14405 : 2004 "Characterization of waste—Leaching behavior test—Up-flow percolation test" [45].

Thirty glass columns (6 cm in diameter × 21 cm in height) were prepared by adding a layer of 21 cm of each of the three types of topsoils (0–15 cm) from Spanish research centers: soil A (Calcic Haploxerept), soil B (Petrocalcic Palexeralf), and soil C (Typic Haploxeralf) (Soil Survey Staff, 2010). Columns were prepared in triplicate for each experiment. The soils were air-dried, crushed, sieved (<2 mm), and homogenized.

Each soil (600 g) was amended with different P sources at an application rate of 100 kg P ha^{-1} (25.5 g of compost and 11.6 g of digestate, resp.), which is considered too high for agricultural needs. Due to the widespread practice of fertilizer application based on N content, in general, these high rates of P are very common in the field. Appropriate controls of soils without waste application were included, and all treatments were performed in triplicate. The columns were carefully packed to avoid the formation of preferential water paths. Fiberglass was placed in the bottom and top of each column to prevent soil loss.

The columns were saturated with distilled water from the bottom upwards, and the saturation was balanced at room temperature for 72 h. The distilled water was then allowed to flow out of the bottoms of the columns. The leaching was transported continuously for 20 d with a constant flow of 22 mLh^{-1} induced by a peristaltic pump from the bottom of each column. The leachate was collected from the top of the columns. Sixteen stages of leachate per column were collected, with liquid-solid (L/S) ranges of 0.1 to 10 L kg^{-1}.

Leaching fractions were analyzed for dissolved reactive phosphorus (DRP), determined from the filtered samples (0.45 μm) without digestion. The P content was determined by ICP-OES.

2.4. Kinetic Model. A variety of kinetic equations including zero-, first-, and second-order, fractionation-power, and parabolic-diffusion and Elovich equations have commonly been employed over the years to describe the kinetics of soil chemical phenomena [46–48].

In the case of the phosphorus leaching experiment data, P leaching (P) was adjusted to a first-order kinetic model:

$$P = P_{max} \cdot \left(1 - e^{klt}\right). \quad (1)$$

Here, P_{max} ($mgkg^{-1}$) is the maximum phosphorus leaching expected, kl (h^{-1}) is the rate of phosphorus leaching, and t (h) is the time.

The behavior of biowaste wettability (W) as a function of time is expressed as follows:

$$W = Mw \cdot \left(1 - e^{-br \cdot t}\right). \quad (2)$$

Here, Mw (g) is the maximum wettability expected, br (s^{-1}) is the adsorption rate, and t is the time (s).

2.5. Statistical Analysis. Analysis of variance (ANOVA) using the F-test at a significance level of 0.05 was performed to establish the possible significant differences between the mean values of leached phosphorus among the different treatments and soil types.

3. Results

Table 1 provides details of some characteristics of the soils used in this study. The main differences between the soils are the higher clay content of soil A (28%) relative to the other soils, which are sandy (≈70%). Soils A and B are slightly basic (pH 7.5–7.9), whereas soil C is acidic (pH 5.9). All three soils have low levels of organic matter. The Fe and Ca concentrations are higher for soil B (5.0% Ca, 1.4% Fe). Values of PSI indicate the retention capacity of P for each soil. Soil B has the highest P adsorption capacity (112 mg kg^{-1}), and soils A and C have similar P adsorption capacities (30 and 27 mg kg^{-1}, resp.).

A summary of the chemical properties of the digestate and compost used in the study is provided in Table 2.

Total solid content is higher in compost (81.9%) than in digestate (28.2%). The digestate has a lower OM content (45.3%) than the compost (62.0%). With respect to acidity, the compost is neutral (pH = 7.5), whereas the digestate is slightly basic (pH = 8.5). The TP concentration of the digestate (7.49 g kg^{-1}) is about twice that of the compost (3.09 g kg^{-1}). The TP concentration, obtained after the calcination and acid extraction of biowaste, is a useful overall indicator of pollution but provides no information about the solubility of P species, which depends on their chemical forms.

Table 2 shows that IP was higher than OP in both digestate (94%) and compost (91%). The Olsen-P and WSP are much higher for the digestate (55% and 49% of the TP) than for compost (20% and 22% of the TP). Significant differences were observed in the calcium content, which was 5 times lower for digestate than for compost (0.8% and 4.5% for digestate and compost, resp.). The hydrosoluble organic matter content was also lower for digestate than for compost. The analyzed biowastes exhibited low concentrations of heavy metals and trace elements (data not shown).

Percentages of WSP, membrane-P, $NaHCO_3$-P, NaOH-P, and HCl-P with respect to total P for digestate and compost are given in Figure 1. The main P fraction for both biowastes was HCl-P, at 49.6% in digestate and 58.0% in compost, followed by $NaHCO_3$-P (16.4%) in digestate and NaOH-P in compost (19.5%). WSP and membrane-P were the smallest fractions for both biowastes.

The sum of the percentages of TP composed of WSP and membrane-P, designated as "loosely bound-P", is higher for digestate than for compost (18.5% and 6.7% of TP, resp.). The sum of the percentages of loosely bound-P and $NaHCO_3$-P, designated as "labile P", is also higher for digestate than for compost (34.8% and 22.4% of total P, resp.). The large amount of this fraction in digestate indicates high vulnerability for both P leaching and availability to plants.

Digestate has a much higher content of P that is easily lost. In contrast, the compost has high P content in the NaOH-P and HCl-P fractions, indicating that the extracted P is more recalcitrant and therefore more difficult to dispose of.

To characterize the wetting of each residue, Figure 2 shows the amount of water absorbed (g) versus time for the two biowastes studied, digestate and compost. The two residues exhibited totally different behaviors. Digestate initially absorbed water rapidly (up to 100 s); later, the amount of water absorbed was fairly constant, indicating a lower wettability. The compost absorbed a large amount of water relative to its weight, with water absorption increasing steadily throughout the trial (1200 s). Wettability results for digestate and compost were well described by a first-order kinetic model (Figure 2). The water adsorption rate (br) for digestate ($17.9 \cdot 10^{-3}$ s^{-1}) was higher than for compost (1.02 10^{-3} s^{-1}) but the maximum wettability (Mw) was much higher for compost (1.97 ± 0.09 g of adsorbed water per g of waste) than for digestate (0.82 ± 0.05 g of adsorbed water per g of waste).

Figures 3 and 4 represent the DRP (mg P kg^{-1} of soil) lost by leaching as a function of time (h) for digestate and compost in each soil. The total DRP concentration (mg P kg^{-1} of soil) accumulated in 10 L of leachate varies for each type of soil, from 43 ± 1.8 mg P kg^{-1} to 49 ± 1.5 mg P kg^{-1} for the mixtures

Table 1: Chemical characteristics of the soils used in this study.

Parameters	Soil A	Soil B	Soil C
USDA classification	Calcic Haploxerepts	Petrocalcic Palexeralfs	Typic Haploxeralfs
Texture	Clay loam	Sandy clay loam	Sandy loam
Sand, %	55.0	70.4	71.0
Silt, %	17.0	8.0	11.0
Clay, %	28.0	21.6	18.0
pH, w extract 1 : 5	7.5	7.9	5.9
OM, %	1.41	2.22	1.03
Ca, %	0.7	5.0	0.06
Fe, %	1.1	1.4	0.6
Olsen-P, mg kg^{-1}	18.8	17.9	10.1
PSI, mg kg^{-1}	29.9	112.2	26.5

Table 2: Biowaste chemical characterization: compost and digestate.

Parameters*	Digestate	Compost
Particle size, mm	10–25	<5
Total solids, %	28.2	81.9
OM, %	45.3	62.0
Hydrosoluble OM, %	1.1	1.9
EC, dS m^{-1}	6.8	4.7
PH	8.5	7.5
Kjeldahl-N, %	3.2	2.8
TP, g kg^{-1}	7.49	3.09
WSP 1 : 250, g kg^{-1}	3.64	0.69
IP, g kg^{-1}	7.04	2.80
OP, g kg^{-1}	0.39	0.25
Olsen-P, g kg^{-1}	4.11	0.61
Ca, %	0.8	4.5
Fe, %	1.4	0.5

*Dry weight basis.

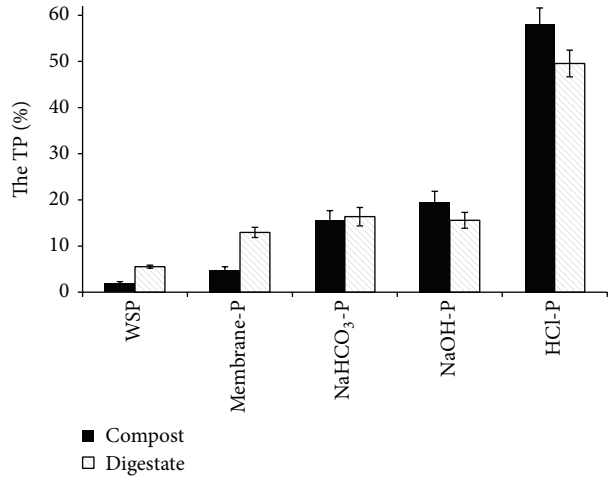

Figure 1: Fractionation of P in compost and digestate.

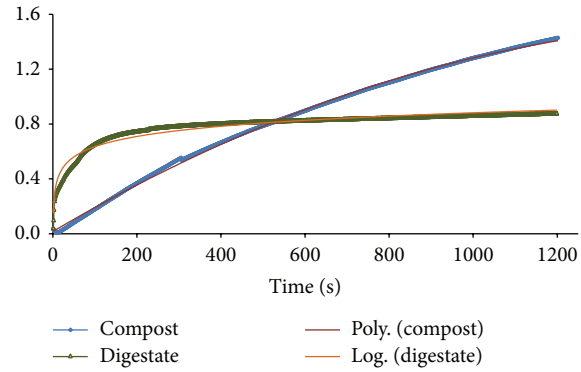

Figure 2: Time evolution of wettability of compost and digestate.

of soil and digestate and from 42 ± 2.1 mg P kg^{-1} to 62 ± 2.3 mg P kg^{-1} for the mixtures of soil and compost. Losses of P vary from 33% to 37% and from 32% to 48% for digestate and compost, respectively.

Losses of DPR in columns amended with compost were more variable and lower for soil B than for soils A and C (Figure 3), which is consistent with the PSI values for each soil type. Soil B has the largest capacity to absorb P (112 mg kg^{-1}) and thus a lower capacity for retention of P, while soils A and C have lower PSI (30 mg kg^{-1} and 27 mg kg^{-1}, resp.). Results in columns amended with digestate were similar for the three soils (Figure 4). Columns of soil with compost, with a lower WSP content (22 % of the TP), lost large amounts of the P applied (from 32% to 47%). In contrast, the DRP losses from the columns treated with the digestate, which have a very high WSP content (49% of the TP), were lower than expected and varied less with the soil type (from 33% to 37%).

The dynamics of phosphorus leaching in the column experiments fitted a first-order kinetic model. Values of kl and P_{max} are shown in Table 3. According to these results, leaching rates (kl) were higher for the soils with digestate (2.3 10^{-3} to 6.7 10^{-3} h^{-1}) than for soils with compost (1.7 10^{-3} to 1.8 10^{-3} h^{-1}).

In all cases, the calculated values for maximum phosphorus leached (P_{max}) were higher for soils with compost (72 to 108 mg kg^{-1}). In soils amended with compost, P_{max} values were significantly higher in soils A and C than in soil B

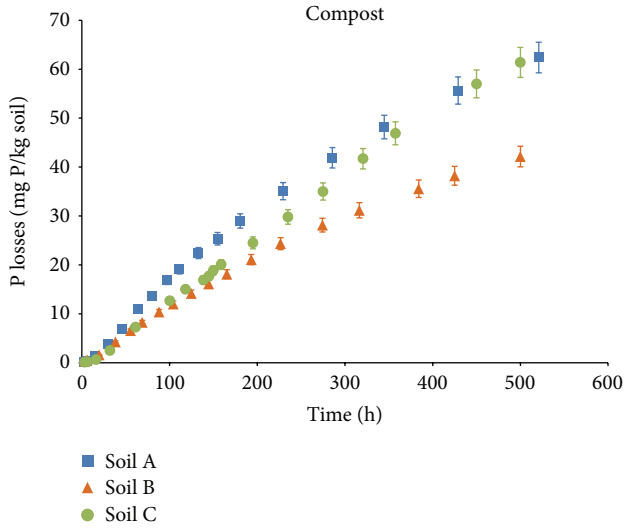

Figure 3: DRP losses by leaching in soil-compost mixtures. Error bars indicate the standard error of the mean ($n = 3$).

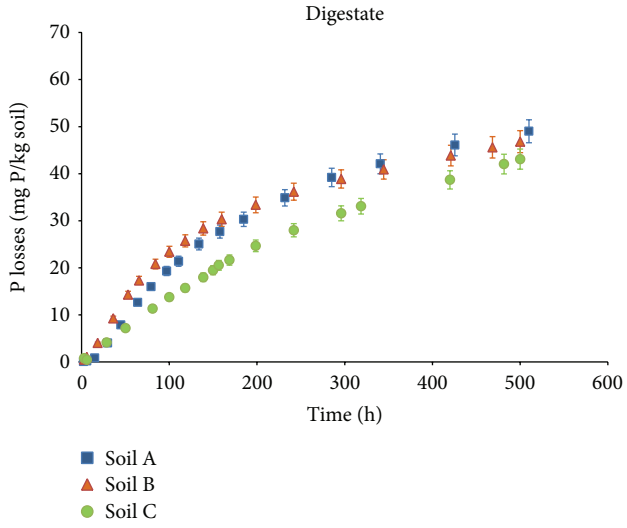

Figure 4: DRP losses by leaching in soil-digestate mixtures. Error bars indicate the standard error of the mean ($n = 3$).

(Table 3). This is consistent with the PSI values (Table 1) that showed lower absorption capacities in soils A and C.

Values of P_{max} for digestate-amended soils ranged from 48 to 62 mg kg^{-1} and again were higher for soils A and C—those two having similar PSI—although the differences from soil B were not statistically significant ($\alpha = 0.05$).

4. Discussion

Leaching of P from soils amended with MSW compost and digestate is a very complex process, involving many factors such as soil properties, waste characteristics, and water transport.

Table 3: First-order kinetic constant (kl) and P maximum leached estimated (P_{max}) for each biowaste and amended soil type.

BIOWASTE	Soil	kl 10^{-3} (h^{-1})	*P_{max} (mg kg^{-1})
Compost	A	1.7	108.0^{Aa}
	B	1.8	72.3^{Ab}
	C	1.7	99.5^{Aa}
Digestate	A	4.4	54.6^{Ba}
	B	6.2	47.8^{Ba}
	C	2.3	61.9^{Ba}

*Same capital letters within a soil type indicate that there were no significant differences between the biowaste type at $\alpha = 0.05$. Same lowercase letters within the same biowaste type indicate that there were no significant differences between soil types.

The application of these wastes produces interactions between P and soil components, depending on the physical and chemical properties of soils and wastes. Water-extractable P (WSP) and Olsen-P determinations are potentially useful to identify sources of P loss, but, in this experiment, none of these factors were correlated with P leaching from the digestate-soil and compost-soil mixtures.

The scientific community has agreed that characterization of P in biowastes is vital to finding indicators that provide significant information about the expected behavior of P when biowastes are applied to soils.

Our results indicate that considering only the biowaste WSP as an indicator of P leaching loss is not a good practice because there was no correlation between the WSP of each residue and the DRP content in the leachate ($r^2 = 0.304$). In almost all the experiments, the losses of P are higher in the compost-soil mixture than in the digestate-soil mixture, which is the opposite of the results expected from P fractionation analysis.

The behavior of the biowastes in wettability experiments can help to explain the results obtained in leaching columns. The digestate presents a lower wettability and consequently a lower interaction between the P in the digestate and the flow leachate. The compost, with a higher wettability, produces higher losses of P by leaching, although its WSP is lower. This demonstrates that the interaction between compost and water in the leaching columns is higher.

It is also important to note that compost has a larger overall surface area in contact with the water than the digestate, because the compost particle size is much smaller.

Kinetic data analysis aids our understanding of the sorption mechanism and prediction of the large-scale behavior of soil systems (Table 3). The rate of phosphorus leaching is similar for the three soils studied when compost is used as the amendment. In the case of digestate application, the constant rates are always higher than for compost, and they are more dependent on soil type. Lower losses were found for soil B (with the highest PSI) than for soil A and C (with similar, lower PSI).

5. Conclusions

As recent works have demonstrated, leaching losses of P by application of organic wastes cannot be neglected. Measuring

biowaste for P indices (WPS, TP, or Olsen-P) that determine soluble or labile P are not useful for assessing P loss by leaching, though this is a practice currently applied in runoff experiments. Instead, it is necessary to evaluate other characteristics of the biowastes. In this experiment, waste wettability has been useful for explaining P losses.

The soil PSI is important for assessing potential P losses by leaching; however, the influence of soils is different for the two types of biowaste. The maximum phosphorus leached in soils amended with compost is significantly dependent on soils and consistent with the PSI values. In contrast, soils amended with digestate present lower total P losses, and the effect of soil is not significant. This phenomenon may be due to the lower soil-waste interaction as a consequence of digestate wettability.

Finally, our overall conclusion is that the P leaching rate depends mainly on the biowaste type and is less dependent on the soil type. However, the maximum amount of P leached depends on both the type of waste and the soil characteristics.

Abbreviations

MSW: Municipal solid waste
WSP: Water-soluble phosphorus
DRP: Dissolved reactive phosphorus
TP: Total phosphorus
FeO-P: Phosphorus extracted by iron oxide
PSI: Soil adsorption index of phosphorus
TS: Total solid
OM: Organic matter
W: Wettability
Mw: Maximum wettability
Br: Biowaste rate
P_{max}: Maximum phosphorus leaching
kl: Rate of phosphorus leaching.

Conflict of Interests

The authors declare that there is no conflict of interests regarding the publication of this paper.

References

[1] COM 235 final, *European Commission*, Communication from the commission to the council and the European Parliament on future step in biowaste management in the European Union, Brussels, Belgium, 2010.

[2] Directive 1999/31/EC of 26 April 1999 on the landfill of waste.

[3] F. Amlinger, S. Nortcliff, K. Weinfurtner, and P. Dreher, "Applying compost—benefits and needs," in *A seminar 22-23 November 2001 (BMLFUW '2003)*, European Commission, Vienna and Brussels, Brussels, Belgium, November 2003.

[4] A. Jones, P. Panago, S. Barcelo et al., 2012, The state of soil in Europe—A contribution of the JRC to the European agency's Environment State and Outlook Report, SOEL 2010.

[5] OECD, *Environmental Indicators For Agriculture*, Organization for Economic Cooperation and Development, Paris, France, 2001.

[6] D. F. Boesch, R. B. Brinsfield, and R. E. Magnien, "Chesapeake bay eutrophication: scientific understanding, ecosystem restoration, and challenges for agriculture," *Journal of Environmental Quality*, vol. 30, no. 2, pp. 303–320, 2001.

[7] B. J. Bush and N. R. Austin, "Landscape and watershed processes: timing of phosphorus fertilizer application within an irrigation cycle for perennial pasture," *Journal of Environmental Quality*, vol. 30, no. 3, pp. 939–946, 2001.

[8] T. C. Daniel, A. N. Sharpley, and J. L. Lemunyon, "Agricultural phosphorus and eutrophication: a symposium overview," *Journal of Environmental Quality*, vol. 27, no. 2, pp. 251–257, 1998.

[9] Science of Enviromental Policity, *Sustainable Phosphorus Use*, European Commission, 2013.

[10] Y. Liu, G. Villalba, R. U. Ayres, and H. Schroder, "Global phosphorus flows and environmental impacts from a consumption perspective," *Journal of Industrial Ecology*, vol. 12, no. 2, pp. 229–247, 2008.

[11] K. C. Van Dijk, J. P. Lesschen, P. A. I. Ehlert, and O. Oenema, "Present and future P use in the EU-27: food system scenario analyses," in *Sustainable Phosphorus Use*, Science for Environment Policy, 2013.

[12] A. N. Sharpley, S. Herron, and T. Daniel, "Overcoming the challenges of phosphorus-based management in poultry farming," *Journal of Soil and Water Conservation*, vol. 62, no. 6, pp. 375–389, 2007.

[13] X.-L. Huang and M. Shenker, "Water-soluble and solid-state speciation of phosphorus in stabilized sewage sludge," *Journal of Environmental Quality*, vol. 33, no. 5, pp. 1895–1903, 2004.

[14] A. N. Sharpley, J. S. Robinson, and S. J. Smith, "Bioavailable phosphorus dynamics in agricultural soils and effects on water quality," *Geoderma*, vol. 67, no. 1-2, pp. 1–15, 1995.

[15] J. T. Sims and S. E. Heckendorn, *Methods of Analysis of the University of Delaware Soil Testing Laboratory*, University of Delaware, Newark, Del, USA, 1991.

[16] D. H. Pote, T. C. Daniel, A. N. Sharpley, P. A. Moore Jr., D. R. Edwards, and D. J. Nichols, "Relating extractable soil phosphorus to phosphorus losses in runoff," *Soil Science Society of America Journal*, vol. 60, no. 3, pp. 855–859, 1996.

[17] H. A. Elliott, R. C. Brandt, and G. A. O'Connor, "Runoff phosphorus losses from surface-applied biosolids," *Journal of Environmental Quality*, vol. 34, no. 5, pp. 1632–1639, 2005.

[18] R. C. Brandt, H. A. Elliott, and G. A. O'Connor, "Water-extractable phosphorus in biosolids: Implications for land-based recycling," *Water Environment Research*, vol. 76, no. 2, pp. 121–129, 2004.

[19] A. Sharpley and B. Moyer, "Phosphorus forms in manure and compost and their release during simulated rainfall," *Journal of Environmental Quality*, vol. 29, no. 5, pp. 1462–1469, 2000.

[20] J. Kang, A. Amoozegar, D. Hesterberg, and D. L. Osmond, "Phosphorus leaching in a sandy soil as affected by organic and inorganic fertilizer sources," *Geoderma*, vol. 161, no. 3-4, pp. 194–201, 2011.

[21] A. J. Peterson, P. E. Speth, R. B. Corey, T. W. Wright, and P. L. Schlecht, "Effect of twelve years of liquid digested sludge application on the soil phosphorus level," in *Sewage Sludge: Land Utilization and the Environment*, C. E. Clapp, Ed., pp. 237–247, SSSA, Madison, Wis, USA, 1994.

[22] P. Lu and G. A. O'Connor, "Biosolids effects on phosphorus retention and release in some sandy Florida soils," *Journal of Environmental Quality*, vol. 30, no. 3, pp. 1059–1063, 2001.

[23] W. G. Harris, R. D. Rhue, G. Kidder, R. B. Brown, and R. Littell, "Phosphorus retention as related to morphology of sandy coastal plain soil materials," *Soil Science Society of America Journal*, vol. 60, no. 5, pp. 1513–1521, 1996.

[24] N. Roussat, J. Méhu, M. Abdelghafour, and P. Brula, "Leaching behaviour of hazardous demolition waste," *Waste Management*, vol. 28, no. 11, pp. 2032–2040, 2008.

[25] P. J. A. Kleinman and A. N. Sharpley, "Effect of broadcast manure on runoff phosphorus concentrations over successive rainfall events," *Journal of Environmental Quality*, vol. 32, no. 3, pp. 1072–1081, 2003.

[26] M.-O. Goebel, S. K. Woche, and J. Bachmann, "Quantitative analysis of liquid penetration kinetics and slaking of aggregates as related to solid-liquid interfacial properties," *Journal of Hydrology*, vol. 442-443, pp. 63–74, 2012.

[27] M.-O. Goebel, J. Bachmann, S. K. Woche, and W. R. Fischer, "Soil wettability, aggregate stability, and the decomposition of soil organic matter," *Geoderma*, vol. 128, no. 1-2, pp. 80–93, 2005.

[28] L. A. Sullivan, "Soil organic matter, air encapsulation and water-stable aggregation," *Journal of Soil Science*, vol. 41, no. 3, pp. 529–534, 1990.

[29] J. M. Tisdall, "Formation of soil aggregates and accumulation of soil organic matter," in *Structure and Organic Matter Storage in Agriculture Soils*, M. R. Carter and B. A. Stewart, Eds., pp. 57–96, Advances in Soil Science, 1996.

[30] J. M. Tisdall and J. M. Oades, "Organic matter and water-stable aggregates in soils," *Journal of Soil Science*, vol. 33, no. 2, pp. 141–163, 1982.

[31] S. H. Doerr and A. D. Thomas, "The role of soil moisture in controlling water repellency: new evidence from forest soils in Portugal," *Journal of Hydrology*, vol. 231-232, pp. 134–147, 2000.

[32] J. Bachmann, M.-O. Goebel, and S. K. Woche, "Small-scale contact angle mapping on undisturbed soil surfaces," *Journal of Hydrology and Hydromechanics*, vol. 61, no. 1, pp. 3–8, 2013.

[33] J. Bachmann, R. Horton, T. Ren, and R. R. Van Der Ploeg, "Comparison of the thermal properties of four wettable and four water-repellent soils," *Soil Science Society of America Journal*, vol. 65, no. 6, pp. 1675–1679, 2001.

[34] R. H. Ellerbrock, H. H. Gerke, J. Bachmann, and M.-O. Goebel, "Composition of organic matter fractions for explaining wettability of three forest soils," *Soil Science Society of America Journal*, vol. 69, no. 1, pp. 57–66, 2005.

[35] P. Capriel, T. Beck, H. Borchert, J. Gronholz, and G. Zachmann, "Hydrophobicity of the organic matter in arable soils," *Soil Biology and Biochemistry*, vol. 27, no. 11, pp. 1453–1458, 1995.

[36] P. D. Hallett, J. Bachmann, H. Czachor, E. Urbanek, and Z. Bin Zhang, "Hydrophobicity of soil," in *Encyclopedia of Agrophysics*, J. Glinski, J. Horabik, and J. Lipiec, Eds., pp. 378–383, Springer, 2010.

[37] J. Murphy and J. P. Riley, "A modified single solution method for the determination of phosphate in natural waters," *Analytica Chimica Acta*, vol. 27, pp. 31–36, 1962.

[38] USEPA, *Process Design Manual: Land Application of Sewage Sludge and Domestic Septage*, Centre for Environmental Research, Cincinnati, Ohio, USA, 1995.

[39] B. W. Bache and E. G. Williams, "A phosphate sorption index for soils," *Journal of Soil Science*, vol. 22, no. 3, pp. 289–301, 1971.

[40] J. D. H. Williams, T. Mayer, and J. O. Nriagu, "Extractability of phosphorus from phosphate minerals common in soils and sediments," *Soil Science Society of America Journal*, vol. 44, no. 3, pp. 462–472, 1980.

[41] M. J. Hedley, J. W. B. Stewart, and B. S. Chauhan, "Changes in inorganic and organic soil phosphorus fractions induced by cultivation practices and by laboratory incubations," *Soil Science Society of America Journal*, vol. 46, no. 5, pp. 970–976, 1982.

[42] Y. Sui, M. L. Thompson, and C. Shang, "Fractionation of phosphorus in a Mollisol amended with biosolids," *Soil Science Society of America Journal*, vol. 63, no. 5, pp. 1174–1180, 1999.

[43] X.-L. Huang, Y. Chen, and M. Shenker, "Chemical fractionation of phosphorus in stabilized biosolids," *Journal of Environmental Quality*, vol. 37, no. 5, pp. 1949–1958, 2008.

[44] L. S. Clesceri, A. E. Greenberg, and A. D. Eaton, *Standards Methods For the Examination of Water and wasteWater*, American Public Health Association, Washington, DC, USA, 20th edition, 1998.

[45] CEN/TS 14405: 2004, Characterization of waste, Leaching behaviour tests, Up-flow percolation test (under specified conditions).

[46] Y. S. Ho and G. McKay, "Sorption of dye from aqueous solution by peat," *Chemical Engineering Journal*, vol. 70, no. 2, pp. 115–124, 1998.

[47] K. P. Raven and L. R. Hossner, "Soil phosphorus desorption kinetics and its relationship with plant growth," *Soil Science Society of America Journal*, vol. 58, no. 2, pp. 416–423, 1994.

[48] D. L. Sparks, *Kinetics of Soil Chemical Processes*, Academic Press, New York, NY, USA, 1989.

Hindawi Publishing Corporation
The Scientific World Journal
Volume 2014, Article ID 856352, 8 pages
http://dx.doi.org/10.1155/2014/856352

Review Article

Soil Physicochemical and Biological Properties of Paddy-Upland Rotation: A Review

Wei Zhou,[1,2] Teng-Fei Lv,[1,3] Yong Chen,[1,2] Anthony P. Westby,[2] and Wan-Jun Ren[1,2]

[1] *Key Laboratory of Crop Eco-Physiology and Farming System in Southwest China, Ministry of P.R. China, Wenjiang, Sichuan 611130, China*
[2] *College of Agronomy, Sichuan Agricultural University, Wenjiang, Sichuan 611130, China*
[3] *Rice Research Institute, Sichuan Agricultural University, Wenjiang, Sichuan 611130, China*

Correspondence should be addressed to Wan-Jun Ren; rwjun@126.com

Received 1 February 2014; Revised 26 April 2014; Accepted 16 May 2014; Published 2 June 2014

Academic Editor: Antonio Paz González

Paddy-upland rotation is an unavoidable cropping system for Asia to meet the increasing demand for food. The reduction in grain yields has increased the research interest on the soil properties of rice-based cropping systems. Paddy-upland rotation fields are unique from other wetland or upland soils, because they are associated with frequent cycling between wetting and drying under anaerobic and aerobic conditions; such rotations affect the soil C and N cycles, make the chemical speciation and biological effectiveness of soil nutrient elements varied with seasons, increase the diversity of soil organisms, and make the soil physical properties more difficult to analyze. Consequently, maintaining or improving soil quality at a desirable level has become a complicated issue. Therefore, fully understanding the soil characteristics of paddy-upland rotation is necessary for the sustainable development of the system. In this paper, we offer helpful insight into the effect of rice-upland combinations on the soil chemical, physical, and biological properties, which could provide guidance for reasonable cultivation management measures and contribute to the improvement of soil quality and crop yield.

1. Introduction

Green Revolution technologies have allowed the food supply of Asia to satisfy the demand of its rapidly growing population in the past decades; however, the pressure on soil and other resources has intensified [1]. The cultivated area is continuously decreasing because of soil pollution, land abandonment, urbanization, and other reasons [2]. Meanwhile, the population and the demand for food continue to increase. Under such a situation, increasing cropping intensity from monoculture to double or triple cropping in a year is an efficient way to guarantee food security on the amount of agricultural land now available.

Paddy-upland rotation is the most important cropping system in southern and eastern Asian countries such as Bangladesh, China, India, Nepal, and Pakistan [3]. This type of rotation has many different sequences, where numerous grain and industrial crops could be rotated with paddy rice. The rotation between rice and dry season crops has a long history; rice-wheat rotation, which is one of the largest and most important agricultural production systems in the world, started during the Tang Dynasty of China [4]. Rice-wheat rotation, which accounts for approximately 13.5 million ha of the Indo-Gangetic Plains of Bangladesh, India, Nepal, and Pakistan and approximately 10.5 million ha of fields in China, is essential to meeting the food demand of the rapidly increasing human population [5, 6]. However, the current situation is not very optimistic, because the cultivated areas of rice and wheat have declined in the last decade [7]. What is worse, previous study of long-term continuous cropping experiments in Asia has reported the yield stagnation or even declination of rice-wheat cropping system [8].

Many studies on this issue have been conducted because the sustainability of rice-based cropping systems is important to the food security of Asia. Changes in soil properties caused by cultivation and management and their consequences to soil productivity have generated significant research concern for many years. Evidence indicates that the degradation of

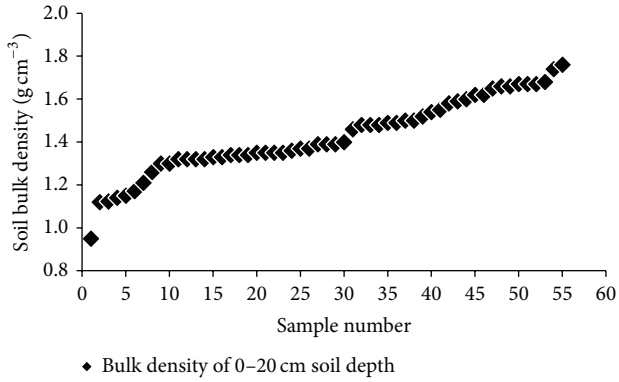

Figure 1: Variation in soil bulk density of paddy-upland rotations. Data are from [2, 13, 14, 19–24].

soil quality is a key factor for the observed declining yield [9]. As a result, researchers have studied the influences of paddy-upland rotation on soil quality and developed effective cultivation and management strategies to sustain soil fertility and maximize crop yield per unit input. In consideration of the unique feature of paddy-upland rotation, all of the soil remediation methods used in this cropping system should consider the different effects on paddy and dry season crops and their interactions with one another. In this study, we reviewed the soil chemical, physical, and biological properties of rice-based cropping systems and identified the aspects that need special attention and consideration to gain guiding references for future research and to contribute to the sustainable development of paddy-upland rotation.

2. Soil Physical Properties of Paddy-Upland Rotation

Rice and upland crops are grown annually in sequence influence each other; however, the soil conditions required by rice growth differ from those required by upland crops. Soil is puddled before rice transplanting and kept flooded to create anaerobic conditions for rice growth. By contrast, upland crops are grown in well-drained soil under tillage and aerobic conditions. Several benefits have been found in rice cultivated under puddled condition. Puddling created a plow layer that reduces hydraulic conductivity to support water ponding, which minimized the water percolation losses and enhanced the water and nutrient use efficiency of rice [10]. Puddling triggered a series of changes in soil physical properties. Puddling deteriorated soil physical properties by breaking down soil aggregates, forming hardpans at shallow depth that leaded to induced changes in pore size distribution; the cone index decreased after puddling and gained strength during the subsidence stage of the puddle soil, and the bulk density (BD) of soil increased and hydraulic conductivity decreased 30 and 60 days after puddling [11]. All of the above mentioned changes are believed to have negative effects on the following upland crop [2].

Paddy-upland rotation could change the soil physical properties of long-term-flooded paddy. Studies have indicated that after the application of paddy-upland rotation, the adverse effects in the long-term-flooded paddy fields have shown slight improvements, such as increased soil granular structure and capillary porosity, improved redox potential of soil, and removed secondary gleization. For instance, Huang and Ding [12] showed that soil water-stable aggregate increased by 12.54% after paddy-upland rotation is applied. However, the influence of paddy-upland rotation on BD had different results. Motschenbacher et al. [13] indicated that BD differed among common rice-based cropping systems; however, even after 10 years of continuous production on a silt-loam soil, increased near-surface soil BD has not been achieved. A successive 10-year experiment showed that the BD of the 0 cm to 10 cm layer soil of paddy-upland rotation was 23.4% higher than that of the continuous cropping of semilate rice [14]. BD, which is an indicator of soil quality, increases with time as particles settle after puddling is halted [10]; this indicator is inversely related to many important soil properties, including water-holding capacity, soil particle size, total porosity, infiltration capacity, hydraulic conductivity, gas exchange, and nutrient mobility, which could influence seedling emergence and root penetration. The compaction of paddy soil leads to low germination rates and limits root development in deep soils for subsequent upland crops [15–17]. Data from rice-wheat systems have shown 8% to 9% reduction in wheat yield when wheat was sown after puddled transplanted rice in comparison with being sown after dry direct-seeded rice without puddling. However, the conflicts between puddled rice and succeeding crops are not consistently observed. Farooq et al. [18] concluded that the effect of puddling on succeeding crops varies for different types of soil and crops and pointed out that much of this response inconsistency is likely related to the site-specific nature of soil puddling.

There is a large variation in soil BD of paddy-upland rotations, which ranges from 0.9 g cm^{-3} to 1.8 g cm^{-3} [2, 13, 14, 19–24] (Figure 1). This difference may be due to different soil types and textures and different cultivation and management measures, such as puddling intensity and depth [25, 26]. Under the condition of paddy-upland rotation, the change of soil physical properties is a complex process, and such change is influenced not only by the soil original properties and crop growth but also by the production and operation practice of farmers. The damaging effect of continuous cultivation with frequent tillage has long been recognized; thus, minimum

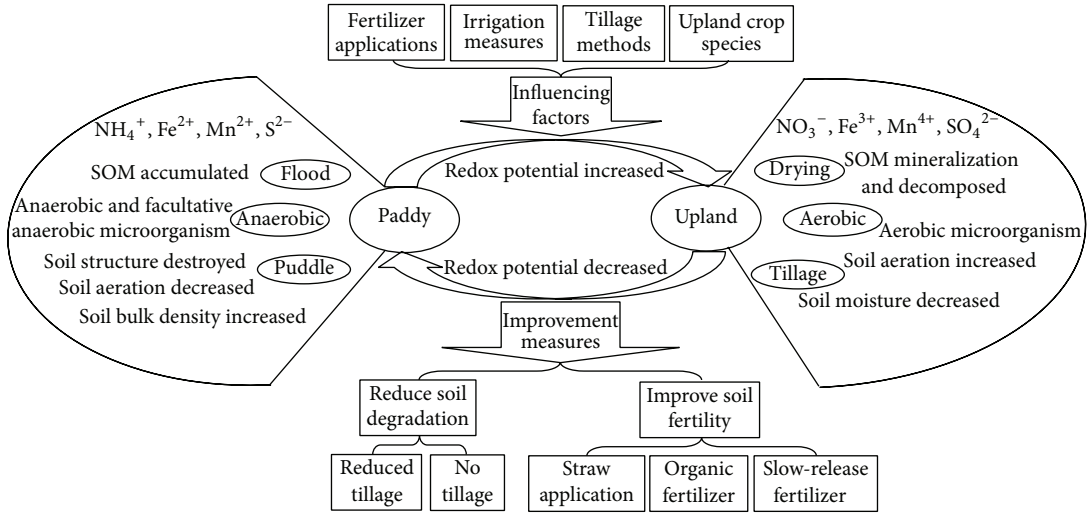

Figure 2: Characteristics of paddy-upland rotation and its improvement measures. SOM: soil organic matter.

tillage systems, namely, no-tillage or zero tillage (ZT), are practiced to maintain and improve the soil quality of paddy-upland rotation. Compared with conventional tillage (CT), ZT, which has minimal soil disturbance and soil structure destruction, promotes the formation of macroaggregates, increases water-stable aggregates, aggregate stability, and least-limiting water range, and decreases BD and soil penetration resistance [27, 28]. However, Gathala et al. [2] indicated that ZT in wheat and CT in rice made the benefits of ZT attained during the wheat phase lost in the rice phase. For paddy-upland rotations, ZT technology is more effective for rice production, upland crop production, or both.

3. Soil Chemical Properties of Paddy-Upland Rotation

3.1. Main Seasonal Changes Driven by Paddy-Upland Rotation. Soil fertility must be maintained to sustain and improve long-term agricultural productivity, that is, crop yields. Comparison of soil under natural vegetation and adjoining cultivated topsoil has revealed that prolonged agricultural land use alters the magnitude, diversity, and spatial variability of a number of soil properties, primarily those related to fertility [1]. Paddy-upland rotation fields are unique from other wetland or upland soils, because of the seasonal alternation of wetting and drying and the frequent alternation of anaerobic and aerobic conditions; the chemical speciation and biological effectiveness of soil nutrient elements vary with seasons (Figure 2). Under flooded conditions, the redox potential of paddy is low and NO_3^-, Fe^{3+}, Mn^{4+}, and SO_4^{2-} are, respectively, reduced to NH_4^+, Fe^{2+}, Mn^{2+}, and S^{2-}. Thus, flooding also improves the availabilities of P, K, Si, Mo, Cu, and Co and reduces the availabilities of N, S, and Zn. By contrast, during the upland crop season, the redox potential is increased, thereby oxidizing the soil nutrient elements and changing the effectiveness of the abovementioned elements [4]. Gupta et al. [29] argued that in most lowland rice soils, P availability initially increased on flooding and rice may meet its P requirement from the residual P applied to the receding wheat. Li et al. [30] indicated that the efficiency of K fertilizer application is affected by various factors, and both rice and the subsequent crop remove enormous amounts of K, resulting in a significant negative K balance in soils regardless of whether K fertilizers are applied at recommended doses. Mn deficiency, which is common in the wheat of rice-wheat rotation systems in China [31] and India [32], leads to the decline in wheat yield. Except for the sporadic use of micronutrients of paddy-upland rotation [20], the decrease in Mn availability in upland field is the main reason for the Mn deficiency [33]. The change in soil moisture content also influences soil pH, thereby affecting the chemical equilibrium and consequently changing the form and effectiveness of soil nutrient elements [34].

3.2. Soil C and N Cycles under Paddy-Upland Rotation Condition. Soil productivity is closely linked with soil organic matter (SOM) status, which is important for nutrient mineralization, soil structural improvements, and favorable soil-water relations [25]. Soil structural degradation is common in intensively cultivated ecosystems because of SOM depletion [35]. Tiessen et al. [36] reported approximately a 1% loss in organic carbon per year during the first 20 years to 30 years in soils under cereal cultivation. SOM decomposition is generally slower in water-logged soil than in well-aerated soil; however, the frequent cycling between anaerobic and aerobic conditions of paddy-upland rotation results in a greater rate of SOM decomposition [13]. During rice season, the number and activity of reducing bacteria are increasing, which not only leads to the lower decomposition of organic matter and contributes to SOM accumulation but also promotes the production of toxic substances such as CH_4 [37]. During upland crop season, the biological N fixation is reduced and SOM mineralization is facilitated, thereby accelerating SOM loss [38]. Kumari et al. [39] posited that soil C is incorporated first into macroaggregates (>0.25 mm) and then forms the core of new microaggregates; this physical protection of C

within macroaggregates limits its oxidation by creating a less favorable environment for microbial activity and thus reduces its decomposition rate by half or more. As a result, the excessive tillage and extractive farming practices reduce SOC stocks. Imbalanced or inappropriate fertilizer practices and intensive cropping with no return of crop residues and other organic inputs also result in SOM loss [40]. Soil types and the choice of crop species could also affect SOM content. Result shows that lighter soil texture had higher decomposable organic C and total C declined than heavy soils [1].

With its negative effects on the environment, the use of N fertilizers and its cycle has received research interest for several years. N fertilizer application is the most important source of soil N, and the three major paths of N losses (ammonia volatilization, denitrification, and leaching) are all influenced by N application, soil moisture state, and tillage practice; consequently, the paddy-upland rotation significantly affects the soil N cycle because of the contrasting soil and water conditions and different nutrients required by the two crops. Research has confirmed that N_2O emission mainly occurs during the drying period of soil rather than during the flooding period, indicating that the alternation of wetting and drying could improve N_2O emission [41]. Other field trials have revealed that the accumulation of inorganic N during upland crop season would be lost to the environment immediately after flooding [42]. Bueno and Ladha [1] found that a clear association exited between organic matter parameters and N uptake and that declining C pools caused lower N uptake. Moreover, soil C and N cycles influence each other through microbiological action.

The interactions between paddy rice and upland crops make the soil C and N cycles more complicated, thereby increasing the difficulty of water and nutrient management of paddy-upland rotation. Paddy-upland rotation is generally harmful for soil C and N storage under the current condition of the cultivation and management practice of farmers. The changes in soil fertilizer before and after experiment under different land utilizing types are shown in Table 1 [14, 19, 20, 40, 43–48]. The effect of the same paddy-upland rotation (rice-wheat) on soil fertilizer varies in different experiments. Compared with other land utilizing types, such as upland-upland rotation, rice-fallow, and fallow, paddy-upland rotation, particularly rice-wheat rotation, is inefficient for maintaining or improving soil fertility. Meanwhile, the rice-Chinese milk vetch rotation could increase soil N content. Researchers have demonstrated that the benefits of legumes in rotation are not only caused by biological N fixation but also by increased nutrient availability, enriched soil fertility, improved soil structure, reduced disease incidence, and increased mycorrhizal colonization, which could help to sustain the long-term productivity of cereal-based cropping systems [49]. Therefore, the rice-wheat cropping system could be diversified by using legumes as substitute crop. The application of organic fertilizers, including green manure, farmyard manure, crop residues or straws, and compost manure, is also an effective measure of improving soil fertility and maintaining land productivity. However, at the present status of organic fertilizer application and the characteristics of nutrient utilization and cycling, three differences should be clarified before using organic fertilizers in paddy-upland rotations: the nutrient content of different organic fertilizers and its release characteristics; the fertilizer requirement rule of different crops, such as require time and amount; and the interactions between rice and different upland crops, such as the influence of residual soil fertility on the following crops. Accordingly, we can guarantee the optimizing timing and doses for using organic fertilizers and ensure the effective utilization of fertilizers.

4. Soil Biological Properties of Paddy-Upland Rotation

Soil microorganisms are involved in various biochemical processes and are vital in maintaining soil fertility and plant yields. The diversity of rhizosphere microorganisms is beneficial to soil health, and the trophic interactions within the rhizosphere affect the aboveground community of plants [50, 51]. Different plants have different soil microbial communities, and crop rotation provides greater concentration and diversity of organic materials, both of which may lead to greater diversity of microbial communities.

Several studies have reported a positive effect of crop rotation on the abundance of beneficial microorganisms. Cropping systems could markedly affect the composition, abundance, diversity, and activity of soil bacterial communities; evidence shows an association between crop type and microbial community composition. For instance, *Bradyrhizobium* sp. and *Herbaspirillum* sp. colonize the interior of rice roots when grown in rotation with a legume crop, which may promote rice growth and productivity [52]. Furthermore, the availability of soil microorganisms increases the availability of plant nutrient elements, especially N and P [53]. Therefore, Xuan et al. [54] indicated that appropriate crop rotation provides a feasible practice for maintaining equilibrium in soil microbial environment for sustainable rice cultivation.

Other effects of crop rotation on soil biological properties are diseases, especially soil-borne diseases, and weed suppression. Different crop species with diverse root exudates and plant residues create varying patterns of resource competition, allelopathic interference, soil disturbance, and mechanical disruptions [55, 56], which lead to an unstable and frequently inhospitable environment where little organisms could survive [57]. Studies have shown that crop rotation is an effective method for reducing crop pests and diseases. The *Sclerotinia* stem rot of oilseed rape, which is caused by *Sclerotinia sclerotiorum*, is one of the most common fungal diseases of rapeseed. Ding [58] indicated that sclerotinias could only survive 20 days under flooded condition and that the paddy-upland rotation could reduce the incidence. Yuan et al. [59] showed that the incidence of the disease of sesame-rape rotation was 32.2% higher than that of rice-rape rotation. *Verticillium* wilt, which is caused by soil-borne fungus, is a worldwide disease affecting temperate and subtropical regions that causes vascular wilt in many plant species [60]. Ebihara et al. [61] demonstrated that paddy-upland rotation could completely control the *Verticillium* wilt of eggplant and strawberry. Marenco and Santos [62] showed

Table 1: Changes in soil fertilizer before and after experiment under different land utilizing types.

Reference	Crop rotation	Before experiment					After experiment				
		Soil depth (cm)	SOC ($g\,kg^{-1}$)	Total N ($g\,kg^{-1}$)	Total P ($g\,kg^{-1}$)	Available P ($mg\,kg^{-1}$)	Soil depth (cm)	SOC ($g\,kg^{-1}$)	Total N ($g\,kg^{-1}$)	Total P ($g\,kg^{-1}$)	Available P ($mg\,kg^{-1}$)
[14]	Rice—fallow	0–20	13.4	1.74	0.75	7.5	0–10	19.94	2.10	1.07	9.40
							10–20	20.47	2.14	0.65	11.10
	Rice—wheat						0–10	18.60	1.82	0.59	20.70
							10–20	17.60	1.78	0.89	19.50
[19]	Rice—fallow	0–20	15.6	2.53	0.62	/	0–10	12.53	2.46	0.53	/
							10–20	12.88	2.36	0.47	
	Rice—rye grass		14.8	2.50	0.63	/	0–10	12.35	2.67	0.67	
							10–20	10.79	2.48	0.54	
	Rice—Chinese milk vetch		16.9	2.46	0.66	/	0–10	14.97	2.92	0.59	
							10–20	12.41	2.61	0.49	
[20]	Rice—wheat	0–15	/	1.35	/	8.5	0–15	/	1.40	/	11.40
[39]			3.6	/	/	10.0	0–15	4.10	/	/	6.40
[42]			3.2	/	/	11.8	0–15	2.90	/	/	16.10
[43]			5.3	/	/	/	0–15	3.75	/	/	/
[44]	Rice—wheat	0–20	12.3	1.70	/	5.2	0–5	17.0	1.80	/	8.25
							5–12	16.30	1.56		6.83
							12–24	11.0	1.05		1.44
[45]	Fallow	0–15	11.4	1.28	/	/	0–5	32.31	2.89	/	/
							5–15	16.42	1.61		
	Rice—wheat						0–5	16.36	1.74		
							5–15	9.92	1.17		
[46]	Wheat—maize	0–20	5.4	0.41	/	8.3	0–20	6.50	0.66	/	22.10
								6.70	0.71		25.20
[47]	Soybean—maize	0–15	5.4	0.45	/	/	0–15	6.80	1.25	/	/
	Centro—maize							6.43	0.67		
	Cowpea—maize							4.86	0.47		
	Fallow—maize							5.07	0.53		

The data in the table are obtained from field experiments using traditional tillage method and cultivation techniques without any application of organic fertilizers or crop straws. A part of SOC data is derived from the conversion of SOM (SOM = 1.724 ∗ SOC, SOC: soil organic carbon; SOM: soil organic matter).

that the rotation of rice with velvet bean or hyacinth bean reduced weed competition and increased the chlorophyll concentration and yield of rice. *Pseudomonas fluorescens* [63] and *Burkholderia vietnamensis* [64] are well documented as beneficial bacteria in rice fields that increase rice yield and act against sheath blight disease, respectively. As cereal crops are good nematode hosts, whereas legume crops are resistant to this parasite, the yield of rice grain when grown after cowpea and/or mungbean is significantly higher than that after cereal crops [65].

The prevention effect of a specific rotation on pest species proliferation may be mediated by impeded drainage and tillage practices, particularly no-till in which plant residues remain on the field [65]. However, soil microorganisms may also include plant pathogens or deleterious rhizosphere microorganisms, which may negatively affect plant growth and yield [66]. For instance, in the rice-wheat cropping system, some of the diseases and insect pests of rice, such as stem borers, stalk rot, and leaf blight, have occurred in wheat [67, 68]. Thus, the effects of paddy-upland rotation on soil properties have advantages and disadvantages; the utilization of such advantages and the control of the disadvantages will be the focus of future research.

5. Conclusions

Paddy-upland rotation is an unavoidable cropping system for Asia to meet the increasing demand for food. However, conventional practices of growing rice and wheat not only deteriorate soil physical properties and decrease water and fertilizer use efficiencies but also cause a stagnation or even reduction in grain yields. Maintaining soil quality at a desirable level is a very complicated and difficult task, because paddy-upland rotation fields are unique from other wetland or upland soils; they are associated with frequent cycling between wetting and drying under anaerobic and aerobic conditions; such rotations change the soil C and N cycles and make the chemical speciation and biological effectiveness of soil nutrient elements varied with seasons, increase the diversity of soil organisms, and make the change of soil physical properties more complicated (Figure 2). Therefore, fully understanding the characteristics of different paddy-upland rotation and its soil properties is necessary in maintaining soil fertility and plant yields. Although new cultivation techniques and nutrient managements, such as minimum tillage systems and combined application of organic and inorganic fertilizers, have been proposed to overcome these problems, extensive investigation and research on potential adverse effects, long-term impacts, and farmer acceptance are still needed. Regardless of the cultivation or management measures used in paddy-upland rotation, the different responses of paddy and upland seasons and their interactions, the long-term effects, the particularity of regions, the differences of ecological conditions, economic and ecological benefits, operability, and the potential of widely use should be considered. By doing so, the paddy-upland rotation can truly achieve sustainable development.

Conflict of Interests

The authors declare that there is no conflict of interests regarding the publication of this paper.

Acknowledgments

This study was financially supported by Sino-German cooperation project (2012DFG91520). The authors would like to gratefully thank all the members of the crop cultivation laboratory of Sichuan agriculture university of China for their suggestions and help.

References

[1] C. S. Bueno and J. K. Ladha, "Comparison of soil properties between continuously cultivated and adjacent uncultivated soils in rice-based systems," *Biology and Fertility of Soils*, vol. 45, no. 5, pp. 499–509, 2009.

[2] M. K. Gathala, J. K. Ladha, Y. S. Saharawat, V. Kumar, V. Kumar, and P. K. Sharma, "Effect of tillage and crop establishment methods on physical properties of a medium-textured soil under a seven-year rice-wheat rotation," *Soil Science Society of America Journal*, vol. 75, no. 5, pp. 1851–1862, 2011.

[3] J. Timsina and D. J. Connor, "Productivity and management of rice-wheat cropping systems: issues and challenges," *Field Crops Research*, vol. 69, no. 2, pp. 93–132, 2001.

[4] M. S. Fan, R. F. Jiang, F. S. Zhang, S. H. Lü, and X. J. Liu, "Nutrient management strategy of paddy rice-upland crop rotation system," *Chinese Journal of Applied Ecology*, vol. 19, no. 2, pp. 424–432, 2008.

[5] J. K. Ladha, K. S. Fischer, M. Hossain, P. R. Hobbs, and B. Hardy, "Improving the productivity of rice-wheat systems of the Indo-Gangetic Plains: a synthesis of NARS-IRRI partnership research," IRRI Discussion Paper 40, IRRI, Los Baños, Philippines, 2000.

[6] D. Dawe, S. Frolking, and C. Li, "Trends in rice-wheat area in China," *Field Crops Research*, vol. 87, no. 1, pp. 89–95, 2004.

[7] China's National Bureau of Statistics, *China Statistical Yearbook 2010*, China Statistics Press, Beijing, China, 2010.

[8] J. K. Ladha, H. Pathak, A. T. Padre, D. Dawe, and R. K. Gupta, "Productivity trends in intensive rice-wheat cropping systems in Asia," in *Improving the Productivity and Sustainability of Rice-Wheat Systems: Issues and Impacts*, J. K. Ladha, Ed., vol. 65 of *Special Publication*, pp. 45–76, 2003.

[9] J. K. Ladha, D. Dawe, H. Pathak et al., "How extensive are yield declines in long-term rice-wheat experiments in Asia?" *Field Crops Research*, vol. 81, no. 2-3, pp. 159–180, 2003.

[10] S. F. Mousavi, S. Yousefi-Moghadam, B. Mostafazadeh-Fard, A. Hemmat, and M. R. Yazdani, "Effect of puddling intensity on physical properties of a silty clay soil under laboratory and field conditions," *Paddy and Water Environment*, vol. 7, no. 1, pp. 45–54, 2009.

[11] B. K. Behera, B. P. Varshney, and A. K. Goel, "Effect of puddling on puddled soil characteristics and performance of self-propelled transplanter in rice crop," *Agricultural Engineering International: CIGRE Journal*, vol. 10, manuscript PM 08 020, 2009.

[12] C. P. Huang and D. L. Ding, "The effects of paddy upland rotation on crop yield and soil physical and chemical characteristics," *Acta Agriculturae Zhejiangensis*, vol. 7, no. 6, pp. 448–450, 1995.

[13] J. M. Motschenbacher, K. R. Brye, and M. M. Anders, "Long-term rice-based cropping system effects on near-surface soil compaction," *Agricultural Sciences*, vol. 2, no. 2, pp. 117–124, 2011.

[14] Z. F. Wang, M. Gao, J. C. Qin, and E. Ci, "Effect of long-term "paddy-upland" rotation on soil fertility of paddy fields," *Journal of Southwest Agricultural University: Natural Science*, vol. 25, no. 6, pp. 514–517, 2003.

[15] A. A. Rahmianna, T. Adisarwanto, G. Kirchhof, and H. B. So, "Crop establishment of legumes in rainfed lowland rice-based cropping systems," *Soil and Tillage Research*, vol. 56, no. 1-2, pp. 67–82, 2000.

[16] H. S. Sur, S. S. Prihar, and S. K. Jalota, "Effect of rice-wheat and maize-wheat rotations on water transmission and wheat root development in a sandy loam of the Punjab, India," *Soil and Tillage Research*, vol. 1, pp. 361–371, 1980.

[17] M. Ishaq, A. Hassan, M. Saeed, M. Ibrahim, and R. Lal, "Subsoil compaction effects on crops in Punjab, Pakistan. I: soil physical properties and crop yield," *Soil and Tillage Research*, vol. 59, no. 1-2, pp. 57–65, 2001.

[18] M. Farooq, S. M. A. Basra, and S. A. Asad, "Comparison of conventional puddling and dry tillage in rice-wheat system," *Paddy and Water Environment*, vol. 6, no. 4, pp. 397–404, 2008.

[19] S. Chen, X. Zheng, D. Wang, L. Chen, C. Xu, and X. Zhang, "Effect of long-term paddy-upland yearly rotations on rice (Oryza sativa) yield, soil properties, and bacteria community diversity," *The Scientific World Journal*, vol. 2012, Article ID 279641, 11 pages, 2012.

[20] P. K. Sharma, J. K. Ladha, T. S. Verma, R. M. Bhagat, and A. T. Padre, "Rice-wheat productivity and nutrient status in a lantana- (Lantana spp.) amended soil," *Biology and Fertility of Soils*, vol. 37, no. 2, pp. 108–114, 2003.

[21] C. Srinivasarao, B. Venkateswarlu, R. Lal et al., "Long-term effects of soil fertility management on carbon sequestration in a rice-lentil cropping system of the indo-gangetic plains," *Soil Science Society of America Journal*, vol. 76, no. 1, pp. 167–178, 2012.

[22] R. M. Wang and Y. S. Ding, "Effect of the paddy-upland yearly rotation on the soil fertility," *Chinese Journal of Rice Science*, vol. 12, no. 2, pp. 85–91, 1998.

[23] K. S. Gangwar, K. K. Singh, and S. K. Sharma, "Effect of tillage on growth, yield and nutrient uptake in wheat after rice in the Indo-Gangetic Plains of India," *Journal of Agricultural Science*, vol. 142, no. 4, pp. 453–459, 2004.

[24] D. K. Benbi, A. S. Toor, and S. Kumar, "Management of organic amendments in rice-wheat cropping system determines the pool where carbon is sequestered," *Plant and Soil*, vol. 360, no. 1-2, pp. 145–162, 2012.

[25] R. K. Gupta and I. K. Jaggi, "Soil physical conditions and paddy yield as influenced by depth of puddling," *Journal of Agronomy and Crop Science*, vol. 148, pp. 329–336, 1979.

[26] J. Y. Zheng, M. A. Shao, and X. C. Zhang, "Spatial variation of surface soil's bulk density and saturated hydraulic conductivity on slope in loess region," *Journal of Soil and Water Conservation*, vol. 18, no. 3, pp. 53–56, 2004.

[27] M. L. Jat, M. K. Gathala, J. K. Ladha et al., "Evaluation of precision land leveling and double zero-till systems in the rice-wheat rotation: water use, productivity, profitability and soil physical properties," *Soil and Tillage Research*, vol. 105, no. 1, pp. 112–121, 2009.

[28] S. Vargas Gil, A. Becker, C. Oddino, M. Zuza, A. Marinelli, and G. March, "Field trial assessment of biological, chemical, and physical responses of soil to tillage intensity, fertilization, and grazing," *Environmental Management*, vol. 44, no. 2, pp. 378–386, 2009.

[29] R. K. Gupta, J. K. Ladha, J. Singh, G. Singh, and H. Pathak, "Yield and phosphorus transformations in a rice-wheat system with crop residue and phosphorus management," *Soil Science Society of America Journal*, vol. 71, no. 5, pp. 1500–1507, 2007.

[30] X. Li, J. Lu, L. Wu, and F. Chen, "The difference of potassium dynamics between yellowish red soil and yellow cinnamon soil under rapeseed (Brassica napus L.)-rice (Oryza sativa L.) rotation," *Plant and Soil*, vol. 320, no. 1-2, pp. 141–151, 2009.

[31] S. H. Lu and F. S. Zhang, "Review and outlook of ten years research on crop Mn nutrition in soils with upland-paddy rotation," *Soil Bulletin*, vol. 12, pp. 1–7, 1997.

[32] V. K. Nayyar, U. S. Sadana, and T. N. Takkar, "Methods and rates of application of Mn and its critical levels for wheat following rice on coarse textured soils," *Fertilizer Research*, vol. 8, no. 2, pp. 173–178, 1985.

[33] X. J. Liu, S. H. Lv, F. S. Zhang, and D. R. Mao, "Effect of water and fertilization on movement of manganese in soils and its uptake by rice," *Acta Pedologica Sinica*, vol. 39, no. 3, pp. 369–375, 1999.

[34] L. A. Morales, E. V. Vázquez, and J. Paz-Ferreiro, "Spatial and temporal variability of Mehlich-1 extractable Fe, Mn and Zn over a rice field as a function of lime amendment," *Stochastic Environmental Research and Risk Assessment*, vol. 25, no. 8, pp. 1039–1048, 2011.

[35] A. Stuart Grandya, G. A. Porter, and M. Susan Erichb, "Organic amendment and rotation crop effects on the recovery of soil organic matter and aggregation in potato cropping systems," *Soil Science Society of America Journal*, vol. 66, no. 4, pp. 1311–1319, 2002.

[36] H. Tiessen, J. W. B. Stewart, and J. R. Bettany, "Cultivation effects on the amounts and concentration of carbon, nitrogen and phosphorus in grassland soils," *Agronomy Journal*, vol. 74, pp. 831–835, 1982.

[37] F. N. Ponnamperuma, "The chemistry of submerged soils," *Advances in Agronomy*, vol. 24, pp. 29–96, 1972.

[38] C. Witt, K. G. Cassman, D. C. Olk et al., "Crop rotation and residue management effects on carbon sequestration, nitrogen cycling and productivity of irrigated rice systems," *Plant and Soil*, vol. 225, no. 1-2, pp. 263–278, 2000.

[39] M. Kumari, D. Chakraborty, M. K. Gathala et al., "Soil aggregation and associated organic carbon fractions as affected by tillage in a rice-wheat rotation in north India," *Soil Science Society of America Journal*, vol. 75, no. 2, pp. 560–567, 2011.

[40] Y. Singh, B. Singh, J. K. Ladha et al., "Long-term effects of organic inputs on yield and soil fertility in the rice-wheat rotation," *Soil Science Society of America Journal*, vol. 68, no. 3, pp. 845–853, 2004.

[41] H. Xu, G. X. Xing, Z. C. Cai, and H. Tsuruta, "Characteristics of N_2O emission from paddy fields in hilly area," *Soil and Environmental Sciences*, vol. 8, no. 4, pp. 266–270, 1999.

[42] B. P. Tripathi, J. K. Ladha, J. Timsina, and S. R. Pascua, "Nitrogen dynamics and balance in intensified rainfed lowland rice-based cropping systems," *Soil Science Society of America Journal*, vol. 61, no. 3, pp. 812–821, 1997.

[43] N. P. S. Yaduvanshi, "Substitution of inorganic fertilizers by organic manures and the effect on soil fertility in a rice-wheat rotation on reclaimed sodic soil in India," *Journal of Agricultural Science*, vol. 140, no. 2, pp. 161–168, 2003.

[44] Y. Singh, B. Singh, J. K. Ladha, C. S. Khind, T. S. Khera, and C. S. Bueno, "Effects of residue decomposition on productivity and soil fertility in rice-wheat rotation," *Soil Science Society of America Journal*, vol. 68, no. 3, pp. 854–864, 2004.

[45] M. S. Fan, X. J. Liu, R. F. Jiang et al., "Crop yields, internal nutrient efficiency, and changes in soil properties in rice-wheat rotations under non-flooded mulching cultivation," *Plant and Soil*, vol. 277, no. 1-2, pp. 265–276, 2005.

[46] S. X. Li, "Effect of long-term fallow and cultivation on soil fertilizer in rice-based cropping system," *Chinese Journal of Eco-Agriculture*, vol. 9, no. 3, pp. 67–69, 2001.

[47] X. Q. Dai, Z. Ouyang, Y. S. Li, and H. M. Wang, "Variation in yield gap induced by nitrogen, phosphorus and potassium fertilizer in north China plain," *PLoS ONE*, vol. 8, no. 12, Article ID e82147, 2013.

[48] M. K. A. Adeboye, E. N. O. Iwuafor, and J. O. Agbenin, "The effects of crop rotation and nitrogen fertilization on soil chemical and microbial properties in a Guinea Savanna Alfisol of Nigeria," *Plant and Soil*, vol. 281, no. 1-2, pp. 97–107, 2006.

[49] V. K. Singh, B. B. Sharma, and B. S. Dwivedi, "The impact of diversification of a rice-wheat cropping system on crop productivity and soil fertility," *Journal of Agricultural Science*, vol. 139, no. 4, pp. 405–412, 2002.

[50] A. Marais, M. Hardy, M. Booyse, and A. Botha, "Effects of monoculture, crop rotation, and soil moisture content on selected soil physicochemical and microbial parameters in wheat fields," *Applied and Environmental Soil Science*, vol. 2012, Article ID 593623, 13 pages, 2012.

[51] J. A. W. Morgan, G. D. Bending, and P. J. White, "Biological costs and benefits to plant-microbe interactions in the rhizosphere," *Journal of Experimental Botany*, vol. 56, no. 417, pp. 1729–1739, 2005.

[52] Y. G. Yanni, R. Y. Rizk, V. Corich et al., "Natural endophytic association between Rhizobium leguminosarum bv. trifolii and rice roots and assessment of its potential to promote rice growth," *Plant and Soil*, vol. 194, no. 1-2, pp. 99–114, 1997.

[53] T. Turmuktini, E. Kantikowati, B. Natalie et al., "Restoring the health of paddy soil by using straw compost and biofertilizers to increase fertilizer efficiency and rice production with Sobari (system of organic based aerobic rice intensification) technology," *Asian Journal of Agriculture and Rural Development*, vol. 2, no. 4, pp. 519–526, 2012.

[54] D. T. Xuan, V. T. Guong, A. Rosling, S. Alström, B. Chai, and N. Högberg, "Different crop rotation systems as drivers of change in soil bacterial community structure and yield of rice, Oryza sativa," *Biology and Fertility of Soils*, vol. 48, no. 2, pp. 217–225, 2012.

[55] N. Ladygina and K. Hedlund, "Plant species influence microbial diversity and carbon allocation in the rhizosphere," *Soil Biology and Biochemistry*, vol. 42, no. 2, pp. 162–168, 2010.

[56] V. O. Biederbeck, C. A. Campbell, and R. P. Zentner, "Effect of crop rotation and fertilization on some biological properties of a loam in southwestern Saskatchewan," *Canadian Journal of Soil Science*, vol. 64, no. 3, pp. 355–367, 1984.

[57] P. A. Roger, K. L. Heong, and P. S. Teng, *Biodiversity and Sustainability of Wetland Rice Production: Role and Potential of Microorganisms and Invertebrates*, IRRI Strategy, 1990–2000 and Beyond, IRRI, Manila, Phillipines, 1989.

[58] Y. M. Ding, *Occurrence of Sclerotinia Stem Rot of Oilseed Rape in Two Farming Systems and Biocontrol Using Coniothyrium minitans*, The Central China Agricultural College, 2010.

[59] W. H. Yuan, N. Liu, X. W. Wang, and H. Zheng, "Effects of cultural measure on resistance and tolerance to scleratinia sclerotiorum in double-low rapeseed," *Acta Agriculturae Universitatis Jiangxiensis*, vol. 31, no. 5, pp. 855–857, 2009.

[60] G. F. Pegg and B. L. Brady, *Verticillium Wilts*, CAB International, Oxford, UK, 2002.

[61] Y. Ebihara, S. Uematsu, and S. Nomiya, "Control of Verticillium dahliae at a strawberry nursery by paddy-upland rotation," *Journal of General Plant Pathology*, vol. 76, no. 1, pp. 7–20, 2010.

[62] R. A. Marenco and Á. M. B. Santos, "Crop rotation reduces weed competition and increases chlorophyll concentration and yield of rice," *Pesquisa Agropecuaria Brasileira*, vol. 34, no. 10, pp. 1881–1887, 1999.

[63] R. Nandakumar, S. Babu, R. Viswanathan, T. Raguchander, and R. Samiyappan, "Induction of systemic resistance in rice against sheath blight disease by Pseudomonas fluorescens," *Soil Biology and Biochemistry*, vol. 33, no. 4-5, pp. 603–612, 2001.

[64] M. Govindarajan, J. Balandreau, S. W. Kwon, H. Y. Weon, and C. Lakshminarasimhan, "Effects of the inoculation of Burkholderia vietnamensis and related endophytic diazotrophic bacteria on grain yield of rice," *Microbial Ecology*, vol. 55, no. 1, pp. 21–37, 2008.

[65] M. M. Mature, "Influence of rice rotation systems on soil nematode trophic groups in Arkansas," *Journal of Agricultural Science*, vol. 4, no. 2, pp. 11–20, 2012.

[66] S. Hilton, A. J. Bennett, G. Keane et al., "Impact of shortened crop rotation of oilseed rape on soil and rhizosphere microbial diversity in relation to yield decline," *PLoS ONE*, vol. 8, no. 4, Article ID e59859, 2013.

[67] S. Nagarajah, H. U. Neue, and M. C. R. Alberto, "Effect of Sesbania, Azolla and rice straw incorporation on the kinetics of NH4, K, Fe, Mn, Zn and P in some flooded rice soils," *Plant and Soil*, vol. 116, no. 1, pp. 37–48, 1989.

[68] S. Chander, R. N. Garg, and G. Singh, "Termite infestation in relation to soil physical property in wheat crop under rice-wheat cropping system," *Annals of Agriculture Research*, vol. 18, pp. 348–350, 1997.